# CONSISTENT ENERGY TREATMENT FOR RADIATION TRANSPORT METHODS

A Dissertation
Presented to
The Academic Faculty

by

Steven James Douglass

In Partial Fulfillment
of the Requirements for the Degree
Doctor of Philosophy in Nuclear Engineering

Georgia Institute of Technology
May 2012

# CONSISTENT ENERGY TREATMENT FOR RADIATION TRANSPORT METHODS

Approved by:


Dr. Farzad Rahnema, Advisor
Nuclear & Radiological Engineering and Medical Physics Programs
George W. Woodruff School
*Georgia Institute of Technology*

Dr. Tom Morley
School of Mathematics
*Georgia Institute of Technology*

Dr. Bojan Petrovic
Nuclear & Radiological Engineering and Medical Physics Programs
George W. Woodruff School
*Georgia Institute of Technology*

Dr. Doron Lubinsky
School of Mathematics
*Georgia Institute of Technology*

Dr. Dingkang Zhang
Nuclear & Radiological Engineering and Medical Physics Programs
George W. Woodruff School
*Georgia Institute of Technology*


Date Approved: March 28, 2012

# ACKNOWLEDGEMENTS

I would first like to thank Dr. Farzad Rahnema, whose guidance, motivation, and tireless patience has been invaluable in the last couple of years. I would not be close to where I am without his support and assistance. I would also like to thank Dr. Dingkang Zhang, for offering insight and assistance throughout my time at Georgia Tech. I also extend my thanks to Dr. Tom Morley, Dr. Doron Lubinsky, and Dr. Bojan Petrovic, who have graciously agreed to serve on my committee.

In addition, I would like to thank my parents, who have always been supportive of my education, and have always been willing to help me in any way they can. I could not have achieved anything without the foundation upon which I was raised.

Lastly, I would like to thank my friends and my brothers. They have been a constant source of encouragement in my graduate endeavors, and on late nights with a pot of coffee, have been the ones sitting next to me offering support. Without them, I doubt I would have had the strength of commitment to achieve what I have over the years.

Thank you all.

# TABLE OF CONTENTS

# LIST OF TABLES

# LIST OF FIGURES

# SUMMARY

The approximations used in the standard multigroup method and cross section condensation procedure introduce several known errors, such those caused by spectral core environment effects and the neglect of the energy and angular coupling of the flux when condensing the total cross section. In this dissertation, a multigroup formulation is developed which maintains direct consistency with the continuous energy or fine-group structure, exhibiting the accuracy of the detailed energy spectrum within the coarse-group calculation.

Two methods are then developed which seek to invert the condensation process – turning the standard one-way condensation (from fine-group to coarse-group) into the first step of a two-way iterative process. The first method is based on the previously published Generalized Energy Condensation, which established a framework for obtaining the fine-group flux by preserving the flux energy spectrum in orthogonal energy expansion functions, but did not maintain a consistent coarse-group formulation. It is demonstrated that with a consistent extension of the GEC, a cross section recondensation scheme can be used to correct for the spectral core environment error. This is then verified numerically in a 1D VHTR core.

In addition, a more practical and efficient new method, termed the "Subgroup Decomposition (SGD) Method," is developed which eliminates the need for expansion functions altogether, and allows the fine-group flux to be decomposed from a consistent coarse-group flux with minimal additional computation or memory requirements. This method, as a special case of a more general spline-approximation for radiation transport, is shown to be highly effective in a cross section recondensation scheme, providing fine-group results in a fraction of the time generally necessary to obtain a fine-group solution.

In addition, a whole-core BWR benchmark problem is generated based on operating reactor parameters, in 2D and 3D. This contributes to the furthering of new methods development from the proof-of-concept level to the whole-core direct 3D transport level . A set of 1D benchmarks is also developed for a BWR, PWR, and VHTR core. These provide significant value both in preliminary testing of the new methods presented in this dissertation and in the future testing of new transport methods.

# CHAPTER 1

# INTRODUCTION

The primary goal of radiation transport methods is to obtain the angular flux as a function of position, angle, and energy. This angular flux is described via the integro-differential Boltzmann radiation transport equation, Eq. (1.1).

$$\begin{aligned}&\hat{\Omega}\cdot\nabla\Psi(\vec{r},\hat{\Omega},E)+\sigma(\vec{r},E)\Psi(\vec{r},\hat{\Omega},E)\\&=\frac{1}{4\pi}\int_0^\infty dE'\int_{4\pi}d\hat{\Omega}'\sigma_s(\vec{r},E'\to E,\hat{\Omega}'\to\hat{\Omega})\Psi(\vec{r},\hat{\Omega},E)+\frac{\chi(\vec{r},E)}{4\pi k}\int_0^\infty dE'\nu\sigma_f(\vec{r},E')\phi(\vec{r},E')\end{aligned} \tag{1}$$

where $\Psi(\vec{r},\hat{\Omega},E)$ is the angular flux, $\phi(\vec{r},E)$ is the scalar flux (the integral of the angular flux over solid angle 4π), and $\sigma(\vec{r},E)$ represents the total macroscopic reaction cross section at position $\vec{r}$ for neutrons with lethargy *u*. The function $\sigma_s(\vec{r},E'\to E,\hat{\Omega}'\to\hat{\Omega})$ is the macroscopic scattering cross section at position $\vec{r}$ with incoming lethargy *E'* and angle $\hat{\Omega}'$ and outgoing lethargy *E* and angle $\hat{\Omega}$. The system multiplication constant is represented by *k* and $\nu\sigma_f(\vec{r},E')$ and $\chi(\vec{r},E)$ are the fission production cross section and fission spectrum, respectively.

This equation can only be solved analytically for extremely simple problems, and numerically solving this equation is highly challenging, particularly for large-scale problems such as reactors, which are composed of thousands of fuel pins of varying material composition, temperature, and exposure. As a result, getting an accurate flux solution with a deterministic method requires such a fine discretization of the phase space that these problems become almost intractable rather quickly. Likewise, stochastic methods such as Monte Carlo are too computationally expensive for practical or timely analysis of full scale cores.

Neutronics analysis has therefore been traditionally limited to homogenized nodal diffusion methods (Smith, 1986 and 1994). However, increases in computational power in recent years have caused a transition to the development of direct transport methods specifically for the analysis of such large-scale problems. This transition is difficult because the large number of unknowns generated from the fine discretization of the phase space results in significant memory and processing time requirements. Another difficulty is that accounting for the steep flux gradients and local anisotropies in the angular flux for a fine discretization requires much higher order approximations than homogenized methods. Even within massively parallel computing systems, the difficulty in scaling transport algorithms to multiple processors restricts the computational advantages of parallelization in whole-core transport.

The research and development of improved whole-core transport methods has been characterized by work along several approaches. Improved data handling techniques and computational acceleration schemes are being developed within parallel computing environments. Adaptive spatial differencing schemes and more advanced phase-space decomposition methods are also being researched in conjunction with improved methods for energy group condensation. These research objectives work towards the goal of a robust framework for whole-core direct transport which allows for accurate and efficient neutronics solutions.

In the energy variable, the multigroup method has become widely used in deterministic transport and diffusion theory because it provides a way of reducing the complexity of the energy dependence through “cross section condensation”. The central

premise of this condensation procedure is that, because one can not solve the problem efficiently with a full energy treatment, an effective cross section can be generated over an energy interval (or "group") *g*, as in Eq. (1.2).

$$\sigma_g(\vec{r}) = \frac{\int_g dE\sigma(\vec{r},E)\phi(\vec{r},E)}{\int_g dE\phi(\vec{r},E)} \tag{1.2}$$

The most obvious source of error is in this process is that introduced by smearing out the detailed energy dependence into a discrete group structure. While the most important physical parameters in reactor core calculations are energy-integrated quantities (e.g. pin power, core eigenvalue), in other applications, such as detection and shielding, the resolution of the energy dependence is highly important. In addition, the spectral dependence of pin-to-pin and neighboring bundle interactions cannot be efficiently calculated with a large number of groups, particularly in fast or optically thin reactors. As a result, extreme care must be taken on a case-by-case basis to ensure that enough groups are used and that their boundaries are appropriate in order to generate solutions with sufficient accuracy.

The reason such care is necessary is that the overall accuracy of the cross section condensation process is determined by how well the physics of the continuous energy spectrum are captured within the multigroup formulation. The vast majority of multigroup transport and diffusion codes use the scalar flux as the weighting function, as in Eq. (1.2), to avoid introducing an angularly dependent total cross section. This effectively assumes that the angular flux is separable in energy and angle within each group, which is frequently not the case. This results in a multigroup formulation which is inconsistent with the physics of the continuous energy transport equation. In the past, the use of spatial homogenization of the cross sections introduced other errors which cancelled out or masked the errors

introduced by this inconsistency. As direct transport without homogenization for large-scale problems becomes more prevalent, however, it is highly important to address it.

Another significant cause of error introduced in the standard condensation process is the use of an incorrect spectrum to condense the cross sections. The angular flux is the desired solution of the transport equation, and therefore the flux spectrum in Eq. (1.2) is not known *a priori.* Instead, a "guess" spectrum is obtained either from the physics of the problem, or from pin-cell or lattice-cell transport calculations with approximate boundary conditions (e.g. specular reflection). As a result of complex core heterogeneity, control rod positions, and core boundary leakage, the exact spectrum in the problem is often extremely different than the guess spectrum, which introduces the so-called "core-environment" error, where both pin-to-pin and bundle-to-bundle effects have been, at best, coarsely approximated. This error can be highly significant in the multigroup calculations, particularly in regions of the problem with sharp flux gradients (e.g. material interfaces, strong absorbers, core periphery).

In this dissertation, a formulation of the multigroup equation is presented which is entirely consistent with the continuous energy physics. This formulation also facilitates a new class of spectral techniques which allow the detailed energy spectrum to be "de-condensed" via orthogonal function expansion or B-Spline approximation. This allows the development of spectral cross section recondensation methods which address the core environment error. In particular, a new "Subgroup Decomposition Method" is derived as a special case of the B-Spline approximation which provides a fundamental advancement in the way whole-core fine-group transport is approached.

In addition to the theoretical development and numerical verification of these methods, this dissertation also includes the development of a set of neutron-transport benchmark problems, provided as tools for the development of neutron transport methods. A GE9-Loaded BWR Benchmark is generated in 2D and 3D with a realistic set of burnup and void distributions based on an operating BWR. While these benchmarks provide a useful set of test problems for future transport methods, new methods benefit from being able to be tested more rapidly and in a simpler physical environment than 2D or 3D reactor problems. This dissertation therefore also includes the development of 1D core benchmark problems for a BWR, PWR, and VHTR which maintain the essential physical characteristics of their 2D counterparts.

# CHAPTER 2

# BACKGROUND

## 2.1 Multigroup Radiation Transport

The steady radiation transport equation, Eq. (1.1), is only solvable analytically for a very restricted class of problems. Outside of geometrically simple problems with mostly uniform material compositions, the equation can only be solved via a computational approach. Because there are very few problems of interest which are that simple, the vast majority of problems are solved via either deterministic computational transport or stochastic (Monte Carlo) simulation. While increased computer power has made Monte Carlo methods more appealing, the increase in computing ability has been paralleled by an increase in the complexity of the problems of interest. For extremely large or complex problems (e.g., large nuclear reactors and shielding problems), a deterministic approach can generally lead to a solution far more quickly than Monte Carlo methods. The deterministic approach requires a discretization of the phase space (position, energy, angular variables), and the majority of deterministic methods begin by discretizing the energy variable using the multigroup method.

### 2.1.1 Phase Space Discretization and Reduction Methods

Deterministic methods establish only an "approximate" solution to the transport equation and how finely one discretizes the phase space determines the level of accuracy of the solution. Spatial discretization schemes break up the geometry of the problem into either 2D or 3D meshes over which the flux is assumed to be constant. Angular approximations treat the angular variable in the transport equation with angular moment expansions (e.g., $P_N$ method) or solve it only for specified directions ($S_N$), and rely on quadrature techniques to

generate angular integrals of the flux (Bell and Glasstone, 1970). The energy variable is typically discretized by generating effective cross sections which are constant over a set of discrete energy intervals and assuming the flux is constant over those intervals (multigroup method).

The difficulty with these approximation schemes is that the large scale, complex spatial heterogeneities, and detailed spectral interactions make the needed discretization prohibitively fine. Even with massively parallel computing systems, modern reactor problems are too complex to be solved efficiently or rapidly. To address this, the industry has long taken the approach of reducing the complexity of the problem by implementing discretization-coarsening schemes.

The most common of these coarsening schemes is the homogenization of cross sections – generating "effective" cross sections which are constant over large subregions of the problem (lattice-cells). For example, in reactor analysis, this is accomplished by performing calculations for a single lattice cell with some sort of approximate boundary condition (e.g., specular reflection or white boundary conditions) using a fine spatial mesh, and then computing a flux-weighted average of the cross section for the entire lattice cell. The whole-core problem can then be solved with a lower-order method (e.g., diffusion theory) to get an approximation of the solution (Smith, 1986).

A large number of advanced methods have been developed over the years to make the cross section homogenization and diffusion calculation more accurate (McKinley and Rahnema, 2000, Rahnema and McKinley, 2002, Smith, 1994). In addition, the increased availability of high-powered computing has reduced the need for these approximations, and made whole-core, fine-mesh transport somewhat more tractable. However, when performing

whole-core transport calculations, most of the available computing resources are used to finely resolve the spatial and angular discretization. As a result, empirically obtained continuous energy (point-wise) cross sections remain unfeasible for use in these whole-core deterministic transport calculations.

### 2.1.2 Energy Group Condensation

The most common method to address this issue is to reduce the complexity of the energy dependence by condensing the continuous energy cross section library into a set of equivalent cross sections which are constant over only a few coarse energy intervals (groups). Before delving too deeply into the detailed workings of new energy methods, it may be helpful to the reader to provide a brief review of this method and its shortcomings.

The standard cross section condensation method simplifies the energy dependence of the problem by reducing the cross sections from a continuous energy point-wise library into a condensed macroscopic library which is constant over a discrete set of energy intervals. In order for the condensed library to be valid, transport calculations with both libraries must produce the same results for relevant physical parameters. In most cases, and especially in reactor analysis, it is the total reaction rate which defines the relevant parameters of the problem (eigenvalue, pin powers, control rod worth, etc.). The cross section condensation process is therefore based on the concept of "reaction rate preservation".

First, the entire energy range is partitioned into a set of $G$ intervals (or "groups") with $G+1$ "group boundaries": $E_0$, $E_1$, ... $E_{G-1}$, $E_G$. Group $g$ is defined as the interval from $E_g$ to $E_{g+1}$, equivalent group cross sections $\sigma_g(\vec{r},\hat{\Omega})$ are defined as a flux-weighted average of the cross section over each energy group, as in Eq. (2.1).

$$\sigma_g(\vec{r},\hat{\Omega}) = \frac{\int_{E_g}^{E_{g+1}} dE\sigma(\vec{r},E)\Psi(\vec{r},\hat{\Omega},E)}{\int_{E_g}^{E_{g+1}} dE\Psi(\vec{r},\hat{\Omega},E)} \tag{2.1}$$

where $\Psi(\vec{r},\hat{\Omega},E)$ is the angular flux at position $\vec{r}$ and energy *E,* moving in direction $\hat{\Omega}$. If the group flux, $\Psi_g(\vec{r},\hat{\Omega})$, is then defined as the integral of the angular flux over group *g* (the denominator in Eq. 1), the total group reaction rate, $R_g(\vec{r},\hat{\Omega})$, is then preserved as the product of group flux and group cross section in Eq. (2.2).

$$R_g(\vec{r},\hat{\Omega}) = \int_{E_g}^{E_{g+1}} dE\sigma(\vec{r},E)\Psi(\vec{r},\hat{\Omega},E) = \sigma_g(\vec{r},\hat{\Omega})\Psi_g(\vec{r},\hat{\Omega}) \tag{2.2}$$

Thus, by defining a set of group cross sections and group fluxes, equations (2.1) and (2.2) represent the fundamental basis of multigroup theory and cross section condensation. However, the central difficulty of the condensation process is also apparent in Eq. (2.1), because the angular flux at every position, energy, and angle is required to generate the group cross sections. This angular flux is the desired solution of the transport equation, and therefore is not known *a priori*. A large amount of research in the field has gone into determining approximate energy spectra with which to generate condensed cross sections that sufficiently reproduce the results of the continuous energy calculation. Over the years, the industry has settled on a multi-layered approach to generate group cross sections for only a few coarse energy groups, visualized in Figure 2.1.

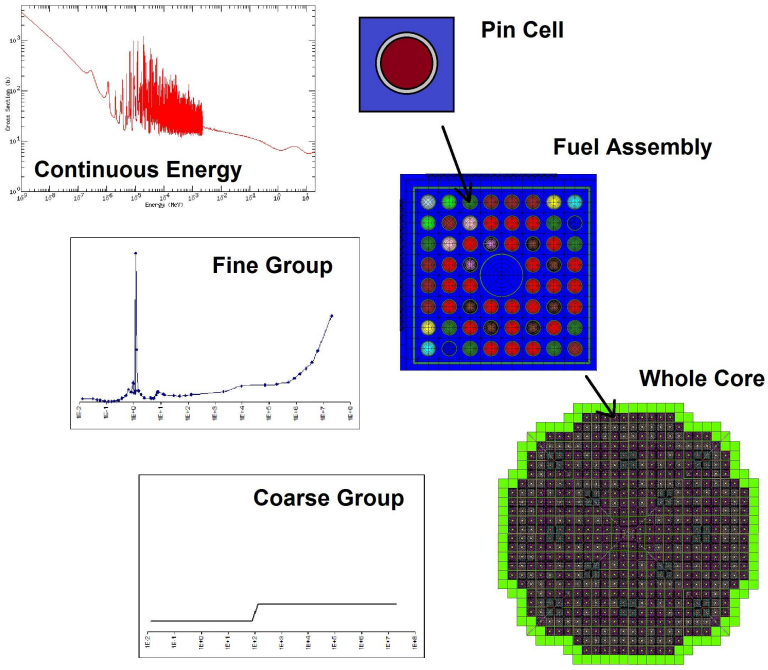


Figure 2.1: Condensation procedure from continuous energy microscopic cross sections to coarse-group macroscopic cross sections.

The first layer of approximation is to use a code such as NJOY (LANL, 1994), which uses a set of approximate flux spectra defined from theoretical considerations to generate ultra-fine (10,000s of groups) or hyper-fine (100,000+ groups) cross sections from empirically obtained continuous-energy cross sections. The flux spectra used for these calculations are typically representative of the general type of system in which the cross sections are most likely to be used. For example, cross sections are generated for typical LWRs by assuming a fission-production spectrum for high energy neutrons, a 1/v spectrum in the slowing down range, and a Maxwellian spectrum in the thermal range. This can become highly-problem specific, however, as the thermal spectrum is dependent on temperature, and generating cross sections at varying temperature is highly challenging, requiring approximations such as thermal-scattering corrections or doppler-broadening resonance corrections.

The next layer of approximation is to use the cross sections from the ultra- or hyper-fine library to perform an ultra- or hyper-fine transport calculation for a highly simplified problem (typically a 1D cylindrical calculation for a single fuel pin). This flux is then used to condense the cross sections further to a fine-group (100s or 1000s of groups) library.

For the next layer of approximation, the fine-group cross sections are then used in a lattice cell (e.g., fuel assemblies, also commonly referred to as bundles, or blocks) transport calculation with specular reflective boundary conditions to obtain a flux with which to generate coarse-group (usually < 10 groups) cross sections. Often, these cross sections are also spatially homogenized over either the pin-cells or material regions. These are then typically used in a whole-core transport (or nodal diffusion) calculation, which introduces an additional layer of approximation in its angular and spatial discretization.

This coarsening procedure allows the whole core problem to be solved more efficiently by greatly reducing the number of unknowns; however, the approximations required to obtain these cross sections can strongly influence the accuracy of the core calculation.

There are two major effects of using this multi-level approximation which introduce errors in the whole core calculation which are well understood, but often neglected in reactor design and analysis. The first significant error introduced is referred to as the "core environment effect," which is caused by the use of specular-reflective boundary conditions in the lattice-cell calculation to obtain the fine-group flux. As mentioned earlier, the cross section condensation process is theoretically designed to preserve the fine-group neutron reaction rates in the coarse-group calculation by defining the coarse-group cross sections as a flux-weighted average over the coarse groups. However, when the lattice is placed into the

core, the environment (neighboring lattices) may be significantly different than the specular reflective (zero-current) boundary conditions, particularly in the case of strong flux gradients across the lattice boundary (due to control blades, varying burnup, peripheral effects, etc.). In these cases, the condensed cross sections do not preserve the fine-group reaction rates of the actual core problem.

The second major error in the condensation process is the handling of a varying angular dependence in the flux within a coarse-group energy interval, which is termed the "energy-angle coupling effect." The overall accuracy of the condensed cross sections is determined by how well the physics of the detailed energy spectrum (continuous energy or fine group) are captured within the coarse group calculation. However, the condensation process introduces an angular dependence in the condensed total cross section because the angular flux is used as the weighting function, as in Eq. (2.1). Because the angular approximation method used in the core calculation is often very different than that used for the lattice-cell calculation, the vast majority of multigroup transport and diffusion codes use the scalar flux as the weighting function to avoid introducing an angularly dependent total cross section. This is accomplished by assuming that the angular flux is separable in energy and angle within each condensed group. Consequently, the coarse-group total cross section does not consistently preserve the total collision reaction rate, resulting in errors in the coarse-group solution (e.g. local flux or global eigenvalues in reactor problems). These errors may be magnified when coarser groups are used or when the angular dependence of the flux varies significantly over a coarse-group interval (common near strong absorbers, material discontinuities, and external boundaries).

## 2.2 Mathematical Background

The new methods developed in this dissertation rely on several mathematical principles, and it is beneficial to review the fundamental elements of these principles as they will appear in the forthcoming derivations. The first mathematical principle we need to review is the concept of orthogonal series expansions, and the second is the concept of Basis-Splines.

### 2.2.1 Orthogonal Series Expansions

A common technique in approximation theory is to approximate a function with a truncated expansion of linearly independent functions, such as a taylor series, or with a complete set of orthogonal functions (known as a Generalized Fourier Series) (Challifour, 1939). It is important to have a basic understanding of the mechanics of these expansion methods, as they play a large role in radiation transport (e.g., spherical harmonics).

Assume a set of orthogonal functions: $\xi_n(x)$, which obey the orthogonality condition in Eq. (2.3) on $x \in [a,b]$ and form a complete set of eigenfunctions on the interval.

$$\int_a^b dx w(x)\xi_n(x)\xi_m(x) = \frac{\delta_{nm}}{\alpha_m} \tag{2.3}$$

where $w(x)$ is a weighting function, $\delta_{nm}$ is the Kronecker Delta, and $\alpha_m$ is a normalization constant determined by the choice of $\xi_n(x)$. Any function $f(x)$ on the interval $[a, b]$ can be then written according to the expansion:

$$f(x) = \sum_{n=0}^{\infty} \alpha_n f_n \xi_n(x) \quad \text{where} \quad f_n = \int_a^b dx w(x)\xi_n(x) f(x) \tag{2.4}$$

A variety of expansion functions are commonly used depending on the desired limits of orthogonality, smoothness, etc. In nuclear engineering, Legendre polynomials are the

most commonly used, though recently other expansion functions have been used, such as the discrete Legendre polynomials (Mosher, 2004, Zhu and Forget, 2010).

### 2.2.2 B-Splines

The use of B-spline approximation in radiation transport applications has been slowly increasing in finite element analysis, particularly because of the computational advantage they possess due to the local support (Hollig, 2003). It is helpful to review the definition and some of the basic properties of B-Splines (deBoor, 2001). Define a non-decreasing knot vector $(t_j) = \{t_0, t_1, \ldots t_J\}$ on the interval $[a, b]$ such that $t_0 = a$, $t_J = b$, and $t_{j-1} \leq t_j$ for all $j \in [1, J]$. On the interval from $a$ to $b$, we then can define the B-spline function $B_{j,k}(x)$ of order $k$ with the recursion relation:

$$B_{j,k}(x) = \frac{x - t_j}{t_{j+k+1} - t_j} B_{j,k-1}(x) + \frac{t_{j+k} - x}{t_{j+k} - t_{j+1}} B_{j+1,k-1}(x) \tag{2.5}$$

with

$$B_{j,1} = \begin{cases} 1 & t_j \leq x \leq t_{j+1} \\ 0 & o.w. \end{cases} \tag{2.6}$$

The B-Spline function defined by Eq. (2.5) possesses the following properties:

1. *Positivity:* $B_{j,k}(x) > 0$, $t_j < x < t_{j+k}$

2. *Local Support:* $B_{j,k}(x) = 0$, $x \notin [t_j, t_{j+k})$

3. *Piecewise Polynomial:* $B_{j,k}(x)$ is a polynomial of degree $k$-1 on the each interval $[t_j, t_{j+1})$ for $j$=1, ... , $k$-1.

It can also be shown (deBoor, 2001) that the functions $B_{j,k}(x)$ are linearly independent on the knot sequence $(t_j)$ and that the linear combination $\$_{k,t}$ spans the space of all polynomials of order $k$, where

$$\$_{k,t} = \left\{ \sum_i \beta_i B_{i,k,t} : \beta_i \quad real, \right\} \tag{2.7}$$

This allows us to construct any piecewise polynomial function *f* as:

$$f(x) = \sum_{i=j-k+1}^{j} \beta_i B_{i,k}(x) \tag{2.8}$$

which requires $N+k$-1 constraints to uniquely determine a piecewise polynomial of degree $k$-1 with $N$+1 break-points. Through appropriate selection of constraints, such as moment-conservation (Pounders and Rahnema, 2010), this may be used to efficiently generate piecewise polynomial approximations of the angular flux.

## 2.3 Advanced Energy Treatments

### 2.3.1 Improved Generation of MG Cross Sections

To date, most of the research that has gone into improving the accuracy of multigroup transport has been focused on improving the transport calculations at the pin-cell and lattice-cell level. Work by M. L. Williams and M. Asgari (1995) formulated a combination of multi-group theory and continuous-energy theory to improve the calculation of the energy spectrum in the resonance region. Their work takes advantage of a Legendre "Sub-moment Expansion" in the scattering transfer function, and breaks the energy spectrum into three regions, using multi-group theory in the fast and thermal ranges, and a point-wise solution in the resonance region, all within a one-dimensional discrete-ordinates framework.

Additionally, M. L. Zerkle has developed methods for solving the neutron transport equation using a near-continuous energy point-wise solution method which collapses the energy dependence to a small number of groups from point-wise data (1997, 1999). Work by M. L. Williams has also provided a solution for thermal neutrons in a reactor using

continuous energy methodology implemented in the CENTRM solution module for the SCALE code system (2001). These advancements have improved the generation of fine-group cross sections for use in lattice cell calculations, but were typically used as part of a homogenization process for nodal diffusion at the whole-core level. As a result, these works have generally neglected both (a) the inconsistent treatment of the energy angle coupling in the condensation process and (b) the core-environment effect on the energy spectrum.

### 2.4.2 Generalized Energy Condensation Theory

Over the last few years, work has also been performed to address these issues within the framework of a generalized energy condensation (GEC) theory developed by Rahnema, Douglass, and Forget (2008). This work allowed an approximation of the fine-group flux at the core level to be generated during the coarse-group calculation by preserving the detailed flux shape during the condensation process within a series of orthogonal expansion moments. This work provides a starting point for the development of the methods in this work, and so it is important to review its development in detail.

The GEC theory is a method whereby the energy spectrum of the neutron flux is produced to a reasonable degree of accuracy during a few-group calculation. This method begins by generating fine-group cross sections, as well as a fine-group transport solution for the individual lattice cells (e.g., fuel assemblies) which make up the system. The fine-group transport solution within each lattice cell is then used as the weighting spectrum in the generation of orthogonal expansion moments for the energy dependence of the cross sections and reaction rates for each region of the assembly for a set of coarse-groups. The essential premise of the GEC theory is to expand the energy dependence of the flux in a complete set

of orthogonal functions $\xi_n(u)$ in lethargy with weighting function *w(u)* within each coarse group, as in Eq. (2.9).

$$\begin{aligned}\Psi(\vec{r},\hat{\Omega},u\in g) &= \sum_n \alpha_n \Psi_{ng}(\vec{r},\hat{\Omega})\xi_n(u\in g)\\ \Psi_{ng}(\vec{r},\hat{\Omega}) &= \int_g du\Psi(\vec{r},\hat{\Omega},u)w(u)\xi_n(u)\end{aligned} \tag{2.9}$$

Because the flux is used as the weighting function in the condensation process, this expansion allows the coarse-group cross sections to include higher-order moments which are not present in the standard condensation. Each coarse group is scaled to the lethargy interval of the group, and when this expansion is incorporated into the transport equation, the generalized condensed transport equation is the result, presented in Eq. (2.10).

$$\begin{aligned}&\hat{\Omega}\cdot\nabla\Psi_{ng}(\vec{r},\hat{\Omega}) + \sigma_g(\vec{r})\Psi_{ng}(\vec{r},\hat{\Omega}) + \delta_{ng}(\vec{r})\Psi_{0g}(\vec{r},\hat{\Omega})\\ &= \sum_{g'=1}^{G}\sum_{l=0}^{\infty}\sum_{m=-l}^{l}\frac{Y_{lm}^{*}(\hat{\Omega})}{4\pi}\int_g duw(u)\xi_n(u)\int_{g'} du'\sigma_{sl}(\vec{r},u'\to u)\phi_{lm}(\vec{r},u')\\ &+ \sum_{g'=1}^{G}\frac{\chi_{ng}(\vec{r})}{4\pi k}\int_{g'} du'\nu\sigma_f(\vec{r},u')\phi(\vec{r},u')\end{aligned} \tag{2.10}$$

where the following non-standard terms are defined:

$$\sigma_{slm}^{n,g'\to g}(\vec{r}) = \frac{\int_g duw(u)\xi_n(u)\int_{g'} du'\sigma_{sl}(\vec{r},u'\to u)\phi_{lm}(\vec{r},u')}{\int_{g'} du'\phi_{lm}(\vec{r},u')} \tag{2.11}$$

$$\delta_{ng}(\vec{r}) = \frac{\int_g du(\sigma(\vec{r},u)-\sigma_g(\vec{r}))w(u)\xi_n(u)\phi(\vec{r},u)}{\int_g du\phi(\vec{r},u)} \tag{2.12}$$

$$\chi_{ng}(\vec{r}) = \int_g du\chi(\vec{r},u)w(u)\xi_n(u) \tag{2.13}$$

This replaces the standard condensation procedure, which uses the ultra-fine or fine-group transport solution to generate fine or coarse-group cross sections that are constant in energy within each coarse group. Using the expansion moments of the cross sections and reaction rates, the problem is then solved via a coupled set of modified transport equations for the whole core. The resultant series of flux moments within each coarse-group can then be used to construct the fine group energy spectrum of the neutron distribution in the entire core. Of note is that the so-called "variation" term $\delta_{ng}(\vec{r})$ defined in Eq. (2.12) was used in the GEC to remove the higher-order moments from the denominator of the total cross section, and in the original implementation of the GEC, as in the above equation, the scalar flux was used to generate $\delta_{ng}(\vec{r})$. In this dissertation, this will be shown to be inconsistent with Eq. (1.1), and an extension of this method will be derived which maintains consistency.

# CHAPTER 3

# THEORY

## 3.1 Group Structure Equivalency

One of the central shortcomings of the standard phase space reduction methods is that the effort to reduce the complexity of the phase space discretization can lead to significant errors. As mentioned previously, the reduction of the energy-dependence of the cross sections from a continuous energy point-wise library into a relatively coarse multigroup structure, results in several approximations. The most significant is that the standard multigroup formulation is not consistent with the continuous energy transport equation.

This inconsistency is related to the manner in which the group total cross section is defined. The standard multigroup definition of the total cross section is as a scalar-flux weighted average of the cross section over an energy range. This ignores the coupling of the energy and angle dependency in the angular flux over that range, and results in a multigroup formulation that does not exactly preserve the reaction rates. This inconsistency has long been recognized (Bell and Glasstone, 1970), and some recent work has begun looking at the energy-angle coupling in more detail (Won and Cho, 2011), but it has generally be neglected by the industry.

This shortcoming has often been overlooked because the other approximations made in the coarsening of the phase space discretization tend to cancel out the errors introduced by neglecting the energy-angle coupling of the flux. However, as whole-core direct transport becomes more common, it is essential that the magnitudes of the energy-angle coupling effect and spectral core environment error be examined in detail and a method developed which addresses these effects in a robust way. This dissertation provides a multigroup

formulation which exactly preserves the energy integrated flux as a function of position and angle, preserving the fission rate, scattering rate, and eigenvalue of the continuous energy problem, and facilitates a cross section recondensation scheme to correct the spectral core environment error.

### 3.1.1 Source-Driven Multigroup Equivalency

The first effect that we address is the consistency of the multigroup formulation with the continuous energy transport equation. This is accomplished by defining an effective source term which maintains equivalency between the multigroup structure and the transport equation independent of the definition of the total group cross section. We start with the transport equation in general geometry in terms of lethargy in Eq. (3.1).

$$\hat{\Omega}\cdot\nabla\Psi(\vec{r},\hat{\Omega},u)+\sigma(\vec{r},u)\Psi(\vec{r},\hat{\Omega},u)-S(\vec{r},\hat{\Omega},u)=0 \tag{3.1}$$

where

$$S(\vec{r},\hat{\Omega},u)=\begin{array}{c}\dfrac{\chi(\vec{r},u)}{4\pi k}\displaystyle\int_0^\infty du'\nu\sigma_f(\vec{r},u')\phi(\vec{r},u') \\ +\displaystyle\sum_{l=0}^{\infty}\sum_{m=-l}^{l}\frac{Y_{lm}^*(\hat{\Omega})}{4\pi}\int_0^\infty du'\sigma_{sl}(\vec{r},u'\to u)\phi_l^m(\vec{r},u')\end{array} \tag{3.2}$$

where $\phi(\vec{r},u')$ is the scalar flux at position $\vec{r}$ and lethargy $u'$, and $\sigma_{sl}(\vec{r},u'\to u)$ and $\phi_l^m(\vec{r},u')$ represent angular moments of the scattering kernel and angular flux:

$$\sigma_{sl}(\vec{r},u'\to u)=\frac{1}{2}\int_{-1}^{1}d\mu_o\sigma_s(\vec{r},u'\to u,\mu_o)P_l(\mu_o) \tag{3.3}$$

$$\phi_l^m(\vec{r},u')=\int_{4\pi}d\hat{\Omega}'Y_{lm}(\hat{\Omega}')\Psi(\vec{r},u',\hat{\Omega}') \tag{3.4}$$

where $Y_{lm}(\hat{\Omega})$ are the normalized spherical harmonics, and $\mu_o=\hat{\Omega}\cdot\hat{\Omega}'$ is the cosine of the scattering angle. It is noted that the method is not dependent on the angular treatment of the

scattering, but for the sake of demonstration, the most common treatment (spherical harmonics) is used. We now define a group structure of $G$ groups with $G$+1 boundaries [$u_0$, $u_1$, ... , $u_{g-1}$, $u_g$, ... , $u_G$]. In order to generate a consistent multigroup formulation, we seek a multigroup source $Q_g(\vec{r},\hat{\Omega})$ such that

$$\hat{\Omega}\cdot\nabla\Psi_g(\vec{r},\hat{\Omega})+\sigma_g(\vec{r})\Psi_g(\vec{r},\hat{\Omega})-Q_g(\vec{r},\hat{\Omega})=0 \tag{3.5}$$

where

$$\Psi_g(\vec{r},\hat{\Omega})=\int_{u_{g-1}}^{u_g} du\Psi(\vec{r},\hat{\Omega},u) \tag{3.6}$$

for some definition of the total group cross section, $\sigma_g(\vec{r})$. By integrating Eq. (3.1) over the boundaries of group $g$, and setting it equal to Eq. (3.5), we can define $Q_g(\vec{r},\hat{\Omega})$ as in Eq. (3.7).

$$Q_g(\vec{r},\hat{\Omega})=S_g(\vec{r},\hat{\Omega})+\sigma_g(\vec{r})\Psi_g(\vec{r},\hat{\Omega})-\int_{u_{g-1}}^{u_g} du\sigma(\vec{r},u)\Psi(\vec{r},\hat{\Omega},u) \tag{3.7}$$

where $S_g(\vec{r},\hat{\Omega})$ is the standard multigroup source definition, as in Eq. (3.8).

$$\begin{aligned} S_g(\vec{r},\hat{\Omega})=&\frac{1}{4\pi k}\int_{u_{g-1}}^{u_g} du\chi(\vec{r},u)\sum_{g'=1}^{G}\int_{u_{g'-1}}^{u_{g'}} du'\nu\sigma_f(\vec{r},u')\phi(\vec{r},u') \\ &+\sum_{l=0}^{\infty}\sum_{m=-l}^{l}\frac{Y_{lm}^*(\hat{\Omega})}{4\pi}\int_{u_{g-1}}^{u_g} du\sum_{g'=1}^{G}\int_{u_{g'-1}}^{u_{g'}} du'\sigma_{sl}(\vec{r},u'\rightarrow u)\phi_l^m(\vec{r},u') \end{aligned} \tag{3.8}$$

The multigroup source therefore consists of the standard multigroup equation plus an additional two terms. These terms may be combined into one term and, by expanding the angular flux in spherical harmonics, simplified as in Eq. (3.9).

$$\sigma_g(\vec{r})\Psi_g(\vec{r},\hat{\Omega}) - \int_{u_{g-1}}^{u_g} du\,\sigma(\vec{r},u)\Psi(\vec{r},\hat{\Omega},u) = \int_{u_{g-1}}^{u_g} du\left(\sigma_g(\vec{r}) - \sigma(\vec{r},u)\right)\Psi(\vec{r},\hat{\Omega},u)$$

$$= \sum_{l=0}^{\infty}\sum_{m=-l}^{l} Y_{lm}(\hat{\Omega}) \int_{u_{g-1}}^{u_g} du\left(\sigma_g(\vec{r}) - \sigma(\vec{r},u)\right)\phi_l^m(\vec{r},u) \tag{3.9}$$

$$= -\sum_{l=0}^{\infty}\sum_{m=-l}^{l} Y_{lm}(\hat{\Omega})\delta_g^{lm}(\vec{r})\phi_g(\vec{r})$$

where $\phi_g(\vec{r})$ is the group scalar flux and $\delta_g^{lm}(\vec{r})$ is defined in Eq. (3.10).

$$\delta_g^{lm}(\vec{r}) = \frac{\int_{u_{g-1}}^{u_g} du\left(\sigma(\vec{r},u) - \sigma_g(\vec{r})\right)\phi_l^m(\vec{r},u)}{\int_{u_{g-1}}^{u_g} du\phi(\vec{r},u)} \tag{3.10}$$

This allows the multigroup transport equation to be rewritten as in Eq. (3.11).

$$\hat{\Omega}\cdot\nabla\Psi_g(\vec{r},\hat{\Omega}) + \sigma_g(\vec{r})\Psi_g(\vec{r},\hat{\Omega}) = S_g(\vec{r},\hat{\Omega}) - \sum_{l=0}^{\infty}\sum_{m=-l}^{l} Y_{lm}(\hat{\Omega})\delta_g^{lm}(\vec{r})\phi_g(\vec{r}) \tag{3.11}$$

Equation (3.11) is essentially the standard multigroup equation, but with an extra source-correction term. The derivation above shows that a consistent multigroup transport equation can be formulated for any definition of the total group cross section as long as this source correction term is included. In order to solve Eq. (3.11), multigroup coefficients are defined in the standard manner, with the total cross section being defined with the standard scalar-flux weighting for consistency with common codes:

$$\sigma_g(\vec{r}) = \frac{\int_{u_{g-1}}^{u_g} du\,\sigma(\vec{r},u)\phi(\vec{r},u)}{\int_{u_{g-1}}^{u_g} du\phi(\vec{r},u)}. \tag{3.12}$$

So far in the derivation, the multigroup formulation and coefficients are described in a general sense, in terms of the continuous energy weighting spectrum and continuous energy

cross sections. This illustrates the utility of a consistent coarse-group formulation, which would allow a direct continuous energy to coarse-group condensation to be performed in theory. However, in practice, it is far more common to perform lattice cell calculations for a fine-group structure and then use the fine-group flux to condense the cross sections into a coarse-group structure.

Let $H$ be the number of groups in a fine-group structure for which the transport solution is desired. It is assumed that for this group structure, the material cross sections are known. Let $C$ be the number of groups in a coarse-group structure for which Eq. (3.11) is efficiently solvable and define the coarse group structure such that every fine group $h$ is entirely contained within some coarse group $c$. Each fine group $h$ is then referred to as a "sub-group" of the coarse group in which it is contained. Eq. (3.11) can then be written as

$$\hat{\Omega}\cdot\nabla\Psi_c(\vec{r},\hat{\Omega})+\sigma_c(\vec{r})\Psi_c(\vec{r},\hat{\Omega})=\frac{\chi_c(\vec{r})}{4\pi k}\sum_{c'=1}^{C}\nu\sigma_{fc'}(\vec{r})\phi_{c'}(\vec{r})-\sum_{l=0}^{\infty}\sum_{m=-l}^{l}\delta_{nc}^{lm}(\vec{r})Y_{lm}(\hat{\Omega})\phi_c(\vec{r})+\sum_{l=0}^{\infty}\sum_{m=-l}^{l}\frac{Y_{lm}^{*}(\hat{\Omega})}{4\pi}\sum_{c'=1}^{C}\sigma_{slmc'\to c}(\vec{r})\phi_{lc'}^{m}(\vec{r}) \tag{3.13}$$

where the coarse-group coefficients are defined in terms of their sub-groups in Eqs. (3.14)–(3.19).

$$\Psi_c(\vec{r},\hat{\Omega})=\sum_{h\in c}\Psi_h(\vec{r},\hat{\Omega}) \tag{3.14}$$

$$\nu\sigma_{fc'}(\vec{r})=\frac{\sum_{h\in c'}\nu\sigma_{fh'}(\vec{r})\phi_{h'}(\vec{r})}{\sum_{h'\in c'}\phi_{h'}(\vec{r})} \tag{3.15}$$

$$\chi_c(\vec{r})=\sum_{h\in c}\chi_h(\vec{r}) \tag{3.16}$$

$$\sigma_{slmc'\to c}(\vec{r})=\frac{\sum_{h\in c}\sum_{h'\in c'}\sigma_{slmh'\to h}(\vec{r})\phi_{lh'}^{m}(\vec{r})}{\sum_{h'\in c'}\phi_{lh'}^{m}(\vec{r})} \tag{3.17}$$

$$\sigma_c(\vec{r}) = \frac{\sum_{h\in c} \sigma_h(\vec{r})\phi_h(\vec{r})}{\sum_{h\in c} \phi_h(\vec{r})} \tag{3.18}$$

$$\delta_c^{lm}(\vec{r}) = \frac{\sum_{h\in c} (\sigma_h(\vec{r}) - \sigma_c(\vec{r}))\phi_{lh}^m(\vec{r})}{\sum_{h\in c} \phi_h(\vec{r})} \tag{3.19}$$

The above derivation establishes the concept of "group structure equivalency" within the framework of cross section condensation. As mentioned earlier, however, there is the problem of the weighting flux within the condensation equations not being known *a priori*. The first step of standard methods is therefore to obtain a fine-group spectrum from the lattice cell calculations. This spectrum is then used to generate the coefficients in Eqs. (3.14)-(3.19), which are used to solve Eq. (3.13) for the core problem. Later in this chapter, two methods are derived which allow the fine-group spectrum to be obtained from this group solution, and these can be used to update the coefficients in Eqs. (3.14)-(3.19).

### 3.1.2 Consistent Generalized Energy Condensation Theory

In the previous section, we defined the condition necessary to establish consistency between the multigroup and the continuous energy formulations (or between a coarse-group and fine-group structure). In this section, we examine the generalized energy condensation theory and extend the principle of cross-section separation used in the original derivation of that method to account physically for the energy-angle coupling of the weighting spectrum. This extension is then shown to satisfy the condition of consistency presented in the previous section.

Within the derivation of the Generalized Energy Condensation Theory (Rahnema, Douglass, and Forget, 2008), the total cross section within each group was separated into two terms: the scalar flux-averaged total group cross section and a "variation" cross section, which is the deviation of the energy dependence of the cross section from the group-average, as in Eq. (3.20). This was done to eliminate the instability that would arise from having an energy-expansion moment near zero in the denominator of the total cross section.

$$\sigma(\vec{r},u) = \sigma_g(\vec{r}) + \delta(\vec{r},u) \tag{3.20}$$

where

$$\sigma_g(\vec{r}) = \frac{\int_g du\sigma(\vec{r},u)\phi(\vec{r},u)}{\int_g du\phi(\vec{r},u)}. \tag{3.21}$$

The essential premise of the GEC theory is to expand the energy dependence of the flux in a complete set of orthogonal functions $\xi_n(u)$ with weighting function *w(u)* within each coarse group, as in Eq. (3).

$$\begin{aligned}\Psi(\vec{r},\hat{\Omega},u\in g) &= \sum_n \alpha_n \Psi_{ng}(\vec{r},\hat{\Omega})\xi_n(u\in g)\\ \Psi_{ng}(\vec{r},\hat{\Omega}) &= \int_g du\Psi(\vec{r},\hat{\Omega},u)w(u)\xi_n(u)\end{aligned} \tag{3.22}$$

Because the flux is used as the weighting function in the condensation process, this expansion allows the coarse-group cross sections to include higher-order moments which are not present in the standard condensation. Each coarse group is scaled to the lethargy interval of the group, and when this expansion is incorporated into the transport equation, the generalized condensed transport equation is the result, presented in Eq. (3.23).

$$\begin{aligned}
&\hat{\Omega}\cdot\nabla\Psi_{ng}(\vec{r},\hat{\Omega})+\sigma_g(\vec{r})\Psi_{ng}(\vec{r},\hat{\Omega})+\delta_{ng}(\vec{r},\hat{\Omega})\Psi_{0g}(\vec{r},\hat{\Omega})\\
&=\sum_{g'=1}^{G}\sum_{l=0}^{\infty}\sum_{m=-l}^{l}\frac{Y_{lm}^{*}(\hat{\Omega})}{4\pi}\int_{g}duw(u)\xi_n(u)\int_{g'}du'\sigma_{sl}(\vec{r},u'\to u)\Psi_{lm}(\vec{r},u')\\
&+\sum_{g'=1}^{G}\frac{\chi_{ng}(\vec{r})}{4\pi k}\int_{g'}du'\nu\sigma_f(\vec{r},u')\phi(\vec{r},u')
\end{aligned}\tag{3.23}$$

In Eq. (3.23), the scattering kernel has been expanded in spherical harmonics for consistency with the group-equivalency above; however, this is not a requirement of the method. Of note in this equation is that, as a result of the separation of the collision cross section into two terms, the coupling of the energy and angular dependence within each coarse group has been entirely shifted from the traditional collision rate into the variation term $\delta_{ng}(\vec{r},\hat{\Omega})\Psi_{0g}(\vec{r},\hat{\Omega})$, which is defined in Eq. (3.24).

$$\delta_{ng}(\vec{r},\hat{\Omega})\Psi_{0g}(\vec{r},\hat{\Omega})=\int_{g}du(\sigma(\vec{r},u)-\sigma_g(\vec{r}))\Psi(\vec{r},\hat{\Omega},u)w(u)\xi_n(u)\tag{3.24}$$

In the original formulation of the GEC theory, this variation term was addressed by assuming that the energy and angular dependence of the flux were separable, just as in standard multigroup theory. Therefore, within the context of the GEC theory, this is the term that must be addressed by the consistent GEC method. The new method begins by approximating the angular flux in Eq. (5) by a series expansion of the angular variable in spherical harmonics (Lewis and Miller, 1993), as in Eq. (3.25). It is noted that other expansion bases may be used to treat this angular dependence (e.g., see Mosher and Rahnema, 2006). The selection of basis may be best determined by optimizing for the specific solution method used to solve the resulting transport equations in the system (e.g., core).

$$\Psi(\vec{r},\hat{\Omega},u)=\sum_{l=0}^{\infty}\sum_{m=-l}^{l}\Psi_{lm}(\vec{r},u)Y_{lm}(\hat{\Omega})\tag{3.25}$$

The angular expansion coefficients of the flux are defined in Eq. (3.26).

$$\phi_{lm}(\vec{r},u)=\int_{4\pi} d\hat{\Omega}\Psi(\vec{r},\hat{\Omega},u)Y_{lm}^{*}(\hat{\Omega}) \quad l=0,...,\infty \quad m=-l,...,l\,. \tag{3.26}$$

When Eqs. (3.25, 3.26) are inserted into the RHS of Eq. (3.24), an expansion (in energy and angle) of the variation term results, as in Eq. (3.28).

$$\delta_{ng}(\vec{r},\hat{\Omega})\Psi_{0g}(\vec{r},\hat{\Omega})=\sum_{l=0}^{\infty}\sum_{m=-l}^{l}\int_{g} du(\sigma(\vec{r},u)-\sigma_{g}(\vec{r}))w(u)\xi_{n}(u)Y_{lm}(\hat{\Omega})\int_{4\pi} d\hat{\Omega}'\Psi(\vec{r},\hat{\Omega}',u)Y_{lm}^{*}(\hat{\Omega}') \tag{3.28}$$

This is then simplified to Eq. (3.29)

$$\delta_{ng}(\vec{r},\hat{\Omega})\Psi_{0g}(\vec{r},\hat{\Omega})=\sum_{l=0}^{\infty}\sum_{m=-l}^{l}\delta_{ng}^{lm}(\vec{r})Y_{lm}(\hat{\Omega})\phi_{g}(\vec{r}) \tag{3.29}$$

by defining the expansion coefficients of the variation cross section as in Eq. (3.30).

$$\delta_{ng}^{lm}(\vec{r})=\frac{\int_{g} du(\sigma(\vec{r},u)-\sigma_{g}(\vec{r}))w(u)\xi_{n}(u)\int_{4\pi} d\hat{\Omega}'\Psi(\vec{r},\hat{\Omega}',u)Y_{lm}^{*}(\hat{\Omega}')}{\int_{g} du\int_{4\pi} d\hat{\Omega}'\Psi(\vec{r},\hat{\Omega}',u)} \tag{3.30}$$

Replacing the variation term in Eq. (3.23) with Eq. (3.29), and moving it to the RHS generates the consistent multigroup equations, presented in Eq. (3.31).

$$\begin{aligned}\hat{\Omega}\cdot\nabla\Psi_{ng}(\vec{r},\hat{\Omega})+\sigma_{g}(\vec{r})\Psi_{ng}(\vec{r},\hat{\Omega})=&\sum_{g'=1}^{G}\sum_{l=0}^{\infty}\sum_{m=-l}^{l}\frac{Y_{lm}^{*}(\hat{\Omega})}{4\pi}\sigma_{slm}^{n,g'\to g}(\vec{r})\phi_{lm,g'}(\vec{r})\\&+\sum_{g'=1}^{G}\frac{\chi_{ng}(\vec{r})}{4\pi k}\nu\sigma_{fg'}(\vec{r})\phi_{g'}(\vec{r})-\sum_{l=0}^{\infty}\sum_{m=-l}^{l}\delta_{ng}^{lm}(\vec{r})Y_{lm}(\hat{\Omega})\phi_{g}(\vec{r})\end{aligned} \tag{3.31}$$

where the multigroup coefficients for the scattering and fission cross sections, and angular flux moments have been defined as in Eqs. (3.32-3.35).

$$\sigma_{slm}^{n,g'\to g}(\vec{r}) = \frac{\int_g du w(u)\xi_n(u) \int_{g'} du' \sigma_{sl}(\vec{r},u'\to u)\phi_{lm}(\vec{r},u')}{\int_{g'} du' \phi_{lm}(\vec{r},u')} \tag{3.32}$$

$$\nu\sigma_{fg'}(\vec{r}) = \frac{\int_{g'} du' \nu\sigma_f(\vec{r},u')\phi(\vec{r},u')}{\int_{g'} du' \phi(\vec{r},u')} \tag{3.33}$$

$$\chi_{ng}(\vec{r}) = \int_g du \chi(\vec{r},u) w(u) \xi_n(u) \tag{3.34}$$

$$\phi_{lm,g'}(\vec{r}) = \int_{g'} du' \phi_{lm}(\vec{r},u') \tag{3.35}$$

Equations (3.31-3.35) represent a multigroup formulation of the transport equation, the solution of which is fully consistent with the fine-group energy and angular dependence. In comparing Eq. (3.31) with Eq. (3.13), it is clear that this formulation of the generalized energy condensation theory is consistent with the continuous energy transport equation. In addition, because the consistent method is based on the GEC theory, the fine-group flux may be extracted from the coarse-group solution using the higher-order moments of the flux and Eq. (3.22). As a result, the consistent GEC theory results in fine-group flux within the coarse-group calculation.

As in the standard multigroup method for whole-core problems, the fine-group (or continuous energy) flux used as the weighting function is computed for a lattice cell (fuel assembly with specular reflective boundaries), and this flux is used to condense the cross sections in Eqs. (3.21, 3.30, 3.32, and 3.33). Once these condensed cross sections and variation coefficients are computed, the coarse-group core flux moments may be obtained from Eq. (3.31) using any solution method (discrete ordinates, characteristics, etc.).

It is noted that if one strictly uses discrete ordinates with the same number of ordinates for both core and assembly level calculations, one could treat the variation term as defined at specific directional values in the same manner as the angular flux instead of using spherical harmonics. Using an expansion of the angular dependence in the variation term (e.g., spherical harmonics), however, provides a more general consistent formulation which is applicable to a wider array of solution methods. Also of note is the fact that the variation term in Eq. (3.31) does not depend on the higher order moments of the flux (in angle or energy), and is dependent only on the scalar group flux. This allows the consistent multigroup method to provide a significantly improved solution over the standard multigroup method without impacting the solution time.

3.1.2.1 Implementation

While the consistent multigroup theory is generalized so that any orthogonal set of functions may be used to expand the energy dependence, in practice, Legendre Polynomials are a logical choice. Because the weighting function $w(u)$ is equal to unity and the non-0th order moments integrate to zero, the RHS of Eq. (3.31) depends only on the $0^{th}$ energy expansion order ($n$=0) flux (Rahnema, Douglass, and Forget, 2008). As a result, the $0^{th}$ energy expansion order equation accounts for the full integral quantities (eigenvalue, coarse-group flux, etc.), and the higher order equations are only used to extract the fine-group flux, as in the GEC theory.

While the consistent multigroup method is sufficiently general to be applicable in any dimensions and with any order of scattering or angular approximation, for the sake of clarity, the method is implemented for testing in this dissertation as 1D with isotropic scattering.

The 1D form of the consistent multigroup equations is presented in Eq. (3.36), with isotropic scattering.

$$\mu \frac{d}{dx}\Psi_{ng}(x,\mu)+\sigma_g(x)\Psi_{ng}(x,\mu)=\frac{1}{2}\sum_{g'=1}^{G}\sigma_s^{n,g'\to g}(x)\phi_{g'}(x) + \sum_{g'=1}^{G}\frac{\chi_{ng}(x)}{2k}\nu\sigma_{fg'}(x)\phi_{g'}(x)-\sum_{l=0}^{L}\delta_{ng}^{l}(x)P_l(\mu)\phi_g(x) \tag{3.36}$$

While either a continuous energy or fine-group structure may serve as the weighting spectrum for the consistent multigroup method, for verification, a fine-group weighting spectrum is used, and the equations are solved in an discrete ordinates framework. The expansion of the variation term is truncated after *L+1* terms of the angular expansion. The number of terms does not significantly affect the solution time in 1D, and the number of terms kept is generally determined by the available order of angular expansion of the fine-group flux. For example, if the fine-group flux is obtained with a discrete ordinates calculation, a maximum of *N* terms (*L*=N-1) may be approximated with the quadrature methods inherent in discrete ordinates calculations.

The consistent generalized energy condensation theory presented above provides an extension of the original GEC theory which is consistent with the detailed energy spectrum (continuous energy or fine-group), and thus provides an improvement over the original GEC. Expansion methods often do not provide the best solution for functional approximation, however, because the order of the expansion and selected coarse-group structure can play a large role. In addition, as the desired resolution of the weighting spectrum increases, the complex resonances of the cross sections and resulting flux makes the use of a truncated series expansion less appealing.

### 3.2 B-Spline Energy Approximation for Neutron Transport

This section presents an extension of the multigroup method via a B-Spline approximation of the intra-group spectral dependence of the angular flux. The standard coarse-group solution is used in conjunction with spectral decomposition cross sections which are defined in addition to the standard coarse-group cross sections. These are then used in a set of subgroup equations to construct the expansion coefficients of the spline approximation.

We begin the derivation with the 1D transport equation in terms of lethargy, with isotropic scattering. This is done for simplicity in the derivation, and not as a restriction to the method.

$$\mu\frac{\partial}{\partial x}\Psi(x,\mu,u)+\sigma(x,u)\Psi(x,\mu,u)=\begin{aligned}&\frac{1}{2\lambda}\int_0^\infty du'\sigma_f(x,u'\to u)\Phi(u')\\&+\int_0^\infty du'\sigma_s(x,u'\to u)\Phi(u')\end{aligned}\tag{3.37}$$

We integrate this over the coarse group $g$, from $u_g$ to $u_{g+1}$, and define the collision term as the sum of an energy dependent term in each group and the deviation from it. This forms the consistent 1D multigroup equation:

$$\mu\frac{\partial}{\partial x}\Psi_g(x,\mu)+\sigma_g(x)\Psi_g(x,\mu)=\begin{aligned}&\frac{1}{2}\sum_{g'=1}^{G}\left(\frac{\sigma_{fg'\to g}(x)}{\lambda}+\sigma_{sg'\to g}(x)\right)\phi_{g'}(x)\\&-\sum_{l=0}^{L}P_l(\mu)\delta_{gl}(x)\phi_g(x)\end{aligned}\tag{3.38}$$

where the cross sections have been defined in the standard manner. As demonstrated above, this represents an exact preservation of the fine-group physics within the coarse-group formulation.

Now, we assume that we have structured our coarse groups so that we have $N_g$ fine groups that are entirely contained within the boundaries of coarse group *g*, not necessarily the same for each coarse group. The fine-group fluxes within these groups are those which are generally used to generate the coarse-group cross sections, as in the previous section and as in standard methods. We now return to the transport equation, and integrate it over the fine-group *h* within coarse-group *g:*

$$\mu\frac{\partial}{\partial x}\int_{u_h}^{u_{h+1}}du\Psi(x,\mu,u)+\sigma_g(x)\int_{u_h}^{u_{h+1}}du\Psi(x,\mu,u)=\begin{aligned}&\frac{1}{2\lambda}\int_{u_h}^{u_{h+1}}du\int_0^{\infty}du'\sigma_f(x,u'\to u)\Phi(u')\\&+\int_{u_h}^{u_{h+1}}du\int_0^{\infty}du'\sigma_s(x,u'\to u)\Phi(u')\\&-\int_{u_h}^{u_{h+1}}du\delta(x,u)\Psi(x,\mu,u)\end{aligned}\tag{3.39}$$

Where $\lambda$ is the multiplication constant. Now, define the cumulative cross section as the integral from the minimum lethargy, or *u=0* to the lethargy *u.*

$$\overline{\Psi}(x,\mu,u)=\int_0^u du'\Psi(x,\mu,u')\tag{3.40}$$

In addition, we define the following terms:

$$\sigma_f^{g'\to h}(x)=\frac{\int_{u_h}^{u_{h+1}}du\int_{u_{g'}}^{u_{g'+1}}du'\sigma_f(x,u'\to u)\phi(u')}{\int_{u_{g'}}^{u_{g'+1}}du'\phi(u')}\tag{3.41}$$

$$\sigma_s^{g'\to h}(x)=\frac{\int_{u_h}^{u_{h+1}}du\int_{u_{g'}}^{u_{g'+1}}du'\sigma_s(x,u'\to u)\phi(u')}{\int_{u_{g'}}^{u_{g'+1}}du'\phi(u')}\tag{3.42}$$

These cross section-like terms are called “fractional group functions” because they represent the fractional impact of the coarse-group flux on the fine-group shape.

With this definition, the fine-group integrated transport equation can be rewritten as

$$\begin{aligned}\mu\frac{\partial}{\partial x}(\overline{\Psi}(x,\mu,u_{h+1})-\overline{\Psi}(x,\mu,u_h)) \\ +\sigma_g(x)(\overline{\Psi}(x,\mu,u_{h+1})-\overline{\Psi}(x,\mu,u_h))\end{aligned} = \sum_{g'=1}^{G}\frac{1}{2}\left(\frac{\sigma_f^{g'\to h}(x)}{\lambda}+\sigma_s^{g'\to h}(x)\right)\phi_{g'}(x) \qquad (3.43)$$

The coarse-group scalar flux is the only flux term on the right hand side of this equation. Therefore, if the coarse-group flux and the eigenvalue were already known, this equation now effectively provides a fixed-source calculation. This coarse-group flux is the $0^{th}$ order energy expansion of the CGEC method in the previous section, and therefore can be solved quickly. Equation (3.43) is therefore an equation for the cumulative flux at the fine-group boundaries. Next, we define the following function:

$$\beta_g(x,\mu,u)=\frac{\overline{\Psi}(x,\mu,u)-\overline{\Psi}(x,\mu,u_g)}{\overline{\Psi}(x,\mu,u_{g+1})-\overline{\Psi}(x,\mu,u_g)} \quad u\in\left[u_g,u_{g+1}\right] \qquad (3.44)$$

This function is referred to as the subgroup shaping function, as it dictates the local spectral shape of the angular flux as a fraction of the coarse-group integrated flux (difference between cumulative flux at the coarse-group boundaries). This function has several important properties: it is everywhere positive, monotonically increasing, and constrained on the unit interval. Rearranging terms of this definition allows us to reframe the cumulative flux as:

$$\overline{\Psi}(x,\mu,u)=\beta_g(x,\mu,u)\Psi_g(x,\mu)+\overline{\Psi}(x,\mu,u_g)=\beta_g(x,\mu,u)\Psi_g(x,\mu)+\sum_{g'=1}^{g}\Psi_{g'}(x,\mu) \qquad (3.45)$$

It is noted here that the summation in the above equation is independent of *u*, and depends only on the coarse-group that the subgroup shaping function is defined in. By inserting this equation into equation (3.43), the left hand side can be rewritten as:

$$\mu\frac{\partial}{\partial x}\left(\Psi_g(x,\mu)(\beta_g(x,\mu,u_{h+1})-\beta_g(x,\mu,u_h))\right) \\ +\sigma_g(x)\left(\Psi_g(x,\mu)(\beta_g(x,\mu,u_{h+1})-\beta_g(x,\mu,u_h))\right) \tag{3.46}$$

Now, on the interval from $u_g$ to $u_{g+1}$, we establish a "knot vector" ($u_i$) composed of the subgroup boundaries, with the boundary points $u_g$ and $u_{g+1}$ possessing multiplicity $k$. This allows us to define a spline approximation for the subgroup shape function (deBoor, 2001):

$$\beta_g(x,\mu,u)=\sum_{i=1}^{N_g+k-1}\beta_g^i(x,\mu)B_{i,k}(u) \tag{3.47}$$

At this point, it is helpful to note a few important features of this approximation. The number of control points $\beta_g^n$ (also called "deBoor points") is dictated by the knots chosen and the order of the expansion. For a spline of order $k$ across $N$ intervals with the endpoints having multiplicity $k$, $N+k-1$ control points are required, and thus the same number of constraints must be satisfied. We can specify $N+1$ of these conditions by declaring that the approximation must be exact at the $N+1$ boundaries of the $N$ intervals. This is equivalent to the following interpolation conditions:

$$\beta_g(x,\mu,u_j)=\sum_{i=1}^{N_g+k-1}\beta_g^i(x,\mu)B_{i,k}(u_j)\quad j=1,\ldots,N_g+1 \tag{3.48}$$

It is clear from having N+1 interpolation conditions and N+k-1 control points, that for the problem to be well defined, $k$ must be greater than 2. This makes physical sense as well, because a spline of order 2 represents a linear approximation to the cumulative flux, which is equivalent to the spectrally flat fine-group flux. $k < 2$ would represent a non-physical spline. In addition, for $k=2$, there are N+1 interpolation conditions and N+1 control points, and thus enough constraints are provided simply by the boundaries. For higher order splines,

additional constraints must be determined (such as moment-conservation), or some knots must be removed to reduce the dimensionality of the spline. For initial studies, we will allow *k* to be equal to 2 and include as future work its extension to continuous energy problems with higher-order splines.

By inserting the spline approximation for the subgroup shape function at the group boundaries in the transport equation, we have:

$$\begin{aligned}&\mu\frac{\partial}{\partial x}\left(\Psi_g(x,\mu)\sum_{i=1}^{N_g+k-1}\beta_g^i(x,\mu)\left(B_{i,k}(u_{h+1})-B_{i,k}(u_h)\right)\right)\\&+\sigma_g(x)\left(\Psi_g(x,\mu)\sum_{i=1}^{N_g+k-1}\beta_g^i(x,\mu)\left(B_{i,k}(u_{h+1})-B_{i,k}(u_h)\right)\right)\end{aligned}=\sum_{g'=1}^{G}\frac{1}{2}\left(\frac{\sigma_f^{g'\to h}(x)}{\lambda}+\sigma_s^{g'\to h}(x)\right)\phi_{g'}(x) \quad (3.49)$$

Note that the correction term is dropped because the integral over the fine-group makes the correction term equal to zero. The primary advantage of the basis spline expansion is in local support, which restricts the number of basis splines which are non-zero at the points $u_n$ and $u_{n+1}$. By reducing the indices of the summation, and extracting the splines themselves, which depend only on the lethargy, we can rewrite the equation as:

$$\sum_{i=n-k}^{n}\left(B_{i,k}(u_{h+1})-B_{i,k}(u_h)\right)\begin{pmatrix}\mu\frac{\partial}{\partial x}\left(\Psi_g(x,\mu)\beta_g^i(x,\mu)\right)\\+\sigma_g(x)\Psi_g(x,\mu)\beta_g^i(x,\mu)\end{pmatrix}=\sum_{g'=1}^{G}\frac{1}{2}\left(\frac{\sigma_f^{g'\to h}(x)}{\lambda}+\sigma_s^{g'\to h}(x)\right)\phi_{g'}(x) \quad (3.50)$$

Now, if we define the following terms:

$$\begin{aligned}Q_g^i(x,\mu)&=\mu\frac{\partial}{\partial x}\left(\Psi_g(x,\mu)\beta_g^i(x,\mu)\right)+\sigma_g(x)\Psi_g(x,\mu)\beta_g^i(x,\mu)\\S_g^i(x,\mu)&=\sum_{g'=1}^{G}\frac{1}{2}\left(\frac{\sigma_f^{g'\to h}(x)}{\lambda}+\sigma_s^{g'\to h}(x)\right)\phi_{g'}(x)\end{aligned} \quad (3.51)$$

the transport equation can be written as a matrix equation:

$$\hat{B}_k\vec{Q}=\vec{S} \quad (3.52)$$

where the elements of the lower triangular matrix $\hat{B}_k$ are defined as:

$$B_{k,ij} = \begin{Bmatrix} B_{i,k}(u_{j+1}) - B_{i,k}(u_j) & j-k \le i \le j \\ 0 & otherwise \end{Bmatrix} \tag{3.53}$$

This $(N_g+1)$ x $(N_g+1)$ matrix is guaranteed to be invertible if and only if the Schoenburg-Whitney conditions (deBoor, 2001) on the knot sequence are satisfied. Also, if $k$=2, this is sufficient to completely define the spline approximation.

Recall that at this point, given an approximate flux (assembly fine-group calculation), the coarse group solution $\Psi_g(x,\mu)$ and eigenvalue are already obtainable from a consistent coarse-group calculation ($0^{th}$ order energy expansion), and the fractional group functions (Eqs. (3.41-43)) are already generated from the initial fine-group calculation. In addition, the $B_k$ matrix and it's inverse may be pre-computed as it depends only on the group structure. The value of the $Q_g$ array are then computed by applying the inverse of the $B$ matrix to the source $S_g$:

$$\vec{Q}_g = \hat{B}_{kg}^{-1}\vec{S}_g \tag{3.54}$$

This results in $N_g$+1 equations for the flux-shape-coefficient $\Psi_g^i(x,\mu) = \beta_g^i(x,\mu)\Psi_g(x,\mu)$:

$$\mu\frac{\partial}{\partial x}\left(\Psi_g^i(x,\mu)\right) + \sigma_g(x)\Psi_g^i(x,\mu) = \left(\hat{B}_{kg}^{-1}\vec{S}_g\right)_i \tag{3.55}$$

which can be solved with $N_g$+1 additional transport sweeps, and dividing out the coarse-group angular flux solution $\Psi_g(x,\mu)$. The fine group cumulative flux solution for the angular flux can then be found with the following equation:

$$\begin{aligned}\overline{\Psi}(x,\mu,u) &= \beta_g(x,\mu,u)\Psi_g(x,\mu) + \sum_{g'=1}^{g}\Psi_{g'}(x,\mu) \\ &= \sum_{i=1}^{N_g+k-1}\beta_g^i(x,\mu)B_{i,k}(u_j)\Psi_g(x,\mu) + \sum_{g'=1}^{g}\Psi_{g'}(x,\mu) \\ &= \sum_{i=1}^{N_g+k-1}\Psi_g^i(x,\mu)B_{i,k}(u_j) + \sum_{g'=1}^{g}\Psi_{g'}(x,\mu)\end{aligned} \tag{3.56}$$

From this equation, the fine-group flux can be calculated by the spline-differentiation formula in deBoor. This method allows for the rapid decomposition of the detailed flux from the coarse group solution via the following procedure:

(1) Generate an assembly-level fine-group flux solution

(2) Generate consistent coarse-group cross sections and the subgroup decomposition functions. Also generate the B-matrix and its inverse.

(3) Solve the consistent coarse-group calculation to obtain the eigenvalue and coarse-group flux for the problem.

(4) Generate the source array by using the decomposition functions with the coarse-group flux solution

(5) Condition the source array with the inverse of the B-matrix to obtain the equations for the spline control points

(6) Perform a single transport sweep for each of these control points.

For example, if one used $k$=2, 47 fine groups, and 2 coarse groups, one would solve the 2-group consistently, and then require 47 additional transport sweeps (not eigenvalue calculations) to fully extract the 47-group flux. This linear spline approximation ($k$ = 2), in fact, represents an extremely practical alternative to the CGEC theory presented in section 3.1.

### 3.3 Subgroup Decomposition Method

Traditionally, the group-collapsing process has been a one-way activity. The resulting solution is only obtained for the coarse-group structure and the detailed spectrum is inaccessible. The CGEC presented in section 3.1 extends the GEC in a way that ensures that the unfolded flux is obtained in a consistent formulation of the transport equation. However, truncation of the expansion means that the unfolding process is not a true "inverse" of the condensation process. The linear spline approximation ($k$=2) from section 3.2, however, *does* meet the fundamental goal of establishing a true "inverse" for the condensation. Because the group flux is an integral over each group, the linear spline approximation represents the multigroup condensation process (e.g., from fine-group to coarse-group), and does so without the need for orthogonal expansions. In this section, we define the linear spline approximation as the "subgroup decomposition method," (SGD) which serves as a highly practical treatment of the energy variable in whole-core transport problems. The new method can be broken into 3 distinct steps.

In the first step, a detailed flux spectrum is used to condense the material cross sections within each region of the problem, generating a coarse-group cross section library. The condensed library is then used within a coarse-group transport equation to obtain a coarse-group flux solution and eigenvalue. It is essential that this coarse-group formulation be consistent, as described in section 3.1. The second step is to perform a set of fixed-source "decomposition sweeps" to obtain the detailed flux spectrum. This is equivalent to solving the Eq. (3.43). For each of these calculations, the source is constructed by decomposing the coarse-group source into a source corresponding to the detailed spectrum via a set of "decomposition cross-sections." As mentioned previously, the detailed spectrum used to

condense the cross sections in the first step is only approximate, generally corresponding to the lattice-cell spectrum.

### 3.2.1 Subgroup Decomposition Sweeps

In order to decompose the flux spectrum after the consistent coarse-group core calculation, two additional "cross sections" are computed when the cross sections are initially condensed:

$$R_{fc'\to h}(\vec{r}) = \chi_h(\vec{r}) \frac{\sum_{h\in c'} \nu\sigma_{fh'}(\vec{r})\phi_{h'}(\vec{r})}{\sum_{h'\in c'} \phi_{h'}(\vec{r})} \tag{3.57}$$

$$R_{slmc'\to h}(\vec{r}) = \frac{\sum_{h'\in c'} \sigma_{slmh'\to h}(\vec{r})\phi^m_{lh'}(\vec{r})}{\sum_{h'\in c'} \phi^m_{lh'}(\vec{r})} \tag{3.58}$$

These coefficients are known as "sub-group decomposition cross sections" because they represent the source in sub-group *h* either by scattering or fission from coarse-group *c'*, and therefore, if the coarse-group flux is known, provide a way of decomposing the source into the fine groups. These are the more practical, multigroup alternative to Eq. (3.44) and Eq. (3.45). It is noted that these cross sections are already computed during the standard condensation calculation, but discarded in favor of the coarse-group cross sections and not used by standard coarse-group transport methods. As a result, the generation of these terms adds negligible time or memory constraints to the condensation procedure and is significantly more efficient than generating energy-expansion moments, as in the GEC theory. The SGD

cross sections allow the fixed-source "decomposition sweep" equation to be written for fine-group *h* as a function of the coarse-group flux and eigenvalue solution.

$$\hat{\Omega}\cdot\nabla\Psi_h(\vec{r},\hat{\Omega})+\sigma_h(\vec{r})\Psi_h(\vec{r},\hat{\Omega})=\frac{1}{4\pi k}\sum_{c'=1}^{C}R_{fc'\to h}\phi_{c'}(\vec{r})+\sum_{l=0}^{\infty}\sum_{m=-l}^{l}\frac{Y_{lm}^{*}(\hat{\Omega})}{4\pi}\sum_{c'=1}^{C}R_{slmc'\to h}(\vec{r})\phi_{lc'}^{m}(\vec{r}) \tag{3.59}$$

Eq. (3.59) is known as a "decomposition sweep" because the eigenvalue and source have already been obtained during the coarse-group calculation, and therefore Eq. (24) requires only a single transport sweep to solve for each subgroup.

### 3.4 Cross Section Recondensation

In order to generate coarse-group cross sections which accurately preserve the fine-group reaction rates, the fine-group flux for the whole-core problem would need to be known. In the standard multigroup method, the lattice cell flux is used as an approximate weighting function; however, this introduces a significant source of error. The specular reflective boundary conditions of the lattice cell calculation are generally not an adequate approximation of the core environment, particularly in the heterogeneous configurations typical of current operating reactors. Because the lattice cell spectrum is not generally a good approximation, improving the coarse-group cross sections requires a different source of fine-group flux. By making use of either the consistent generalized condensation theory or the subgroup decomposition method presented in the previous sections, a new core-level fine-group flux can be found which is closer to the fine-group core spectrum than it is to the lattice cell spectrum. As demonstrated by Douglass, Rahnema, and Forget (2008), the expanded fine-group flux for a 1D BWR problem with a high order expansion (> 10 energy moments) resulted in less than 3% average RMS error, in comparison with 15% RMS error

for the lattice spectrum, even when using an inconsistent coarse-group formulation and the expansion based method.

The basis of the recondensation methodology is therefore to treat the lattice spectrum merely as an initial guess for the weighting function, and to use one of the inverse condensation techniques (either CGEC theory or the SGD method) to generate a new approximation to core-level fine group flux. The new spectrum, which is a better approximation for the core-level flux than the lattice cell spectrum, is then used to generate new cross section moments, and the method is repeated.

Thus, the recondensation method is described by the following procedure.

(1) Select an initial fine-group energy spectrum. This is typically the spectrum obtained with lattice cell calculations with specular boundary conditions.

(2) Generate coarse-group cross sections weighted with the initial spectrum.

    a. If using the CGEC, also generate the higher-order cross section moments.

    b. If using the SGD, generate the subgroup decomposition cross sections.

(3) Perform a coarse-group whole-core calculation to obtain an approximation of the eigenvalue and coarse-group flux.

    a. This calculation must be performed with a consistent formulation, including the correction term (Eq. (3.19), (3.29)).

(4) Obtain the fine-group flux from the coarse-group flux and eigenvalue.

    a. If using the CGEC, this consists of the higher-order flux moment calculations based on the zeroth-order coarse-group flux solution.

    b. If using the SGD, this consists of the “decomposition sweeps” for each fine-group.

(5) Use the flux from step (4) to generate updated coarse-group cross sections and higher order moments / decomposition cross sections.

(6) Repeat steps (2)-(5) until the coarse-group calculations converge.

There are a few important factors which must be noted with regards to practical implementation of a recondensation scheme based on either the CGEC or the SGD method.

The first is that a criteria must be defined to determine when the solution is sufficiently converged. Repeating the recondensation procedure until the decomposed/unfolded fine-group flux in successive iterations differ by less than some fixed parameter is the most natural convergence parameter. However, in practice, converging the detailed spectrum to within a very fine parameter is generally less important than converging the coarse-group cross sections, and therefore the reaction rates. For a wide class of problems, small changes in the fine-group flux spectrum do not dramatically effect the reaction rate or eigenvalue. For example, continuing the recondensation procedure until the fine-group flux at the periphery of a large VHTR problem (where large reflectors and shields around the core attenuate the flux to near zero) is highly converged is an inefficient use of computational power. As a result, for it is generally preferred that recondensation procedure is performed until the coarse-group cross sections in successive iterations differ by no more than some criterion. However, converging 2-group cross sections to a given criterion, for example, does not result in as accurate a solution as converging 8-group cross sections to the same criteria, and therefore it is expected that if too few groups are used, it may be necessary to tighten the convergence criteria for some problems. In this dissertation, the default

convergence for the cross sections is 0.1%, and when further convergence is needed, it is stated.

The second factor is the effect of the coarse-group structure chosen on the recondensation scheme. Using the SGD method within a consistent coarse-group formulation ensures that the coarse-group and fine-group calculations are entirely consistent independent of the group structure chosen, because each fine-group is entirely contained within a coarse-group. In the CGEC based recondensation, the group structure and order of expansion would both play a significant role in the accuracy of the solution. In either case, when calculating the core-level coarse-group flux, using a larger number of coarse-groups or more spectrally appropriate group boundaries may result in fewer recondensation iterations being necessary. Therefore, there is a complex trade-off between using more groups or higher order expansions to lower the number of iterations and the extra time required to solve the coarse-group calculation with more groups.

In general, the recondensation method allows for a corrected flux solution at the whole-core level which does not contain the error generated from the use of specular boundary conditions in the lattice cell calculation. An interesting property of the recondensation methodology is that it uses the lattice cell calculation as only an initial guess for the iterative procedure. As in most iterative processes, while the speed of convergence is strongly affected by the use of a good initial guess, the final converged solution of the iterative process is independent, and will be the same for any initial guess. This makes the recondensation methodology essentially independent of the lattice cell calculation, and by iterating between the expanded spectrum and the coarse-group core calculations, the core solution could be obtained without performing the lattice calculation. As a result, the

recondensation solution can be thought of as an intrinsic solution of the core, depending only on the cross section mesh, fine-group structure (and order of expansion in the CGEC), rather than as a merely a correction to the lattice cell spectrum.

The implementation of the recondensation methodology results in the need to balance the optimization of the initial guess versus the data handling and storage requirements.

While the lattice solution does generate a more rapid convergence, the computational requirements (solution time and memory requirements) of the lattice calculation may cause the solution of the lattice problem to be more expensive than the added iterations from a non-optimized initial guess. A detailed analysis of this optimization problem is outside the scope of this paper, and within the implementation presented in the next section, the lattice cell flux is the initial guess.

# CHAPTER 4

# BENCHMARK PROBLEM DEVLOPMENT

For much of the history of the nuclear industry, solving the neutron transport equation required numerical methods based on a variety of simplifications (such as homogenization and diffusion theory) because the computer technology was not advanced enough to allow engineers and scientists to use direct neutron transport for a whole-core problem. In recent years, there has been a renewed interest in utilizing the improvements in computer technology to develop new methods, such as those presented in the previous chapter, for treating more complicated reactor problems with direct transport. Validating codes which implement these methods requires testing with relevant benchmark problems; however, there is a lack of full-scale, heterogeneous neutronics benchmarks for whole-core transport problems. Thus, new benchmarks are necessary that possess a high degree of heterogeneity at both the assembly and core levels, and with geometry and materials which are characteristic of real-world designs. In addition to the methods developed in the previous section, this dissertation seeks to address this knowledge gap by providing a 2D and 3D benchmark for a BWR core, and 1D benchmarks for LWR and VHTR problems intended for early methods development.

The benchmark problems presented in this dissertation are intended to be somewhat representative of operational reactors. In order to make the benchmark specifications useable by methods developers with a wide variety of available computing power and at different points in the development process, several simplifications have been made while retaining the significant physics features of the core. For example, operational reactor lifetime vastly exceeds the life of a fuel assembly design, as engineers constantly upgrade the assemblies to

allow higher burnup, increased stability, and improved power-density. As a result, operating reactors use several different fuel assembly types during a given cycle, but for simplicity, the specifications in this dissertation are all based on somewhat restricted assembly designs. The burnups, state parameters, and enrichments may vary throughout the core (to retain the physical effects of that trend in operating reactors), but the geometric design is consistent.

In addition, the nodal distribution of void and burnup parameters in the BWR has been reduced to only three burnups and three void fractions. These kinds of simplifications may introduce unrealistic gradients; however, the benchmark problems are intended to challenge whole-core transport methods while maintaining computational simplicity and are not intended to explicitly model a specific reactor.

## 4.1 GE9-Loaded BWR with Operational State Parameters

### 4.1.1 Core Description

The core geometry is based on a large BWR consisting of 560 fuel bundles laid out in a 26x26 grid with an assembly pitch of 15.24 cm. The layout of the core is based on a nodal state parameter distribution from an operating reactor (Sutton, 2007). While this distribution contains radial and axial heterogeneity in both void fraction and exposure, the benchmark specification is simplified to contain an axially uniform burnup distribution. Figure 4.1 contains the burnup layout of the core. The bundles are numbered according to the figure, and these numbers will be used later in the section to reference specific bundles. The core is surrounded by a row of assembly-width square moderator regions and vacuum boundary conditions.

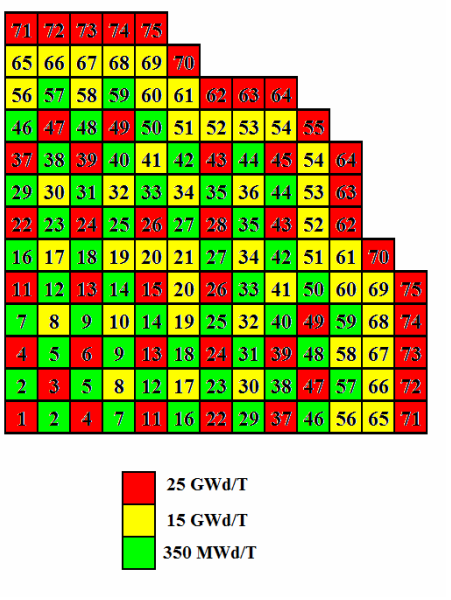


Figure 4.1: BWR Radial Core Layout

The burnups for the benchmark problem were calculated by axially averaging the exposure of the nodal state parameter distribution and setting each bundle to the batch-average burnup. The operating reactor uses a 4-batch cycle, however to reduce the size of the cross section library, the two highest exposure batches were averaged together to produce a three-batch layout.

While an operating reactor has a continuously varying void distribution, generating multigroup cross sections for each explicit void state would make the cross section library prohibitively large. Therefore, each void state in the benchmark specification, is binned into one of three values (0%, 40%, and 70%) as seen in Table 4.1. The benchmark layout consists of five axial void zones as seen in Figure 4.2, within which the void distribution is axially uniform. Each of these zones consists of 5 axial nodes 15.24 cm thick.

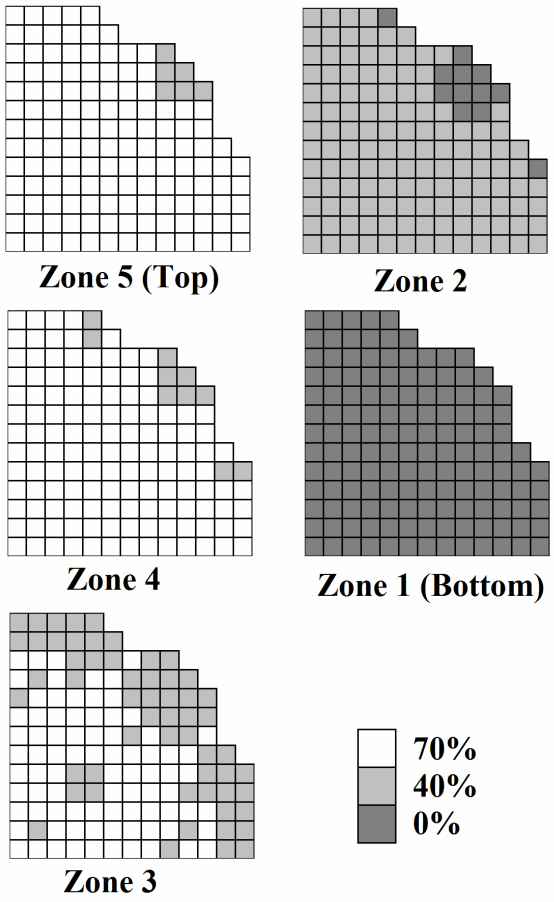


Figure 4.2: BWR Axial Core Layout

Table 4.1: BWR Void and Burnup State Point Intervals

| | Operating Reactor Nodal Distribution Interval | Benchmark Value |
|---|---|---|
| Void Fraction | < 20% | 0% |
| | 20 – 60% | 40% |
| | > 60% | 70% |
| Burnup | Batch 3: 250 – 400 MWd/T | 350 MWd/T |
| | Batch 2: 13 GWd/T – 17 GWd/T | 15 GWd/T |
| | Batch 1: 20 GWd/T – 30 GWd/T | 25 GWd/T |

The benchmark problem consists of 25 axial nodes of thickness 15.24 cm, 23 of which are active fuel nodes and 2 of which are top and bottom blankets of natural Uranium fuel nodes. Three different control rod configurations are examined in this paper:

1. ARO - All Rods Out
2. ARI - All Rods In – control blades are inserted the full 48 notches (first 24 nodes)
3. SRI – Some Rods In – Operating condition: control blades are inserted according to the control rod insertion map obtained for the operating reactor near the beginning of cycle.

Figure 4.3 contains the control blade insertion pattern for this configuration. The insertion values represent the number of notches (½ axial nodes) that the control blades are inserted**.**

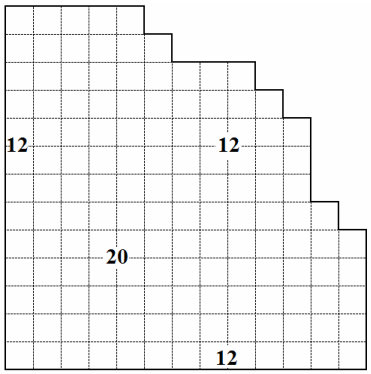


Figure 4.3: SRI Configuration Control Blade Insertion Map

### 4.1.2 Bundle Configuration

The bundle used in the core is a GE9 BWR bundle specification from work on BWR bundle depletion using RACER (Kelley, 1995). The geometric and state parameters of the GE9 bundle are presented in Table 4.2. The model used in this benchmark is simplified by squaring the corners of the bundle casing.

Table 4.2. GE9 Bundle Parameters

| Bundle Specification (Kelley, 1995) | | Control Blade Specification (Solis et. al., 2001) | |
|---|---|---|---|
| Number of Fuel Pins | 60 | Sheath Half-Span | 12.3825 cm |
| Fuel Pin Radius | 0.53213 cm | Sheath Center-Cross Standoff | 1.98501 cm |
| Fuel Pin Clad Radius | 0.61341 cm | Sheath Thickness | 0.79248 cm |
| Central Water Tube Radius | 1.6002 cm | Sheath Material | SS304 |
| Central Water Tube Clad Radius | 1.7018 cm | Control Tube Material | B4C (70% density) |
| Fuel Pin Pitch | 1.6256 cm | Control Tube Radius | 0.23876 cm |
| Large Water Gap Thickness | 0.9525 cm | Control Tube Pitch | 0.57764 cm |
| Small Water Gap Thickness | 0.47498 cm | | |
| Zr Assembly Casing Thickness | 0.2032 cm | | |
| Fuel Temperature | 833 K | | |
| Clad / Mod Temperature | 600 K | | |

The GE9 bundle consists of 10 different fuel enrichments, and 2 enrichments of gadded fuel rods, laid out as in Figure 4.4. The fresh material compositions are located in Appendix A.

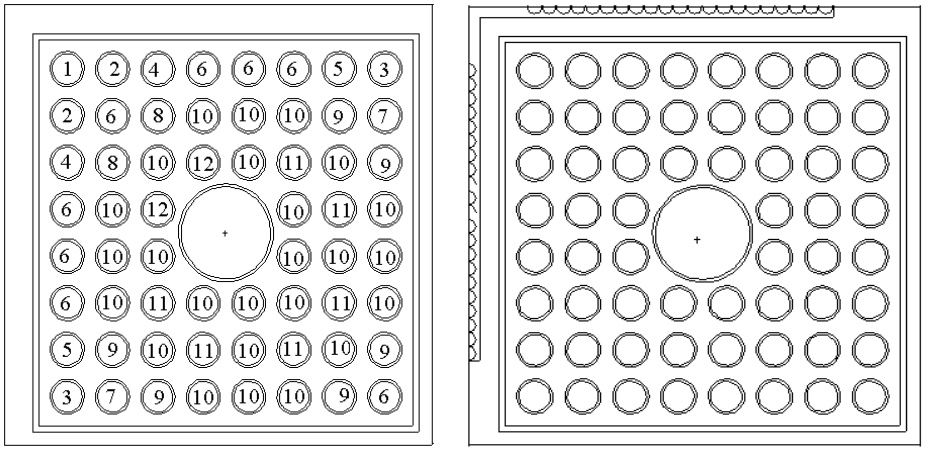


Figure 4.4: GE9 Bundle Layout

### 4.1.3 Dimensional Reduction to 2D

When developing and testing new transport methods and codes, it is often impractical to begin with a fully heterogeneous, whole-core 3D benchmark problem. This results in preliminary tests of new methods being done in simple 1D problems, and then moving up to simple 2D problems. It is still desirable, however, for these problems to possess the physics

and geometries characteristic of operating reactors as closely as possible. To facilitate this, a 2D benchmark problem has been generated by reducing the 3D problem and maintaining the relevant physics and geometry.

The 2D void distribution is generated by axially averaging the nodal void distribution of the operating reactor, and then binning each bundle into the same intervals as in the 3D problem (see Table 4.1). This results in each bundle falling within the 40% void interval; therefore, the 2D benchmark model possesses a uniform void of 40%. The burnup map for the 2D benchmark is the same as the 3D model (see Figure 4.1). The same three control configurations are chosen for the 2D benchmark problem (ARO, ARI, SRI). Because of the difficulty in modeling partially inserted control blades in a two-dimensional problem, the 2D SRI configuration contains control blades in each location used for partial control blades in the 3D problem.

### 4.1.4 Cross Section Generation

The GE9 bundle was modeled with diagonal symmetry and fully specular reflective boundary conditions using the lattice depletion code HELIOS v1.10 (Simenov, 2003). The 47-group unadjusted production library was used to deplete the bundle to 25 GWd/T in 50 burnup steps. A specific power level of 24.3249 W/g, obtained from the real-world BWR state parameters, was used to deplete the bundle. Depleted fuel isotopics were dumped for each of the burnup points in the benchmark problem (350 MWd/T, 15 GWd/T, and 25GWd/T), and branch calculations were performed to generate 2-group cross sections for each void state (0%, 40%, and 70% void), with and without a $1/8^{th}$-slice of the control blade. Voiding is only performed for the coolant in the fuel lattice; the bypass coolant and the central water column remain un-voided. A second set of depletion and branch-off

calculations was performed for the natural Uranium bundles present in the top and bottom blankets of the core. Natural Uranium bundles are identical to the active fuel bundles, but all fuel pins are replaced with natural $UO_2$. The HELIOS model, including the computational mesh, is presented in Figure 4.5.

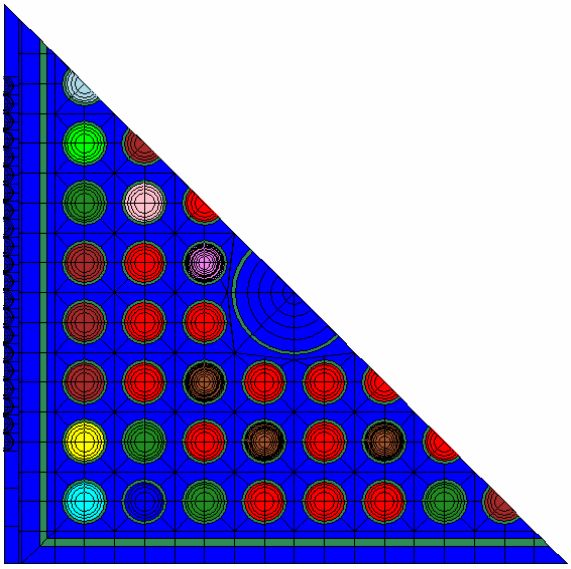

Figure 4.5: GE9 Fuel Bundle HELIOS Model

The fuel pins were meshed with 5 annular regions and 4 azimuthal regions. In order to correctly model pin fission rates, gadded fuel rods were meshed with 10 annular regions. Cross sections were output for each material type used in the bundle (10 fuels, 2 gadded fuels, Zr structure, voided coolant, unvoided coolant). The 2-group thermal boundary used for the cross section generation was 0.62506 eV, as is standard for LWR analysis.

The bundle eigenvalues for each state (burnup, void, control) obtained in the HELIOS calculations are presented in Table 4.3. The 2-group macroscopic cross sections for each material region of the bundles are presented in Appendix A.

Table 4.3: HELIOS k-infinity values for each BWR bundle type.

| Burnup (GWd/T) | 0% Void | 40% Void | 70% Void |
|---|---|---|---|
| | GE9 Bundle | | |
| 0.350 | 1.05712 | 1.04269 | 1.02220 |
| 15 | 1.15211 | 1.12788 | 1.09605 |
| 25 | 1.04030 | 1.01705 | 0.98695 |
| | Controlled GE9 Bundle | | |
| 0.350 | 0.95287 | 0.93104 | 0.90523 |
| 15 | 1.05704 | 1.01901 | 0.97289 |
| 25 | 0.95139 | 0.91467 | 0.87064 |
| | Natural Uranium Bundle | | |
| 0.350 | 0.84095 | 0.85796 | 0.86223 |
| 15 | 0.79422 | 0.79196 | 0.78034 |
| 25 | 0.75524 | 0.74988 | 0.73627 |
| | Controlled Natural Uranium Bundle | | |
| 0.350 | 0.72977 | 0.72741 | 0.71247 |
| 15 | 0.70691 | 0.69132 | 0.66612 |
| 25 | 0.67393 | 0.65636 | 0.63026 |

### 4.1.5 MCNP Core Models

Each configuration was modeled in MCNP5 (LANL, 2005) using 1/8th symmetry, with specular boundary conditions on the diagonal and west faces, laid out radially as in Figure 4.6. The top, bottom, and north faces are modeled with vacuum boundary conditions. A 15.24 cm thick layer of additional moderator surrounds the core (same cross section as bypass coolant in the periphery bundles). Note that this model does not treat reentrant particles in the MCNP simulation. The 2D configurations were modeled in the same manner as the 3D cores in the radial direction, but with specular reflective boundary conditions on the top and bottom faces and axially uniform state parameters.

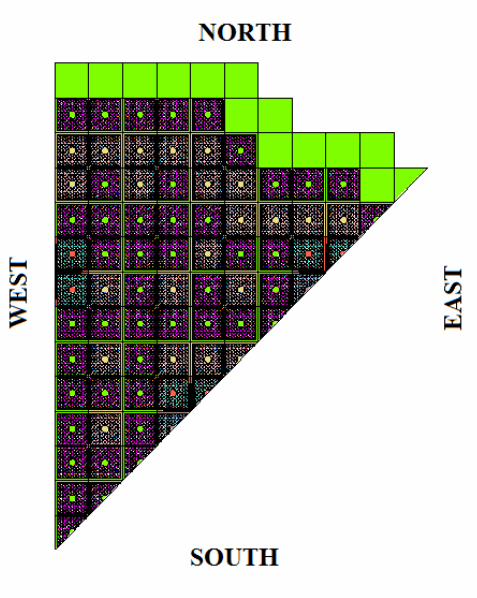


Figure 4.6: 1/8$^{th}$ Core Layout for MCNP Model of BWR

### 4.1.6. MCNP Core Simulation

Calculations were performed for each core configuration (ARO, ARI, SRI) with MCNP5 using a 128 node cluster. An initial calculation was performed with 1.05 billion histories (250,000 histories per cycle for 4200 cycles) to obtain a converged source distribution. For each configuration, the solution was obtained with an additional 1.05 billion histories were simulated (250,000 histories for 4000 active and 200 inactive cycles). Tallies were made for the average energy-integrated fission density in all fission producing pins in each mesh.

In order to ensure that the benchmark is useable for a wide variety of transport methods, the MCNP calculation was performed with the multigroup option, as opposed to continuous energy.

Table 4.4: MCNP Eigenvalue for all three configurations

| | | ARO | ARI | SRI |
|---|---|---|---|---|
| 3D | Eigenvalue | 1.03955 | 0.94557 | 1.03396 |
| | Std. Deviation | 0.00001 | 0.00001 | 0.00001 |
| 2D | Eigenvalue | 1.04230 | 0.93955 | 1.03344 |
| | Std. Deviation | 0.00001 | 0.00001 | 0.00001 |

Figure 4.7 contains the axial relative fission density, integrated over the each axial core layer for all three configurations of the 3D problem.

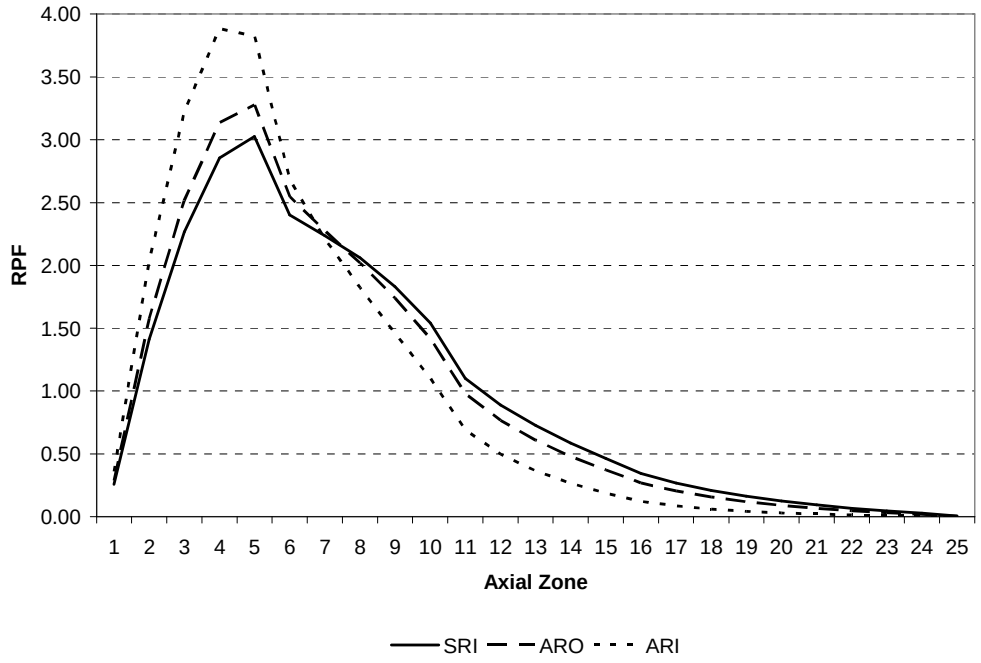


Figure 4.7: Layer-Averaged Relative Fission Density
for SRI, ARO, and ARI Configurations

For each control configuration, bundle-integrated fission densities for every axial layer are presented in Appendix A. These are produced by normalizing the tally result $f_i$ for every axial layer of each pin to the total number of fuel assemblies in the core (560), as in Eq. (4.1).

$$P_i = \frac{\bar{f}_i \cdot 560}{\sum_i \bar{f}_i} \tag{4.1}$$

Axially-integrated pin fission densities are plotted, along with axially-integrated bundle fission densities, for each configuration and these are presented in the following sections. In addition, while providing individual fission densities for each pin is impractical due to the large number of fuel pins in the core, a detailed description of pin fission densities (PFD) is desirable to fully test new codes' ability to accurately model local transport effects. To satisfy this need, four bundles were chosen which highlight the more challenging regions of the benchmark for methods: a high-power fresh bundle which is controlled in the SRI configuration (bundle 14), a medium burnup bundle adjacent to a controlled bundle in the SRI configuration (bundle 30), a peripheral bundle (bundle 70), and the peak bundle in the ARO configuration (bundle 21). The axially-integrated fission densities are presented in the following sections for each pin in the bundles, normalized to the total number of fuel pins in the bundle (60), as in Eq. (4.2).

$$P_n = \frac{f_n \cdot 60}{\sum_n f_n} \tag{4.2}$$

Pin Fission Density results as well as an analysis of the uncertainty in the results are presented in sections 4.2.5.1 – 4.2.5.6 for the various configurations.

4.2.5.1 BWR Pin Fission Density Results – 3D ARO

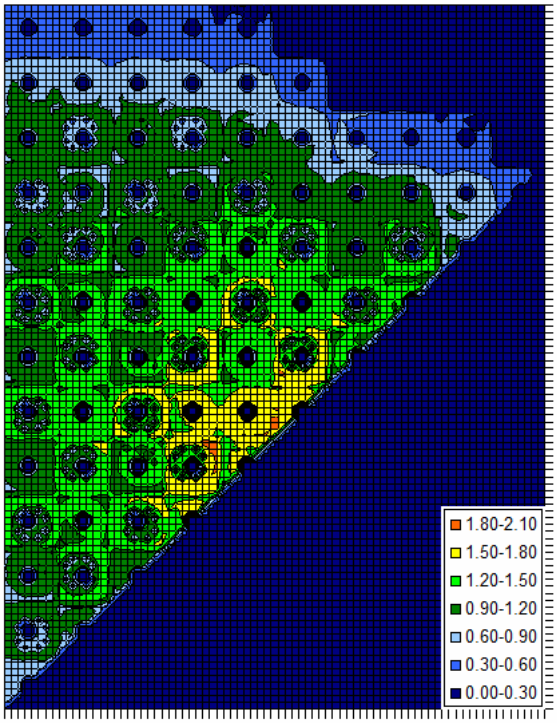


| | | | | | | | | | |
|---|---|---|---|---|---|---|---|---|---|
| 0.43 (0.50) | 0.42 (0.50) | 0.40 (0.51) | 0.37 (0.53) | 0.34 (0.58) | | | | | |
| 0.82 (0.39) | 0.79 (0.39) | 0.78 (0.40) | 0.74 (0.41) | 0.67 (0.43) | 0.47 (0.47) | | | | |
| 0.97 (0.35) | 0.92 (0.35) | 0.95 (0.35) | 0.92 (0.36) | 0.94 (0.36) | 0.83 (0.38) | 0.58 (0.42) | 0.45 (0.48) | 0.35 (0.57) | |
| 0.97 (0.35) | 0.88 (0.34) | 0.99 (0.34) | 0.92 (0.33) | 1.05 (0.33) | 1.04 (0.33) | 0.98 (0.35) | 0.91 (0.38) | 0.72 (0.43) | 0.42 (0.55) |
| 0.92 (0.34) | 1.05 (0.33) | 0.96 (0.32) | 1.16 (0.31) | 1.24 (0.31) | 1.17 (0.31) | 0.99 (0.32) | 1.09 (0.34) | 0.83 (0.39) | |
| 1.09 (0.33) | 1.18 (0.32) | 1.20 (0.31) | 1.32 (0.30) | 1.32 (0.29) | 1.34 (0.29) | 1.21 (0.31) | 1.19 (0.34) | | |
| 1.00 (0.32) | 1.21 (0.31) | 1.13 (0.30) | 1.37 (0.29) | 1.26 (0.28) | 1.42 (0.28) | 1.18 (0.31) | | | |
| 1.16 (0.32) | 1.28 (0.30) | 1.33 (0.29) | 1.50 (0.28) | 1.64 (0.27) | 1.63 (0.28) | | | | |
| 1.02 (0.32) | 1.23 (0.31) | 1.16 (0.29) | 1.47 (0.28) | 1.43 (0.28) | | | | | |
| 1.11 (0.32) | 1.22 (0.31) | 1.27 (0.30) | 1.45 (0.31) | | | | | | |
| 0.91 (0.34) | 1.09 (0.33) | 1.04 (0.33) | | | | | | | |
| 0.95 (0.35) | 0.90 (0.36) | | | | | | | | |
| 0.79 (0.38) | | | | | | | | | |

Figure 4.8: 3D ARO Configuration: PFD distribution and bundle fission density with statistical uncertainty (%)

Table 4.5: Selected pin fission density results
and % uncertainty (in parentheses) for BWR – 3D ARO Configuration

| Bundle 14 | | | | | | | | Bundle 30 | | | | | | | |
|---|---|---|---|---|---|---|---|---|---|---|---|---|---|---|---|
| 1.10 | 1.18 | 1.10 | 1.11 | 1.13 | 1.26 | 1.26 | 1.23 | 0.86 | 0.90 | 0.92 | 0.92 | 0.94 | 0.89 | 0.84 | 0.82 |
| (0.28) | (0.29) | (0.30) | (0.30) | (0.30) | (0.28) | (0.27) | (0.25) | (0.30) | (0.30) | (0.31) | (0.31) | (0.30) | (0.30) | (0.28) | (0.28) |
| 1.17 | 0.93 | 0.36 | 0.87 | 0.37 | 0.99 | 1.26 | 1.25 | 0.93 | 1.02 | 1.05 | 1.06 | 1.09 | 1.03 | 0.94 | 0.86 |
| (0.30) | (0.32) | (0.22) | (0.32) | (0.22) | (0.30) | (0.28) | (0.26) | (0.31) | (0.32) | (0.32) | (0.32) | (0.31) | (0.31) | (0.29) | (0.28) |
| 1.06 | 0.35 | 0.82 | 0.96 | 0.92 | 0.38 | 1.15 | 1.24 | 1.02 | 0.97 | 1.03 | 1.08 | 1.06 | 1.08 | 1.04 | 0.91 |
| (0.31) | (0.22) | (0.33) | (0.32) | (0.33) | (0.22) | (0.29) | (0.26) | (0.32) | (0.33) | (0.33) | (0.32) | (0.32) | (0.32) | (0.31) | (0.29) |
| 1.05 | 0.84 | 0.94 | | | 0.99 | 1.15 | 1.22 | 1.03 | 0.98 | 1.03 | | | 1.07 | 1.12 | 0.98 |
| (0.31) | (0.33) | (0.33) | | | (0.32) | (0.29) | (0.26) | (0.33) | (0.33) | (0.33) | | | (0.32) | (0.31) | (0.30) |
| 1.06 | 0.35 | 0.90 | | | 0.36 | 1.15 | 1.23 | 1.01 | 0.93 | 1.02 | | | 1.10 | 1.10 | 0.97 |
| (0.31) | (0.23) | (0.33) | | | (0.22) | (0.29) | (0.26) | (0.33) | (0.33) | (0.33) | | | (0.32) | (0.31) | (0.30) |
| 1.16 | 0.93 | 0.36 | 0.96 | 0.35 | 1.02 | 1.21 | 1.17 | 1.03 | 0.97 | 0.94 | 1.03 | 1.05 | 1.07 | 1.10 | 0.99 |
| (0.29) | (0.32) | (0.22) | (0.32) | (0.22) | (0.30) | (0.28) | (0.26) | (0.33) | (0.34) | (0.33) | (0.33) | (0.33) | (0.32) | (0.31) | (0.29) |
| 1.15 | 1.16 | 1.08 | 1.10 | 1.12 | 1.19 | 1.18 | 1.13 | 1.03 | 0.97 | 0.98 | 0.95 | 1.02 | 1.03 | 1.09 | 0.97 |
| (0.28) | (0.29) | (0.30) | (0.30) | (0.29) | (0.28) | (0.26) | (0.25) | (0.32) | (0.33) | (0.33) | (0.33) | (0.33) | (0.32) | (0.31) | (0.29) |
| 1.11 | 1.14 | 1.15 | 1.15 | 1.18 | 1.14 | 1.12 | 1.10 | 0.91 | 1.04 | 1.06 | 1.05 | 1.08 | 1.09 | 1.01 | 0.94 |
| (0.26) | (0.27) | (0.27) | (0.27) | (0.27) | (0.26) | (0.25) | (0.24) | (0.31) | (0.32) | (0.33) | (0.33) | (0.32) | (0.31) | (0.30) | (0.28) |
| Bundle 21 | | | | | | | | Bundle 70 | | | | | | | |
| 0.93 | 0.96 | 0.97 | 0.96 | 0.97 | 0.90 | 0.84 | 0.81 | 0.81 | 0.83 | 0.83 | 0.79 | 0.77 | 0.68 | 0.62 | 0.59 |
| (0.25) | (0.25) | (0.26) | (0.26) | (0.26) | (0.26) | (0.27) | (0.34) | (0.46) | (0.47) | (0.48) | (0.49) | (0.50) | (0.50) | (0.50) | (0.48) |
| 1.02 | 1.09 | 1.11 | 1.11 | 1.12 | 1.04 | 0.94 | 0.84 | 0.89 | 0.95 | 0.97 | 0.93 | 0.92 | 0.80 | 0.70 | 0.64 |
| (0.26) | (0.26) | (0.27) | (0.27) | (0.27) | (0.28) | (0.36) | (0.27) | (0.47) | (0.49) | (0.51) | (0.52) | (0.52) | (0.52) | (0.51) | (0.48) |
| 1.13 | 1.06 | 1.09 | 1.13 | 1.10 | 1.10 | 1.04 | 0.90 | 1.03 | 0.97 | 0.98 | 0.96 | 0.90 | 0.90 | 0.83 | 0.74 |
| (0.27) | (0.27) | (0.28) | (0.28) | (0.29) | (0.38) | (0.28) | (0.26) | (0.48) | (0.50) | (0.52) | (0.52) | (0.53) | (0.53) | (0.51) | (0.48) |
| 1.15 | 1.08 | 1.10 | | | 1.10 | 1.12 | 0.97 | 1.12 | 1.04 | 1.01 | | | 0.93 | 0.99 | 0.87 |
| (0.27) | (0.28) | (0.28) | | | (0.29) | (0.27) | (0.26) | (0.48) | (0.50) | (0.50) | | | (0.51) | (0.50) | (0.47) |
| 1.14 | 1.02 | 1.10 | | | 1.13 | 1.11 | 0.96 | 1.18 | 1.03 | 1.05 | | | 1.03 | 1.05 | 0.93 |
| (0.27) | (0.28) | (0.29) | | | (0.28) | (0.27) | (0.26) | (0.47) | (0.48) | (0.49) | | | (0.50) | (0.49) | (0.45) |
| 1.17 | 1.07 | 1.02 | 1.10 | 1.10 | 1.09 | 1.11 | 0.97 | 1.27 | 1.16 | 1.04 | 1.08 | 1.07 | 1.09 | 1.12 | 1.00 |
| (0.27) | (0.29) | (0.39) | (0.29) | (0.28) | (0.28) | (0.27) | (0.26) | (0.45) | (0.47) | (0.48) | (0.48) | (0.49) | (0.49) | (0.47) | (0.44) |
| 1.16 | 1.08 | 1.07 | 1.02 | 1.08 | 1.06 | 1.09 | 0.96 | 1.31 | 1.22 | 1.19 | 1.08 | 1.14 | 1.10 | 1.14 | 1.02 |
| (0.28) | (0.39) | (0.29) | (0.28) | (0.28) | (0.27) | (0.26) | (0.25) | (0.43) | (0.45) | (0.46) | (0.47) | (0.47) | (0.47) | (0.45) | (0.42) |
| 1.02 | 1.16 | 1.17 | 1.14 | 1.15 | 1.13 | 1.02 | 0.93 | 1.19 | 1.34 | 1.34 | 1.28 | 1.26 | 1.20 | 1.08 | 1.01 |
| (0.36) | (0.28) | (0.27) | (0.27) | (0.27) | (0.27) | (0.26) | (0.25) | (0.41) | (0.42) | (0.44) | (0.45) | (0.45) | (0.44) | (0.43) | (0.41) |

4.2.5.2 BWR Pin Fission Density Results – 3D ARI

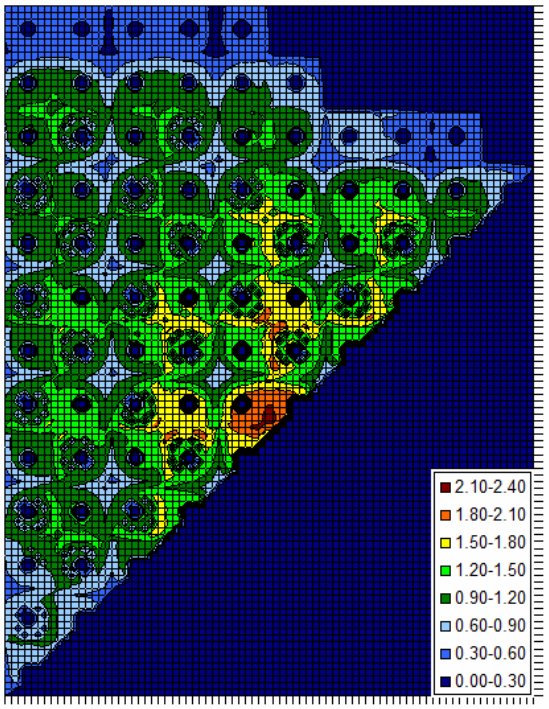


| | | | | | | | | | |
|---|---|---|---|---|---|---|---|---|---|
| 0.44 (0.47) | 0.43 (0.47) | 0.42 (0.48) | 0.39 (0.49) | 0.37 (0.53) | | | | | |
| 0.92 (0.34) | 0.89 (0.35) | 0.89 (0.35) | 0.86 (0.36) | 0.80 (0.37) | 0.66 (0.39) | | | | |
| 1.04 (0.32) | 0.95 (0.33) | 1.02 (0.32) | 0.97 (0.33) | 1.05 (0.32) | 0.96 (0.34) | 0.64 (0.38) | 0.51 (0.43) | 0.40 (0.51) | |
| 0.95 (0.33) | 0.87 (0.33) | 0.99 (0.32) | 0.95 (0.31) | 1.12 (0.30) | 1.18 (0.30) | 1.13 (0.31) | 1.12 (0.32) | 0.92 (0.36) | 0.65 (0.43) |
| 0.87 (0.33) | 0.98 (0.32) | 0.94 (0.31) | 1.12 (0.30) | 1.29 (0.28) | 1.23 (0.28) | 1.08 (0.29) | 1.21 (0.31) | 0.98 (0.34) | |
| 1.00 (0.32) | 1.12 (0.31) | 1.14 (0.30) | 1.31 (0.28) | 1.32 (0.27) | 1.41 (0.27) | 1.26 (0.28) | 1.29 (0.31) | | |
| 0.92 (0.31) | 1.08 (0.31) | 1.07 (0.29) | 1.29 (0.28) | 1.26 (0.26) | 1.41 (0.27) | 1.21 (0.29) | | | |
| 1.03 (0.32) | 1.16 (0.30) | 1.22 (0.29) | 1.45 (0.27) | 1.67 (0.25) | 1.69 (0.26) | | | | |
| 0.90 (0.32) | 1.07 (0.31) | 1.07 (0.29) | 1.35 (0.28) | 1.41 (0.27) | | | | | |
| 0.94 (0.33) | 1.06 (0.32) | 1.11 (0.30) | 1.31 (0.31) | | | | | | |
| 0.77 (0.34) | 0.91 (0.33) | 0.92 (0.33) | | | | | | | |
| 0.76 (0.37) | 0.74 (0.38) | | | | | | | | |
| 0.65 (0.40) | | | | | | | | | |

Figure 4.9: 3D ARI Configuration: PFD distribution and bundle fission density with statistical uncertainty (%)

Table 4.6: Selected pin fission density results
and % uncertainty (in parentheses) for BWR – 3D ARI Configuration

| Bundle 14 | | | | | | | | Bundle 30 | | | | | | | |
|---|---|---|---|---|---|---|---|---|---|---|---|---|---|---|---|
| 1.31 | 1.45 | 1.33 | 1.33 | 1.33 | 1.44 | 1.37 | 1.29 | 0.85 | 0.82 | 0.78 | 0.74 | 0.73 | 0.64 | 0.57 | 0.50 |
| (0.26) | (0.27) | (0.27) | (0.27) | (0.27) | (0.26) | (0.25) | (0.24) | (0.29) | (0.30) | (0.31) | (0.32) | (0.32) | (0.32) | (0.32) | (0.32) |
| 1.42 | 1.13 | 0.42 | 1.03 | 0.43 | 1.11 | 1.33 | 1.19 | 0.97 | 1.03 | 1.02 | 1.00 | 0.99 | 0.86 | 0.72 | 0.57 |
| (0.27) | (0.29) | (0.20) | (0.30) | (0.20) | (0.29) | (0.27) | (0.26) | (0.30) | (0.31) | (0.32) | (0.32) | (0.32) | (0.32) | (0.32) | (0.32) |
| 1.27 | 0.41 | 0.97 | 1.12 | 1.05 | 0.42 | 1.16 | 1.08 | 1.11 | 1.05 | 1.09 | 1.11 | 1.05 | 1.01 | 0.87 | 0.66 |
| (0.28) | (0.20) | (0.31) | (0.30) | (0.30) | (0.20) | (0.28) | (0.27) | (0.31) | (0.31) | (0.31) | (0.31) | (0.31) | (0.32) | (0.32) | (0.32) |
| 1.24 | 0.98 | 1.10 | | | 1.05 | 1.11 | 1.00 | 1.16 | 1.10 | 1.14 | | | 1.07 | 1.01 | 0.76 |
| (0.29) | (0.30) | (0.30) | | | (0.30) | (0.29) | (0.28) | (0.31) | (0.31) | (0.31) | | | (0.31) | (0.32) | (0.32) |
| 1.21 | 0.40 | 1.01 | | | 0.38 | 1.05 | 0.96 | 1.17 | 1.07 | 1.15 | | | 1.14 | 1.04 | 0.78 |
| (0.29) | (0.20) | (0.31) | | | (0.20) | (0.30) | (0.28) | (0.30) | (0.31) | (0.31) | | | (0.31) | (0.31) | (0.31) |
| 1.28 | 1.01 | 0.39 | 1.00 | 0.37 | 0.95 | 1.01 | 0.85 | 1.20 | 1.13 | 1.08 | 1.17 | 1.16 | 1.13 | 1.07 | 0.84 |
| (0.28) | (0.30) | (0.21) | (0.31) | (0.21) | (0.31) | (0.29) | (0.28) | (0.30) | (0.31) | (0.31) | (0.30) | (0.30) | (0.31) | (0.31) | (0.30) |
| 1.20 | 1.18 | 1.05 | 1.04 | 1.00 | 0.99 | 0.90 | 0.75 | 1.21 | 1.14 | 1.14 | 1.09 | 1.14 | 1.10 | 1.09 | 0.89 |
| (0.27) | (0.29) | (0.30) | (0.30) | (0.30) | (0.30) | (0.29) | (0.28) | (0.30) | (0.30) | (0.31) | (0.31) | (0.31) | (0.31) | (0.30) | (0.29) |
| 1.10 | 1.04 | 0.96 | 0.91 | 0.90 | 0.81 | 0.74 | 0.65 | 1.06 | 1.22 | 1.23 | 1.21 | 1.21 | 1.18 | 1.05 | 0.93 |
| (0.26) | (0.28) | (0.29) | (0.29) | (0.29) | (0.29) | (0.28) | (0.28) | (0.29) | (0.29) | (0.30) | (0.30) | (0.30) | (0.30) | (0.29) | (0.28) |
| Bundle 21 | | | | | | | | Bundle 70 | | | | | | | |
| 0.91 | 0.87 | 0.82 | 0.77 | 0.74 | 0.64 | 0.56 | 0.48 | 0.78 | 0.81 | 0.83 | 0.79 | 0.77 | 0.68 | 0.62 | 0.59 |
| (0.23) | (0.24) | (0.25) | (0.26) | (0.27) | (0.27) | (0.28) | (0.75) | (0.37) | (0.38) | (0.39) | (0.40) | (0.40) | (0.40) | (0.40) | (0.39) |
| 1.06 | 1.10 | 1.08 | 1.04 | 1.01 | 0.87 | 0.71 | 0.56 | 0.87 | 0.95 | 0.97 | 0.94 | 0.93 | 0.80 | 0.70 | 0.64 |
| (0.24) | (0.24) | (0.25) | (0.26) | (0.27) | (0.28) | (0.75) | (0.28) | (0.39) | (0.40) | (0.41) | (0.42) | (0.42) | (0.42) | (0.41) | (0.39) |
| 1.22 | 1.14 | 1.15 | 1.16 | 1.09 | 1.03 | 0.87 | 0.64 | 1.02 | 0.97 | 1.00 | 0.98 | 0.91 | 0.91 | 0.84 | 0.74 |
| (0.24) | (0.25) | (0.25) | (0.25) | (0.27) | (0.73) | (0.28) | (0.27) | (0.39) | (0.41) | (0.42) | (0.42) | (0.42) | (0.42) | (0.41) | (0.39) |
| 1.29 | 1.20 | 1.21 | | | 1.09 | 1.01 | 0.74 | 1.13 | 1.06 | 1.03 | | | 0.94 | 0.99 | 0.86 |
| (0.24) | (0.25) | (0.25) | | | (0.27) | (0.27) | (0.27) | (0.39) | (0.40) | (0.41) | | | (0.42) | (0.41) | (0.38) |
| 1.31 | 1.17 | 1.24 | | | 1.16 | 1.04 | 0.77 | 1.19 | 1.04 | 1.08 | | | 1.04 | 1.04 | 0.91 |
| (0.24) | (0.25) | (0.26) | | | (0.25) | (0.26) | (0.26) | (0.38) | (0.39) | (0.39) | | | (0.41) | (0.40) | (0.37) |
| 1.36 | 1.24 | 1.17 | 1.24 | 1.21 | 1.15 | 1.08 | 0.82 | 1.29 | 1.18 | 1.06 | 1.10 | 1.08 | 1.09 | 1.10 | 0.98 |
| (0.24) | (0.25) | (0.69) | (0.26) | (0.25) | (0.25) | (0.25) | (0.25) | (0.36) | (0.38) | (0.39) | (0.39) | (0.39) | (0.40) | (0.39) | (0.36) |
| 1.36 | 1.26 | 1.24 | 1.17 | 1.20 | 1.14 | 1.10 | 0.87 | 1.32 | 1.23 | 1.21 | 1.09 | 1.14 | 1.09 | 1.10 | 0.98 |
| (0.24) | (0.67) | (0.25) | (0.25) | (0.25) | (0.25) | (0.24) | (0.24) | (0.35) | (0.36) | (0.37) | (0.38) | (0.39) | (0.39) | (0.37) | (0.35) |
| 1.19 | 1.36 | 1.36 | 1.31 | 1.29 | 1.22 | 1.06 | 0.91 | 1.20 | 1.35 | 1.35 | 1.28 | 1.25 | 1.16 | 1.03 | 0.95 |
| (0.62) | (0.24) | (0.24) | (0.24) | (0.24) | (0.24) | (0.24) | (0.23) | (0.33) | (0.34) | (0.36) | (0.36) | (0.37) | (0.37) | (0.36) | (0.34) |

4.2.5.3 BWR Pin Fission Density Results – 3D SRI

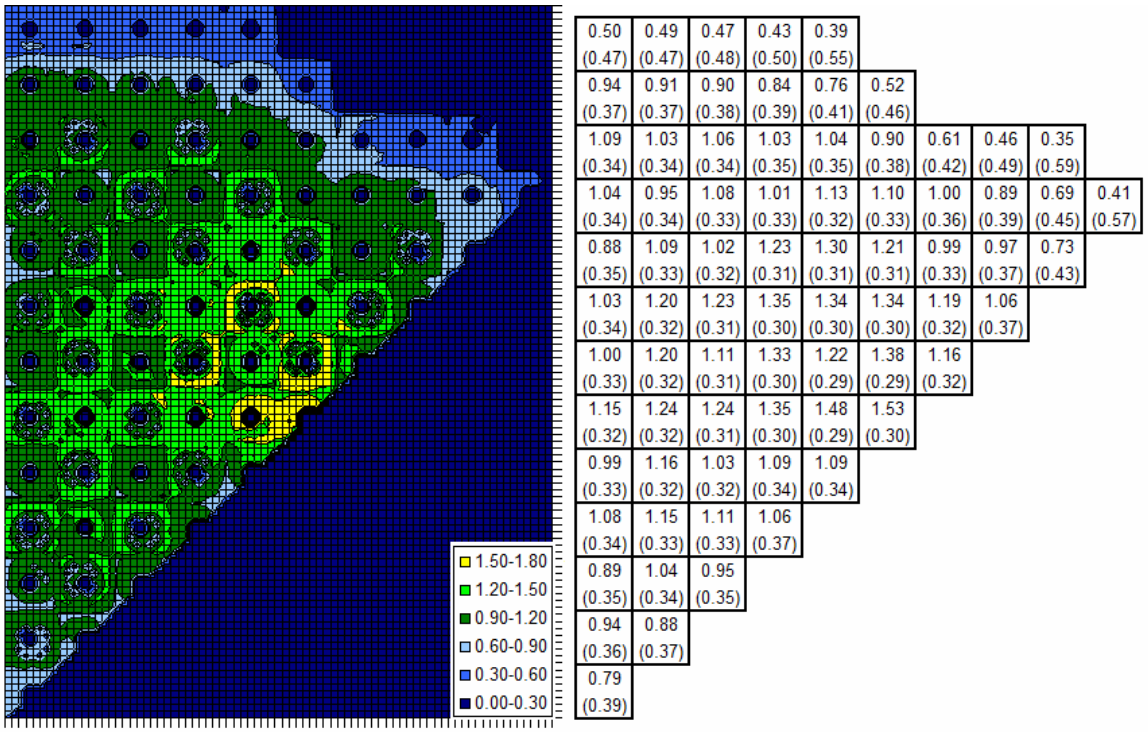


| | | | | | | | | | |
|---|---|---|---|---|---|---|---|---|---|
| 0.50 (0.47) | 0.49 (0.47) | 0.47 (0.48) | 0.43 (0.50) | 0.39 (0.55) | | | | | |
| 0.94 (0.37) | 0.91 (0.37) | 0.90 (0.38) | 0.84 (0.39) | 0.76 (0.41) | 0.52 (0.46) | | | | |
| 1.09 (0.34) | 1.03 (0.34) | 1.06 (0.34) | 1.03 (0.35) | 1.04 (0.35) | 0.90 (0.38) | 0.61 (0.42) | 0.46 (0.49) | 0.35 (0.59) | |
| 1.04 (0.34) | 0.95 (0.34) | 1.08 (0.33) | 1.01 (0.33) | 1.13 (0.32) | 1.10 (0.33) | 1.00 (0.36) | 0.89 (0.39) | 0.69 (0.45) | 0.41 (0.57) |
| 0.88 (0.35) | 1.09 (0.33) | 1.02 (0.32) | 1.23 (0.31) | 1.30 (0.31) | 1.21 (0.31) | 0.99 (0.33) | 0.97 (0.37) | 0.73 (0.43) | |
| 1.03 (0.34) | 1.20 (0.32) | 1.23 (0.31) | 1.35 (0.30) | 1.34 (0.30) | 1.34 (0.30) | 1.19 (0.32) | 1.06 (0.37) | | |
| 1.00 (0.33) | 1.20 (0.32) | 1.11 (0.31) | 1.33 (0.30) | 1.22 (0.29) | 1.38 (0.29) | 1.16 (0.32) | | | |
| 1.15 (0.32) | 1.24 (0.32) | 1.24 (0.31) | 1.35 (0.30) | 1.48 (0.29) | 1.53 (0.30) | | | | |
| 0.99 (0.33) | 1.16 (0.32) | 1.03 (0.32) | 1.09 (0.34) | 1.09 (0.34) | | | | | |
| 1.08 (0.34) | 1.15 (0.33) | 1.11 (0.33) | 1.06 (0.37) | | | | | | |
| 0.89 (0.35) | 1.04 (0.34) | 0.95 (0.35) | | | | | | | |
| 0.94 (0.36) | 0.88 (0.37) | | | | | | | | |
| 0.79 (0.39) | | | | | | | | | |

Figure 4.10: 3D SRI Configuration: PFD distribution and bundle fission density with statistical uncertainty (%)

Table 4.7. Selected pin fission density results
and % uncertainty (in parentheses) for BWR – 3D SRI Configuration

| Bundle 14 | | | | | | | | Bundle 30 | | | | | | | |
|---|---|---|---|---|---|---|---|---|---|---|---|---|---|---|---|
| 1.28 | 1.39 | 1.28 | 1.28 | 1.29 | 1.40 | 1.36 | 1.29 | 0.85 | 0.89 | 0.92 | 0.92 | 0.95 | 0.90 | 0.86 | 0.84 |
| (0.31) | (0.32) | (0.33) | (0.34) | (0.33) | (0.32) | (0.31) | (0.29) | (0.31) | (0.31) | (0.31) | (0.31) | (0.31) | (0.30) | (0.29) | (0.28) |
| 1.37 | 1.09 | 0.42 | 0.99 | 0.42 | 1.08 | 1.31 | 1.21 | 0.92 | 1.01 | 1.04 | 1.06 | 1.10 | 1.04 | 0.95 | 0.87 |
| (0.33) | (0.35) | (0.25) | (0.36) | (0.25) | (0.35) | (0.33) | (0.31) | (0.32) | (0.33) | (0.33) | (0.32) | (0.32) | (0.31) | (0.30) | (0.29) |
| 1.23 | 0.41 | 0.93 | 1.07 | 1.01 | 0.41 | 1.14 | 1.11 | 1.01 | 0.97 | 1.03 | 1.08 | 1.07 | 1.09 | 1.05 | 0.92 |
| (0.34) | (0.25) | (0.37) | (0.36) | (0.37) | (0.25) | (0.35) | (0.33) | (0.33) | (0.34) | (0.34) | (0.33) | (0.32) | (0.32) | (0.31) | (0.29) |
| 1.21 | 0.95 | 1.05 | | | 1.02 | 1.10 | 1.04 | 1.02 | 0.98 | 1.02 | | | 1.08 | 1.13 | 0.99 |
| (0.35) | (0.37) | (0.37) | | | (0.37) | (0.36) | (0.34) | (0.34) | (0.34) | (0.34) | | | (0.32) | (0.31) | (0.30) |
| 1.19 | 0.40 | 0.98 | | | 0.38 | 1.05 | 1.01 | 1.01 | 0.93 | 1.02 | | | 1.10 | 1.11 | 0.98 |
| (0.35) | (0.26) | (0.38) | | | (0.26) | (0.36) | (0.35) | (0.34) | (0.34) | (0.34) | | | (0.32) | (0.32) | (0.30) |
| 1.28 | 1.00 | 0.39 | 0.98 | 0.37 | 0.95 | 1.04 | 0.91 | 1.03 | 0.96 | 0.94 | 1.03 | 1.05 | 1.07 | 1.10 | 0.99 |
| (0.34) | (0.36) | (0.26) | (0.38) | (0.26) | (0.38) | (0.36) | (0.35) | (0.34) | (0.34) | (0.34) | (0.33) | (0.33) | (0.33) | (0.32) | (0.30) |
| 1.22 | 1.19 | 1.06 | 1.04 | 1.01 | 1.02 | 0.95 | 0.83 | 1.03 | 0.97 | 0.97 | 0.95 | 1.02 | 1.02 | 1.08 | 0.97 |
| (0.33) | (0.35) | (0.36) | (0.37) | (0.37) | (0.36) | (0.35) | (0.34) | (0.33) | (0.33) | (0.34) | (0.34) | (0.33) | (0.33) | (0.31) | (0.30) |
| 1.14 | 1.08 | 1.01 | 0.97 | 0.96 | 0.88 | 0.82 | 0.76 | 0.90 | 1.04 | 1.05 | 1.04 | 1.07 | 1.08 | 1.01 | 0.94 |
| (0.31) | (0.33) | (0.35) | (0.35) | (0.36) | (0.35) | (0.35) | (0.34) | (0.32) | (0.33) | (0.33) | (0.33) | (0.33) | (0.32) | (0.30) | (0.29) |
| Bundle 21 | | | | | | | | Bundle 70 | | | | | | | |
| 0.94 | 0.97 | 0.99 | 0.97 | 0.99 | 0.92 | 0.87 | 0.84 | 0.82 | 0.84 | 0.84 | 0.80 | 0.78 | 0.68 | 0.62 | 0.59 |
| (0.26) | (0.27) | (0.27) | (0.27) | (0.27) | (0.27) | (0.28) | (0.35) | (0.44) | (0.45) | (0.46) | (0.47) | (0.48) | (0.48) | (0.48) | (0.47) |
| 1.02 | 1.10 | 1.12 | 1.12 | 1.14 | 1.06 | 0.96 | 0.87 | 0.90 | 0.97 | 0.98 | 0.94 | 0.92 | 0.80 | 0.70 | 0.64 |
| (0.27) | (0.28) | (0.29) | (0.29) | (0.29) | (0.29) | (0.38) | (0.28) | (0.45) | (0.47) | (0.49) | (0.50) | (0.50) | (0.50) | (0.49) | (0.46) |
| 1.12 | 1.06 | 1.10 | 1.13 | 1.11 | 1.12 | 1.06 | 0.92 | 1.04 | 0.98 | 0.99 | 0.97 | 0.90 | 0.90 | 0.83 | 0.74 |
| (0.28) | (0.29) | (0.29) | (0.29) | (0.31) | (0.40) | (0.29) | (0.27) | (0.46) | (0.48) | (0.50) | (0.50) | (0.50) | (0.51) | (0.49) | (0.46) |
| 1.14 | 1.06 | 1.10 | | | 1.11 | 1.14 | 0.99 | 1.14 | 1.05 | 1.01 | | | 0.93 | 0.99 | 0.87 |
| (0.29) | (0.30) | (0.30) | | | (0.31) | (0.29) | (0.27) | (0.46) | (0.48) | (0.49) | | | (0.50) | (0.48) | (0.45) |
| 1.12 | 1.00 | 1.08 | | | 1.13 | 1.12 | 0.97 | 1.18 | 1.03 | 1.05 | | | 1.02 | 1.04 | 0.92 |
| (0.29) | (0.30) | (0.31) | | | (0.29) | (0.29) | (0.27) | (0.45) | (0.47) | (0.48) | | | (0.49) | (0.47) | (0.44) |
| 1.14 | 1.05 | 1.00 | 1.08 | 1.10 | 1.10 | 1.12 | 0.99 | 1.28 | 1.16 | 1.04 | 1.08 | 1.06 | 1.08 | 1.11 | 0.99 |
| (0.30) | (0.31) | (0.42) | (0.31) | (0.30) | (0.29) | (0.29) | (0.27) | (0.43) | (0.45) | (0.46) | (0.47) | (0.47) | (0.47) | (0.46) | (0.42) |
| 1.12 | 1.05 | 1.05 | 1.00 | 1.06 | 1.06 | 1.10 | 0.97 | 1.31 | 1.22 | 1.19 | 1.08 | 1.13 | 1.09 | 1.12 | 1.01 |
| (0.30) | (0.41) | (0.31) | (0.30) | (0.30) | (0.29) | (0.28) | (0.27) | (0.41) | (0.43) | (0.45) | (0.45) | (0.46) | (0.45) | (0.44) | (0.41) |
| 0.99 | 1.12 | 1.14 | 1.12 | 1.14 | 1.12 | 1.02 | 0.94 | 1.19 | 1.34 | 1.33 | 1.27 | 1.25 | 1.18 | 1.06 | 1.00 |
| (0.39) | (0.30) | (0.30) | (0.29) | (0.29) | (0.28) | (0.27) | (0.26) | (0.39) | (0.41) | (0.42) | (0.43) | (0.44) | (0.43) | (0.42) | (0.40) |

4.2.5.4 BWR Pin Fission Density Results – 2D ARO

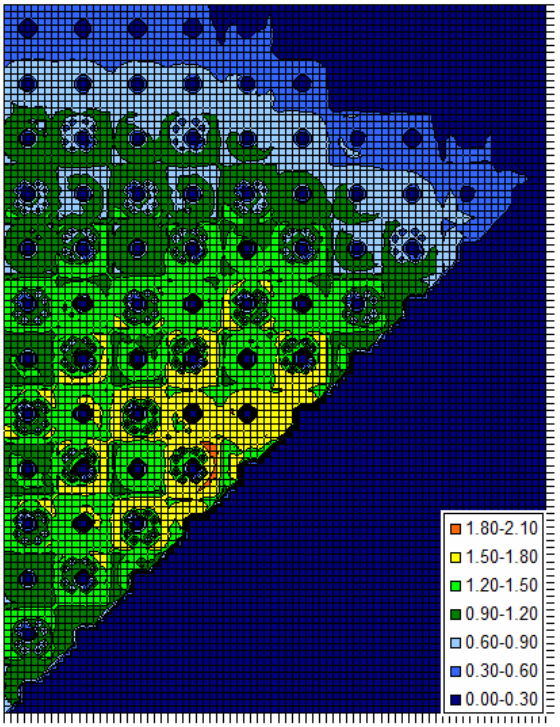


| | | | | | | | | | |
|---|---|---|---|---|---|---|---|---|---|
| 0.41 (0.12) | 0.40 (0.12) | 0.38 (0.13) | 0.35 (0.13) | 0.30 (0.14) | | | | | |
| 0.76 (0.10) | 0.74 (0.10) | 0.72 (0.10) | 0.66 (0.11) | 0.59 (0.11) | 0.43 (0.12) | | | | |
| 0.95 (0.09) | 0.90 (0.09) | 0.91 (0.09) | 0.85 (0.09) | 0.84 (0.09) | 0.74 (0.10) | 0.53 (0.11) | 0.39 (0.13) | 0.28 (0.15) | |
| 0.99 (0.09) | 0.87 (0.08) | 0.99 (0.08) | 0.88 (0.08) | 1.00 (0.08) | 0.96 (0.09) | 0.84 (0.09) | 0.68 (0.10) | 0.51 (0.12) | 0.32 (0.15) |
| 0.94 (0.08) | 1.10 (0.08) | 0.98 (0.08) | 1.16 (0.08) | 1.21 (0.08) | 1.11 (0.08) | 0.87 (0.08) | 0.84 (0.09) | 0.60 (0.11) | |
| 1.17 (0.08) | 1.25 (0.08) | 1.26 (0.07) | 1.34 (0.07) | 1.32 (0.07) | 1.30 (0.08) | 1.14 (0.08) | 1.03 (0.09) | | |
| 1.10 (0.08) | 1.30 (0.07) | 1.19 (0.07) | 1.42 (0.07) | 1.27 (0.07) | 1.40 (0.07) | 1.12 (0.08) | | | |
| 1.29 (0.07) | 1.39 (0.07) | 1.42 (0.07) | 1.56 (0.07) | 1.66 (0.07) | 1.62 (0.07) | | | | |
| 1.14 (0.07) | 1.36 (0.07) | 1.26 (0.07) | 1.52 (0.07) | 1.43 (0.07) | | | | | |
| 1.27 (0.07) | 1.37 (0.07) | 1.40 (0.07) | 1.52 (0.07) | | | | | | |
| 1.05 (0.08) | 1.25 (0.08) | 1.16 (0.08) | | | | | | | |
| 1.12 (0.08) | 1.02 (0.08) | | | | | | | | |
| 0.94 (0.09) | | | | | | | | | |

Figure 4.11: 2D ARO Configuration: PFD distribution and bundle fission density with statistical uncertainty (%)

Table 4.8: Selected pin fission density results
and % uncertainty (in parentheses) for BWR – 2D ARO Configuration

| Bundle 14 | | | | | | | | Bundle 30 | | | | | | | |
|---|---|---|---|---|---|---|---|---|---|---|---|---|---|---|---|
| 1.10 | 1.18 | 1.10 | 1.11 | 1.13 | 1.26 | 1.26 | 1.23 | 0.86 | 0.90 | 0.92 | 0.92 | 0.94 | 0.89 | 0.84 | 0.82 |
| (0.07) | (0.07) | (0.30) | (0.30) | (0.30) | (0.28) | (0.27) | (0.25) | (0.30) | (0.30) | (0.31) | (0.31) | (0.30) | (0.30) | (0.28) | (0.28) |
| 1.17 | 0.93 | 0.36 | 0.87 | 0.37 | 0.99 | 1.26 | 1.25 | 0.93 | 1.02 | 1.05 | 1.06 | 1.09 | 1.03 | 0.94 | 0.86 |
| (0.07) | (0.07) | (0.22) | (0.32) | (0.22) | (0.30) | (0.28) | (0.26) | (0.31) | (0.32) | (0.32) | (0.32) | (0.31) | (0.31) | (0.29) | (0.28) |
| 1.07 | 0.36 | 0.82 | 0.96 | 0.92 | 0.38 | 1.15 | 1.24 | 1.02 | 0.97 | 1.03 | 1.08 | 1.06 | 1.08 | 1.04 | 0.91 |
| (0.07) | (0.05) | (0.33) | (0.32) | (0.33) | (0.22) | (0.29) | (0.26) | (0.32) | (0.33) | (0.33) | (0.32) | (0.32) | (0.32) | (0.31) | (0.29) |
| 1.06 | 0.84 | 0.94 | | | 0.99 | 1.15 | 1.22 | 1.03 | 0.98 | 1.03 | | | 1.07 | 1.12 | 0.98 |
| (0.07) | (0.08) | (0.33) | | | (0.32) | (0.29) | (0.26) | (0.33) | (0.33) | (0.33) | | | (0.32) | (0.31) | (0.30) |
| 1.07 | 0.37 | 0.90 | | | 0.36 | 1.15 | 1.23 | 1.01 | 0.93 | 1.02 | | | 1.10 | 1.10 | 0.97 |
| (0.07) | (0.05) | (0.33) | | | (0.22) | (0.29) | (0.26) | (0.33) | (0.33) | (0.33) | | | (0.32) | (0.31) | (0.30) |
| 1.18 | 0.95 | 0.36 | 0.96 | 0.35 | 1.02 | 1.21 | 1.17 | 1.03 | 0.97 | 0.94 | 1.03 | 1.05 | 1.07 | 1.10 | 0.99 |
| (0.07) | (0.07) | (0.22) | (0.32) | (0.22) | (0.30) | (0.28) | (0.26) | (0.33) | (0.34) | (0.33) | (0.33) | (0.33) | (0.32) | (0.31) | (0.29) |
| 1.16 | 1.18 | 1.08 | 1.10 | 1.12 | 1.19 | 1.18 | 1.13 | 1.03 | 0.97 | 0.98 | 0.95 | 1.02 | 1.03 | 1.09 | 0.97 |
| (0.07) | (0.07) | (0.30) | (0.30) | (0.29) | (0.28) | (0.26) | (0.25) | (0.32) | (0.33) | (0.33) | (0.33) | (0.33) | (0.32) | (0.31) | (0.29) |
| 1.13 | 1.15 | 1.15 | 1.15 | 1.18 | 1.14 | 1.12 | 1.10 | 0.91 | 1.04 | 1.06 | 1.05 | 1.08 | 1.09 | 1.01 | 0.94 |
| (0.06) | (0.06) | (0.27) | (0.27) | (0.27) | (0.26) | (0.25) | (0.24) | (0.31) | (0.32) | (0.33) | (0.33) | (0.32) | (0.31) | (0.30) | (0.28) |
| Bundle 21 | | | | | | | | Bundle 70 | | | | | | | |
| 0.82 | 0.85 | 0.97 | 0.96 | 0.97 | 0.90 | 0.84 | 0.81 | 0.81 | 0.83 | 0.83 | 0.79 | 0.77 | 0.68 | 0.62 | 0.59 |
| (0.11) | (0.12) | (0.26) | (0.26) | (0.26) | (0.26) | (0.27) | (0.34) | (0.46) | (0.47) | (0.48) | (0.49) | (0.50) | (0.50) | (0.50) | (0.48) |
| 0.89 | 0.97 | 1.11 | 1.11 | 1.12 | 1.04 | 0.94 | 0.84 | 0.89 | 0.95 | 0.97 | 0.93 | 0.92 | 0.80 | 0.70 | 0.64 |
| (0.12) | (0.12) | (0.27) | (0.27) | (0.27) | (0.28) | (0.36) | (0.27) | (0.47) | (0.49) | (0.51) | (0.52) | (0.52) | (0.52) | (0.51) | (0.48) |
| 1.01 | 0.96 | 1.09 | 1.13 | 1.10 | 1.10 | 1.04 | 0.90 | 1.03 | 0.97 | 0.98 | 0.96 | 0.90 | 0.90 | 0.83 | 0.74 |
| (0.12) | (0.13) | (0.28) | (0.28) | (0.29) | (0.38) | (0.28) | (0.26) | (0.48) | (0.50) | (0.52) | (0.52) | (0.53) | (0.53) | (0.51) | (0.48) |
| 1.10 | 1.02 | 1.10 | | | 1.10 | 1.12 | 0.97 | 1.12 | 1.04 | 1.01 | | | 0.93 | 0.99 | 0.87 |
| (0.12) | (0.13) | (0.28) | | | (0.29) | (0.27) | (0.26) | (0.48) | (0.50) | (0.50) | | | (0.51) | (0.50) | (0.47) |
| 1.14 | 1.00 | 1.10 | | | 1.13 | 1.11 | 0.96 | 1.18 | 1.03 | 1.05 | | | 1.03 | 1.05 | 0.93 |
| (0.12) | (0.12) | (0.29) | | | (0.28) | (0.27) | (0.26) | (0.47) | (0.48) | (0.49) | | | (0.50) | (0.49) | (0.45) |
| 1.23 | 1.12 | 1.02 | 1.10 | 1.10 | 1.09 | 1.11 | 0.97 | 1.27 | 1.16 | 1.04 | 1.08 | 1.07 | 1.09 | 1.12 | 1.00 |
| (0.12) | (0.12) | (0.39) | (0.29) | (0.28) | (0.28) | (0.27) | (0.26) | (0.45) | (0.47) | (0.48) | (0.48) | (0.49) | (0.49) | (0.47) | (0.44) |
| 1.26 | 1.17 | 1.07 | 1.02 | 1.08 | 1.06 | 1.09 | 0.96 | 1.31 | 1.22 | 1.19 | 1.08 | 1.14 | 1.10 | 1.14 | 1.02 |
| (0.11) | (0.12) | (0.29) | (0.28) | (0.28) | (0.27) | (0.26) | (0.25) | (0.43) | (0.45) | (0.46) | (0.47) | (0.47) | (0.47) | (0.45) | (0.42) |
| 1.14 | 1.29 | 1.17 | 1.14 | 1.15 | 1.13 | 1.02 | 0.93 | 1.19 | 1.34 | 1.34 | 1.28 | 1.26 | 1.20 | 1.08 | 1.01 |
| (0.11) | (0.11) | (0.27) | (0.27) | (0.27) | (0.27) | (0.26) | (0.25) | (0.41) | (0.42) | (0.44) | (0.45) | (0.45) | (0.44) | (0.43) | (0.41) |

4.2.5.5 BWR Pin Fission Density Results – 2D ARI

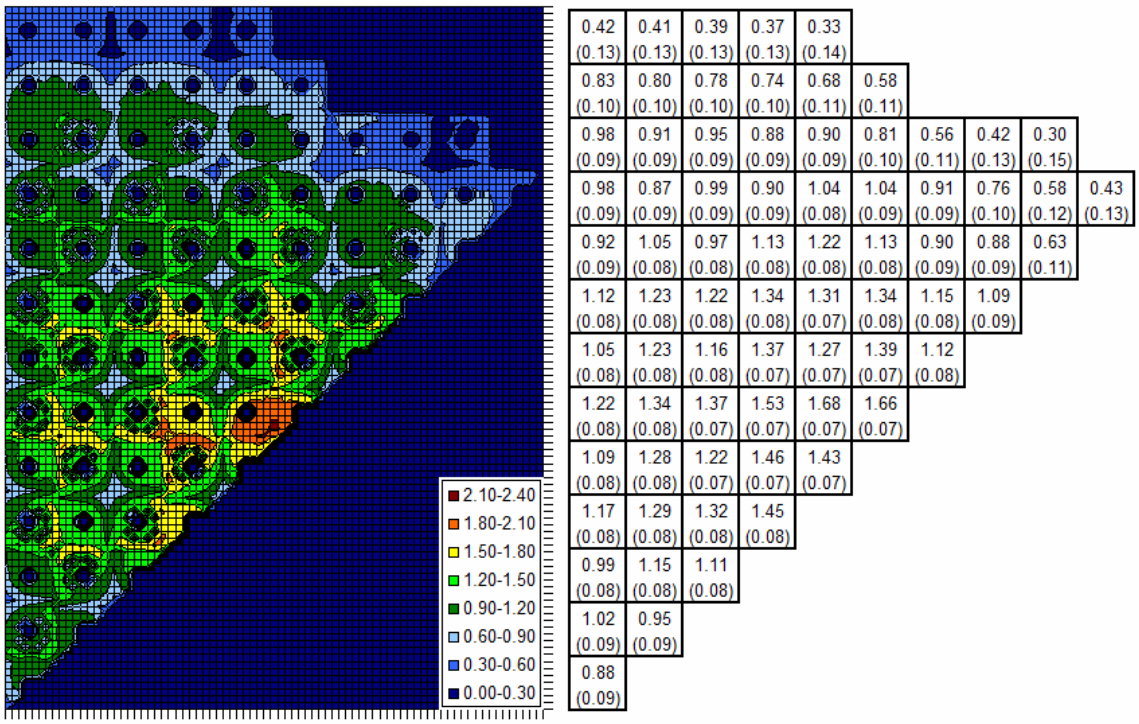


Figure 4.12: 2D ARI Configuration: PFD distribution and bundle fission density with statistical uncertainty (%)

Table 4.9: Selected pin fission density results
and % uncertainty (in parentheses) for BWR – 2D ARI Configuration

| Bundle 14 | | | | | | | | Bundle 30 | | | | | | | |
|---|---|---|---|---|---|---|---|---|---|---|---|---|---|---|---|
| 1.30 | 1.43 | 1.31 | 1.29 | 1.29 | 1.39 | 1.33 | 1.24 | 0.86 | 0.83 | 0.79 | 0.74 | 0.73 | 0.64 | 0.57 | 0.50 |
| (0.07) | (0.07) | (0.07) | (0.07) | (0.07) | (0.07) | (0.07) | (0.06) | (0.08) | (0.08) | (0.08) | (0.08) | (0.08) | (0.08) | (0.08) | (0.08) |
| 1.41 | 1.13 | 0.45 | 1.02 | 0.45 | 1.10 | 1.29 | 1.16 | 0.98 | 1.03 | 1.02 | 1.00 | 0.98 | 0.86 | 0.72 | 0.58 |
| (0.07) | (0.07) | (0.05) | (0.08) | (0.05) | (0.07) | (0.07) | (0.07) | (0.08) | (0.08) | (0.08) | (0.08) | (0.08) | (0.08) | (0.08) | (0.08) |
| 1.27 | 0.44 | 0.97 | 1.10 | 1.05 | 0.44 | 1.13 | 1.05 | 1.11 | 1.05 | 1.08 | 1.10 | 1.04 | 1.01 | 0.87 | 0.66 |
| (0.07) | (0.05) | (0.08) | (0.08) | (0.08) | (0.05) | (0.07) | (0.07) | (0.08) | (0.08) | (0.08) | (0.08) | (0.08) | (0.08) | (0.08) | (0.08) |
| 1.24 | 0.99 | 1.09 | | | 1.04 | 1.09 | 0.98 | 1.16 | 1.10 | 1.13 | | | 1.06 | 1.01 | 0.76 |
| (0.07) | (0.08) | (0.08) | | | (0.08) | (0.07) | (0.07) | (0.08) | (0.08) | (0.08) | | | (0.08) | (0.08) | (0.08) |
| 1.22 | 0.43 | 1.02 | | | 0.41 | 1.04 | 0.95 | 1.17 | 1.06 | 1.15 | | | 1.13 | 1.04 | 0.79 |
| (0.07) | (0.05) | (0.08) | | | (0.05) | (0.07) | (0.07) | (0.08) | (0.08) | (0.08) | | | (0.08) | (0.08) | (0.08) |
| 1.30 | 1.03 | 0.42 | 1.02 | 0.40 | 0.96 | 1.00 | 0.84 | 1.21 | 1.12 | 1.08 | 1.16 | 1.16 | 1.13 | 1.08 | 0.84 |
| (0.07) | (0.08) | (0.05) | (0.08) | (0.05) | (0.08) | (0.07) | (0.07) | (0.08) | (0.08) | (0.08) | (0.08) | (0.08) | (0.08) | (0.08) | (0.08) |
| 1.23 | 1.21 | 1.07 | 1.05 | 1.01 | 0.99 | 0.90 | 0.75 | 1.22 | 1.14 | 1.14 | 1.09 | 1.14 | 1.10 | 1.10 | 0.90 |
| (0.07) | (0.07) | (0.07) | (0.08) | (0.08) | (0.07) | (0.07) | (0.07) | (0.08) | (0.08) | (0.08) | (0.08) | (0.08) | (0.08) | (0.08) | (0.08) |
| 1.13 | 1.07 | 0.99 | 0.93 | 0.91 | 0.82 | 0.74 | 0.66 | 1.06 | 1.23 | 1.23 | 1.21 | 1.21 | 1.18 | 1.05 | 0.94 |
| (0.07) | (0.07) | (0.07) | (0.07) | (0.07) | (0.07) | (0.07) | (0.07) | (0.07) | (0.08) | (0.08) | (0.08) | (0.08) | (0.08) | (0.07) | (0.07) |
| Bundle 21 | | | | | | | | Bundle 70 | | | | | | | |
| 0.93 | 0.88 | 0.83 | 0.78 | 0.75 | 0.65 | 0.57 | 0.49 | 0.79 | 0.84 | 0.86 | 0.83 | 0.82 | 0.73 | 0.67 | 0.64 |
| (0.06) | (0.07) | (0.07) | (0.07) | (0.07) | (0.07) | (0.08) | (0.20) | (0.11) | (0.11) | (0.11) | (0.11) | (0.11) | (0.11) | (0.11) | (0.11) |
| 1.06 | 1.11 | 1.08 | 1.04 | 1.01 | 0.87 | 0.72 | 0.57 | 0.87 | 0.96 | 1.00 | 0.97 | 0.97 | 0.85 | 0.75 | 0.69 |
| (0.07) | (0.07) | (0.07) | (0.07) | (0.07) | (0.08) | (0.20) | (0.08) | (0.11) | (0.11) | (0.11) | (0.12) | (0.12) | (0.11) | (0.11) | (0.11) |
| 1.22 | 1.13 | 1.15 | 1.16 | 1.08 | 1.03 | 0.87 | 0.65 | 1.00 | 0.97 | 1.00 | 0.99 | 0.93 | 0.95 | 0.89 | 0.78 |
| (0.07) | (0.07) | (0.07) | (0.07) | (0.08) | (0.20) | (0.08) | (0.07) | (0.11) | (0.11) | (0.12) | (0.12) | (0.12) | (0.12) | (0.11) | (0.11) |
| 1.29 | 1.19 | 1.21 | | | 1.08 | 1.01 | 0.75 | 1.09 | 1.03 | 1.01 | | | 0.96 | 1.04 | 0.91 |
| (0.07) | (0.07) | (0.07) | | | (0.08) | (0.07) | (0.07) | (0.11) | (0.11) | (0.12) | | | (0.12) | (0.11) | (0.10) |
| 1.30 | 1.16 | 1.23 | | | 1.16 | 1.04 | 0.78 | 1.14 | 1.01 | 1.04 | | | 1.05 | 1.07 | 0.95 |
| (0.07) | (0.07) | (0.07) | | | (0.07) | (0.07) | (0.07) | (0.11) | (0.11) | (0.11) | | | (0.11) | (0.11) | (0.10) |
| 1.34 | 1.23 | 1.16 | 1.23 | 1.21 | 1.15 | 1.08 | 0.83 | 1.22 | 1.13 | 1.02 | 1.07 | 1.06 | 1.09 | 1.13 | 1.01 |
| (0.07) | (0.07) | (0.20) | (0.07) | (0.07) | (0.07) | (0.07) | (0.07) | (0.11) | (0.11) | (0.11) | (0.11) | (0.11) | (0.11) | (0.11) | (0.10) |
| 1.35 | 1.25 | 1.23 | 1.16 | 1.19 | 1.13 | 1.11 | 0.88 | 1.25 | 1.17 | 1.15 | 1.05 | 1.11 | 1.08 | 1.11 | 1.00 |
| (0.07) | (0.18) | (0.07) | (0.07) | (0.07) | (0.07) | (0.07) | (0.07) | (0.10) | (0.10) | (0.11) | (0.11) | (0.11) | (0.11) | (0.10) | (0.10) |
| 1.18 | 1.35 | 1.34 | 1.30 | 1.29 | 1.22 | 1.06 | 0.93 | 1.13 | 1.28 | 1.28 | 1.22 | 1.21 | 1.14 | 1.03 | 0.96 |
| (0.18) | (0.07) | (0.07) | (0.07) | (0.07) | (0.07) | (0.07) | (0.06) | (0.10) | (0.10) | (0.10) | (0.11) | (0.11) | (0.10) | (0.10) | (0.10) |

4.2.5.6 BWR Pin Fission Density Results – 2D SRI

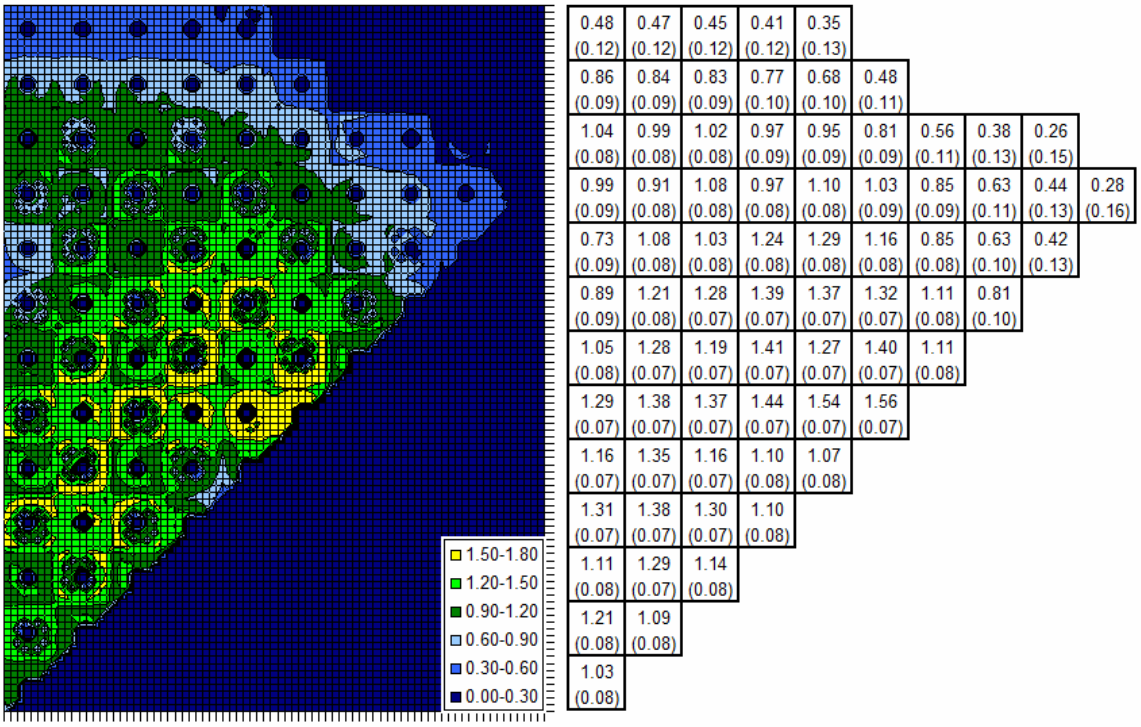


Figure 4.13: 2D SRI Configuration: PFD distribution and bundle fission density with statistical uncertainty (%)

Table 4.10. Selected pin fission density results
and % uncertainty (in parentheses) for BWR – 2D SRI Configuration

| Bundle 14 | | | | | | | | Bundle 30 | | | | | | | |
|---|---|---|---|---|---|---|---|---|---|---|---|---|---|---|---|
| 1.34 | 1.46 | 1.33 | 1.31 | 1.32 | 1.43 | 1.37 | 1.29 | 0.80 | 0.86 | 0.90 | 0.91 | 0.95 | 0.90 | 0.87 | 0.85 |
| (0.07) | (0.07) | (0.08) | (0.08) | (0.08) | (0.07) | (0.07) | (0.07) | (0.08) | (0.08) | (0.08) | (0.08) | (0.07) | (0.07) | (0.07) | (0.07) |
| 1.45 | 1.15 | 0.45 | 1.02 | 0.45 | 1.10 | 1.30 | 1.17 | 0.88 | 0.98 | 1.02 | 1.05 | 1.10 | 1.04 | 0.96 | 0.88 |
| (0.08) | (0.08) | (0.05) | (0.08) | (0.05) | (0.08) | (0.08) | (0.07) | (0.08) | (0.08) | (0.08) | (0.08) | (0.08) | (0.08) | (0.07) | (0.07) |
| 1.30 | 0.44 | 0.97 | 1.09 | 1.03 | 0.43 | 1.12 | 1.04 | 0.96 | 0.94 | 1.01 | 1.07 | 1.07 | 1.10 | 1.07 | 0.94 |
| (0.08) | (0.05) | (0.08) | (0.08) | (0.08) | (0.05) | (0.08) | (0.08) | (0.08) | (0.08) | (0.08) | (0.08) | (0.08) | (0.08) | (0.07) | (0.07) |
| 1.27 | 1.00 | 1.08 | | | 1.02 | 1.06 | 0.96 | 0.98 | 0.95 | 1.01 | | | 1.09 | 1.15 | 1.01 |
| (0.08) | (0.08) | (0.08) | | | (0.09) | (0.08) | (0.08) | (0.08) | (0.08) | (0.08) | | | (0.08) | (0.08) | (0.07) |
| 1.26 | 0.43 | 1.01 | | | 0.39 | 1.00 | 0.91 | 0.98 | 0.91 | 1.00 | | | 1.12 | 1.13 | 1.00 |
| (0.08) | (0.05) | (0.09) | | | (0.06) | (0.08) | (0.08) | (0.08) | (0.08) | (0.08) | | | (0.08) | (0.08) | (0.07) |
| 1.35 | 1.05 | 0.42 | 1.00 | 0.39 | 0.93 | 0.96 | 0.80 | 1.00 | 0.95 | 0.93 | 1.03 | 1.06 | 1.09 | 1.13 | 1.01 |
| (0.08) | (0.08) | (0.06) | (0.09) | (0.06) | (0.09) | (0.08) | (0.08) | (0.08) | (0.08) | (0.08) | (0.08) | (0.08) | (0.08) | (0.08) | (0.07) |
| 1.28 | 1.23 | 1.07 | 1.03 | 0.98 | 0.95 | 0.86 | 0.72 | 1.02 | 0.96 | 0.97 | 0.95 | 1.03 | 1.05 | 1.12 | 1.00 |
| (0.07) | (0.08) | (0.08) | (0.08) | (0.08) | (0.08) | (0.08) | (0.08) | (0.08) | (0.08) | (0.08) | (0.08) | (0.08) | (0.08) | (0.07) | (0.07) |
| 1.19 | 1.09 | 0.99 | 0.91 | 0.89 | 0.79 | 0.71 | 0.63 | 0.90 | 1.04 | 1.05 | 1.06 | 1.09 | 1.11 | 1.04 | 0.97 |
| (0.07) | (0.08) | (0.08) | (0.08) | (0.08) | (0.08) | (0.08) | (0.08) | (0.08) | (0.08) | (0.08) | (0.08) | (0.08) | (0.08) | (0.07) | (0.07) |
| Bundle 21 | | | | | | | | Bundle 70 | | | | | | | |
| 0.94 | 0.97 | 0.99 | 0.98 | 0.99 | 0.92 | 0.87 | 0.84 | 0.83 | 0.86 | 0.87 | 0.83 | 0.81 | 0.72 | 0.65 | 0.63 |
| (0.06) | (0.06) | (0.07) | (0.07) | (0.07) | (0.07) | (0.07) | (0.18) | (0.11) | (0.11) | (0.11) | (0.11) | (0.12) | (0.12) | (0.11) | (0.11) |
| 1.03 | 1.10 | 1.12 | 1.12 | 1.14 | 1.06 | 0.96 | 0.87 | 0.90 | 0.98 | 1.00 | 0.97 | 0.96 | 0.84 | 0.74 | 0.67 |
| (0.07) | (0.07) | (0.07) | (0.07) | (0.07) | (0.07) | (0.18) | (0.07) | (0.11) | (0.12) | (0.12) | (0.12) | (0.12) | (0.12) | (0.12) | (0.11) |
| 1.12 | 1.06 | 1.10 | 1.13 | 1.11 | 1.12 | 1.06 | 0.92 | 1.03 | 0.97 | 1.00 | 0.98 | 0.91 | 0.93 | 0.87 | 0.77 |
| (0.07) | (0.07) | (0.07) | (0.07) | (0.07) | (0.20) | (0.07) | (0.07) | (0.12) | (0.12) | (0.12) | (0.12) | (0.12) | (0.12) | (0.12) | (0.11) |
| 1.13 | 1.06 | 1.09 | | | 1.11 | 1.14 | 0.99 | 1.11 | 1.03 | 1.00 | | | 0.94 | 1.02 | 0.89 |
| (0.07) | (0.07) | (0.07) | | | (0.07) | (0.07) | (0.07) | (0.12) | (0.12) | (0.12) | | | (0.12) | (0.12) | (0.11) |
| 1.12 | 1.00 | 1.08 | | | 1.13 | 1.12 | 0.98 | 1.15 | 1.00 | 1.03 | | | 1.03 | 1.06 | 0.94 |
| (0.07) | (0.07) | (0.08) | | | (0.07) | (0.07) | (0.07) | (0.11) | (0.12) | (0.12) | | | (0.12) | (0.12) | (0.11) |
| 1.13 | 1.04 | 1.00 | 1.08 | 1.09 | 1.10 | 1.12 | 0.99 | 1.24 | 1.13 | 1.02 | 1.06 | 1.05 | 1.08 | 1.12 | 1.01 |
| (0.07) | (0.08) | (0.20) | (0.08) | (0.07) | (0.07) | (0.07) | (0.07) | (0.11) | (0.11) | (0.12) | (0.12) | (0.12) | (0.12) | (0.11) | (0.10) |
| 1.12 | 1.05 | 1.04 | 1.00 | 1.06 | 1.06 | 1.10 | 0.97 | 1.27 | 1.18 | 1.15 | 1.05 | 1.11 | 1.08 | 1.13 | 1.02 |
| (0.07) | (0.20) | (0.08) | (0.07) | (0.07) | (0.07) | (0.07) | (0.06) | (0.11) | (0.11) | (0.11) | (0.11) | (0.12) | (0.11) | (0.11) | (0.10) |
| 0.98 | 1.12 | 1.13 | 1.12 | 1.13 | 1.12 | 1.03 | 0.94 | 1.14 | 1.29 | 1.29 | 1.23 | 1.22 | 1.16 | 1.06 | 1.00 |
| (0.20) | (0.07) | (0.07) | (0.07) | (0.07) | (0.07) | (0.07) | (0.06) | (0.10) | (0.10) | (0.11) | (0.11) | (0.11) | (0.11) | (0.10) | (0.10) |

## 4.4 BWR Pin Fission Density Uncertainty Analysis

Due to the large number of fuel pins in the core, providing individual fission densities for each pin is impractical, so in order to provide a good understanding of the statistical uncertainty present in the pin fission density distribution, three statistical data types (Smith et al., 2005) are used to analyze the pin fission distribution in each assembly as in Eq. (4.3), Eq. (4.4) and Eq. (4.5).

$$AVG = \frac{\sum_{i=1}^{N} |e_i|}{N} \tag{4.3}$$

$$RMS = \sqrt{\frac{\sum_{i=1}^{N} e_n{}^2}{N}} \tag{4.4}$$

$$MRE = \frac{\sum_{i=1}^{N} |e_i| \cdot f_i}{N \cdot f_{avg}} \tag{4.5}$$

Where $e_n$ is the statistical uncertainty (relative error) of the fission density $f_n$. These data types are presented in Tables 4.11-4.16 for the axially integrated fuel pins (fuel and blanket layers) within each bundle of the BWR problem.

Table 4.11: Axially integrated pin fission density uncertainty analysis for the 3D ARO configuration

| | | | | | | | | | | |
|---|---|---|---|---|---|---|---|---|---|---|
| AVG | 0.5034 | 0.5062 | 0.5169 | 0.5389 | 0.5884 | | | | | |
| RMS | 0.5059 | 0.5088 | 0.5197 | 0.5419 | 0.5931 | | | | | |
| MRE | 0.4996 | 0.5027 | 0.5130 | 0.5340 | 0.5796 | | | | | |
| AVG | 0.3884 | 0.3933 | 0.3966 | 0.4093 | 0.4361 | 0.4774 | | | | |
| RMS | 0.3888 | 0.3936 | 0.3971 | 0.4096 | 0.4371 | 0.4783 | | | | |
| MRE | 0.3878 | 0.3931 | 0.3960 | 0.4087 | 0.4335 | 0.4745 | | | | |
| AVG | 0.3486 | 0.3488 | 0.3523 | 0.3551 | 0.3619 | 0.3853 | 0.4204 | 0.4869 | 0.5783 | |
| RMS | 0.3491 | 0.3510 | 0.3528 | 0.3575 | 0.3627 | 0.3864 | 0.4223 | 0.4892 | 0.5830 | |
| MRE | 0.3490 | 0.3534 | 0.3527 | 0.3594 | 0.3616 | 0.3837 | 0.4187 | 0.4828 | 0.5700 | |
| AVG | 0.3403 | 0.3429 | 0.3348 | 0.3341 | 0.3244 | 0.3339 | 0.3529 | 0.3761 | 0.4325 | 0.5705 |
| RMS | 0.3422 | 0.3433 | 0.3367 | 0.3345 | 0.3263 | 0.3341 | 0.3533 | 0.3764 | 0.4339 | 0.5781 |
| MRE | 0.3453 | 0.3439 | 0.3399 | 0.3350 | 0.3295 | 0.3345 | 0.3528 | 0.3756 | 0.4291 | 0.5460 |
| AVG | 0.3374 | 0.3264 | 0.3219 | 0.3098 | 0.3058 | 0.3063 | 0.3213 | 0.3349 | 0.3993 | |
| RMS | 0.3379 | 0.3286 | 0.3224 | 0.3119 | 0.3063 | 0.3082 | 0.3219 | 0.3370 | 0.4046 | |
| MRE | 0.3381 | 0.3304 | 0.3224 | 0.3131 | 0.3060 | 0.3102 | 0.3218 | 0.3391 | 0.3866 | |
| AVG | 0.3214 | 0.3151 | 0.3032 | 0.2967 | 0.2877 | 0.2938 | 0.3020 | 0.3472 | | |
| RMS | 0.3232 | 0.3155 | 0.3049 | 0.2971 | 0.2894 | 0.2941 | 0.3038 | 0.3506 | | |
| MRE | 0.3265 | 0.3157 | 0.3079 | 0.2972 | 0.2921 | 0.2945 | 0.3061 | 0.3375 | | |
| AVG | 0.3167 | 0.3036 | 0.2965 | 0.2834 | 0.2786 | 0.2787 | 0.3198 | | | |
| RMS | 0.3170 | 0.3056 | 0.2968 | 0.2853 | 0.2791 | 0.2804 | 0.3234 | | | |
| MRE | 0.3173 | 0.3076 | 0.2972 | 0.2869 | 0.2791 | 0.2823 | 0.3106 | | | |
| AVG | 0.3108 | 0.3031 | 0.2887 | 0.2786 | 0.2650 | 0.2893 | | | | |
| RMS | 0.3126 | 0.3036 | 0.2903 | 0.2790 | 0.2652 | 0.2921 | | | | |
| MRE | 0.3156 | 0.3036 | 0.2930 | 0.2789 | 0.2656 | 0.2812 | | | | |
| AVG | 0.3152 | 0.3015 | 0.2926 | 0.2800 | 0.2911 | | | | | |
| RMS | 0.3154 | 0.3034 | 0.2928 | 0.2818 | 0.2939 | | | | | |
| MRE | 0.3159 | 0.3056 | 0.2934 | 0.2837 | 0.2833 | | | | | |
| AVG | 0.3197 | 0.3119 | 0.2972 | 0.3165 | | | | | | |
| RMS | 0.3215 | 0.3124 | 0.2990 | 0.3201 | | | | | | |
| MRE | 0.3243 | 0.3121 | 0.3014 | 0.3071 | | | | | | |
| AVG | 0.3351 | 0.3218 | 0.3393 | | | | | | | |
| RMS | 0.3353 | 0.3237 | 0.3426 | | | | | | | |
| MRE | 0.3359 | 0.3263 | 0.3301 | | | | | | | |
| AVG | 0.3481 | 0.3722 | | | | | | | | |
| RMS | 0.3502 | 0.3763 | | | | | | | | |
| MRE | 0.3529 | 0.3616 | | | | | | | | |
| AVG | 0.3952 | | | | | | | | | |
| RMS | 0.3991 | | | | | | | | | |
| MRE | 0.3838 | | | | | | | | | |

Table 4.12: Axially integrated pin fission density uncertainty analysis for the 3D ARI configuration

| | | | | | | | | | | |
|---|---|---|---|---|---|---|---|---|---|---|
| AVG | 0.4704 | 0.4725 | 0.4801 | 0.4959 | 0.5341 | | | | | |
| RMS | 0.4715 | 0.4737 | 0.4812 | 0.4974 | 0.5364 | | | | | |
| MRE | 0.4690 | 0.4713 | 0.4794 | 0.4932 | 0.5300 | | | | | |
| AVG | 0.3495 | 0.3539 | 0.3551 | 0.3631 | 0.3814 | 0.3875 | | | | |
| RMS | 0.3504 | 0.3547 | 0.3560 | 0.3641 | 0.3828 | 0.3882 | | | | |
| MRE | 0.3442 | 0.3491 | 0.3499 | 0.3573 | 0.3745 | 0.3854 | | | | |
| AVG | 0.3191 | 0.3188 | 0.3213 | 0.3223 | 0.3241 | 0.3407 | 0.3775 | 0.4384 | 0.5131 | |
| RMS | 0.3192 | 0.3208 | 0.3215 | 0.3244 | 0.3242 | 0.3411 | 0.3779 | 0.4399 | 0.5150 | |
| MRE | 0.3180 | 0.3250 | 0.3205 | 0.3291 | 0.3237 | 0.3387 | 0.3784 | 0.4341 | 0.5115 | |
| AVG | 0.3223 | 0.3276 | 0.3140 | 0.3130 | 0.2938 | 0.2985 | 0.3148 | 0.3297 | 0.3700 | 0.4449 |
| RMS | 0.3243 | 0.3277 | 0.3161 | 0.3132 | 0.2959 | 0.2988 | 0.3153 | 0.3306 | 0.3711 | 0.4505 |
| MRE | 0.3285 | 0.3270 | 0.3196 | 0.3122 | 0.2985 | 0.2963 | 0.3119 | 0.3242 | 0.3643 | 0.4269 |
| AVG | 0.3301 | 0.3152 | 0.3091 | 0.2928 | 0.2841 | 0.2792 | 0.2938 | 0.3010 | 0.3530 | |
| RMS | 0.3303 | 0.3172 | 0.3093 | 0.2946 | 0.2842 | 0.2810 | 0.2939 | 0.3030 | 0.3567 | |
| MRE | 0.3291 | 0.3218 | 0.3084 | 0.2992 | 0.2833 | 0.2847 | 0.2937 | 0.3068 | 0.3414 | |
| AVG | 0.3145 | 0.3081 | 0.2914 | 0.2835 | 0.2691 | 0.2724 | 0.2776 | 0.3198 | | |
| RMS | 0.3166 | 0.3082 | 0.2934 | 0.2837 | 0.2709 | 0.2726 | 0.2794 | 0.3234 | | |
| MRE | 0.3198 | 0.3072 | 0.2962 | 0.2827 | 0.2740 | 0.2713 | 0.2828 | 0.3076 | | |
| AVG | 0.3147 | 0.2990 | 0.2890 | 0.2721 | 0.2637 | 0.2602 | 0.3010 | | | |
| RMS | 0.3149 | 0.3008 | 0.2892 | 0.2738 | 0.2638 | 0.2619 | 0.3042 | | | |
| MRE | 0.3135 | 0.3051 | 0.2879 | 0.2779 | 0.2632 | 0.2652 | 0.2912 | | | |
| AVG | 0.3099 | 0.3013 | 0.2820 | 0.2685 | 0.2497 | 0.2704 | | | | |
| RMS | 0.3120 | 0.3014 | 0.2840 | 0.2686 | 0.2500 | 0.2735 | | | | |
| MRE | 0.3154 | 0.3009 | 0.2868 | 0.2682 | 0.2480 | 0.2596 | | | | |
| AVG | 0.3184 | 0.3015 | 0.2902 | 0.2734 | 0.2792 | | | | | |
| RMS | 0.3186 | 0.3035 | 0.2904 | 0.2753 | 0.2826 | | | | | |
| MRE | 0.3168 | 0.3074 | 0.2885 | 0.2787 | 0.2678 | | | | | |
| AVG | 0.3250 | 0.3166 | 0.2969 | 0.3160 | | | | | | |
| RMS | 0.3272 | 0.3167 | 0.2988 | 0.3192 | | | | | | |
| MRE | 0.3310 | 0.3165 | 0.3023 | 0.3056 | | | | | | |
| AVG | 0.3459 | 0.3291 | 0.3439 | | | | | | | |
| RMS | 0.3462 | 0.3313 | 0.3479 | | | | | | | |
| MRE | 0.3436 | 0.3347 | 0.3302 | | | | | | | |
| AVG | 0.3627 | 0.3913 | | | | | | | | |
| RMS | 0.3650 | 0.3954 | | | | | | | | |
| MRE | 0.3696 | 0.3787 | | | | | | | | |
| AVG | 0.4152 | | | | | | | | | |
| RMS | 0.4200 | | | | | | | | | |
| MRE | 0.3990 | | | | | | | | | |

Table 4.13: Axially integrated pin fission density uncertainty analysis for the 3D SRI configuration

| | | | | | | | | | | |
|---|---|---|---|---|---|---|---|---|---|---|
| AVG | 0.4728 | 0.4754 | 0.4862 | 0.5082 | 0.5569 | | | | | |
| RMS | 0.4751 | 0.4777 | 0.4888 | 0.5109 | 0.5613 | | | | | |
| MRE | 0.4695 | 0.4724 | 0.4828 | 0.5038 | 0.5491 | | | | | |
| AVG | 0.3680 | 0.3728 | 0.3761 | 0.3890 | 0.4172 | 0.4604 | | | | |
| RMS | 0.3683 | 0.3731 | 0.3766 | 0.3893 | 0.4182 | 0.4613 | | | | |
| MRE | 0.3676 | 0.3727 | 0.3757 | 0.3885 | 0.4149 | 0.4579 | | | | |
| AVG | 0.3355 | 0.3346 | 0.3379 | 0.3409 | 0.3498 | 0.3766 | 0.4184 | 0.4930 | 0.5926 | |
| RMS | 0.3359 | 0.3366 | 0.3383 | 0.3432 | 0.3506 | 0.3777 | 0.4203 | 0.4951 | 0.5972 | |
| MRE | 0.3360 | 0.3392 | 0.3383 | 0.3454 | 0.3497 | 0.3752 | 0.4167 | 0.4892 | 0.5850 | |
| AVG | 0.3364 | 0.3358 | 0.3260 | 0.3254 | 0.3180 | 0.3317 | 0.3573 | 0.3891 | 0.4540 | 0.5948 |
| RMS | 0.3384 | 0.3362 | 0.3279 | 0.3258 | 0.3198 | 0.3319 | 0.3578 | 0.3893 | 0.4554 | 0.6025 |
| MRE | 0.3413 | 0.3367 | 0.3309 | 0.3262 | 0.3229 | 0.3324 | 0.3572 | 0.3887 | 0.4512 | 0.5701 |
| AVG | 0.3538 | 0.3271 | 0.3197 | 0.3069 | 0.3051 | 0.3084 | 0.3311 | 0.3625 | 0.4383 | |
| RMS | 0.3539 | 0.3292 | 0.3201 | 0.3089 | 0.3056 | 0.3103 | 0.3318 | 0.3645 | 0.4434 | |
| MRE | 0.3545 | 0.3313 | 0.3204 | 0.3105 | 0.3054 | 0.3126 | 0.3315 | 0.3683 | 0.4253 | |
| AVG | 0.3411 | 0.3205 | 0.3063 | 0.3007 | 0.2925 | 0.3006 | 0.3135 | 0.3796 | | |
| RMS | 0.3420 | 0.3209 | 0.3080 | 0.3010 | 0.2943 | 0.3009 | 0.3156 | 0.3834 | | |
| MRE | 0.3436 | 0.3210 | 0.3111 | 0.3011 | 0.2970 | 0.3013 | 0.3177 | 0.3679 | | |
| AVG | 0.3248 | 0.3114 | 0.3063 | 0.2951 | 0.2908 | 0.2891 | 0.3313 | | | |
| RMS | 0.3252 | 0.3134 | 0.3066 | 0.2970 | 0.2912 | 0.2909 | 0.3351 | | | |
| MRE | 0.3255 | 0.3157 | 0.3071 | 0.2992 | 0.2915 | 0.2932 | 0.3216 | | | |
| AVG | 0.3197 | 0.3154 | 0.3065 | 0.3033 | 0.2884 | 0.3077 | | | | |
| RMS | 0.3216 | 0.3158 | 0.3084 | 0.3038 | 0.2887 | 0.3108 | | | | |
| MRE | 0.3247 | 0.3158 | 0.3110 | 0.3035 | 0.2890 | 0.2990 | | | | |
| AVG | 0.3268 | 0.3172 | 0.3209 | 0.3351 | 0.3493 | | | | | |
| RMS | 0.3271 | 0.3191 | 0.3213 | 0.3371 | 0.3533 | | | | | |
| MRE | 0.3276 | 0.3219 | 0.3218 | 0.3408 | 0.3359 | | | | | |
| AVG | 0.3317 | 0.3294 | 0.3271 | 0.3851 | | | | | | |
| RMS | 0.3337 | 0.3299 | 0.3291 | 0.3892 | | | | | | |
| MRE | 0.3365 | 0.3298 | 0.3317 | 0.3725 | | | | | | |
| AVG | 0.3468 | 0.3371 | 0.3648 | | | | | | | |
| RMS | 0.3471 | 0.3391 | 0.3686 | | | | | | | |
| MRE | 0.3477 | 0.3422 | 0.3548 | | | | | | | |
| AVG | 0.3571 | 0.3848 | | | | | | | | |
| RMS | 0.3592 | 0.3890 | | | | | | | | |
| MRE | 0.3622 | 0.3739 | | | | | | | | |
| AVG | 0.4038 | | | | | | | | | |
| RMS | 0.4078 | | | | | | | | | |
| MRE | 0.3920 | | | | | | | | | |

Table 4.14: Axially integrated pin fission density uncertainty analysis for the 2D ARO configuration

| | | | | | | | | | | |
|---|---|---|---|---|---|---|---|---|---|---|
| AVG | 0.1238 | 0.1245 | 0.1273 | 0.1335 | 0.1438 | | | | | |
| RMS | 0.1244 | 0.1251 | 0.1279 | 0.1341 | 0.1447 | | | | | |
| MRE | 0.1232 | 0.1239 | 0.1268 | 0.1326 | 0.1426 | | | | | |
| AVG | 0.0982 | 0.0987 | 0.1007 | 0.1057 | 0.1112 | 0.1203 | | | | |
| RMS | 0.0982 | 0.0987 | 0.1009 | 0.1058 | 0.1115 | 0.1205 | | | | |
| MRE | 0.0980 | 0.0987 | 0.1006 | 0.1056 | 0.1106 | 0.1200 | | | | |
| AVG | 0.0875 | 0.0865 | 0.0895 | 0.0893 | 0.0927 | 0.0997 | 0.1078 | 0.1265 | 0.1483 | |
| RMS | 0.0876 | 0.0872 | 0.0898 | 0.0901 | 0.0929 | 0.1000 | 0.1083 | 0.1269 | 0.1492 | |
| MRE | 0.0876 | 0.0880 | 0.0895 | 0.0905 | 0.0925 | 0.0992 | 0.1075 | 0.1258 | 0.1472 | |
| AVG | 0.0833 | 0.0845 | 0.0827 | 0.0837 | 0.0820 | 0.0872 | 0.0933 | 0.1040 | 0.1197 | 0.1527 |
| RMS | 0.0841 | 0.0847 | 0.0834 | 0.0838 | 0.0827 | 0.0873 | 0.0936 | 0.1041 | 0.1200 | 0.1544 |
| MRE | 0.0852 | 0.0847 | 0.0844 | 0.0839 | 0.0837 | 0.0875 | 0.0931 | 0.1039 | 0.1188 | 0.1475 |
| AVG | 0.0810 | 0.0790 | 0.0785 | 0.0765 | 0.0765 | 0.0777 | 0.0835 | 0.0897 | 0.1103 | |
| RMS | 0.0812 | 0.0796 | 0.0787 | 0.0771 | 0.0767 | 0.0783 | 0.0838 | 0.0904 | 0.1120 | |
| MRE | 0.0811 | 0.0803 | 0.0786 | 0.0774 | 0.0766 | 0.0788 | 0.0834 | 0.0910 | 0.1066 | |
| AVG | 0.0768 | 0.0765 | 0.0728 | 0.0738 | 0.0710 | 0.0753 | 0.0777 | 0.0918 | | |
| RMS | 0.0773 | 0.0766 | 0.0736 | 0.0740 | 0.0716 | 0.0755 | 0.0783 | 0.0927 | | |
| MRE | 0.0781 | 0.0767 | 0.0748 | 0.0739 | 0.0727 | 0.0755 | 0.0788 | 0.0894 | | |
| AVG | 0.0755 | 0.0717 | 0.0720 | 0.0692 | 0.0685 | 0.0690 | 0.0806 | | | |
| RMS | 0.0757 | 0.0724 | 0.0722 | 0.0698 | 0.0686 | 0.0696 | 0.0815 | | | |
| MRE | 0.0756 | 0.0734 | 0.0721 | 0.0705 | 0.0686 | 0.0704 | 0.0783 | | | |
| AVG | 0.0720 | 0.0725 | 0.0685 | 0.0677 | 0.0667 | 0.0730 | | | | |
| RMS | 0.0727 | 0.0727 | 0.0691 | 0.0678 | 0.0668 | 0.0738 | | | | |
| MRE | 0.0739 | 0.0725 | 0.0699 | 0.0678 | 0.0669 | 0.0710 | | | | |
| AVG | 0.0740 | 0.0702 | 0.0690 | 0.0663 | 0.0712 | | | | | |
| RMS | 0.0742 | 0.0708 | 0.0691 | 0.0669 | 0.0720 | | | | | |
| MRE | 0.0741 | 0.0717 | 0.0692 | 0.0674 | 0.0694 | | | | | |
| AVG | 0.0732 | 0.0735 | 0.0697 | 0.0758 | | | | | | |
| RMS | 0.0738 | 0.0737 | 0.0703 | 0.0766 | | | | | | |
| MRE | 0.0748 | 0.0735 | 0.0712 | 0.0736 | | | | | | |
| AVG | 0.0767 | 0.0737 | 0.0797 | | | | | | | |
| RMS | 0.0768 | 0.0743 | 0.0805 | | | | | | | |
| MRE | 0.0770 | 0.0752 | 0.0776 | | | | | | | |
| AVG | 0.0782 | 0.0836 | | | | | | | | |
| RMS | 0.0787 | 0.0847 | | | | | | | | |
| MRE | 0.0795 | 0.0812 | | | | | | | | |
| AVG | 0.0891 | | | | | | | | | |
| RMS | 0.0899 | | | | | | | | | |
| MRE | 0.0866 | | | | | | | | | |

Table 4.15: Axially integrated pin fission density uncertainty analysis for the 2D ARI configuration

| | | | | | | | | | | |
|---|---|---|---|---|---|---|---|---|---|---|
| AVG | 0.1267 | 0.1268 | 0.1305 | 0.1348 | 0.1435 | | | | | |
| RMS | 0.1269 | 0.1270 | 0.1307 | 0.1351 | 0.1440 | | | | | |
| MRE | 0.1265 | 0.1267 | 0.1305 | 0.1343 | 0.1426 | | | | | |
| AVG | 0.0990 | 0.1003 | 0.1010 | 0.1040 | 0.1085 | 0.1092 | | | | |
| RMS | 0.0992 | 0.1006 | 0.1012 | 0.1043 | 0.1088 | 0.1093 | | | | |
| MRE | 0.0976 | 0.0991 | 0.0997 | 0.1025 | 0.1069 | 0.1089 | | | | |
| AVG | 0.0897 | 0.0875 | 0.0898 | 0.0888 | 0.0922 | 0.0978 | 0.1092 | 0.1270 | 0.1485 | |
| RMS | 0.0897 | 0.0883 | 0.0898 | 0.0896 | 0.0923 | 0.0980 | 0.1093 | 0.1274 | 0.1488 | |
| MRE | 0.0897 | 0.0897 | 0.0898 | 0.0909 | 0.0922 | 0.0974 | 0.1092 | 0.1257 | 0.1484 | |
| AVG | 0.0850 | 0.0880 | 0.0843 | 0.0865 | 0.0828 | 0.0867 | 0.0937 | 0.1030 | 0.1175 | 0.1382 |
| RMS | 0.0857 | 0.0881 | 0.0850 | 0.0866 | 0.0834 | 0.0868 | 0.0938 | 0.1033 | 0.1178 | 0.1396 |
| MRE | 0.0869 | 0.0879 | 0.0860 | 0.0862 | 0.0842 | 0.0862 | 0.0930 | 0.1015 | 0.1161 | 0.1337 |
| AVG | 0.0860 | 0.0817 | 0.0803 | 0.0790 | 0.0795 | 0.0793 | 0.0873 | 0.0900 | 0.1112 | |
| RMS | 0.0861 | 0.0822 | 0.0804 | 0.0795 | 0.0795 | 0.0799 | 0.0874 | 0.0908 | 0.1125 | |
| MRE | 0.0857 | 0.0834 | 0.0803 | 0.0805 | 0.0795 | 0.0808 | 0.0876 | 0.0918 | 0.1076 | |
| AVG | 0.0805 | 0.0795 | 0.0755 | 0.0777 | 0.0732 | 0.0772 | 0.0788 | 0.0930 | | |
| RMS | 0.0811 | 0.0795 | 0.0762 | 0.0778 | 0.0739 | 0.0773 | 0.0794 | 0.0942 | | |
| MRE | 0.0818 | 0.0795 | 0.0772 | 0.0774 | 0.0746 | 0.0769 | 0.0804 | 0.0891 | | |
| AVG | 0.0793 | 0.0748 | 0.0770 | 0.0708 | 0.0698 | 0.0707 | 0.0845 | | | |
| RMS | 0.0794 | 0.0755 | 0.0771 | 0.0714 | 0.0698 | 0.0713 | 0.0854 | | | |
| MRE | 0.0794 | 0.0769 | 0.0768 | 0.0725 | 0.0698 | 0.0722 | 0.0818 | | | |
| AVG | 0.0755 | 0.0782 | 0.0722 | 0.0698 | 0.0690 | 0.0755 | | | | |
| RMS | 0.0761 | 0.0783 | 0.0728 | 0.0698 | 0.0691 | 0.0762 | | | | |
| MRE | 0.0771 | 0.0781 | 0.0735 | 0.0698 | 0.0689 | 0.0729 | | | | |
| AVG | 0.0788 | 0.0740 | 0.0737 | 0.0693 | 0.0748 | | | | | |
| RMS | 0.0789 | 0.0747 | 0.0738 | 0.0699 | 0.0757 | | | | | |
| MRE | 0.0788 | 0.0758 | 0.0731 | 0.0709 | 0.0722 | | | | | |
| AVG | 0.0777 | 0.0788 | 0.0735 | 0.0791 | | | | | | |
| RMS | 0.0783 | 0.0789 | 0.0742 | 0.0801 | | | | | | |
| MRE | 0.0793 | 0.0789 | 0.0751 | 0.0762 | | | | | | |
| AVG | 0.0823 | 0.0782 | 0.0848 | | | | | | | |
| RMS | 0.0824 | 0.0788 | 0.0857 | | | | | | | |
| MRE | 0.0817 | 0.0797 | 0.0821 | | | | | | | |
| AVG | 0.0837 | 0.0918 | | | | | | | | |
| RMS | 0.0843 | 0.0928 | | | | | | | | |
| MRE | 0.0853 | 0.0889 | | | | | | | | |
| AVG | 0.0967 | | | | | | | | | |
| RMS | 0.0976 | | | | | | | | | |
| MRE | 0.0934 | | | | | | | | | |

Table 4.16: Axially integrated pin fission density uncertainty analysis for the 2D SRI configuration

| | | | | | | | | | | |
|---|---|---|---|---|---|---|---|---|---|---|
| AVG | 0.1157 | 0.1162 | 0.1182 | 0.1243 | 0.1340 | | | | | |
| RMS | 0.1162 | 0.1167 | 0.1187 | 0.1249 | 0.1348 | | | | | |
| MRE | 0.1151 | 0.1157 | 0.1176 | 0.1236 | 0.1328 | | | | | |
| AVG | 0.0927 | 0.0942 | 0.0950 | 0.0980 | 0.1040 | 0.1138 | | | | |
| RMS | 0.0928 | 0.0943 | 0.0952 | 0.0981 | 0.1042 | 0.1140 | | | | |
| MRE | 0.0926 | 0.0941 | 0.0948 | 0.0980 | 0.1035 | 0.1136 | | | | |
| AVG | 0.0847 | 0.0832 | 0.0847 | 0.0840 | 0.0883 | 0.0952 | 0.1065 | 0.1277 | 0.1555 | |
| RMS | 0.0848 | 0.0840 | 0.0849 | 0.0849 | 0.0887 | 0.0955 | 0.1070 | 0.1281 | 0.1563 | |
| MRE | 0.0847 | 0.0848 | 0.0847 | 0.0856 | 0.0882 | 0.0947 | 0.1060 | 0.1269 | 0.1546 | |
| AVG | 0.0833 | 0.0830 | 0.0795 | 0.0788 | 0.0788 | 0.0852 | 0.0927 | 0.1080 | 0.1283 | 0.1652 |
| RMS | 0.0841 | 0.0832 | 0.0801 | 0.0789 | 0.0794 | 0.0853 | 0.0930 | 0.1081 | 0.1288 | 0.1669 |
| MRE | 0.0851 | 0.0831 | 0.0810 | 0.0790 | 0.0803 | 0.0854 | 0.0924 | 0.1078 | 0.1277 | 0.1597 |
| AVG | 0.0902 | 0.0798 | 0.0768 | 0.0745 | 0.0755 | 0.0775 | 0.0850 | 0.1017 | 0.1306 | |
| RMS | 0.0902 | 0.0805 | 0.0770 | 0.0751 | 0.0757 | 0.0781 | 0.0853 | 0.1026 | 0.1321 | |
| MRE | 0.0899 | 0.0812 | 0.0770 | 0.0755 | 0.0755 | 0.0786 | 0.0849 | 0.1031 | 0.1264 | |
| AVG | 0.0843 | 0.0775 | 0.0723 | 0.0727 | 0.0700 | 0.0747 | 0.0783 | 0.1039 | | |
| RMS | 0.0850 | 0.0776 | 0.0730 | 0.0729 | 0.0706 | 0.0748 | 0.0790 | 0.1054 | | |
| MRE | 0.0859 | 0.0776 | 0.0742 | 0.0727 | 0.0716 | 0.0748 | 0.0794 | 0.0991 | | |
| AVG | 0.0772 | 0.0730 | 0.0723 | 0.0695 | 0.0688 | 0.0697 | 0.0812 | | | |
| RMS | 0.0773 | 0.0738 | 0.0725 | 0.0702 | 0.0690 | 0.0703 | 0.0822 | | | |
| MRE | 0.0772 | 0.0743 | 0.0724 | 0.0710 | 0.0690 | 0.0712 | 0.0787 | | | |
| AVG | 0.0723 | 0.0732 | 0.0700 | 0.0717 | 0.0687 | 0.0748 | | | | |
| RMS | 0.0730 | 0.0734 | 0.0706 | 0.0719 | 0.0688 | 0.0757 | | | | |
| MRE | 0.0742 | 0.0732 | 0.0716 | 0.0717 | 0.0688 | 0.0726 | | | | |
| AVG | 0.0737 | 0.0703 | 0.0732 | 0.0758 | 0.0827 | | | | | |
| RMS | 0.0738 | 0.0710 | 0.0734 | 0.0765 | 0.0837 | | | | | |
| MRE | 0.0737 | 0.0720 | 0.0733 | 0.0774 | 0.0795 | | | | | |
| AVG | 0.0718 | 0.0733 | 0.0718 | 0.0876 | | | | | | |
| RMS | 0.0725 | 0.0736 | 0.0726 | 0.0886 | | | | | | |
| MRE | 0.0736 | 0.0734 | 0.0736 | 0.0844 | | | | | | |
| AVG | 0.0750 | 0.0725 | 0.0800 | | | | | | | |
| RMS | 0.0752 | 0.0732 | 0.0808 | | | | | | | |
| MRE | 0.0752 | 0.0743 | 0.0778 | | | | | | | |
| AVG | 0.0763 | 0.0821 | | | | | | | | |
| RMS | 0.0768 | 0.0830 | | | | | | | | |
| MRE | 0.0775 | 0.0799 | | | | | | | | |
| AVG | 0.0855 | | | | | | | | | |
| RMS | 0.0863 | | | | | | | | | |
| MRE | 0.0831 | | | | | | | | | |

## 4.2 Generation of 1D Benchmarks

When developing new computational methods, it is often beneficial to have a set of simple problems which are significantly smaller in scope than a 2D core and which can be used to establish proof-of-concept implementations. For these problems, it is desirable to have full control over the problem, easily obtained reference solutions, and enough flexibility in the specification that one can rapidly obtain solutions and highlight specific effects. In addition to being extremely time-consuming, implementing a new spectral method within a full, 2 or 3-dimensional, fine-mesh transport code could mask some of the specific effects that new spectral methods are intended to address. At the same time, it is important for these simpler problems to possess, as much as possible, the physical characteristics of the larger, more complicated problems for which the method is ultimately intended.

Therefore, in addition to the benchmark problems presented in the previous section, this dissertation includes the development of a set of 1D benchmark problems which are representative of some of the various reactor types for which new transport methods might be applied. The intention of this work is to provide a set of tools for the industry to use in benchmarking new methods, and to use some of these tools to test the new methods presented in this dissertation.

It is not possible to fully represent a 2D or 3D problem within a 1D framework, but it is possible to select some important physical features which we most care about, and work to preserve them as best as possible within the 1D problem. There are two substantively different ways to reduce a benchmark problem to 1D that are generally relevant for radiation transport methods. The first type is by dividing the 2D model into columns, and performing

a flux-weighted transverse-integration over each column of the 2D problem to produce 1D cross sections, shown visually in Figure 4.14 for a controlled GE9 Lattice.

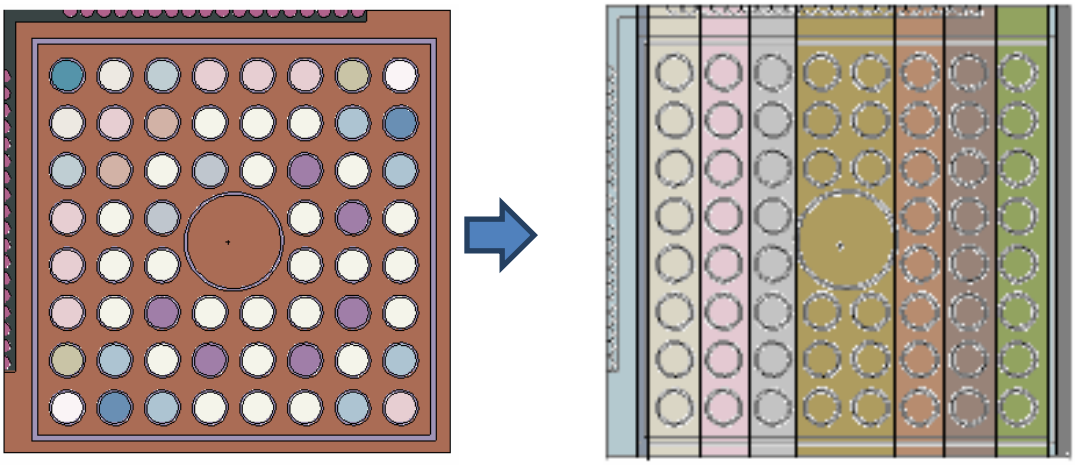

Figure 4.14: Transverse Integration of a GE9 Lattice

For this type of 1D cross section generation, a lattice calculation (with specular reflective boundary conditions) is performed for each bundle type, just as one would to generate core level cross sections in a 2D or 3D problem, and for each column *i*, a homogenized cross section is generated for each energy group *g* according to Eq. (4.6).

$$\sigma_{gi} = \frac{\int_{u_{g-1}}^{u_g} du \int_i d\vec{r}\,\sigma(\vec{r},u)\phi(\vec{r},u)}{\int_{u_{g-1}}^{u_g} du \int_i d\vec{r}\,\phi(\vec{r},u)} \tag{4.6}$$

This method of homogenizing over each column is effective at capturing the overall reaction rates by distributing the effect of control rods or gadolinium pins over the column, and weighting it by the local reaction rates despite the fact that the actual path a particle (such as a neutron) sees moving through the 1D bundle is not the same as the 2D problem.

Much of the current and future research in the industry, however, is focused on more

advanced reactor types, such as optically-thin, gas-cooled, graphite-moderated prismatic cores. These reactors have a hexagonal lattice structure, such as that presented in figure 4.15.

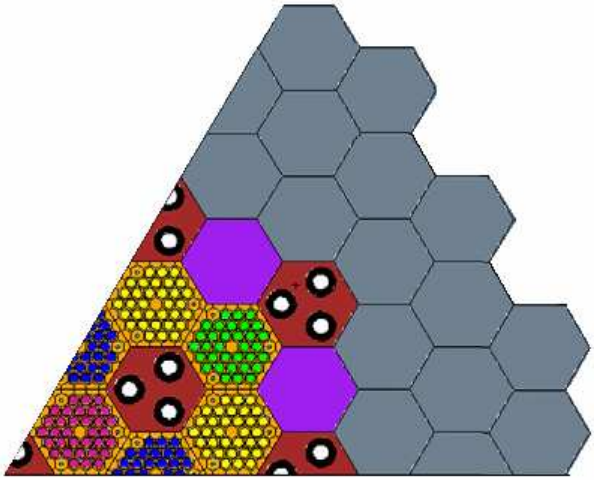

Figure 4.15: Hexagonal-Lattice Core Structure

The difficulty in generating a 1D benchmark problem using the transverse-integration method presented above is that there is no obvious manner for establishing a division of this problem into column-wise segments. As a result, a second method is used to reduce the problem into 1D. In this method, the hexagonal lattices are converted into equivalent-area circles, a volume-fraction preservation of the isotopic number densities in each annular region of the lattice to obtain an equivalent "concentric lattice," demonstrated for an HTTR control block in Figure 4.16.

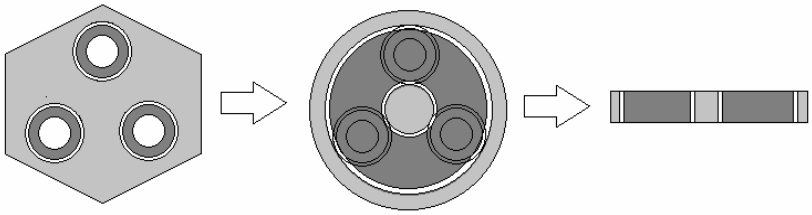

Figure 4.16: Reduction to 1D of HTTR Control Block

Each annular region of the concentric lattice consists of a uniform material constructed by volume-averaging the number densities of each isotope in the region. This method of 1D reduction is not as effective at capturing local 2D effects (such as pin-to-pin interaction) as the transverse integration. For optically thin problems, however, it does a good job of capturing the longer mean free paths, increased streaming effects, and bundle-to-bundle effects, and therefore represents a reasonable method for 1D reduction.

In the following sections, these methods are used to generate 1D benchmark problems for a BWR, PWR, and HTTR core.

### 4.2.1 Transverse-Integrated GE9-Loaded 1D BWR Problem

This benchmark is generated by starting with a 2D fuel assembly problem with full heterogeneity and performing a transport calculation to obtain the neutron flux distribution in a fine-group structure. This distribution is used to generate 1D region-wise cross sections by performing a flux-weighted transverse integration of the cross sections over slab regions of the 2D model, as described above.

In order to generate a BWR benchmark problem that is representative of realistic reactors, fuel assemblies must be included that possess several burn-up and coolant void parameters, and possess a large number of different fuel types. A GE9 BWR lattice (Kelley, 1995) was chosen as representative of BWR assemblies, which consists of 12 fuel types, including four pins which possess 5.84 at% Gd. It was modeled in ½ symmetry with full heterogeneity and a 47-group calculation was performed to deplete the assembly to 17 MWd/t for three void parameters (0, 40, 70%). The lattice depletion code HELIOS (Simeonov, 2003) was used to perform transport calculations in this work. In this calculation, control blades were modeled with full detail (sheath and rods).

For each unique state (burn-up, coolant void fraction, presence of control blades), cross sections are generated in 47 groups for each fuel pin, the averaged control blade, the structure, the coolant, center channel, and moderator. To ensure consistent solutions for each condensed group structure, the 47-group cross sections generated at each burn up point are then used in full bundle calculations to generate flux-weighted, transversely integrated 1D cross sections. An illustration of this process is shown in Figure 4.17.

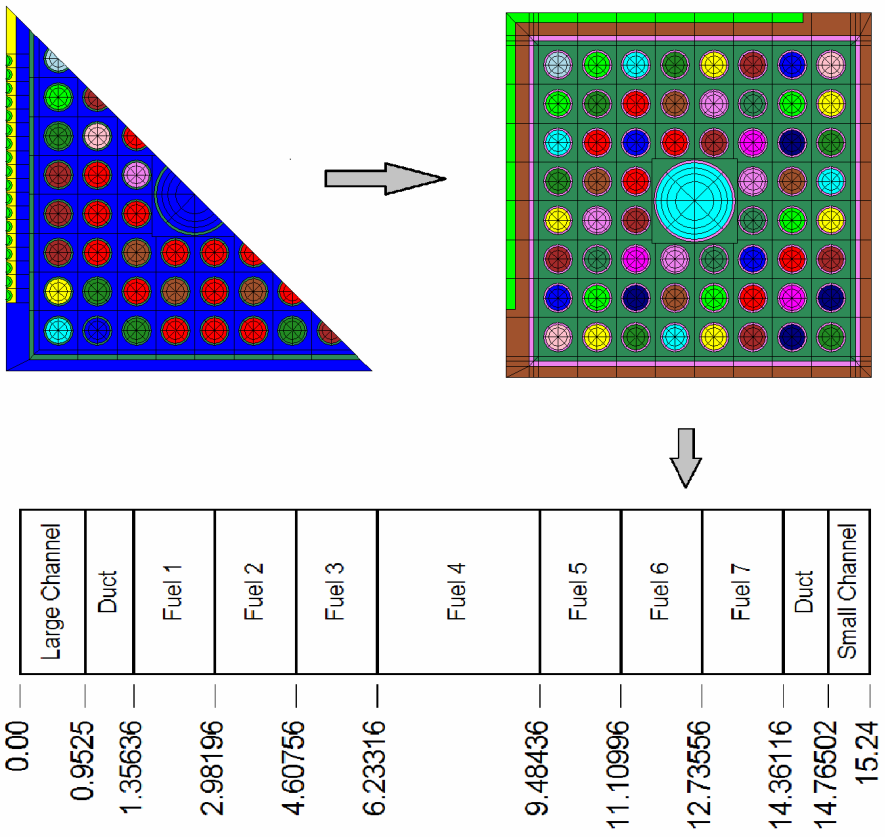


Figure 4.17: Generation of the 1D GE9 layout from the 2D Heterogeneous Assembly.

In order to determine a core layout that is somewhat representative of BWR problems, a whole core layout was determined by generating a 1D equivalent of a modified HAFAS benchmark specification (Forget and Rahnema, 2006). The burn-up and void distributions of the HAFAS problem were retained to include higher levels of heterogeneity in the core than

in typical reactors in order to present a more challenging problem for new methods and codes. For each unique set of state parameters (0, 40, 70% void; fresh, depleted to 17 GWd/T; controlled and uncontrolled), cross sections were generated for each column in 47 groups.

The 1D cross sections were verified by comparing the eigenvalue of 2D, single assembly calculations in 47 groups with the same assembly calculated with 47 groups in 1D. The results of this comparison are presented for each void fraction in Table 4.17 (fresh assemblies are labeled A, depleted assemblies are labeled B, and + specifies a controlled assembly).

Table 4.17: Single BWR Assembly Comparison: 1D and 2D

| Assembly Type | $K_{eff}$ 2D, 47G | $K_{eff}$ 1D, 47G | Error[a] (pcm) |
|---|---|---|---|
| 0% A | 1.05012 | 1.05388 | -376 |
| 40% A | 1.03692 | 1.03978 | -286 |
| 70% A | 1.01677 | 1.01918 | -241 |
| 0% B | 1.13419 | 1.13127 | 292 |
| 40% B | 1.11702 | 1.11444 | 258 |
| 70% B | 1.08886 | 1.08624 | 262 |
| 0% A + | 0.94801 | 0.94853 | -52 |
| 40% A + | 0.92639 | 0.92578 | 61 |
| 70% A + | 0.89941 | 0.89805 | 136 |
| 0% B + | 1.04658 | 1.04381 | 277 |
| 40% B + | 1.02044 | 1.01696 | 348 |
| 70% B + | 0.98257 | 0.97847 | 410 |

[a] $(K_{2D} - K_{1D})*10^5$

4.2.1.1 Benchmark Core Description

The 1D benchmark problem is laid out in slab geometry, with specular reflective boundary conditions on the left and vacuum conditions on the right. Generation of 1D controlled assemblies via transverse-integration does not accurately represent the physics of control assemblies in a 2D core, as it represents a full column of control assemblies in the

core. Despite this drawback, a controlled configuration is included as it possesses increased flux heterogeneity and serves to additionally stress transport methods.

The 1D core is composed of 20 assemblies of width 15.24 cm, modeled with ½ symmetry. The benchmark is specified at operating temperature, wherein all non-fuel materials are evaluated at a temperature of 600 K, and fuel materials are evaluated at a temperature of 833 K. A power level of 25.6 W/g was used to generate all cross sections.

The transverse-integration method was used to generate cross sections for the lattice at varying void fraction (0%, 40%, and 70%) and exposure (0 GWd/t, 17GWd/t). These lattices were then laid end to end for two control configurations: All-Rods-Out (ARO) and Some-Rods-In (SRI), with the burnup and void distribution presented in Figure 4.18. In the latter case, the rods were used to make the SRI configuration near critical. In the figure, the void fraction of each lattice is given, lattices labeled "A" are fresh, lattices labeled "B" are depleted to 17 GWd/T, and lattices that include a "+" are controlled. The outer lattice is a uniform reflector lattice composed of unvoided moderator with 47-group cross sections from the fresh lattice, labeled "MOD" in the figure.

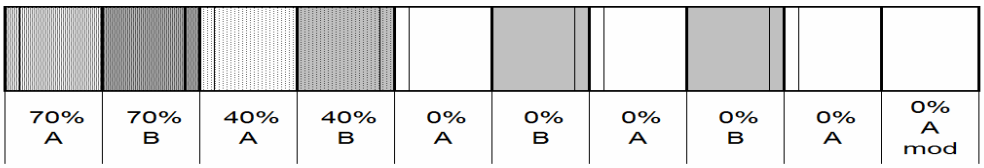


(a)

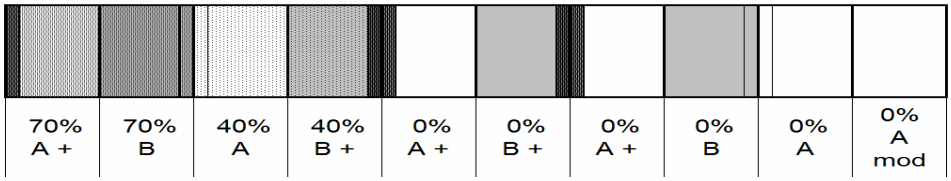


(b)

Figure 4.18: BWR 1D Core layout for the (a) ARO and (b) SRI configuration.

4.2.1.2 Benchmark Calculation

The whole core 1D benchmark problem was modeled in HELIOS in 47 groups and a solution was generated for the average neutron flux in each material slab and the effective core eigenvalue. Solutions were for both the ARO and SRI configurations. The eigenvalue for the ARO configuration was 1.06825 and for the controlled state was 1.00579. The 2-group flux for both core configurations is presented in Figure 4.19. Note that for this paper, the solution is not intended as a reference, but rather to highlight the heterogeneity of the problem via the neutron flux solution.

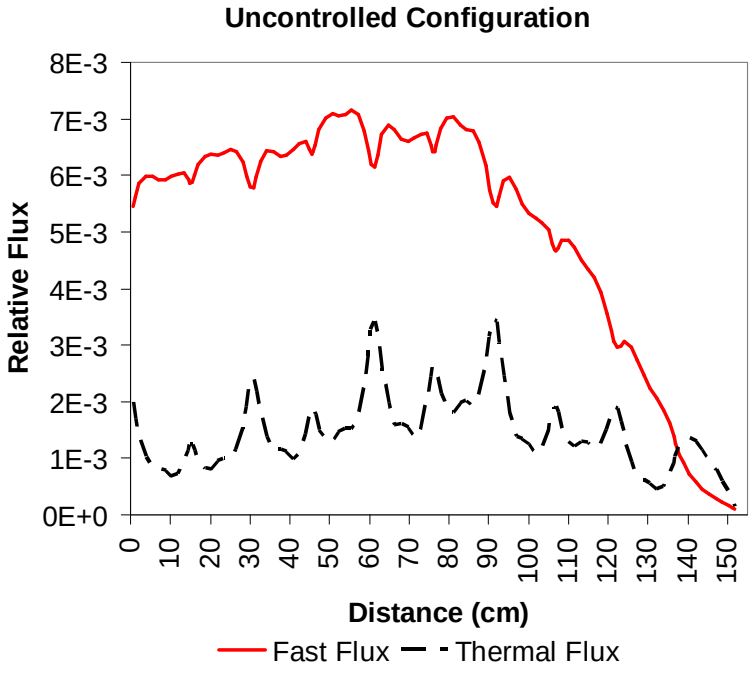


(a)

Figure 4.19: 2-group neutron flux distribution for the (a) ARO and (b) SRI BWR configurations.

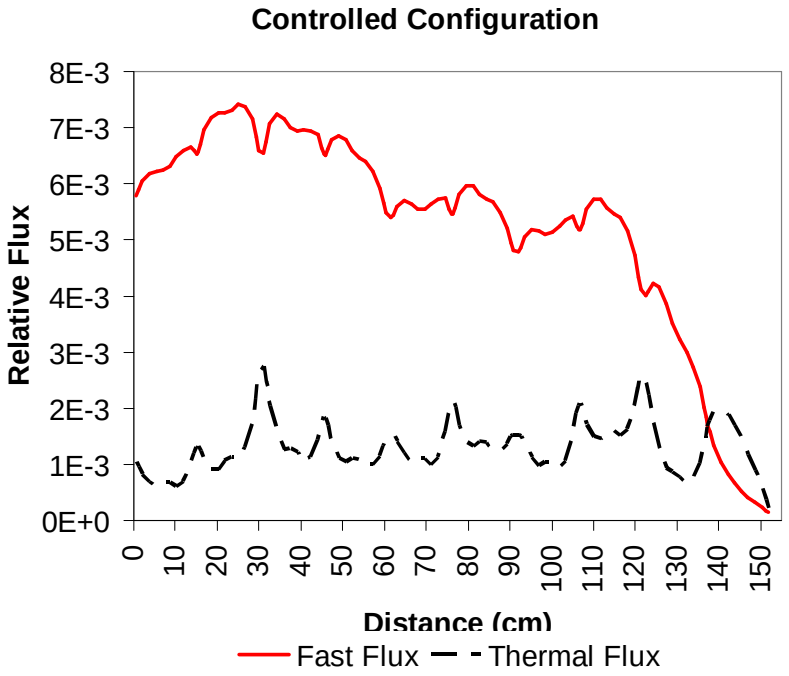


(b)

Figure 4.19 (continued)

### 4.2.2 Transverse-Integrated C5G7-Loaded 1D PWR Problem

In order to generate a PWR benchmark problem that is representative of realistic reactors, fuel assemblies must include a large number of closely spaced fuel pins, burnable-absorber in the moderator, and control pins spaced throughout the assembly. To make the problem more relevant for future reactor work, both UO2 and MOX assemblies should be included in the core. Assemblies from the C5G7 benchmark specification (Kozlowski and Downar, 2003, and Cathalau et. al., 1996) were modeled in $1/8^{th}$ symmetry with full heterogeneity. A 47-group calculation was performed to deplete both MOX and UO2 assemblies to generate cross sections at burn-up values of 0, 17, and 28 MWd/T. As before, the lattice depletion code HELIOS (Simeonov, 2003) was used to perform 2D transport calculations in this work.

For each unique state (MOX/UO2, burn-up, presence of control pins), cross sections were generated in 47 groups for each unique material region (fuel, clad, moderator, control pins, fission chamber). To ensure consistent solutions for each condensed group structure, the 47-group cross sections generated at each burn up point are then used in $1/4^{th}$ assembly calculations to generate flux-weighted, transversely integrated 1D cross sections. An illustration of this process is shown in figure 4.20.

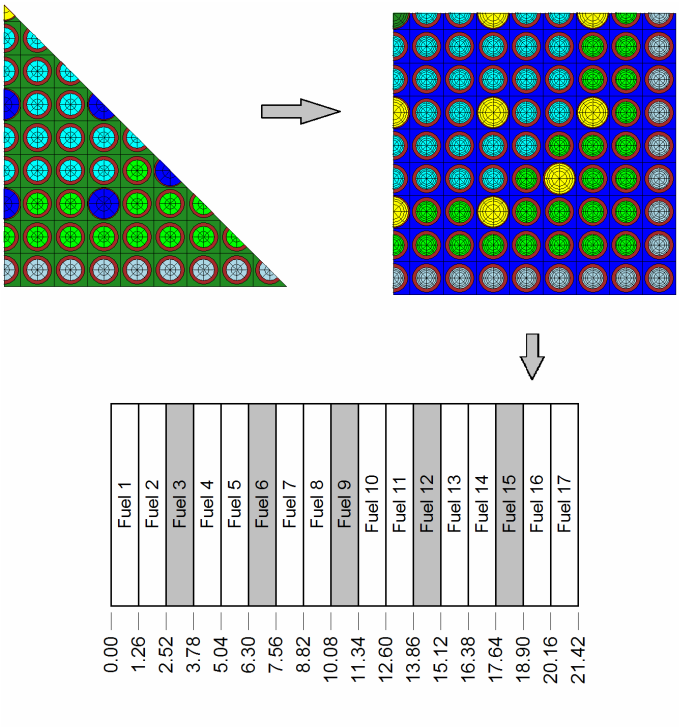


Figure 4.20: Generation of the 1D PWR assembly layout from the 2D Heterogeneous Assembly. In controlled assemblies, the shaded regions of the assembly contain the control material.

In order to determine a core layout that is representative of PWR problems, a whole core layout was determined by generating a 1D equivalent of a modified 2-loop Westinghouse reactor design (Nath, 1971) with every other UO2 assembly replaced by MOX assemblies. For each unique set of state parameters (burn-up, presence of control pins), 1D cross sections were generated in 47 groups.

The 1D cross sections were verified by comparing the eigenvalue of 2D, single assembly calculations in 47 groups with the same assembly calculated with 47 groups in 1D. The results of this comparison are presented for each burn-up in Table 4.18 (+ specify a controlled assembly).

Table 4.18: Single PWR Assembly Comparison: 1D and 2D

| Assembly Type | Burnup (MWD/t) | $K_{eff}$ -2D | $K_{eff}$ -1D | Error[a] (pcm) |
|---|---|---|---|---|
| $UO_2$ | 0 | 1.06998 | 1.07 | -2 |
| | 17 | 1.11665 | 1.11657 | 8 |
| | 28 | 1.01821 | 1.01811 | 10 |
| $UO_2$ + | 0 | 0.60743 | 0.60417 | 326 |
| | 17 | 0.63361 | 0.63069 | 292 |
| | 28 | 0.60801 | 0.60532 | 269 |
| MOX | 0 | 1.08359 | 1.08346 | 13 |
| | 17 | 1.07039 | 1.0702 | 19 |
| | 28 | 1.03593 | 1.03574 | 19 |
| MOX + | 0 | 0.72732 | 0.72561 | 171 |
| | 17 | 0.70947 | 0.70789 | 158 |
| | 28 | 0.69058 | 0.68905 | 153 |

[a] $(K_{2D} - K_{1D})*10^5$

4.2.2.1 Benchmark Core Description

The 1D benchmark problem is laid out in slab geometry, with specular reflective boundary conditions on the left and vacuum conditions on the right. As in the BWR problem, 1D controlled assemblies do not accurately represent the physics of control assemblies in a 2D core, as it represents a full column of control assemblies in the core. It is nonetheless included due to the increased flux heterogeneity, and it serves to additionally stress transport methods.

The 1D core is composed of 17 assemblies of width 21.42 cm, modeled with ½ symmetry. The benchmark is specified at operating temperature, wherein the moderator region on the right side of the core is evaluated at a temperature of 600 K, and all fuel

materials are evaluated at a temperature of 900 K. A power level of 34.8 W/g was used to generate all cross sections. Each assembly is composed of 17 macroscopic cross section regions, laid out with the All-Rods-Out (ARO) and Some-Rods-In (SRI) configurations in Figure 4.21.

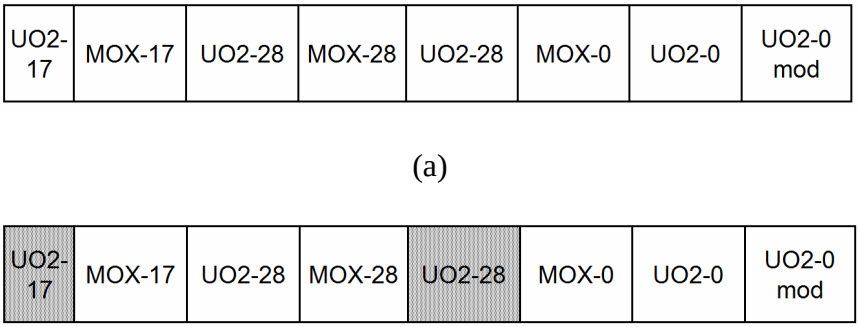


Figure 4.21: 1D Core layout for the (a) ARO and (b) ARI PWR configuration. The number indicates the burn-up value. Shaded assemblies are controlled. The mod regions are composed entirely of moderator.

4.2.2.2 Benchmark Calculation

The whole core 1D benchmark problem was modeled in HELIOS and a solution was generated for the average neutron flux in each material slab and the effective core eigenvalue. Solutions were obtained for both a controlled and uncontrolled configuration. The eigenvalue for the uncontrolled state was 1.05396 and for the controlled state was 0.98961. The 2-group flux for both core configurations is presented in Figure 4.22.

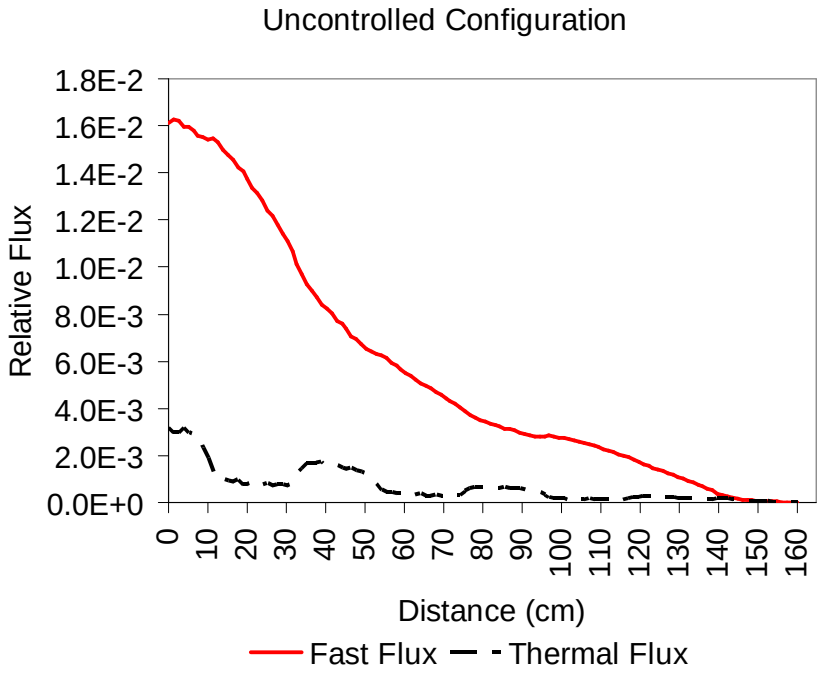


(a)

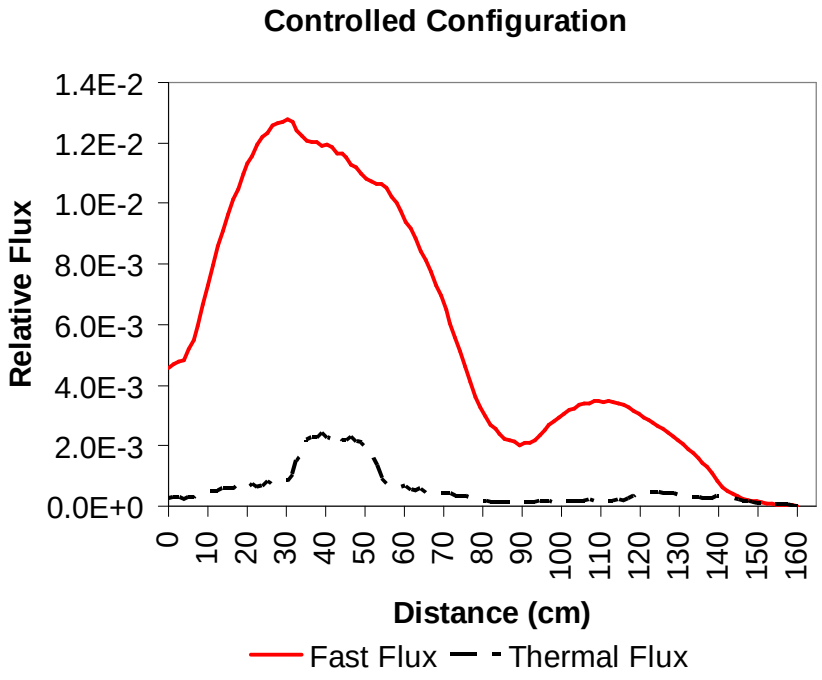


(b)

Figure 4.22: 2-group neutron flux distribution for the (a) ARO and (b) SRI PWR configurations.

### 4.2.3 Volume-Fraction Preserved 1D HTTR Problem

In order to construct a 1D benchmark problem which is representative of the physics of VHTRs, a 3D model of the HTTR (Zhang et. al., 2011) was chosen as the starting point for this work. The following method was used to generate the 1D geometry, illustrated in Figure 4.23.

1. The width of the 1D blocks (fuel, control, and reflectors) was set as 37.8027 cm, which is the diameter of a circle with the same area as the 2D hexagonal blocks in the HTTR specification.
2. The 1D fuel block geometry was obtained by preserving the volume of the fuel elements, helium regions, and burnable poisons (BP).

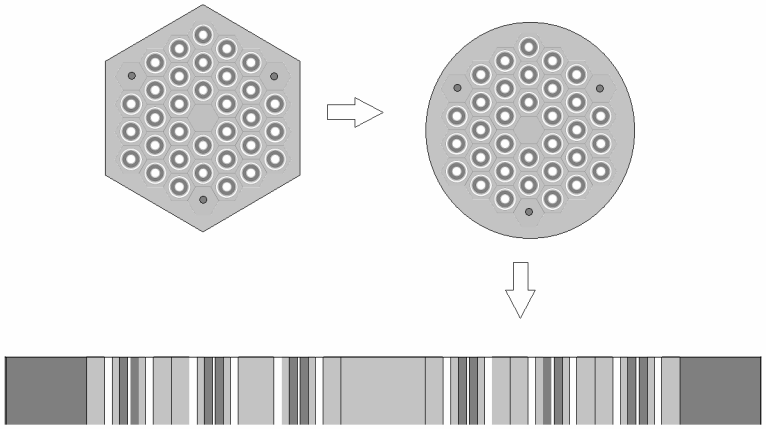

Figure 4.23: Illustration of 1D HTTR Block Generation

The control rod block (CRB) geometry was obtained by dividing the 2D CRB into annular regions and preserving the volume of these regions to generate the 1D CRB (as was illustrated in Figure 4.16. Each block in the 1D core model represents a hexagonal "ring" in the core. The number densities within each 1D block were obtained by performing a volume-weighted homogenization over the hexagonal rings of the 2D HTTR core layout seen in

Figure 4.24. The fuel material in each of the 4 fuel zones was obtained by a volume-weighted axial averaging of the fuel material in a 3D HTTR specification (Zhang et. al., 2011).

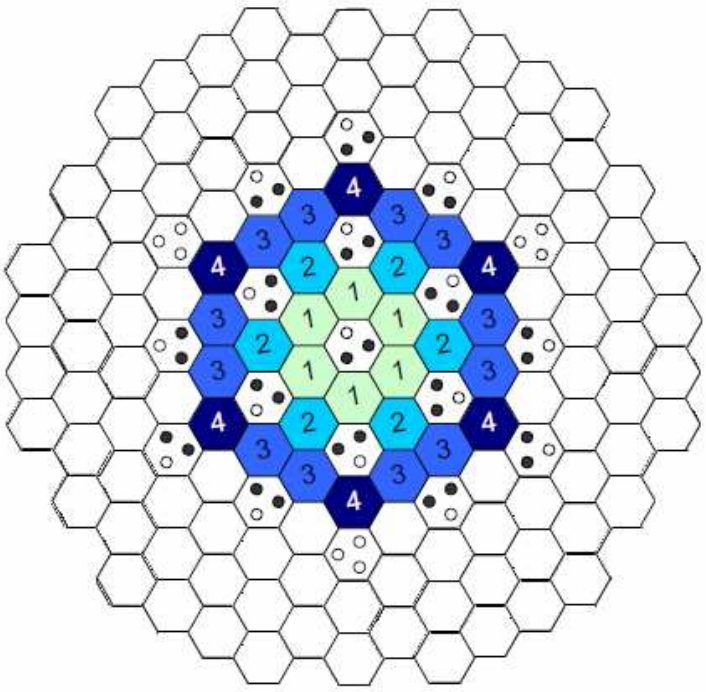


Figure 4.24: Layout of 2D HTTR Model

For the 3rd core ring, where control rod blocks and fuel blocks are present, the number densities were obtained as follows. First, the control block number densities were volume-smeared over the whole block. Second, this material was then smeared into the graphite moderator regions of the fuel 2 blocks, resulting in a controlled and uncontrolled 1D block.

The 2D fuel blocks in the HTTR specification include 3 BP holes (2 filled). In order to represent this in the 1D problem, the BP material is smeared into the outer graphite regions of the 1D fuel block. When going from 2D to 1D, preserving the volume fraction of burnable poison in the block overestimates the absorption in the 1D model. To compensate for this, the amount of BP in the block is reduced by 50%.

4.2.3.1 Benchmark Core Description

The 1D core consists of 15 blocks of width 37.8027 cm of 6 different types: Center Control, Fuel 1, Fuel 2 + Control, Fuel 3, Outer Control, and Reflector. Each fuel block (2, 3, and 4) consists of 6 fuel pins, a center graphite region, and outer graphite regions. Control Rod Blocks (1 and 5) consists of 2 control rods, surrounded by tube regions, with center and outer graphite slabs. In the uncontrolled case, the tube material (graphite + helium gas) fills the control regions. As mentioned in the previous section, the number densities of the control blocks of ring 3 have been smeared into the graphite of fuel 2, resulting in a controlled and uncontrolled state for that block. Surrounding the core are 3 blocks of pure graphite reflector. The geometric parameters for the problem and number densities for all materials are presented in Appendix B. The core is laid out (with ½ symmetry) as in Figure 4.25.

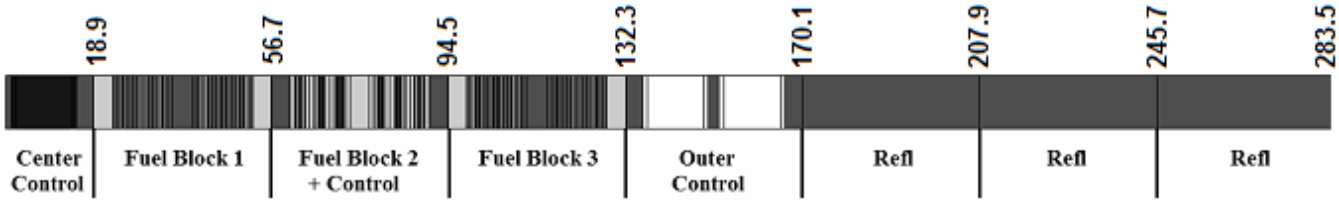


Figure 4.25: HTTR 1D Core Layout

An All-Rods-Out (ARO) and All-Rods-In (ARI) configuration was generated for this problem. The ARI configuration has control rods inserted in the outer control regions and in fuel block 2. The center control block is only used for loading the HTTR, and is dismantled after core loading is completed, and is not considered when computing controllable reactivity (Kim et. al., 1996).

4.2.3.2 Benchmark Calculation

One difficulty in using HELIOS is that the native cross section library is designed with LWR problems in mind, and thus the cross sections are not optimized for VHTR problems. As a result, it is more appropriate to calculate the solution with MCNP. The 1D core was modeled for both configurations (ARO and ARI) in MCNP5 (LANL, 2003), using the ENDF-VII continuous energy library at 293.6K, with S(α,β) cross sections used for all graphite in the problem. A converged source distribution was obtained using 10,000 particles per cycle for 500 cycles (5 million histories). The problem was solved with 500 million histories (250,000 per cycle for 2000 active cycles). The spatial flux distribution was tallied in 6 groups and is presented in Figure 4.26. The eigenvalue of the uncontrolled configuration was found to be 1.09310 ± 0.00003 and the eigenvalue of the controlled case was found to be 0.81298 ± 0.00003.

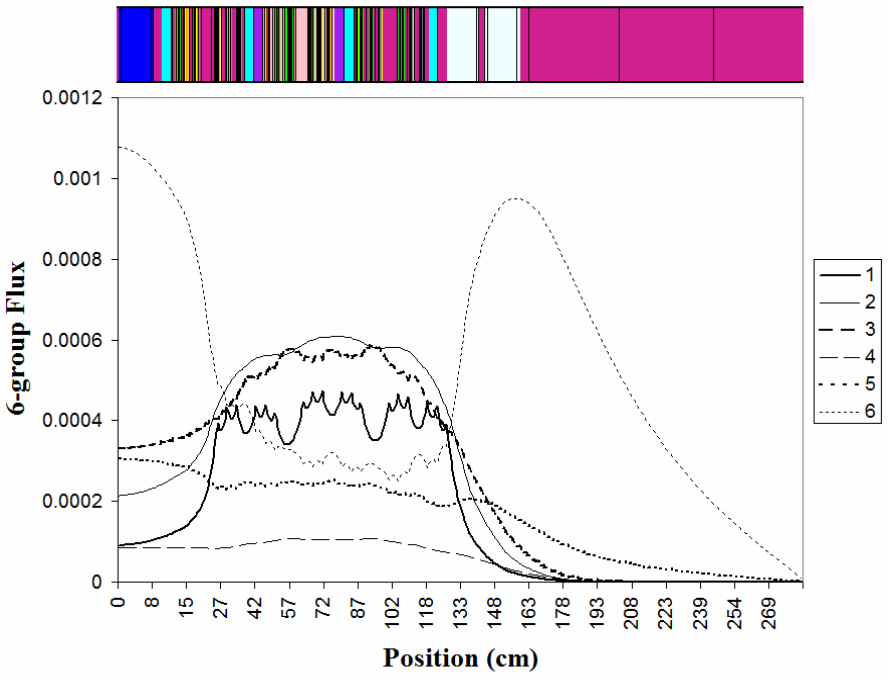


(a)

Figure 4.26: 6-group flux for (a) ARO and (b) ARI configurations.

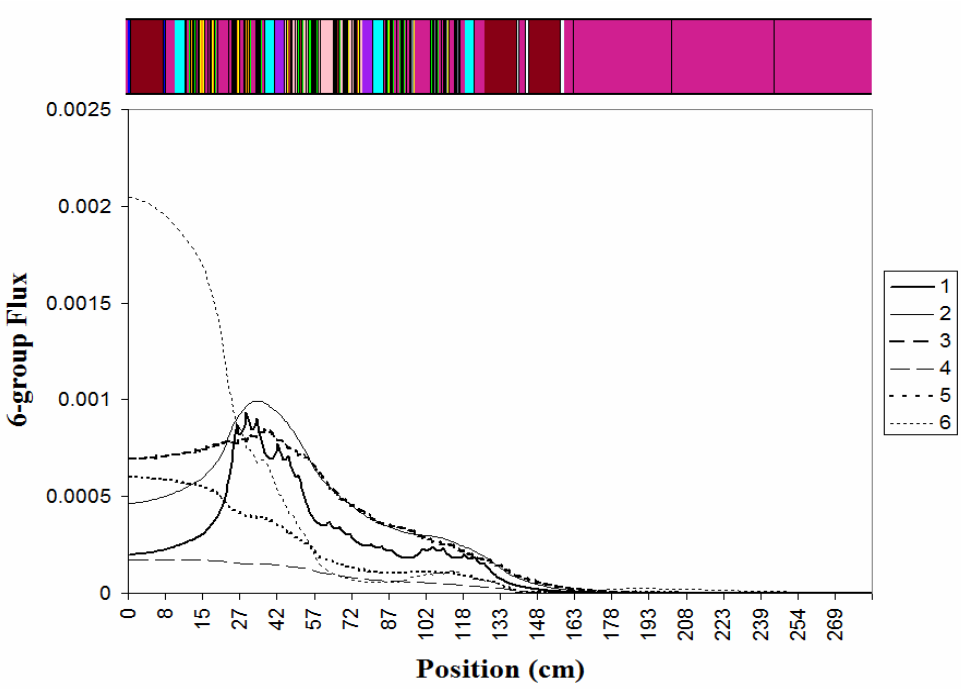


(b)

Figure 4.26 (Continued)

The sharp flux gradients induced by control rods provides a challenging problem for methods developers. It is therefore desirable for the effect of control rods in the 1D problem to be similar to the effect in a full 3D model. The controllable reactivity margin of the 3D HTTR problem (Kim et. al., 1996) was specified as >18%. The 1D model results in an estimated 24% controllable reactivity margin. This indicates that the worth of control rods is captured reasonably well in the 1D model, given the approximations made in the dimensional reduction.

### 4.2.4 Pin-Cell Homogenized GE9 Test Cores

In addition to the 1D benchmark cores developed in the previous three sections, it is often convenient to have a versatile set of cross sections and easily constructed cores without the rigor associated with preserving the physical characteristics of a 2D bundle. Preliminary

tests of new methods benefit from having a highly simple mechanism for generating challenging transport problems in order to prove that the methods are robust and accurate.

In order to accomplish this, a new set of 1D benchmark problems at both the lattice and core level has been developed in this paper. The benchmark problems are composed of the different pin cells used in the GE9 BWR bundle (Kelly, 1995), but without a specific lattice structure. The pin cell was modeled in the lattice cell depletion code HELIOS (Simeonov, 2003), with $1/8^{th}$ symmetry and full specular reflection on all sides, as seen in Figure 4.27. For each of the fuel enrichments in the GE9 lattice, 47-group homogenized cross sections (flux-weighted) were generated for the entire pin cell from a 47-group transport calculation with the HELIOS 47-group cross section library.

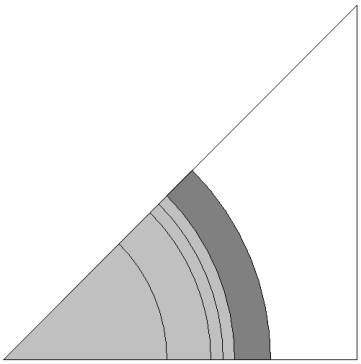

| | |
|---|---|
| Cell Pitch | 1.62560 cm |
| Fuel Radius | 0.53213 cm |
| Incremental Fuel Radii | 0.37627 cm |
| | 0.47595 cm |
| | 0.50482 cm |
| Clad Radius | 0.61341 cm |

Figure 4.27: GE9 Pin Cell Geometry

Twelve different fuel types (10 enrichments + 2 gadded) were used to generate cross sections, corresponding to the 12 fuel pin types used in the GE9 bundle. The number densities of the fuel materials are presented in Appendix A. Fuels 11 and 12 contain Gd with the number densities labeled "Gad" in the Table. In order to add heterogeneity to the 1D problems, an additional cross section set was generated for the moderator region of the pin cell for fuel type 1.

These calculations result in 13 cross section sets (12 fuel types and 1 moderator) and allow the buildup of a variety of 1D benchmark problems. By varying the amount and location of Gd and moderator slabs, strong flux gradients representing the more challenging aspects of 2D and 3D core models can be simulated in a straightforward and flexible way. In order to provide an example of the utility of this method for generating challenging problems, the homogenized cell cross sections produced from the GE9 pins were used to generate three simple 1D Core Benchmark problems composed of 4 different 1D assembly types.

Each assembly is composed of 10 material regions (8 fuel-pin regions + moderator region on both sides). The fuel regions are each 1.6256 cm in width, and the outside moderator regions are 1.1176 cm in width, accounting for 15.24 cm total bundle width (typical of BWR bundles). Table 4.19 contains the layout of each bundle type by fuel type, with moderator regions shaded and labeled with an M and gadded pins striped. The bundle problems were modeled with specular reflective boundaries on both sides using a 1D discrete ordinates code ($S_8$) with isotropic scattering, and the eigenvalue results (47-group $S_8$ calculation) are presented in the table.

Table 4.19: 1D BWR Test Bundle Layouts

| Bundle # | Bundle Layout | | | | | | | | | | $k_{inf}$ |
|---|---|---|---|---|---|---|---|---|---|---|---|
| 1 | M | 3 | 3 | 8 | 8 | 8 | 8 | 3 | 3 | M | 1.32802 |
| 2 | M | 3 | 3 | 3 | 3 | 3 | 3 | 3 | 3 | M | 1.27464 |
| 3 | M | 3 | 3 | 11 | 11 | 11 | 11 | 3 | 3 | M | 0.73029 |
| 4 | M | 11 | 11 | 11 | 11 | 11 | 11 | 11 | 11 | M | 0.31612 |

The 1D core geometries are composed of seven assemblies, with vacuum boundaries on both sides. Table 4.20 contains the core layout of three cores of increasing complexity, as well as the effective eigenvalue for each core, computed with a 47-group $S_8$ approximation.

Table 4.20. 1D BWR Test Core Layouts by Bundle Type

| Core # | Core Layout | | | | | | | $k_{eff}$ |
|---|---|---|---|---|---|---|---|---|
| 1 | 1 | 2 | 1 | 2 | 1 | 2 | 1 | 1.26528 |
| 2 | 1 | 3 | 1 | 3 | 1 | 3 | 1 | 1.03427 |
| 3 | 1 | 4 | 1 | 4 | 1 | 4 | 1 | 0.85857 |

Core 1 represents a relatively simple reactor problem, without sharp flux gradients due to the lack of highly absorbing regions and relative homogeneity. Core 2 includes 4 gadded fuel pins in 3 of the assemblies, introducing sharper thermal flux gradients and creating a more challenging problem for methods. Core 3 is a highly challenging configuration, as it includes 3 bundles made up entirely of gadded pins, and contains very sharp thermal flux gradients at the boundary interfaces. The cores were modeled with ½ symmetry (specular boundary condition on the right side, vacuum on the right), and the 2-group flux of each core, computed by integrating the 47-group solution over the standard 2-group range (thermal boundary 0.62506 eV), is presented in Figure 4.28.

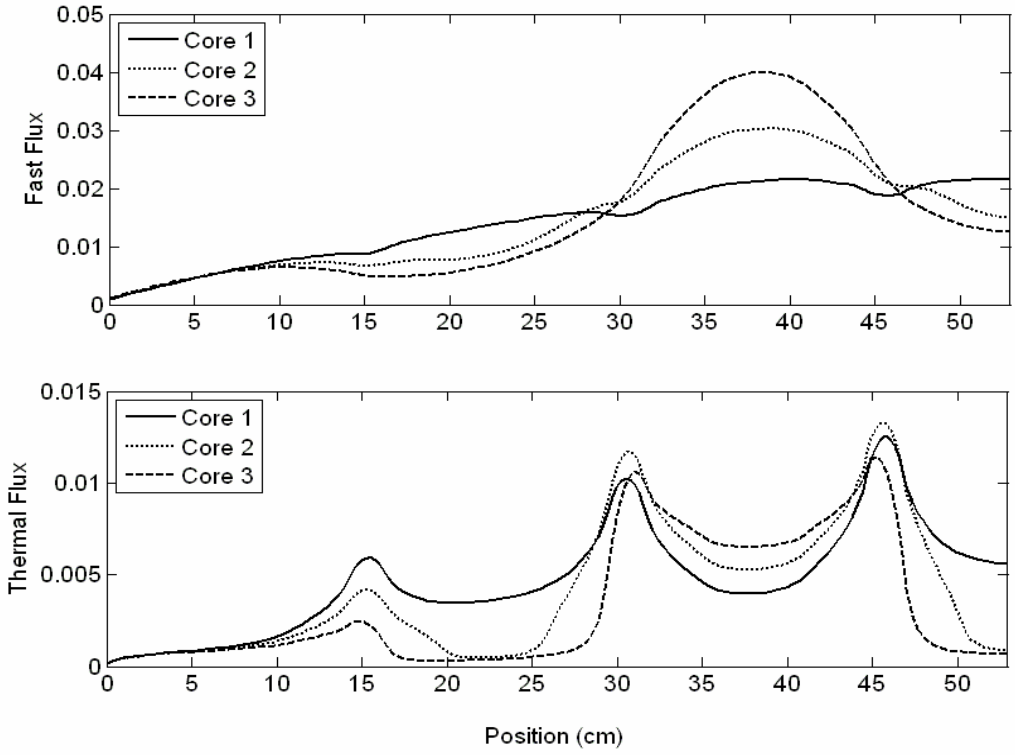


Figure 4.28: 2-Group Flux (47-group calculation) for BWR Test Cores

The figure demonstrates the effectiveness of the method at generating flux gradients of varying strength with a characteristic BWR flux spectrum. These cores, generated from a small set of cross sections, provide an extremely efficient mechanism to test new benchmark methods.

# CHAPTER 5

# NUMERICAL VERIFICATION

## 5.1 Consistent Generalized Energy Condensation Theory Verification

The primary objective of the consistent multigroup method, within the framework of GEC theory, is to allow for the generation of the detailed spectrum of the angular flux within an arbitrarily coarse multigroup energy structure. There are two orders of expansion contained within the CGEC equation (Eq. 3.31). The first, *N*, is the number of higher order energy moments that are preserved to allow unfolding the detailed energy dependence during the coarse-group calculation. The second, *L*, is the order of the coupling correction included in the source term of the coarse-group calculation. As a result, *L* dictates the accuracy of the coarse-group calculation, and *N* dictates the degree of detailed flux spectrum that may be unfolded from it. The ability to vary *L* is important as it allows the consistent formulation to maintain the angular accuracy of the fine-group spectrum, even if the coarse-group calculation uses a different angular method (i.e., if the detailed spectrum is only determined for first order angular flux, such as with CPM, that information can be preserved in the correction term for an $S_8$ calculation, even though the $S_8$ calculation has angular order 7).

The first phase of verification is to examine the accuracy of the coarse-group calculation without unfolding (*N*=0). This is presented in section 5.1.1 for several 1D transport problems by comparing the accuracy of the coarse-group transport solution (eigenvalue, flux) using the consistent multigroup method with that obtained using the standard method. This verifies that the coarse-group formulation is equivalent to the fine-group structure. The second phase of verification is to determine the accuracy of the

unfolded flux spectrum obtained from the higher order flux moments ($N>0$) for varying orders of coupling correction. This is presented in section 5.1.2 for one of the problems of section 5.1.1. Section 5.1.3 extends section 5.1.2 by examining the unfolded flux spectrum in the 1D HTTR Benchmark problem. Finally, section 5.1.4 examines the use of the CGEC method in a cross section recondensation scheme to correct for the spectral core environment error.

### 5.1.1 CGEC Test Problems (N=0)

In order to examine the CGEC in the kind of environment in which it would be applied, the first test of the method uses 1D bundle problems with boundary conditions taken from the interface flux in a core calculation. This provides small, simple problems which isolate the consistent condensation method from the effect of core environment error and increases the anisotropy of the flux distribution, creating a more challenging problem and highlighting the influence of the energy-angle coupling effect.

For this first test, two of the bundle types are selected from the Pin-Cell Homogenized GE9 Test Cores in section 4.2.4. Each bundle is composed of 10 material regions (8 fuel-pin regions + moderator region on both sides). The fuel regions are each 1.6256 cm in width, and the outside moderator regions are 1.1176 cm in width, accounting for 15.24 cm total bundle width (typical of BWR bundles). The two bundle types are laid out in Figure 5.1. Bundle A is composed of low-enriched pins (“L”), high-enriched pins (“H”), and moderator (“M”). Bundle B is composed of both low-enriched fuel pins and gadded fuel pins (“G”).

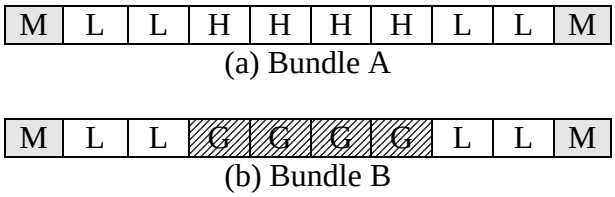


Figure 5.1: Single Bundle Layout for Bundles A and B

In order to obtain boundary conditions for the bundles which are representative of a core environment, Test Core 2 from section 4.2.4 is used. This core possesses steep flux gradients and highly anisotropic flux across the assembly interfaces due to alternating fuel bundles and partially gadded fuel bundles. Also of note is that this benchmark problem, which was constructed by layering pin-cell homogenized cross sections, does not represent a 1D core directly, but can more accurately represent local transport effects (e.g., flux at a gadded pin-cell interface). The core is composed of seven bundles, with vacuum boundaries on both sides, shown with the 2-group flux, calculated with an $S_{16}$ calculation, in Figure 5.2. The 47-group reference eigenvalue, computed with an $S_{16}$ approximation and transport-corrected scattering, was 1.05595.

The core calculation was used only to provide 47-group core-level boundary conditions for the bundles. Because the boundary conditions vary by bundle position in the core, there are four unique bundles labeled in Figure 5.2: (B1) Periphery, (B2) Outer Gadded, (B3) Inner Fuel, and (B4) Center Gadded.

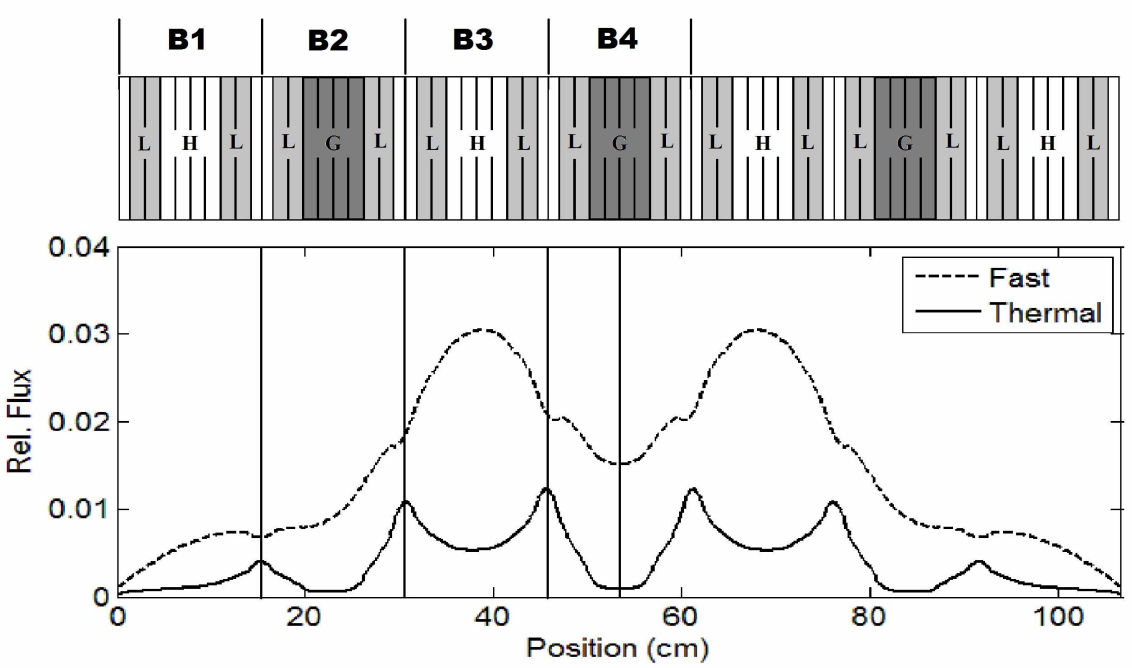


Figure 5.2: 1D Test Core Layout and 2g Flux. Vertical lines on the flux graph represent bundle interfaces. Center line is the symmetry line of the core.

For each bundle, the following method is used to verify the consistent multigroup method.

1. A 47-group transport calculation is performed with an $S_{16}$ approximation and albedo boundary conditions from the core calculation. This flux is the reference solution for the bundle.
2. The 47-group reference angular flux is used to generate 2-group cross sections using both the standard method (assuming separable energy and angle) and the consistent condensation theory (with energy-angle coupling correction).
3. These cross sections are then used to solve the bundle problem in a 2-group, $S_{16}$ calculation with boundary conditions obtained by integrating the 47-group boundary conditions into the 2-group structure.
4. The 2-group solution is compared to the 47-group reference solution (eigenvalue, scalar and angular flux integrated into the 2-group structure).

Because the accuracy of the new method is determined by how well the 2-group solution matches the 47-group solution, an initial verification of the method is obtained by comparing the eigenvalue of the 2-group calculation ($k_2$) with the 47-group reference eigenvalue ($k_{47}$). The eigenvalue results of the calculations are presented in Table 5.1. Because the 47-group solution was computed with an $S_{16}$ calculation, the variation term is limited to 15th order, and is therefore truncated at $L$=15. The standard multigroup method corresponds to the 0th-order energy-angle correction ($L$=0).

Table 5.1. Eigenvalue results for Bundles 1-4 for increasing angular expansion order.

| | Bundle 1 | | Bundle 2 | | Bundle 3 | | Bundle 4 | |
|---|---|---|---|---|---|---|---|---|
| $k_{47}ref$[1] | 1.05597 | | 1.05599 | | 1.05599 | | 1.05599 | |
| | $k_2$ | $\delta k^*$ (pcm) | $k_2$ | $\delta k^*$ (pcm) | $k_2$ | $\delta k^*$ (pcm) | $k_2$ | $\delta k^*$ (pcm) |
| Standard Method | 1.10384 | 4787 | 1.17632 | 12034 | 1.07804 | 2205 | 1.08593 | 2994 |
| L = 1 | 1.05565 | -33 | 1.05135 | -464 | 1.05526 | -73 | 1.05163 | -436 |
| L = 2 | 1.05653 | 56 | 1.05564 | -35 | 1.05618 | 19 | 1.05572 | -27 |
| L = 3 | 1.05608 | 11 | 1.05560 | -39 | 1.05608 | 9 | 1.05565 | -34 |
| L = 4 | 1.05594 | -3 | 1.05609 | 10 | 1.05595 | -4 | 1.05607 | 7 |
| L = 5 | 1.05599 | 1 | 1.05593 | -5 | 1.05600 | 1 | 1.05594 | -5 |
| L = 6 | 1.05594 | -3 | 1.05604 | 6 | 1.05597 | -2 | 1.05604 | 5 |
| L = 7 | 1.05597 | -1 | 1.05598 | -1 | 1.05599 | 0 | 1.05598 | -1 |
| L = 8 | 1.05596 | -1 | 1.05600 | 2 | 1.05598 | -1 | 1.05600 | 1 |
| L = 9 | 1.05597 | -1 | 1.05598 | 0 | 1.05599 | 0 | 1.05599 | 0 |
| L = 10 | 1.05596 | -1 | 1.05599 | 0 | 1.05598 | -1 | 1.05599 | 0 |
| L = 11 | 1.05597 | 0 | 1.05598 | 0 | 1.05599 | 0 | 1.05599 | 0 |
| L = 12 | 1.05597 | 0 | 1.05598 | 0 | 1.05599 | 0 | 1.05599 | 0 |
| L = 13 | 1.05597 | 0 | 1.05598 | 0 | 1.05599 | 0 | 1.05599 | 0 |
| L = 14 | 1.05597 | 0 | 1.05598 | 0 | 1.05599 | 0 | 1.05599 | 0 |
| L = 15 | 1.05597 | 0 | 1.05599 | 0 | 1.05599 | 0 | 1.05599 | 0 |

$\delta k^* = 10^5 (k_2 - k_{47}ref)$

[1] The 47 group reference eigenvalue is determined from the single bundle calculation with boundary conditions obtained from the core calculation, and is expected to match the core eigenvalue within numerical convergence criteria.

Table 5.1 clearly demonstrates both the magnitude of error introduced by assuming the energy and angular dependence are separable and the effectiveness of the consistent method to correct this error. Particularly in the gadded bundles (2 and 4), the anisotropy introduced by the strong absorber resulted in significant errors. As seen in the table, a 3$^{rd}$ order correction is sufficient to account for most of the effect of the energy-angle coupling, and a 7$^{th}$ order correction is sufficient to fully account for it.

In addition to the eigenvalues, verification of the consistent multigroup method requires an examination of the accuracy of the flux solution, both with the standard and consistent multigroup methods. For each bundle, the 2-group flux (angular and scalar) is compared with the 2-group flux obtained by integrating the 47-group reference into the 2-group structure.

#### 5.1.1.1 Bundle 1 Flux Comparison

Because the consistent method is designed to better account for flux anisotropy in the coarse-group calculation, both the scalar and angular flux accuracy must be examined. Figure 5.3 contains the 2-group reference scalar flux as a function of position in the bundle and the 2-group reference angular flux, averaged over the bundle, for each discrete direction. The angular flux is normalized such that the magnitude of each arrow in the figure represents the fraction of the angular flux in that direction (i.e. the sum of the magnitude for all directions is 100 for each group).

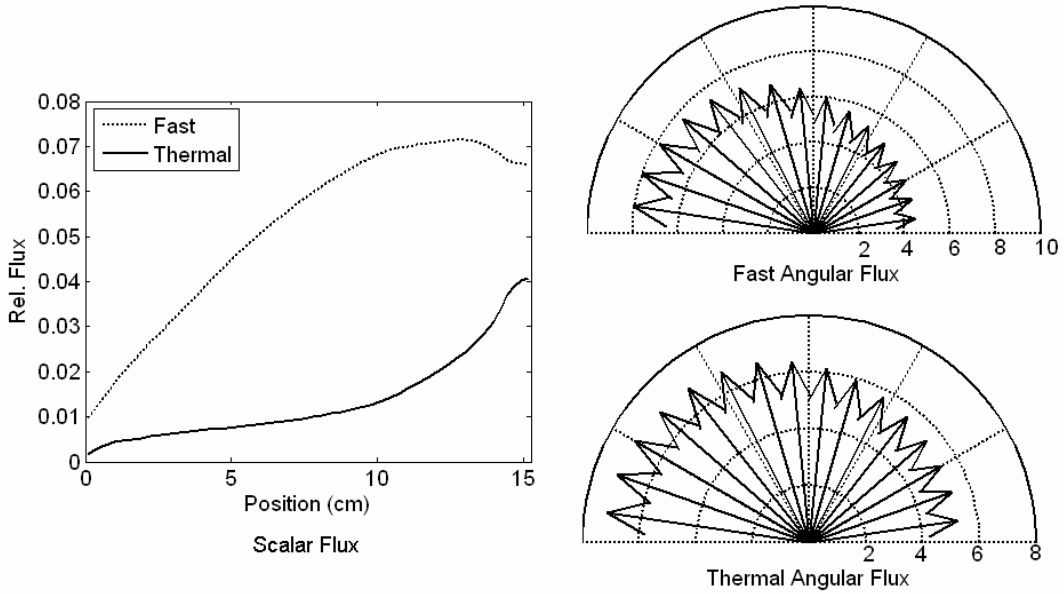


Figure 5.3: Bundle 1 - Reference Scalar Flux and Spatially Averaged Angular Flux (2g)

The anisotropy of the flux in this bundle is clearly seen in Figure 5.3, particularly in the fast group, wherein neutrons are streaming towards the vacuum boundary on the left hand side. In order to examine the accuracy of the coarse group calculation using both the standard method and the consistent multigroup method, the 2g flux error is presented in Figure 5.4. The scalar flux error is presented for the standard method, a first-order coupling correction ($L$=1), and the full coupling correction ($L$=15). For the angular flux, only the standard method and the $L$=1 case are presented because the error of the fully corrected ($L$=15) solution is too small to be visible on the figure.

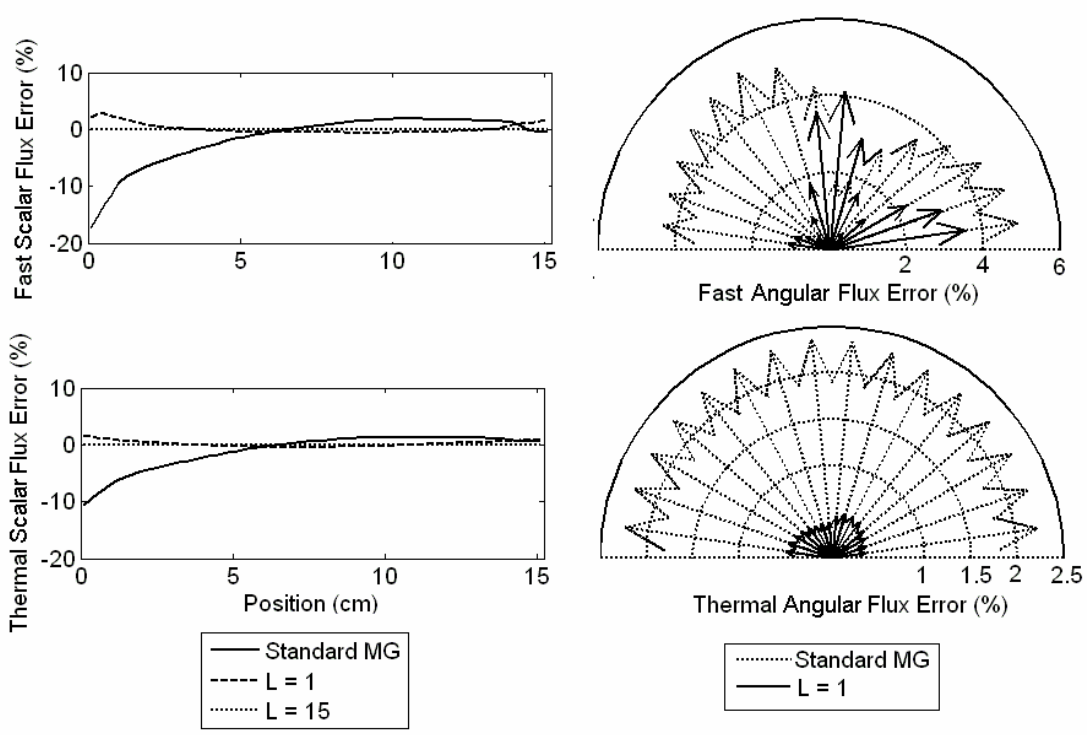


Figure 5.4: 2g Scalar and Average Angular Flux %-Error for Bundle 1.

As seen in Figure 5.4, the standard multigroup method results in significant errors in both the scalar and angular flux distributions. In the scalar flux, it is clearly seen that this error increases towards the vacuum boundary where the flux is more anisotropic. In addition, the angular distribution shows that the error in the fast group is, as expected, highly dependent on the direction. Figure 5.4 also demonstrates that even the 1st order corrected solution generates significant improvement over the standard multigroup method in both the scalar and angular fluxes and that the 15th order correction was able to reproduce the reference solution exactly. Note that in order to allow for easy viewing of the angular flux errors, it was necessary to use a different scale for the fast and the thermal flux errors.

In order to gain a more thorough understanding of the error present in the scalar flux distribution, the 2-group scalar flux from the condensed calculation $\tilde{\phi}_g(x)$ was compared

with the reference 2-group scalar flux $\phi_g(x)$ within each group using the spatial average error ($AVG_g$), the root-mean-square spatial error ($RMS_g$), and the flux-weighted spatial average error ($FWE_g$), defined in Eqs. (5.1)-(5.3). Table 5.2 presents these errors for increasing order of coupling correction in Bundle 1.

$$AVG_g = \frac{\int dx \left| e_g(x) \right|}{\int dx} \tag{5.1}$$

$$RMS_g = \sqrt{\frac{\int dx e_g^2(x)}{\int dx}} \tag{5.2}$$

$$FWE_g = \frac{\int dx \left| e_g(x) \right| \tilde{\phi}_g(x)}{\int dx \phi_g(x)} \tag{5.3}$$

Where

$$e_g(x) = 100 \frac{\tilde{\phi}_g(x) - \phi_g(x)}{\phi_g(x)} \tag{5.4}$$

As is seen in Table 5.2, the flux results are quite poor for the standard multigroup method, resulting in an spatial average error greater than 2%. When using even a 1st order coupling correction, this is reduced to less than 1%, and by the 3rd order the consistent multigroup method has reproduced the reference solution with high accuracy. It is also evident from the results in Table 5.2 that the energy-angle coupling of the total cross section can be fully accounted for with accuracy sufficient for the vast majority of purposes by a 4th or 5th order correction. This is true of Bundle 1, presented here, as well as for the other bundles, which are shown in the next sections.

Table 5.2: Scalar Flux Error Analysis – Bundle 1

| | $AVG_q$ | | $RMS_q$ | | $MRE_q$ | |
|---|---|---|---|---|---|---|
| L | Fast | Thermal | Fast | Thermal | Fast | Thermal |
| 0* | 2.92 | 2.15 | 4.58 | 3.15 | 1.83 | 1.34 |
| 1 | 0.67 | 0.40 | 0.90 | 0.50 | 0.56 | 0.42 |
| 2 | 0.13 | 0.07 | 0.21 | 0.10 | 0.13 | 0.12 |
| 3 | 0.06 | 0.03 | 0.10 | 0.04 | 0.05 | 0.03 |
| 4 | 0.04 | 0.01 | 0.07 | 0.02 | 0.04 | 0.02 |
| 5 | 0.02 | 0.00 | 0.04 | 0.01 | 0.02 | 0.00 |
| 6 | 0.02 | 0.00 | 0.04 | 0.01 | 0.02 | 0.01 |
| 7 | 0.01 | 0.00 | 0.03 | 0.00 | 0.01 | 0.00 |
| 8 | 0.02 | 0.00 | 0.03 | 0.00 | 0.02 | 0.00 |
| 9 | 0.01 | 0.00 | 0.02 | 0.00 | 0.01 | 0.00 |
| 10 | 0.01 | 0.00 | 0.02 | 0.00 | 0.01 | 0.00 |
| 11 | 0.01 | 0.00 | 0.01 | 0.00 | 0.01 | 0.00 |
| 12 | 0.01 | 0.00 | 0.01 | 0.00 | 0.01 | 0.00 |
| 13 | 0.00 | 0.00 | 0.01 | 0.00 | 0.00 | 0.00 |
| 14 | 0.00 | 0.00 | 0.01 | 0.00 | 0.00 | 0.00 |
| 15 | 0.00 | 0.00 | 0.00 | 0.00 | 0.00 | 0.00 |

* L = 0 is the Standard Multigroup Method

5.1.1.2 Bundle 2 Flux Comparison

Figure 5.5 contains the 2-group reference scalar flux as a function of position in bundle 2 and the 2-group reference angular flux, averaged over the bundle, for each discrete direction.

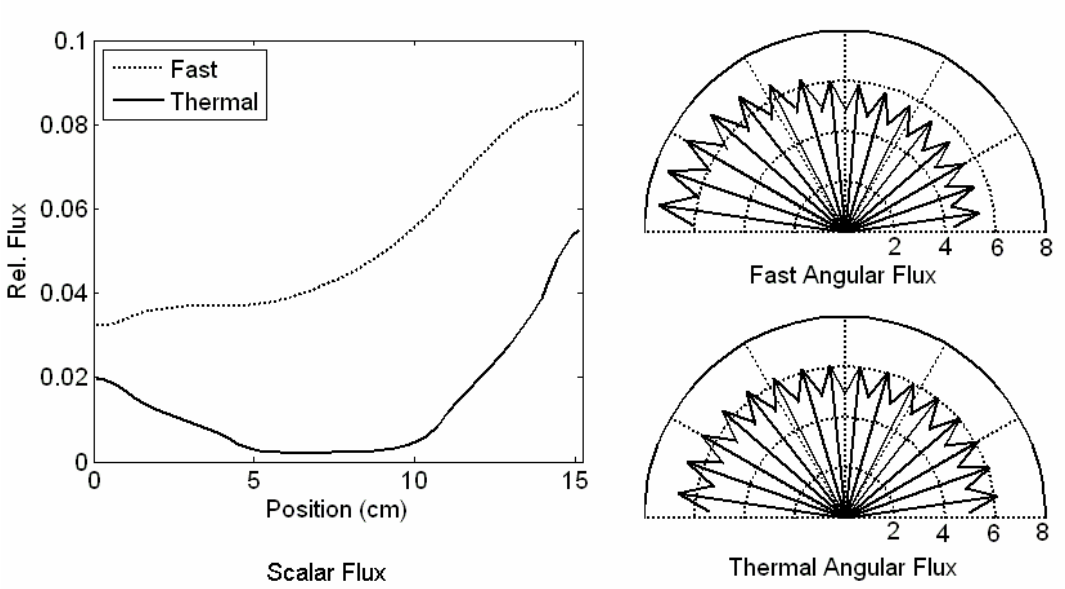


Figure 5.5: Bundle 2 - Reference Scalar Flux and Spatially Averaged Angular Flux (2g)

In this bundle, there is a significantly high anisotropy in the angular flux because of the presence of the gadolinium. (This anisotropy is not evident in Figure 5.5 because the strong gradients on both sides of the bundle result in a highly anisotropic flux in opposite directions.) This results in much larger flux errors than in Bundle 1. The scalar flux error is presented for the standard method, a first-order coupling correction (L = 1), and the full coupling correction (L=15) in Figure 5.6.

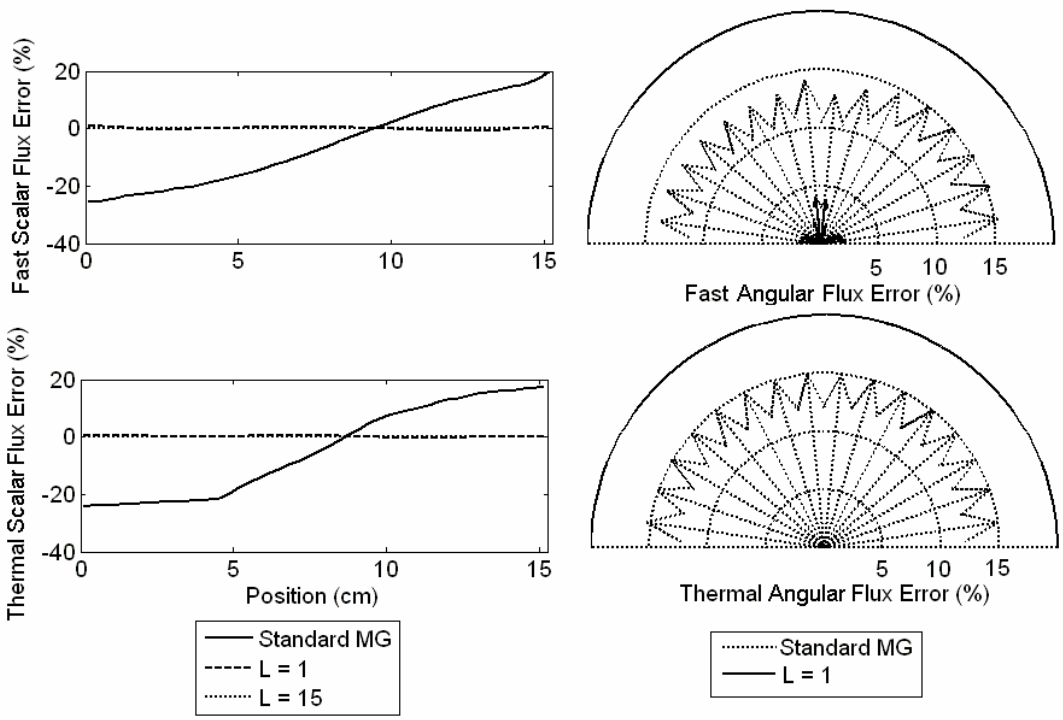


Figure 5.6: 2g Scalar and Average Angular Flux %-Error for Bundle 2.

As seen in Figure 5.6, the standard multigroup method results in much larger errors in the flux than in Bundle 1. This is due to the increased effect of local anisotropies generated by the strong flux gradient across the bundle. It is also evident that in this bundle, the 1st order coupling correction results in significant improvement. It is noted that the 1st order error in the thermal angular flux is too small to be visible on the graph. Table 5.3 presents the $AVG_g$, $RMS_g$, and $FWE_g$ errors for increasing order of coupling correction in Bundle 2.

Table 5.3: Scalar Flux Error Analysis – Bundle 2

| | $AVG_q$ | | $RMS_q$ | | $MRE_q$ | |
|---|---|---|---|---|---|---|
| L | Fast | Thermal | Fast | Thermal | Fast | Thermal |
| 0* | 13.42 | 14.71 | 15.25 | 16.28 | 12.11 | 16.98 |
| 1 | 0.42 | 0.27 | 0.50 | 0.31 | 0.44 | 0.18 |
| 2 | 0.17 | 0.09 | 0.21 | 0.10 | 0.18 | 0.09 |
| 3 | 0.07 | 0.03 | 0.09 | 0.03 | 0.08 | 0.03 |
| 4 | 0.05 | 0.02 | 0.09 | 0.02 | 0.06 | 0.02 |
| 5 | 0.03 | 0.00 | 0.04 | 0.01 | 0.03 | 0.00 |
| 6 | 0.03 | 0.01 | 0.05 | 0.01 | 0.03 | 0.01 |
| 7 | 0.02 | 0.00 | 0.03 | 0.00 | 0.02 | 0.00 |
| 8 | 0.02 | 0.00 | 0.04 | 0.01 | 0.02 | 0.00 |
| 9 | 0.01 | 0.00 | 0.02 | 0.00 | 0.01 | 0.00 |
| 10 | 0.01 | 0.00 | 0.02 | 0.00 | 0.01 | 0.00 |
| 11 | 0.01 | 0.00 | 0.01 | 0.00 | 0.01 | 0.00 |
| 12 | 0.01 | 0.00 | 0.02 | 0.00 | 0.01 | 0.00 |
| 13 | 0.00 | 0.00 | 0.01 | 0.00 | 0.00 | 0.00 |
| 14 | 0.00 | 0.00 | 0.01 | 0.00 | 0.00 | 0.00 |
| 15 | 0.00 | 0.00 | 0.00 | 0.00 | 0.00 | 0.00 |

* L = 0 is the Standard Multigroup Method

It is clear from Table 5.3 that Bundle 2 is much more greatly affected by neglecting the energy angle coupling using the standard method; however, a 1$^{st}$ order coupling correction is sufficient to reproduce the fine-group results very well.

5.1.1.3 Bundle 3 Flux Comparison

Figure 5.7 contains the 2-group reference scalar flux as a function of position in bundle 3 and the 2-group reference angular flux, averaged over the bundle, for each discrete direction.

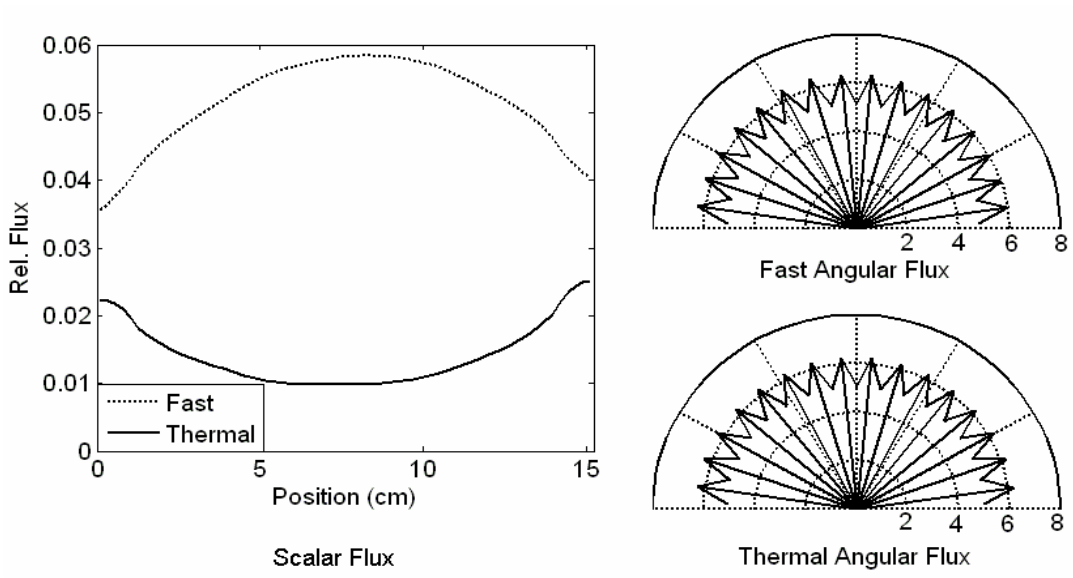


Figure 5.7: Bundle 3 - Reference Scalar Flux and Spatially Averaged Angular Flux (2g)

Because the position of Bundle 3 in the core results in a roughly symmetric flux distribution, and because the bundle does not possess any gadded pins, Bundle 3 is the least anisotropic. This is clearly seen in the angular flux graphs in Figure 5.7. The scalar and angular flux errors are presented in Figure 5.8.

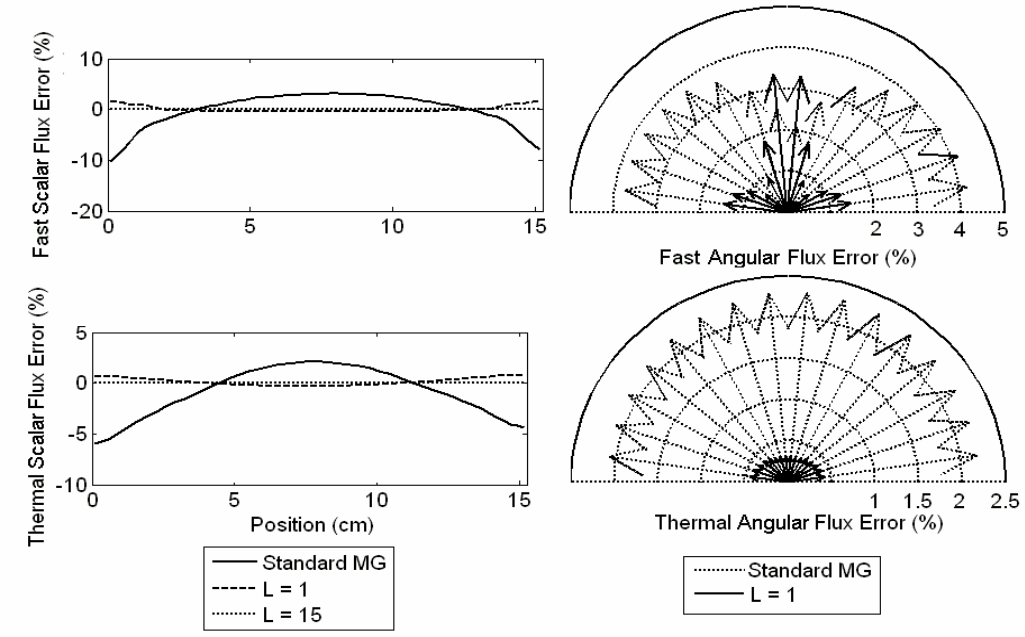


Figure 5.8: 2g Scalar and Average Angular Flux %-Error for Bundle 3.

As seen in Figure 8, while the flux error in this bundle is less significant than in bundles 1 and 2, the error is still significant in both the scalar and angular flux distributions using the standard method. As in bundles 1 and 2, the 1st order coupling correction provides a significant improvement over the standard method. Table 5.4 presents the $AVG_g$, $RMS_g$, and $FWE_g$ errors for Bundle 3, demonstrating similar behavior as previous bundles.

Table 5.4: Scalar Flux Error Analysis – Bundle 3

| | $AVG_g$ | | $RMS_g$ | | $MRE_g$ | |
|---|---|---|---|---|---|---|
| L | Fast | Thermal | Fast | Thermal | Fast | Thermal |
| 0* | 2.65 | 2.07 | 3.36 | 2.52 | 2.49 | 2.34 |
| 1 | 0.49 | 0.32 | 0.61 | 0.39 | 0.46 | 0.38 |
| 2 | 0.14 | 0.06 | 0.21 | 0.09 | 0.12 | 0.08 |
| 3 | 0.06 | 0.02 | 0.09 | 0.03 | 0.05 | 0.03 |
| 4 | 0.04 | 0.01 | 0.08 | 0.02 | 0.04 | 0.01 |
| 5 | 0.02 | 0.00 | 0.04 | 0.00 | 0.02 | 0.00 |
| 6 | 0.03 | 0.00 | 0.05 | 0.01 | 0.02 | 0.01 |
| 7 | 0.02 | 0.00 | 0.03 | 0.00 | 0.02 | 0.00 |
| 8 | 0.02 | 0.00 | 0.04 | 0.00 | 0.02 | 0.00 |
| 9 | 0.01 | 0.00 | 0.02 | 0.00 | 0.01 | 0.00 |
| 10 | 0.01 | 0.00 | 0.02 | 0.00 | 0.01 | 0.00 |
| 11 | 0.01 | 0.00 | 0.01 | 0.00 | 0.01 | 0.00 |
| 12 | 0.01 | 0.00 | 0.02 | 0.00 | 0.01 | 0.00 |
| 13 | 0.00 | 0.00 | 0.01 | 0.00 | 0.00 | 0.00 |
| 14 | 0.00 | 0.00 | 0.01 | 0.00 | 0.00 | 0.00 |
| 15 | 0.00 | 0.00 | 0.00 | 0.00 | 0.00 | 0.00 |

* L = 0 is the Standard Multigroup Method

5.1.1.4 Bundle 4 Flux Comparison

Figure 5.9 contains the 2-group reference scalar flux as a function of position in bundle 4 and the 2-group reference angular flux, averaged over the bundle, for each discrete direction. Whereas the previous bundles have included the full bundle, due to the symmetry of Bundle 4, only half of the bundle was modeled. This allows the local anisotropies present in the bundle to be apparent, as seen in Figure 5.9.

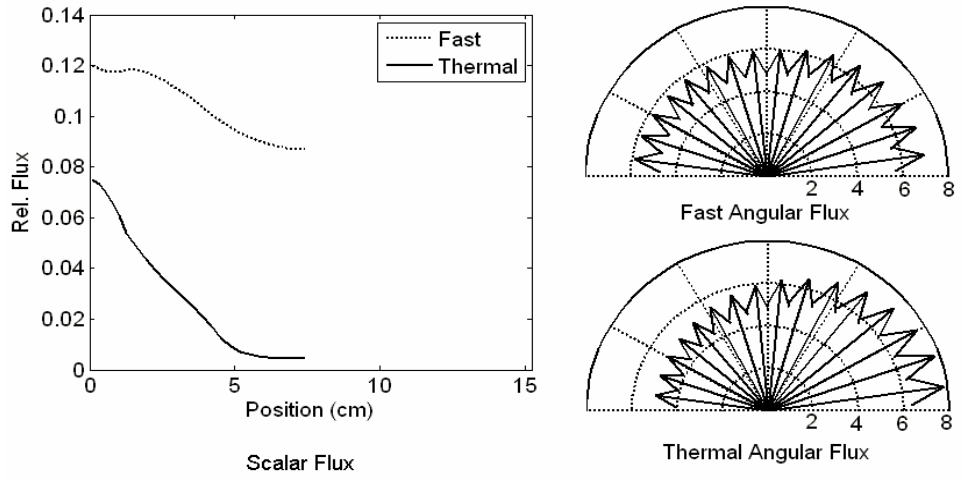


Figure 5.9: Bundle 4 - Reference Scalar Flux and Spatially Averaged Angular Flux (2g)

As seen in Figure 5.9, the angular flux (particularly thermal), is highly directed due to the presence of strong absorbers (gadded pins). In Bundle 2, this effect was averaged out over the whole bundle, but because only the left half of the bundle is used here, the local anisotropy is more apparent.

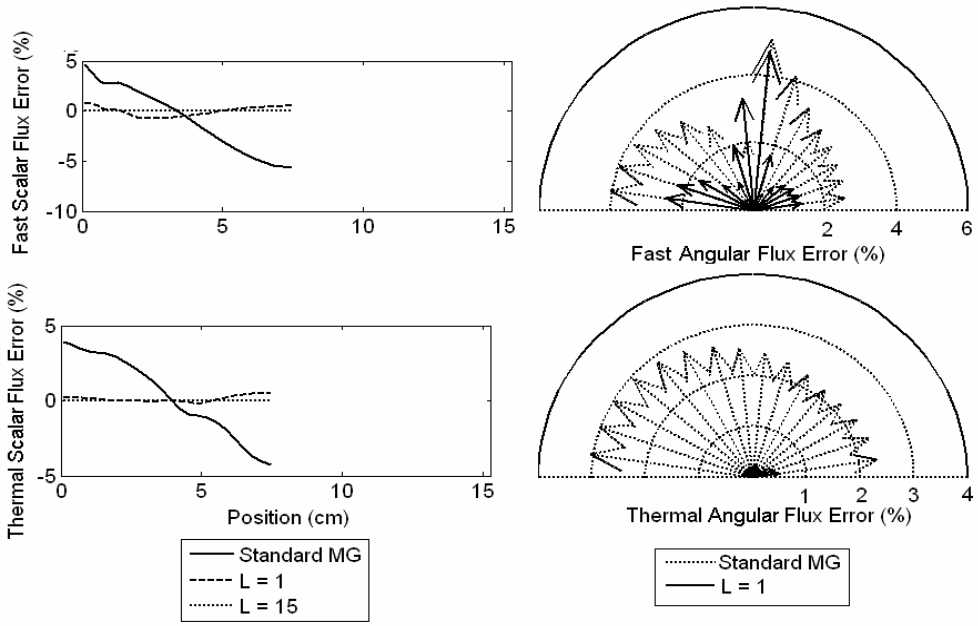


Figure 5.10: 2g Scalar and Average Angular Flux %-Error for Bundle 4.

This indicates that even in the case of specular boundary conditions, local anisotropies may still introduce energy-angle coupling effects that must be considered. The flux errors for Bundle 4 are presented in Figure 5.10.

As in previous bundles, the 1st order coupling correction greatly improved the solution, and the 15th order coupling correction reproduced the reference calculation exactly. Table 5.5 presents the $AVG_g$, $RMS_g$, and $FWE_g$ errors for increasing order of coupling correction in Bundle 4.

Table 5.5: Scalar Flux Error Analysis – Bundle 4

| | $AVG_g$ | | $RMS_g$ | | $MRE_g$ | |
|---|---|---|---|---|---|---|
| L | Fast | Thermal | Fast | Thermal | Fast | Thermal |
| 0* | 1.47 | 1.17 | 2.40 | 1.87 | 2.79 | 2.77 |
| 1 | 0.21 | 0.08 | 0.33 | 0.16 | 0.42 | 0.12 |
| 2 | 0.09 | 0.03 | 0.14 | 0.05 | 0.18 | 0.05 |
| 3 | 0.04 | 0.01 | 0.06 | 0.02 | 0.08 | 0.03 |
| 4 | 0.03 | 0.01 | 0.06 | 0.01 | 0.06 | 0.02 |
| 5 | 0.01 | 0.00 | 0.03 | 0.00 | 0.03 | 0.00 |
| 6 | 0.01 | 0.00 | 0.04 | 0.01 | 0.03 | 0.01 |
| 7 | 0.01 | 0.00 | 0.02 | 0.00 | 0.02 | 0.00 |
| 8 | 0.01 | 0.00 | 0.03 | 0.00 | 0.02 | 0.00 |
| 9 | 0.01 | 0.00 | 0.02 | 0.00 | 0.01 | 0.00 |
| 10 | 0.01 | 0.00 | 0.02 | 0.00 | 0.01 | 0.00 |
| 11 | 0.00 | 0.00 | 0.01 | 0.00 | 0.01 | 0.00 |
| 12 | 0.00 | 0.00 | 0.01 | 0.00 | 0.01 | 0.00 |
| 13 | 0.00 | 0.00 | 0.01 | 0.00 | 0.00 | 0.00 |
| 14 | 0.00 | 0.00 | 0.01 | 0.00 | 0.00 | 0.00 |
| 15 | 0.00 | 0.00 | 0.00 | 0.00 | 0.00 | 0.00 |

* L = 0 is the Standard Multigroup Method

### 5.1.2 CGEC Test Problems with Fine-Group Unfolding (N > 0)

By incorporating the energy-angle coupling within the GEC framework, the consistent method provides the means to fully unfold the energy dependence of the angular flux. In order to verify the accuracy of the unfolded angular flux, Bundle 3 was chosen as an example problem. For this bundle, the 47-group $S_{16}$ solution was used to condense the cross

sections, and the consistent multigroup method was used to solve the 2-group problem with a $50^{th}$ order energy expansion. From the coarse-group expansion moments, the 47-group flux was then expanded and compared with the 47-group reference solution. If the condensation and unfolding method is fully consistent, the unfolded flux and the reference flux (used to condense the cross sections) should be identical up to the expansion order chosen.

Table 5.6 presents an error analysis of the unfolded fine-group flux $\tilde{\Psi}_{gp}(x)$ in group $g$ for discrete ordinate (direction) $p$, in comparison with the 47-group reference flux $\Psi_{gp}(x)$. The ordinates are indexed by $p$ because the more standard discrete ordinates index $n$ is used to describe the energy expansion moment index. The goal in this comparison is to determine how well the angular dependence of the fine-group spectrum is unfolded by the expansion by averaging over the spatial and energy variables. The analysis is presented as $Eavg_p$, $Erms_p$, and $Efwe_p$ errors for each discrete ordinate $p$, defined in Eqs. (5.5)-(5.7), for both the uncorrected (L=0) and fully corrected (L=15) cases. The fully corrected case (i.e. L=K-1) is chosen here to highlight the full effect of energy-angle coupling even though as will be demonstrated later, a $5^{th}$ order coupling correction is generally sufficient for the level of anisotropy present in this bundle.

$$Eavg_p = \frac{\int dx \sum_{g=1}^{47} e_{gp}(x)\Delta u_g}{\int dx \sum_{g=1}^{47} \Delta u_g} \tag{5.5}$$

$$Erms_p = \sqrt{\frac{\int dx \sum_{g=1}^{47} e_{gp}^2(x)\Delta u_g}{\int dx \sum_{g=1}^{47} \Delta u_g}} \tag{5.6}$$

$$MRE_p = \frac{\int dx \sum_{g=1}^{47} e_{gp}(x)\Delta u_g \cdot \tilde{\Psi}_{gp}(x)}{\int dx \sum_{g=1}^{47} \Delta u_g \cdot \Psi_{gp}(x)} \tag{5.7}$$

where

$$e_{gp}(x) = 100\frac{\left|\tilde{\Psi}_{gp}(x) - \Psi_{gp}(x)\right|}{\Psi_{gp}(x)} \tag{5.8}$$

Table 5.6. Unfolded Fine-Group Flux Error for Bundle 3, 50$^{th}$ order Energy Expansion as a Function of Discrete Direction *p*

| *Discrete direction p* | $Eavg_p$ | | $Erms_p$ | | $Efwe_p$ | |
|---|---|---|---|---|---|---|
| | L = 0 | L = 15 | L = 0 | L = 15 | L = 0 | L = 15 |
| 1 | 6.17 | 3.14 | 12.31 | 5.93 | 5.80 | 1.45 |
| 2 | 6.08 | 3.15 | 11.96 | 5.93 | 5.67 | 1.46 |
| 3 | 5.92 | 3.17 | 11.36 | 5.93 | 5.43 | 1.48 |
| 4 | 5.70 | 3.20 | 10.54 | 5.92 | 5.11 | 1.50 |
| 5 | 5.44 | 3.22 | 9.58 | 5.91 | 4.72 | 1.53 |
| 6 | 5.13 | 3.26 | 8.52 | 5.88 | 4.27 | 1.57 |
| 7 | 4.84 | 3.28 | 7.68 | 5.84 | 3.89 | 1.60 |
| 8 | 4.93 | 3.30 | 9.43 | 5.83 | 4.04 | 1.62 |
| 9 | 4.93 | 3.30 | 9.42 | 5.83 | 4.17 | 1.63 |
| 10 | 4.75 | 3.30 | 7.42 | 5.84 | 3.96 | 1.62 |
| 11 | 4.90 | 3.29 | 7.84 | 5.86 | 4.19 | 1.59 |
| 12 | 5.03 | 3.26 | 8.25 | 5.86 | 4.43 | 1.57 |
| 13 | 5.14 | 3.24 | 8.56 | 5.85 | 4.59 | 1.55 |
| 14 | 5.38 | 3.22 | 8.87 | 5.84 | 4.71 | 1.53 |
| 15 | 5.25 | 3.21 | 8.83 | 5.83 | 4.75 | 1.52 |
| 16 | 5.26 | 3.21 | 8.88 | 5.82 | 4.77 | 1.51 |

As seen in Table 5.6, the uncorrected case (L=0) showed significant errors in the unfolded angular flux as a result of the inconsistent treatment of the energy-angle coupling. This was significantly improved in the fully corrected case. Of note is that the $Efwe_p$ error in the table is the most effective indicator of the accuracy of the unfolded flux because small

absolute errors in groups and spatial meshes with very low magnitude fluxes introduce large relative errors which do not accurately reflect the overall accuracy.

The improvement in the flux spectrum in Table 5.6 demonstrates the effect of fully accounting for the energy angle coupling, and the remaining error in the corrected case is a direct result of the truncation of the energy-expansion order. In order to confirm this, the bundle problem was solved again with varying expansion order and the 47-group angular flux was compared with the reference solution. For each order, the angular-average of the $Efwe_p$ values was calculated, resulting in one number describing the average "error" in the unfolded spectrum for both the uncorrected (standard method, L=0) and fully corrected (L=15) cases, and these are presented in Figure 5.11 for varying energy expansion order *N*.

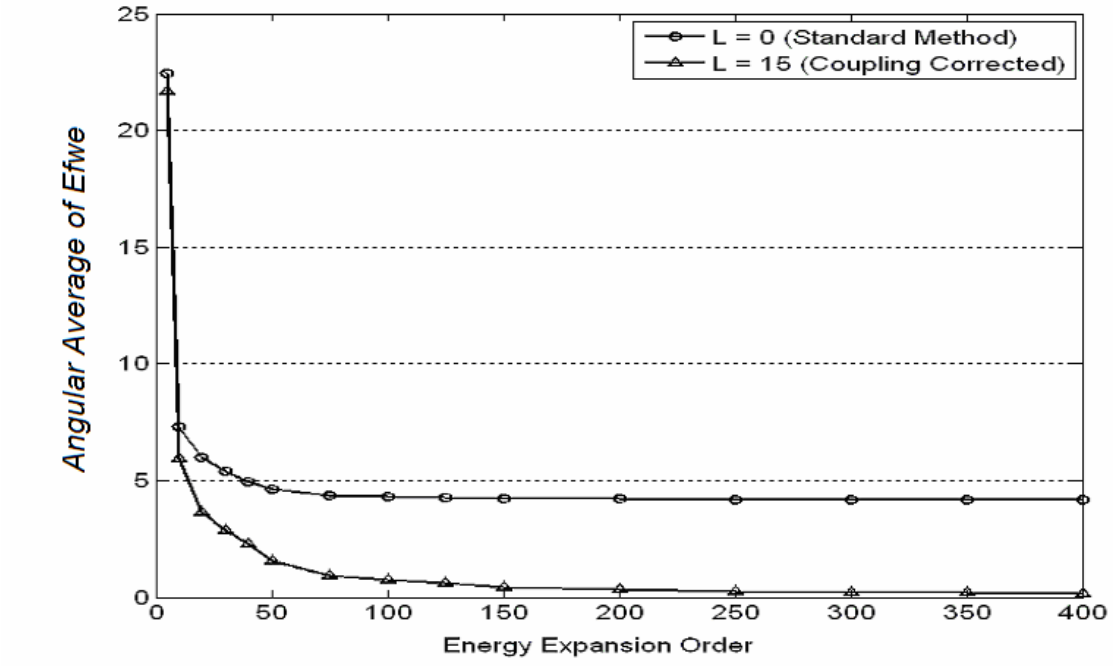


Figure 5.11: Average *Efwe* as a function of energy expansion order

As demonstrated in Figure 5.11, the standard generalized energy condensation theory without coupling correction (L=0) is not able to improve the average *Efwe* beyond ~4.1%. When the energy-angle coupling is fully corrected (L=15), the consistent method is able to reproduce the flux with arbitrary accuracy, depending only on the truncation order of the energy expansion. This result is summarized in Table 5.7, which contains the $Efwe_p$ error for both the uncorrected and fully corrected unfolded flux at several expansion orders for each direction *p*.

Table 5.7: Unfolded Angular Flux Error ($Efwe_p$) for Selected Energy Expansion Orders

| *Discrete direction p* | N = 50 | | N = 100 | | N = 200 | | N = 400 | |
|---|---|---|---|---|---|---|---|---|
| | L = 0 | L = 15 | L = 0 | L = 15 | L = 0 | L = 15 | L = 0 | L = 15 |
| 1 | 5.80 | 1.45 | 5.50 | 0.69 | 5.43 | 0.34 | 5.41 | 0.16 |
| 2 | 5.67 | 1.46 | 5.37 | 0.69 | 5.29 | 0.34 | 5.27 | 0.17 |
| 3 | 5.43 | 1.48 | 5.13 | 0.70 | 5.05 | 0.34 | 5.03 | 0.17 |
| 4 | 5.11 | 1.50 | 4.80 | 0.71 | 4.72 | 0.35 | 4.70 | 0.17 |
| 5 | 4.72 | 1.53 | 4.40 | 0.73 | 4.32 | 0.36 | 4.30 | 0.17 |
| 6 | 4.27 | 1.57 | 3.93 | 0.74 | 3.84 | 0.36 | 3.82 | 0.18 |
| 7 | 3.89 | 1.60 | 3.46 | 0.76 | 3.33 | 0.37 | 3.31 | 0.18 |
| 8 | 4.04 | 1.62 | 3.55 | 0.77 | 3.38 | 0.38 | 3.34 | 0.18 |
| 9 | 4.17 | 1.63 | 3.69 | 0.77 | 3.52 | 0.38 | 3.48 | 0.18 |
| 10 | 3.96 | 1.62 | 3.54 | 0.76 | 3.41 | 0.37 | 3.38 | 0.18 |
| 11 | 4.19 | 1.59 | 3.85 | 0.75 | 3.75 | 0.37 | 3.72 | 0.18 |
| 12 | 4.43 | 1.57 | 4.11 | 0.74 | 4.02 | 0.36 | 4.00 | 0.18 |
| 13 | 4.59 | 1.55 | 4.29 | 0.73 | 4.21 | 0.36 | 4.19 | 0.17 |
| 14 | 4.71 | 1.53 | 4.42 | 0.73 | 4.34 | 0.36 | 4.32 | 0.17 |
| 15 | 4.75 | 1.52 | 4.46 | 0.72 | 4.38 | 0.35 | 4.36 | 0.17 |
| 16 | 4.77 | 1.51 | 4.48 | 0.72 | 4.40 | 0.35 | 4.39 | 0.17 |

As expected, Table 5.7 suggests that as one extends the energy expansion to high order, the unfolded flux is obtained to arbitrary accuracy, dependent only on the truncation order. In order to confirm that the remaining error in the unfolded flux is a consequence of truncation, the 47-group reference solution was truncated to various expansion orders. This

was done by computing the energy expansion moments of the reference flux and unfolding them to order $N$ via Eq. (5.9).

$$\begin{aligned}\Psi_{gp}^{Trunc,N}(x) &= \sum_{n=0}^{N}(2n+1)\int_{g} du\overline{P}_{n}(u)\cdot\Psi_{Gnp}^{REF}(x) \\ &= \sum_{n=0}^{N}(2n+1)\int_{g} du\overline{P}_{n}(u)\cdot\left(\sum_{g\in G}\Psi_{gp}^{REF}(x)\int_{g} du\overline{P}_{n}(u)\right)\end{aligned} \tag{5.9}$$

In order for the new method to be considered accurate, it must be able to exactly reproduce the reference solution up to the order of expansion. Thus, the truncated reference solution of Eq. 5.9 represents the best possible CGEC solution for order $N$ and is exact as $N \rightarrow \infty$. It is therefore this solution that the consistent method should reproduce. This was verified by comparing the 50$^{th}$ order unfolded flux with the 50$^{th}$ order truncated reference flux for Bundle 3. This is presented in Table 5.8 as $Efwe_p$, obtained with Eq. (5.7) for both the uncorrected (L=0) case and several orders of coupling correction, using the truncated flux of Eq. (5.9) as the reference solution.

As seen in Table 5.8, the fully corrected flux (L=15) exactly reproduces the truncated fine-group flux. It is also clear that, as in the scalar flux, one does not necessarily need to use the full correction order because a 4$^{th}$ or 5$^{th}$ order coupling correction is sufficient to account for the coupling of the energy and angular dependence. Because of the decoupling of the higher-order energy expansion moments from the zeroth-order, consistent coarse-group calculation, the energy expansion truncation order may be increased with minimal impact on the overall solution time (Rahnema, Douglass, and Forget, 2008). As a result, the new consistent generalized energy condensation theory provides a robust method for generating the a good approximation fine-group flux within a coarse-group calculation.

Table 5.8. Comparison ($Efwe_p$) of $50^{th}$ order unfolded angular flux with $50^{th}$ order truncated reference 47-group flux.

| *Discrete Direction p* | L=0 | L=1 | L=2 | L=3 | L=4 | L=5 | L=10 | L=15 |
|---|---|---|---|---|---|---|---|---|
| 1 | 5.06 | 1.81 | 0.86 | 0.53 | 0.35 | 0.23 | 0.08 | 0.00 |
| 2 | 4.96 | 1.64 | 0.69 | 0.34 | 0.17 | 0.06 | 0.07 | 0.00 |
| 3 | 4.79 | 1.34 | 0.43 | 0.12 | 0.09 | 0.12 | 0.02 | 0.00 |
| 4 | 4.54 | 0.96 | 0.23 | 0.24 | 0.20 | 0.13 | 0.05 | 0.00 |
| 5 | 4.23 | 0.59 | 0.40 | 0.35 | 0.18 | 0.08 | 0.07 | 0.00 |
| 6 | 3.84 | 0.83 | 0.64 | 0.34 | 0.17 | 0.20 | 0.05 | 0.00 |
| 7 | 3.35 | 1.40 | 0.77 | 0.32 | 0.36 | 0.25 | 0.15 | 0.00 |
| 8 | 3.23 | 2.18 | 0.94 | 0.86 | 0.65 | 0.57 | 0.28 | 0.00 |
| 9 | 3.35 | 2.23 | 0.97 | 0.89 | 0.67 | 0.59 | 0.28 | 0.00 |
| 10 | 3.44 | 1.44 | 0.78 | 0.33 | 0.37 | 0.26 | 0.15 | 0.00 |
| 11 | 3.79 | 0.86 | 0.66 | 0.34 | 0.18 | 0.20 | 0.05 | 0.00 |
| 12 | 4.03 | 0.62 | 0.42 | 0.35 | 0.18 | 0.08 | 0.07 | 0.00 |
| 13 | 4.16 | 0.96 | 0.24 | 0.24 | 0.20 | 0.14 | 0.05 | 0.00 |
| 14 | 4.27 | 1.32 | 0.42 | 0.12 | 0.09 | 0.12 | 0.02 | 0.00 |
| 15 | 4.27 | 1.59 | 0.69 | 0.35 | 0.16 | 0.06 | 0.06 | 0.00 |
| 16 | 4.28 | 1.75 | 0.86 | 0.53 | 0.33 | 0.23 | 0.07 | 0.00 |

5.1.2.1 Additional Verification

In order to verify that the consistent multigroup method is a fully robust method, it is important that the method provides accurate calculations independent of the solution method (e.g., discretization of the phase space). In order to verify this, the Bundle 3 problem in section was solved again, starting from the whole core, using a varying number of discrete ordinates. For each number of discrete ordinates, the eigenvalue of the 2g calculation, both with the standard and the consistent method, is compared with the 47g reference. The consistent method in each case is implemented for increasing coupling correction order, and the results are presented in Table 5.9.

Table 5.9. Eigenvalue Results for Varying Angular Resolution

| | S2 | | S4 | | S8 | | S16 | |
|---|---|---|---|---|---|---|---|---|
| $k_{47}ref$ | 1.05017 | | 1.05559 | | 1.05589 | | 1.05599 | |
| | $k_2$ | $\delta k^*$ | $k_2$ | $\delta k^*$ | $k_2$ | $\delta k^*$ | $k_2$ | $\delta k^*$ |
| Standard Method | 1.07559 | 2542 | 1.07746 | 2187 | 1.07782 | 2192 | 1.07804 | 2205 |
| L = 1 | 1.05017 | 0 | 1.05451 | -108 | 1.05487 | -102 | 1.05526 | -73 |
| L = 2 | | | 1.05563 | 4 | 1.05600 | 11 | 1.05618 | 19 |
| L = 3 | | | 1.05559 | 0 | 1.05590 | 1 | 1.05608 | 9 |
| L = 4 | | | | | 1.05581 | -8 | 1.05595 | -4 |
| L = 5 | | | | | 1.05587 | -2 | 1.05600 | 1 |
| L = 6 | | | | | 1.05586 | -4 | 1.05597 | -2 |
| L = 7 | | | | | 1.05589 | 0 | 1.05599 | 0 |
| L = 8 | | | | | | | 1.05598 | -1 |
| L = 9 | | | | | | | 1.05599 | 0 |
| L = 10 | | | | | | | 1.05598 | -1 |
| L = 11 | | | | | | | 1.05599 | 0 |
| L = 12 | | | | | | | 1.05599 | 0 |
| L = 13 | | | | | | | 1.05599 | 0 |
| L = 14 | | | | | | | 1.05599 | 0 |
| L = 15 | | | | | | | 1.05599 | 0 |

$\delta k^* = 10^5 (k_2 - k_{47}ref)$

As seen in the table, the consistent multigroup method results in the same behavior, independent of the number of ordinates used. Of note is that, in each case, the use of the full coupling correction with the maximum value of *L* that is accessible for that number of ordinates, the 47g solution is reproduced exactly. This is because the 47g reference solution can only vary with energy up to that order, and thus no additional terms are neglected by the truncation of the coupling correction order. It is also noted that the consistent method is unaffected by the refinement of the spatial mesh or number of coarse groups.

### 5.1.3 Application to an Optically Thin Benchmark problem

One of the most challenging aspects of optically thin reactors is that the increased anisotropy and longer mean free paths of these systems generate significant spectral errors in

the condensed cross sections. As a result, a larger number of coarse groups are generally required to generate accurate core solutions. While this requires more than 20 coarse groups in some systems (e.g., high temperature gas cooled reactors), as few as 6 groups are often used to obtain more rapid solutions; however, the 2-group structure generally used in LWR problems is unable to accurately represent the optically thin spectrum with the standard method. One of the advantages of the consistent method is that, because the condensed solution exactly reproduces the fine-group reaction rates, the accuracy of the solution becomes much less dependent on the coarse-group structure.

In order to demonstrate the effectiveness of the consistent method to accurately treat an optically thin problem with a coarse-group structure that is not optimal for the problem, the 1D HTTR benchmark problem in section 4.2.3. Testing this method requires a fine-group cross section set, rather than the MCNP solution, and so 47-group cross sections were generated for each unique material by modeling the entire ARO configuration of the core with HELIOS (Simeonov, 2003).

As in the previous example, these cross sections were used to generate a 47-group $S_{16}$ reference solution for the core, and 47-group interface fluxes were used to obtain albedo boundary conditions for each of the 3 fuel blocks in the HTTR core. The eigenvalue of this discrete ordinates fine-group reference core calculation was 1.10826.

The same process used in the BWR problem was used to examine the consistent method in each block. The core interface fluxes were used to establish the boundary conditions for a 47-group $S_{16}$ assembly calculation, which is considered the reference flux for the blocks. As before, the cross sections were condensed with increasing order of angular correction from $L$=0 (no correction) to $L$=15 (full correction). The same coarse-group

structure was used as in the BWR problem (0.625 eV thermal boundary), which is known to be insufficient for standard multigroup calculations in gas cooled reactors. Table 5.10 presents the eigenvalue results of the calculations, analogous to the Table 5.1 results for the BWR case.

Table 5.10: Eigenvalue results for Blocks 1-3 for increasing angular expansion order.

| | Block 1 | | Block 2 | | Block 3 | |
|---|---|---|---|---|---|---|
| $k_{47}ref$ | 1.10828 | | 1.10827 | | 1.10826 | |
| | $k_2$ | $\delta k^*$ *(pcm)* | $k_2$ | $\delta k^*$ *(pcm)* | $k_2$ | $\delta k^*$ *(pcm)* |
| Standard Method | 1.11737 | 908 | 1.10948 | 122 | 1.11983 | 1156 |
| L = 1 | 1.10809 | -20 | 1.10821 | -5 | 1.10805 | -22 |
| L = 2 | 1.10786 | -43 | 1.10789 | -37 | 1.10788 | -39 |
| L = 3 | 1.10816 | -13 | 1.10814 | -12 | 1.10815 | -12 |
| L = 4 | 1.10800 | -29 | 1.10801 | -25 | 1.10801 | -26 |
| L = 5 | 1.10815 | -14 | 1.10814 | -12 | 1.10814 | -13 |
| L = 6 | 1.10808 | -21 | 1.10808 | -18 | 1.10808 | -19 |
| L = 7 | 1.10817 | -12 | 1.10816 | -10 | 1.10816 | -11 |
| L = 8 | 1.10814 | -15 | 1.10813 | -13 | 1.10813 | -14 |
| L = 9 | 1.10820 | -9 | 1.10819 | -7 | 1.10818 | -9 |
| L = 10 | 1.10818 | -11 | 1.10817 | -9 | 1.10817 | -10 |
| L = 11 | 1.10823 | -6 | 1.10822 | -4 | 1.10821 | -6 |
| L = 12 | 1.10822 | -7 | 1.10821 | -5 | 1.10820 | -7 |
| L = 13 | 1.10826 | -3 | 1.10824 | -2 | 1.10823 | -4 |
| L = 14 | 1.10825 | -4 | 1.10824 | -2 | 1.10823 | -4 |
| L = 15 | 1.10829 | 0 | 1.10827 | 1 | 1.10826 | -1 |

$\delta k^* = 10^5 (k_2 - k_{47}ref)$

As seen in the table, the degree of anisotropy in the boundary flux influences the accuracy of the standard condensation method. Blocks 1 and 3 both border a control block without rods inserted (which are thus effectively moderator blocks). This results in fluxes which at high energy are directed outward towards the control block (neutrons generated from fission) and at low energy are directed inward towards the fuel block (thermalized in the moderator). Block 2, on the other hand, borders additional fuel blocks on either side, which is most similar to a zero-current (specular reflective) boundary condition, leading to a

more isotropic flux and more accurate result with the standard method. However, independent of the boundary conditions and isotropy of the flux, the consistent method was able to exactly match the reference solution.

In order to examine the accuracy of the flux solution, a flux analysis analogous to that performed for the BWR problem was performed for Block 3, as it exhibits the largest error using the standard method. Figure 5.12 contains the reference flux for fuel block 3. Included in the figure are (a) the 2-group scalar flux, obtained by summing the 47-group reference into the 2-group structure and (b) the fast and thermal angular flux for each discrete direction at the block boundaries and the center region of the block

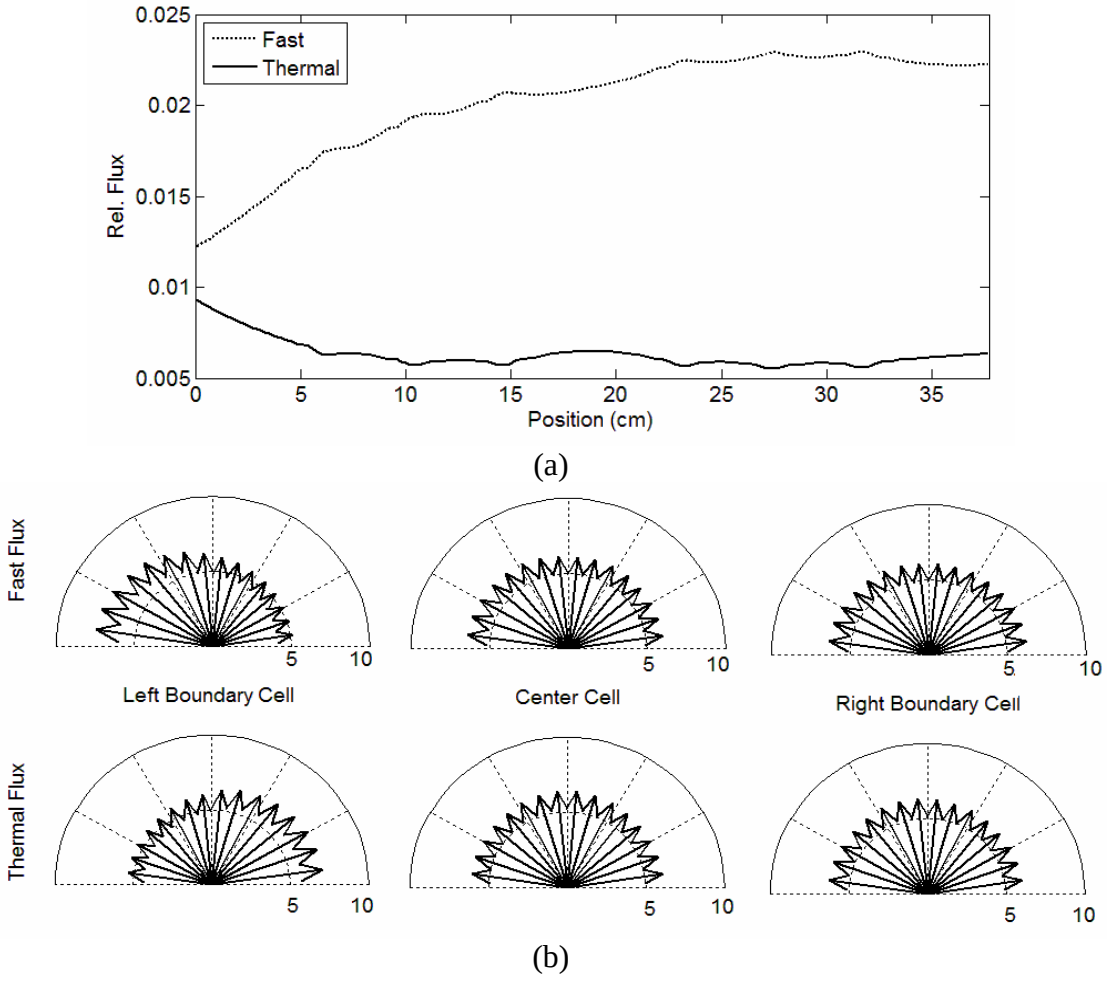


Figure 5.12: Block 3 - Reference Scalar (a) and Selected Angular Flux (b)

As is evident in Figure 5.12, the left side of the fuel block, which borders an uncontrolled CRB (moderator), causes a flux gradient at that boundary and introduces anisotropy in both the thermal and fast angular flux. This results in errors in the coarse-group cross sections and the coarse-group solution from neglecting the angular effect. The error in the 2-group scalar flux and angular flux are presented in Figure 5.13.

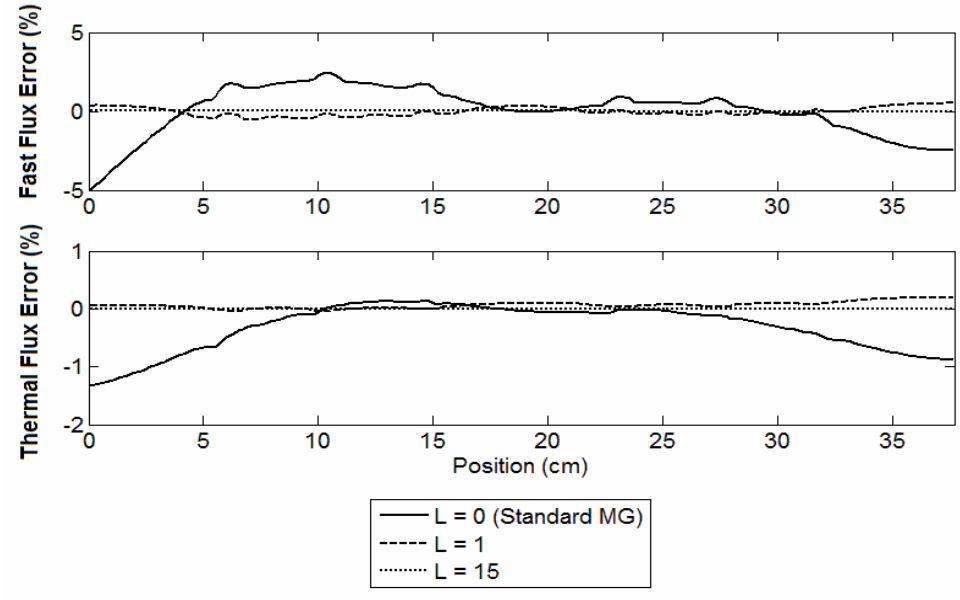


(a)

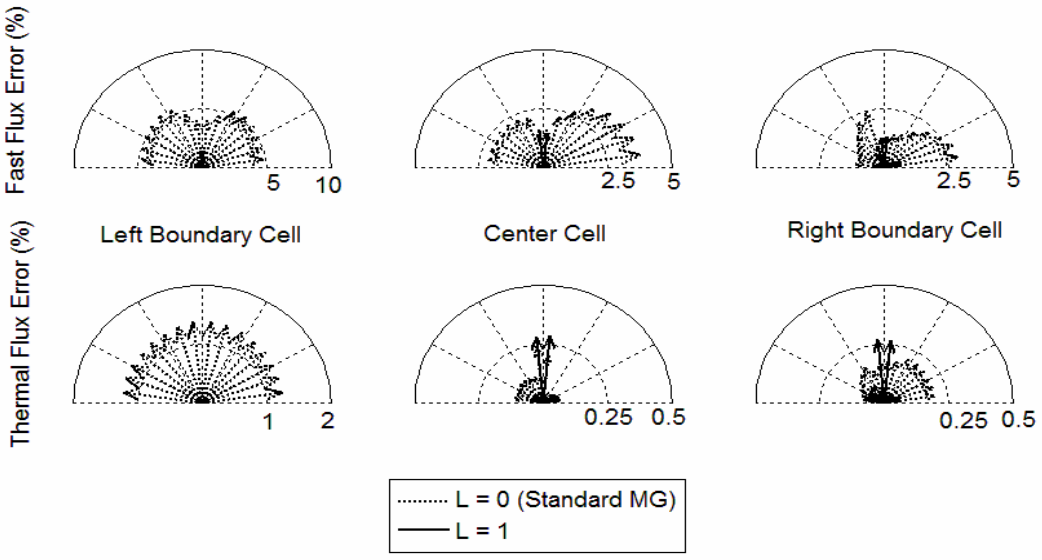


(b)

Figure 5.13: 2g Scalar and Selected Angular Flux %-Error for Block 3.

As seen in Figure 5.13, the standard multigroup method results errors in the angular and scalar flux of up to 5%, particularly in the fast group and near the boundary. This is due to the effect of local anisotropy generated by the neighboring CRB. It is also evident that in this block, the 1st order coupling correction results in significant improvement. It is noted that the 1st order error in the thermal angular flux is too small to be visible on the graph of the left boundary cell angular flux error. Table 5.11 presents the $AVG_g$, $RMS_g$, and $FWE_g$ errors for increasing order of coupling correction in Block 3.

Table 5.11: Scalar Flux Error Analysis – Block 3

| | $AVG_g$ | | $RMS_g$ | | $MRE_g$ | |
|---|---|---|---|---|---|---|
| L | Fast | Thermal | Fast | Thermal | Fast | Thermal |
| 0* | 1.18 | 0.35 | 1.54 | 0.51 | 1.10 | 0.38 |
| 1 | 0.23 | 0.07 | 0.27 | 0.09 | 0.23 | 0.07 |
| 2 | 0.10 | 0.02 | 0.14 | 0.02 | 0.10 | 0.02 |
| 3 | 0.06 | 0.01 | 0.07 | 0.01 | 0.06 | 0.01 |
| 4 | 0.06 | 0.01 | 0.09 | 0.01 | 0.06 | 0.01 |
| 5 | 0.04 | 0.00 | 0.05 | 0.00 | 0.04 | 0.00 |
| 6 | 0.05 | 0.00 | 0.07 | 0.00 | 0.05 | 0.00 |
| 7 | 0.03 | 0.00 | 0.04 | 0.00 | 0.03 | 0.00 |
| 8 | 0.04 | 0.00 | 0.05 | 0.00 | 0.04 | 0.00 |
| 9 | 0.02 | 0.00 | 0.03 | 0.00 | 0.02 | 0.00 |
| 10 | 0.03 | 0.00 | 0.04 | 0.00 | 0.03 | 0.00 |
| 11 | 0.02 | 0.00 | 0.02 | 0.00 | 0.02 | 0.00 |
| 12 | 0.02 | 0.00 | 0.02 | 0.00 | 0.02 | 0.00 |
| 13 | 0.01 | 0.00 | 0.01 | 0.00 | 0.01 | 0.00 |
| 14 | 0.01 | 0.00 | 0.01 | 0.00 | 0.01 | 0.00 |
| 15 | 0.00 | 0.00 | 0.00 | 0.00 | 0.00 | 0.00 |

* L = 0 is the Standard Multigroup Method

Table 5.11 clearly demonstrates that the consistent method is able to explicitly correct for the coupling effects, and reproduce the reference solution exactly, despite flux anisotropy and a highly non-optimal group structure. The results in Table 5.11 would seem to indicate that the standard method has not done as poorly as one might have expected for these problems. This is because gas cooled reactors possess complicated geometries (e.g.,

asymmetric burnable absorber pins, control rods in non-fissionable assemblies) which cannot be accurately modeled in a 1D system. While the 1D problem adequately accounts for the global physics parameters of the HTTR, the effect of smearing the number densities eliminates the local transport effects that were seen in the BWR problem.

Consequently, the results in Table 5.11 underestimate the errors that result from using the standard condensation method in higher-dimensional models (2D or 3D), where explicit modeling of the burnable absorber pins and control rods introduce local effects that are not captured in the 1D model. However, as shown in the BWR problem and in the optically thin problem, the consistent method can accurately account for these effects, and the analysis of this method in higher-dimensional optically thin problems is considered in future work.

In addition, it is known that the spectrum of the fuel block is greatly affected by the type of blocks surrounding it, resulting in a large spectral core environment error. The new CGEC method provides a framework for consistently condensing the cross sections, despite group structure or anisotropy in the weighting function, and provides a way of approximately inverting the condensation process by unfolding the detailed spectrum to within the accuracy of the expansion order.

### 5.1.4 Cross Section Recondensation via CGEC Theory

#### 5.1.4.1 Flux Update Procedure

The results in the previous section indicate that the unfolded flux is able to reproduce the solution up to the order of truncation. However, one of the consequences of using an orthogonal expansion to approximate the flux is the introduction of random computational noise in the fine-group flux. Because the fine-group flux used to condense the next iteration of the recondensation procedure is the integral of the coarse expansion over the fine-group,

negative fluxes can result for some fine groups which are non-physical and can introduce errors in the condensed cross sections. (Zhu and Forget, 2011) In addition, the unconverged portion of the coarse-group flux can introduce very small non-physical errors in the unfolded flux. These errors and the flux negativity can introduce instabilities in a recondensation scheme, and must be corrected for the re-condensation scheme to converge.

A flux update procedure was initially introduced by Zhu and Forget (2011) to address flux negativity issues from truncation in a discrete Legendre Polynomial application of the GEC, and additionally serves to filter out the numerical noise from the unconverged portion of the coarse-group flux, even when there is no flux negativity. The procedure consists of using the unfolded multigroup flux to generate a neutron-balance eigenvalue (ratio of fission to absorption and leakage) and a multigroup source. This source is then used in a fixed-source transport sweep through the core for each group to provide an updated flux. It is then this flux which is used to re-condense the cross sections. Performing this update during each iteration helps to reduce the noise and stabilize the recondensation procedure and eliminates flux negativity. In some situations, it may be necessary to perform this flux update several times during an iteration to eliminate the flux negativity (Zhu and Forget, 2011).

#### 5.1.4.2 CGEC Recondensation for 1D HTTR

The previous sections have demonstrated that the CGEC theory is able to reproduce the fine-group spectrum to a good approximation when the exact flux spectrum is used to generate the cross sections and expansion moments. As mentioned earlier, however, this flux is not known before hand, and so a guess of the flux (e.g., lattice cell flux) is used to produce the cross sections for the coarse-group calculation. The unfolded flux from this coarse-group calculation has been shown (Rahnema, Douglass, and Forget, 2008) to be a significantly

improved approximation to the core-level flux than the lattice cell flux is. As a result, using the unfolded flux as a new weighting flux to update the coarse-group cross sections and re-calculate the core solution would provide an improved result. In order to verify this method, the 1D HTTR problem is used as a benchmark problem, which is of significant interest for this type of method.

Optically thin systems like the HTTR typically maintain reactor control via separate "control blocks" which contain graphite moderator and control rods, but no fuel. In addition, the longer neutron mean free paths in these systems require several rings of reflector and/or shield blocks to reduce leakage and preserve neutron economy.

The absence of fuel in these blocks makes generating coarse-group cross sections highly challenging for the materials contained therein, because lattice cell calculations with specular boundary conditions cannot be performed for these assemblies. This is typically addressed by either performing an "extended" lattice calculation, which includes part of a control block in a fuel block calculation (Zhang et. al., 2011), or by assuming an "average" spectrum from the fuel lattice calculations. Neither of these provide a good approximation for the actual spectrum in these lattices when placed in the core environment, particularly for shield or reflector blocks located far from the core. Therefore, the CGEC recondensation described in section 3.4 will provide a core-level spectral correction to the collapsed cross sections in the core, thereby providing a dramatic improvement to the cross sections in the non-fissionable lattice cells.

The HTTR 1D benchmark problem consists of three fissionable lattices (Fuel Blocks 1, 2, and 3) and five non-fissionable lattices (Center Control, Outer Control, and three reflector blocks). This problem therefore presents a significant challenge in generating a

good weighting spectrum with lattice-cell calculations, particularly in the outer reflector blocks. For these lattices, the attenuation of the flux results in a spectrum which is dramatically different than that of the fissionable lattices. In the case that the outer control rods are inserted, this becomes an even more significant effect.

In this section, the group structure chosen as the fine-group structure is the HELIOS 47-group structure. All calculations are performed in $S_8$, and all cross sections are condensed for each spatial mesh (i.e., no spatial homogenization). While spatial homogenization is commonly used in core analysis, this dissertation is focused on the spectral effects and intended primarily for whole-core fine-mesh transport problems. A 6-group structure was chosen from VHTR literature (Zhang et. al., 2011) and aligned as closely as possible to the 47-group boundaries to provide a condensed group structure. This is provided in Table 5.12.

Table 5.12: VHTR 6-Group Structure

| Groups | Lower Bound (eV) | Upper Bound (eV) |
|---|---|---|
| 1 | 1.8316E+05 | 2.0000E+07 |
| 2 | 2.0347E+03 | 1.8316E+05 |
| 3 | 2.3824E+00 | 2.0347E+03 |
| 4 | 6.2506E-01 | 2.3824E+00 |
| 5 | 1.1157E-01 | 6.2506E-01 |
| 6 | 1.0000E-04 | 1.1157E-01 |

In order to examine the effectiveness of the consistent recondensation methodology, the accuracy of the coarse-group calculation is examined both before recondensation (standard method) and after enough recondensation iterations to converge the cross sections to within 0.1%. Both the ARO and ARI configurations are examined. Figure 5.15 presents the 6-group scalar flux reference for both configurations as well as the spatial relative error,

$E_g(x)$ defined in Eq. (5.10), for both the standard method (no recondensation, lattice-cell flux for condensation), and the consistent recondensation solution ($10^{th}$ and $40^{th}$ order).

$$E_g(x) = 100 \frac{\left| \tilde{\phi}_g(x) - \phi_g^{REF}(x) \right|}{\left\langle \phi_g^{REF}(x) \right\rangle} \tag{5.10}$$

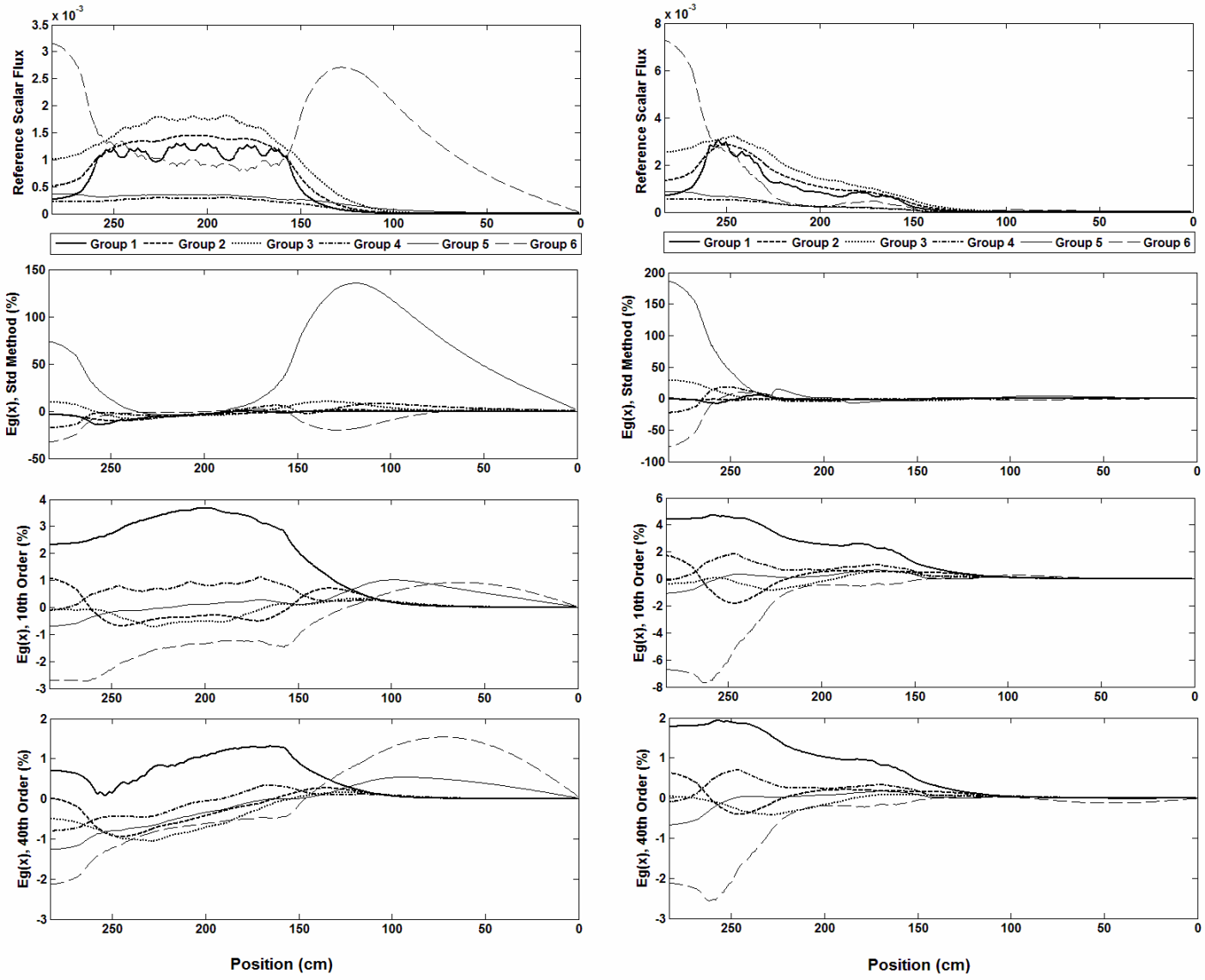


Figure 5.14: Spatial relative error for the standard method, $10^{th}$ order, and $40^{th}$ order CGEC Recondensation

The results in Figure 5.14 clearly demonstrate the errors introduced in the flux solution by use of an average moderator spectrum to condense the cross sections in the reflector regions. In group 5, this resulted in relative errors over 100% in the uncontrolled case and approaching 200% in the controlled case. As expected the flux errors were largest in the reflector regions where the energy spectrum is not well represented by the spectrum in the moderator of the lattice-cell calculations.

Figure 5.14 also clearly demonstrates the effectiveness of the recondensation methodology to improve the solutions. With a $40^{th}$ order energy expansion, the largest relative errors in the 6-group flux were on the order of 2%. Even with a $10^{th}$ order expansion, the largest relative flux error in the uncontrolled case was under 4% and under 8% for the controlled case. This highlights the value of the consistent recondensation method for optically thin problems, as even a low-order energy expansion can dramatically improve the flux distribution.

As is demonstrated in Tables 5.13 and 5.14, the consistent recondensation method is also able to dramatically improve the eigenvalue and reaction rates of the core solution. The Table presents the results for the eigenvalue, block fission density, and block absorption density as compared to the 47-group reference solution as well as the standard method. Both the absorption and fission densities are normalized to the average block fission density in the core.

As expected, the standard method was very poor at reproducing the absorption rate in the non-fissionable lattices. The consistent recondensation method was able to dramatically improve the solution. For example, the error in the center control block was lowered from 14.3% to 1.1% with a $10^{th}$ order expansion, and to 0.0% with a $40^{th}$ order expansion. The

method improved the coarse-group eigenvalue error from 702 pcm to 53 pcm with a 40th order calculation. This was also demonstrated in the controlled cases, where the absorption rate in the outer control block, which has a large reactivity effect, was reduced from 4.8% to 0.3% with a 10th order expansion, and to 0.0% with a 40th order expansion. The eigenvalue in the controlled case was improved from an error of 1301 pcm to 68 pcm.

Table 5.13: Reaction Rate Results of CGEC Recondensation for 1D HTTR

| | | | Center Cont. | FB 1 | FB 2 | FB 3 | Outer Cont. | Refl | Refl | Refl |
|---|---|---|---|---|---|---|---|---|---|---|
| **ARO** | 47g Ref | Fiss | | **1.011** | **0.929** | **1.060** | | | | |
| | | Abs | **0.038** | **2.277** | **1.866** | **2.186** | **0.081** | **0.072** | **0.033** | **0.010** |
| | 6g Std | Fiss | | -2.7% | 0.4% | 2.2% | | | | |
| | | Abs | -14.3% | -3.1% | 0.2% | 1.5% | -11.8% | -9.1% | -2.1% | 3.1% |
| | 6g 10th Ord | Fiss | | -0.1% | 0.0% | 0.1% | | | | |
| | | Abs | 1.1% | -0.1% | -0.1% | 0.1% | 2.3% | 3.1% | 4.0% | 4.9% |
| | 6g 40th Ord | Fiss | | -0.2% | 0.0% | 0.2% | | | | |
| | | Abs | 0.0% | -0.3% | -0.1% | 0.2% | 1.3% | 2.0% | 3.3% | 4.4% |
| | | | Center Cont. | FB 1 | FB 2 | FB 3 | Outer Cont. | Refl | Refl | Refl |
| **ARI** | 47g Ref | Fiss | | **2.025** | **0.461** | **0.514** | | | | |
| | | Abs | **0.095** | **4.587** | **2.530** | **1.072** | **0.444** | **0.004** | **0.002** | **0.001** |
| | 6g Std | Fiss | | 0.9% | -2.8% | -1.0% | | | | |
| | | Abs | -11.4% | 0.1% | -2.8% | -1.1% | -4.8% | -25.4% | -22.5% | -20.5% |
| | 6g 10th Ord | Fiss | | -0.1% | -0.4% | 0.6% | | | | |
| | | Abs | 1.2% | -0.1% | -0.5% | 0.5% | 0.3% | 4.7% | 3.4% | 1.5% |
| | 6g 40th Ord | Fiss | | 0.0% | -0.1% | 0.2% | | | | |
| | | Abs | 0.4% | 0.0% | -0.2% | 0.1% | 0.0% | 0.7% | -0.9% | -2.7% |

Table 5.14: Eigenvalue Results of CGEC Recondensation for 1D HTTR

| ARO | | ARI | |
|---|---|---|---|
| *k* | d*k* (pcm) | *k* | d*k* (pcm) |
| **1.1079** | - | **0.8369** | - |
| 1.1157 | 702 | 0.8478 | 1301 |
| 1.1070 | -88 | 0.8378 | 112 |
| 1.1074 | -53 | 0.8374 | 68 |

The consistent recondensation method has been shown in this paper to be highly effective at correcting the errors associated with the use of approximate spectra in non-fissionable assemblies in optically thin reactor systems like the HTTR. As one would expect, increasing the order of the energy expansion improves the solution. However in many, if not most, cases, it is not necessarily practical to perform high order calculations, and one will often trade off some degree of accuracy for speed. The results in demonstrate that even for relatively low order calculations, a dramatic improvement may be seen in the eigenvalue, reaction rates, and flux solution in a coarse-group core calculation. However, the necessity of performing a flux update at every iteration to ensure positivity may become prohibitively time consuming in addition to the calculation of higher-order cross section moments and higher-order flux moment calculations. Also, the reader will note that the entirety of the SGD method presented in section 3.3 requires only a fixed source transport sweep for each fine group, and therefore is computationally equivalent to the flux update, but without the need for any expansion moment calculations.

## 5.2 Subgroup Decomposition Method Verification

It is noted that the condensed formulation of both the SGD and CGEC methods is essentially the same as long as the correction term is included. Therefore, in order to verify the accuracy of the SGD method, we begin with the recondensation procedure in section 3.4, applied to both the 1D Transverse-Integrated BWR Core and 1D HTTR core problems. As normally done, the coarse group cross sections are initially obtained from the lattice cell calculations for the fissionable lattices with specular reflective boundary conditions on both sides. For the outer moderator lattice in the BWR problem, the spectrum used to generate the initial cross sections is that of the small channel of the fresh, unvoided lattice. For the non-fissionable lattices in the HTTR problem (reflectors and control lattices), the corresponding cross sections are obtained using the average moderator spectrum of the nearest fissionable lattice. All transport calculations in this section are performed in $S_8$ with linear diamond differencing with negative flux fix-up, flux convergence of $10^{-4}$, eigenvalue convergence of $10^{-6}$, and Gauss-Legendre angular quadrature. All calculations in this section are performed with transport-corrected isotropic scattering (Bell and Glasstone, 1970).

### 5.2.1 BWR Discrete Ordinates Reference Solution

The benchmark solution in section 4.3 for this problem consisted of a HELIOS calculation, and in order to maintain consistency in the coarse-group and fine-group methods, a discrete-ordinates reference calculation is first calculated for both configurations of the BWR core. The reference solution for both configurations was generated using a 47-group $S_8$ calculation with linear diamond differencing. The calculated eigenvalue of the ARO configuration was 1.0668 and of the SRI configuration

was 1.0034. The 47-group reference scalar flux for both configurations is presented as a function of position and lethargy in Figure 5.15 with the specular reflective boundary at position 0 cm.

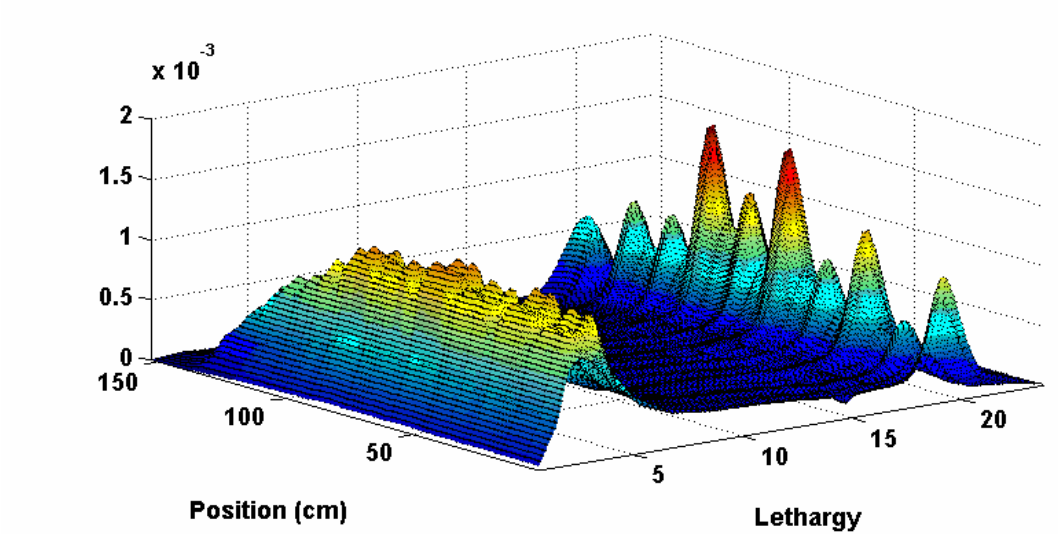


(a)

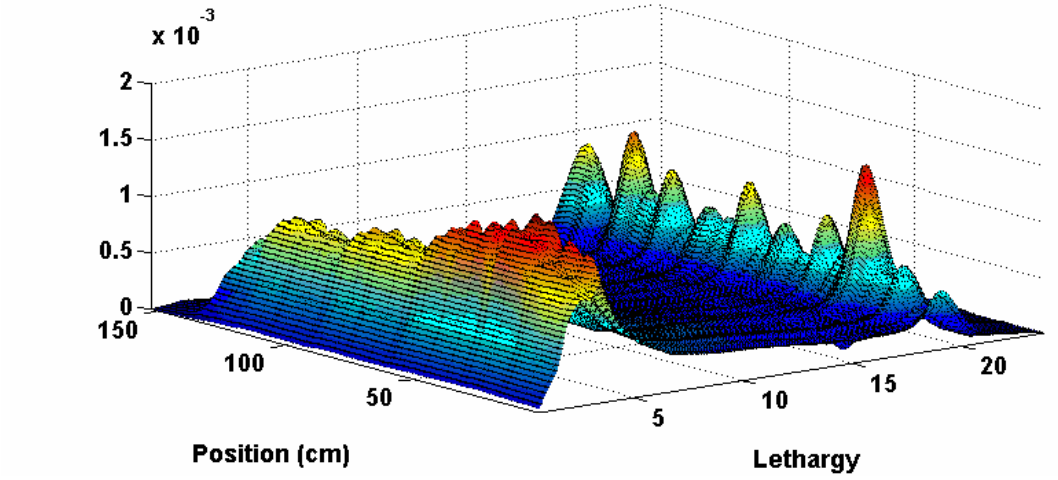


(b)

Figure 5.15: Reference 47-group scalar flux for BWR benchmark problem for the (a) ARO and (b) SRI configurations.

In Figure 5.16, the reference pin fission density (PFD) is presented in addition to the 2-group flux for both configurations. The 2-group reference is computed by integrating the 47-group reference solution into the standard thermal 2-group structure

(0.625 eV thermal boundary). The PFD is normalized to the number of fissionable pins (i.e. the average PFD = 1).

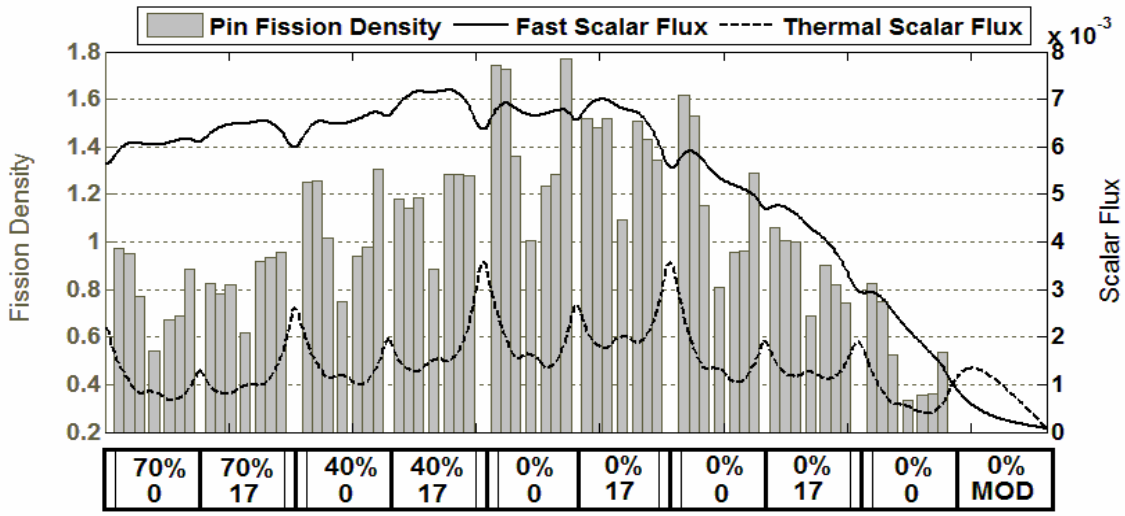


(a)

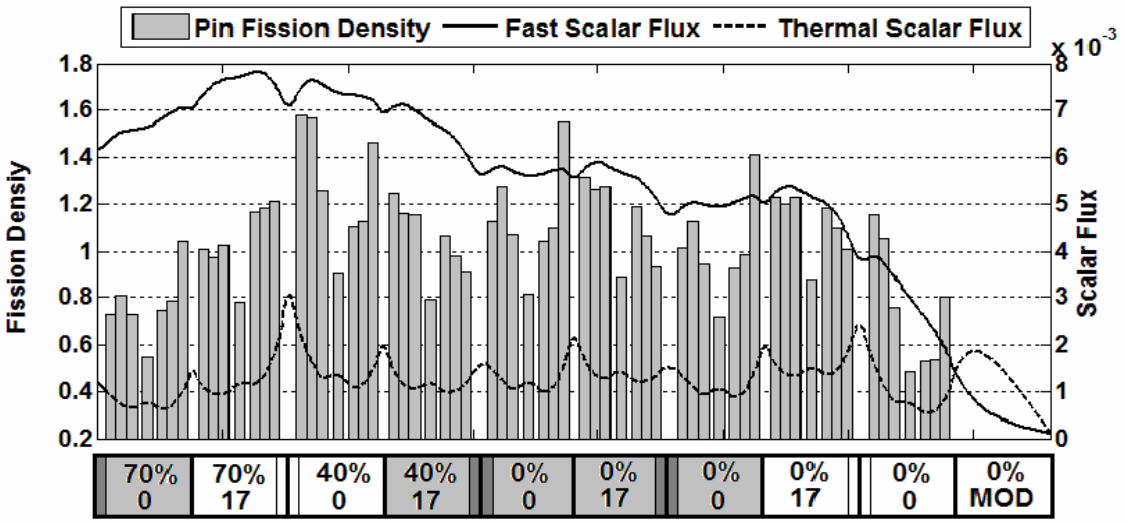


(b)

Figure 5.16: Reference 2-group flux and pin fission density for the (a) ARO and (b) SRI configurations.

### 5.2.2 SGD Verification with Transverse Integrated BWR Core

In order to compare the SGD method with standard condensation method, the SGD method for the BWR core was applied using the standard 2-group structure (0.625

eV thermal boundary) for the coarse-group calculations. The results of these calculations are presented in Table 5.15 (shaded cells represent controlled lattices). In the table, the bundle-averaged fission density ("fd"), capture density ("cd"), and eigenvalues are compared to the reference for both the ARO and SRI configuration. In the table, the bundle-averaged fission and capture densities are normalized to the average fission density in the core.

Table 5.15. BWR Core SGD Results

| VF | 70% | 70% | 40% | 40% | 0% | 0% | 0% | 0% | 0% | 0% |
|---|---|---|---|---|---|---|---|---|---|---|
| BU | 0 | 17 | 0 | 17 | 0 | 17 | 0 | 17 | 0 | 0 mod |
| ARO CONFIGURATION | | | | | | | | | | |
| | 47g Reference | | | | | | | | | |
| *fd** | **0.75** | **0.81** | **1.03** | **1.14** | **1.39** | **1.37** | **1.14** | **0.86** | **0.50** | |
| *cd** | **1.07** | **1.13** | **1.42** | **1.52** | **1.86** | **1.78** | **1.51** | **1.11** | **0.64** | **0.16** |
| | 2g Standard Method | | | | | | | | | |
| *fd %-err** | -15.04 | -12.12 | -9.00 | -3.46 | 0.10 | 6.18 | 8.14 | 12.41 | 11.34 | |
| *cd %-err** | -15.08 | -11.80 | -9.18 | -3.24 | 0.03 | 6.21 | 8.17 | 12.40 | 12.19 | -13.31 |
| | 2g SGD Recondensation Method (30 Itns) | | | | | | | | | |
| *fd %-err** | 0.26 | 0.23 | 0.17 | 0.09 | 0.00 | -0.09 | -0.15 | -0.22 | -0.35 | |
| *cd %-err** | 0.26 | 0.22 | 0.17 | 0.09 | 0.01 | -0.09 | -0.15 | -0.21 | -0.34 | -0.86 |
| | Reference *k* | | 2g Std Meth | | d*k* (pcm) | | 2g SGD Rec. | | d*k* (pcm) | |
| | **1.0668** | | 1.0704 | | 336 | | 1.0669 | | 5 | |
| SRI CONFIGURATION | | | | | | | | | | |
| | 47g Reference | | | | | | | | | |
| *fd* | **0.74** | **1.02** | **1.24** | **1.01** | **1.10** | **1.10** | **0.98** | **1.09** | **0.73** | |
| *cd* | **1.29** | **1.43** | **1.71** | **1.58** | **1.75** | **1.64** | **1.56** | **1.41** | **0.93** | **0.24** |
| | 2g Standard Method | | | | | | | | | |
| *fd %-err** | -19.04 | -14.24 | -12.63 | -11.62 | -8.98 | -0.12 | 12.09 | 28.45 | 31.95 | |
| *cd %-err** | -19.22 | -13.92 | -12.85 | -11.43 | -9.30 | 0.34 | 11.52 | 28.52 | 33.11 | 3.05 |
| | 2g SGD Recondensation Method (30 Itns) | | | | | | | | | |
| *fd %-err** | -0.42 | -0.40 | -0.35 | -0.25 | -0.05 | 0.13 | 0.36 | 0.50 | 0.57 | |
| *cd %-err** | -0.42 | -0.39 | -0.35 | -0.24 | -0.06 | 0.14 | 0.36 | 0.51 | 0.57 | 0.61 |
| | Reference *k* | | 2g Std Meth | | d*k* (pcm) | | 2g SGD Rec. | | d*k* (pcm) | |
| | **1.0034** | | 1.0088 | | 531 | | 1.0034 | | -5 | |

* *fd* = bundle averaged fission density, *cd* = bundle averaged non-fission capture density
*fd %-err* = % difference between fission density and reference *fd*,
*cd %-err* = % difference between non-fission capture density and reference *cd*

In Table 5.15, the "2g Standard Method" refer to the initial calculation of the core-level coarse group flux, prior to any recondensation iterations. For this calculation, the cross sections were condensed with the lattice-cell spectrum and the whole-core calculation is then performed in 2 groups. As expected, the spectral core environment effect results in large errors in the bundle fission density, particularly when the flux spectrum in the core is different than the lattice-cell spectrum.

In the ARO configuration, this effect is seen towards the center of the core and towards the outer periphery, where the fission density error was greater than 10%, but lower towards the higher-power regions of the core, where the flux is not as strongly varying. In the SRI configuration, the error in the standard method is even more apparent, as the spectral difference between controlled and uncontrolled lattices is significant, particularly towards the periphery. This results in errors which are much larger than in the ARO configuration, staying over 10% for most of the lattices, and reaching over 28% for uncontrolled lattices neighboring controlled lattices near the periphery.

As demonstrated in the Table 5.15, after converging the cross sections to within 0.1%, the SGD method was shown to be highly accurate. In the ARO configuration, the maximum bundle-averaged fission density error was reduced from 15.04% to 0.35%, and in the SRI configuration, it was reduced from 31.95% to 0.57%. The average capture density showed similar improvement, going from 15.08% to 0.86% error in the ARO configuration and from 33.11% to 0.61% in the SRI configuration.

Also as seen in the table, because of error cancellation, integral quantities such as the eigenvalue may exhibit smaller errors than those for local quantities such as the flux

when using the standard method. Using the SGD recondensation method, these errors are significantly reduced. As one would expect, these errors can be completely eliminated if a tight enough convergence on the flux and cross sections is employed.

One challenge of BWR analysis is adequately capturing local spectral effects in condensation, such as absorption rate in Gd pins. Therefore, in addition to the bundle-averaged quantities presented above, it is beneficial to have an understanding of more spatially detailed results. Figure 5.17 presents the pin-fission density error and the %-error in the 2-group scalar flux distribution for the standard method and the 2-group SGD recondensation method. In both configurations, the SGD recondensation provides a dramatic improvement in the solution.

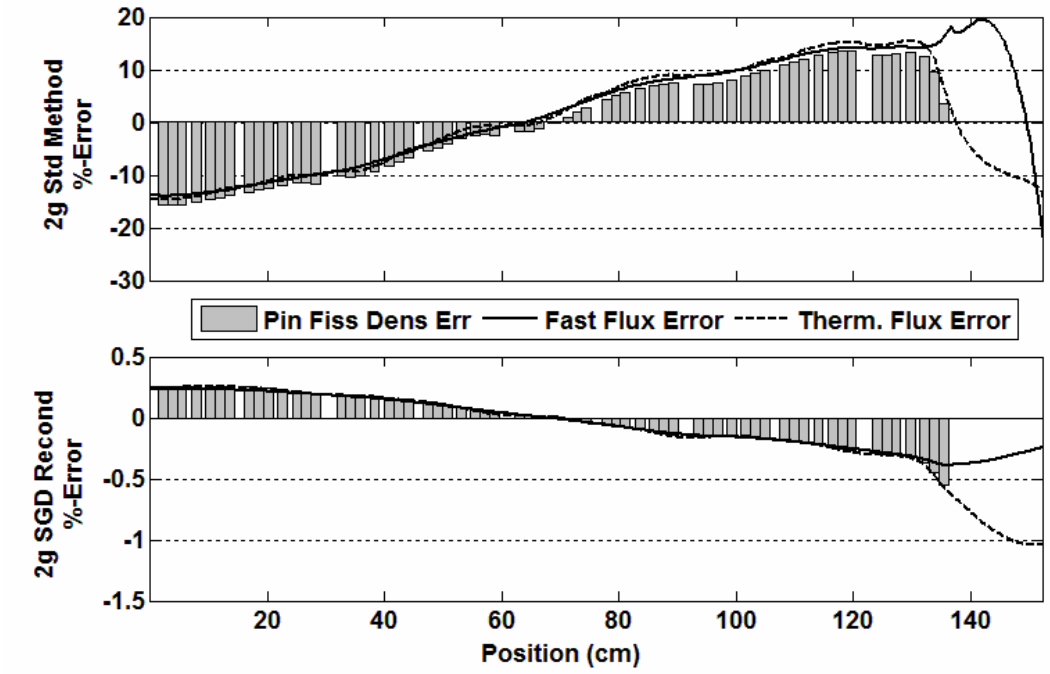


(a)

Figure 5.17: Pin fission density error and 2-group flux error of the standard and SGD recondensation methods for the (a) ARO and (b) SRI configurations

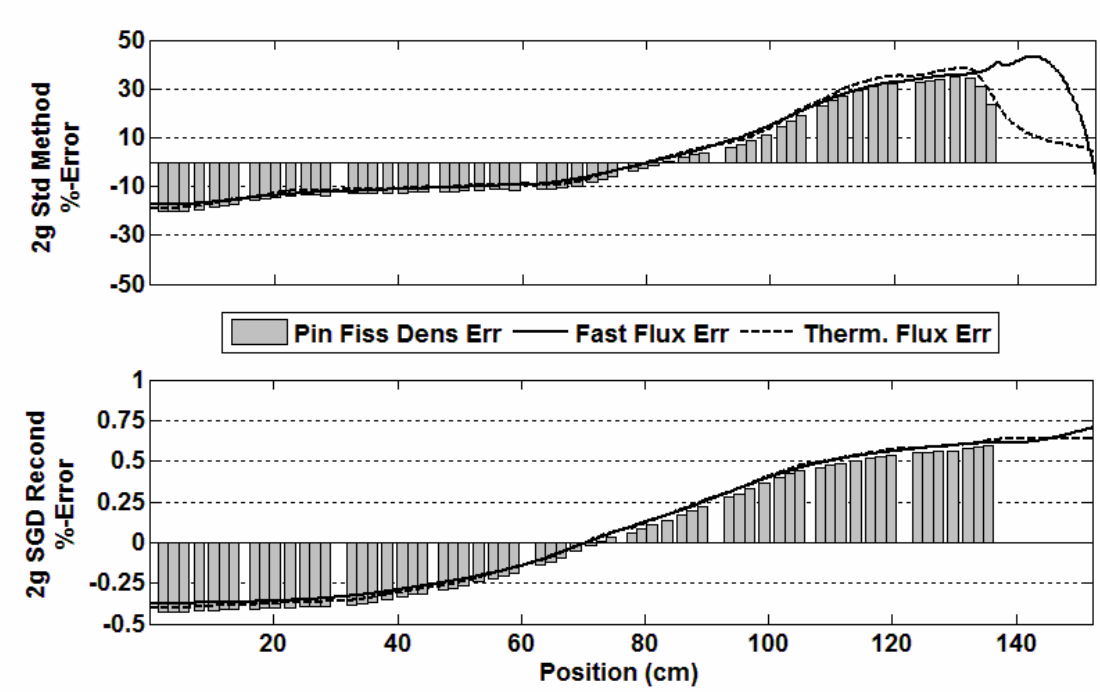


(b)

Figure 5.17 (continued)

A summary of the error in the pin fission densities for both the standard and SGD recondensation method is presented in Table 5.16, where the *Favg*, *Frms*, *Ffwe*, and *Fmax* error are defined in Eqs. (5.11)-(5.15). In the equations, $\tilde{f}_i$ is the calculated fission density and $f_i$ is the reference fission density of pin *i*.

$$e_i = 100\frac{\tilde{f}_i - f_i}{f_i} \tag{5.11}$$

$$Favg = \frac{\sum_i |e_i|}{I} \tag{5.12}$$

$$Frms = \sqrt{\frac{\sum_i |e_i|^2}{I}} \tag{5.13}$$

$$Ffwe = \frac{\sum_i |e_i| \tilde{f}_i}{\sum_i f_i} \tag{5.14}$$

$$Fmax = \max(|e_i|) \tag{5.15}$$

Table 5.16: BWR pin fission density error analysis

| | *Favg* | *Frms* | *Ffwe* | *Fmax* |
|---|---|---|---|---|
| ARO – 2g Std Method | 8.80 | 9.84 | 7.78 | 15.68 |
| ARO – 2g SGD Recond | 0.18 | 0.21 | 0.15 | 0.55 |
| SRI – 2g Std Method | 15.71 | 18.18 | 15.92 | 34.79 |
| SRI – 2g SGD Recond | 0.34 | 0.37 | 0.33 | 0.59 |

As demonstrated in Table 5.16, the SGD method provides a dramatic improvement in the accuracy of the pin fission densities, reducing the maximum error in the pin fission density from over 15% in the ARO configuration and over 34% in the SRI configuration to under 0.6%. The *Ffwe* is a PFD-weighted error and is the most physically relevant assessment of the average error. In the ARO configuration, the *Ffwe* is reduced from 7.8% to 0.15%, and in the SRI configuration, it is reduced from 15.9% to 0.33%.

### 5.2.3 HTTR Discrete Ordinates Reference Solution

As in the BWR problem, an $S_N$ reference solution is required to compare the results of the method. A 47-group cross section set was therefore obtained by modeling the HTTR core in HELIOS for both configurations (ARO and ARI) and generating cross sections for each material. The reference solution for both configurations was generated using a 47-group $S_8$ calculation with linear diamond differencing. The calculated eigenvalue of the ARO configuration was 1.1080 and of the ARI configuration was 0.8370. The 47-group reference scalar flux for both configurations is presented as a

function of position and lethargy in Figure 5.18 with the specular reflective boundary at position 283.51935 cm.

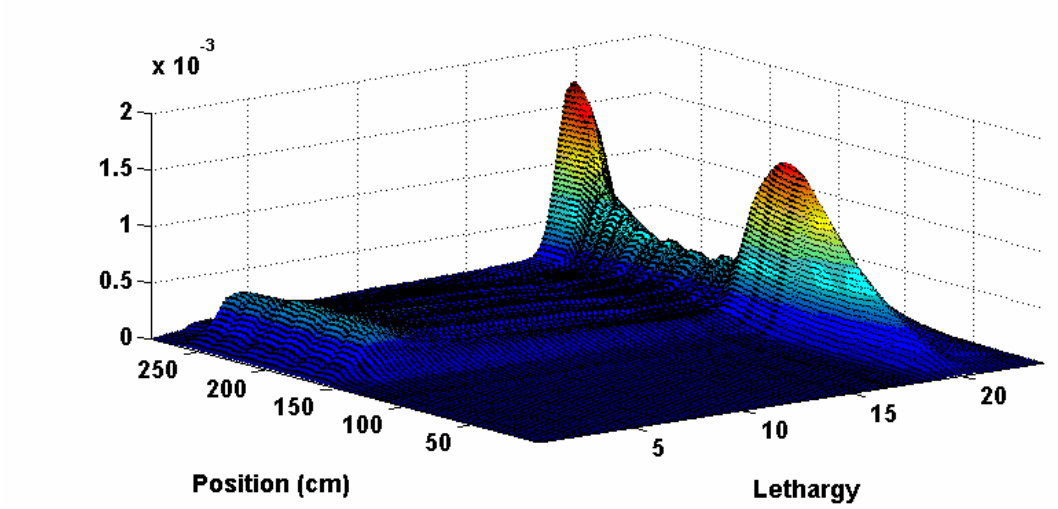


(a)

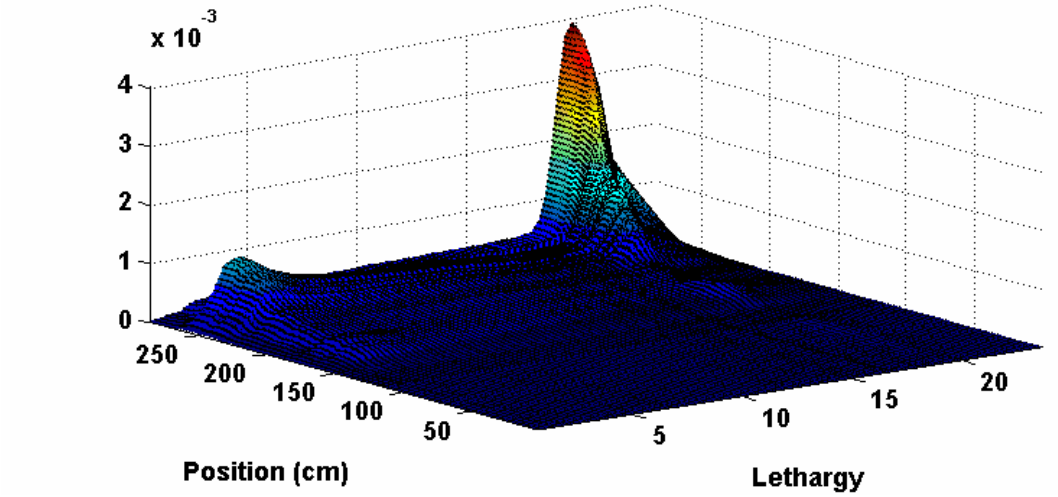


(b)

Figure 5.18. Reference 47-group scalar flux for HTTR benchmark problem for the (a) ARO and (b) ARI configurations.

In Figure 5.19, the reference pin fission density (PFD) is presented along with the 3-group reference flux. This flux consists of the thermal flux ($E < 0.625$ eV), the resonance region flux (0.625 eV $< E <$ 2.0347 keV) and the fission region ($E >$ 2.0347 keV). These boundaries correspond to the appropriate boundaries in the 6-group

structure commonly used in VHTR analysis (Zhang et. al., 2011). As before, the PFD is normalized to the number of fissionable pins (i.e. the average PFD = 1).

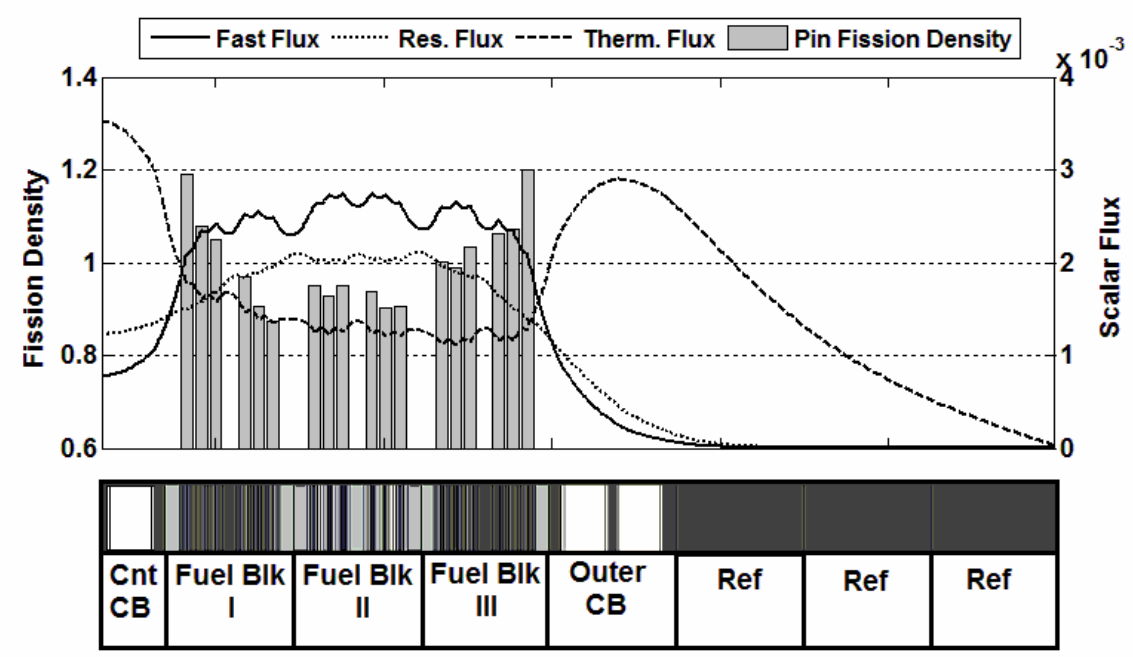


(a)

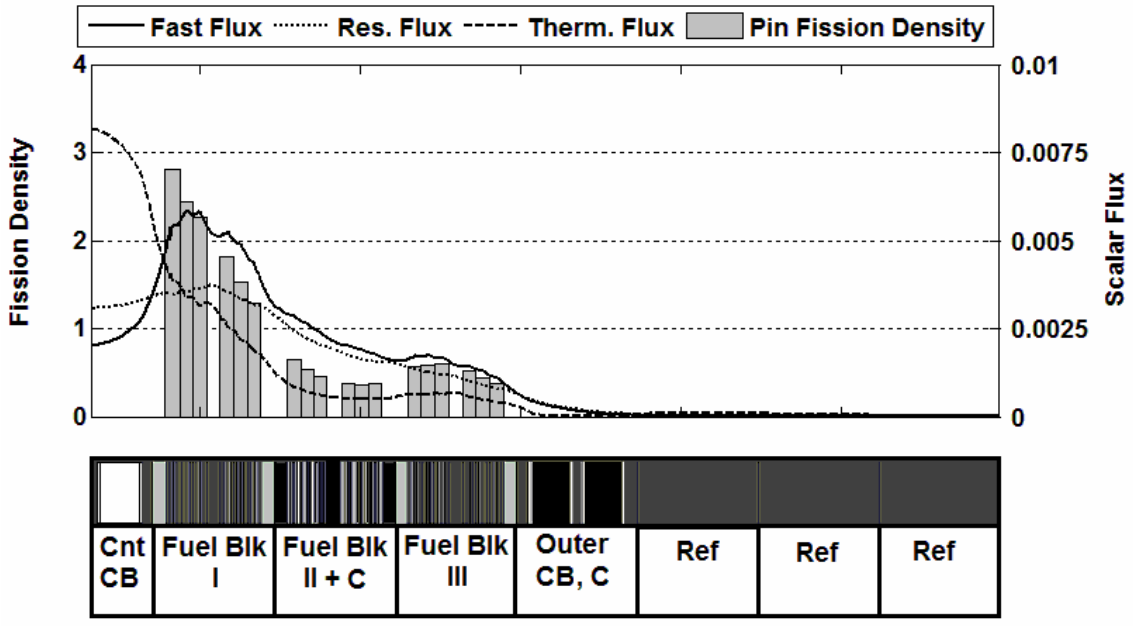


(b)

Figure 5.19. Reference 3-group flux and pin fission density for the (a) ARO and (b) SRI configurations.

### 5.2.4 SGD Verification with Transverse Integrated HTTR Core

In order to compare the SGD method with standard condensation method for the HTTR problem, the 2-group structure used in the BWR problem is insufficient. Instead, a common 6-group structure from VHTR literature is used for the coarse-group calculations (Zhang et. al, 2011). The results of these calculations are presented in Table 5.17. As in Table 5.15, the bundle-averaged fission density, capture density, and eigenvalue solutions are compared for both the ARO and ARI configuration.

Table 5.17. HTTR Core SGD Results

| | Center Cont | Fuel I | Fuel II | Fuel III | Outer Cont | Refl | Refl | Refl |
|---|---|---|---|---|---|---|---|---|
| **ARO CONFIGURATION** | | | | | | | | |
| | 47g Reference | | | | | | | |
| *fd* | | **1.01** | **0.93** | **1.06** | | | | |
| *cd* | **0.08** | **1.27** | **0.94** | **1.13** | **0.08** | **0.07** | **0.03** | **0.01** |
| | 6g Standard Method | | | | | | | |
| *fd %-err** | | -2.65 | 0.31 | 2.26 | | | | |
| *cd %-err** | -14.50 | -3.40 | -0.04 | 0.87 | -11.92 | -9.50 | -2.52 | 2.68 |
| | 6g SGD Recondensation Method (59 Itns) | | | | | | | |
| *fd %-err** | | -0.27 | 0.02 | 0.24 | | | | |
| *cd %-err** | -0.44 | -0.24 | 0.07 | 0.27 | 0.40 | 0.80 | 1.80 | 2.81 |
| | Reference k | | 6g Std Method | | dk (pcm) | 6g SGD Recond | | dk (pcm) |
| | 1.1080 | | 1.1160 | | 725 | 1.1074 | | -51 |
| **ARI CONFIGURATION** | | | | | | | | |
| | 47g Reference | | | | | | | |
| *fd* | | **2.03** | **0.46** | **0.51** | | | | |
| *cd* | **0.19** | **2.56** | **0.75** | **0.56** | **0.44** | **0.004** | **0.002** | **0.001** |
| | 6g Standard Method | | | | | | | |
| *fd %-err** | | 0.98 | -2.92 | -1.23 | | | | |
| *cd %-err** | -11.60 | -0.46 | -2.64 | -1.51 | -4.91 | -27.78 | -25.26 | -23.32 |
| | 6g SGD Recondensation Method | | | | | | | |
| *fd %-err** | | 0.05 | -0.05 | -0.15 | | | | |
| *cd %-err** | 0.10 | 0.04 | -0.05 | -0.15 | -0.20 | -0.93 | -2.25 | -3.74 |
| | Reference k | | 6g Std Method | | dk (pcm) | 6g SGD Recond | | dk (pcm) |
| | **0.8370** | | 0.8483 | | 1354 | 0.8371 | | 21 |

* *fd* = bundle averaged fission density, *cd* = bundle averaged non-fission capture density
*fd %-err* = % difference between fission density and reference *fd*
*cd %-err* = % difference between non-fission capture density and reference *cd*

As expected, the standard method results in large errors in the bundle fission density for the HTTR core particularly when the flux spectrum is most different from the lattice-cell spectrum. This was significant in this problem towards the periphery, where the large amount of reflector has attenuated the outgoing flux. In the ARI configuration, this is even more apparent, resulting in 27% error in the capture density within the reflectors.

As seen in the table, the errors in the capture density using the SGD method were larger (3%) than in the BWR problem (< 1%). It was found that this was because a convergence criteria of 0.1% for the cross sections was not tight enough for this type of problem, which exhibits a harder thermal spectrum than the BWR. As will be seen in the next section, this can be corrected by tightening the convergence criteria of the cross sections. However, it is noted that the flux in the outer two reflector blocks of the problem is negligibly small, and thus the 3% error in the capture density has a negligible effect on the overall core solution. Improving the solution in that region by tightening the convergence criteria, while possible, is not computationally efficient.

As in BWR analysis, effectively capturing the local transport results is important in VHTR analysis, particularly for reactivity effects of burnable poisons. Figure 5.20 presents the pin-fission density error and the %-error in the 3-group scalar flux distribution for the standard method and the 6-group SGD recondensation method. For the sake of clarity, both the 47-group reference and the results of the 6-group standard method and SGD recondensation are integrated into the 3-group structure (thermal, resonance, fast) described in the previous section.

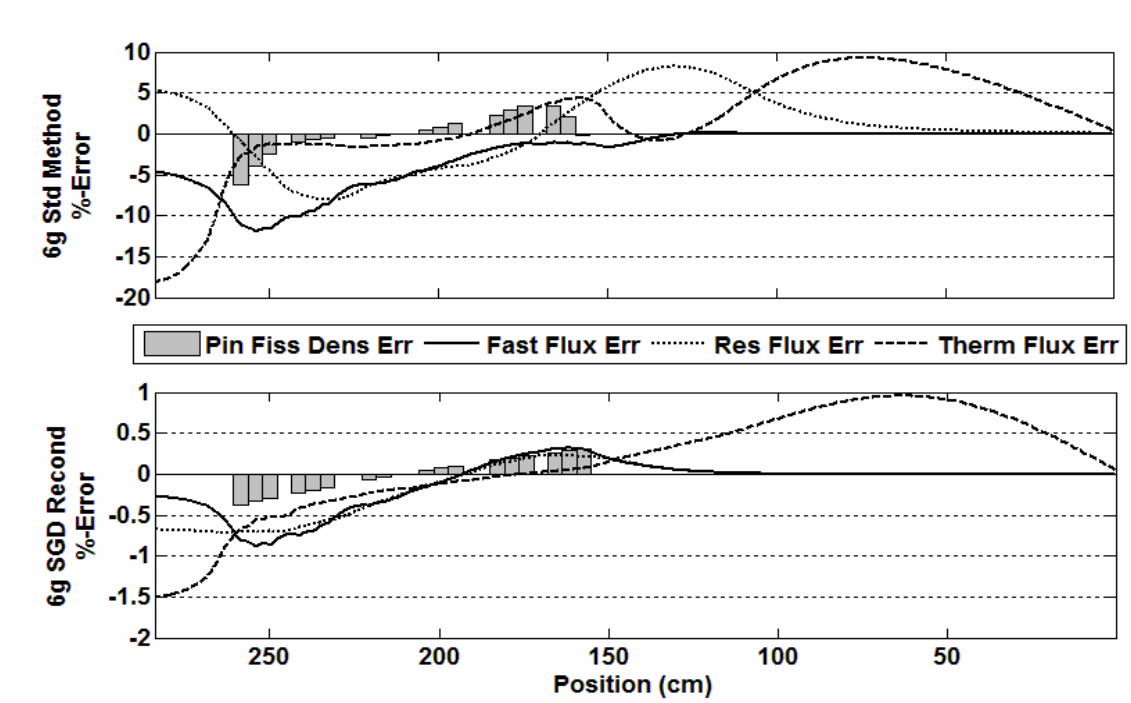


(a)

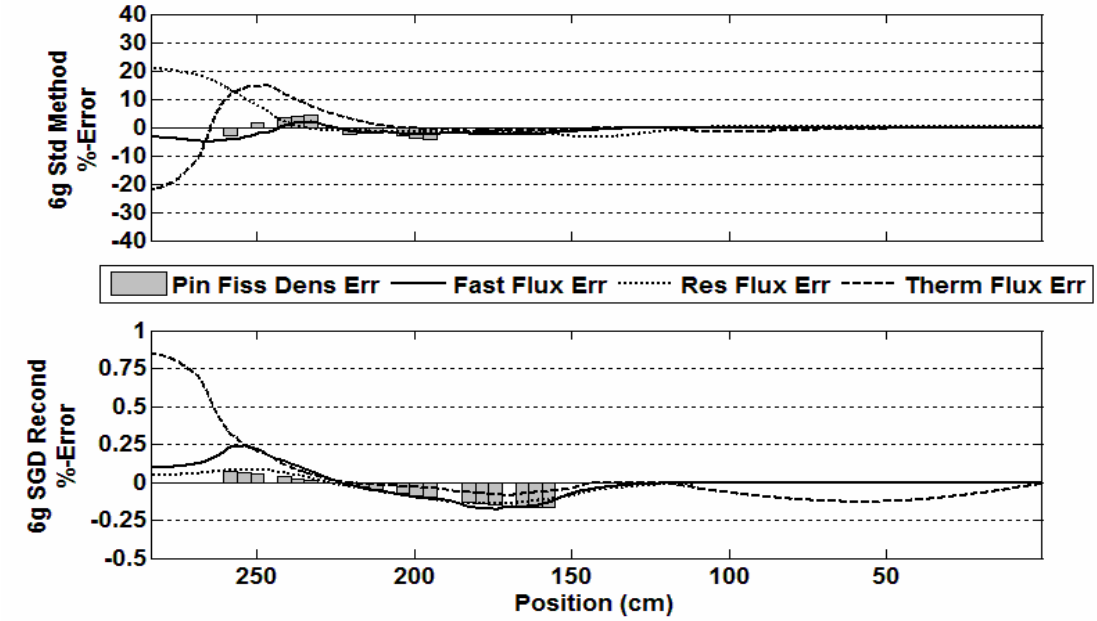


(b)

Figure 5.20: Pin fission density error and 3-group flux error of the standard and SGD recondensation methods for the (a) ARO and (b) ARI configurations

As in the BWR case, an error analysis of the pin fission density is presented in Table 5.18.

Table 5.18: HTTR pin fission density error analysis

| | *Favg* | *Frms* | *Ffwe* | *Fmax* |
|---|---|---|---|---|
| ARO – 6g Std Method | 1.81 | 2.43 | 1.89 | 6.19 |
| ARO – 6g SGD Recond | 0.19 | 0.22 | 0.19 | 0.37 |
| ARI – 6g Std Method | 2.34 | 2.66 | 2.29 | 4.51 |
| ARI – 6g SGD Recond | 0.09 | 0.10 | 0.07 | 0.17 |

As demonstrated in the table, the SGD method provides a dramatic improvement in the accuracy of the pin fission densities, reducing the maximum error in the pin fission density from over 6% in the ARO configuration and over 4% in the ARI configuration to under 0.4% and 0.2% respectively.

### 5.2.5 Decomposed Spectrum Error

In the previous sections, the recondensed coarse-group solution with the SGD method was compared for the BWR and HTTR problems. In this section, the decomposed fine-group flux obtained with the SGD recondensation procedure is compared to the reference fine-group solution. This is done with a "decomposed flux error" function, $DFE(x, p)$, defined in Eqs. (5.16) and (5.17).

$$e_h(x,\mu_p) = \frac{\tilde{\Psi}_h(x,\mu_p) - \Psi_h^{REF}(x,\mu_p)}{\Psi_h^{REF}(x,\mu_p)} \tag{5.16}$$

$$DFE(x, p) = 100 \frac{\sum_{h=1}^{H} \left| e_h(x,\mu_p) \right| \tilde{\Psi}_h(x,\mu_p)}{\sum_{h=1}^{H} \Psi_h^{REF}(x,\mu_p)} \tag{1.17}$$

where $\tilde{\Psi}_h(x,\mu_p)$ is the decomposed angular flux in direction $\mu_p$ and fine-group $h$ produced with the SGD method, $\Psi_h^{REF}(x,\mu_p)$ is the fine-group reference solution for the

problem, and $e_h(x,\mu_p)$ is the relative error of the decomposed solution. *DFE* is therefore a flux-weighted relative error function, and it is plotted in Figure 5.21 for the controlled configurations of the BWR (SRI) and HTTR (ARI) problem.

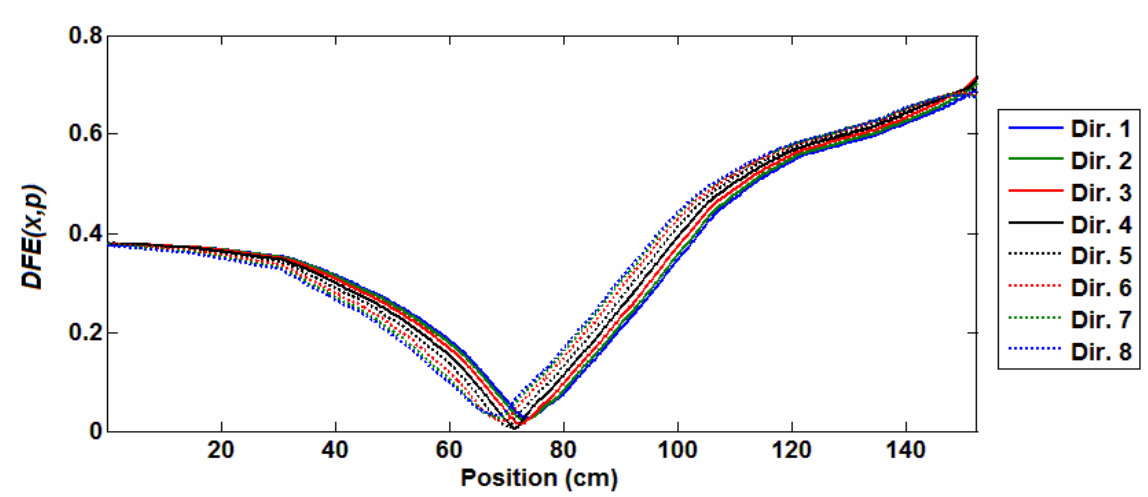


(a)

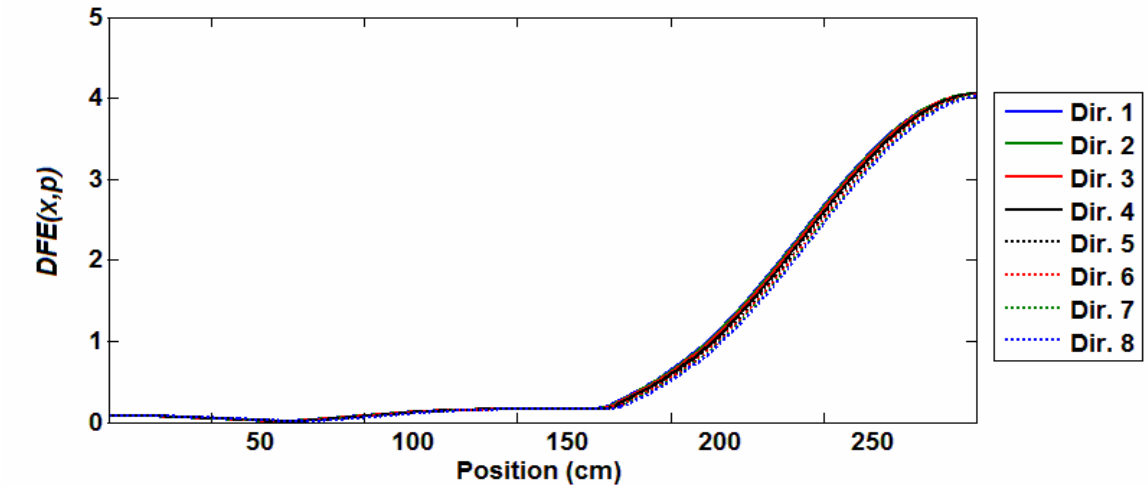


(b)

Figure 5.21: Plot of $DFE(x, p)$ for each direction $p$ for the
(a) BWR – SRI configuration and the (b) HTTR – ARI configuration

As seen in the figure, the SGD decomposed spectrum is highly accurate for both cores. In the BWR, the decomposed flux error is less than 0.8% for all directions

throughout the core. For the HTTR, the spectrum is highly accurate and within 0.5% error for the fissionable and control regions, but approaches 4% error towards the periphery. As discussed previously, this does not significantly affect the coarse-group cross sections, which are converged to within 0.1%, and further convergence is possible, but not generally necessary.

### 5.2.6. SGD Group Structure Dependence

The major benefit of the SGD method is that, instead of solving the fine-group transport equation, which is overly time consuming because one must converge a fine-group source and eigenvalue, the coarse-group transport equation can be solved, the fine-group flux decomposed, and the coarse-group cross sections recondensed more rapidly. As mentioned earlier, because the condensation process in the SGD method consistently treats the energy angle coupling in the coarse-group solution and decomposes the flux from that solution, the final solution of the SGD method is independent of the coarse group structure chosen. As a result, if the reference solution is used to condense the cross sections, the coarse group structure is irrelevant. This is demonstrated by calculating the lattice-cell spectrum for the fresh, unvoided bundle of the BWR problem with specular boundary conditions and using this exact spectrum to condense the cross sections into five different group structures presented in Figure 5.22. The 2, 4, and 8 group structures are commonly used in LWR analysis (Douglass and Rahnema, 2010b), and the 6-group structure is common in VHTR analysis (Zhang et. al, 2011).

| 1-Group | 2-Group | 4-Group | 6-Group | 8-Group | Energy (eV) |
|---|---|---|---|---|---|
| --- | --- | --- | --- | --- | 2.0000E+07 |
| | | | | --- | 2.2313E+06 |
| | | | | --- | 8.2085E+05 |
| | | | --- | | 1.8316E+05 |
| | | --- | | --- | 9.1188E+03 |
| | | | --- | | 2.0347E+03 |
| | | | | --- | 1.3007E+02 |
| | | --- | | --- | 3.9279E+00 |
| | | | --- | | 2.3824E+00 |
| | --- | --- | --- | --- | 6.2506E-01 |
| | | | | --- | 1.4572E-01 |
| | | | --- | | 1.1157E-01 |
| --- | --- | --- | --- | --- | 1.0000E-04 |

Figure 5.22. Coarse-group Structures

The SGD method is then used for only this lattice, so no core-environment effects are present, and the fine-group flux is decomposed. In this case, the SGD method is expected to exactly reproduce the fine-group lattice cell flux to within the convergence criteria of the coarse-group calculation. In order to determine the accuracy of the decomposed flux for each group structure, the decomposed flux error function, *DFE* was averaged over the discrete directions, and the results are presented in Figure 5.23.

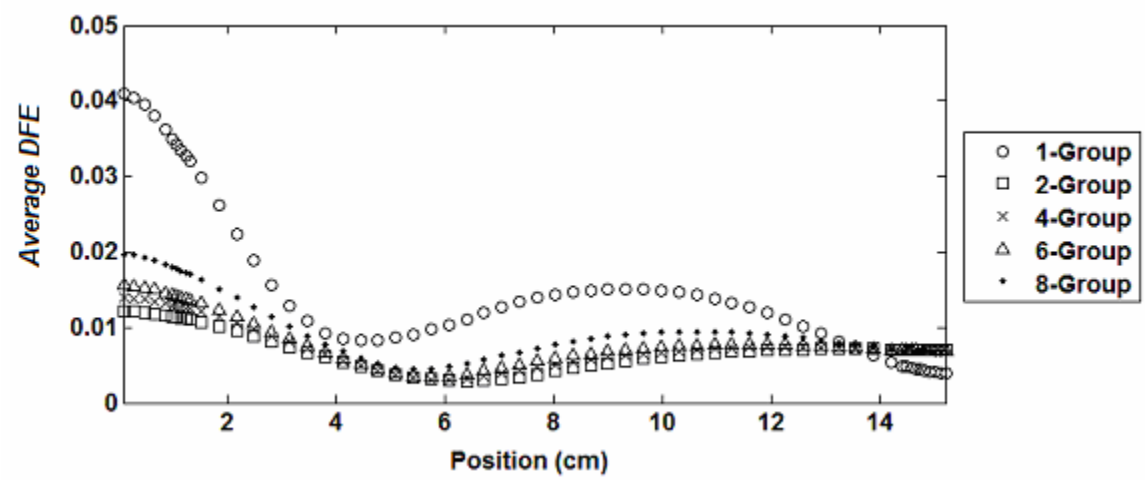


Figure 5.23: Directional Average of *DFE(x,p)* for the SGD spectrum using various coarse-group structures

It is clear from Figure 5.24 that the group structure chosen does not have a significant effect on the accuracy of the decomposed spectrum. For all group structures except the 1-group, the error function had a maximum value of 0.02%, which is within convergence. As was mentioned in section 3.4, if very few groups are used, convergence to a specified convergence criteria does not produce as accurate a solution as converging several groups to the same convergence criteria. In this problem, this results in the 1-group decomposed spectrum having slightly more error when the flux convergence of the transport calculation was $10^{-4}$. To demonstrate that this can be eliminated by tighter convergence, Table 5.19 contains the results of the SGD calculation for the bundle for each group structure using the $10^{-6}$ eigenvalue convergence criteria and $10^{-4}$ flux convergence criteria that is used for all other calculations in this paper, as well as the result of a 1-group SGD calculation with the flux converged further to a criterion of $10^{-5}$.

Table 5.19: GE9 1D lattice-cell SGD results varying group structure.

| | $k_{inf}$ | d$k_{inf}$ (pcm) | max(*DFE(x,p)*) | avg(*DFE(x,p)*) | Time (s) |
|---|---|---|---|---|---|
| Reference | 1.0533 | - | - | - | 111.8 |
| 1G + Decomp | 1.0533 | -1 | 0.0469 | 0.0145 | 1.4 |
| 2G + Decomp | 1.0533 | -1 | 0.0131 | 0.0065 | 2.0 |
| 4G + Decomp | 1.0533 | -1 | 0.0153 | 0.0071 | 2.5 |
| 6G + Decomp | 1.0533 | -1 | 0.0174 | 0.0076 | 2.9 |
| 8G + Decomp | 1.0533 | -2 | 0.0224 | 0.0092 | 3.1 |
| 1G + Decomp* | 1.0533 | 0 | 0.0125 | 0.0067 | 1.5 |

* flux convergence of $10^{-5}$

As demonstrated in the table, the SGD method is highly effective in reproducing the reference spectrum from a coarse-group calculation independent of the coarse-group structure chosen. Even for a 1-group calculation with standard convergence criteria, the maximum mean relative error was less than 0.05%, but with a tighter convergence, this was reduced to 0.0125%.

As described in section 3.4, the SGD recondensation method will eventually result in the same solution independent of group structure if a tight enough convergence is used, though the number of coarse-groups can significantly impact the number of iterations required to converge the coarse-group cross sections and the length of time needed for each coarse-group calculation. In order to examine this effect for each problem, the SGD recondensation procedure was used with the 5 different group structures in Figure 5.22 to solve the BWR and HTTR Cores.

It is noted that the 6-group structure would generally not result in good solutions for the LWR problem and vice-versa, however, one of the benefits of the SGD method is that the converged solution is independent of the coarse-group structure, and it is desired to determine how the method performs when an inappropriate coarse-group structure is used. Therefore, every coarse-group structure is used for both of the problems to

demonstrate the effect on the convergence rate and on the accuracy of the final converged solution. In order to examine the effect of the coarse-group structure on the convergence rate, Figure 5.24 presents the maximum %-difference between successive iterations of the coarse-group cross sections is plotted as a function of iteration and computation time for both configurations of the BWR core.

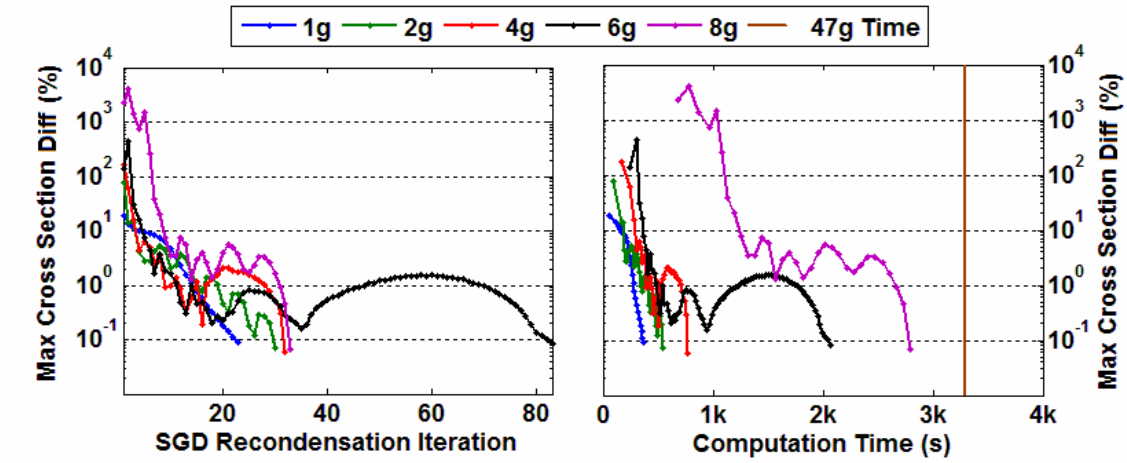


(a)

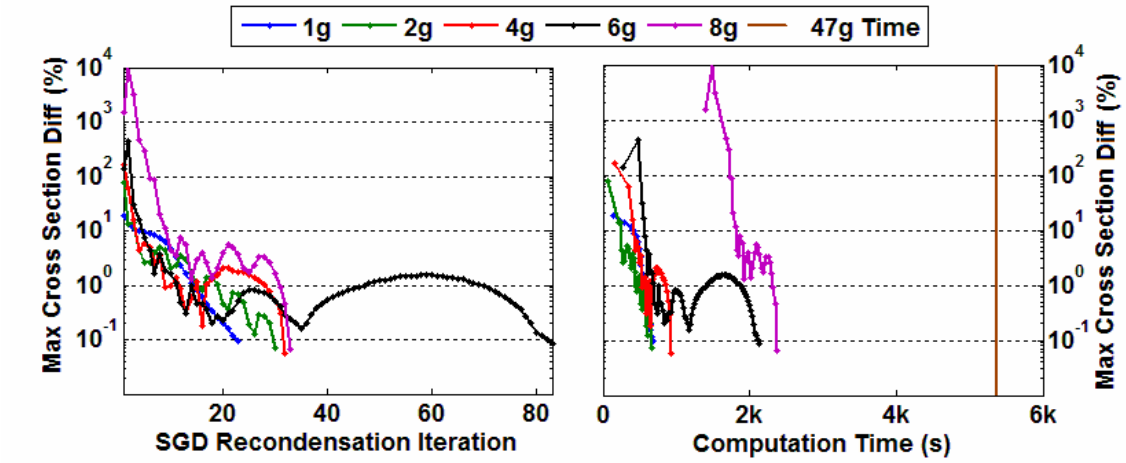


(b)

Figure 5.24: Cross section convergence vs. iteration and computation time for the (a) ARO and (b) SRI configurations of the BWR core.

As seen in the figure, the group structure chosen can have a very significant effect on the convergence of the cross sections. The 6-group structure is known to be a poor structure for LWR analysis, which necessitated many more iterations to successfully converge the cross sections. The other group structures, which were designed for LWRs, performed better in terms of iterations, but as seen on the right side of the graphs, did not necessarily perform as well in computation time. In the ARO configuration, using an 8-group structure required almost as much time to generate the solution as the 47-group reference. However, using a 1-group or 2-group structure produced a converged set of coarse-group cross sections much more rapidly.

In order to examine the effect of group structure on the final converged solution, the directional average of the decomposed flux error function, *DFE*, was calculated for the final decomposed flux spectrum for each coarse-group structure. These are presented in Figure 5.25 for both configurations of the BWR core.

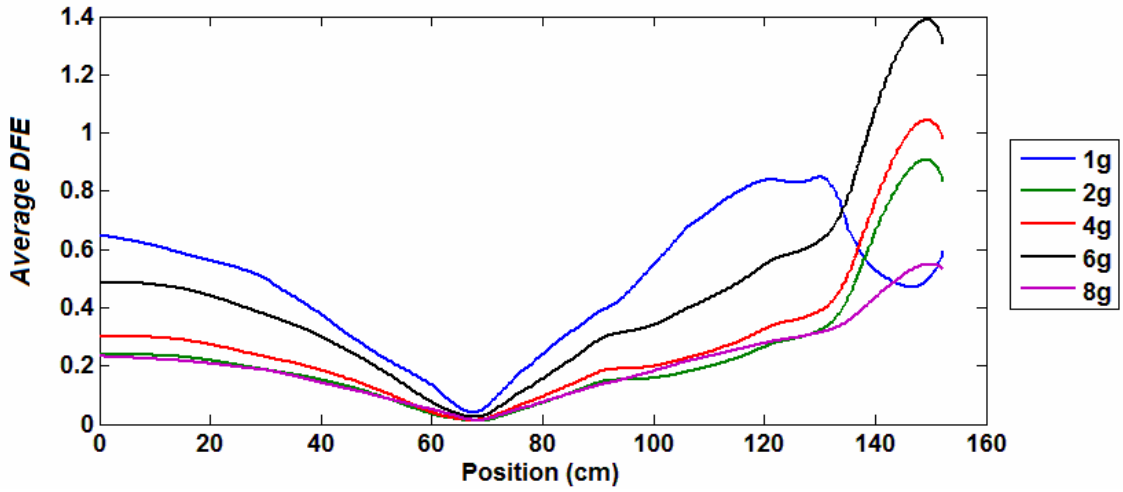


(a)

Figure 5.25: Directional Average of *DFE(x,p)* for each coarse-group structure of the (a) ARO and (b) SRI configuration of the BWR core.

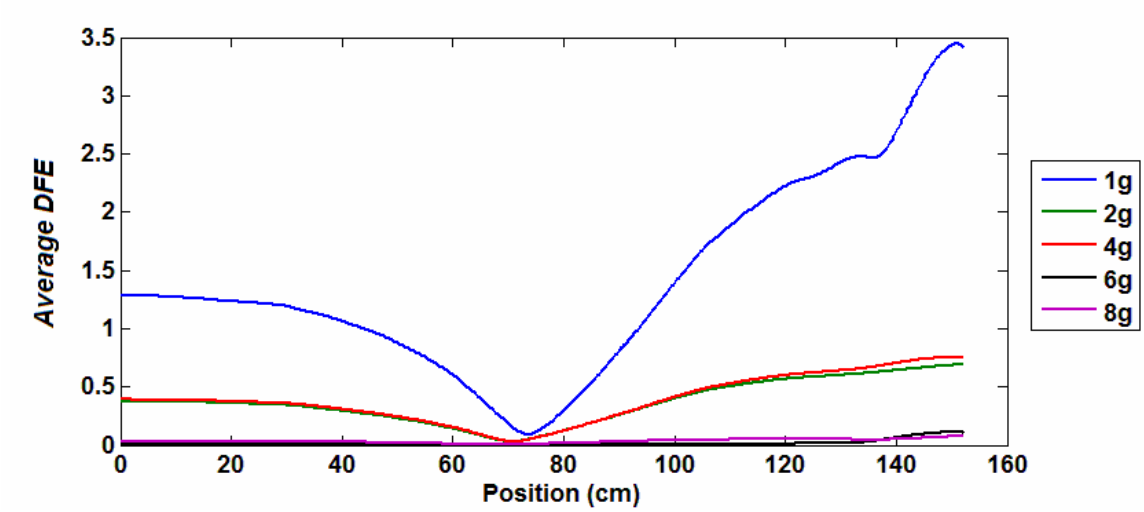


(b)

Figure 5.25 (continued)

As seen in the figure, and as expected, while the SGD recondensation results in the correct solution independent of group structure given a tight enough convergence criteria, when that criteria is fixed, using more groups generally results in more accurate results for the final solution. The results for the ARO core also indicate that the appropriateness of the group boundaries can play a significant role in the accuracy of the converged solution. The 6-group structure is not generally appropriate for LWR problems, and in the ARO configuration, it resulted in a marginally less accurate solution than the 2, 4, and 8-group structures. Table 5.20 presents the SGD recondensation eigenvalue for the BWR core for both configurations. The table highlights the benefit of the SGD recondensation method as a design tool. As expected, the standard method performs better with increasing coarse group structure, and the eigenvalue converges more rapidly as the number of coarse groups increases. If one does not possess the time or capacity to generate a fine-group solution, even 5 iterations of the SGD method can provide a dramatically improved eigenvalue with as few as 2 groups.

Table 5.20: BWR SGD eigenvalue results for various group structures.

| | ARO CONFIGURATION | | | | | | | | | |
|---|---|---|---|---|---|---|---|---|---|---|
| | 1g | | 2g | | 4g | | 6g | | 8g | |
| itn | *k* | d*k* (pcm) | *k* | d*k* (pcm) | *k* | d*k* (pcm) | *K* | d*k* (pcm) | *k* | d*k* (pcm) |
| 1* | 1.0744 | 712 | 1.0704 | 336 | 1.0690 | 208 | 1.0681 | 119 | 1.0674 | 53 |
| 2 | 1.0686 | 165 | 1.0674 | 51 | 1.0670 | 16 | 1.0669 | 8 | 1.0669 | 6 |
| 3 | 1.0678 | 94 | 1.0670 | 16 | 1.0667 | -10 | 1.0667 | -7 | 1.0668 | -1 |
| 4 | 1.0677 | 83 | 1.0671 | 25 | 1.0667 | -14 | 1.0667 | -6 | 1.0668 | -1 |
| 5 | 1.0677 | 80 | 1.0670 | 20 | 1.0667 | -13 | 1.0667 | -9 | 1.0668 | 1 |
| 10 | 1.0673 | 43 | 1.0667 | -14 | 1.0668 | -4 | 1.0668 | -5 | 1.0668 | 3 |
| 15 | 1.0670 | 21 | 1.0668 | 0 | 1.0668 | 1 | 1.0668 | -1 | 1.0668 | 3 |
| 20 | 1.0669 | 11 | 1.0668 | 3 | 1.0668 | 4 | 1.0668 | 2 | 1.0668 | 3 |
| Final | 1.0669 | 8 | 1.0669 | 5 | 1.0669 | 7 | 1.0669 | 9 | 1.0668 | 3 |
| itns: | 23 | | 30 | | 32 | | 83 | | 33 | |
| | SRI CONFIGURATION | | | | | | | | | |
| | 1g | | 2g | | 4g | | 6g | | 8g | |
| itn | *k* | d*k* (pcm) | *k* | d*k* (pcm) | *k* | d*k* (pcm) | *k* | d*k* (pcm) | *k* | d*k* (pcm) |
| 1* | 1.0188 | 1537 | 1.0088 | 531 | 1.0061 | 269 | 1.0047 | 131 | 1.0042 | 76 |
| 2 | 1.0062 | 274 | 1.0044 | 98 | 1.0036 | 21 | 1.0034 | -8 | 1.0034 | 2 |
| 3 | 1.0050 | 160 | 1.0039 | 44 | 1.0033 | -11 | 1.0032 | -24 | 1.0033 | -10 |
| 4 | 1.0048 | 137 | 1.0039 | 46 | 1.0032 | -19 | 1.0032 | -20 | 1.0034 | -5 |
| 5 | 1.0048 | 132 | 1.0038 | 32 | 1.0032 | -21 | 1.0032 | -24 | 1.0034 | -3 |
| 10 | 1.0040 | 61 | 1.0032 | -21 | 1.0033 | -15 | 1.0032 | -20 | 1.0034 | -3 |
| 15 | 1.0036 | 22 | 1.0034 | -7 | 1.0033 | -11 | 1.0033 | -16 | 1.0034 | -2 |
| 20 | 1.0034 | -4 | 1.0034 | -6 | 1.0033 | -8 | 1.0033 | -13 | 1.0034 | -1 |
| Final | 1.0033 | -10 | 1.0034 | -5 | 1.0034 | -4 | 1.0034 | 1 | 1.0034 | 0 |
| itns: | 23 | | 30 | | 32 | | 83 | | 33 | |

*the 1st iteration represents the standard coarse-group condensation method

Another important conclusion which can be drawn from the table is that for this problem, converging the cross sections to within 0.1% resulted in an eigenvalue error of < 10 pcm in the final solution, independent of group structure. In addition, noting the computation time in Figure 5.24, performing the 1-group SGD calculation can be done more quickly and result in a more accurate solution than performing a standard 8-group calculation.

Because the HTTR core presents a different set of challenges than the BWR core, it is important to examine the effects of the coarse-group structure on the convergence rate and final solution for that problem as well. Figure 5.26 presents the cross section convergence rate, Figure 5.27 presents the directional average of *DFE(x,p)*, and Table 5.21 presents the eigenvalue results for each group structure in the ARO and ARI configuration of the HTTR problem.

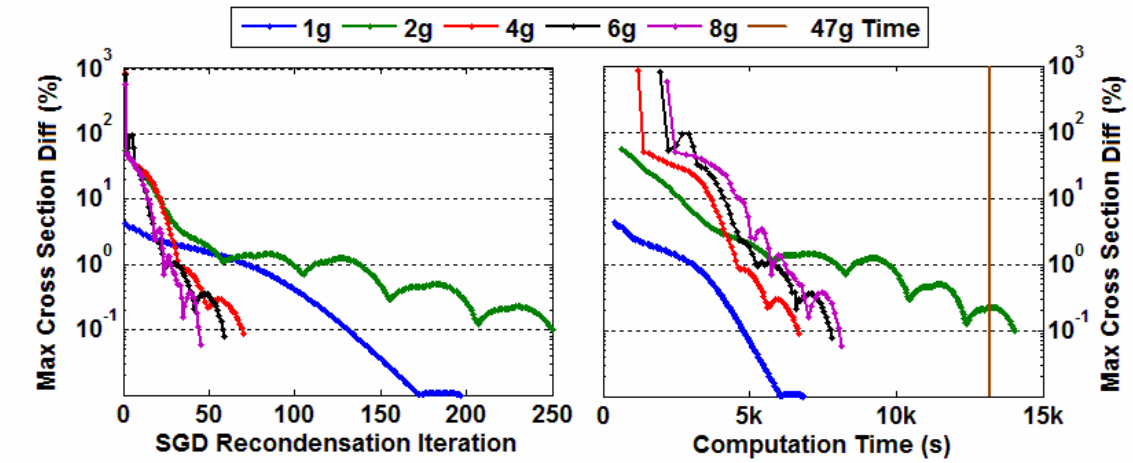


(a)

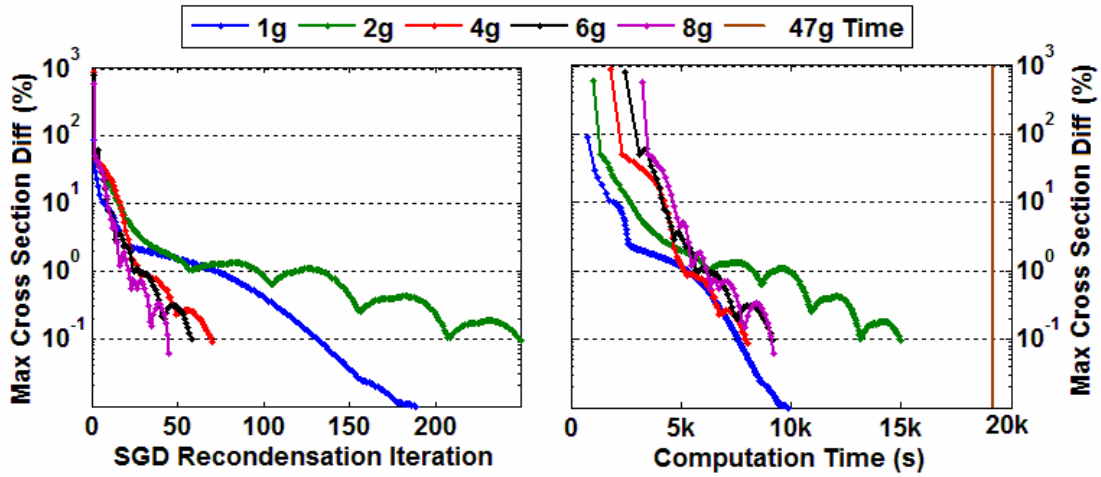


(b)

Figure 5.26: Cross section convergence vs. iteration and computation time for the (a) ARO and (b) ARI configurations of the HTTR core.

Of note in Figure 5.26 is that the 1-group cross sections were converged beyond the 0.1% that the other coarse-group cross sections were converged to. As mentioned in section 3.4, using a very small number of groups may require a tighter convergence of the cross sections to obtain a converged flux spectrum. In this problem, with the 1-group structure, the eigenvalue and flux distribution still varied significantly after the cross sections had converged to 0.1% and so the convergence was tightened in this case to 0.01% for the cross sections. Also of note in Figure 5.26 is that, except for the 2-group structure, the computation time is roughly independent of the group structure chosen. For the 4, 6, and 8-group structures, increasing the number of groups necessitates fewer SGD iterations, but each iteration takes longer. For the 1-group case, the need to perform additional iterations compensated for the faster calculation of each iteration, resulting in a similar computational time as the 4, 6, and 8-group structures.

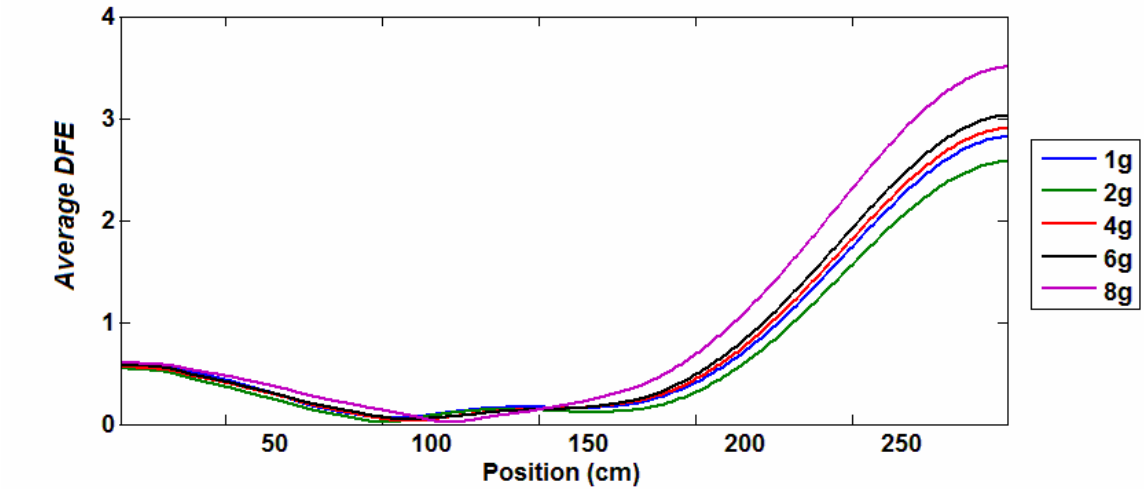


(a)

Figure 5.27: Directional Average of *DFE(x,p)* for each coarse-group structure of the (a) ARO and (b) ARI configuration of the HTTR core.

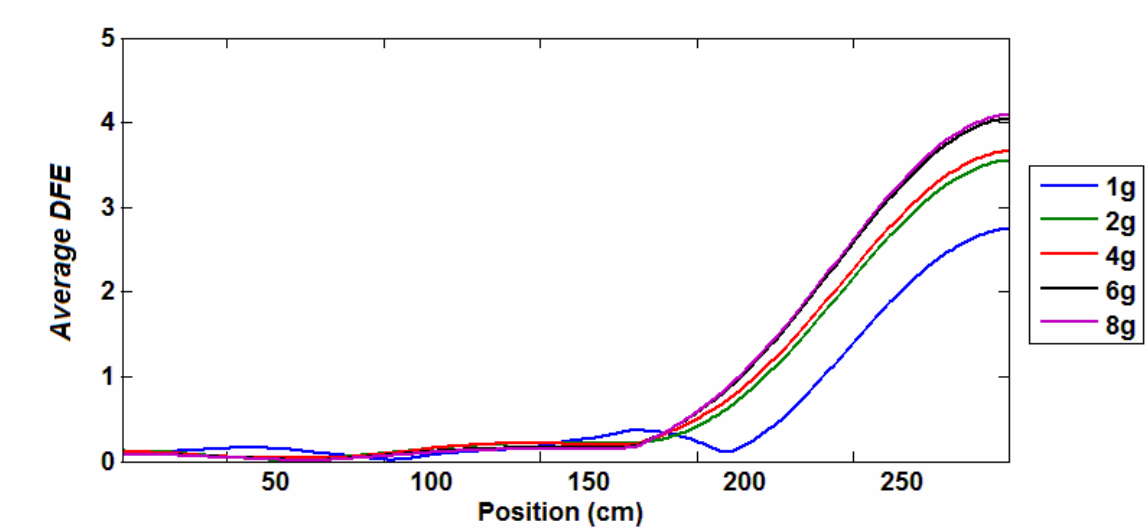


(b)

Figure 5.27 (continued)

As seen in Figure 5.27, the decomposed flux spectrum of the converged SGD calculation is essentially independent of the group structure chosen. Even the 2-group structure, which took the longest to converge, produced a final result with similar accuracy as the other group structures.

Unlike in the BWR problem, the long mean free path, reduced capture rate, and large quantity of non-fissionable regions in the HTTR problem result in a much slower convergence. As is seen in Table 5.21, the HTTR problem required significantly more iterations than the BWR problem to converge, and the initial iterations did not approach the final solution as rapidly. Nonetheless, the SGD method with an appropriately chosen group structure is a more efficient method than the fine-group calculation, and converges to the correct solution independent of the coarse-group structure chosen.

Table 5.21: HTTR SGD eigenvalue results for various group structures.

| | ARO CONFIGURATION | | | | | | | | | |
|---|---|---|---|---|---|---|---|---|---|---|
| | 1g[+] | | 2g | | 4g | | 6g | | 8g | |
| itn | *k* | d*k* (pcm) | *k* | d*k* (pcm) | *k* | d*k* (pcm) | *k* | d*k* (pcm) | *k* | d*k* (pcm) |
| 1* | 1.1296 | 1954 | 1.1229 | 1344 | 1.1205 | 1124 | 1.1160 | 725 | 1.1148 | 612 |
| 2 | 1.1268 | 1697 | 1.1211 | 1180 | 1.1185 | 951 | 1.1134 | 485 | 1.1122 | 378 |
| 3 | 1.1257 | 1599 | 1.1200 | 1081 | 1.1172 | 827 | 1.1118 | 341 | 1.1110 | 267 |
| 4 | 1.1246 | 1499 | 1.1189 | 986 | 1.1161 | 729 | 1.1107 | 244 | 1.1100 | 183 |
| 5 | 1.1235 | 1404 | 1.1179 | 898 | 1.1151 | 643 | 1.1100 | 180 | 1.1093 | 117 |
| 10 | 1.1190 | 993 | 1.1142 | 558 | 1.1116 | 325 | 1.1085 | 48 | 1.1075 | -44 |
| 20 | 1.1125 | 411 | 1.1117 | 332 | 1.1081 | 13 | 1.1075 | -41 | 1.1072 | -71 |
| 30 | 1.1104 | 216 | 1.11087 | 259 | 1.1073 | -66 | 1.1073 | -60 | 1.1075 | -47 |
| 40 | 1.1097 | 154 | 1.1100 | 176 | 1.1073 | -60 | 1.1075 | -48 | 1.1075 | -47 |
| Final | 1.1073 | -61 | 1.1077 | -29 | 1.1076 | -35 | 1.1074 | -51 | 1.1075 | -46 |
| itns: | 197 | | 250 | | 70 | | 59 | | 45 | |
| | ARI CONFIGURATION | | | | | | | | | |
| | 1g[+] | | 2g | | 4g | | 6g | | 8g | |
| itn | *k* | d*k* (pcm) | *k* | d*k* (pcm) | *k* | d*k* (pcm) | *k* | d*k* (pcm) | *k* | d*k* (pcm) |
| 1* | 0.8791 | 5034 | 0.8628 | 3092 | 0.8550 | 2163 | 0.8483 | 1354 | 0.8462 | 1106 |
| 2 | 0.8654 | 3407 | 0.8574 | 2446 | 0.8498 | 1534 | 0.8441 | 857 | 0.8434 | 772 |
| 3 | 0.8602 | 2774 | 0.8557 | 2242 | 0.8481 | 1329 | 0.8426 | 679 | 0.8419 | 590 |
| 4 | 0.8563 | 2311 | 0.8539 | 2030 | 0.8467 | 1161 | 0.8415 | 550 | 0.8408 | 462 |
| 5 | 0.8532 | 1945 | 0.8523 | 1835 | 0.8454 | 1015 | 0.8407 | 451 | 0.8400 | 362 |
| 10 | 0.8435 | 783 | 0.8466 | 1153 | 0.8412 | 512 | 0.8388 | 223 | 0.8378 | 105 |
| 20 | 0.8342 | -325 | 0.8431 | 742 | 0.8380 | 131 | 0.8376 | 74 | 0.8370 | 7 |
| 30 | 0.8303 | -795 | 0.8421 | 622 | 0.8372 | 31 | 0.8371 | 18 | 0.8371 | 19 |
| 40 | 0.8305 | -774 | 0.8408 | 459 | 0.8370 | 12 | 0.8370 | 5 | 0.8371 | 17 |
| Final | 0.8364 | -70 | 0.8371 | 23 | 0.8372 | 26 | 0.8371 | 21 | 0.8371 | 15 |
| itns: | 188 | | 249 | | 70 | | 58 | | 45 | |

*the 1st iteration represents the standard coarse-group condensation method

[+]the 1-group SGD recondensation was converged to 0.01% cross section difference

# CHAPTER 6

# CONCLUSIONS

This dissertation has presented the development of two new methods for treating the energy variable in radiation transport applications. Both of these methods operate within the context of "consistent" group condensation. This would be more generally referred to as a concept of "group structure equivalency," as it describes the multigroup formulation which exactly preserves the detailed spectrum of the equation. The standard practice in radiation transport has been to somewhat neglect this equivalency, preferring the ease of implementation from ignoring the energy-angle coupling of the angular flux in the definition of the total cross section.

This lack of consistency in the multigroup / coarse-group formulation is not a new revelation, and has been at least acknowledged since the 1970s. It is only now, however, that computational power has increased to the point that other approximations, which have traditionally masked or cancelled out the effects, have been, or are on the way to being eliminated. It is therefore now, that the industry must begin to examine the manner in which the multigroup method is applied, and take care to ensure consistency at every level of group condensation. The results in this dissertation have indicated that the error introduced when the energy variable is treated inconsistently in coarse-group whole-core transport, can be very large, but that by implementing a consistent multigroup formulation, the detailed spectral effects can be preserved, independent of the group structure.

The two multigroup methods that have been presented in this dissertation, the CGEC theory and the SGD method, are primarily designed as an "inverse" of the group

condensation process. The CGEC method, by expanding the flux in orthogonal functions, can result in an approximate "unfolded" flux spectrum, and due to the decoupling of the higher-order terms, can do so relatively quickly, but is only accurate up to the order of expansion. The SGD method provides a significant improvement over the CGEC method because, unlike expansion-based methods, it is accurate up to the convergence criteria of the transport equation, and does not require the generation of any expansion moments. In fact, the fundamental data that must be stored for the SGD method, the "Subgroup Decomposition Cross Sections," are already computed by the vast majority of transport codes.

The utility of both of these methods has been examined as a way of approaching the spectral core environment error caused by using lattice cell (with specular boundary conditions) spectra to condense the cross sections. In both, a recondensation scheme has been developed which can correct for this error by updating the cross sections, recondensing with core-level fine-group spectra. However, the flux update procedure that is necessary to ensure positivity and convergence for expansion based methods like the CGEC (continuous or discrete expansions), requires the same number of operations as the entirety of the SGD method, not including the calculation of cross section expansion moments or higher-order flux moment calculations.

The primary conclusion that can be drawn from this dissertation is that, while expansion based methods may be used for rapid, low-order correction of the spectral core environment error, the SGD method provides a much more efficient and accurate solution. In fact, a very-coarse-group (1 or 2 groups) SGD recondensation calculation

has been shown in a BWR to be able to produce a solution as accurate as a 47-group solution in less time than it would take to generate a standard 8-group solution.

The SGD method also has the advantage of having been derived from a B-Spline formulation of the transport equation, and is in fact, the lowest-order B-Spline approximation that has physical meaning. This dissertation has presented the theoretical framework to examine a consistent continuous-energy to fine-group formulation as well through higher-order B-Splines. This is not as relevant to the practical application of the multigroup method, but the further examination of the B-Spline formulation has the potential to lead to a deterministic, coarse-group transport formulation with fully continuous-energy accuracy. This would be highly interesting to explore as future work.

In order to facilitate future examination of this, as well as other methods development, this dissertation has also presented the development of a highly simplified, yet physically realistic 2D and 3D BWR Benchmark Suite. By basing the core geometry and state parameters on an operating reactor, methods developers may use these problems to benchmark their own whole-core transport codes on a system which possesses the same neutron physics as the types of problems that engineers will need the codes to solve. In addition, the development of three 1D benchmark problems for LWR and VHTR reactor types provides the tools necessary for methods developers to test their codes in the early stages, long before they are developed enough to make use of large 2D and 3D benchmark problems. The development of good benchmarks is an ongoing task in the industry, and the problems presented in this dissertation are intended to contribute towards that effort.

# APPENDIX A

# SUPPLEMENTAL INFORMATION - 2D/3D BWR BENCHMARK

Table A.1: Fresh Material Composition – GE9 Lattice

| | Number Densities (10^24 at/cm^3) | | | | |
|---|---|---|---|---|---|
| Nuclide | Fuel 01 | Fuel 02 | Fuel 03 | Fuel 04 | Fuel 05 |
| U-234 | 3.1503E-6 | 4.0177E-6 | 4.4514E-6 | 4.8851E-6 | 5.3189E-6 |
| U-235 | 3.6369E-4 | 4.5461E-4 | 5.0007E-4 | 5.4553E-4 | 5.9099E-4 |
| U-238 | 2.2081E-2 | 2.1991E-2 | 2.1945E-2 | 2.1900E-2 | 2.1854E-2 |
| O | 4.4896E-2 | 4.4898E-2 | 4.4899E-2 | 4.4900E-2 | 4.4901E-2 |
| | | | | | |
| | Fuel 06 | Fuel 07 | Fuel 08 | Fuel 09 | Fuel 10 |
| U-234 | 5.7526E-6 | 6.1863E-6 | 7.4874E-6 | 7.9211E-6 | 8.2406E-6 |
| U-235 | 6.3645E-4 | 6.8190E-4 | 8.1828E-4 | 8.6374E-4 | 8.9783E-4 |
| U-238 | 2.1809E-2 | 2.1764E-2 | 2.1628E-2 | 2.1582E-2 | 2.1548E-2 |
| O | 4.4902E-2 | 4.4903E-2 | 4.4907E-2 | 4.4908E-2 | 4.4908E-2 |
| | | | | | |
| | Fuel 11 | Fuel 12 | | H | O-16 |
| U-234 | 7.8127E-6 | 7.0985E-6 | | Water at 600 K, No Void | |
| U-235 | 8.5120E-4 | 7.7578E-4 | | 4.9316E-2 | 2.4658E-2 |
| U-238 | 2.0429E-2 | 2.0504E-2 | | Water at 600 K, 40% Void | |
| O | 4.4558E-2 | 4.4556E-2 | | 3.0588E-2 | 1.5294E-2 |
| Gd-154 | 2.8746E-5 | 2.8746E-5 | | Water at 600 K, 70% Void | |
| Gd-155 | 1.9550E-4 | 1.9550E-4 | | 1.6542E-2 | 8.2712E-3 |
| Gd-156 | 2.7045E-4 | 2.7045E-4 | | Zirconium Cladding | |
| Gd-157 | 2.0677E-4 | 2.0677E-4 | | Nat Zr | 4.3239E-2 |
| Gd-158 | 3.2819E-4 | 3.2819E-4 | | | |
| Gd-160 | 2.9121E-4 | 2.9121E-4 | | | |

## A.1. 2-Group Cross Sections – 2D / 3D BWR Benchmark Problem

The cross sections presented in this appendix are provided for use in testing transport codes for whole-core calculations. They are provided in the following format.

$$\left\{\sigma_{cg}\right\}_{g=1}^{G}, \left\{\sigma_{fg}\right\}_{g=1}^{G}, \left\{\nu_{g}\right\}_{g=1}^{G}, \left\{\chi_{g}\right\}_{g=1}^{G}, \left\{\left\{\left\{\sigma_{sn}^{g'\to g}\right\}_{g'=1}^{G}\right\}_{g=1}^{G}\right\}_{n=1}^{N}$$

where, for $G$ energy groups, $\sigma_{cg}$ is the group $g$ capture cross section, $\sigma_{fg}$ is the group $g$ fission cross section, $\nu_{g}$ is the group $g$ fission yield (i.e. $\nu\sigma_{fg} = \nu_{g}\sigma_{fg}$), $\chi_{g}$ is the fission spectrum corresponding to group $g$, and $\sigma_{sn}^{g'\to g}$ is the $n^{\text{th}}$ (of $N$) Legendre moment of the scattering cross section from group $g'$ to group $g$.

**GE9 Bundle - Void Fraction: 0%, Burnup: 0.350 GWd/T, Uncontrolled**

```
 Region # 1 - Fuel 01
  2.5721E-02  1.7250E-01  5.9040E-03  1.0989E-01  2.6080E+00  2.4457E+00
  1.0000E+00  0.0000E+00  3.7734E-01  9.4965E-04  6.7848E-04  3.9213E-01
  4.3978E-02 -2.2306E-04 -6.4236E-05  8.4560E-03
 Region # 2 - Fuel 02
  2.5479E-02  2.0178E-01  6.5563E-03  1.3427E-01  2.5941E+00  2.4426E+00
  1.0000E+00  0.0000E+00  3.7544E-01  8.8662E-04  7.9457E-04  3.9226E-01
  4.4710E-02 -2.0830E-04 -7.4292E-05  8.4777E-03
 Region # 3 - Fuel 03
  2.6959E-02  2.1754E-01  6.9697E-03  1.4715E-01  2.5821E+00  2.4419E+00
  1.0000E+00  0.0000E+00  3.7720E-01  9.0545E-04  8.4530E-04  3.9242E-01
  4.4179E-02 -2.1279E-04 -7.8480E-05  8.4840E-03
 Region # 4 - Fuel 04
  2.6181E-02  2.3090E-01  7.2134E-03  1.5843E-01  2.5803E+00  2.4409E+00
  1.0000E+00  0.0000E+00  3.7522E-01  8.5566E-04  9.0313E-04  3.9246E-01
  4.4906E-02 -2.0108E-04 -8.3581E-05  8.4960E-03
 Region # 5 - Fuel 05
  2.6863E-02  2.4569E-01  7.5945E-03  1.7061E-01  2.5733E+00  2.4403E+00
  1.0000E+00  0.0000E+00  3.7532E-01  8.5960E-04  9.4483E-04  3.9259E-01
  4.4825E-02 -2.0204E-04 -8.7097E-05  8.5030E-03
 Region # 6 - Fuel 06
  2.7128E-02  2.5935E-01  7.8951E-03  1.8208E-01  2.5678E+00  2.4397E+00
  1.0000E+00  0.0000E+00  3.7538E-01  8.4249E-04  1.0107E-03  3.9267E-01
  4.4885E-02 -1.9804E-04 -9.2730E-05  8.5133E-03
 Region # 7 - Fuel 07
  2.7584E-02  2.7346E-01  8.2459E-03  1.9377E-01  2.5630E+00  2.4392E+00
  1.0000E+00  0.0000E+00  3.7523E-01  8.3731E-04  1.0577E-03  3.9280E-01
  4.4928E-02 -1.9683E-04 -9.6732E-05  8.5211E-03
 Region # 8 - Fuel 08
  2.7584E-02  3.1183E-01  9.0658E-03  2.2610E-01  2.5543E+00  2.4380E+00
  1.0000E+00  0.0000E+00  3.7315E-01  7.8637E-04  1.2123E-03  3.9307E-01
  4.5650E-02 -1.8486E-04 -1.1015E-04  8.5494E-03
 Region # 9 - Fuel 09
  2.9100E-02  3.2636E-01  9.5341E-03  2.3816E-01  2.5464E+00  2.4378E+00
  1.0000E+00  0.0000E+00  3.7506E-01  8.0809E-04  1.2843E-03  3.9322E-01
  4.5028E-02 -1.9003E-04 -1.1601E-04  8.5565E-03
 Region #10 - Fuel 10
  2.9356E-02  3.2853E-01  9.7477E-03  2.4134E-01  2.5423E+00  2.4375E+00
  1.0000E+00  0.0000E+00  3.7615E-01  7.9580E-04  1.5474E-03  3.9287E-01
  4.4737E-02 -1.8724E-04 -1.3820E-04  8.5868E-03
 Region #11 - Fuel 11
  4.0202E-02  2.9556E+00  9.2394E-03  1.4226E-01  2.5360E+00  2.4402E+00
```

1.0000E+00 0.0000E+00 3.7919E-01 7.8144E-04 5.0115E-03 3.9967E-01
4.3577E-02 -1.8332E-04 -4.1881E-04 9.0079E-03
Region #12 - Fuel 12
4.0336E-02 3.0860E+00 8.7745E-03 1.3301E-01 2.5405E+00 2.4410E+00
1.0000E+00 0.0000E+00 3.7999E-01 8.0637E-04 4.6395E-03 4.0042E-01
4.3346E-02 -1.8913E-04 -3.9027E-04 8.9785E-03
Region #13 - Zirconium Clad
1.7326E-03 4.4617E-03 0.0000E+00 0.0000E+00 0.0000E+00 0.0000E+00
0.0000E+00 0.0000E+00 3.1255E-01 3.2590E-04 4.9390E-04 2.7648E-01
3.8496E-02 -7.6534E-05 -6.1191E-05 2.5069E-03
Region #14 - Moderator
3.2088E-04 9.0287E-03 0.0000E+00 0.0000E+00 0.0000E+00 0.0000E+00
0.0000E+00 0.0000E+00 6.2620E-01 2.9994E-02 1.6607E-03 1.9202E+00
3.7310E-01 8.8930E-03 1.0297E-03 5.4633E-01
Region #15 - Bypass/Central Water Rod
3.4505E-04 9.4577E-03 0.0000E+00 0.0000E+00 0.0000E+00 0.0000E+00
0.0000E+00 0.0000E+00 6.5128E-01 3.4639E-02 1.2007E-03 1.9753E+00
3.9004E-01 1.0272E-02 7.4128E-04 5.4380E-01

**GE9 Bundle - Void Fraction: 0%, Burnup: 0.350 GWd/T, Controlled**

Region # 1 - Fuel 01
2.6842E-02 1.6442E-01 5.7497E-03 1.0473E-01 2.5896E+00 2.4467E+00
1.0000E+00 0.0000E+00 3.8481E-01 9.6799E-04 1.1823E-03 3.9107E-01
4.1689E-02 -2.2779E-04 -1.0700E-04 8.5127E-03
Region # 2 - Fuel 02
2.6693E-02 1.9315E-01 6.4976E-03 1.2854E-01 2.5779E+00 2.4433E+00
1.0000E+00 0.0000E+00 3.8214E-01 9.2115E-04 1.2631E-03 3.9130E-01
4.2563E-02 -2.1673E-04 -1.1393E-04 8.5291E-03
Region # 3 - Fuel 03
2.7410E-02 2.1537E-01 6.9861E-03 1.4568E-01 2.5778E+00 2.4420E+00
1.0000E+00 0.0000E+00 3.7897E-01 9.2548E-04 9.5785E-04 3.9219E-01
4.3562E-02 -2.1757E-04 -8.7996E-05 8.4962E-03
Region # 4 - Fuel 04
2.7297E-02 2.2139E-01 7.2131E-03 1.5195E-01 2.5671E+00 2.4413E+00
1.0000E+00 0.0000E+00 3.8085E-01 8.8767E-04 1.3497E-03 3.9155E-01
4.3079E-02 -2.0886E-04 -1.2132E-04 8.5446E-03
Region # 5 - Fuel 05
2.7387E-02 2.4111E-01 7.6086E-03 1.6745E-01 2.5676E+00 2.4405E+00
1.0000E+00 0.0000E+00 3.7782E-01 8.7598E-04 1.1407E-03 3.9219E-01
4.4007E-02 -2.0600E-04 -1.0367E-04 8.5245E-03
Region # 6 - Fuel 06
2.7911E-02 2.5186E-01 7.9229E-03 1.7687E-01 2.5594E+00 2.4399E+00
1.0000E+00 0.0000E+00 3.7912E-01 8.6400E-04 1.3232E-03 3.9204E-01
4.3675E-02 -2.0326E-04 -1.1912E-04 8.5471E-03
Region # 7 - Fuel 07
2.7972E-02 2.7150E-01 8.2915E-03 1.9241E-01 2.5600E+00 2.4393E+00
1.0000E+00 0.0000E+00 3.7645E-01 8.5559E-04 1.1465E-03 3.9263E-01
4.4484E-02 -2.0116E-04 -1.0419E-04 8.5302E-03
Region # 8 - Fuel 08
2.8796E-02 3.0234E-01 9.2231E-03 2.1934E-01 2.5444E+00 2.4382E+00
1.0000E+00 0.0000E+00 3.7753E-01 8.2951E-04 1.5827E-03 3.9239E-01
4.4138E-02 -1.9514E-04 -1.4121E-04 8.5868E-03
Region # 9 - Fuel 09
2.9357E-02 3.2468E-01 9.5792E-03 2.3695E-01 2.5448E+00 2.4379E+00
1.0000E+00 0.0000E+00 3.7575E-01 8.1966E-04 1.3509E-03 3.9310E-01
4.4772E-02 -1.9277E-04 -1.2158E-04 8.5631E-03
Region #10 - Fuel 10
2.9732E-02 3.2580E-01 9.8136E-03 2.3939E-01 2.5398E+00 2.4376E+00
1.0000E+00 0.0000E+00 3.7723E-01 8.1140E-04 1.6543E-03 3.9269E-01
4.4343E-02 -1.9094E-04 -1.4712E-04 8.5972E-03
Region #11 - Fuel 11
4.0594E-02 2.9128E+00 9.2855E-03 1.4157E-01 2.5344E+00 2.4402E+00
1.0000E+00 0.0000E+00 3.7986E-01 7.9345E-04 5.1037E-03 3.9928E-01
4.3326E-02 -1.8614E-04 -4.2579E-04 9.0139E-03
Region #12 - Fuel 12

```
 4.1478E-02  2.9446E+00  8.8875E-03  1.3089E-01  2.5356E+00  2.4411E+00
 1.0000E+00  0.0000E+00  3.8209E-01  8.3638E-04  4.9485E-03  3.9914E-01
 4.2577E-02 -1.9622E-04 -4.1364E-04  8.9985E-03
Region #13 - Zirconium Clad
 1.7614E-03  4.3634E-03  0.0000E+00  0.0000E+00  0.0000E+00  0.0000E+00
 0.0000E+00  0.0000E+00  3.1378E-01  3.2930E-04  6.0751E-04  2.7632E-01
 3.7949E-02 -7.7334E-05 -7.5177E-05  2.5244E-03
Region #14 - Blade Sheath
 5.3568E-03  1.3932E-01  0.0000E+00  0.0000E+00  0.0000E+00  0.0000E+00
 0.0000E+00  0.0000E+00  5.9825E-01  1.5280E-03  2.2586E-03  8.7596E-01
 3.6109E-02  0.0000E+00  0.0000E+00  1.1872E-02
Region #15 - Control Rod
 8.2516E-03  3.0261E-01  0.0000E+00  0.0000E+00  0.0000E+00  0.0000E+00
 0.0000E+00  0.0000E+00  3.3836E-03  2.4535E-05  1.2331E-05  4.3440E-03
 2.8057E-04 -1.2488E-06  1.4692E-08  2.6276E-04
Region #16 - Moderator
 3.2153E-04  8.8575E-03  0.0000E+00  0.0000E+00  0.0000E+00  0.0000E+00
 0.0000E+00  0.0000E+00  6.3369E-01  3.0632E-02  1.9681E-03  1.8982E+00
 3.7793E-01  9.0768E-03  1.2229E-03  5.4718E-01
Region #17 - Bypass/Central Water Rod
 3.4064E-04  9.2315E-03  0.0000E+00  0.0000E+00  0.0000E+00  0.0000E+00
 0.0000E+00  0.0000E+00  6.5669E-01  3.4534E-02  1.5229E-03  1.9462E+00
 3.9337E-01  1.0223E-02  9.4348E-04  5.4502E-01
```

**GE9 Bundle - Void Fraction: 0%, Burnup: 15 GWd/T, Uncontrolled**

```
Region # 1 - Fuel 01
 3.0750E-02  1.7838E-01  4.4845E-03  8.7764E-02  2.7353E+00  2.7015E+00
 1.0000E+00  0.0000E+00  3.7872E-01  9.1494E-04  6.4764E-04  3.8980E-01
 4.3236E-02 -2.1076E-04 -6.0401E-05  8.4227E-03
Region # 2 - Fuel 02
 2.9421E-02  2.0209E-01  4.9698E-03  1.0708E-01  2.7070E+00  2.6578E+00
 1.0000E+00  0.0000E+00  3.7678E-01  8.5085E-04  7.4685E-04  3.8993E-01
 4.3914E-02 -1.9608E-04 -6.8722E-05  8.4401E-03
Region # 3 - Fuel 03
 3.1013E-02  2.1461E-01  5.1865E-03  1.1612E-01  2.6954E+00  2.6493E+00
 1.0000E+00  0.0000E+00  3.7860E-01  8.7451E-04  7.9342E-04  3.8992E-01
 4.3368E-02 -2.0188E-04 -7.2563E-05  8.4449E-03
Region # 4 - Fuel 04
 2.9530E-02  2.2734E-01  5.4640E-03  1.2720E-01  2.6829E+00  2.6281E+00
 1.0000E+00  0.0000E+00  3.7632E-01  8.2075E-04  8.3661E-04  3.9007E-01
 4.4139E-02 -1.8939E-04 -7.6227E-05  8.4549E-03
Region # 5 - Fuel 05
 3.0112E-02  2.3842E-01  5.6908E-03  1.3566E-01  2.6734E+00  2.6190E+00
 1.0000E+00  0.0000E+00  3.7663E-01  8.2732E-04  8.7403E-04  3.9009E-01
 4.3985E-02 -1.9101E-04 -7.9323E-05  8.4602E-03
Region # 6 - Fuel 06
 3.0006E-02  2.5281E-01  5.9797E-03  1.4741E-01  2.6624E+00  2.6062E+00
 1.0000E+00  0.0000E+00  3.7620E-01  8.0620E-04  9.2601E-04  3.9020E-01
 4.4195E-02 -1.8624E-04 -8.3679E-05  8.4690E-03
Region # 7 - Fuel 07
 3.0276E-02  2.6520E-01  6.2398E-03  1.5718E-01  2.6540E+00  2.5974E+00
 1.0000E+00  0.0000E+00  3.7604E-01  8.0109E-04  9.6818E-04  3.9027E-01
 4.4226E-02 -1.8512E-04 -8.7184E-05  8.4755E-03
Region # 8 - Fuel 08
 2.9392E-02  3.0180E-01  6.9909E-03  1.8786E-01  2.6311E+00  2.5678E+00
 1.0000E+00  0.0000E+00  3.7344E-01  7.4552E-04  1.0578E-03  3.9066E-01
 4.5060E-02 -1.7222E-04 -9.4772E-05  8.4958E-03
Region # 9 - Fuel 09
 3.0898E-02  3.1776E-01  7.3312E-03  1.9978E-01  2.6223E+00  2.5659E+00
 1.0000E+00  0.0000E+00  3.7515E-01  7.6637E-04  1.1351E-03  3.9070E-01
 4.4532E-02 -1.7735E-04 -1.0111E-04  8.5039E-03
Region #10 - Fuel 10
 3.0587E-02  3.3729E-01  7.7560E-03  2.1670E-01  2.6125E+00  2.5570E+00
 1.0000E+00  0.0000E+00  3.7466E-01  7.4154E-04  1.2575E-03  3.9088E-01
 4.4813E-02 -1.7179E-04 -1.1134E-04  8.5228E-03
```

```
 Region #11 - Fuel 11
  3.1270E-02  3.5997E-01  8.0141E-03  2.3021E-01  2.5977E+00  2.5435E+00
  1.0000E+00  0.0000E+00  3.7322E-01  7.2035E-04  1.3717E-03  3.8465E-01
  4.4981E-02 -1.6627E-04 -1.1802E-04  8.4719E-03
 Region #12 - Fuel 12
  3.1500E-02  3.2924E-01  7.4066E-03  2.0645E-01  2.6113E+00  2.5539E+00
  1.0000E+00  0.0000E+00  3.7363E-01  7.4500E-04  1.1720E-03  3.8448E-01
  4.4806E-02 -1.7185E-04 -1.0188E-04  8.4431E-03
 Region #13 - Zirconium Clad
  1.7213E-03  4.5261E-03  0.0000E+00  0.0000E+00  0.0000E+00  0.0000E+00
  0.0000E+00  0.0000E+00  3.1206E-01  3.1252E-04  4.4950E-04  2.7656E-01
  3.8800E-02 -7.3380E-05 -5.5694E-05  2.4993E-03
 Region #14 - Moderator
  3.1746E-04  9.2015E-03  0.0000E+00  0.0000E+00  0.0000E+00  0.0000E+00
  0.0000E+00  0.0000E+00  6.2245E-01  2.8630E-02  1.4696E-03  1.9424E+00
  3.7059E-01  8.4385E-03  9.1060E-04  5.4535E-01
 Region #15 - Bypass/Central Water Rod
  3.4320E-04  9.5102E-03  0.0000E+00  0.0000E+00  0.0000E+00  0.0000E+00
  0.0000E+00  0.0000E+00  6.4836E-01  3.3744E-02  1.1365E-03  1.9820E+00
  3.8810E-01  9.9765E-03  7.0120E-04  5.4351E-01
GE9 Bundle - Void Fraction: 0%, Burnup: 15 GWd/T, Controlled
 Region # 1 - Fuel 01
  3.1758E-02  1.7647E-01  4.2537E-03  8.7207E-02  2.7250E+00  2.7077E+00
  1.0000E+00  0.0000E+00  3.8574E-01  9.1637E-04  1.1411E-03  3.8879E-01
  4.1190E-02 -2.1140E-04 -1.0166E-04  8.4779E-03
 Region # 2 - Fuel 02
  3.0601E-02  1.9953E-01  4.8111E-03  1.0590E-01  2.6963E+00  2.6637E+00
  1.0000E+00  0.0000E+00  3.8312E-01  8.7087E-04  1.1971E-03  3.8904E-01
  4.1972E-02 -2.0094E-04 -1.0625E-04  8.4895E-03
 Region # 3 - Fuel 03
  3.1543E-02  2.1395E-01  5.1604E-03  1.1579E-01  2.6921E+00  2.6508E+00
  1.0000E+00  0.0000E+00  3.8044E-01  8.9211E-04  9.0100E-04  3.8971E-01
  4.2755E-02 -2.0599E-04 -8.1532E-05  8.4565E-03
 Region # 4 - Fuel 04
  3.0602E-02  2.2413E-01  5.3625E-03  1.2545E-01  2.6732E+00  2.6335E+00
  1.0000E+00  0.0000E+00  3.8169E-01  8.4065E-04  1.2536E-03  3.8924E-01
  4.2484E-02 -1.9417E-04 -1.1091E-04  8.5004E-03
 Region # 5 - Fuel 05
  3.0655E-02  2.3680E-01  5.6529E-03  1.3474E-01  2.6689E+00  2.6215E+00
  1.0000E+00  0.0000E+00  3.7914E-01  8.3946E-04  1.0571E-03  3.8972E-01
  4.3203E-02 -1.9389E-04 -9.4579E-05  8.4803E-03
 Region # 6 - Fuel 06
  3.0755E-02  2.5048E-01  5.9324E-03  1.4606E-01  2.6557E+00  2.6099E+00
  1.0000E+00  0.0000E+00  3.7975E-01  8.2025E-04  1.2098E-03  3.8964E-01
  4.3094E-02 -1.8961E-04 -1.0727E-04  8.4998E-03
 Region # 7 - Fuel 07
  3.0742E-02  2.6443E-01  6.2458E-03  1.5671E-01  2.6512E+00  2.5984E+00
  1.0000E+00  0.0000E+00  3.7741E-01  8.1853E-04  1.0510E-03  3.9012E-01
  4.3757E-02 -1.8918E-04 -9.4048E-05  8.4840E-03
 Region # 8 - Fuel 08
  3.0608E-02  2.9780E-01  7.0212E-03  1.8524E-01  2.6222E+00  2.5711E+00
  1.0000E+00  0.0000E+00  3.7770E-01  7.8051E-04  1.3723E-03  3.9008E-01
  4.3660E-02 -1.8043E-04 -1.2076E-04  8.5279E-03
 Region # 9 - Fuel 09
  3.1209E-02  3.1708E-01  7.3505E-03  1.9931E-01  2.6205E+00  2.5666E+00
  1.0000E+00  0.0000E+00  3.7597E-01  7.7779E-04  1.1938E-03  3.9059E-01
  4.4248E-02 -1.8001E-04 -1.0597E-04  8.5097E-03
 Region #10 - Fuel 10
  3.0991E-02  3.3654E-01  7.7873E-03  2.1624E-01  2.6100E+00  2.5578E+00
  1.0000E+00  0.0000E+00  3.7579E-01  7.5551E-04  1.3436E-03  3.9074E-01
  4.4427E-02 -1.7505E-04 -1.1845E-04  8.5315E-03
 Region #11 - Fuel 11
  3.1527E-02  3.5934E-01  8.0436E-03  2.2980E-01  2.5964E+00  2.5439E+00
  1.0000E+00  0.0000E+00  3.7378E-01  7.3033E-04  1.4182E-03  3.8457E-01
```

```
 4.4772E-02 -1.6858E-04 -1.2176E-04  8.4763E-03
Region #12 - Fuel 12
 3.2331E-02  3.2744E-01  7.4682E-03  2.0531E-01  2.6066E+00  2.5551E+00
 1.0000E+00  0.0000E+00  3.7577E-01  7.7200E-04  1.3009E-03  3.8426E-01
 4.4059E-02 -1.7813E-04 -1.1224E-04  8.4552E-03
Region #13 - Zirconium Clad
 1.7482E-03  4.4437E-03  0.0000E+00  0.0000E+00  0.0000E+00  0.0000E+00
 0.0000E+00  0.0000E+00  3.1326E-01  3.1479E-04  5.4449E-04  2.7642E-01
 3.8306E-02 -7.3914E-05 -6.7384E-05  2.5140E-03
Region #14 - Blade Sheath
 5.3082E-03  1.4007E-01  0.0000E+00  0.0000E+00  0.0000E+00  0.0000E+00
 0.0000E+00  0.0000E+00  5.9738E-01  1.4820E-03  2.2055E-03  8.7606E-01
 3.6311E-02  0.0000E+00  0.0000E+00  1.1871E-02
Region #15 - Control Rod
 8.1226E-03  3.0446E-01  0.0000E+00  0.0000E+00  0.0000E+00  0.0000E+00
 0.0000E+00  0.0000E+00  3.3780E-03  2.3650E-05  1.1980E-05  4.3457E-03
 2.8060E-04 -1.1997E-06  1.4915E-08  2.6272E-04
Region #16 - Moderator
 3.1735E-04  9.0622E-03  0.0000E+00  0.0000E+00  0.0000E+00  0.0000E+00
 0.0000E+00  0.0000E+00  6.2940E-01  2.9165E-02  1.7174E-03  1.9244E+00
 3.7506E-01  8.5900E-03  1.0663E-03  5.4604E-01
Region #17 - Bypass/Central Water Rod
 3.3817E-04  9.3106E-03  0.0000E+00  0.0000E+00  0.0000E+00  0.0000E+00
 0.0000E+00  0.0000E+00  6.5346E-01  3.3551E-02  1.4215E-03  1.9564E+00
 3.9122E-01  9.8998E-03  8.8012E-04  5.4459E-01
```

**GE9 Bundle - Void Fraction: 0%, Burnup: 25 GWd/T, Uncontrolled**

```
Region # 1 - Fuel 01
 3.2855E-02  1.6804E-01  4.0158E-03  7.2563E-02  2.7852E+00  2.7906E+00
 1.0000E+00  0.0000E+00  3.7907E-01  9.1942E-04  6.0580E-04  3.8849E-01
 4.2739E-02 -2.1057E-04 -5.6688E-05  8.4064E-03
Region # 2 - Fuel 02
 3.1194E-02  1.8583E-01  4.3452E-03  8.6336E-02  2.7608E+00  2.7457E+00
 1.0000E+00  0.0000E+00  3.7724E-01  8.5293E-04  6.8813E-04  3.8860E-01
 4.3378E-02 -1.9524E-04 -6.3546E-05  8.4201E-03
Region # 3 - Fuel 03
 3.2906E-02  1.9565E-01  4.4672E-03  9.2803E-02  2.7528E+00  2.7380E+00
 1.0000E+00  0.0000E+00  3.7913E-01  8.7985E-04  7.3250E-04  3.8849E-01
 4.2792E-02 -2.0179E-04 -6.7170E-05  8.4236E-03
Region # 4 - Fuel 04
 3.1134E-02  2.0599E-01  4.6972E-03  1.0161E-01  2.7382E+00  2.7112E+00
 1.0000E+00  0.0000E+00  3.7678E-01  8.2244E-04  7.6321E-04  3.8867E-01
 4.3580E-02 -1.8844E-04 -6.9769E-05  8.4315E-03
Region # 5 - Fuel 05
 3.1697E-02  2.1436E-01  4.8407E-03  1.0755E-01  2.7301E+00  2.7015E+00
 1.0000E+00  0.0000E+00  3.7718E-01  8.3014E-04  7.9721E-04  3.8861E-01
 4.3395E-02 -1.9028E-04 -7.2553E-05  8.4355E-03
Region # 6 - Fuel 06
 3.1477E-02  2.2703E-01  5.0770E-03  1.1749E-01  2.7177E+00  2.6842E+00
 1.0000E+00  0.0000E+00  3.7665E-01  8.0767E-04  8.4075E-04  3.8872E-01
 4.3618E-02 -1.8521E-04 -7.6171E-05  8.4429E-03
Region # 7 - Fuel 07
 3.1681E-02  2.3730E-01  5.2700E-03  1.2518E-01  2.7091E+00  2.6733E+00
 1.0000E+00  0.0000E+00  3.7647E-01  8.0250E-04  8.7794E-04  3.8874E-01
 4.3637E-02 -1.8406E-04 -7.9230E-05  8.4481E-03
Region # 8 - Fuel 08
 3.0398E-02  2.6825E-01  5.8889E-03  1.5053E-01  2.6809E+00  2.6322E+00
 1.0000E+00  0.0000E+00  3.7374E-01  7.4324E-04  9.4081E-04  3.8909E-01
 4.4483E-02 -1.7028E-04 -8.4522E-05  8.4637E-03
Region # 9 - Fuel 09
 3.1985E-02  2.8360E-01  6.1513E-03  1.6131E-01  2.6725E+00  2.6302E+00
 1.0000E+00  0.0000E+00  3.7545E-01  7.6522E-04  1.0214E-03  3.8904E-01
 4.3952E-02 -1.7567E-04 -9.1081E-05  8.4717E-03
Region #10 - Fuel 10
 3.1577E-02  3.0625E-01  6.6010E-03  1.8010E-01  2.6584E+00  2.6157E+00
```

```
 1.0000E+00  0.0000E+00  3.7478E-01  7.3717E-04  1.1287E-03  3.8931E-01
 4.4308E-02 -1.6935E-04 -9.9987E-05  8.4893E-03
Region #11 - Fuel 11
 3.2341E-02  3.3010E-01  6.8582E-03  1.9554E-01  2.6404E+00  2.5975E+00
 1.0000E+00  0.0000E+00  3.7326E-01  7.1351E-04  1.2282E-03  3.8318E-01
 4.4522E-02 -1.6321E-04 -1.0567E-04  8.4369E-03
Region #12 - Fuel 12
 3.2733E-02  2.9583E-01  6.2315E-03  1.6883E-01  2.6595E+00  2.6147E+00
 1.0000E+00  0.0000E+00  3.7387E-01  7.4285E-04  1.0473E-03  3.8292E-01
 4.4262E-02 -1.6991E-04 -9.1165E-05  8.4099E-03
Region #13 - Zirconium Clad
 1.7329E-03  4.5608E-03  0.0000E+00  0.0000E+00  0.0000E+00  0.0000E+00
 0.0000E+00  0.0000E+00  3.1207E-01  3.1528E-04  4.1804E-04  2.7661E-01
 3.8479E-02 -7.4021E-05 -5.1822E-05  2.4941E-03
Region #14 - Moderator
 3.2096E-04  9.2839E-03  0.0000E+00  0.0000E+00  0.0000E+00  0.0000E+00
 0.0000E+00  0.0000E+00  6.2544E-01  2.8805E-02  1.3611E-03  1.9530E+00
 3.7261E-01  8.4718E-03  8.4248E-04  5.4489E-01
Region #15 - Bypass/Central Water Rod
 3.4805E-04  9.5450E-03  0.0000E+00  0.0000E+00  0.0000E+00  0.0000E+00
 0.0000E+00  0.0000E+00  6.5144E-01  3.4257E-02  1.0809E-03  1.9865E+00
 3.9021E-01  1.0122E-02  6.6629E-04  5.4333E-01
```

**GE9 Bundle - Void Fraction: 0%, Burnup: 25 GWd/T, Controlled**

```
Region # 1 - Fuel 01
 3.3890E-02  1.6714E-01  3.7659E-03  7.2820E-02  2.7792E+00  2.7938E+00
 1.0000E+00  0.0000E+00  3.8609E-01  9.1826E-04  1.0758E-03  3.8752E-01
 4.0714E-02 -2.1060E-04 -9.5913E-05  8.4593E-03
Region # 2 - Fuel 02
 3.2422E-02  1.8457E-01  4.1556E-03  8.6182E-02  2.7538E+00  2.7498E+00
 1.0000E+00  0.0000E+00  3.8356E-01  8.7088E-04  1.1132E-03  3.8775E-01
 4.1456E-02 -1.9959E-04 -9.8894E-05  8.4670E-03
Region # 3 - Fuel 03
 3.3479E-02  1.9533E-01  4.4266E-03  9.2743E-02  2.7508E+00  2.7391E+00
 1.0000E+00  0.0000E+00  3.8101E-01  8.9722E-04  8.3715E-04  3.8828E-01
 4.2177E-02 -2.0583E-04 -7.5872E-05  8.4350E-03
Region # 4 - Fuel 04
 3.2246E-02  2.0432E-01  4.5609E-03  1.0108E-01  2.7311E+00  2.7155E+00
 1.0000E+00  0.0000E+00  3.8217E-01  8.4063E-04  1.1541E-03  3.8789E-01
 4.1938E-02 -1.9278E-04 -1.0221E-04  8.4745E-03
Region # 5 - Fuel 05
 3.2263E-02  2.1351E-01  4.7837E-03  1.0723E-01  2.7268E+00  2.7036E+00
 1.0000E+00  0.0000E+00  3.7967E-01  8.4151E-04  9.7021E-04  3.8826E-01
 4.2616E-02 -1.9296E-04 -8.6928E-05  8.4547E-03
Region # 6 - Fuel 06
 3.2250E-02  2.2606E-01  5.0018E-03  1.1718E-01  2.7125E+00  2.6876E+00
 1.0000E+00  0.0000E+00  3.8021E-01  8.2060E-04  1.1065E-03  3.8819E-01
 4.2526E-02 -1.8829E-04 -9.8205E-05  8.4720E-03
Region # 7 - Fuel 07
 3.2188E-02  2.3687E-01  5.2585E-03  1.2498E-01  2.7070E+00  2.6742E+00
 1.0000E+00  0.0000E+00  3.7788E-01  8.2001E-04  9.5957E-04  3.8859E-01
 4.3162E-02 -1.8811E-04 -8.5978E-05  8.4565E-03
Region # 8 - Fuel 08
 3.1688E-02  2.6587E-01  5.8648E-03  1.4917E-01  2.6730E+00  2.6356E+00
 1.0000E+00  0.0000E+00  3.7811E-01  7.7806E-04  1.2370E-03  3.8854E-01
 4.3071E-02 -1.7839E-04 -1.0893E-04  8.4942E-03
Region # 9 - Fuel 09
 3.2320E-02  2.8321E-01  6.1571E-03  1.6108E-01  2.6710E+00  2.6311E+00
 1.0000E+00  0.0000E+00  3.7629E-01  7.7665E-04  1.0804E-03  3.8893E-01
 4.3664E-02 -1.7831E-04 -9.5944E-05  8.4776E-03
Region #10 - Fuel 10
 3.2011E-02  3.0612E-01  6.6150E-03  1.8011E-01  2.6562E+00  2.6166E+00
 1.0000E+00  0.0000E+00  3.7594E-01  7.5109E-04  1.2152E-03  3.8917E-01
 4.3917E-02 -1.7258E-04 -1.0710E-04  8.4981E-03
Region #11 - Fuel 11
```

```
 3.2621E-02  3.2970E-01  6.8771E-03  1.9534E-01  2.6392E+00  2.5980E+00
 1.0000E+00  0.0000E+00  3.7384E-01  7.2342E-04  1.2777E-03  3.8310E-01
 4.4311E-02 -1.6549E-04 -1.0963E-04  8.4416E-03
Region #12 - Fuel 12
 3.3647E-02  2.9458E-01  6.2582E-03  1.6813E-01  2.6551E+00  2.6162E+00
 1.0000E+00  0.0000E+00  3.7612E-01  7.7047E-04  1.1775E-03  3.8269E-01
 4.3491E-02 -1.7628E-04 -1.0159E-04  8.4223E-03
Region #13 - Zirconium Clad
 1.7599E-03  4.4822E-03  0.0000E+00  0.0000E+00  0.0000E+00  0.0000E+00
 0.0000E+00  0.0000E+00  3.1327E-01  3.1738E-04  5.0869E-04  2.7648E-01
 3.7982E-02 -7.4517E-05 -6.2979E-05  2.5082E-03
Region #14 - Blade Sheath
 5.3786E-03  1.4068E-01  0.0000E+00  0.0000E+00  0.0000E+00  0.0000E+00
 0.0000E+00  0.0000E+00  6.0061E-01  1.5034E-03  2.1144E-03  8.7620E-01
 3.6143E-02  0.0000E+00  0.0000E+00  1.1870E-02
Region #15 - Control Rod
 8.2502E-03  3.0593E-01  0.0000E+00  0.0000E+00  0.0000E+00  0.0000E+00
 0.0000E+00  0.0000E+00  3.3851E-03  2.3946E-05  1.1459E-05  4.3473E-03
 2.8049E-04 -1.2133E-06  1.2332E-08  2.6269E-04
Region #16 - Moderator
 3.2091E-04  9.1497E-03  0.0000E+00  0.0000E+00  0.0000E+00  0.0000E+00
 0.0000E+00  0.0000E+00  6.3244E-01  2.9337E-02  1.5992E-03  1.9357E+00
 3.7710E-01  8.6220E-03  9.9219E-04  5.4556E-01
Region #17 - Bypass/Central Water Rod
 3.4300E-04  9.3511E-03  0.0000E+00  0.0000E+00  0.0000E+00  0.0000E+00
 0.0000E+00  0.0000E+00  6.5658E-01  3.4046E-02  1.3562E-03  1.9616E+00
 3.9336E-01  1.0039E-02  8.3913E-04  5.4438E-01
```

**GE9 Bundle - Void Fraction: 40%, Burnup: 0.350 GWd/T, Uncontrolled**

```
Region # 1 - Fuel 01
 2.5359E-02  1.6985E-01  5.7451E-03  1.0819E-01  2.6012E+00  2.4460E+00
 1.0000E+00  0.0000E+00  3.8016E-01  9.2688E-04  8.2673E-04  3.9179E-01
 4.3215E-02 -2.1786E-04 -7.6787E-05  8.4741E-03
Region # 2 - Fuel 02
 2.4859E-02  1.9772E-01  6.3854E-03  1.3154E-01  2.5881E+00  2.4429E+00
 1.0000E+00  0.0000E+00  3.7789E-01  8.6309E-04  9.6935E-04  3.9184E-01
 4.4024E-02 -2.0289E-04 -8.9077E-05  8.4999E-03
Region # 3 - Fuel 03
 2.6505E-02  2.1309E-01  6.7843E-03  1.4413E-01  2.5756E+00  2.4421E+00
 1.0000E+00  0.0000E+00  3.8032E-01  8.7380E-04  1.0476E-03  3.9197E-01
 4.3380E-02 -2.0551E-04 -9.5538E-05  8.5077E-03
Region # 4 - Fuel 04
 2.5471E-02  2.2551E-01  7.0278E-03  1.5471E-01  2.5750E+00  2.4411E+00
 1.0000E+00  0.0000E+00  3.7753E-01  8.2874E-04  1.1041E-03  3.9198E-01
 4.4269E-02 -1.9487E-04 -1.0055E-04  8.5212E-03
Region # 5 - Fuel 05
 2.6200E-02  2.3972E-01  7.3953E-03  1.6645E-01  2.5674E+00  2.4405E+00
 1.0000E+00  0.0000E+00  3.7807E-01  8.2955E-04  1.1673E-03  3.9208E-01
 4.4081E-02 -1.9511E-04 -1.0583E-04  8.5299E-03
Region # 6 - Fuel 06
 2.6353E-02  2.5251E-01  7.6837E-03  1.7727E-01  2.5626E+00  2.4399E+00
 1.0000E+00  0.0000E+00  3.7785E-01  8.1046E-04  1.2449E-03  3.9213E-01
 4.4230E-02 -1.9063E-04 -1.1245E-04  8.5419E-03
Region # 7 - Fuel 07
 2.6804E-02  2.6591E-01  8.0235E-03  1.8843E-01  2.5576E+00  2.4394E+00
 1.0000E+00  0.0000E+00  3.7789E-01  8.0297E-04  1.3105E-03  3.9223E-01
 4.4224E-02 -1.8889E-04 -1.1798E-04  8.5514E-03
Region # 8 - Fuel 08
 2.6473E-02  3.0200E-01  8.8255E-03  2.1897E-01  2.5505E+00  2.4382E+00
 1.0000E+00  0.0000E+00  3.7490E-01  7.5819E-04  1.4585E-03  3.9246E-01
 4.5152E-02 -1.7832E-04 -1.3085E-04  8.5810E-03
Region # 9 - Fuel 09
 2.8111E-02  3.1524E-01  9.2616E-03  2.3008E-01  2.5419E+00  2.4380E+00
 1.0000E+00  0.0000E+00  3.7763E-01  7.6846E-04  1.5983E-03  3.9253E-01
 4.4367E-02 -1.8084E-04 -1.4228E-04  8.5932E-03
```

```
 Region #10 - Fuel 10
  2.8023E-02  3.1582E-01  9.4165E-03  2.3204E-01  2.5393E+00  2.4378E+00
  1.0000E+00  0.0000E+00  3.7799E-01  7.4854E-04  1.8964E-03  3.9211E-01
  4.4325E-02 -1.7624E-04 -1.6725E-04  8.6275E-03
 Region #11 - Fuel 11
  3.7939E-02  2.6581E+00  8.8658E-03  1.3799E-01  2.5352E+00  2.4403E+00
  1.0000E+00  0.0000E+00  3.7983E-01  7.2301E-04  5.5335E-03  3.9729E-01
  4.3545E-02 -1.6971E-04 -4.5773E-04  9.0408E-03
 Region #12 - Fuel 12
  3.8253E-02  2.8388E+00  8.4504E-03  1.2972E-01  2.5399E+00  2.4411E+00
  1.0000E+00  0.0000E+00  3.8042E-01  7.5290E-04  5.0590E-03  3.9848E-01
  4.3376E-02 -1.7668E-04 -4.2179E-04  9.0051E-03
 Region #13 - Zirconium Clad
  1.7539E-03  4.3523E-03  0.0000E+00  0.0000E+00  0.0000E+00  0.0000E+00
  0.0000E+00  0.0000E+00  3.1535E-01  3.0624E-04  6.1589E-04  2.7631E-01
  3.8580E-02 -7.1919E-05 -7.6197E-05  2.5259E-03
 Region #14 - Moderator
  1.8801E-04  5.4385E-03  0.0000E+00  0.0000E+00  0.0000E+00  0.0000E+00
  0.0000E+00  0.0000E+00  3.8959E-01  1.7509E-02  1.2715E-03  1.1702E+00
  2.3180E-01  5.1819E-03  7.9047E-04  3.3974E-01
 Region #15 - Bypass/Central Water Rod
  3.2879E-04  9.2896E-03  0.0000E+00  0.0000E+00  0.0000E+00  0.0000E+00
  0.0000E+00  0.0000E+00  6.5536E-01  3.2973E-02  1.4758E-03  1.9536E+00
  3.9212E-01  9.7520E-03  9.1407E-04  5.4466E-01
```

**GE9 Bundle - Void Fraction: 40%, Burnup: 0.350 GWd/T, Controlled**

```
 Region # 1 - Fuel 01
  2.6175E-02  1.5909E-01  5.5319E-03  1.0131E-01  2.5822E+00  2.4473E+00
  1.0000E+00  0.0000E+00  3.8791E-01  9.1322E-04  1.4968E-03  3.9037E-01
  4.0980E-02 -2.1512E-04 -1.3344E-04  8.5498E-03
 Region # 2 - Fuel 02
  2.5832E-02  1.8589E-01  6.2620E-03  1.2369E-01  2.5710E+00  2.4438E+00
  1.0000E+00  0.0000E+00  3.8505E-01  8.6950E-04  1.6146E-03  3.9052E-01
  4.1840E-02 -2.0477E-04 -1.4344E-04  8.5707E-03
 Region # 3 - Fuel 03
  2.6990E-02  2.1031E-01  6.7884E-03  1.4226E-01  2.5701E+00  2.4423E+00
  1.0000E+00  0.0000E+00  3.8254E-01  8.9156E-04  1.1959E-03  3.9168E-01
  4.2634E-02 -2.0977E-04 -1.0801E-04  8.5235E-03
 Region # 4 - Fuel 04
  2.6402E-02  2.1248E-01  6.9639E-03  1.4583E-01  2.5606E+00  2.4418E+00
  1.0000E+00  0.0000E+00  3.8379E-01  8.3842E-04  1.7238E-03  3.9072E-01
  4.2336E-02 -1.9745E-04 -1.5267E-04  8.5885E-03
 Region # 5 - Fuel 05
  2.6691E-02  2.3377E-01  7.3878E-03  1.6235E-01  2.5608E+00  2.4408E+00
  1.0000E+00  0.0000E+00  3.8097E-01  8.3949E-04  1.4262E-03  3.9155E-01
  4.3167E-02 -1.9758E-04 -1.2762E-04  8.5583E-03
 Region # 6 - Fuel 06
  2.7035E-02  2.4230E-01  7.6683E-03  1.7017E-01  2.5532E+00  2.4403E+00
  1.0000E+00  0.0000E+00  3.8210E-01  8.1906E-04  1.6786E-03  3.9126E-01
  4.2907E-02 -1.9285E-04 -1.4888E-04  8.5885E-03
 Region # 7 - Fuel 07
  2.7279E-02  2.6308E-01  8.0663E-03  1.8646E-01  2.5532E+00  2.4395E+00
  1.0000E+00  0.0000E+00  3.7971E-01  8.2143E-04  1.4437E-03  3.9198E-01
  4.3593E-02 -1.9329E-04 -1.2910E-04  8.5647E-03
 Region # 8 - Fuel 08
  2.7635E-02  2.8764E-01  8.9286E-03  2.0873E-01  2.5389E+00  2.4385E+00
  1.0000E+00  0.0000E+00  3.8032E-01  7.8537E-04  2.0262E-03  3.9142E-01
  4.3378E-02 -1.8492E-04 -1.7821E-04  8.6381E-03
 Region # 9 - Fuel 09
  2.8477E-02  3.1263E-01  9.3164E-03  2.2822E-01  2.5390E+00  2.4381E+00
  1.0000E+00  0.0000E+00  3.7886E-01  7.8212E-04  1.7055E-03  3.9234E-01
  4.3934E-02 -1.8409E-04 -1.5119E-04  8.6036E-03
 Region #10 - Fuel 10
  2.8509E-02  3.1142E-01  9.4878E-03  2.2890E-01  2.5353E+00  2.4378E+00
  1.0000E+00  0.0000E+00  3.7975E-01  7.6446E-04  2.0762E-03  3.9180E-01
```

```
 4.3720E-02 -1.8004E-04 -1.8213E-04  8.6448E-03
Region #11 - Fuel 11
 3.8510E-02  2.5903E+00  8.9242E-03  1.3686E-01  2.5323E+00  2.4403E+00
 1.0000E+00  0.0000E+00  3.8104E-01  7.3723E-04  5.6911E-03  3.9666E-01
 4.3113E-02 -1.7308E-04 -4.6950E-04  9.0510E-03
Region #12 - Fuel 12
 3.9492E-02  2.6307E+00  8.5454E-03  1.2657E-01  2.5331E+00  2.4412E+00
 1.0000E+00  0.0000E+00  3.8346E-01  7.7599E-04  5.5294E-03  3.9657E-01
 4.2340E-02 -1.8220E-04 -4.5712E-04  9.0354E-03
Region #13 - Zirconium Clad
 1.7923E-03  4.2276E-03  0.0000E+00  0.0000E+00  0.0000E+00  0.0000E+00
 0.0000E+00  0.0000E+00  3.1709E-01  3.0833E-04  7.7086E-04  2.7609E-01
 3.7895E-02 -7.2413E-05 -9.5261E-05  2.5495E-03
Region #14 - Blade Sheath
 5.2142E-03  1.3597E-01  0.0000E+00  0.0000E+00  0.0000E+00  0.0000E+00
 0.0000E+00  0.0000E+00  6.0057E-01  1.4373E-03  2.7727E-03  8.7521E-01
 3.5289E-02  0.0000E+00  0.0000E+00  1.1878E-02
Region #15 - Control Rod
 7.9505E-03  2.9507E-01  0.0000E+00  0.0000E+00  0.0000E+00  0.0000E+00
 0.0000E+00  0.0000E+00  3.4087E-03  2.3116E-05  1.5126E-05  4.3357E-03
 2.8071E-04 -1.1776E-06  2.9146E-08  2.6292E-04
Region #16 - Moderator
 1.8741E-04  5.2949E-03  0.0000E+00  0.0000E+00  0.0000E+00  0.0000E+00
 0.0000E+00  0.0000E+00  3.9561E-01  1.7860E-02  1.5439E-03  1.1517E+00
 2.3564E-01  5.2793E-03  9.6184E-04  3.4043E-01
Region #17 - Bypass/Central Water Rod
 3.2318E-04  9.0178E-03  0.0000E+00  0.0000E+00  0.0000E+00  0.0000E+00
 0.0000E+00  0.0000E+00  6.6268E-01  3.2846E-02  1.8898E-03  1.9187E+00
 3.9664E-01  9.6941E-03  1.1741E-03  5.4610E-01
```

**GE9 Bundle - Void Fraction: 40%, Burnup: 15 GWd/T, Uncontrolled**

```
Region # 1 - Fuel 01
 3.0058E-02  1.7761E-01  4.3243E-03  8.7470E-02  2.7310E+00  2.7033E+00
 1.0000E+00  0.0000E+00  3.8134E-01  8.8234E-04  7.8793E-04  3.8949E-01
 4.2570E-02 -2.0317E-04 -7.2051E-05  8.4395E-03
Region # 2 - Fuel 02
 2.8419E-02  2.0063E-01  4.8041E-03  1.0633E-01  2.7026E+00  2.6600E+00
 1.0000E+00  0.0000E+00  3.7894E-01  8.1636E-04  9.0822E-04  3.8956E-01
 4.3338E-02 -1.8793E-04 -8.2068E-05  8.4603E-03
Region # 3 - Fuel 03
 3.0163E-02  2.1306E-01  5.0087E-03  1.1530E-01  2.6907E+00  2.6518E+00
 1.0000E+00  0.0000E+00  3.8132E-01  8.3245E-04  9.8026E-04  3.8952E-01
 4.2720E-02 -1.9209E-04 -8.8013E-05  8.4666E-03
Region # 4 - Fuel 04
 2.8451E-02  2.2523E-01  5.2907E-03  1.2598E-01  2.6788E+00  2.6306E+00
 1.0000E+00  0.0000E+00  3.7837E-01  7.8354E-04  1.0182E-03  3.8965E-01
 4.3607E-02 -1.8059E-04 -9.1200E-05  8.4775E-03
Region # 5 - Fuel 05
 2.9054E-02  2.3602E-01  5.5032E-03  1.3423E-01  2.6688E+00  2.6217E+00
 1.0000E+00  0.0000E+00  3.7900E-01  7.8707E-04  1.0759E-03  3.8964E-01
 4.3380E-02 -1.8154E-04 -9.5955E-05  8.4845E-03
Region # 6 - Fuel 06
 2.8854E-02  2.4987E-01  5.7868E-03  1.4559E-01  2.6583E+00  2.6088E+00
 1.0000E+00  0.0000E+00  3.7833E-01  7.6479E-04  1.1352E-03  3.8973E-01
 4.3660E-02 -1.7647E-04 -1.0088E-04  8.4944E-03
Region # 7 - Fuel 07
 2.9096E-02  2.6192E-01  6.0357E-03  1.5512E-01  2.6497E+00  2.6002E+00
 1.0000E+00  0.0000E+00  3.7831E-01  7.5732E-04  1.1937E-03  3.8978E-01
 4.3660E-02 -1.7481E-04 -1.0571E-04  8.5024E-03
Region # 8 - Fuel 08
 2.7952E-02  2.9708E-01  6.7796E-03  1.8471E-01  2.6277E+00  2.5702E+00
 1.0000E+00  0.0000E+00  3.7500E-01  7.0885E-04  1.2689E-03  3.9016E-01
 4.4620E-02 -1.6337E-04 -1.1202E-04  8.5229E-03
Region # 9 - Fuel 09
 2.9563E-02  3.1232E-01  7.0927E-03  1.9612E-01  2.6184E+00  2.5688E+00
```

```
 1.0000E+00  0.0000E+00  3.7738E-01  7.2001E-04  1.4052E-03  3.9011E-01
 4.3982E-02 -1.6639E-04 -1.2319E-04  8.5357E-03
Region #10 - Fuel 10
 2.9072E-02  3.3065E-01  7.4925E-03  2.1212E-01  2.6095E+00  2.5600E+00
 1.0000E+00  0.0000E+00  3.7646E-01  6.9348E-04  1.5411E-03  3.9026E-01
 4.4380E-02 -1.6037E-04 -1.3444E-04  8.5565E-03
Region #11 - Fuel 11
 2.9702E-02  3.5120E-01  7.7344E-03  2.2456E-01  2.5950E+00  2.5466E+00
 1.0000E+00  0.0000E+00  3.7496E-01  6.7136E-04  1.6826E-03  3.8397E-01
 4.4563E-02 -1.5464E-04 -1.4261E-04  8.5080E-03
Region #12 - Fuel 12
 3.0079E-02  3.2344E-01  7.1692E-03  2.0275E-01  2.6086E+00  2.5564E+00
 1.0000E+00  0.0000E+00  3.7527E-01  7.0027E-04  1.4107E-03  3.8395E-01
 4.4421E-02 -1.6122E-04 -1.2085E-04  8.4712E-03
Region #13 - Zirconium Clad
 1.7428E-03  4.4339E-03  0.0000E+00  0.0000E+00  0.0000E+00  0.0000E+00
 0.0000E+00  0.0000E+00  3.1483E-01  2.9198E-04  5.5739E-04  2.7641E-01
 3.8878E-02 -6.8558E-05 -6.8956E-05  2.5160E-03
Region #14 - Moderator
 1.8579E-04  5.5735E-03  0.0000E+00  0.0000E+00  0.0000E+00  0.0000E+00
 0.0000E+00  0.0000E+00  3.8742E-01  1.6599E-02  1.1196E-03  1.1876E+00
 2.3034E-01  4.8746E-03  6.9583E-04  3.3897E-01
Region #15 - Bypass/Central Water Rod
 3.2686E-04  9.3612E-03  0.0000E+00  0.0000E+00  0.0000E+00  0.0000E+00
 0.0000E+00  0.0000E+00  6.5246E-01  3.2020E-02  1.3885E-03  1.9628E+00
 3.9019E-01  9.4336E-03  8.5968E-04  5.4426E-01
```

**GE9 Bundle - Void Fraction: 40%, Burnup: 15 GWd/T, Controlled**

```
Region # 1 - Fuel 01
 3.0615E-02  1.7489E-01  4.0581E-03  8.6611E-02  2.7199E+00  2.7115E+00
 1.0000E+00  0.0000E+00  3.8854E-01  8.5307E-04  1.4420E-03  3.8815E-01
 4.0574E-02 -1.9674E-04 -1.2650E-04  8.5130E-03
Region # 2 - Fuel 02
 2.9248E-02  1.9695E-01  4.6019E-03  1.0459E-01  2.6910E+00  2.6681E+00
 1.0000E+00  0.0000E+00  3.8573E-01  8.0933E-04  1.5265E-03  3.8833E-01
 4.1365E-02 -1.8657E-04 -1.3333E-04  8.5281E-03
Region # 3 - Fuel 03
 3.0721E-02  2.1218E-01  4.9685E-03  1.1486E-01  2.6866E+00  2.6537E+00
 1.0000E+00  0.0000E+00  3.8360E-01  8.4795E-04  1.1241E-03  3.8924E-01
 4.1979E-02 -1.9573E-04 -9.9947E-05  8.4820E-03
Region # 4 - Fuel 04
 2.9262E-02  2.2063E-01  5.1429E-03  1.2344E-01  2.6679E+00  2.6380E+00
 1.0000E+00  0.0000E+00  3.8433E-01  7.8204E-04  1.5959E-03  3.8851E-01
 4.1849E-02 -1.8045E-04 -1.3899E-04  8.5403E-03
Region # 5 - Fuel 05
 2.9541E-02  2.3381E-01  5.4472E-03  1.3297E-01  2.6634E+00  2.6249E+00
 1.0000E+00  0.0000E+00  3.8189E-01  7.9301E-04  1.3199E-03  3.8915E-01
 4.2502E-02 -1.8300E-04 -1.1615E-04  8.5112E-03
Region # 6 - Fuel 06
 2.9470E-02  2.4638E-01  5.7059E-03  1.4354E-01  2.6505E+00  2.6140E+00
 1.0000E+00  0.0000E+00  3.8243E-01  7.6677E-04  1.5312E-03  3.8896E-01
 4.2439E-02 -1.7706E-04 -1.3359E-04  8.5372E-03
Region # 7 - Fuel 07
 2.9649E-02  2.6074E-01  6.0324E-03  1.5439E-01  2.6457E+00  2.6017E+00
 1.0000E+00  0.0000E+00  3.8026E-01  7.7482E-04  1.3211E-03  3.8955E-01
 4.3015E-02 -1.7890E-04 -1.1621E-04  8.5153E-03
Region # 8 - Fuel 08
 2.9085E-02  2.9079E-01  6.7639E-03  1.8058E-01  2.6171E+00  2.5753E+00
 1.0000E+00  0.0000E+00  3.8027E-01  7.2875E-04  1.7549E-03  3.8927E-01
 4.2964E-02 -1.6814E-04 -1.5196E-04  8.5723E-03
Region # 9 - Fuel 09
 2.9993E-02  3.1114E-01  7.1128E-03  1.9532E-01  2.6154E+00  2.5699E+00
 1.0000E+00  0.0000E+00  3.7873E-01  7.3361E-04  1.5047E-03  3.8994E-01
 4.3523E-02 -1.6956E-04 -1.3136E-04  8.5454E-03
Region #10 - Fuel 10
```

```
 2.9603E-02  3.2904E-01  7.5230E-03  2.1108E-01  2.6055E+00  2.5614E+00
 1.0000E+00  0.0000E+00  3.7829E-01  7.0849E-04  1.6944E-03  3.9000E-01
 4.3775E-02 -1.6389E-04 -1.4701E-04  8.5716E-03
Region #11 - Fuel 11
 3.0130E-02  3.4976E-01  7.7747E-03  2.2364E-01  2.5923E+00  2.5474E+00
 1.0000E+00  0.0000E+00  3.7617E-01  6.8495E-04  1.7797E-03  3.8381E-01
 4.4142E-02 -1.5780E-04 -1.5034E-04  8.5171E-03
Region #12 - Fuel 12
 3.1060E-02  3.2014E-01  7.2163E-03  2.0067E-01  2.6017E+00  2.5587E+00
 1.0000E+00  0.0000E+00  3.7854E-01  7.2352E-04  1.6446E-03  3.8355E-01
 4.3338E-02 -1.6668E-04 -1.3953E-04  8.4930E-03
Region #13 - Zirconium Clad
 1.7799E-03  4.3267E-03  0.0000E+00  0.0000E+00  0.0000E+00  0.0000E+00
 0.0000E+00  0.0000E+00  3.1653E-01  2.9323E-04  6.9062E-04  2.7622E-01
 3.8225E-02 -6.8853E-05 -8.5340E-05  2.5364E-03
Region #14 - Blade Sheath
 5.1548E-03  1.3699E-01  0.0000E+00  0.0000E+00  0.0000E+00  0.0000E+00
 0.0000E+00  0.0000E+00  5.9959E-01  1.3823E-03  2.6988E-03  8.7536E-01
 3.5488E-02  0.0000E+00  0.0000E+00  1.1876E-02
Region #15 - Control Rod
 7.7962E-03  2.9763E-01  0.0000E+00  0.0000E+00  0.0000E+00  0.0000E+00
 0.0000E+00  0.0000E+00  3.4028E-03  2.2052E-05  1.4640E-05  4.3381E-03
 2.8074E-04 -1.1181E-06  2.9523E-08  2.6285E-04
Region #16 - Moderator
 1.8489E-04  5.4524E-03  0.0000E+00  0.0000E+00  0.0000E+00  0.0000E+00
 0.0000E+00  0.0000E+00  3.9324E-01  1.6908E-02  1.3469E-03  1.1720E+00
 2.3405E-01  4.9586E-03  8.3886E-04  3.3956E-01
Region #17 - Bypass/Central Water Rod
 3.2079E-04  9.1173E-03  0.0000E+00  0.0000E+00  0.0000E+00  0.0000E+00
 0.0000E+00  0.0000E+00  6.5960E-01  3.1822E-02  1.7623E-03  1.9314E+00
 3.9459E-01  9.3514E-03  1.0945E-03  5.4556E-01
```

**GE9 Bundle - Void Fraction: 40%, Burnup: 25 GWd/T, Uncontrolled**

```
Region # 1 - Fuel 01
 3.2091E-02  1.6759E-01  3.8540E-03  7.2521E-02  2.7819E+00  2.7915E+00
 1.0000E+00  0.0000E+00  3.8181E-01  8.8566E-04  7.3841E-04  3.8820E-01
 4.2042E-02 -2.0271E-04 -6.7681E-05  8.4223E-03
Region # 2 - Fuel 02
 3.0072E-02  1.8493E-01  4.1821E-03  8.6032E-02  2.7570E+00  2.7473E+00
 1.0000E+00  0.0000E+00  3.7946E-01  8.1653E-04  8.3825E-04  3.8825E-01
 4.2776E-02 -1.8664E-04 -7.5943E-05  8.4390E-03
Region # 3 - Fuel 03
 3.1942E-02  1.9476E-01  4.2938E-03  9.2506E-02  2.7488E+00  2.7398E+00
 1.0000E+00  0.0000E+00  3.8186E-01  8.3566E-04  9.0708E-04  3.8811E-01
 4.2126E-02 -1.9153E-04 -8.1575E-05  8.4441E-03
Region # 4 - Fuel 04
 2.9922E-02  2.0467E-01  4.5308E-03  1.0104E-01  2.7343E+00  2.7132E+00
 1.0000E+00  0.0000E+00  3.7888E-01  7.8293E-04  9.3025E-04  3.8828E-01
 4.3023E-02 -1.7909E-04 -8.3524E-05  8.4525E-03
Region # 5 - Fuel 05
 3.0501E-02  2.1290E-01  4.6613E-03  1.0688E-01  2.7258E+00  2.7038E+00
 1.0000E+00  0.0000E+00  3.7957E-01  7.8757E-04  9.8364E-04  3.8819E-01
 4.2770E-02 -1.8028E-04 -8.7876E-05  8.4582E-03
Region # 6 - Fuel 06
 3.0181E-02  2.2515E-01  4.8958E-03  1.1653E-01  2.7137E+00  2.6865E+00
 1.0000E+00  0.0000E+00  3.7881E-01  7.6382E-04  1.0323E-03  3.8828E-01
 4.3060E-02 -1.7487E-04 -9.1889E-05  8.4664E-03
Region # 7 - Fuel 07
 3.0347E-02  2.3525E-01  5.0796E-03  1.2411E-01  2.7049E+00  2.6758E+00
 1.0000E+00  0.0000E+00  3.7880E-01  7.5620E-04  1.0844E-03  3.8828E-01
 4.3052E-02 -1.7317E-04 -9.6152E-05  8.4729E-03
Region # 8 - Fuel 08
 2.8786E-02  2.6514E-01  5.6973E-03  1.4867E-01  2.6772E+00  2.6346E+00
 1.0000E+00  0.0000E+00  3.7539E-01  7.0400E-04  1.1304E-03  3.8864E-01
 4.4011E-02 -1.6081E-04 -9.9983E-05  8.4884E-03
```

Region # 9 - Fuel 09
3.0486E-02 2.8003E-01 5.9357E-03 1.5917E-01 2.6684E+00 2.6331E+00
1.0000E+00 0.0000E+00 3.7772E-01 7.1639E-04 1.2663E-03 3.8850E-01
4.3377E-02 -1.6414E-04 -1.1104E-04 8.5009E-03
Region #10 - Fuel 10
2.9899E-02 3.0166E-01 6.3677E-03 1.7718E-01 2.6550E+00 2.6186E+00
1.0000E+00 0.0000E+00 3.7667E-01 6.8696E-04 1.3829E-03 3.8875E-01
4.3838E-02 -1.5743E-04 -1.2063E-04 8.5199E-03
Region #11 - Fuel 11
3.0604E-02 3.2394E-01 6.6142E-03 1.9182E-01 2.6372E+00 2.6007E+00
1.0000E+00 0.0000E+00 3.7510E-01 6.6269E-04 1.5058E-03 3.8257E-01
4.4060E-02 -1.5116E-04 -1.2754E-04 8.4697E-03
Region #12 - Fuel 12
3.1149E-02 2.9193E-01 6.0237E-03 1.6659E-01 2.6563E+00 2.6172E+00
1.0000E+00 0.0000E+00 3.7560E-01 6.9567E-04 1.2602E-03 3.8244E-01
4.3842E-02 -1.5871E-04 -1.0804E-04 8.4354E-03
Region #13 - Zirconium Clad
1.7566E-03 4.4754E-03 0.0000E+00 0.0000E+00 0.0000E+00 0.0000E+00
0.0000E+00 0.0000E+00 3.1491E-01 2.9394E-04 5.1837E-04 2.7647E-01
3.8526E-02 -6.9010E-05 -6.4157E-05 2.5097E-03
Region #14 - Moderator
1.8754E-04 5.6358E-03 0.0000E+00 0.0000E+00 0.0000E+00 0.0000E+00
0.0000E+00 0.0000E+00 3.8956E-01 1.6659E-02 1.0360E-03 1.1956E+00
2.3177E-01 4.8783E-03 6.4333E-04 3.3863E-01
Region #15 - Bypass/Central Water Rod
3.3130E-04 9.4036E-03 0.0000E+00 0.0000E+00 0.0000E+00 0.0000E+00
0.0000E+00 0.0000E+00 6.5597E-01 3.2505E-02 1.3216E-03 1.9683E+00
3.9257E-01 9.5670E-03 8.1763E-04 5.4405E-01

**GE9 Bundle - Void Fraction: 40%, Burnup: 25 GWd/T, Controlled**

Region # 1 - Fuel 01
3.2620E-02 1.6621E-01 3.5744E-03 7.2744E-02 2.7750E+00 2.7958E+00
1.0000E+00 0.0000E+00 3.8901E-01 8.5324E-04 1.3615E-03 3.8691E-01
4.0064E-02 -1.9557E-04 -1.1945E-04 8.4928E-03
Region # 2 - Fuel 02
3.0905E-02 1.8301E-01 3.9551E-03 8.5691E-02 2.7491E+00 2.7529E+00
1.0000E+00 0.0000E+00 3.8623E-01 8.0697E-04 1.4218E-03 3.8708E-01
4.0819E-02 -1.8469E-04 -1.2424E-04 8.5034E-03
Region # 3 - Fuel 03
3.2549E-02 1.9430E-01 4.2371E-03 9.2406E-02 2.7461E+00 2.7412E+00
1.0000E+00 0.0000E+00 3.8421E-01 8.5115E-04 1.0481E-03 3.8783E-01
4.1376E-02 -1.9514E-04 -9.3242E-05 8.4593E-03
Region # 4 - Fuel 04
3.0737E-02 2.0217E-01 4.3532E-03 1.0016E-01 2.7262E+00 2.7191E+00
1.0000E+00 0.0000E+00 3.8488E-01 7.7933E-04 1.4721E-03 3.8720E-01
4.1274E-02 -1.7845E-04 -1.2826E-04 8.5120E-03
Region # 5 - Fuel 05
3.1006E-02 2.1167E-01 4.5861E-03 1.0639E-01 2.7217E+00 2.7064E+00
1.0000E+00 0.0000E+00 3.8248E-01 7.9280E-04 1.2153E-03 3.8772E-01
4.1888E-02 -1.8155E-04 -1.0701E-04 8.4838E-03
Region # 6 - Fuel 06
3.0804E-02 2.2349E-01 4.7891E-03 1.1589E-01 2.7074E+00 2.6912E+00
1.0000E+00 0.0000E+00 3.8296E-01 7.6452E-04 1.4039E-03 3.8755E-01
4.1841E-02 -1.7514E-04 -1.2251E-04 8.5069E-03
Region # 7 - Fuel 07
3.0950E-02 2.3456E-01 5.0544E-03 1.2377E-01 2.7016E+00 2.6772E+00
1.0000E+00 0.0000E+00 3.8082E-01 7.7400E-04 1.2103E-03 3.8805E-01
4.2392E-02 -1.7729E-04 -1.0650E-04 8.4858E-03
Region # 8 - Fuel 08
2.9970E-02 2.6130E-01 5.6279E-03 1.4647E-01 2.6675E+00 2.6398E+00
1.0000E+00 0.0000E+00 3.8077E-01 7.2336E-04 1.5863E-03 3.8779E-01
4.2341E-02 -1.6542E-04 -1.3736E-04 8.5353E-03
Region # 9 - Fuel 09
3.0952E-02 2.7932E-01 5.9361E-03 1.5873E-01 2.6657E+00 2.6344E+00
1.0000E+00 0.0000E+00 3.7915E-01 7.3025E-04 1.3660E-03 3.8832E-01

```
 4.2906E-02 -1.6735E-04 -1.1920E-04  8.5108E-03
Region #10 - Fuel 10
 3.0471E-02  3.0100E-01  6.3743E-03  1.7687E-01  2.6513E+00  2.6202E+00
 1.0000E+00  0.0000E+00  3.7857E-01  7.0215E-04  1.5355E-03  3.8849E-01
 4.3219E-02 -1.6096E-04 -1.3309E-04  8.5352E-03
Region #11 - Fuel 11
 3.1072E-02  3.2296E-01  6.6364E-03  1.9129E-01  2.6345E+00  2.6016E+00
 1.0000E+00  0.0000E+00  3.7637E-01  6.7650E-04  1.6062E-03  3.8240E-01
 4.3626E-02 -1.5433E-04 -1.3551E-04  8.4792E-03
Region #12 - Fuel 12
 3.2212E-02  2.8965E-01  6.0287E-03  1.6532E-01  2.6498E+00  2.6198E+00
 1.0000E+00  0.0000E+00  3.7901E-01  7.1954E-04  1.4926E-03  3.8204E-01
 4.2728E-02 -1.6426E-04 -1.2655E-04  8.4574E-03
Region #13 - Zirconium Clad
 1.7943E-03  4.3721E-03  0.0000E+00  0.0000E+00  0.0000E+00  0.0000E+00
 0.0000E+00  0.0000E+00  3.1662E-01  2.9508E-04  6.4617E-04  2.7629E-01
 3.7861E-02 -6.9278E-05 -7.9877E-05  2.5292E-03
Region #14 - Blade Sheath
 5.2258E-03  1.3771E-01  0.0000E+00  0.0000E+00  0.0000E+00  0.0000E+00
 0.0000E+00  0.0000E+00  6.0321E-01  1.4006E-03  2.5920E-03  8.7552E-01
 3.5273E-02  0.0000E+00  0.0000E+00  1.1875E-02
Region #15 - Control Rod
 7.9232E-03  2.9936E-01  0.0000E+00  0.0000E+00  0.0000E+00  0.0000E+00
 0.0000E+00  0.0000E+00  3.4113E-03  2.2285E-05  1.4025E-05  4.3400E-03
 2.8059E-04 -1.1282E-06  2.6356E-08  2.6282E-04
Region #16 - Moderator
 1.8666E-04  5.5183E-03  0.0000E+00  0.0000E+00  0.0000E+00  0.0000E+00
 0.0000E+00  0.0000E+00  3.9548E-01  1.6973E-02  1.2551E-03  1.1804E+00
 2.3555E-01  4.9628E-03  7.8118E-04  3.3920E-01
Region #17 - Bypass/Central Water Rod
 3.2518E-04  9.1655E-03  0.0000E+00  0.0000E+00  0.0000E+00  0.0000E+00
 0.0000E+00  0.0000E+00  6.6326E-01  3.2295E-02  1.6849E-03  1.9376E+00
 3.9708E-01  9.4796E-03  1.0459E-03  5.4531E-01
```

**GE9 Bundle - Void Fraction: 70%, Burnup: 0.350 GWd/T, Uncontrolled**

```
Region # 1 - Fuel 01
 2.4730E-02  1.6659E-01  5.5501E-03  1.0609E-01  2.5943E+00  2.4464E+00
 1.0000E+00  0.0000E+00  3.8296E-01  8.9098E-04  1.0131E-03  3.9137E-01
 4.2523E-02 -2.0957E-04 -9.2467E-05  8.4966E-03
Region # 2 - Fuel 02
 2.3938E-02  1.9289E-01  6.1691E-03  1.2830E-01  2.5821E+00  2.4432E+00
 1.0000E+00  0.0000E+00  3.8026E-01  8.2776E-04  1.1856E-03  3.9132E-01
 4.3402E-02 -1.9473E-04 -1.0720E-04  8.5271E-03
Region # 3 - Fuel 03
 2.5665E-02  2.0771E-01  6.5339E-03  1.4048E-01  2.5696E+00  2.4425E+00
 1.0000E+00  0.0000E+00  3.8324E-01  8.2491E-04  1.2991E-03  3.9143E-01
 4.2710E-02 -1.9417E-04 -1.1659E-04  8.5368E-03
Region # 4 - Fuel 04
 2.4433E-02  2.1913E-01  6.7841E-03  1.5031E-01  2.5696E+00  2.4414E+00
 1.0000E+00  0.0000E+00  3.7979E-01  7.9160E-04  1.3499E-03  3.9139E-01
 4.3693E-02 -1.8626E-04 -1.2110E-04  8.5519E-03
Region # 5 - Fuel 05
 2.5144E-02  2.3269E-01  7.1242E-03  1.6157E-01  2.5620E+00  2.4408E+00
 1.0000E+00  0.0000E+00  3.8068E-01  7.8420E-04  1.4417E-03  3.9147E-01
 4.3451E-02 -1.8459E-04 -1.2869E-04  8.5626E-03
Region # 6 - Fuel 06
 2.5178E-02  2.4453E-01  7.3983E-03  1.7166E-01  2.5579E+00  2.4402E+00
 1.0000E+00  0.0000E+00  3.8013E-01  7.6555E-04  1.5289E-03  3.9148E-01
 4.3694E-02 -1.8020E-04 -1.3609E-04  8.5761E-03
Region # 7 - Fuel 07
 2.5567E-02  2.5723E-01  7.7134E-03  1.8229E-01  2.5531E+00  2.4397E+00
 1.0000E+00  0.0000E+00  3.8032E-01  7.5298E-04  1.6171E-03  3.9155E-01
 4.3678E-02 -1.7728E-04 -1.4345E-04  8.5873E-03
Region # 8 - Fuel 08
 2.4988E-02  2.9137E-01  8.5139E-03  2.1124E-01  2.5469E+00  2.4384E+00
```

```
 1.0000E+00  0.0000E+00  3.7652E-01  7.2247E-04  1.7392E-03  3.9178E-01
 4.4730E-02 -1.7002E-04 -1.5406E-04  8.6168E-03
Region # 9 - Fuel 09
 2.6589E-02  3.0270E-01  8.8732E-03  2.2097E-01  2.5383E+00  2.4383E+00
 1.0000E+00  0.0000E+00  3.7984E-01  7.1347E-04  1.9730E-03  3.9173E-01
 4.3900E-02 -1.6804E-04 -1.7321E-04  8.6362E-03
Region #10 - Fuel 10
 2.6208E-02  3.0229E-01  8.9837E-03  2.2213E-01  2.5370E+00  2.4380E+00
 1.0000E+00  0.0000E+00  3.7947E-01  6.9187E-04  2.2897E-03  3.9126E-01
 4.4076E-02 -1.6303E-04 -1.9944E-04  8.6727E-03
Region #11 - Fuel 11
 3.5187E-02  2.3988E+00  8.4097E-03  1.3401E-01  2.5346E+00  2.4404E+00
 1.0000E+00  0.0000E+00  3.8037E-01  6.5956E-04  6.0679E-03  3.9512E-01
 4.3580E-02 -1.5494E-04 -4.9653E-04  9.0747E-03
Region #12 - Fuel 12
 3.5837E-02  2.6230E+00  8.0721E-03  1.2670E-01  2.5389E+00  2.4412E+00
 1.0000E+00  0.0000E+00  3.8082E-01  6.9883E-04  5.4749E-03  3.9673E-01
 4.3403E-02 -1.6409E-04 -4.5224E-04  9.0317E-03
Region #13 - Zirconium Clad
 1.7717E-03  4.2196E-03  0.0000E+00  0.0000E+00  0.0000E+00  0.0000E+00
 0.0000E+00  0.0000E+00  3.1871E-01  2.8310E-04  7.6613E-04  2.7609E-01
 3.8804E-02 -6.6488E-05 -9.4658E-05  2.5492E-03
Region #14 - Moderator
 9.4757E-05  2.8405E-03  0.0000E+00  0.0000E+00  0.0000E+00  0.0000E+00
 0.0000E+00  0.0000E+00  2.1122E-01  8.7903E-03  8.4438E-04  6.1994E-01
 1.2545E-01  2.5971E-03  5.2622E-04  1.8427E-01
Region #15 - Bypass/Central Water Rod
 3.0960E-04  9.0884E-03  0.0000E+00  0.0000E+00  0.0000E+00  0.0000E+00
 0.0000E+00  0.0000E+00  6.5957E-01  3.0976E-02  1.8062E-03  1.9277E+00
 3.9416E-01  9.1345E-03  1.1218E-03  5.4570E-01
```

**GE9 Bundle - Void Fraction: 70%, Burnup: 0.350 GWd/T, Controlled**

```
Region # 1 - Fuel 01
 2.5105E-02  1.5284E-01  5.2601E-03  9.7297E-02  2.5755E+00  2.4482E+00
 1.0000E+00  0.0000E+00  3.9087E-01  8.3714E-04  1.8838E-03  3.8954E-01
 4.0404E-02 -1.9742E-04 -1.6562E-04  8.5945E-03
Region # 2 - Fuel 02
 2.4517E-02  1.7737E-01  5.9532E-03  1.1800E-01  2.5647E+00  2.4445E+00
 1.0000E+00  0.0000E+00  3.8789E-01  7.9658E-04  2.0490E-03  3.8958E-01
 4.1251E-02 -1.8783E-04 -1.7946E-04  8.6212E-03
Region # 3 - Fuel 03
 2.6178E-02  2.0425E-01  6.5146E-03  1.3816E-01  2.5624E+00  2.4427E+00
 1.0000E+00  0.0000E+00  3.8618E-01  8.3669E-04  1.4947E-03  3.9105E-01
 4.1773E-02 -1.9706E-04 -1.3291E-04  8.5572E-03
Region # 4 - Fuel 04
 2.5021E-02  2.0204E-01  6.6256E-03  1.3866E-01  2.5546E+00  2.4423E+00
 1.0000E+00  0.0000E+00  3.8662E-01  7.6908E-04  2.1881E-03  3.8973E-01
 4.1731E-02 -1.8133E-04 -1.9106E-04  8.6419E-03
Region # 5 - Fuel 05
 2.5570E-02  2.2526E-01  7.0785E-03  1.5644E-01  2.5540E+00  2.4411E+00
 1.0000E+00  0.0000E+00  3.8420E-01  7.8367E-04  1.7806E-03  3.9079E-01
 4.2386E-02 -1.8463E-04 -1.5697E-04  8.5990E-03
Region # 6 - Fuel 06
 2.5668E-02  2.3116E-01  7.3154E-03  1.6236E-01  2.5475E+00  2.4407E+00
 1.0000E+00  0.0000E+00  3.8501E-01  7.5466E-04  2.1187E-03  3.9033E-01
 4.2270E-02 -1.7789E-04 -1.8521E-04  8.6386E-03
Region # 7 - Fuel 07
 2.6112E-02  2.5325E-01  7.7385E-03  1.7951E-01  2.5468E+00  2.4398E+00
 1.0000E+00  0.0000E+00  3.8301E-01  7.6690E-04  1.8150E-03  3.9120E-01
 4.2799E-02 -1.8065E-04 -1.5984E-04  8.6067E-03
Region # 8 - Fuel 08
 2.5899E-02  2.7098E-01  8.5102E-03  1.9670E-01  2.5340E+00  2.4389E+00
 1.0000E+00  0.0000E+00  3.8289E-01  7.2173E-04  2.5628E-03  3.9029E-01
 4.2788E-02 -1.7014E-04 -2.2226E-04  8.6989E-03
Region # 9 - Fuel 09
```

```
 2.7068E-02  2.9877E-01  8.9270E-03  2.1817E-01  2.5336E+00  2.4384E+00
 1.0000E+00  0.0000E+00  3.8194E-01  7.2592E-04  2.1450E-03  3.9143E-01
 4.3206E-02 -1.7104E-04 -1.8736E-04  8.6526E-03
Region #10 - Fuel 10
 2.6759E-02  2.9556E-01  9.0393E-03  2.1732E-01  2.5312E+00  2.4381E+00
 1.0000E+00  0.0000E+00  3.8214E-01  7.0257E-04  2.5800E-03  3.9078E-01
 4.3209E-02 -1.6564E-04 -2.2323E-04  8.7001E-03
Region #11 - Fuel 11
 3.5909E-02  2.2973E+00  8.4662E-03  1.3226E-01  2.5299E+00  2.4404E+00
 1.0000E+00  0.0000E+00  3.8242E-01  6.7152E-04  6.3215E-03  3.9416E-01
 4.2895E-02 -1.5781E-04 -5.1522E-04  9.0910E-03
Region #12 - Fuel 12
 3.6968E-02  2.3392E+00  8.1113E-03  1.2235E-01  2.5305E+00  2.4413E+00
 1.0000E+00  0.0000E+00  3.8489E-01  7.0531E-04  6.1404E-03  3.9410E-01
 4.2122E-02 -1.6579E-04 -5.0177E-04  9.0744E-03
Region #13 - Zirconium Clad
 1.8229E-03  4.0640E-03  0.0000E+00  0.0000E+00  0.0000E+00  0.0000E+00
 0.0000E+00  0.0000E+00  3.2117E-01  2.8187E-04  9.7681E-04  2.7581E-01
 3.7949E-02 -6.6202E-05 -1.2055E-04  2.5808E-03
Region #14 - Blade Sheath
 5.0201E-03  1.3203E-01  0.0000E+00  0.0000E+00  0.0000E+00  0.0000E+00
 0.0000E+00  0.0000E+00  6.0256E-01  1.3209E-03  3.3961E-03  8.7432E-01
 3.4369E-02  0.0000E+00  0.0000E+00  1.1885E-02
Region #15 - Control Rod
 7.5346E-03  2.8618E-01  0.0000E+00  0.0000E+00  0.0000E+00  0.0000E+00
 0.0000E+00  0.0000E+00  3.4372E-03  2.1281E-05  1.8527E-05  4.3258E-03
 2.8113E-04 -1.0854E-06  4.7861E-08  2.6310E-04
Region #16 - Moderator
 9.3470E-05  2.7389E-03  0.0000E+00  0.0000E+00  0.0000E+00  0.0000E+00
 0.0000E+00  0.0000E+00  2.1536E-01  8.8955E-03  1.0522E-03  6.0682E-01
 1.2806E-01  2.6220E-03  6.5707E-04  1.8474E-01
Region #17 - Bypass/Central Water Rod
 3.0188E-04  8.7665E-03  0.0000E+00  0.0000E+00  0.0000E+00  0.0000E+00
 0.0000E+00  0.0000E+00  6.6943E-01  3.0700E-02  2.3339E-03  1.8863E+00
 4.0024E-01  9.0265E-03  1.4535E-03  5.4736E-01
GE9 Bundle - Void Fraction: 70%, Burnup: 15 GWd/T, Uncontrolled
Region # 1 - Fuel 01
 2.9031E-02  1.7660E-01  4.1447E-03  8.7067E-02  2.7264E+00  2.7055E+00
 1.0000E+00  0.0000E+00  3.8383E-01  8.3843E-04  9.6257E-04  3.8911E-01
 4.1981E-02 -1.9290E-04 -8.6454E-05  8.4604E-03
Region # 2 - Fuel 02
 2.7065E-02  1.9875E-01  4.6107E-03  1.0534E-01  2.6981E+00  2.6626E+00
 1.0000E+00  0.0000E+00  3.8104E-01  7.7263E-04  1.1068E-03  3.8911E-01
 4.2822E-02 -1.7756E-04 -9.8321E-05  8.4850E-03
Region # 3 - Fuel 03
 2.8882E-02  2.1108E-01  4.7948E-03  1.1424E-01  2.6862E+00  2.6548E+00
 1.0000E+00  0.0000E+00  3.8377E-01  7.7647E-04  1.2101E-03  3.8904E-01
 4.2183E-02 -1.7902E-04 -1.0686E-04  8.4934E-03
Region # 4 - Fuel 04
 2.7002E-02  2.2251E-01  5.0788E-03  1.2441E-01  2.6745E+00  2.6334E+00
 1.0000E+00  0.0000E+00  3.8035E-01  7.3814E-04  1.2390E-03  3.8915E-01
 4.3126E-02 -1.6979E-04 -1.0920E-04  8.5051E-03
Region # 5 - Fuel 05
 2.7565E-02  2.3300E-01  5.2735E-03  1.3244E-01  2.6645E+00  2.6247E+00
 1.0000E+00  0.0000E+00  3.8125E-01  7.3449E-04  1.3229E-03  3.8910E-01
 4.2875E-02 -1.6915E-04 -1.1606E-04  8.5140E-03
Region # 6 - Fuel 06
 2.7274E-02  2.4619E-01  5.5479E-03  1.4332E-01  2.6543E+00  2.6118E+00
 1.0000E+00  0.0000E+00  3.8030E-01  7.1310E-04  1.3879E-03  3.8917E-01
 4.3215E-02 -1.6422E-04 -1.2140E-04  8.5251E-03
Region # 7 - Fuel 07
 2.7439E-02  2.5789E-01  5.7794E-03  1.5259E-01  2.6458E+00  2.6033E+00
 1.0000E+00  0.0000E+00  3.8037E-01  7.0139E-04  1.4647E-03  3.8920E-01
 4.3219E-02 -1.6160E-04 -1.2770E-04  8.5345E-03
```

```
 Region # 8 - Fuel 08
  2.6097E-02  2.9152E-01  6.5171E-03  1.8100E-01  2.6244E+00  2.5727E+00
  1.0000E+00  0.0000E+00  3.7642E-01  6.6624E-04  1.5131E-03  3.8959E-01
  4.4239E-02 -1.5302E-04 -1.3162E-04  8.5542E-03
 Region # 9 - Fuel 09
  2.7689E-02  3.0578E-01  6.7816E-03  1.9174E-01  2.6151E+00  2.5720E+00
  1.0000E+00  0.0000E+00  3.7928E-01  6.6134E-04  1.7263E-03  3.8943E-01
  4.3577E-02 -1.5248E-04 -1.4905E-04  8.5732E-03
 Region #10 - Fuel 10
  2.7039E-02  3.2285E-01  7.1544E-03  2.0677E-01  2.6069E+00  2.5630E+00
  1.0000E+00  0.0000E+00  3.7798E-01  6.3639E-04  1.8680E-03  3.8956E-01
  4.4073E-02 -1.4673E-04 -1.6058E-04  8.5952E-03
 Region #11 - Fuel 11
  2.7592E-02  3.4119E-01  7.3720E-03  2.1810E-01  2.5928E+00  2.5495E+00
  1.0000E+00  0.0000E+00  3.7639E-01  6.1356E-04  2.0365E-03  3.8321E-01
  4.4275E-02 -1.4085E-04 -1.6999E-04  8.5489E-03
 Region #12 - Fuel 12
  2.8200E-02  3.1658E-01  6.8723E-03  1.9836E-01  2.6059E+00  2.5590E+00
  1.0000E+00  0.0000E+00  3.7665E-01  6.5014E-04  1.6781E-03  3.8336E-01
  4.4111E-02 -1.4919E-04 -1.4172E-04  8.5032E-03
 Region #13 - Zirconium Clad
  1.7616E-03  4.3219E-03  0.0000E+00  0.0000E+00  0.0000E+00  0.0000E+00
  0.0000E+00  0.0000E+00  3.1815E-01  2.6841E-04  6.8969E-04  2.7621E-01
  3.9081E-02 -6.3020E-05 -8.5199E-05  2.5364E-03
 Region #14 - Moderator
  9.3470E-05  2.9302E-03  0.0000E+00  0.0000E+00  0.0000E+00  0.0000E+00
  0.0000E+00  0.0000E+00  2.1020E-01  8.2612E-03  7.4072E-04  6.3144E-01
  1.2476E-01  2.4161E-03  4.6164E-04  1.8377E-01
 Region #15 - Bypass/Central Water Rod
  3.0775E-04  9.1836E-03  0.0000E+00  0.0000E+00  0.0000E+00  0.0000E+00
  0.0000E+00  0.0000E+00  6.5684E-01  2.9994E-02  1.6893E-03  1.9399E+00
  3.9235E-01  8.8008E-03  1.0489E-03  5.4517E-01
GE9 Bundle - Void Fraction: 70%, Burnup: 15 GWd/T, Controlled
 Region # 1 - Fuel 01
  2.8999E-02  1.7285E-01  3.8334E-03  8.5785E-02  2.7150E+00  2.7157E+00
  1.0000E+00  0.0000E+00  3.9127E-01  7.7259E-04  1.8063E-03  3.8738E-01
  4.0065E-02 -1.7804E-04 -1.5620E-04  8.5550E-03
 Region # 2 - Fuel 02
  2.7390E-02  1.9361E-01  4.3497E-03  1.0286E-01  2.6859E+00  2.6730E+00
  1.0000E+00  0.0000E+00  3.8825E-01  7.3122E-04  1.9287E-03  3.8748E-01
  4.0853E-02 -1.6830E-04 -1.6595E-04  8.5747E-03
 Region # 3 - Fuel 03
  2.9467E-02  2.0991E-01  4.7310E-03  1.1364E-01  2.6807E+00  2.6572E+00
  1.0000E+00  0.0000E+00  3.8679E-01  7.8716E-04  1.4029E-03  3.8867E-01
  4.1242E-02 -1.8157E-04 -1.2274E-04  8.5135E-03
 Region # 4 - Fuel 04
  2.7388E-02  2.1615E-01  4.8683E-03  1.2086E-01  2.6627E+00  2.6431E+00
  1.0000E+00  0.0000E+00  3.8688E-01  7.0723E-04  2.0159E-03  3.8763E-01
  4.1314E-02 -1.6289E-04 -1.7293E-04  8.5888E-03
 Region # 5 - Fuel 05
  2.7971E-02  2.3008E-01  5.1862E-03  1.3075E-01  2.6578E+00  2.6287E+00
  1.0000E+00  0.0000E+00  3.8476E-01  7.3133E-04  1.6453E-03  3.8847E-01
  4.1831E-02 -1.6851E-04 -1.4252E-04  8.5488E-03
 Region # 6 - Fuel 06
  2.7665E-02  2.4123E-01  5.4189E-03  1.4037E-01  2.6454E+00  2.6186E+00
  1.0000E+00  0.0000E+00  3.8504E-01  6.9770E-04  1.9293E-03  3.8813E-01
  4.1867E-02 -1.6081E-04 -1.6572E-04  8.5828E-03
 Region # 7 - Fuel 07
  2.8066E-02  2.5611E-01  5.7548E-03  1.5149E-01  2.6400E+00  2.6054E+00
  1.0000E+00  0.0000E+00  3.8318E-01  7.1525E-04  1.6590E-03  3.8885E-01
  4.2320E-02 -1.6488E-04 -1.4358E-04  8.5538E-03
 Region # 8 - Fuel 08
  2.6943E-02  2.8216E-01  6.4252E-03  1.7486E-01  2.6122E+00  2.5800E+00
  1.0000E+00  0.0000E+00  3.8265E-01  6.6055E-04  2.2227E-03  3.8831E-01
```

```
 4.2396E-02 -1.5194E-04 -1.8942E-04  8.6258E-03
Region # 9 - Fuel 09
 2.8248E-02  3.0379E-01  6.7936E-03  1.9040E-01  2.6103E+00  2.5737E+00
 1.0000E+00  0.0000E+00  3.8153E-01  6.7458E-04  1.8944E-03  3.8915E-01
 4.2849E-02 -1.5559E-04 -1.6273E-04  8.5893E-03
Region #10 - Fuel 10
 2.7657E-02  3.1984E-01  7.1691E-03  2.0480E-01  2.6010E+00  2.5654E+00
 1.0000E+00  0.0000E+00  3.8078E-01  6.4769E-04  2.1289E-03  3.8912E-01
 4.3180E-02 -1.4942E-04 -1.8176E-04  8.6205E-03
Region #11 - Fuel 11
 2.8184E-02  3.3837E-01  7.4123E-03  2.1631E-01  2.5881E+00  2.5510E+00
 1.0000E+00  0.0000E+00  3.7856E-01  6.2688E-04  2.2236E-03  3.8291E-01
 4.3551E-02 -1.4397E-04 -1.8473E-04  8.5660E-03
Region #12 - Fuel 12
 2.9172E-02  3.1109E-01  6.8759E-03  1.9491E-01  2.5970E+00  2.5626E+00
 1.0000E+00  0.0000E+00  3.8114E-01  6.5980E-04  2.0682E-03  3.8270E-01
 4.2709E-02 -1.5159E-04 -1.7259E-04  8.5391E-03
Region #13 - Zirconium Clad
 1.8127E-03  4.1844E-03  0.0000E+00  0.0000E+00  0.0000E+00  0.0000E+00
 0.0000E+00  0.0000E+00  3.2059E-01  2.6695E-04  8.7584E-04  2.7596E-01
 3.8224E-02 -6.2680E-05 -1.0807E-04  2.5645E-03
Region #14 - Blade Sheath
 4.9576E-03  1.3343E-01  0.0000E+00  0.0000E+00  0.0000E+00  0.0000E+00
 0.0000E+00  0.0000E+00  6.0164E-01  1.2613E-03  3.2877E-03  8.7452E-01
 3.4561E-02  0.0000E+00  0.0000E+00  1.1883E-02
Region #15 - Control Rod
 7.3779E-03  2.8967E-01  0.0000E+00  0.0000E+00  0.0000E+00  0.0000E+00
 0.0000E+00  0.0000E+00  3.4321E-03  2.0116E-05  1.7829E-05  4.3291E-03
 2.8115E-04 -1.0193E-06  4.8164E-08  2.6301E-04
Region #16 - Moderator
 9.2158E-05  2.8414E-03  0.0000E+00  0.0000E+00  0.0000E+00  0.0000E+00
 0.0000E+00  0.0000E+00  2.1435E-01  8.3675E-03  9.1996E-04  6.1998E-01
 1.2738E-01  2.4406E-03  5.7456E-04  1.8418E-01
Region #17 - Bypass/Central Water Rod
 2.9990E-04  8.8890E-03  0.0000E+00  0.0000E+00  0.0000E+00  0.0000E+00
 0.0000E+00  0.0000E+00  6.6681E-01  2.9702E-02  2.1755E-03  1.9020E+00
 3.9850E-01  8.6845E-03  1.3547E-03  5.4669E-01
```

**GE9 Bundle - Void Fraction: 70%, Burnup: 25 GWd/T, Uncontrolled**

```
Region # 1 - Fuel 01
 3.0965E-02  1.6695E-01  3.6760E-03  7.2429E-02  2.7782E+00  2.7927E+00
 1.0000E+00  0.0000E+00  3.8438E-01  8.4048E-04  9.0385E-04  3.8783E-01
 4.1417E-02 -1.9216E-04 -8.1310E-05  8.4423E-03
Region # 2 - Fuel 02
 2.8572E-02  1.8370E-01  3.9958E-03  8.5579E-02  2.7530E+00  2.7491E+00
 1.0000E+00  0.0000E+00  3.8163E-01  7.7105E-04  1.0237E-03  3.8783E-01
 4.2228E-02 -1.7585E-04 -9.1121E-05  8.4623E-03
Region # 3 - Fuel 03
 3.0517E-02  1.9355E-01  4.0921E-03  9.2070E-02  2.7448E+00  2.7420E+00
 1.0000E+00  0.0000E+00  3.8440E-01  7.7753E-04  1.1226E-03  3.8765E-01
 4.1564E-02 -1.7798E-04 -9.9223E-05  8.4694E-03
Region # 4 - Fuel 04
 2.8315E-02  2.0289E-01  4.3320E-03  1.0022E-01  2.7302E+00  2.7154E+00
 1.0000E+00  0.0000E+00  3.8097E-01  7.3544E-04  1.1345E-03  3.8781E-01
 4.2510E-02 -1.6780E-04 -1.0016E-04  8.4784E-03
Region # 5 - Fuel 05
 2.8845E-02  2.1096E-01  4.4492E-03  1.0595E-01  2.7216E+00  2.7063E+00
 1.0000E+00  0.0000E+00  3.8184E-01  7.3280E-04  1.2128E-03  3.8769E-01
 4.2238E-02 -1.6739E-04 -1.0652E-04  8.4860E-03
Region # 6 - Fuel 06
 2.8429E-02  2.2269E-01  4.6781E-03  1.1525E-01  2.7095E+00  2.6891E+00
 1.0000E+00  0.0000E+00  3.8085E-01  7.0986E-04  1.2649E-03  3.8776E-01
 4.2585E-02 -1.6209E-04 -1.1076E-04  8.4950E-03
Region # 7 - Fuel 07
 2.8508E-02  2.3261E-01  4.8489E-03  1.2269E-01  2.7008E+00  2.6786E+00
```

```
 1.0000E+00  0.0000E+00  3.8091E-01  6.9793E-04  1.3336E-03  3.8774E-01
 4.2582E-02 -1.5942E-04 -1.1633E-04  8.5029E-03
Region # 8 - Fuel 08
 2.6731E-02  2.6125E-01  5.4644E-03  1.4634E-01  2.6734E+00  2.6369E+00
 1.0000E+00  0.0000E+00  3.7689E-01  6.5931E-04  1.3522E-03  3.8811E-01
 4.3591E-02 -1.4994E-04 -1.1778E-04  8.5174E-03
Region # 9 - Fuel 09
 2.8419E-02  2.7556E-01  5.6644E-03  1.5645E-01  2.6645E+00  2.6361E+00
 1.0000E+00  0.0000E+00  3.7969E-01  6.5546E-04  1.5582E-03  3.8788E-01
 4.2939E-02 -1.4971E-04 -1.3449E-04  8.5356E-03
Region #10 - Fuel 10
 2.7673E-02  2.9603E-01  6.0748E-03  1.7360E-01  2.6518E+00  2.6216E+00
 1.0000E+00  0.0000E+00  3.7826E-01  6.2788E-04  1.6768E-03  3.8810E-01
 4.3485E-02 -1.4332E-04 -1.4407E-04  8.5555E-03
Region #11 - Fuel 11
 2.8291E-02  3.1659E-01  6.3029E-03  1.8736E-01  2.6343E+00  2.6036E+00
 1.0000E+00  0.0000E+00  3.7662E-01  6.0323E-04  1.8222E-03  3.8188E-01
 4.3720E-02 -1.3697E-04 -1.5197E-04  8.5071E-03
Region #12 - Fuel 12
 2.9074E-02  2.8708E-01  5.7679E-03  1.6378E-01  2.6530E+00  2.6198E+00
 1.0000E+00  0.0000E+00  3.7706E-01  6.4333E-04  1.5001E-03  3.8190E-01
 4.3487E-02 -1.4615E-04 -1.2673E-04  8.4648E-03
Region #13 - Zirconium Clad
 1.7782E-03  4.3709E-03  0.0000E+00  0.0000E+00  0.0000E+00  0.0000E+00
 0.0000E+00  0.0000E+00  3.1831E-01  2.6957E-04  6.4139E-04  2.7629E-01
 3.8693E-02 -6.3283E-05 -7.9266E-05  2.5287E-03
Region #14 - Moderator
 9.4157E-05  2.9703E-03  0.0000E+00  0.0000E+00  0.0000E+00  0.0000E+00
 0.0000E+00  0.0000E+00  2.1154E-01  8.2643E-03  6.8510E-04  6.3660E-01
 1.2564E-01  2.4077E-03  4.2666E-04  1.8355E-01
Region #15 - Bypass/Central Water Rod
 3.1170E-04  9.2342E-03  0.0000E+00  0.0000E+00  0.0000E+00  0.0000E+00
 0.0000E+00  0.0000E+00  6.6087E-01  3.0441E-02  1.6093E-03  1.9465E+00
 3.9506E-01  8.9191E-03  9.9869E-04  5.4491E-01
```

**GE9 Bundle - Void Fraction: 70%, Burnup: 25 GWd/T, Controlled**

```
Region # 1 - Fuel 01
 3.0841E-02  1.6490E-01  3.3590E-03  7.2519E-02  2.7708E+00  2.7981E+00
 1.0000E+00  0.0000E+00  3.9180E-01  7.7091E-04  1.7071E-03  3.8618E-01
 3.9510E-02 -1.7650E-04 -1.4760E-04  8.5329E-03
Region # 2 - Fuel 02
 2.8846E-02  1.8085E-01  3.7195E-03  8.4910E-02  2.7444E+00  2.7563E+00
 1.0000E+00  0.0000E+00  3.8884E-01  7.2662E-04  1.7988E-03  3.8627E-01
 4.0268E-02 -1.6594E-04 -1.5480E-04  8.5477E-03
Region # 3 - Fuel 03
 3.1156E-02  1.9292E-01  4.0092E-03  9.1909E-02  2.7409E+00  2.7438E+00
 1.0000E+00  0.0000E+00  3.8751E-01  7.8848E-04  1.3132E-03  3.8728E-01
 4.0601E-02 -1.8057E-04 -1.1489E-04  8.4895E-03
Region # 4 - Fuel 04
 2.8660E-02  1.9925E-01  4.1010E-03  9.8827E-02  2.7210E+00  2.7231E+00
 1.0000E+00  0.0000E+00  3.8750E-01  7.0201E-04  1.8629E-03  3.8637E-01
 4.0700E-02 -1.6035E-04 -1.5982E-04  8.5577E-03
Region # 5 - Fuel 05
 2.9263E-02  2.0925E-01  4.3426E-03  1.0524E-01  2.7163E+00  2.7097E+00
 1.0000E+00  0.0000E+00  3.8544E-01  7.2902E-04  1.5208E-03  3.8708E-01
 4.1176E-02 -1.6660E-04 -1.3175E-04  8.5195E-03
Region # 6 - Fuel 06
 2.8806E-02  2.2008E-01  4.5279E-03  1.1413E-01  2.7021E+00  2.6951E+00
 1.0000E+00  0.0000E+00  3.8565E-01  6.9302E-04  1.7737E-03  3.8677E-01
 4.1227E-02 -1.5835E-04 -1.5233E-04  8.5499E-03
Region # 7 - Fuel 07
 2.9191E-02  2.3154E-01  4.7979E-03  1.2216E-01  2.6959E+00  2.6807E+00
 1.0000E+00  0.0000E+00  3.8385E-01  7.1231E-04  1.5262E-03  3.8739E-01
 4.1656E-02 -1.6279E-04 -1.3205E-04  8.5222E-03
Region # 8 - Fuel 08
```

2.7594E-02 2.5539E-01 5.3280E-03 1.4295E-01 2.6621E+00 2.6443E+00
1.0000E+00 0.0000E+00 3.8321E-01 6.5262E-04 2.0153E-03 3.8689E-01
4.1731E-02 -1.4863E-04 -1.7171E-04 8.5853E-03
Region # 9 - Fuel 09
2.9026E-02 2.7429E-01 5.6496E-03 1.5568E-01 2.6600E+00 2.6381E+00
1.0000E+00 0.0000E+00 3.8205E-01 6.6925E-04 1.7265E-03 3.8758E-01
4.2185E-02 -1.5292E-04 -1.4816E-04 8.5520E-03
Region #10 - Fuel 10
2.8337E-02 2.9445E-01 6.0602E-03 1.7273E-01 2.6461E+00 2.6241E+00
1.0000E+00 0.0000E+00 3.8118E-01 6.3958E-04 1.9345E-03 3.8767E-01
4.2565E-02 -1.4608E-04 -1.6494E-04 8.5808E-03
Region #11 - Fuel 11
2.8935E-02 3.1459E-01 6.3178E-03 1.8622E-01 2.6296E+00 2.6054E+00
1.0000E+00 0.0000E+00 3.7892E-01 6.1709E-04 2.0123E-03 3.8157E-01
4.2969E-02 -1.4018E-04 -1.6691E-04 8.5248E-03
Region #12 - Fuel 12
3.0116E-02 2.8326E-01 5.7286E-03 1.6164E-01 2.6444E+00 2.6239E+00
1.0000E+00 0.0000E+00 3.8172E-01 6.5343E-04 1.8828E-03 3.8124E-01
4.2047E-02 -1.4862E-04 -1.5697E-04 8.5008E-03
Region #13 - Zirconium Clad
1.8307E-03 4.2372E-03 0.0000E+00 0.0000E+00 0.0000E+00 0.0000E+00
0.0000E+00 0.0000E+00 3.2078E-01 2.6803E-04 8.2083E-04 2.7604E-01
3.7810E-02 -6.2925E-05 -1.0132E-04 2.5558E-03
Region #14 - Blade Sheath
5.0292E-03 1.3426E-01 0.0000E+00 0.0000E+00 0.0000E+00 0.0000E+00
0.0000E+00 0.0000E+00 6.0572E-01 1.2759E-03 3.1629E-03 8.7471E-01
3.4293E-02 0.0000E+00 0.0000E+00 1.1882E-02
Region #15 - Control Rod
7.5039E-03 2.9168E-01 0.0000E+00 0.0000E+00 0.0000E+00 0.0000E+00
0.0000E+00 0.0000E+00 3.4424E-03 2.0280E-05 1.7107E-05 4.3313E-03
2.8096E-04 -1.0256E-06 4.4190E-08 2.6297E-04
Region #16 - Moderator
9.2843E-05 2.8834E-03 0.0000E+00 0.0000E+00 0.0000E+00 0.0000E+00
0.0000E+00 0.0000E+00 2.1581E-01 8.3763E-03 8.5826E-04 6.2539E-01
1.2834E-01 2.4333E-03 5.3573E-04 1.8396E-01
Region #17 - Bypass/Central Water Rod
3.0380E-04 8.9446E-03 0.0000E+00 0.0000E+00 0.0000E+00 0.0000E+00
0.0000E+00 0.0000E+00 6.7115E-01 3.0148E-02 2.0849E-03 1.9092E+00
4.0142E-01 8.8001E-03 1.2978E-03 5.4641E-01

**GE9 Blanket - Void Fraction: 0%, Burnup: 0.350 GWd/T, Uncontrolled**

Region # 1 - Natural UO2
2.2480E-02 1.0270E-01 4.1150E-03 5.2172E-02 2.6778E+00 2.4721E+00
1.0000E+00 0.0000E+00 3.7846E-01 9.7320E-04 4.9446E-04 3.9173E-01
4.3588E-02 -2.2828E-04 -4.8590E-05 8.4242E-03
Region # 2 - Zirconium Clad
1.7563E-03 4.6968E-03 0.0000E+00 0.0000E+00 0.0000E+00 0.0000E+00
0.0000E+00 0.0000E+00 3.1231E-01 3.7733E-04 2.2977E-04 2.7687E-01
3.7295E-02 -8.8598E-05 -2.8680E-05 2.4658E-03
Region # 3 - Moderator
3.4385E-04 9.6105E-03 0.0000E+00 0.0000E+00 0.0000E+00 0.0000E+00
0.0000E+00 0.0000E+00 6.3618E-01 3.3923E-02 7.4709E-04 1.9951E+00
3.8017E-01 1.0118E-02 4.5574E-04 5.4329E-01
Region # 4 - Bypass/Central Water Rod
3.6499E-04 9.7596E-03 0.0000E+00 0.0000E+00 0.0000E+00 0.0000E+00
0.0000E+00 0.0000E+00 6.6026E-01 3.8044E-02 6.6821E-04 2.0142E+00
3.9637E-01 1.1333E-02 4.0673E-04 5.4230E-01

**GE9 Blanket - Void Fraction: 0%, Burnup: 0.350 GWd/T, Controlled**

Region # 1 - Natural UO2
2.2896E-02 1.0196E-01 4.0684E-03 5.1802E-02 2.6739E+00 2.4725E+00
1.0000E+00 0.0000E+00 3.8044E-01 9.9964E-04 5.8295E-04 3.9154E-01
4.2869E-02 -2.3460E-04 -5.6120E-05 8.4342E-03
Region # 2 - Zirconium Clad
1.7856E-03 4.6480E-03 0.0000E+00 0.0000E+00 0.0000E+00 0.0000E+00
0.0000E+00 0.0000E+00 3.1344E-01 3.8370E-04 2.8033E-04 2.7679E-01

```
 3.6676E-02 -9.0097E-05 -3.4911E-05  2.4738E-03
 Region # 3 - Blade Sheath
 5.6947E-03  1.4445E-01  0.0000E+00  0.0000E+00  0.0000E+00  0.0000E+00
 0.0000E+00  0.0000E+00  6.0846E-01  1.7124E-03  1.4319E-03  8.7713E-01
 3.5429E-02  0.0000E+00  0.0000E+00  1.1863E-02
 Region # 4 - Control Rod
 8.9825E-03  3.1451E-01  0.0000E+00  0.0000E+00  0.0000E+00  0.0000E+00
 0.0000E+00  0.0000E+00  3.4081E-03  2.7614E-05  7.6858E-06  4.3571E-03
 2.8021E-04 -1.4027E-06 -8.8118E-09  2.6255E-04
 Region # 5 - Moderator
 3.4687E-04  9.5291E-03  0.0000E+00  0.0000E+00  0.0000E+00  0.0000E+00
 0.0000E+00  0.0000E+00  6.4407E-01  3.4820E-02  8.8176E-04  1.9846E+00
 3.8531E-01  1.0382E-02  5.4028E-04  5.4370E-01
 Region # 6 - Bypass/Central Water Rod
 3.6302E-04  9.6203E-03  0.0000E+00  0.0000E+00  0.0000E+00  0.0000E+00
 0.0000E+00  0.0000E+00  6.6629E-01  3.8212E-02  8.3722E-04  1.9963E+00
 4.0017E-01  1.1369E-02  5.1264E-04  5.4309E-01
GE9 Blanket - Void Fraction: 0%, Burnup: 15 GWd/T, Uncontrolled
 Region # 1 - Natural UO2
 2.8993E-02  1.5180E-01  3.7817E-03  6.3235E-02  2.8079E+00  2.8313E+00
 1.0000E+00  0.0000E+00  3.7791E-01  8.5372E-04  6.2252E-04  3.8921E-01
 4.3583E-02 -1.9509E-04 -5.8187E-05  8.4161E-03
 Region # 2 - Zirconium Clad
 1.7538E-03  4.6814E-03  0.0000E+00  0.0000E+00  0.0000E+00  0.0000E+00
 0.0000E+00  0.0000E+00  3.1172E-01  3.4665E-04  2.8859E-04  2.7680E-01
 3.7483E-02 -8.1379E-05 -3.5896E-05  2.4738E-03
 Region # 3 - Moderator
 3.4092E-04  9.5693E-03  0.0000E+00  0.0000E+00  0.0000E+00  0.0000E+00
 0.0000E+00  0.0000E+00  6.3411E-01  3.1405E-02  9.2668E-04  1.9897E+00
 3.7871E-01  9.2582E-03  5.6940E-04  5.4338E-01
 Region # 4 - Bypass/Central Water Rod
 3.6663E-04  9.6969E-03  0.0000E+00  0.0000E+00  0.0000E+00  0.0000E+00
 0.0000E+00  0.0000E+00  6.5839E-01  3.6712E-02  8.1463E-04  2.0061E+00
 3.9516E-01  1.0875E-02  4.9900E-04  5.4257E-01
GE9 Blanket - Void Fraction: 0%, Burnup: 15 GWd/T, Controlled
 Region # 1 - Natural UO2
 2.9519E-02  1.5226E-01  3.7229E-03  6.3771E-02  2.8082E+00  2.8309E+00
 1.0000E+00  0.0000E+00  3.7988E-01  8.7144E-04  7.3176E-04  3.8901E-01
 4.2919E-02 -1.9921E-04 -6.7314E-05  8.4283E-03
 Region # 2 - Zirconium Clad
 1.7817E-03  4.6256E-03  0.0000E+00  0.0000E+00  0.0000E+00  0.0000E+00
 0.0000E+00  0.0000E+00  3.1291E-01  3.5002E-04  3.5118E-04  2.7671E-01
 3.6936E-02 -8.2173E-05 -4.3604E-05  2.4836E-03
 Region # 3 - Blade Sheath
 5.5932E-03  1.4315E-01  0.0000E+00  0.0000E+00  0.0000E+00  0.0000E+00
 0.0000E+00  0.0000E+00  6.0676E-01  1.6093E-03  1.7108E-03  8.7677E-01
 3.5881E-02  0.0000E+00  0.0000E+00  1.1865E-02
 Region # 4 - Control Rod
 8.7072E-03  3.1170E-01  0.0000E+00  0.0000E+00  0.0000E+00  0.0000E+00
 0.0000E+00  0.0000E+00  3.3989E-03  2.5717E-05  9.1787E-06  4.3537E-03
 2.8034E-04 -1.3011E-06  4.8665E-10  2.6258E-04
 Region # 5 - Moderator
 3.4228E-04  9.4746E-03  0.0000E+00  0.0000E+00  0.0000E+00  0.0000E+00
 0.0000E+00  0.0000E+00  6.4154E-01  3.2070E-02  1.0917E-03  1.9775E+00
 3.8351E-01  9.4476E-03  6.7311E-04  5.4385E-01
 Region # 6 - Bypass/Central Water Rod
 3.6279E-04  9.5421E-03  0.0000E+00  0.0000E+00  0.0000E+00  0.0000E+00
 0.0000E+00  0.0000E+00  6.6396E-01  3.6610E-02  1.0197E-03  1.9862E+00
 3.9861E-01  1.0823E-02  6.2767E-04  5.4343E-01
GE9 Blanket - Void Fraction: 0%, Burnup: 25 GWd/T, Uncontrolled
 Region # 1 - Natural UO2
 3.1001E-02  1.6020E-01  3.7297E-03  6.2974E-02  2.8296E+00  2.8725E+00
 1.0000E+00  0.0000E+00  3.7735E-01  8.2916E-04  6.3480E-04  3.8772E-01
 4.3325E-02 -1.8871E-04 -5.9025E-05  8.4086E-03
```

Region # 2 - Zirconium Clad
1.7575E-03 4.6758E-03 0.0000E+00 0.0000E+00 0.0000E+00 0.0000E+00
0.0000E+00 0.0000E+00 3.1172E-01 3.4076E-04 2.9544E-04 2.7679E-01
3.7458E-02 -7.9993E-05 -3.6742E-05 2.4748E-03
Region # 3 - Moderator
3.4062E-04 9.5567E-03 0.0000E+00 0.0000E+00 0.0000E+00 0.0000E+00
0.0000E+00 0.0000E+00 6.3440E-01 3.0916E-02 9.4850E-04 1.9881E+00
3.7887E-01 9.0955E-03 5.8310E-04 5.4344E-01
Region # 4 - Bypass/Central Water Rod
3.6763E-04 9.6864E-03 0.0000E+00 0.0000E+00 0.0000E+00 0.0000E+00
0.0000E+00 0.0000E+00 6.5888E-01 3.6512E-02 8.3396E-04 2.0047E+00
3.9549E-01 1.0804E-02 5.1114E-04 5.4262E-01

**GE9 Blanket - Void Fraction: 0%, Burnup: 25 GWd/T, Controlled**

Region # 1 - Natural UO2
3.1557E-02 1.6078E-01 3.6714E-03 6.3581E-02 2.8308E+00 2.8719E+00
1.0000E+00 0.0000E+00 3.7931E-01 8.4492E-04 7.4644E-04 3.8752E-01
4.2681E-02 -1.9236E-04 -6.8315E-05 8.4211E-03
Region # 2 - Zirconium Clad
1.7849E-03 4.6188E-03 0.0000E+00 0.0000E+00 0.0000E+00 0.0000E+00
0.0000E+00 0.0000E+00 3.1290E-01 3.4340E-04 3.5970E-04 2.7670E-01
3.6929E-02 -8.0616E-05 -4.4656E-05 2.4848E-03
Region # 3 - Blade Sheath
5.5817E-03 1.4294E-01 0.0000E+00 0.0000E+00 0.0000E+00 0.0000E+00
0.0000E+00 0.0000E+00 6.0711E-01 1.5916E-03 1.7458E-03 8.7672E-01
3.5932E-02 0.0000E+00 0.0000E+00 1.1866E-02
Region # 4 - Control Rod
8.6608E-03 3.1123E-01 0.0000E+00 0.0000E+00 0.0000E+00 0.0000E+00
0.0000E+00 0.0000E+00 3.3985E-03 2.5394E-05 9.3655E-06 4.3532E-03
2.8038E-04 -1.2845E-06 1.3761E-09 2.6259E-04
Region # 5 - Moderator
3.4183E-04 9.4599E-03 0.0000E+00 0.0000E+00 0.0000E+00 0.0000E+00
0.0000E+00 0.0000E+00 6.4168E-01 3.1526E-02 1.1179E-03 1.9756E+00
3.8357E-01 9.2678E-03 6.8957E-04 5.4392E-01
Region # 6 - Bypass/Central Water Rod
3.6353E-04 9.5288E-03 0.0000E+00 0.0000E+00 0.0000E+00 0.0000E+00
0.0000E+00 0.0000E+00 6.6429E-01 3.6340E-02 1.0444E-03 1.9845E+00
3.9883E-01 1.0730E-02 6.4316E-04 5.4350E-01

**GE9 Blanket - Void Fraction: 40%, Burnup: 0.350 GWd/T, Uncontrolled**

Region # 1 - Natural UO2
2.1594E-02 1.0131E-01 3.9427E-03 5.1453E-02 2.6702E+00 2.4730E+00
1.0000E+00 0.0000E+00 3.8064E-01 9.5090E-04 6.0216E-04 3.9142E-01
4.2969E-02 -2.2312E-04 -5.7895E-05 8.4402E-03
Region # 2 - Zirconium Clad
1.7787E-03 4.6351E-03 0.0000E+00 0.0000E+00 0.0000E+00 0.0000E+00
0.0000E+00 0.0000E+00 3.1508E-01 3.6433E-04 2.8255E-04 2.7678E-01
3.7273E-02 -8.5547E-05 -3.5190E-05 2.4745E-03
Region # 3 - Moderator
2.0336E-04 5.8727E-03 0.0000E+00 0.0000E+00 0.0000E+00 0.0000E+00
0.0000E+00 0.0000E+00 3.9659E-01 2.0297E-02 5.6300E-04 1.2262E+00
2.3675E-01 6.0506E-03 3.4508E-04 3.3749E-01
Region # 4 - Bypass/Central Water Rod
3.4988E-04 9.6633E-03 0.0000E+00 0.0000E+00 0.0000E+00 0.0000E+00
0.0000E+00 0.0000E+00 6.6509E-01 3.6822E-02 8.0612E-04 2.0018E+00
3.9898E-01 1.0953E-02 4.9321E-04 5.4282E-01

**GE9 Blanket - Void Fraction: 40%, Burnup: 0.350 GWd/T, Controlled**

Region # 1 - Natural UO2
2.2080E-02 1.0018E-01 3.8687E-03 5.0886E-02 2.6637E+00 2.4736E+00
1.0000E+00 0.0000E+00 3.8339E-01 9.7978E-04 7.3655E-04 3.9113E-01
4.1998E-02 -2.3004E-04 -6.9310E-05 8.4554E-03
Region # 2 - Zirconium Clad
1.8199E-03 4.5686E-03 0.0000E+00 0.0000E+00 0.0000E+00 0.0000E+00
0.0000E+00 0.0000E+00 3.1674E-01 3.7175E-04 3.5521E-04 2.7668E-01
3.6441E-02 -8.7294E-05 -4.4143E-05 2.4859E-03
Region # 3 - Blade Sheath

5.5959E-03 1.4228E-01 0.0000E+00 0.0000E+00 0.0000E+00 0.0000E+00
0.0000E+00 0.0000E+00 6.1181E-01 1.6505E-03 1.7327E-03 8.7668E-01
3.4454E-02 0.0000E+00 0.0000E+00 1.1867E-02
Region # 4 - Control Rod
8.7859E-03 3.0976E-01 0.0000E+00 0.0000E+00 0.0000E+00 0.0000E+00
0.0000E+00 0.0000E+00 3.4364E-03 2.6667E-05 9.2764E-06 4.3520E-03
2.8027E-04 -1.3553E-06 -1.5798E-09 2.6265E-04
Region # 5 - Moderator
2.0463E-04 5.7986E-03 0.0000E+00 0.0000E+00 0.0000E+00 0.0000E+00
0.0000E+00 0.0000E+00 4.0335E-01 2.0933E-02 6.8817E-04 1.2166E+00
2.4112E-01 6.2360E-03 4.2368E-04 3.3786E-01
Region # 6 - Bypass/Central Water Rod
3.4734E-04 9.4898E-03 0.0000E+00 0.0000E+00 0.0000E+00 0.0000E+00
0.0000E+00 0.0000E+00 6.7375E-01 3.7164E-02 1.0343E-03 1.9795E+00
4.0446E-01 1.1038E-02 6.3630E-04 5.4378E-01

**GE9 Blanket - Void Fraction: 40%, Burnup: 15 GWd/T, Uncontrolled**

Region # 1 - Natural UO2
2.7627E-02 1.5119E-01 3.6013E-03 6.3148E-02 2.8041E+00 2.8319E+00
1.0000E+00 0.0000E+00 3.8026E-01 8.1241E-04 7.6439E-04 3.8888E-01
4.2927E-02 -1.8520E-04 -6.9968E-05 8.4345E-03
Region # 2 - Zirconium Clad
1.7814E-03 4.6189E-03 0.0000E+00 0.0000E+00 0.0000E+00 0.0000E+00
0.0000E+00 0.0000E+00 3.1467E-01 3.2770E-04 3.5819E-04 2.7670E-01
3.7420E-02 -7.6926E-05 -4.4462E-05 2.4847E-03
Region # 3 - Moderator
1.9971E-04 5.8485E-03 0.0000E+00 0.0000E+00 0.0000E+00 0.0000E+00
0.0000E+00 0.0000E+00 3.9585E-01 1.8404E-02 7.0464E-04 1.2230E+00
2.3616E-01 5.4024E-03 4.3486E-04 3.3750E-01
Region # 4 - Bypass/Central Water Rod
3.4985E-04 9.5888E-03 0.0000E+00 0.0000E+00 0.0000E+00 0.0000E+00
0.0000E+00 0.0000E+00 6.6419E-01 3.5223E-02 9.9482E-04 1.9921E+00
3.9837E-01 1.0396E-02 6.1223E-04 5.4312E-01

**GE9 Blanket - Void Fraction: 40%, Burnup: 15 GWd/T, Controlled**

Region # 1 - Natural UO2
2.8215E-02 1.5157E-01 3.5120E-03 6.3734E-02 2.8037E+00 2.8317E+00
1.0000E+00 0.0000E+00 3.8300E-01 8.2900E-04 9.3154E-04 3.8856E-01
4.2029E-02 -1.8906E-04 -8.3874E-05 8.4531E-03
Region # 2 - Zirconium Clad
1.8209E-03 4.5432E-03 0.0000E+00 0.0000E+00 0.0000E+00 0.0000E+00
0.0000E+00 0.0000E+00 3.1640E-01 3.3085E-04 4.4834E-04 2.7657E-01
3.6679E-02 -7.7668E-05 -5.5558E-05 2.4986E-03
Region # 3 - Blade Sheath
5.4729E-03 1.4074E-01 0.0000E+00 0.0000E+00 0.0000E+00 0.0000E+00
0.0000E+00 0.0000E+00 6.1053E-01 1.5219E-03 2.0914E-03 8.7622E-01
3.4857E-02 0.0000E+00 0.0000E+00 1.1870E-02
Region # 4 - Control Rod
8.4557E-03 3.0646E-01 0.0000E+00 0.0000E+00 0.0000E+00 0.0000E+00
0.0000E+00 0.0000E+00 3.4291E-03 2.4288E-05 1.1195E-05 4.3479E-03
2.8034E-04 -1.2276E-06 1.1096E-08 2.6269E-04
Region # 5 - Moderator
1.9965E-04 5.7630E-03 0.0000E+00 0.0000E+00 0.0000E+00 0.0000E+00
0.0000E+00 0.0000E+00 4.0225E-01 1.8841E-02 8.5886E-04 1.2119E+00
2.4026E-01 5.5234E-03 5.3183E-04 3.3792E-01
Region # 6 - Bypass/Central Water Rod
3.4495E-04 9.3962E-03 0.0000E+00 0.0000E+00 0.0000E+00 0.0000E+00
0.0000E+00 0.0000E+00 6.7224E-01 3.5198E-02 1.2716E-03 1.9674E+00
4.0339E-01 1.0363E-02 7.8601E-04 5.4417E-01

**GE9 Blanket - Void Fraction: 40%, Burnup: 25 GWd/T, Uncontrolled**

Region # 1 - Natural UO2
2.9490E-02 1.5959E-01 3.5466E-03 6.2930E-02 2.8263E+00 2.8725E+00
1.0000E+00 0.0000E+00 3.7974E-01 7.8385E-04 7.7832E-04 3.8738E-01
4.2662E-02 -1.7793E-04 -7.0907E-05 8.4272E-03
Region # 2 - Zirconium Clad
1.7868E-03 4.6124E-03 0.0000E+00 0.0000E+00 0.0000E+00 0.0000E+00

0.0000E+00 0.0000E+00 3.1474E-01 3.2030E-04 3.6629E-04 2.7669E-01
3.7388E-02 -7.5187E-05 -4.5463E-05 2.4859E-03
Region # 3 - Moderator
1.9886E-04 5.8396E-03 0.0000E+00 0.0000E+00 0.0000E+00 0.0000E+00
0.0000E+00 0.0000E+00 3.9615E-01 1.8017E-02 7.2035E-04 1.2218E+00
2.3632E-01 5.2748E-03 4.4472E-04 3.3755E-01
Region # 4 - Bypass/Central Water Rod
3.5007E-04 9.5760E-03 0.0000E+00 0.0000E+00 0.0000E+00 0.0000E+00
0.0000E+00 0.0000E+00 6.6493E-01 3.4934E-02 1.0187E-03 1.9905E+00
3.9884E-01 1.0296E-02 6.2723E-04 5.4319E-01

**GE9 Blanket - Void Fraction: 40%, Burnup: 25 GWd/T, Controlled**

Region # 1 - Natural UO2
3.0109E-02 1.6012E-01 3.4569E-03 6.3607E-02 2.8270E+00 2.8718E+00
1.0000E+00 0.0000E+00 3.8248E-01 7.9788E-04 9.4871E-04 3.8706E-01
4.1784E-02 -1.8119E-04 -8.5029E-05 8.4460E-03
Region # 2 - Zirconium Clad
1.8261E-03 4.5352E-03 0.0000E+00 0.0000E+00 0.0000E+00 0.0000E+00
0.0000E+00 0.0000E+00 3.1647E-01 3.2249E-04 4.5860E-04 2.7656E-01
3.6665E-02 -7.5703E-05 -5.6826E-05 2.5001E-03
Region # 3 - Blade Sheath
5.4538E-03 1.4048E-01 0.0000E+00 0.0000E+00 0.0000E+00 0.0000E+00
0.0000E+00 0.0000E+00 6.1100E-01 1.4977E-03 2.1337E-03 8.7616E-01
3.4884E-02 0.0000E+00 0.0000E+00 1.1870E-02
Region # 4 - Control Rod
8.3936E-03 3.0590E-01 0.0000E+00 0.0000E+00 0.0000E+00 0.0000E+00
0.0000E+00 0.0000E+00 3.4298E-03 2.3863E-05 1.1421E-05 4.3473E-03
2.8033E-04 -1.2057E-06 1.2179E-08 2.6270E-04
Region # 5 - Moderator
1.9859E-04 5.7523E-03 0.0000E+00 0.0000E+00 0.0000E+00 0.0000E+00
0.0000E+00 0.0000E+00 4.0247E-01 1.8410E-02 8.7828E-04 1.2106E+00
2.4036E-01 5.3819E-03 5.4402E-04 3.3798E-01
Region # 6 - Bypass/Central Water Rod
3.4472E-04 9.3801E-03 0.0000E+00 0.0000E+00 0.0000E+00 0.0000E+00
0.0000E+00 0.0000E+00 6.7284E-01 3.4820E-02 1.3021E-03 1.9653E+00
4.0376E-01 1.0235E-02 8.0519E-04 5.4424E-01

**GE9 Blanket - Void Fraction: 70%, Burnup: 0.350 GWd/T, Uncontrolled**

Region # 1 - Natural UO2
2.0382E-02 9.9485E-02 3.7509E-03 5.0506E-02 2.6626E+00 2.4741E+00
1.0000E+00 0.0000E+00 3.8259E-01 9.2290E-04 7.3742E-04 3.9101E-01
4.2445E-02 -2.1660E-04 -6.9551E-05 8.4610E-03
Region # 2 - Zirconium Clad
1.7989E-03 4.5515E-03 0.0000E+00 0.0000E+00 0.0000E+00 0.0000E+00
0.0000E+00 0.0000E+00 3.1832E-01 3.4997E-04 3.4958E-04 2.7667E-01
3.7335E-02 -8.2177E-05 -4.3457E-05 2.4858E-03
Region # 3 - Moderator
1.0407E-04 3.1128E-03 0.0000E+00 0.0000E+00 0.0000E+00 0.0000E+00
0.0000E+00 0.0000E+00 2.1561E-01 1.0537E-02 3.7269E-04 6.5501E-01
1.2854E-01 3.1411E-03 2.2937E-04 1.8289E-01
Region # 4 - Bypass/Central Water Rod
3.3316E-04 9.5378E-03 0.0000E+00 0.0000E+00 0.0000E+00 0.0000E+00
0.0000E+00 0.0000E+00 6.7039E-01 3.5432E-02 9.7757E-04 1.9856E+00
4.0181E-01 1.0524E-02 6.0071E-04 5.4350E-01

**GE9 Blanket - Void Fraction: 70%, Burnup: 0.350 GWd/T, Controlled**

Region # 1 - Natural UO2
2.0919E-02 9.7783E-02 3.6391E-03 4.9648E-02 2.6528E+00 2.4751E+00
1.0000E+00 0.0000E+00 3.8637E-01 9.5076E-04 9.4110E-04 3.9058E-01
4.1156E-02 -2.2333E-04 -8.6795E-05 8.4841E-03
Region # 2 - Zirconium Clad
1.8567E-03 4.4598E-03 0.0000E+00 0.0000E+00 0.0000E+00 0.0000E+00
0.0000E+00 0.0000E+00 3.2075E-01 3.5736E-04 4.5542E-04 2.7652E-01
3.6217E-02 -8.3917E-05 -5.6492E-05 2.5022E-03
Region # 3 - Blade Sheath
5.4718E-03 1.3961E-01 0.0000E+00 0.0000E+00 0.0000E+00 0.0000E+00
0.0000E+00 0.0000E+00 6.1546E-01 1.5766E-03 2.0990E-03 8.7612E-01

3.3361E-02 0.0000E+00 0.0000E+00 1.1872E-02
Region # 4 - Control Rod
8.5371E-03 3.0383E-01 0.0000E+00 0.0000E+00 0.0000E+00 0.0000E+00
0.0000E+00 0.0000E+00 3.4694E-03 2.5553E-05 1.1241E-05 4.3456E-03
2.8058E-04 -1.2993E-06 7.5093E-09 2.6279E-04
Region # 5 - Moderator
1.0421E-04 3.0542E-03 0.0000E+00 0.0000E+00 0.0000E+00 0.0000E+00
0.0000E+00 0.0000E+00 2.2053E-01 1.0893E-02 4.7451E-04 6.4746E-01
1.3171E-01 3.2427E-03 2.9333E-04 1.8318E-01
Region # 6 - Bypass/Central Water Rod
3.2979E-04 9.3179E-03 0.0000E+00 0.0000E+00 0.0000E+00 0.0000E+00
0.0000E+00 0.0000E+00 6.8267E-01 3.5916E-02 1.2898E-03 1.9573E+00
4.0958E-01 1.0649E-02 7.9664E-04 5.4469E-01

**GE9 Blanket - Void Fraction: 70%, Burnup: 15 GWd/T, Uncontrolled**

Region # 1 - Natural UO2
2.5792E-02 1.5027E-01 3.3999E-03 6.2942E-02 2.8003E+00 2.8325E+00
1.0000E+00 0.0000E+00 3.8240E-01 7.6136E-04 9.3889E-04 3.8846E-01
4.2358E-02 -1.7289E-04 -8.4317E-05 8.4576E-03
Region # 2 - Zirconium Clad
1.8080E-03 4.5394E-03 0.0000E+00 0.0000E+00 0.0000E+00 0.0000E+00
0.0000E+00 0.0000E+00 3.1817E-01 3.0583E-04 4.4524E-04 2.7657E-01
3.7444E-02 -7.1786E-05 -5.5170E-05 2.4983E-03
Region # 3 - Moderator
1.0075E-04 3.1049E-03 0.0000E+00 0.0000E+00 0.0000E+00 0.0000E+00
0.0000E+00 0.0000E+00 2.1555E-01 9.2806E-03 4.6812E-04 6.5393E-01
1.2841E-01 2.7105E-03 2.9000E-04 1.8284E-01
Region # 4 - Bypass/Central Water Rod
3.3072E-04 9.4549E-03 0.0000E+00 0.0000E+00 0.0000E+00 0.0000E+00
0.0000E+00 0.0000E+00 6.7062E-01 3.3455E-02 1.2153E-03 1.9749E+00
4.0188E-01 9.8332E-03 7.5088E-04 5.4382E-01

**GE9 Blanket - Void Fraction: 70%, Burnup: 15 GWd/T, Controlled**

Region # 1 - Natural UO2
2.6400E-02 1.5049E-01 3.2691E-03 6.3559E-02 2.7989E+00 2.8326E+00
1.0000E+00 0.0000E+00 3.8618E-01 7.7237E-04 1.1924E-03 3.8797E-01
4.1156E-02 -1.7550E-04 -1.0528E-04 8.4854E-03
Region # 2 - Zirconium Clad
1.8640E-03 4.4363E-03 0.0000E+00 0.0000E+00 0.0000E+00 0.0000E+00
0.0000E+00 0.0000E+00 3.2068E-01 3.0734E-04 5.7612E-04 2.7639E-01
3.6436E-02 -7.2143E-05 -7.1268E-05 2.5183E-03
Region # 3 - Blade Sheath
5.3199E-03 1.3787E-01 0.0000E+00 0.0000E+00 0.0000E+00 0.0000E+00
0.0000E+00 0.0000E+00 6.1467E-01 1.4156E-03 2.5520E-03 8.7556E-01
3.3694E-02 0.0000E+00 0.0000E+00 1.1875E-02
Region # 4 - Control Rod
8.1338E-03 3.0014E-01 0.0000E+00 0.0000E+00 0.0000E+00 0.0000E+00
0.0000E+00 0.0000E+00 3.4645E-03 2.2563E-05 1.3656E-05 4.3408E-03
2.8058E-04 -1.1386E-06 2.4615E-08 2.6282E-04
Region # 5 - Moderator
9.9947E-05 3.0383E-03 0.0000E+00 0.0000E+00 0.0000E+00 0.0000E+00
0.0000E+00 0.0000E+00 2.2025E-01 9.4911E-03 5.9347E-04 6.4535E-01
1.3141E-01 2.7652E-03 3.6887E-04 1.8316E-01
Region # 6 - Bypass/Central Water Rod
3.2434E-04 9.2131E-03 0.0000E+00 0.0000E+00 0.0000E+00 0.0000E+00
0.0000E+00 0.0000E+00 6.8219E-01 3.3459E-02 1.5912E-03 1.9438E+00
4.0911E-01 9.8017E-03 9.8705E-04 5.4509E-01

**GE9 Blanket - Void Fraction: 70%, Burnup: 25 GWd/T, Uncontrolled**

Region # 1 - Natural UO2
2.7467E-02 1.5867E-01 3.3420E-03 6.2769E-02 2.8229E+00 2.8723E+00
1.0000E+00 0.0000E+00 3.8193E-01 7.2855E-04 9.5304E-04 3.8695E-01
4.2088E-02 -1.6468E-04 -8.5246E-05 8.4503E-03
Region # 2 - Zirconium Clad
1.8154E-03 4.5323E-03 0.0000E+00 0.0000E+00 0.0000E+00 0.0000E+00
0.0000E+00 0.0000E+00 3.1833E-01 2.9671E-04 4.5411E-04 2.7656E-01
3.7410E-02 -6.9642E-05 -5.6266E-05 2.4997E-03

```
 Region # 3 - Moderator
  9.9878E-05  3.0998E-03  0.0000E+00  0.0000E+00  0.0000E+00  0.0000E+00
  0.0000E+00  0.0000E+00  2.1577E-01  9.0173E-03  4.7721E-04  6.5327E-01
  1.2853E-01  2.6247E-03  2.9570E-04  1.8287E-01
 Region # 4 - Bypass/Central Water Rod
  3.2996E-04  9.4401E-03  0.0000E+00  0.0000E+00  0.0000E+00  0.0000E+00
  0.0000E+00  0.0000E+00  6.7162E-01  3.3048E-02  1.2433E-03  1.9730E+00
  4.0250E-01  9.6947E-03  7.6842E-04  5.4389E-01
```

**GE9 Blanket - Void Fraction: 70%, Burnup: 25 GWd/T, Controlled**

```
 Region # 1 - Natural UO2
  2.8099E-02  1.5906E-01  3.2097E-03  6.3503E-02  2.8230E+00  2.8717E+00
  1.0000E+00  0.0000E+00  3.8573E-01  7.3626E-04  1.2103E-03  3.8648E-01
  4.0906E-02 -1.6652E-04 -1.0645E-04  8.4785E-03
 Region # 2 - Zirconium Clad
  1.8716E-03  4.4276E-03  0.0000E+00  0.0000E+00  0.0000E+00  0.0000E+00
  0.0000E+00  0.0000E+00  3.2086E-01  2.9697E-04  5.8748E-04  2.7637E-01
  3.6419E-02 -6.9704E-05 -7.2674E-05  2.5200E-03
 Region # 3 - Blade Sheath
  5.2907E-03  1.3759E-01  0.0000E+00  0.0000E+00  0.0000E+00  0.0000E+00
  0.0000E+00  0.0000E+00  6.1528E-01  1.3836E-03  2.6008E-03  8.7549E-01
  3.3696E-02  0.0000E+00  0.0000E+00  1.1876E-02
 Region # 4 - Control Rod
  8.0465E-03  2.9952E-01  0.0000E+00  0.0000E+00  0.0000E+00  0.0000E+00
  0.0000E+00  0.0000E+00  3.4659E-03  2.2002E-05  1.3912E-05  4.3401E-03
  2.8056E-04 -1.1099E-06  2.5807E-08  2.6283E-04
 Region # 5 - Moderator
  9.8886E-05  3.0321E-03  0.0000E+00  0.0000E+00  0.0000E+00  0.0000E+00
  0.0000E+00  0.0000E+00  2.2044E-01  9.1965E-03  6.0497E-04  6.4455E-01
  1.3150E-01  2.6694E-03  3.7608E-04  1.8319E-01
 Region # 6 - Bypass/Central Water Rod
  3.2294E-04  9.1948E-03  0.0000E+00  0.0000E+00  0.0000E+00  0.0000E+00
  0.0000E+00  0.0000E+00  6.8308E-01  3.2940E-02  1.6268E-03  1.9414E+00
  4.0964E-01  9.6281E-03  1.0094E-03  5.4518E-01
```

## A.2. Bundle-Node-Average Fission Densities – 3D BWR Benchmark

Table A.2: 3D Node Averaged Fission Density (ARO) and MCNP % Uncertainty

| | | | | | | | | | | | | | |
|---|---|---|---|---|---|---|---|---|---|---|---|---|---|
| Layer 1 | | | | | | | | | | | | | |
| **1** | 9.25E-3 | (0.63) | **16** | 1.35E-2 | (0.46) | **31** | 1.41E-2 | (0.45) | **46** | 1.14E-2 | (0.50) | **61** | 8.64E-3 (0.61) |
| **2** | 1.03E-2 | (0.53) | **17** | 1.48E-2 | (0.47) | **32** | 1.56E-2 | (0.45) | **47** | 1.11E-2 | (0.53) | **62** | 6.41E-3 (0.70) |
| **3** | 1.07E-2 | (0.58) | **18** | 1.56E-2 | (0.43) | **33** | 1.58E-2 | (0.42) | **48** | 1.15E-2 | (0.50) | **63** | 4.60E-3 (0.82) |
| **4** | 1.10E-2 | (0.54) | **19** | 1.76E-2 | (0.43) | **34** | 1.58E-2 | (0.45) | **49** | 1.17E-2 | (0.52) | **64** | 3.18E-3 (0.99) |
| **5** | 1.21E-2 | (0.48) | **20** | 1.86E-2 | (0.42) | **35** | 1.41E-2 | (0.45) | **50** | 1.24E-2 | (0.48) | **65** | 8.76E-3 (0.61) |
| **6** | 1.31E-2 | (0.52) | **21** | 1.89E-2 | (0.44) | **36** | 1.29E-2 | (0.53) | **51** | 1.18E-2 | (0.52) | **66** | 8.60E-3 (0.61) |
| **7** | 1.26E-2 | (0.48) | **22** | 1.27E-2 | (0.50) | **37** | 1.13E-2 | (0.53) | **52** | 9.97E-3 | (0.57) | **67** | 8.36E-3 (0.62) |
| **8** | 1.38E-2 | (0.48) | **23** | 1.40E-2 | (0.45) | **38** | 1.21E-2 | (0.48) | **53** | 8.16E-3 | (0.63) | **68** | 7.89E-3 (0.64) |
| **9** | 1.46E-2 | (0.44) | **24** | 1.47E-2 | (0.46) | **39** | 1.24E-2 | (0.50) | **54** | 5.92E-3 | (0.74) | **69** | 6.84E-3 (0.68) |
| **10** | 1.64E-2 | (0.47) | **25** | 1.63E-2 | (0.42) | **40** | 1.37E-2 | (0.46) | **55** | 3.71E-3 | (0.97) | **70** | 5.03E-3 (0.79) |
| **11** | 1.27E-2 | (0.50) | **26** | 1.66E-2 | (0.44) | **41** | 1.47E-2 | (0.47) | **56** | 1.11E-2 | (0.54) | **71** | 4.74E-3 (0.82) |
| **12** | 1.41E-2 | (0.45) | **27** | 1.69E-2 | (0.41) | **42** | 1.38E-2 | (0.45) | **57** | 1.07E-2 | (0.51) | **72** | 4.66E-3 (0.82) |
| **13** | 1.50E-2 | (0.46) | **28** | 1.52E-2 | (0.48) | **43** | 1.20E-2 | (0.51) | **58** | 1.09E-2 | (0.54) | **73** | 4.46E-3 (0.84) |
| **14** | 1.70E-2 | (0.41) | **29** | 1.26E-2 | (0.48) | **44** | 1.06E-2 | (0.52) | **59** | 1.05E-2 | (0.52) | **74** | 4.07E-3 (0.88) |
| **15** | 1.79E-2 | (0.45) | **30** | 1.36E-2 | (0.48) | **45** | 8.19E-3 | (0.66) | **60** | 1.03E-2 | (0.56) | **75** | 3.36E-3 (0.96) |
| Layer 2 | | | | | | | | | | | | | |
| **1** | 4.61E-2 | (0.41) | **16** | 7.32E-2 | (0.34) | **31** | 7.77E-2 | (0.33) | **46** | 6.21E-2 | (0.36) | **61** | 5.18E-2 (0.40) |
| **2** | 5.60E-2 | (0.38) | **17** | 8.26E-2 | (0.32) | **32** | 8.75E-2 | (0.31) | **47** | 5.46E-2 | (0.36) | **62** | 3.41E-2 (0.45) |
| **3** | 5.25E-2 | (0.38) | **18** | 8.59E-2 | (0.31) | **33** | 8.74E-2 | (0.31) | **48** | 6.35E-2 | (0.36) | **63** | 2.45E-2 (0.53) |
| **4** | 5.47E-2 | (0.36) | **19** | 9.99E-2 | (0.29) | **34** | 8.89E-2 | (0.31) | **49** | 5.82E-2 | (0.35) | **64** | 1.66E-2 (0.64) |
| **5** | 6.67E-2 | (0.35) | **20** | 1.11E-1 | (0.27) | **35** | 7.77E-2 | (0.32) | **50** | 6.84E-2 | (0.35) | **65** | 5.28E-2 (0.40) |
| **6** | 6.47E-2 | (0.35) | **21** | 1.11E-1 | (0.29) | **36** | 7.21E-2 | (0.36) | **51** | 6.82E-2 | (0.35) | **66** | 5.08E-2 (0.40) |
| **7** | 6.84E-2 | (0.35) | **22** | 6.30E-2 | (0.33) | **37** | 5.62E-2 | (0.35) | **52** | 5.96E-2 | (0.37) | **67** | 5.01E-2 (0.41) |
| **8** | 7.71E-2 | (0.33) | **23** | 7.71E-2 | (0.33) | **38** | 6.65E-2 | (0.35) | **53** | 4.82E-2 | (0.42) | **68** | 4.67E-2 (0.42) |
| **9** | 8.05E-2 | (0.32) | **24** | 7.28E-2 | (0.31) | **39** | 6.14E-2 | (0.34) | **54** | 3.58E-2 | (0.48) | **69** | 4.15E-2 (0.45) |
| **10** | 9.17E-2 | (0.32) | **25** | 9.00E-2 | (0.30) | **40** | 7.54E-2 | (0.33) | **55** | 2.01E-2 | (0.62) | **70** | 2.74E-2 (0.50) |
| **11** | 6.33E-2 | (0.33) | **26** | 8.37E-2 | (0.29) | **41** | 8.26E-2 | (0.32) | **56** | 6.45E-2 | (0.36) | **71** | 2.51E-2 (0.53) |
| **12** | 7.77E-2 | (0.32) | **27** | 9.37E-2 | (0.30) | **42** | 7.65E-2 | (0.33) | **57** | 5.98E-2 | (0.37) | **72** | 2.44E-2 (0.53) |
| **13** | 7.47E-2 | (0.31) | **28** | 7.53E-2 | (0.32) | **43** | 6.05E-2 | (0.34) | **58** | 6.23E-2 | (0.37) | **73** | 2.35E-2 (0.54) |
| **14** | 9.41E-2 | (0.30) | **29** | 6.85E-2 | (0.35) | **44** | 5.88E-2 | (0.37) | **59** | 5.85E-2 | (0.37) | **74** | 2.14E-2 (0.57) |
| **15** | 9.29E-2 | (0.29) | **30** | 7.63E-2 | (0.33) | **45** | 4.21E-2 | (0.43) | **60** | 5.97E-2 | (0.37) | **75** | 1.76E-2 (0.62) |
| Layer 3 | | | | | | | | | | | | | |
| **1** | 7.38E-2 | (0.33) | **16** | 1.16E-1 | (0.27) | **31** | 1.23E-1 | (0.26) | **46** | 9.81E-2 | (0.29) | **61** | 8.37E-2 (0.31) |
| **2** | 8.85E-2 | (0.30) | **17** | 1.32E-1 | (0.25) | **32** | 1.39E-1 | (0.25) | **47** | 8.73E-2 | (0.28) | **62** | 5.50E-2 (0.35) |
| **3** | 8.40E-2 | (0.30) | **18** | 1.36E-1 | (0.25) | **33** | 1.39E-1 | (0.24) | **48** | 1.00E-1 | (0.29) | **63** | 3.98E-2 (0.42) |
| **4** | 8.76E-2 | (0.28) | **19** | 1.59E-1 | (0.23) | **34** | 1.42E-1 | (0.24) | **49** | 9.29E-2 | (0.27) | **64** | 2.72E-2 (0.50) |
| **5** | 1.05E-1 | (0.28) | **20** | 1.79E-1 | (0.22) | **35** | 1.23E-1 | (0.26) | **50** | 1.09E-1 | (0.28) | **65** | 8.51E-2 (0.31) |
| **6** | 1.03E-1 | (0.28) | **21** | 1.78E-1 | (0.23) | **36** | 1.15E-1 | (0.28) | **51** | 1.10E-1 | (0.28) | **66** | 8.18E-2 (0.32) |
| **7** | 1.08E-1 | (0.28) | **22** | 1.01E-1 | (0.26) | **37** | 8.99E-2 | (0.28) | **52** | 9.62E-2 | (0.29) | **67** | 8.04E-2 (0.32) |
| **8** | 1.23E-1 | (0.26) | **23** | 1.22E-1 | (0.26) | **38** | 1.05E-1 | (0.28) | **53** | 7.80E-2 | (0.33) | **68** | 7.52E-2 (0.33) |
| **9** | 1.27E-1 | (0.25) | **24** | 1.16E-1 | (0.25) | **39** | 9.79E-2 | (0.27) | **54** | 5.81E-2 | (0.38) | **69** | 6.69E-2 (0.35) |
| **10** | 1.46E-1 | (0.25) | **25** | 1.43E-1 | (0.24) | **40** | 1.19E-1 | (0.26) | **55** | 3.30E-2 | (0.48) | **70** | 4.43E-2 (0.40) |

| | | | | | | | | | | | | | | | |
|---|---|---|---|---|---|---|---|---|---|---|---|---|---|---|---|
| **11** | 1.01E-1 | (0.26) | **26** | 1.34E-1 | (0.23) | **41** | 1.32E-1 | (0.25) | **56** | 1.03E-1 | (0.29) | **71** | 4.05E-2 | (0.41) |
| **12** | 1.23E-1 | (0.26) | **27** | 1.49E-1 | (0.23) | **42** | 1.21E-1 | (0.26) | **57** | 9.47E-2 | (0.29) | **72** | 3.96E-2 | (0.42) |
| **13** | 1.19E-1 | (0.24) | **28** | 1.20E-1 | (0.25) | **43** | 9.74E-2 | (0.27) | **58** | 9.93E-2 | (0.29) | **73** | 3.79E-2 | (0.43) |
| **14** | 1.49E-1 | (0.23) | **29** | 1.08E-1 | (0.28) | **44** | 9.37E-2 | (0.30) | **59** | 9.26E-2 | (0.30) | **74** | 3.46E-2 | (0.45) |
| **15** | 1.49E-1 | (0.23) | **30** | 1.21E-1 | (0.26) | **45** | 6.84E-2 | (0.34) | **60** | 9.62E-2 | (0.29) | **75** | 2.85E-2 | (0.49) |
| Layer 4 | | | | | | | | | | | | | | |
| **1** | 9.31E-2 | (0.29) | **16** | 1.44E-1 | (0.24) | **31** | 1.53E-1 | (0.23) | **46** | 1.22E-1 | (0.26) | **61** | 1.04E-1 | (0.28) |
| **2** | 1.12E-1 | (0.27) | **17** | 1.64E-1 | (0.23) | **32** | 1.73E-1 | (0.22) | **47** | 1.09E-1 | (0.25) | **62** | 6.91E-2 | (0.32) |
| **3** | 1.06E-1 | (0.27) | **18** | 1.69E-1 | (0.22) | **33** | 1.72E-1 | (0.22) | **48** | 1.25E-1 | (0.26) | **63** | 5.04E-2 | (0.37) |
| **4** | 1.10E-1 | (0.25) | **19** | 1.98E-1 | (0.21) | **34** | 1.76E-1 | (0.22) | **49** | 1.15E-1 | (0.25) | **64** | 3.47E-2 | (0.45) |
| **5** | 1.32E-1 | (0.25) | **20** | 2.22E-1 | (0.19) | **35** | 1.53E-1 | (0.23) | **50** | 1.35E-1 | (0.25) | **65** | 1.06E-1 | (0.28) |
| **6** | 1.29E-1 | (0.24) | **21** | 2.21E-1 | (0.20) | **36** | 1.45E-1 | (0.25) | **51** | 1.37E-1 | (0.25) | **66** | 1.01E-1 | (0.29) |
| **7** | 1.36E-1 | (0.25) | **22** | 1.26E-1 | (0.24) | **37** | 1.12E-1 | (0.25) | **52** | 1.21E-1 | (0.26) | **67** | 9.98E-2 | (0.29) |
| **8** | 1.54E-1 | (0.23) | **23** | 1.52E-1 | (0.23) | **38** | 1.31E-1 | (0.25) | **53** | 9.87E-2 | (0.29) | **68** | 9.33E-2 | (0.30) |
| **9** | 1.59E-1 | (0.23) | **24** | 1.45E-1 | (0.22) | **39** | 1.22E-1 | (0.24) | **54** | 7.41E-2 | (0.33) | **69** | 8.31E-2 | (0.32) |
| **10** | 1.82E-1 | (0.23) | **25** | 1.77E-1 | (0.21) | **40** | 1.48E-1 | (0.24) | **55** | 4.22E-2 | (0.43) | **70** | 5.53E-2 | (0.35) |
| **11** | 1.27E-1 | (0.24) | **26** | 1.66E-1 | (0.21) | **41** | 1.64E-1 | (0.23) | **56** | 1.28E-1 | (0.26) | **71** | 5.04E-2 | (0.37) |
| **12** | 1.53E-1 | (0.23) | **27** | 1.85E-1 | (0.21) | **42** | 1.52E-1 | (0.23) | **57** | 1.17E-1 | (0.26) | **72** | 4.93E-2 | (0.37) |
| **13** | 1.48E-1 | (0.22) | **28** | 1.50E-1 | (0.23) | **43** | 1.22E-1 | (0.24) | **58** | 1.23E-1 | (0.26) | **73** | 4.71E-2 | (0.38) |
| **14** | 1.85E-1 | (0.21) | **29** | 1.35E-1 | (0.25) | **44** | 1.18E-1 | (0.26) | **59** | 1.15E-1 | (0.27) | **74** | 4.31E-2 | (0.40) |
| **15** | 1.85E-1 | (0.20) | **30** | 1.52E-1 | (0.23) | **45** | 8.66E-2 | (0.30) | **60** | 1.19E-1 | (0.26) | **75** | 3.56E-2 | (0.44) |
| Layer 5 | | | | | | | | | | | | | | |
| **1** | 9.99E-2 | (0.28) | **16** | 1.52E-1 | (0.23) | **31** | 1.60E-1 | (0.23) | **46** | 1.28E-1 | (0.25) | **61** | 1.08E-1 | (0.28) |
| **2** | 1.20E-1 | (0.26) | **17** | 1.71E-1 | (0.22) | **32** | 1.80E-1 | (0.22) | **47** | 1.13E-1 | (0.25) | **62** | 7.31E-2 | (0.31) |
| **3** | 1.12E-1 | (0.26) | **18** | 1.77E-1 | (0.21) | **33** | 1.79E-1 | (0.21) | **48** | 1.30E-1 | (0.25) | **63** | 5.44E-2 | (0.36) |
| **4** | 1.17E-1 | (0.24) | **19** | 2.05E-1 | (0.20) | **34** | 1.83E-1 | (0.21) | **49** | 1.20E-1 | (0.24) | **64** | 3.85E-2 | (0.42) |
| **5** | 1.40E-1 | (0.24) | **20** | 2.27E-1 | (0.19) | **35** | 1.61E-1 | (0.23) | **50** | 1.40E-1 | (0.24) | **65** | 1.08E-1 | (0.28) |
| **6** | 1.36E-1 | (0.24) | **21** | 2.27E-1 | (0.20) | **36** | 1.54E-1 | (0.24) | **51** | 1.42E-1 | (0.24) | **66** | 1.04E-1 | (0.28) |
| **7** | 1.43E-1 | (0.24) | **22** | 1.32E-1 | (0.23) | **37** | 1.18E-1 | (0.24) | **52** | 1.27E-1 | (0.25) | **67** | 1.02E-1 | (0.28) |
| **8** | 1.61E-1 | (0.23) | **23** | 1.59E-1 | (0.22) | **38** | 1.37E-1 | (0.24) | **53** | 1.07E-1 | (0.28) | **68** | 9.59E-2 | (0.29) |
| **9** | 1.66E-1 | (0.22) | **24** | 1.51E-1 | (0.21) | **39** | 1.27E-1 | (0.23) | **54** | 8.19E-2 | (0.32) | **69** | 8.59E-2 | (0.31) |
| **10** | 1.89E-1 | (0.22) | **25** | 1.84E-1 | (0.21) | **40** | 1.54E-1 | (0.23) | **55** | 4.70E-2 | (0.40) | **70** | 5.80E-2 | (0.34) |
| **11** | 1.33E-1 | (0.23) | **26** | 1.72E-1 | (0.20) | **41** | 1.70E-1 | (0.22) | **56** | 1.32E-1 | (0.25) | **71** | 5.26E-2 | (0.36) |
| **12** | 1.61E-1 | (0.22) | **27** | 1.91E-1 | (0.21) | **42** | 1.58E-1 | (0.23) | **57** | 1.21E-1 | (0.26) | **72** | 5.15E-2 | (0.37) |
| **13** | 1.55E-1 | (0.21) | **28** | 1.56E-1 | (0.22) | **43** | 1.28E-1 | (0.23) | **58** | 1.27E-1 | (0.26) | **73** | 4.93E-2 | (0.37) |
| **14** | 1.92E-1 | (0.21) | **29** | 1.42E-1 | (0.24) | **44** | 1.28E-1 | (0.25) | **59** | 1.19E-1 | (0.26) | **74** | 4.52E-2 | (0.39) |
| **15** | 1.91E-1 | (0.20) | **30** | 1.58E-1 | (0.23) | **45** | 9.51E-2 | (0.29) | **60** | 1.23E-1 | (0.26) | **75** | 3.79E-2 | (0.43) |
| Layer 6 | | | | | | | | | | | | | | |
| **1** | 7.97E-2 | (0.29) | **16** | 1.19E-1 | (0.24) | **31** | 1.23E-1 | (0.23) | **46** | 9.83E-2 | (0.26) | **61** | 8.16E-2 | (0.29) |
| **2** | 9.54E-2 | (0.27) | **17** | 1.31E-1 | (0.23) | **32** | 1.36E-1 | (0.23) | **47** | 8.68E-2 | (0.26) | **62** | 5.96E-2 | (0.32) |
| **3** | 8.87E-2 | (0.27) | **18** | 1.36E-1 | (0.22) | **33** | 1.36E-1 | (0.22) | **48** | 1.00E-1 | (0.26) | **63** | 4.65E-2 | (0.36) |
| **4** | 9.17E-2 | (0.25) | **19** | 1.54E-1 | (0.21) | **34** | 1.38E-1 | (0.23) | **49** | 9.14E-2 | (0.26) | **64** | 3.87E-2 | (0.42) |
| **5** | 1.10E-1 | (0.25) | **20** | 1.69E-1 | (0.20) | **35** | 1.25E-1 | (0.23) | **50** | 1.06E-1 | (0.25) | **65** | 7.97E-2 | (0.30) |
| **6** | 1.05E-1 | (0.25) | **21** | 1.68E-1 | (0.22) | **36** | 1.21E-1 | (0.25) | **51** | 1.06E-1 | (0.26) | **66** | 7.71E-2 | (0.30) |
| **7** | 1.12E-1 | (0.25) | **22** | 1.02E-1 | (0.24) | **37** | 9.10E-2 | (0.26) | **52** | 9.87E-2 | (0.27) | **67** | 7.58E-2 | (0.30) |
| **8** | 1.24E-1 | (0.24) | **23** | 1.23E-1 | (0.23) | **38** | 1.07E-1 | (0.25) | **53** | 1.02E-1 | (0.28) | **68** | 7.13E-2 | (0.31) |
| **9** | 1.29E-1 | (0.23) | **24** | 1.16E-1 | (0.23) | **39** | 9.81E-2 | (0.25) | **54** | 8.22E-2 | (0.32) | **69** | 6.52E-2 | (0.33) |
| **10** | 1.43E-1 | (0.23) | **25** | 1.41E-1 | (0.22) | **40** | 1.19E-1 | (0.24) | **55** | 4.77E-2 | (0.40) | **70** | 4.65E-2 | (0.36) |

| | | | | | | | | | | | | |
|---|---|---|---|---|---|---|---|---|---|---|---|---|
| **11** | 1.04E-1 | (0.24) | **26** | 1.30E-1 | (0.21) | **41** | 1.27E-1 | (0.23) | **56** | 9.78E-2 | (0.27) | **71** | 4.21E-2 | (0.38) |
| **12** | 1.25E-1 | (0.23) | **27** | 1.46E-1 | (0.22) | **42** | 1.20E-1 | (0.24) | **57** | 9.22E-2 | (0.27) | **72** | 4.14E-2 | (0.38) |
| **13** | 1.19E-1 | (0.22) | **28** | 1.20E-1 | (0.24) | **43** | 1.01E-1 | (0.24) | **58** | 9.49E-2 | (0.27) | **73** | 3.97E-2 | (0.39) |
| **14** | 1.47E-1 | (0.22) | **29** | 1.11E-1 | (0.25) | **44** | 1.22E-1 | (0.26) | **59** | 9.02E-2 | (0.27) | **74** | 3.70E-2 | (0.40) |
| **15** | 1.43E-1 | (0.22) | **30** | 1.21E-1 | (0.24) | **45** | 9.46E-2 | (0.29) | **60** | 9.16E-2 | (0.28) | **75** | 3.61E-2 | (0.43) |
| Layer 7 | | | | | | | | | | | | | | |
| **1** | 7.30E-2 | (0.30) | **16** | 1.07E-1 | (0.25) | **31** | 1.10E-1 | (0.25) | **46** | 8.78E-2 | (0.28) | **61** | 7.22E-2 | (0.31) |
| **2** | 8.75E-2 | (0.28) | **17** | 1.17E-1 | (0.24) | **32** | 1.20E-1 | (0.24) | **47** | 7.74E-2 | (0.27) | **62** | 5.40E-2 | (0.33) |
| **3** | 8.09E-2 | (0.28) | **18** | 1.21E-1 | (0.24) | **33** | 1.21E-1 | (0.24) | **48** | 8.96E-2 | (0.27) | **63** | 4.29E-2 | (0.37) |
| **4** | 8.35E-2 | (0.27) | **19** | 1.35E-1 | (0.23) | **34** | 1.22E-1 | (0.24) | **49** | 8.10E-2 | (0.27) | **64** | 3.68E-2 | (0.43) |
| **5** | 9.98E-2 | (0.26) | **20** | 1.47E-1 | (0.22) | **35** | 1.12E-1 | (0.25) | **50** | 9.43E-2 | (0.27) | **65** | 6.95E-2 | (0.32) |
| **6** | 9.46E-2 | (0.26) | **21** | 1.47E-1 | (0.23) | **36** | 1.09E-1 | (0.27) | **51** | 9.38E-2 | (0.27) | **66** | 6.74E-2 | (0.32) |
| **7** | 1.02E-1 | (0.26) | **22** | 9.20E-2 | (0.25) | **37** | 8.14E-2 | (0.27) | **52** | 8.83E-2 | (0.28) | **67** | 6.64E-2 | (0.32) |
| **8** | 1.11E-1 | (0.25) | **23** | 1.10E-1 | (0.25) | **38** | 9.57E-2 | (0.27) | **53** | 9.52E-2 | (0.29) | **68** | 6.29E-2 | (0.33) |
| **9** | 1.15E-1 | (0.24) | **24** | 1.03E-1 | (0.24) | **39** | 8.75E-2 | (0.26) | **54** | 7.77E-2 | (0.33) | **69** | 5.75E-2 | (0.35) |
| **10** | 1.27E-1 | (0.25) | **25** | 1.25E-1 | (0.23) | **40** | 1.05E-1 | (0.25) | **55** | 4.54E-2 | (0.41) | **70** | 4.17E-2 | (0.38) |
| **11** | 9.33E-2 | (0.25) | **26** | 1.15E-1 | (0.23) | **41** | 1.12E-1 | (0.25) | **56** | 8.58E-2 | (0.29) | **71** | 3.77E-2 | (0.40) |
| **12** | 1.12E-1 | (0.24) | **27** | 1.29E-1 | (0.23) | **42** | 1.07E-1 | (0.25) | **57** | 8.14E-2 | (0.29) | **72** | 3.70E-2 | (0.40) |
| **13** | 1.06E-1 | (0.24) | **28** | 1.06E-1 | (0.25) | **43** | 9.02E-2 | (0.26) | **58** | 8.37E-2 | (0.29) | **73** | 3.55E-2 | (0.41) |
| **14** | 1.30E-1 | (0.23) | **29** | 9.96E-2 | (0.26) | **44** | 1.13E-1 | (0.27) | **59** | 7.99E-2 | (0.29) | **74** | 3.32E-2 | (0.42) |
| **15** | 1.25E-1 | (0.23) | **30** | 1.08E-1 | (0.26) | **45** | 8.92E-2 | (0.30) | **60** | 8.05E-2 | (0.29) | **75** | 3.33E-2 | (0.45) |
| Layer 8 | | | | | | | | | | | | | | |
| **1** | 6.63E-2 | (0.32) | **16** | 9.54E-2 | (0.27) | **31** | 9.74E-2 | (0.26) | **46** | 7.78E-2 | (0.30) | **61** | 6.40E-2 | (0.33) |
| **2** | 7.91E-2 | (0.29) | **17** | 1.04E-1 | (0.26) | **32** | 1.06E-1 | (0.26) | **47** | 6.87E-2 | (0.29) | **62** | 4.81E-2 | (0.35) |
| **3** | 7.26E-2 | (0.30) | **18** | 1.07E-1 | (0.25) | **33** | 1.06E-1 | (0.25) | **48** | 7.94E-2 | (0.29) | **63** | 3.86E-2 | (0.39) |
| **4** | 7.50E-2 | (0.28) | **19** | 1.20E-1 | (0.24) | **34** | 1.08E-1 | (0.25) | **49** | 7.18E-2 | (0.29) | **64** | 3.32E-2 | (0.45) |
| **5** | 8.95E-2 | (0.27) | **20** | 1.29E-1 | (0.23) | **35** | 9.89E-2 | (0.26) | **50** | 8.34E-2 | (0.28) | **65** | 6.14E-2 | (0.34) |
| **6** | 8.46E-2 | (0.28) | **21** | 1.29E-1 | (0.25) | **36** | 9.72E-2 | (0.28) | **51** | 8.31E-2 | (0.29) | **66** | 5.96E-2 | (0.34) |
| **7** | 9.14E-2 | (0.27) | **22** | 8.20E-2 | (0.27) | **37** | 7.27E-2 | (0.29) | **52** | 7.86E-2 | (0.30) | **67** | 5.88E-2 | (0.34) |
| **8** | 9.94E-2 | (0.26) | **23** | 9.83E-2 | (0.26) | **38** | 8.51E-2 | (0.28) | **53** | 8.52E-2 | (0.31) | **68** | 5.56E-2 | (0.35) |
| **9** | 1.03E-1 | (0.26) | **24** | 9.11E-2 | (0.25) | **39** | 7.76E-2 | (0.28) | **54** | 7.01E-2 | (0.34) | **69** | 5.10E-2 | (0.37) |
| **10** | 1.13E-1 | (0.26) | **25** | 1.10E-1 | (0.25) | **40** | 9.33E-2 | (0.27) | **55** | 4.10E-2 | (0.43) | **70** | 3.71E-2 | (0.40) |
| **11** | 8.33E-2 | (0.27) | **26** | 1.01E-1 | (0.24) | **41** | 9.92E-2 | (0.27) | **56** | 7.58E-2 | (0.30) | **71** | 3.35E-2 | (0.42) |
| **12** | 1.00E-1 | (0.26) | **27** | 1.13E-1 | (0.24) | **42** | 9.46E-2 | (0.27) | **57** | 7.20E-2 | (0.31) | **72** | 3.29E-2 | (0.42) |
| **13** | 9.38E-2 | (0.25) | **28** | 9.35E-2 | (0.26) | **43** | 8.04E-2 | (0.27) | **58** | 7.40E-2 | (0.31) | **73** | 3.16E-2 | (0.43) |
| **14** | 1.15E-1 | (0.24) | **29** | 8.87E-2 | (0.28) | **44** | 1.01E-1 | (0.28) | **59** | 7.06E-2 | (0.31) | **74** | 2.95E-2 | (0.45) |
| **15** | 1.10E-1 | (0.24) | **30** | 9.57E-2 | (0.27) | **45** | 8.01E-2 | (0.31) | **60** | 7.11E-2 | (0.31) | **75** | 2.97E-2 | (0.48) |
| Layer 9 | | | | | | | | | | | | | | |
| **1** | 5.78E-2 | (0.34) | **16** | 8.23E-2 | (0.29) | **31** | 8.35E-2 | (0.28) | **46** | 6.73E-2 | (0.32) | **61** | 5.53E-2 | (0.35) |
| **2** | 6.90E-2 | (0.31) | **17** | 8.92E-2 | (0.28) | **32** | 9.07E-2 | (0.28) | **47** | 5.93E-2 | (0.31) | **62** | 4.16E-2 | (0.38) |
| **3** | 6.32E-2 | (0.32) | **18** | 9.21E-2 | (0.27) | **33** | 9.08E-2 | (0.27) | **48** | 6.83E-2 | (0.31) | **63** | 3.34E-2 | (0.42) |
| **4** | 6.52E-2 | (0.30) | **19** | 1.02E-1 | (0.26) | **34** | 9.19E-2 | (0.28) | **49** | 6.17E-2 | (0.31) | **64** | 2.88E-2 | (0.49) |
| **5** | 7.76E-2 | (0.29) | **20** | 1.10E-1 | (0.25) | **35** | 8.49E-2 | (0.28) | **50** | 7.16E-2 | (0.31) | **65** | 5.31E-2 | (0.36) |
| **6** | 7.31E-2 | (0.30) | **21** | 1.10E-1 | (0.27) | **36** | 8.36E-2 | (0.30) | **51** | 7.15E-2 | (0.31) | **66** | 5.16E-2 | (0.37) |
| **7** | 7.91E-2 | (0.29) | **22** | 7.06E-2 | (0.29) | **37** | 6.27E-2 | (0.31) | **52** | 6.78E-2 | (0.32) | **67** | 5.09E-2 | (0.37) |
| **8** | 8.57E-2 | (0.29) | **23** | 8.44E-2 | (0.28) | **38** | 7.34E-2 | (0.30) | **53** | 7.35E-2 | (0.34) | **68** | 4.81E-2 | (0.38) |
| **9** | 8.88E-2 | (0.28) | **24** | 7.80E-2 | (0.27) | **39** | 6.67E-2 | (0.30) | **54** | 6.06E-2 | (0.37) | **69** | 4.43E-2 | (0.40) |
| **10** | 9.72E-2 | (0.28) | **25** | 9.44E-2 | (0.27) | **40** | 8.00E-2 | (0.29) | **55** | 3.56E-2 | (0.47) | **70** | 3.22E-2 | (0.43) |

| | | | | | | | | | | | | |
|---|---|---|---|---|---|---|---|---|---|---|---|---|
| **11** | 7.19E-2 | (0.29) | **26** | 8.62E-2 | (0.26) | **41** | 8.49E-2 | (0.29) | **56** | 6.55E-2 | (0.33) | **71** | 2.91E-2 | (0.45) |
| **12** | 8.63E-2 | (0.28) | **27** | 9.69E-2 | (0.26) | **42** | 8.11E-2 | (0.29) | **57** | 6.22E-2 | (0.33) | **72** | 2.85E-2 | (0.45) |
| **13** | 8.06E-2 | (0.27) | **28** | 7.99E-2 | (0.29) | **43** | 6.89E-2 | (0.29) | **58** | 6.38E-2 | (0.33) | **73** | 2.74E-2 | (0.46) |
| **14** | 9.88E-2 | (0.26) | **29** | 7.64E-2 | (0.30) | **44** | 8.69E-2 | (0.30) | **59** | 6.09E-2 | (0.33) | **74** | 2.56E-2 | (0.48) |
| **15** | 9.43E-2 | (0.26) | **30** | 8.23E-2 | (0.29) | **45** | 6.90E-2 | (0.33) | **60** | 6.14E-2 | (0.34) | **75** | 2.57E-2 | (0.52) |
| Layer 10 | | | | | | | | | | | | | | |
| **1** | 4.77E-2 | (0.37) | **16** | 6.68E-2 | (0.32) | **31** | 6.75E-2 | (0.31) | **46** | 5.53E-2 | (0.35) | **61** | 4.60E-2 | (0.39) |
| **2** | 5.69E-2 | (0.34) | **17** | 7.21E-2 | (0.31) | **32** | 7.28E-2 | (0.31) | **47** | 4.90E-2 | (0.34) | **62** | 3.43E-2 | (0.41) |
| **3** | 5.26E-2 | (0.35) | **18** | 7.43E-2 | (0.30) | **33** | 7.31E-2 | (0.30) | **48** | 5.61E-2 | (0.34) | **63** | 2.76E-2 | (0.46) |
| **4** | 5.32E-2 | (0.33) | **19** | 8.21E-2 | (0.29) | **34** | 7.39E-2 | (0.31) | **49** | 5.10E-2 | (0.34) | **64** | 2.37E-2 | (0.54) |
| **5** | 6.36E-2 | (0.32) | **20** | 8.83E-2 | (0.28) | **35** | 6.90E-2 | (0.31) | **50** | 5.87E-2 | (0.34) | **65** | 4.47E-2 | (0.40) |
| **6** | 5.95E-2 | (0.33) | **21** | 8.76E-2 | (0.30) | **36** | 6.85E-2 | (0.34) | **51** | 5.82E-2 | (0.34) | **66** | 4.33E-2 | (0.40) |
| **7** | 6.45E-2 | (0.32) | **22** | 5.71E-2 | (0.32) | **37** | 5.20E-2 | (0.34) | **52** | 5.57E-2 | (0.35) | **67** | 4.27E-2 | (0.40) |
| **8** | 6.94E-2 | (0.32) | **23** | 6.83E-2 | (0.31) | **38** | 6.00E-2 | (0.33) | **53** | 5.96E-2 | (0.37) | **68** | 4.06E-2 | (0.41) |
| **9** | 7.23E-2 | (0.30) | **24** | 6.29E-2 | (0.30) | **39** | 5.40E-2 | (0.33) | **54** | 4.87E-2 | (0.41) | **69** | 3.72E-2 | (0.43) |
| **10** | 8.01E-2 | (0.31) | **25** | 7.59E-2 | (0.30) | **40** | 6.49E-2 | (0.32) | **55** | 2.88E-2 | (0.52) | **70** | 2.71E-2 | (0.47) |
| **11** | 5.84E-2 | (0.32) | **26** | 6.90E-2 | (0.29) | **41** | 6.83E-2 | (0.32) | **56** | 5.38E-2 | (0.36) | **71** | 2.45E-2 | (0.49) |
| **12** | 7.01E-2 | (0.31) | **27** | 7.80E-2 | (0.29) | **42** | 6.57E-2 | (0.32) | **57** | 5.13E-2 | (0.36) | **72** | 2.42E-2 | (0.49) |
| **13** | 6.53E-2 | (0.30) | **28** | 6.53E-2 | (0.32) | **43** | 5.66E-2 | (0.32) | **58** | 5.25E-2 | (0.36) | **73** | 2.31E-2 | (0.50) |
| **14** | 8.09E-2 | (0.29) | **29** | 6.23E-2 | (0.33) | **44** | 7.06E-2 | (0.34) | **59** | 5.11E-2 | (0.36) | **74** | 2.18E-2 | (0.52) |
| **15** | 7.66E-2 | (0.29) | **30** | 6.66E-2 | (0.32) | **45** | 5.57E-2 | (0.37) | **60** | 5.14E-2 | (0.37) | **75** | 2.16E-2 | (0.56) |
| Layer 11 | | | | | | | | | | | | | | |
| **1** | 3.16E-2 | (0.42) | **16** | 4.35E-2 | (0.36) | **31** | 4.39E-2 | (0.36) | **46** | 3.76E-2 | (0.39) | **61** | 3.66E-2 | (0.43) |
| **2** | 3.82E-2 | (0.39) | **17** | 4.61E-2 | (0.36) | **32** | 4.64E-2 | (0.36) | **47** | 3.78E-2 | (0.39) | **62** | 2.47E-2 | (0.46) |
| **3** | 4.05E-2 | (0.40) | **18** | 4.81E-2 | (0.34) | **33** | 4.69E-2 | (0.34) | **48** | 3.81E-2 | (0.38) | **63** | 2.16E-2 | (0.52) |
| **4** | 3.49E-2 | (0.38) | **19** | 5.32E-2 | (0.33) | **34** | 4.72E-2 | (0.35) | **49** | 3.96E-2 | (0.38) | **64** | 1.67E-2 | (0.60) |
| **5** | 4.22E-2 | (0.36) | **20** | 5.68E-2 | (0.32) | **35** | 4.65E-2 | (0.35) | **50** | 3.95E-2 | (0.38) | **65** | 3.59E-2 | (0.44) |
| **6** | 3.87E-2 | (0.38) | **21** | 5.54E-2 | (0.34) | **36** | 5.20E-2 | (0.39) | **51** | 3.86E-2 | (0.39) | **66** | 3.50E-2 | (0.44) |
| **7** | 4.21E-2 | (0.36) | **22** | 3.71E-2 | (0.37) | **37** | 4.04E-2 | (0.38) | **52** | 4.28E-2 | (0.40) | **67** | 3.45E-2 | (0.45) |
| **8** | 4.47E-2 | (0.36) | **23** | 4.43E-2 | (0.35) | **38** | 4.05E-2 | (0.37) | **53** | 3.82E-2 | (0.43) | **68** | 3.33E-2 | (0.46) |
| **9** | 4.77E-2 | (0.34) | **24** | 4.04E-2 | (0.35) | **39** | 3.52E-2 | (0.38) | **54** | 3.05E-2 | (0.48) | **69** | 3.03E-2 | (0.48) |
| **10** | 6.23E-2 | (0.35) | **25** | 4.88E-2 | (0.34) | **40** | 4.27E-2 | (0.36) | **55** | 1.90E-2 | (0.59) | **70** | 2.22E-2 | (0.51) |
| **11** | 3.78E-2 | (0.36) | **26** | 4.40E-2 | (0.34) | **41** | 4.37E-2 | (0.37) | **56** | 3.58E-2 | (0.41) | **71** | 2.03E-2 | (0.54) |
| **12** | 4.54E-2 | (0.35) | **27** | 5.08E-2 | (0.33) | **42** | 4.31E-2 | (0.36) | **57** | 3.49E-2 | (0.40) | **72** | 1.99E-2 | (0.54) |
| **13** | 4.28E-2 | (0.34) | **28** | 4.92E-2 | (0.36) | **43** | 4.33E-2 | (0.37) | **58** | 3.57E-2 | (0.41) | **73** | 1.92E-2 | (0.55) |
| **14** | 6.28E-2 | (0.32) | **29** | 4.15E-2 | (0.37) | **44** | 4.61E-2 | (0.38) | **59** | 4.09E-2 | (0.40) | **74** | 1.78E-2 | (0.57) |
| **15** | 5.88E-2 | (0.33) | **30** | 4.30E-2 | (0.37) | **45** | 3.50E-2 | (0.43) | **60** | 4.13E-2 | (0.41) | **75** | 1.59E-2 | (0.61) |
| Layer 12 | | | | | | | | | | | | | | |
| **1** | 2.51E-2 | (0.47) | **16** | 3.40E-2 | (0.40) | **31** | 3.42E-2 | (0.40) | **46** | 2.98E-2 | (0.44) | **61** | 2.93E-2 | (0.49) |
| **2** | 3.05E-2 | (0.43) | **17** | 3.57E-2 | (0.40) | **32** | 3.58E-2 | (0.40) | **47** | 3.03E-2 | (0.44) | **62** | 1.95E-2 | (0.51) |
| **3** | 3.24E-2 | (0.44) | **18** | 3.74E-2 | (0.38) | **33** | 3.62E-2 | (0.39) | **48** | 3.02E-2 | (0.43) | **63** | 1.70E-2 | (0.59) |
| **4** | 2.74E-2 | (0.42) | **19** | 4.11E-2 | (0.38) | **34** | 3.63E-2 | (0.40) | **49** | 3.16E-2 | (0.43) | **64** | 1.30E-2 | (0.67) |
| **5** | 3.33E-2 | (0.41) | **20** | 4.37E-2 | (0.37) | **35** | 3.62E-2 | (0.39) | **50** | 3.10E-2 | (0.42) | **65** | 2.89E-2 | (0.49) |
| **6** | 3.02E-2 | (0.43) | **21** | 4.25E-2 | (0.39) | **36** | 4.06E-2 | (0.43) | **51** | 3.00E-2 | (0.44) | **66** | 2.82E-2 | (0.49) |
| **7** | 3.31E-2 | (0.41) | **22** | 2.88E-2 | (0.41) | **37** | 3.23E-2 | (0.42) | **52** | 3.36E-2 | (0.45) | **67** | 2.80E-2 | (0.50) |
| **8** | 3.49E-2 | (0.41) | **23** | 3.46E-2 | (0.40) | **38** | 3.19E-2 | (0.42) | **53** | 2.94E-2 | (0.49) | **68** | 2.69E-2 | (0.51) |
| **9** | 3.74E-2 | (0.39) | **24** | 3.13E-2 | (0.40) | **39** | 2.76E-2 | (0.42) | **54** | 2.34E-2 | (0.55) | **69** | 2.45E-2 | (0.53) |
| **10** | 4.93E-2 | (0.39) | **25** | 3.79E-2 | (0.38) | **40** | 3.33E-2 | (0.41) | **55** | 1.47E-2 | (0.67) | **70** | 1.80E-2 | (0.57) |

| | | | | | | | | | | | | |
|---|---|---|---|---|---|---|---|---|---|---|---|---|
| **11** | 2.95E-2 | (0.41) | **26** | 3.37E-2 | (0.38) | **41** | 3.37E-2 | (0.41) | **56** | 2.82E-2 | (0.46) | **71** | 1.65E-2 | (0.60) |
| **12** | 3.54E-2 | (0.39) | **27** | 3.92E-2 | (0.38) | **42** | 3.34E-2 | (0.41) | **57** | 2.78E-2 | (0.45) | **72** | 1.62E-2 | (0.60) |
| **13** | 3.33E-2 | (0.39) | **28** | 3.84E-2 | (0.41) | **43** | 3.40E-2 | (0.41) | **58** | 2.83E-2 | (0.46) | **73** | 1.56E-2 | (0.61) |
| **14** | 4.95E-2 | (0.36) | **29** | 3.26E-2 | (0.41) | **44** | 3.57E-2 | (0.43) | **59** | 3.30E-2 | (0.45) | **74** | 1.45E-2 | (0.64) |
| **15** | 4.63E-2 | (0.37) | **30** | 3.34E-2 | (0.42) | **45** | 2.67E-2 | (0.49) | **60** | 3.32E-2 | (0.46) | **75** | 1.28E-2 | (0.68) |
| Layer 13 | | | | | | | | | | | | | | |
| **1** | 2.03E-2 | (0.52) | **16** | 2.71E-2 | (0.45) | **31** | 2.71E-2 | (0.45) | **46** | 2.38E-2 | (0.49) | **61** | 2.32E-2 | (0.54) |
| **2** | 2.44E-2 | (0.48) | **17** | 2.84E-2 | (0.45) | **32** | 2.83E-2 | (0.45) | **47** | 2.42E-2 | (0.49) | **62** | 1.54E-2 | (0.58) |
| **3** | 2.61E-2 | (0.49) | **18** | 2.96E-2 | (0.43) | **33** | 2.86E-2 | (0.44) | **48** | 2.41E-2 | (0.48) | **63** | 1.34E-2 | (0.66) |
| **4** | 2.20E-2 | (0.47) | **19** | 3.24E-2 | (0.42) | **34** | 2.85E-2 | (0.45) | **49** | 2.51E-2 | (0.48) | **64** | 1.02E-2 | (0.76) |
| **5** | 2.67E-2 | (0.45) | **20** | 3.44E-2 | (0.41) | **35** | 2.85E-2 | (0.44) | **50** | 2.46E-2 | (0.48) | **65** | 2.31E-2 | (0.55) |
| **6** | 2.42E-2 | (0.48) | **21** | 3.33E-2 | (0.44) | **36** | 3.19E-2 | (0.49) | **51** | 2.38E-2 | (0.50) | **66** | 2.26E-2 | (0.55) |
| **7** | 2.65E-2 | (0.46) | **22** | 2.30E-2 | (0.46) | **37** | 2.58E-2 | (0.47) | **52** | 2.64E-2 | (0.51) | **67** | 2.24E-2 | (0.56) |
| **8** | 2.79E-2 | (0.46) | **23** | 2.75E-2 | (0.45) | **38** | 2.55E-2 | (0.47) | **53** | 2.31E-2 | (0.55) | **68** | 2.15E-2 | (0.57) |
| **9** | 2.98E-2 | (0.43) | **24** | 2.48E-2 | (0.44) | **39** | 2.19E-2 | (0.47) | **54** | 1.82E-2 | (0.62) | **69** | 1.96E-2 | (0.60) |
| **10** | 3.91E-2 | (0.44) | **25** | 2.99E-2 | (0.43) | **40** | 2.64E-2 | (0.46) | **55** | 1.15E-2 | (0.76) | **70** | 1.43E-2 | (0.64) |
| **11** | 2.35E-2 | (0.46) | **26** | 2.65E-2 | (0.43) | **41** | 2.66E-2 | (0.47) | **56** | 2.25E-2 | (0.51) | **71** | 1.32E-2 | (0.67) |
| **12** | 2.82E-2 | (0.44) | **27** | 3.08E-2 | (0.42) | **42** | 2.64E-2 | (0.46) | **57** | 2.22E-2 | (0.50) | **72** | 1.30E-2 | (0.67) |
| **13** | 2.65E-2 | (0.43) | **28** | 3.02E-2 | (0.46) | **43** | 2.67E-2 | (0.47) | **58** | 2.27E-2 | (0.51) | **73** | 1.26E-2 | (0.68) |
| **14** | 3.92E-2 | (0.41) | **29** | 2.60E-2 | (0.46) | **44** | 2.80E-2 | (0.49) | **59** | 2.63E-2 | (0.50) | **74** | 1.16E-2 | (0.71) |
| **15** | 3.66E-2 | (0.42) | **30** | 2.65E-2 | (0.47) | **45** | 2.09E-2 | (0.56) | **60** | 2.64E-2 | (0.51) | **75** | 1.02E-2 | (0.76) |
| Layer 14 | | | | | | | | | | | | | | |
| **1** | 1.62E-2 | (0.59) | **16** | 2.15E-2 | (0.51) | **31** | 2.14E-2 | (0.51) | **46** | 1.88E-2 | (0.55) | **61** | 1.81E-2 | (0.62) |
| **2** | 1.95E-2 | (0.53) | **17** | 2.25E-2 | (0.51) | **32** | 2.23E-2 | (0.51) | **47** | 1.91E-2 | (0.55) | **62** | 1.20E-2 | (0.65) |
| **3** | 2.08E-2 | (0.55) | **18** | 2.34E-2 | (0.48) | **33** | 2.25E-2 | (0.49) | **48** | 1.89E-2 | (0.54) | **63** | 1.05E-2 | (0.75) |
| **4** | 1.75E-2 | (0.53) | **19** | 2.55E-2 | (0.48) | **34** | 2.23E-2 | (0.51) | **49** | 1.98E-2 | (0.54) | **64** | 7.98E-3 | (0.86) |
| **5** | 2.13E-2 | (0.51) | **20** | 2.69E-2 | (0.47) | **35** | 2.22E-2 | (0.50) | **50** | 1.92E-2 | (0.54) | **65** | 1.82E-2 | (0.62) |
| **6** | 1.92E-2 | (0.53) | **21** | 2.61E-2 | (0.50) | **36** | 2.48E-2 | (0.56) | **51** | 1.86E-2 | (0.56) | **66** | 1.78E-2 | (0.62) |
| **7** | 2.11E-2 | (0.51) | **22** | 1.83E-2 | (0.52) | **37** | 2.05E-2 | (0.53) | **52** | 2.07E-2 | (0.58) | **67** | 1.76E-2 | (0.63) |
| **8** | 2.21E-2 | (0.51) | **23** | 2.17E-2 | (0.50) | **38** | 2.02E-2 | (0.53) | **53** | 1.80E-2 | (0.62) | **68** | 1.68E-2 | (0.64) |
| **9** | 2.36E-2 | (0.48) | **24** | 1.96E-2 | (0.50) | **39** | 1.73E-2 | (0.53) | **54** | 1.42E-2 | (0.70) | **69** | 1.53E-2 | (0.67) |
| **10** | 3.09E-2 | (0.50) | **25** | 2.35E-2 | (0.48) | **40** | 2.08E-2 | (0.52) | **55** | 8.95E-3 | (0.86) | **70** | 1.12E-2 | (0.73) |
| **11** | 1.87E-2 | (0.51) | **26** | 2.08E-2 | (0.48) | **41** | 2.09E-2 | (0.53) | **56** | 1.78E-2 | (0.58) | **71** | 1.04E-2 | (0.76) |
| **12** | 2.24E-2 | (0.49) | **27** | 2.41E-2 | (0.48) | **42** | 2.06E-2 | (0.52) | **57** | 1.76E-2 | (0.56) | **72** | 1.02E-2 | (0.76) |
| **13** | 2.09E-2 | (0.49) | **28** | 2.36E-2 | (0.52) | **43** | 2.08E-2 | (0.53) | **58** | 1.79E-2 | (0.58) | **73** | 9.86E-3 | (0.77) |
| **14** | 3.07E-2 | (0.46) | **29** | 2.06E-2 | (0.52) | **44** | 2.18E-2 | (0.55) | **59** | 2.07E-2 | (0.57) | **74** | 9.10E-3 | (0.80) |
| **15** | 2.85E-2 | (0.48) | **30** | 2.10E-2 | (0.52) | **45** | 1.62E-2 | (0.63) | **60** | 2.08E-2 | (0.58) | **75** | 8.00E-3 | (0.86) |
| Layer 15 | | | | | | | | | | | | | | |
| **1** | 1.29E-2 | (0.66) | **16** | 1.69E-2 | (0.57) | **31** | 1.67E-2 | (0.57) | **46** | 1.46E-2 | (0.62) | **61** | 1.36E-2 | (0.71) |
| **2** | 1.54E-2 | (0.60) | **17** | 1.78E-2 | (0.57) | **32** | 1.74E-2 | (0.58) | **47** | 1.47E-2 | (0.62) | **62** | 9.10E-3 | (0.75) |
| **3** | 1.63E-2 | (0.63) | **18** | 1.83E-2 | (0.55) | **33** | 1.75E-2 | (0.56) | **48** | 1.46E-2 | (0.62) | **63** | 7.91E-3 | (0.86) |
| **4** | 1.39E-2 | (0.59) | **19** | 1.98E-2 | (0.54) | **34** | 1.73E-2 | (0.58) | **49** | 1.51E-2 | (0.62) | **64** | 6.13E-3 | (0.98) |
| **5** | 1.68E-2 | (0.57) | **20** | 2.09E-2 | (0.53) | **35** | 1.70E-2 | (0.57) | **50** | 1.48E-2 | (0.61) | **65** | 1.37E-2 | (0.71) |
| **6** | 1.51E-2 | (0.60) | **21** | 2.01E-2 | (0.57) | **36** | 1.85E-2 | (0.64) | **51** | 1.42E-2 | (0.64) | **66** | 1.34E-2 | (0.71) |
| **7** | 1.67E-2 | (0.57) | **22** | 1.44E-2 | (0.58) | **37** | 1.58E-2 | (0.60) | **52** | 1.54E-2 | (0.67) | **67** | 1.32E-2 | (0.72) |
| **8** | 1.75E-2 | (0.57) | **23** | 1.71E-2 | (0.57) | **38** | 1.57E-2 | (0.59) | **53** | 1.34E-2 | (0.72) | **68** | 1.27E-2 | (0.74) |
| **9** | 1.85E-2 | (0.55) | **24** | 1.53E-2 | (0.57) | **39** | 1.35E-2 | (0.60) | **54** | 1.09E-2 | (0.80) | **69** | 1.16E-2 | (0.77) |
| **10** | 2.37E-2 | (0.57) | **25** | 1.84E-2 | (0.55) | **40** | 1.62E-2 | (0.58) | **55** | 6.91E-3 | (0.97) | **70** | 8.46E-3 | (0.83) |

| | | | | | | | | | | | | |
|---|---|---|---|---|---|---|---|---|---|---|---|---|
| **11** | 1.48E-2 | (0.58) | **26** | 1.62E-2 | (0.55) | **41** | 1.62E-2 | (0.60) | **56** | 1.37E-2 | (0.66) | **71** | 7.85E-3 | (0.87) |
| **12** | 1.77E-2 | (0.56) | **27** | 1.86E-2 | (0.54) | **42** | 1.59E-2 | (0.59) | **57** | 1.34E-2 | (0.64) | **72** | 7.78E-3 | (0.87) |
| **13** | 1.64E-2 | (0.55) | **28** | 1.80E-2 | (0.60) | **43** | 1.56E-2 | (0.61) | **58** | 1.36E-2 | (0.66) | **73** | 7.49E-3 | (0.89) |
| **14** | 2.37E-2 | (0.53) | **29** | 1.62E-2 | (0.59) | **44** | 1.63E-2 | (0.64) | **59** | 1.56E-2 | (0.65) | **74** | 6.91E-3 | (0.92) |
| **15** | 2.17E-2 | (0.54) | **30** | 1.65E-2 | (0.59) | **45** | 1.24E-2 | (0.73) | **60** | 1.56E-2 | (0.66) | **75** | 6.14E-3 | (0.98) |
| Layer 16 | | | | | | | | | | | | | | |
| **1** | 1.01E-2 | (0.74) | **16** | 1.33E-2 | (0.64) | **31** | 1.30E-2 | (0.65) | **46** | 1.09E-2 | (0.72) | **61** | 8.49E-3 | (0.83) |
| **2** | 1.20E-2 | (0.68) | **17** | 1.39E-2 | (0.64) | **32** | 1.35E-2 | (0.65) | **47** | 9.52E-3 | (0.72) | **62** | 6.56E-3 | (0.88) |
| **3** | 1.08E-2 | (0.71) | **18** | 1.43E-2 | (0.62) | **33** | 1.35E-2 | (0.64) | **48** | 1.09E-2 | (0.71) | **63** | 5.21E-3 | (0.99) |
| **4** | 1.09E-2 | (0.67) | **19** | 1.51E-2 | (0.62) | **34** | 1.32E-2 | (0.66) | **49** | 9.66E-3 | (0.71) | **64** | 4.61E-3 | (1.13) |
| **5** | 1.30E-2 | (0.65) | **20** | 1.58E-2 | (0.61) | **35** | 1.23E-2 | (0.67) | **50** | 1.09E-2 | (0.71) | **65** | 8.35E-3 | (0.84) |
| **6** | 1.17E-2 | (0.68) | **21** | 1.55E-2 | (0.65) | **36** | 1.16E-2 | (0.75) | **51** | 1.04E-2 | (0.75) | **66** | 8.16E-3 | (0.85) |
| **7** | 1.32E-2 | (0.65) | **22** | 1.13E-2 | (0.66) | **37** | 1.02E-2 | (0.70) | **52** | 9.50E-3 | (0.78) | **67** | 8.06E-3 | (0.85) |
| **8** | 1.37E-2 | (0.65) | **23** | 1.34E-2 | (0.64) | **38** | 1.18E-2 | (0.68) | **53** | 8.21E-3 | (0.85) | **68** | 7.74E-3 | (0.87) |
| **9** | 1.42E-2 | (0.62) | **24** | 1.20E-2 | (0.64) | **39** | 1.04E-2 | (0.69) | **54** | 8.12E-3 | (0.92) | **69** | 8.38E-3 | (0.90) |
| **10** | 1.52E-2 | (0.66) | **25** | 1.43E-2 | (0.62) | **40** | 1.23E-2 | (0.67) | **55** | 5.23E-3 | (1.12) | **70** | 5.54E-3 | (0.96) |
| **11** | 1.16E-2 | (0.65) | **26** | 1.26E-2 | (0.62) | **41** | 1.24E-2 | (0.68) | **56** | 1.01E-2 | (0.76) | **71** | 5.06E-3 | (1.00) |
| **12** | 1.38E-2 | (0.63) | **27** | 1.42E-2 | (0.62) | **42** | 1.19E-2 | (0.68) | **57** | 9.84E-3 | (0.75) | **72** | 5.00E-3 | (1.01) |
| **13** | 1.25E-2 | (0.63) | **28** | 1.17E-2 | (0.69) | **43** | 9.70E-3 | (0.71) | **58** | 9.87E-3 | (0.76) | **73** | 4.83E-3 | (1.02) |
| **14** | 1.52E-2 | (0.60) | **29** | 1.24E-2 | (0.67) | **44** | 1.01E-2 | (0.74) | **59** | 9.70E-3 | (0.75) | **74** | 4.51E-3 | (1.06) |
| **15** | 1.39E-2 | (0.63) | **30** | 1.28E-2 | (0.67) | **45** | 9.10E-3 | (0.84) | **60** | 9.67E-3 | (0.78) | **75** | 4.64E-3 | (1.13) |
| Layer 17 | | | | | | | | | | | | | | |
| **1** | 7.88E-3 | (0.84) | **16** | 1.04E-2 | (0.73) | **31** | 1.00E-2 | (0.74) | **46** | 8.25E-3 | (0.82) | **61** | 6.26E-3 | (0.96) |
| **2** | 9.38E-3 | (0.77) | **17** | 1.08E-2 | (0.73) | **32** | 1.04E-2 | (0.75) | **47** | 7.15E-3 | (0.83) | **62** | 4.94E-3 | (1.01) |
| **3** | 8.35E-3 | (0.81) | **18** | 1.11E-2 | (0.70) | **33** | 1.04E-2 | (0.73) | **48** | 8.30E-3 | (0.81) | **63** | 3.91E-3 | (1.13) |
| **4** | 8.54E-3 | (0.76) | **19** | 1.17E-2 | (0.70) | **34** | 1.01E-2 | (0.76) | **49** | 7.23E-3 | (0.82) | **64** | 3.51E-3 | (1.30) |
| **5** | 1.01E-2 | (0.74) | **20** | 1.21E-2 | (0.69) | **35** | 9.36E-3 | (0.77) | **50** | 8.26E-3 | (0.82) | **65** | 6.14E-3 | (0.98) |
| **6** | 9.18E-3 | (0.77) | **21** | 1.20E-2 | (0.74) | **36** | 8.60E-3 | (0.87) | **51** | 7.82E-3 | (0.86) | **66** | 6.01E-3 | (0.98) |
| **7** | 1.03E-2 | (0.73) | **22** | 8.77E-3 | (0.75) | **37** | 7.76E-3 | (0.80) | **52** | 7.00E-3 | (0.91) | **67** | 5.92E-3 | (0.99) |
| **8** | 1.07E-2 | (0.73) | **23** | 1.04E-2 | (0.72) | **38** | 9.07E-3 | (0.78) | **53** | 6.05E-3 | (0.98) | **68** | 5.69E-3 | (1.01) |
| **9** | 1.09E-2 | (0.71) | **24** | 9.26E-3 | (0.73) | **39** | 8.00E-3 | (0.78) | **54** | 6.08E-3 | (1.06) | **69** | 6.26E-3 | (1.04) |
| **10** | 1.15E-2 | (0.75) | **25** | 1.11E-2 | (0.70) | **40** | 9.39E-3 | (0.76) | **55** | 3.94E-3 | (1.29) | **70** | 4.17E-3 | (1.10) |
| **11** | 9.06E-3 | (0.74) | **26** | 9.70E-3 | (0.71) | **41** | 9.53E-3 | (0.78) | **56** | 7.65E-3 | (0.87) | **71** | 3.78E-3 | (1.16) |
| **12** | 1.08E-2 | (0.71) | **27** | 1.09E-2 | (0.71) | **42** | 9.05E-3 | (0.78) | **57** | 7.41E-3 | (0.86) | **72** | 3.73E-3 | (1.16) |
| **13** | 9.70E-3 | (0.71) | **28** | 8.88E-3 | (0.79) | **43** | 7.22E-3 | (0.82) | **58** | 7.43E-3 | (0.88) | **73** | 3.62E-3 | (1.18) |
| **14** | 1.16E-2 | (0.69) | **29** | 9.61E-3 | (0.76) | **44** | 7.47E-3 | (0.86) | **59** | 7.21E-3 | (0.87) | **74** | 3.36E-3 | (1.22) |
| **15** | 1.05E-2 | (0.72) | **30** | 9.93E-3 | (0.76) | **45** | 6.82E-3 | (0.97) | **60** | 7.12E-3 | (0.90) | **75** | 3.52E-3 | (1.29) |
| Layer 18 | | | | | | | | | | | | | | |
| **1** | 6.13E-3 | (0.95) | **16** | 8.08E-3 | (0.83) | **31** | 7.72E-3 | (0.84) | **46** | 6.33E-3 | (0.94) | **61** | 4.74E-3 | (1.10) |
| **2** | 7.27E-3 | (0.87) | **17** | 8.39E-3 | (0.83) | **32** | 7.97E-3 | (0.85) | **47** | 5.48E-3 | (0.94) | **62** | 3.73E-3 | (1.16) |
| **3** | 6.56E-3 | (0.91) | **18** | 8.58E-3 | (0.80) | **33** | 7.92E-3 | (0.83) | **48** | 6.30E-3 | (0.93) | **63** | 2.94E-3 | (1.31) |
| **4** | 6.64E-3 | (0.86) | **19** | 8.98E-3 | (0.80) | **34** | 7.72E-3 | (0.86) | **49** | 5.52E-3 | (0.94) | **64** | 2.65E-3 | (1.49) |
| **5** | 7.88E-3 | (0.83) | **20** | 9.38E-3 | (0.78) | **35** | 7.08E-3 | (0.88) | **50** | 6.26E-3 | (0.94) | **65** | 4.64E-3 | (1.12) |
| **6** | 7.11E-3 | (0.88) | **21** | 9.17E-3 | (0.84) | **36** | 6.49E-3 | (1.00) | **51** | 5.92E-3 | (0.99) | **66** | 4.52E-3 | (1.13) |
| **7** | 7.92E-3 | (0.83) | **22** | 6.80E-3 | (0.85) | **37** | 5.97E-3 | (0.91) | **52** | 5.34E-3 | (1.04) | **67** | 4.45E-3 | (1.13) |
| **8** | 8.27E-3 | (0.83) | **23** | 8.04E-3 | (0.82) | **38** | 6.95E-3 | (0.89) | **53** | 4.58E-3 | (1.13) | **68** | 4.30E-3 | (1.16) |
| **9** | 8.49E-3 | (0.80) | **24** | 7.14E-3 | (0.83) | **39** | 6.11E-3 | (0.89) | **54** | 4.61E-3 | (1.22) | **69** | 4.74E-3 | (1.20) |
| **10** | 8.89E-3 | (0.85) | **25** | 8.47E-3 | (0.80) | **40** | 7.17E-3 | (0.87) | **55** | 3.01E-3 | (1.47) | **70** | 3.14E-3 | (1.26) |

| | | | | | | | | | | | | |
|---|---|---|---|---|---|---|---|---|---|---|---|---|
| **11** | 7.02E-3 | (0.84) | **26** | 7.44E-3 | (0.81) | **41** | 7.25E-3 | (0.89) | **56** | 5.78E-3 | (1.00) | **71** | 2.86E-3 | (1.33) |
| **12** | 8.35E-3 | (0.81) | **27** | 8.37E-3 | (0.81) | **42** | 6.88E-3 | (0.89) | **57** | 5.60E-3 | (0.99) | **72** | 2.83E-3 | (1.33) |
| **13** | 7.47E-3 | (0.81) | **28** | 6.75E-3 | (0.90) | **43** | 5.49E-3 | (0.94) | **58** | 5.63E-3 | (1.01) | **73** | 2.72E-3 | (1.36) |
| **14** | 8.96E-3 | (0.78) | **29** | 7.41E-3 | (0.86) | **44** | 5.68E-3 | (0.98) | **59** | 5.46E-3 | (1.00) | **74** | 2.56E-3 | (1.41) |
| **15** | 8.15E-3 | (0.82) | **30** | 7.68E-3 | (0.87) | **45** | 5.19E-3 | (1.12) | **60** | 5.40E-3 | (1.04) | **75** | 2.67E-3 | (1.48) |
| Layer 19 | | | | | | | | | | | | | | |
| **1** | 4.70E-3 | (1.09) | **16** | 6.19E-3 | (0.95) | **31** | 5.90E-3 | (0.96) | **46** | 4.79E-3 | (1.07) | **61** | 3.57E-3 | (1.27) |
| **2** | 5.63E-3 | (0.99) | **17** | 6.41E-3 | (0.95) | **32** | 6.09E-3 | (0.97) | **47** | 4.13E-3 | (1.09) | **62** | 2.81E-3 | (1.33) |
| **3** | 5.04E-3 | (1.04) | **18** | 6.54E-3 | (0.91) | **33** | 6.03E-3 | (0.96) | **48** | 4.78E-3 | (1.07) | **63** | 2.21E-3 | (1.51) |
| **4** | 5.13E-3 | (0.98) | **19** | 6.88E-3 | (0.92) | **34** | 5.87E-3 | (0.99) | **49** | 4.14E-3 | (1.09) | **64** | 1.98E-3 | (1.72) |
| **5** | 6.06E-3 | (0.95) | **20** | 7.18E-3 | (0.90) | **35** | 5.39E-3 | (1.01) | **50** | 4.72E-3 | (1.08) | **65** | 3.48E-3 | (1.29) |
| **6** | 5.43E-3 | (1.00) | **21** | 6.98E-3 | (0.96) | **36** | 4.95E-3 | (1.14) | **51** | 4.44E-3 | (1.14) | **66** | 3.41E-3 | (1.30) |
| **7** | 6.13E-3 | (0.95) | **22** | 5.21E-3 | (0.97) | **37** | 4.54E-3 | (1.04) | **52** | 4.01E-3 | (1.20) | **67** | 3.32E-3 | (1.32) |
| **8** | 6.39E-3 | (0.95) | **23** | 6.15E-3 | (0.94) | **38** | 5.29E-3 | (1.02) | **53** | 3.46E-3 | (1.29) | **68** | 3.26E-3 | (1.33) |
| **9** | 6.53E-3 | (0.92) | **24** | 5.47E-3 | (0.95) | **39** | 4.65E-3 | (1.03) | **54** | 3.49E-3 | (1.41) | **69** | 3.55E-3 | (1.38) |
| **10** | 6.82E-3 | (0.97) | **25** | 6.48E-3 | (0.92) | **40** | 5.45E-3 | (1.00) | **55** | 2.25E-3 | (1.70) | **70** | 2.35E-3 | (1.46) |
| **11** | 5.41E-3 | (0.95) | **26** | 5.68E-3 | (0.93) | **41** | 5.50E-3 | (1.02) | **56** | 4.38E-3 | (1.15) | **71** | 2.14E-3 | (1.54) |
| **12** | 6.43E-3 | (0.92) | **27** | 6.37E-3 | (0.93) | **42** | 5.19E-3 | (1.03) | **57** | 4.24E-3 | (1.14) | **72** | 2.11E-3 | (1.54) |
| **13** | 5.74E-3 | (0.92) | **28** | 5.14E-3 | (1.03) | **43** | 4.14E-3 | (1.08) | **58** | 4.22E-3 | (1.17) | **73** | 2.05E-3 | (1.57) |
| **14** | 6.90E-3 | (0.89) | **29** | 5.64E-3 | (0.99) | **44** | 4.31E-3 | (1.13) | **59** | 4.11E-3 | (1.15) | **74** | 1.92E-3 | (1.62) |
| **15** | 6.24E-3 | (0.94) | **30** | 5.85E-3 | (0.99) | **45** | 3.91E-3 | (1.28) | **60** | 4.07E-3 | (1.20) | **75** | 2.00E-3 | (1.71) |
| Layer 20 | | | | | | | | | | | | | | |
| **1** | 3.64E-3 | (1.24) | **16** | 4.70E-3 | (1.08) | **31** | 4.46E-3 | (1.11) | **46** | 3.59E-3 | (1.24) | **61** | 2.64E-3 | (1.48) |
| **2** | 4.29E-3 | (1.13) | **17** | 4.90E-3 | (1.09) | **32** | 4.59E-3 | (1.12) | **47** | 3.09E-3 | (1.26) | **62** | 2.10E-3 | (1.55) |
| **3** | 3.80E-3 | (1.20) | **18** | 4.98E-3 | (1.05) | **33** | 4.54E-3 | (1.10) | **48** | 3.58E-3 | (1.24) | **63** | 1.65E-3 | (1.75) |
| **4** | 3.92E-3 | (1.12) | **19** | 5.22E-3 | (1.05) | **34** | 4.40E-3 | (1.14) | **49** | 3.11E-3 | (1.25) | **64** | 1.48E-3 | (1.99) |
| **5** | 4.63E-3 | (1.09) | **20** | 5.44E-3 | (1.03) | **35** | 4.04E-3 | (1.17) | **50** | 3.54E-3 | (1.24) | **65** | 2.58E-3 | (1.50) |
| **6** | 4.13E-3 | (1.15) | **21** | 5.31E-3 | (1.10) | **36** | 3.71E-3 | (1.32) | **51** | 3.32E-3 | (1.32) | **66** | 2.53E-3 | (1.51) |
| **7** | 4.68E-3 | (1.09) | **22** | 3.93E-3 | (1.12) | **37** | 3.40E-3 | (1.20) | **52** | 2.98E-3 | (1.39) | **67** | 2.49E-3 | (1.52) |
| **8** | 4.87E-3 | (1.09) | **23** | 4.67E-3 | (1.08) | **38** | 3.99E-3 | (1.17) | **53** | 2.59E-3 | (1.50) | **68** | 2.40E-3 | (1.55) |
| **9** | 4.95E-3 | (1.05) | **24** | 4.14E-3 | (1.09) | **39** | 3.50E-3 | (1.18) | **54** | 2.62E-3 | (1.62) | **69** | 2.60E-3 | (1.61) |
| **10** | 5.15E-3 | (1.12) | **25** | 4.90E-3 | (1.06) | **40** | 4.13E-3 | (1.15) | **55** | 1.70E-3 | (1.97) | **70** | 1.74E-3 | (1.69) |
| **11** | 4.12E-3 | (1.09) | **26** | 4.29E-3 | (1.07) | **41** | 4.13E-3 | (1.18) | **56** | 3.26E-3 | (1.34) | **71** | 1.58E-3 | (1.78) |
| **12** | 4.87E-3 | (1.06) | **27** | 4.81E-3 | (1.07) | **42** | 3.86E-3 | (1.19) | **57** | 3.16E-3 | (1.32) | **72** | 1.56E-3 | (1.79) |
| **13** | 4.37E-3 | (1.06) | **28** | 3.84E-3 | (1.19) | **43** | 3.09E-3 | (1.26) | **58** | 3.15E-3 | (1.35) | **73** | 1.52E-3 | (1.82) |
| **14** | 5.25E-3 | (1.02) | **29** | 4.26E-3 | (1.14) | **44** | 3.22E-3 | (1.31) | **59** | 3.04E-3 | (1.34) | **74** | 1.42E-3 | (1.88) |
| **15** | 4.75E-3 | (1.08) | **30** | 4.42E-3 | (1.14) | **45** | 2.95E-3 | (1.48) | **60** | 3.03E-3 | (1.39) | **75** | 1.46E-3 | (2.00) |
| Layer 21 | | | | | | | | | | | | | | |
| **1** | 2.73E-3 | (1.43) | **16** | 3.52E-3 | (1.25) | **31** | 3.34E-3 | (1.28) | **46** | 2.65E-3 | (1.44) | **61** | 1.94E-3 | (1.72) |
| **2** | 3.22E-3 | (1.31) | **17** | 3.64E-3 | (1.26) | **32** | 3.41E-3 | (1.30) | **47** | 2.29E-3 | (1.46) | **62** | 1.54E-3 | (1.81) |
| **3** | 2.87E-3 | (1.38) | **18** | 3.72E-3 | (1.21) | **33** | 3.38E-3 | (1.28) | **48** | 2.64E-3 | (1.44) | **63** | 1.22E-3 | (2.03) |
| **4** | 2.93E-3 | (1.30) | **19** | 3.88E-3 | (1.22) | **34** | 3.25E-3 | (1.33) | **49** | 2.28E-3 | (1.47) | **64** | 1.09E-3 | (2.32) |
| **5** | 3.47E-3 | (1.25) | **20** | 4.02E-3 | (1.20) | **35** | 2.97E-3 | (1.36) | **50** | 2.60E-3 | (1.45) | **65** | 1.91E-3 | (1.75) |
| **6** | 3.11E-3 | (1.33) | **21** | 3.90E-3 | (1.28) | **36** | 2.70E-3 | (1.55) | **51** | 2.46E-3 | (1.53) | **66** | 1.86E-3 | (1.76) |
| **7** | 3.50E-3 | (1.25) | **22** | 2.95E-3 | (1.29) | **37** | 2.54E-3 | (1.39) | **52** | 2.20E-3 | (1.62) | **67** | 1.83E-3 | (1.78) |
| **8** | 3.64E-3 | (1.26) | **23** | 3.47E-3 | (1.25) | **38** | 2.95E-3 | (1.36) | **53** | 1.90E-3 | (1.75) | **68** | 1.72E-3 | (1.83) |
| **9** | 3.71E-3 | (1.22) | **24** | 3.08E-3 | (1.26) | **39** | 2.58E-3 | (1.38) | **54** | 1.89E-3 | (1.91) | **69** | 1.60E-3 | (1.91) |
| **10** | 3.83E-3 | (1.29) | **25** | 3.65E-3 | (1.22) | **40** | 3.04E-3 | (1.34) | **55** | 1.23E-3 | (2.30) | **70** | 1.27E-3 | (1.99) |

| | | | | | | | | | | | | |
|---|---|---|---|---|---|---|---|---|---|---|---|---|
| **11** | 3.08E-3 | (1.27) | **26** | 3.19E-3 | (1.24) | **41** | 3.06E-3 | (1.37) | **56** | 2.42E-3 | (1.55) | **71** | 1.17E-3 | (2.08) |
| **12** | 3.66E-3 | (1.23) | **27** | 3.55E-3 | (1.24) | **42** | 2.88E-3 | (1.38) | **57** | 2.33E-3 | (1.54) | **72** | 1.15E-3 | (2.09) |
| **13** | 3.27E-3 | (1.23) | **28** | 2.84E-3 | (1.39) | **43** | 2.26E-3 | (1.47) | **58** | 2.30E-3 | (1.58) | **73** | 1.10E-3 | (2.13) |
| **14** | 3.88E-3 | (1.19) | **29** | 3.14E-3 | (1.32) | **44** | 2.35E-3 | (1.53) | **59** | 2.23E-3 | (1.57) | **74** | 1.03E-3 | (2.22) |
| **15** | 3.51E-3 | (1.25) | **30** | 3.28E-3 | (1.32) | **45** | 2.13E-3 | (1.74) | **60** | 2.18E-3 | (1.63) | **75** | 9.53E-4 | (2.32) |
| Layer 22 | | | | | | | | | | | | | | |
| **1** | 1.99E-3 | (1.68) | **16** | 2.52E-3 | (1.48) | **31** | 2.38E-3 | (1.51) | **46** | 1.90E-3 | (1.71) | **61** | 1.38E-3 | (2.04) |
| **2** | 2.34E-3 | (1.54) | **17** | 2.64E-3 | (1.48) | **32** | 2.45E-3 | (1.53) | **47** | 1.64E-3 | (1.73) | **62** | 1.10E-3 | (2.14) |
| **3** | 2.08E-3 | (1.62) | **18** | 2.68E-3 | (1.43) | **33** | 2.42E-3 | (1.51) | **48** | 1.88E-3 | (1.70) | **63** | 8.64E-4 | (2.41) |
| **4** | 2.11E-3 | (1.53) | **19** | 2.78E-3 | (1.44) | **34** | 2.33E-3 | (1.57) | **49** | 1.62E-3 | (1.73) | **64** | 7.89E-4 | (2.74) |
| **5** | 2.50E-3 | (1.48) | **20** | 2.87E-3 | (1.42) | **35** | 2.14E-3 | (1.60) | **50** | 1.87E-3 | (1.71) | **65** | 1.36E-3 | (2.06) |
| **6** | 2.25E-3 | (1.56) | **21** | 2.80E-3 | (1.52) | **36** | 1.94E-3 | (1.83) | **51** | 1.76E-3 | (1.81) | **66** | 1.31E-3 | (2.10) |
| **7** | 2.54E-3 | (1.48) | **22** | 2.11E-3 | (1.53) | **37** | 1.82E-3 | (1.65) | **52** | 1.58E-3 | (1.91) | **67** | 1.30E-3 | (2.11) |
| **8** | 2.61E-3 | (1.48) | **23** | 2.50E-3 | (1.48) | **38** | 2.12E-3 | (1.61) | **53** | 1.36E-3 | (2.07) | **68** | 1.21E-3 | (2.18) |
| **9** | 2.67E-3 | (1.43) | **24** | 2.21E-3 | (1.49) | **39** | 1.86E-3 | (1.62) | **54** | 1.34E-3 | (2.26) | **69** | 1.11E-3 | (2.28) |
| **10** | 2.77E-3 | (1.52) | **25** | 2.62E-3 | (1.44) | **40** | 2.20E-3 | (1.58) | **55** | 8.70E-4 | (2.75) | **70** | 8.89E-4 | (2.36) |
| **11** | 2.22E-3 | (1.49) | **26** | 2.28E-3 | (1.46) | **41** | 2.19E-3 | (1.62) | **56** | 1.71E-3 | (1.85) | **71** | 8.31E-4 | (2.47) |
| **12** | 2.62E-3 | (1.45) | **27** | 2.55E-3 | (1.47) | **42** | 2.06E-3 | (1.63) | **57** | 1.66E-3 | (1.82) | **72** | 8.12E-4 | (2.48) |
| **13** | 2.36E-3 | (1.44) | **28** | 2.06E-3 | (1.63) | **43** | 1.63E-3 | (1.73) | **58** | 1.64E-3 | (1.88) | **73** | 7.77E-4 | (2.53) |
| **14** | 2.81E-3 | (1.40) | **29** | 2.27E-3 | (1.56) | **44** | 1.70E-3 | (1.80) | **59** | 1.58E-3 | (1.86) | **74** | 7.30E-4 | (2.63) |
| **15** | 2.50E-3 | (1.48) | **30** | 2.35E-3 | (1.57) | **45** | 1.52E-3 | (2.06) | **60** | 1.53E-3 | (1.94) | **75** | 6.67E-4 | (2.77) |
| Layer 23 | | | | | | | | | | | | | | |
| **1** | 1.36E-3 | (2.03) | **16** | 1.69E-3 | (1.81) | **31** | 1.62E-3 | (1.84) | **46** | 1.27E-3 | (2.10) | **61** | 9.27E-4 | (2.50) |
| **2** | 1.58E-3 | (1.87) | **17** | 1.77E-3 | (1.81) | **32** | 1.64E-3 | (1.87) | **47** | 1.09E-3 | (2.11) | **62** | 7.39E-4 | (2.61) |
| **3** | 1.39E-3 | (1.98) | **18** | 1.79E-3 | (1.74) | **33** | 1.63E-3 | (1.83) | **48** | 1.26E-3 | (2.08) | **63** | 5.89E-4 | (2.93) |
| **4** | 1.42E-3 | (1.87) | **19** | 1.87E-3 | (1.75) | **34** | 1.57E-3 | (1.92) | **49** | 1.08E-3 | (2.12) | **64** | 5.26E-4 | (3.36) |
| **5** | 1.68E-3 | (1.80) | **20** | 1.93E-3 | (1.73) | **35** | 1.44E-3 | (1.95) | **50** | 1.24E-3 | (2.10) | **65** | 9.13E-4 | (2.53) |
| **6** | 1.51E-3 | (1.91) | **21** | 1.87E-3 | (1.85) | **36** | 1.30E-3 | (2.23) | **51** | 1.19E-3 | (2.20) | **66** | 8.77E-4 | (2.56) |
| **7** | 1.69E-3 | (1.80) | **22** | 1.42E-3 | (1.86) | **37** | 1.23E-3 | (2.00) | **52** | 1.06E-3 | (2.32) | **67** | 8.71E-4 | (2.58) |
| **8** | 1.75E-3 | (1.81) | **23** | 1.67E-3 | (1.80) | **38** | 1.41E-3 | (1.96) | **53** | 9.14E-4 | (2.53) | **68** | 8.00E-4 | (2.68) |
| **9** | 1.80E-3 | (1.74) | **24** | 1.49E-3 | (1.81) | **39** | 1.26E-3 | (1.97) | **54** | 9.03E-4 | (2.76) | **69** | 7.37E-4 | (2.79) |
| **10** | 1.86E-3 | (1.86) | **25** | 1.75E-3 | (1.77) | **40** | 1.47E-3 | (1.93) | **55** | 5.77E-4 | (3.37) | **70** | 5.94E-4 | (2.90) |
| **11** | 1.48E-3 | (1.83) | **26** | 1.54E-3 | (1.79) | **41** | 1.46E-3 | (1.98) | **56** | 1.15E-3 | (2.24) | **71** | 5.57E-4 | (3.00) |
| **12** | 1.76E-3 | (1.76) | **27** | 1.71E-3 | (1.79) | **42** | 1.39E-3 | (1.99) | **57** | 1.10E-3 | (2.22) | **72** | 5.43E-4 | (3.04) |
| **13** | 1.58E-3 | (1.76) | **28** | 1.37E-3 | (2.00) | **43** | 1.11E-3 | (2.11) | **58** | 1.10E-3 | (2.29) | **73** | 5.23E-4 | (3.09) |
| **14** | 1.89E-3 | (1.70) | **29** | 1.53E-3 | (1.90) | **44** | 1.13E-3 | (2.21) | **59** | 1.06E-3 | (2.28) | **74** | 4.79E-4 | (3.24) |
| **15** | 1.69E-3 | (1.80) | **30** | 1.56E-3 | (1.91) | **45** | 1.01E-3 | (2.52) | **60** | 1.03E-3 | (2.37) | **75** | 4.51E-4 | (3.37) |
| Layer 24 | | | | | | | | | | | | | | |
| **1** | 7.91E-4 | (2.66) | **16** | 1.01E-3 | (2.33) | **31** | 9.57E-4 | (2.39) | **46** | 7.72E-4 | (2.69) | **61** | 5.51E-4 | (3.26) |
| **2** | 9.37E-4 | (2.44) | **17** | 1.04E-3 | (2.35) | **32** | 9.71E-4 | (2.44) | **47** | 6.51E-4 | (2.75) | **62** | 4.29E-4 | (3.43) |
| **3** | 8.23E-4 | (2.58) | **18** | 1.08E-3 | (2.26) | **33** | 9.63E-4 | (2.40) | **48** | 7.55E-4 | (2.70) | **63** | 3.36E-4 | (3.85) |
| **4** | 8.37E-4 | (2.43) | **19** | 1.12E-3 | (2.28) | **34** | 9.26E-4 | (2.51) | **49** | 6.45E-4 | (2.75) | **64** | 2.96E-4 | (4.43) |
| **5** | 1.00E-3 | (2.35) | **20** | 1.14E-3 | (2.26) | **35** | 8.47E-4 | (2.55) | **50** | 7.42E-4 | (2.73) | **65** | 5.45E-4 | (3.29) |
| **6** | 9.08E-4 | (2.47) | **21** | 1.10E-3 | (2.43) | **36** | 7.55E-4 | (2.92) | **51** | 6.97E-4 | (2.88) | **66** | 5.19E-4 | (3.34) |
| **7** | 1.02E-3 | (2.34) | **22** | 8.43E-4 | (2.44) | **37** | 7.28E-4 | (2.61) | **52** | 6.21E-4 | (3.05) | **67** | 5.01E-4 | (3.39) |
| **8** | 1.05E-3 | (2.36) | **23** | 1.01E-3 | (2.34) | **38** | 8.41E-4 | (2.56) | **53** | 5.27E-4 | (3.33) | **68** | 4.60E-4 | (3.53) |
| **9** | 1.08E-3 | (2.25) | **24** | 8.82E-4 | (2.35) | **39** | 7.45E-4 | (2.57) | **54** | 5.27E-4 | (3.61) | **69** | 4.25E-4 | (3.68) |
| **10** | 1.10E-3 | (2.41) | **25** | 1.04E-3 | (2.30) | **40** | 8.81E-4 | (2.50) | **55** | 3.39E-4 | (4.38) | **70** | 3.46E-4 | (3.79) |

| | | | | | | | | | | | | |
|---|---|---|---|---|---|---|---|---|---|---|---|---|
| **11** | 8.80E-4 | (2.36) | **26** | 8.99E-4 | (2.33) | **41** | 8.73E-4 | (2.57) | **56** | 6.88E-4 | (2.91) | **71** | 3.18E-4 | (3.98) |
| **12** | 1.04E-3 | (2.30) | **27** | 1.01E-3 | (2.34) | **42** | 8.28E-4 | (2.58) | **57** | 6.61E-4 | (2.89) | **72** | 3.15E-4 | (3.98) |
| **13** | 9.32E-4 | (2.29) | **28** | 8.00E-4 | (2.62) | **43** | 6.52E-4 | (2.74) | **58** | 6.52E-4 | (2.97) | **73** | 3.03E-4 | (4.07) |
| **14** | 1.14E-3 | (2.21) | **29** | 9.23E-4 | (2.46) | **44** | 6.74E-4 | (2.88) | **59** | 6.38E-4 | (2.94) | **74** | 2.71E-4 | (4.30) |
| **15** | 1.00E-3 | (2.34) | **30** | 9.45E-4 | (2.47) | **45** | 5.86E-4 | (3.33) | **60** | 6.01E-4 | (3.09) | **75** | 2.65E-4 | (4.42) |
| Layer 25 | | | | | | | | | | | | | | |
| **1** | 1.81E-4 | (3.83) | **16** | 2.06E-4 | (3.09) | **31** | 1.91E-4 | (3.18) | **46** | 1.51E-4 | (3.60) | **61** | 1.05E-4 | (4.64) |
| **2** | 1.92E-4 | (3.20) | **17** | 2.17E-4 | (3.24) | **32** | 2.02E-4 | (3.37) | **47** | 1.50E-4 | (3.88) | **62** | 8.84E-5 | (5.05) |
| **3** | 1.95E-4 | (3.64) | **18** | 2.17E-4 | (2.98) | **33** | 1.90E-4 | (3.20) | **48** | 1.51E-4 | (3.57) | **63** | 7.02E-5 | (5.67) |
| **4** | 1.96E-4 | (3.41) | **19** | 2.29E-4 | (3.15) | **34** | 1.94E-4 | (3.45) | **49** | 1.53E-4 | (3.88) | **64** | 6.07E-5 | (6.63) |
| **5** | 2.00E-4 | (3.09) | **20** | 2.21E-4 | (3.23) | **35** | 1.71E-4 | (3.36) | **50** | 1.47E-4 | (3.62) | **65** | 1.02E-4 | (4.77) |
| **6** | 2.13E-4 | (3.48) | **21** | 2.13E-4 | (3.49) | **36** | 1.58E-4 | (4.08) | **51** | 1.37E-4 | (4.10) | **66** | 1.02E-4 | (4.73) |
| **7** | 2.03E-4 | (3.09) | **22** | 1.95E-4 | (3.43) | **37** | 1.67E-4 | (3.71) | **52** | 1.17E-4 | (4.41) | **67** | 9.79E-5 | (4.86) |
| **8** | 2.18E-4 | (3.24) | **23** | 2.00E-4 | (3.10) | **38** | 1.68E-4 | (3.39) | **53** | 1.05E-4 | (4.72) | **68** | 9.14E-5 | (5.01) |
| **9** | 2.15E-4 | (3.00) | **24** | 2.05E-4 | (3.32) | **39** | 1.72E-4 | (3.63) | **54** | 9.78E-5 | (5.28) | **69** | 8.02E-5 | (5.31) |
| **10** | 2.40E-4 | (3.30) | **25** | 2.06E-4 | (3.05) | **40** | 1.76E-4 | (3.30) | **55** | 6.65E-5 | (6.74) | **70** | 7.24E-5 | (5.61) |
| **11** | 2.04E-4 | (3.38) | **26** | 2.05E-4 | (3.31) | **41** | 1.77E-4 | (3.61) | **56** | 1.37E-4 | (4.14) | **71** | 6.81E-5 | (5.86) |
| **12** | 2.10E-4 | (3.02) | **27** | 2.00E-4 | (3.11) | **42** | 1.65E-4 | (3.44) | **57** | 1.30E-4 | (3.83) | **72** | 6.57E-5 | (5.87) |
| **13** | 2.17E-4 | (3.24) | **28** | 1.92E-4 | (3.69) | **43** | 1.50E-4 | (3.90) | **58** | 1.35E-4 | (4.12) | **73** | 6.31E-5 | (5.93) |
| **14** | 2.27E-4 | (2.92) | **29** | 1.83E-4 | (3.25) | **44** | 1.34E-4 | (3.80) | **59** | 1.22E-4 | (3.97) | **74** | 5.69E-5 | (6.32) |
| **15** | 2.19E-4 | (3.43) | **30** | 1.94E-4 | (3.42) | **45** | 1.27E-4 | (4.87) | **60** | 1.20E-4 | (4.38) | **75** | 5.29E-5 | (6.65) |

Table A.3: 3D Node Averaged Fission Density (ARI) and MCNP % Uncertainty

| Layer 1 | | | | | | | | | | | | |
|---|---|---|---|---|---|---|---|---|---|---|---|---|
| **1** | 9.65E-3 | (0.64) | **16** | 1.49E-2 | (0.45) | **31** | 1.68E-2 | (0.42) | **46** | 1.40E-2 | (0.47) | **61** | 1.26E-2 | (0.52) |
| **2** | 1.06E-2 | (0.54) | **17** | 1.66E-2 | (0.46) | **32** | 1.90E-2 | (0.43) | **47** | 1.38E-2 | (0.50) | **62** | 8.84E-3 | (0.62) |
| **3** | 1.11E-2 | (0.59) | **18** | 1.81E-2 | (0.41) | **33** | 1.98E-2 | (0.39) | **48** | 1.46E-2 | (0.46) | **63** | 6.51E-3 | (0.72) |
| **4** | 1.19E-2 | (0.54) | **19** | 2.11E-2 | (0.41) | **34** | 2.04E-2 | (0.41) | **49** | 1.52E-2 | (0.47) | **64** | 4.37E-3 | (0.88) |
| **5** | 1.30E-2 | (0.48) | **20** | 2.35E-2 | (0.39) | **35** | 1.81E-2 | (0.41) | **50** | 1.67E-2 | (0.43) | **65** | 1.27E-2 | (0.52) |
| **6** | 1.45E-2 | (0.52) | **21** | 2.41E-2 | (0.40) | **36** | 1.74E-2 | (0.47) | **51** | 1.68E-2 | (0.45) | **66** | 1.25E-2 | (0.53) |
| **7** | 1.34E-2 | (0.48) | **22** | 1.45E-2 | (0.49) | **37** | 1.35E-2 | (0.50) | **52** | 1.42E-2 | (0.49) | **67** | 1.22E-2 | (0.53) |
| **8** | 1.49E-2 | (0.48) | **23** | 1.58E-2 | (0.44) | **38** | 1.43E-2 | (0.46) | **53** | 1.22E-2 | (0.53) | **68** | 1.19E-2 | (0.54) |
| **9** | 1.62E-2 | (0.43) | **24** | 1.73E-2 | (0.45) | **39** | 1.51E-2 | (0.48) | **54** | 8.98E-3 | (0.62) | **69** | 1.06E-2 | (0.57) |
| **10** | 1.86E-2 | (0.46) | **25** | 1.92E-2 | (0.40) | **40** | 1.65E-2 | (0.43) | **55** | 6.94E-3 | (0.75) | **70** | 9.35E-3 | (0.61) |
| **11** | 1.42E-2 | (0.49) | **26** | 2.06E-2 | (0.41) | **41** | 1.89E-2 | (0.43) | **56** | 1.49E-2 | (0.49) | **71** | 6.30E-3 | (0.74) |
| **12** | 1.55E-2 | (0.44) | **27** | 2.11E-2 | (0.38) | **42** | 1.81E-2 | (0.41) | **57** | 1.42E-2 | (0.46) | **72** | 6.19E-3 | (0.74) |
| **13** | 1.73E-2 | (0.44) | **28** | 1.91E-2 | (0.45) | **43** | 1.58E-2 | (0.46) | **58** | 1.47E-2 | (0.49) | **73** | 5.98E-3 | (0.75) |
| **14** | 1.98E-2 | (0.39) | **29** | 1.45E-2 | (0.46) | **44** | 1.44E-2 | (0.46) | **59** | 1.42E-2 | (0.46) | **74** | 5.60E-3 | (0.78) |
| **15** | 2.21E-2 | (0.42) | **30** | 1.59E-2 | (0.47) | **45** | 1.13E-2 | (0.58) | **60** | 1.43E-2 | (0.49) | **75** | 4.73E-3 | (0.85) |
| Layer 2 | | | | | | | | | | | | |
| **1** | 5.00E-2 | (0.41) | **16** | 8.33E-2 | (0.32) | **31** | 9.46E-2 | (0.30) | **46** | 7.84E-2 | (0.33) | **61** | 7.89E-2 | (0.34) |
| **2** | 5.89E-2 | (0.38) | **17** | 9.67E-2 | (0.30) | **32** | 1.11E-1 | (0.28) | **47** | 7.11E-2 | (0.33) | **62** | 4.86E-2 | (0.39) |
| **3** | 5.66E-2 | (0.38) | **18** | 1.02E-1 | (0.29) | **33** | 1.12E-1 | (0.28) | **48** | 8.20E-2 | (0.33) | **63** | 3.58E-2 | (0.46) |
| **4** | 6.14E-2 | (0.35) | **19** | 1.24E-1 | (0.27) | **34** | 1.20E-1 | (0.27) | **49** | 7.82E-2 | (0.31) | **64** | 2.39E-2 | (0.56) |
| **5** | 7.28E-2 | (0.35) | **20** | 1.46E-1 | (0.25) | **35** | 1.02E-1 | (0.29) | **50** | 9.45E-2 | (0.30) | **65** | 7.94E-2 | (0.34) |
| **6** | 7.46E-2 | (0.34) | **21** | 1.49E-1 | (0.26) | **36** | 1.02E-1 | (0.31) | **51** | 1.00E-1 | (0.30) | **66** | 7.65E-2 | (0.34) |
| **7** | 7.51E-2 | (0.34) | **22** | 7.46E-2 | (0.32) | **37** | 6.97E-2 | (0.33) | **52** | 8.81E-2 | (0.32) | **67** | 7.60E-2 | (0.34) |
| **8** | 8.68E-2 | (0.32) | **23** | 8.89E-2 | (0.31) | **38** | 8.01E-2 | (0.33) | **53** | 7.50E-2 | (0.35) | **68** | 7.27E-2 | (0.35) |
| **9** | 9.11E-2 | (0.31) | **24** | 8.90E-2 | (0.29) | **39** | 7.74E-2 | (0.31) | **54** | 5.64E-2 | (0.40) | **69** | 6.64E-2 | (0.37) |
| **10** | 1.08E-1 | (0.30) | **25** | 1.09E-1 | (0.28) | **40** | 9.34E-2 | (0.31) | **55** | 3.84E-2 | (0.47) | **70** | 5.16E-2 | (0.39) |
| **11** | 7.29E-2 | (0.32) | **26** | 1.08E-1 | (0.26) | **41** | 1.11E-1 | (0.28) | **56** | 9.02E-2 | (0.32) | **71** | 3.44E-2 | (0.47) |
| **12** | 8.73E-2 | (0.32) | **27** | 1.20E-1 | (0.27) | **42** | 1.03E-1 | (0.29) | **57** | 8.12E-2 | (0.33) | **72** | 3.39E-2 | (0.47) |
| **13** | 8.92E-2 | (0.29) | **28** | 9.86E-2 | (0.29) | **43** | 8.39E-2 | (0.30) | **58** | 8.81E-2 | (0.32) | **73** | 3.26E-2 | (0.48) |
| **14** | 1.12E-1 | (0.28) | **29** | 8.09E-2 | (0.33) | **44** | 8.23E-2 | (0.32) | **59** | 8.13E-2 | (0.33) | **74** | 3.06E-2 | (0.49) |
| **15** | 1.20E-1 | (0.26) | **30** | 9.30E-2 | (0.31) | **45** | 6.13E-2 | (0.37) | **60** | 8.78E-2 | (0.32) | **75** | 2.57E-2 | (0.54) |
| Layer 3 | | | | | | | | | | | | |
| **1** | 7.94E-2 | (0.33) | **16** | 1.30E-1 | (0.26) | **31** | 1.48E-1 | (0.24) | **46** | 1.22E-1 | (0.27) | **61** | 1.26E-1 | (0.27) |
| **2** | 9.22E-2 | (0.31) | **17** | 1.52E-1 | (0.24) | **32** | 1.75E-1 | (0.23) | **47** | 1.12E-1 | (0.26) | **62** | 7.82E-2 | (0.31) |
| **3** | 8.96E-2 | (0.31) | **18** | 1.59E-1 | (0.23) | **33** | 1.75E-1 | (0.22) | **48** | 1.28E-1 | (0.26) | **63** | 5.78E-2 | (0.36) |
| **4** | 9.69E-2 | (0.28) | **19** | 1.96E-1 | (0.21) | **34** | 1.89E-1 | (0.22) | **49** | 1.24E-1 | (0.25) | **64** | 3.88E-2 | (0.44) |
| **5** | 1.14E-1 | (0.28) | **20** | 2.33E-1 | (0.20) | **35** | 1.61E-1 | (0.23) | **50** | 1.48E-1 | (0.24) | **65** | 1.27E-1 | (0.27) |
| **6** | 1.18E-1 | (0.27) | **21** | 2.36E-1 | (0.21) | **36** | 1.62E-1 | (0.25) | **51** | 1.59E-1 | (0.24) | **66** | 1.22E-1 | (0.27) |
| **7** | 1.17E-1 | (0.27) | **22** | 1.18E-1 | (0.25) | **37** | 1.10E-1 | (0.26) | **52** | 1.41E-1 | (0.25) | **67** | 1.21E-1 | (0.27) |
| **8** | 1.37E-1 | (0.26) | **23** | 1.39E-1 | (0.25) | **38** | 1.25E-1 | (0.26) | **53** | 1.21E-1 | (0.27) | **68** | 1.16E-1 | (0.28) |
| **9** | 1.42E-1 | (0.25) | **24** | 1.41E-1 | (0.23) | **39** | 1.22E-1 | (0.25) | **54** | 9.15E-2 | (0.31) | **69** | 1.06E-1 | (0.29) |
| **10** | 1.70E-1 | (0.24) | **25** | 1.70E-1 | (0.23) | **40** | 1.46E-1 | (0.25) | **55** | 6.27E-2 | (0.37) | **70** | 8.25E-2 | (0.30) |
| **11** | 1.15E-1 | (0.26) | **26** | 1.70E-1 | (0.21) | **41** | 1.75E-1 | (0.23) | **56** | 1.43E-1 | (0.25) | **71** | 5.49E-2 | (0.37) |
| **12** | 1.37E-1 | (0.25) | **27** | 1.87E-1 | (0.22) | **42** | 1.61E-1 | (0.23) | **57** | 1.28E-1 | (0.26) | **72** | 5.38E-2 | (0.37) |
| **13** | 1.41E-1 | (0.23) | **28** | 1.56E-1 | (0.23) | **43** | 1.34E-1 | (0.24) | **58** | 1.40E-1 | (0.25) | **73** | 5.19E-2 | (0.38) |

| | | | | | | | | | | | | | | | |
|---|---|---|---|---|---|---|---|---|---|---|---|---|---|---|---|
| **14** | 1.75E-1 | (0.22) | **29** | 1.27E-1 | (0.26) | **44** | 1.31E-1 | (0.26) | **59** | 1.28E-1 | (0.26) | **74** | 4.88E-2 | (0.39) |
| **15** | 1.91E-1 | (0.21) | **30** | 1.47E-1 | (0.25) | **45** | 9.89E-2 | (0.29) | **60** | 1.40E-1 | (0.25) | **75** | 4.09E-2 | (0.43) |
| Layer 4 | | | | | | | | | | | | | | | |
| **1** | 9.69E-2 | (0.30) | **16** | 1.58E-1 | (0.24) | **31** | 1.79E-1 | (0.22) | **46** | 1.47E-1 | (0.24) | **61** | 1.52E-1 | (0.24) |
| **2** | 1.12E-1 | (0.28) | **17** | 1.84E-1 | (0.22) | **32** | 2.11E-1 | (0.21) | **47** | 1.35E-1 | (0.24) | **62** | 9.50E-2 | (0.28) |
| **3** | 1.09E-1 | (0.28) | **18** | 1.91E-1 | (0.21) | **33** | 2.10E-1 | (0.20) | **48** | 1.54E-1 | (0.24) | **63** | 7.10E-2 | (0.32) |
| **4** | 1.18E-1 | (0.25) | **19** | 2.35E-1 | (0.20) | **34** | 2.27E-1 | (0.20) | **49** | 1.48E-1 | (0.23) | **64** | 4.84E-2 | (0.39) |
| **5** | 1.38E-1 | (0.25) | **20** | 2.79E-1 | (0.18) | **35** | 1.94E-1 | (0.21) | **50** | 1.78E-1 | (0.22) | **65** | 1.51E-1 | (0.24) |
| **6** | 1.42E-1 | (0.24) | **21** | 2.83E-1 | (0.19) | **36** | 1.97E-1 | (0.23) | **51** | 1.92E-1 | (0.22) | **66** | 1.45E-1 | (0.25) |
| **7** | 1.42E-1 | (0.25) | **22** | 1.42E-1 | (0.23) | **37** | 1.32E-1 | (0.24) | **52** | 1.72E-1 | (0.23) | **67** | 1.45E-1 | (0.25) |
| **8** | 1.66E-1 | (0.23) | **23** | 1.68E-1 | (0.23) | **38** | 1.51E-1 | (0.24) | **53** | 1.48E-1 | (0.25) | **68** | 1.38E-1 | (0.26) |
| **9** | 1.72E-1 | (0.23) | **24** | 1.69E-1 | (0.21) | **39** | 1.47E-1 | (0.23) | **54** | 1.14E-1 | (0.28) | **69** | 1.28E-1 | (0.26) |
| **10** | 2.05E-1 | (0.22) | **25** | 2.04E-1 | (0.21) | **40** | 1.76E-1 | (0.22) | **55** | 7.82E-2 | (0.33) | **70** | 9.93E-2 | (0.28) |
| **11** | 1.39E-1 | (0.23) | **26** | 2.04E-1 | (0.19) | **41** | 2.10E-1 | (0.21) | **56** | 1.71E-1 | (0.23) | **71** | 6.58E-2 | (0.34) |
| **12** | 1.65E-1 | (0.23) | **27** | 2.25E-1 | (0.20) | **42** | 1.94E-1 | (0.21) | **57** | 1.53E-1 | (0.24) | **72** | 6.47E-2 | (0.34) |
| **13** | 1.69E-1 | (0.21) | **28** | 1.88E-1 | (0.21) | **43** | 1.63E-1 | (0.22) | **58** | 1.67E-1 | (0.23) | **73** | 6.23E-2 | (0.35) |
| **14** | 2.10E-1 | (0.20) | **29** | 1.53E-1 | (0.24) | **44** | 1.60E-1 | (0.23) | **59** | 1.53E-1 | (0.24) | **74** | 5.85E-2 | (0.36) |
| **15** | 2.29E-1 | (0.19) | **30** | 1.77E-1 | (0.23) | **45** | 1.23E-1 | (0.26) | **60** | 1.68E-1 | (0.23) | **75** | 4.94E-2 | (0.39) |
| Layer 5 | | | | | | | | | | | | | | | |
| **1** | 9.74E-2 | (0.29) | **16** | 1.57E-1 | (0.24) | **31** | 1.76E-1 | (0.22) | **46** | 1.45E-1 | (0.25) | **61** | 1.47E-1 | (0.25) |
| **2** | 1.13E-1 | (0.28) | **17** | 1.82E-1 | (0.22) | **32** | 2.06E-1 | (0.21) | **47** | 1.32E-1 | (0.24) | **62** | 9.53E-2 | (0.28) |
| **3** | 1.09E-1 | (0.28) | **18** | 1.89E-1 | (0.21) | **33** | 2.06E-1 | (0.20) | **48** | 1.51E-1 | (0.24) | **63** | 7.29E-2 | (0.32) |
| **4** | 1.18E-1 | (0.25) | **19** | 2.29E-1 | (0.20) | **34** | 2.22E-1 | (0.20) | **49** | 1.45E-1 | (0.23) | **64** | 5.17E-2 | (0.38) |
| **5** | 1.38E-1 | (0.25) | **20** | 2.68E-1 | (0.18) | **35** | 1.93E-1 | (0.21) | **50** | 1.74E-1 | (0.22) | **65** | 1.44E-1 | (0.25) |
| **6** | 1.41E-1 | (0.24) | **21** | 2.72E-1 | (0.19) | **36** | 1.96E-1 | (0.22) | **51** | 1.87E-1 | (0.22) | **66** | 1.39E-1 | (0.25) |
| **7** | 1.42E-1 | (0.25) | **22** | 1.41E-1 | (0.23) | **37** | 1.31E-1 | (0.24) | **52** | 1.71E-1 | (0.23) | **67** | 1.39E-1 | (0.25) |
| **8** | 1.65E-1 | (0.23) | **23** | 1.66E-1 | (0.23) | **38** | 1.49E-1 | (0.24) | **53** | 1.53E-1 | (0.24) | **68** | 1.33E-1 | (0.26) |
| **9** | 1.70E-1 | (0.23) | **24** | 1.66E-1 | (0.21) | **39** | 1.45E-1 | (0.23) | **54** | 1.21E-1 | (0.27) | **69** | 1.23E-1 | (0.27) |
| **10** | 2.01E-1 | (0.22) | **25** | 2.01E-1 | (0.21) | **40** | 1.73E-1 | (0.22) | **55** | 8.42E-2 | (0.32) | **70** | 9.73E-2 | (0.28) |
| **11** | 1.39E-1 | (0.23) | **26** | 1.99E-1 | (0.19) | **41** | 2.05E-1 | (0.21) | **56** | 1.65E-1 | (0.23) | **71** | 6.43E-2 | (0.34) |
| **12** | 1.64E-1 | (0.23) | **27** | 2.20E-1 | (0.20) | **42** | 1.91E-1 | (0.21) | **57** | 1.48E-1 | (0.24) | **72** | 6.33E-2 | (0.34) |
| **13** | 1.67E-1 | (0.21) | **28** | 1.85E-1 | (0.21) | **43** | 1.62E-1 | (0.22) | **58** | 1.61E-1 | (0.24) | **73** | 6.12E-2 | (0.35) |
| **14** | 2.06E-1 | (0.21) | **29** | 1.52E-1 | (0.24) | **44** | 1.65E-1 | (0.23) | **59** | 1.48E-1 | (0.24) | **74** | 5.76E-2 | (0.36) |
| **15** | 2.21E-1 | (0.19) | **30** | 1.74E-1 | (0.23) | **45** | 1.30E-1 | (0.26) | **60** | 1.62E-1 | (0.24) | **75** | 4.96E-2 | (0.39) |
| Layer 6 | | | | | | | | | | | | | | | |
| **1** | 6.97E-2 | (0.32) | **16** | 1.10E-1 | (0.25) | **31** | 1.22E-1 | (0.24) | **46** | 1.01E-1 | (0.27) | **61** | 9.84E-2 | (0.28) |
| **2** | 8.19E-2 | (0.29) | **17** | 1.24E-1 | (0.25) | **32** | 1.39E-1 | (0.23) | **47** | 9.08E-2 | (0.26) | **62** | 7.04E-2 | (0.30) |
| **3** | 7.77E-2 | (0.30) | **18** | 1.31E-1 | (0.23) | **33** | 1.42E-1 | (0.22) | **48** | 1.05E-1 | (0.26) | **63** | 5.60E-2 | (0.34) |
| **4** | 8.27E-2 | (0.28) | **19** | 1.53E-1 | (0.22) | **34** | 1.50E-1 | (0.22) | **49** | 9.93E-2 | (0.25) | **64** | 4.98E-2 | (0.39) |
| **5** | 9.79E-2 | (0.27) | **20** | 1.77E-1 | (0.21) | **35** | 1.35E-1 | (0.23) | **50** | 1.19E-1 | (0.24) | **65** | 9.35E-2 | (0.28) |
| **6** | 9.79E-2 | (0.27) | **21** | 1.79E-1 | (0.22) | **36** | 1.37E-1 | (0.25) | **51** | 1.25E-1 | (0.24) | **66** | 9.07E-2 | (0.29) |
| **7** | 1.00E-1 | (0.27) | **22** | 9.83E-2 | (0.25) | **37** | 9.10E-2 | (0.26) | **52** | 1.21E-1 | (0.25) | **67** | 9.04E-2 | (0.29) |
| **8** | 1.13E-1 | (0.26) | **23** | 1.16E-1 | (0.25) | **38** | 1.05E-1 | (0.26) | **53** | 1.37E-1 | (0.25) | **68** | 8.70E-2 | (0.29) |
| **9** | 1.19E-1 | (0.24) | **24** | 1.14E-1 | (0.23) | **39** | 1.00E-1 | (0.25) | **54** | 1.16E-1 | (0.28) | **69** | 8.19E-2 | (0.30) |
| **10** | 1.36E-1 | (0.25) | **25** | 1.39E-1 | (0.23) | **40** | 1.20E-1 | (0.24) | **55** | 8.19E-2 | (0.32) | **70** | 6.99E-2 | (0.31) |
| **11** | 9.65E-2 | (0.26) | **26** | 1.35E-1 | (0.22) | **41** | 1.38E-1 | (0.23) | **56** | 1.08E-1 | (0.26) | **71** | 4.61E-2 | (0.37) |
| **12** | 1.15E-1 | (0.25) | **27** | 1.51E-1 | (0.22) | **42** | 1.31E-1 | (0.23) | **57** | 9.98E-2 | (0.27) | **72** | 4.54E-2 | (0.37) |
| **13** | 1.15E-1 | (0.23) | **28** | 1.27E-1 | (0.24) | **43** | 1.16E-1 | (0.23) | **58** | 1.06E-1 | (0.26) | **73** | 4.40E-2 | (0.38) |

| | | | | | | | | | | | | | | | |
|---|---|---|---|---|---|---|---|---|---|---|---|---|---|---|---|
| **14** | 1.42E-1 | (0.22) | **29** | 1.07E-1 | (0.26) | **44** | 1.48E-1 | (0.24) | **59** | 1.00E-1 | (0.27) | **74** | 4.17E-2 | (0.39) |
| **15** | 1.47E-1 | (0.22) | **30** | 1.19E-1 | (0.25) | **45** | 1.23E-1 | (0.26) | **60** | 1.07E-1 | (0.26) | **75** | 4.42E-2 | (0.41) |
| Layer 7 | | | | | | | | | | | | | | | |
| **1** | 5.92E-2 | (0.34) | **16** | 9.20E-2 | (0.28) | **31** | 1.01E-1 | (0.26) | **46** | 8.27E-2 | (0.29) | **61** | 7.96E-2 | (0.30) |
| **2** | 6.97E-2 | (0.32) | **17** | 1.03E-1 | (0.27) | **32** | 1.13E-1 | (0.26) | **47** | 7.45E-2 | (0.29) | **62** | 5.92E-2 | (0.33) |
| **3** | 6.55E-2 | (0.33) | **18** | 1.07E-1 | (0.25) | **33** | 1.16E-1 | (0.25) | **48** | 8.65E-2 | (0.28) | **63** | 4.82E-2 | (0.36) |
| **4** | 6.93E-2 | (0.30) | **19** | 1.24E-1 | (0.24) | **34** | 1.22E-1 | (0.25) | **49** | 8.09E-2 | (0.28) | **64** | 4.49E-2 | (0.41) |
| **5** | 8.20E-2 | (0.29) | **20** | 1.41E-1 | (0.23) | **35** | 1.12E-1 | (0.25) | **50** | 9.67E-2 | (0.27) | **65** | 7.40E-2 | (0.32) |
| **6** | 8.11E-2 | (0.29) | **21** | 1.43E-1 | (0.24) | **36** | 1.15E-1 | (0.27) | **51** | 1.02E-1 | (0.27) | **66** | 7.21E-2 | (0.32) |
| **7** | 8.42E-2 | (0.29) | **22** | 8.16E-2 | (0.28) | **37** | 7.53E-2 | (0.29) | **52** | 1.00E-1 | (0.27) | **67** | 7.18E-2 | (0.32) |
| **8** | 9.36E-2 | (0.28) | **23** | 9.67E-2 | (0.27) | **38** | 8.70E-2 | (0.28) | **53** | 1.19E-1 | (0.27) | **68** | 6.94E-2 | (0.33) |
| **9** | 9.86E-2 | (0.27) | **24** | 9.37E-2 | (0.26) | **39** | 8.23E-2 | (0.28) | **54** | 1.04E-1 | (0.29) | **69** | 6.57E-2 | (0.34) |
| **10** | 1.12E-1 | (0.27) | **25** | 1.14E-1 | (0.25) | **40** | 9.87E-2 | (0.26) | **55** | 7.42E-2 | (0.34) | **70** | 5.72E-2 | (0.34) |
| **11** | 8.01E-2 | (0.28) | **26** | 1.09E-1 | (0.24) | **41** | 1.12E-1 | (0.26) | **56** | 8.62E-2 | (0.29) | **71** | 3.76E-2 | (0.41) |
| **12** | 9.55E-2 | (0.27) | **27** | 1.24E-1 | (0.24) | **42** | 1.08E-1 | (0.26) | **57** | 8.06E-2 | (0.29) | **72** | 3.72E-2 | (0.41) |
| **13** | 9.39E-2 | (0.26) | **28** | 1.04E-1 | (0.26) | **43** | 9.65E-2 | (0.26) | **58** | 8.52E-2 | (0.29) | **73** | 3.60E-2 | (0.42) |
| **14** | 1.16E-1 | (0.25) | **29** | 8.91E-2 | (0.28) | **44** | 1.28E-1 | (0.26) | **59** | 8.11E-2 | (0.29) | **74** | 3.43E-2 | (0.43) |
| **15** | 1.18E-1 | (0.24) | **30** | 9.83E-2 | (0.27) | **45** | 1.09E-1 | (0.28) | **60** | 8.57E-2 | (0.29) | **75** | 3.74E-2 | (0.45) |
| Layer 8 | | | | | | | | | | | | | | | |
| **1** | 5.01E-2 | (0.38) | **16** | 7.62E-2 | (0.30) | **31** | 8.31E-2 | (0.29) | **46** | 6.79E-2 | (0.32) | **61** | 6.54E-2 | (0.34) |
| **2** | 5.87E-2 | (0.35) | **17** | 8.46E-2 | (0.30) | **32** | 9.31E-2 | (0.28) | **47** | 6.11E-2 | (0.32) | **62** | 4.93E-2 | (0.36) |
| **3** | 5.48E-2 | (0.35) | **18** | 8.83E-2 | (0.28) | **33** | 9.48E-2 | (0.27) | **48** | 7.09E-2 | (0.31) | **63** | 4.06E-2 | (0.40) |
| **4** | 5.80E-2 | (0.33) | **19** | 1.02E-1 | (0.27) | **34** | 1.00E-1 | (0.27) | **49** | 6.63E-2 | (0.31) | **64** | 3.83E-2 | (0.44) |
| **5** | 6.84E-2 | (0.32) | **20** | 1.15E-1 | (0.25) | **35** | 9.28E-2 | (0.27) | **50** | 7.92E-2 | (0.30) | **65** | 5.99E-2 | (0.35) |
| **6** | 6.73E-2 | (0.32) | **21** | 1.16E-1 | (0.27) | **36** | 9.55E-2 | (0.29) | **51** | 8.37E-2 | (0.30) | **66** | 5.85E-2 | (0.36) |
| **7** | 7.02E-2 | (0.32) | **22** | 6.76E-2 | (0.31) | **37** | 6.23E-2 | (0.32) | **52** | 8.35E-2 | (0.30) | **67** | 5.83E-2 | (0.36) |
| **8** | 7.78E-2 | (0.31) | **23** | 7.99E-2 | (0.29) | **38** | 7.18E-2 | (0.31) | **53** | 1.00E-1 | (0.30) | **68** | 5.64E-2 | (0.36) |
| **9** | 8.14E-2 | (0.29) | **24** | 7.70E-2 | (0.29) | **39** | 6.77E-2 | (0.30) | **54** | 8.85E-2 | (0.32) | **69** | 5.36E-2 | (0.37) |
| **10** | 9.21E-2 | (0.30) | **25** | 9.29E-2 | (0.27) | **40** | 8.12E-2 | (0.29) | **55** | 6.35E-2 | (0.37) | **70** | 4.70E-2 | (0.37) |
| **11** | 6.65E-2 | (0.31) | **26** | 8.93E-2 | (0.27) | **41** | 9.16E-2 | (0.28) | **56** | 7.00E-2 | (0.33) | **71** | 3.06E-2 | (0.45) |
| **12** | 7.90E-2 | (0.30) | **27** | 1.01E-1 | (0.26) | **42** | 8.88E-2 | (0.28) | **57** | 6.56E-2 | (0.33) | **72** | 3.03E-2 | (0.45) |
| **13** | 7.72E-2 | (0.28) | **28** | 8.59E-2 | (0.29) | **43** | 8.01E-2 | (0.28) | **58** | 6.94E-2 | (0.33) | **73** | 2.93E-2 | (0.46) |
| **14** | 9.48E-2 | (0.27) | **29** | 7.39E-2 | (0.31) | **44** | 1.07E-1 | (0.28) | **59** | 6.61E-2 | (0.33) | **74** | 2.80E-2 | (0.47) |
| **15** | 9.62E-2 | (0.27) | **30** | 8.14E-2 | (0.30) | **45** | 9.26E-2 | (0.30) | **60** | 7.00E-2 | (0.32) | **75** | 3.07E-2 | (0.49) |
| Layer 9 | | | | | | | | | | | | | | | |
| **1** | 4.07E-2 | (0.42) | **16** | 6.11E-2 | (0.34) | **31** | 6.62E-2 | (0.32) | **46** | 5.44E-2 | (0.36) | **61** | 5.24E-2 | (0.38) |
| **2** | 4.77E-2 | (0.38) | **17** | 6.78E-2 | (0.33) | **32** | 7.41E-2 | (0.32) | **47** | 4.89E-2 | (0.36) | **62** | 3.97E-2 | (0.40) |
| **3** | 4.46E-2 | (0.39) | **18** | 7.05E-2 | (0.31) | **33** | 7.53E-2 | (0.30) | **48** | 5.67E-2 | (0.35) | **63** | 3.28E-2 | (0.44) |
| **4** | 4.69E-2 | (0.36) | **19** | 8.07E-2 | (0.30) | **34** | 7.98E-2 | (0.30) | **49** | 5.30E-2 | (0.34) | **64** | 3.11E-2 | (0.49) |
| **5** | 5.52E-2 | (0.35) | **20** | 9.09E-2 | (0.28) | **35** | 7.43E-2 | (0.31) | **50** | 6.33E-2 | (0.33) | **65** | 4.78E-2 | (0.39) |
| **6** | 5.39E-2 | (0.36) | **21** | 9.19E-2 | (0.30) | **36** | 7.67E-2 | (0.33) | **51** | 6.69E-2 | (0.33) | **66** | 4.67E-2 | (0.40) |
| **7** | 5.65E-2 | (0.35) | **22** | 5.41E-2 | (0.34) | **37** | 5.00E-2 | (0.35) | **52** | 6.71E-2 | (0.33) | **67** | 4.65E-2 | (0.40) |
| **8** | 6.26E-2 | (0.34) | **23** | 6.39E-2 | (0.33) | **38** | 5.75E-2 | (0.35) | **53** | 8.07E-2 | (0.33) | **68** | 4.51E-2 | (0.40) |
| **9** | 6.52E-2 | (0.33) | **24** | 6.14E-2 | (0.32) | **39** | 5.42E-2 | (0.34) | **54** | 7.17E-2 | (0.35) | **69** | 4.30E-2 | (0.42) |
| **10** | 7.36E-2 | (0.33) | **25** | 7.40E-2 | (0.31) | **40** | 6.47E-2 | (0.33) | **55** | 5.15E-2 | (0.41) | **70** | 3.77E-2 | (0.41) |
| **11** | 5.34E-2 | (0.34) | **26** | 7.07E-2 | (0.30) | **41** | 7.31E-2 | (0.32) | **56** | 5.59E-2 | (0.36) | **71** | 2.46E-2 | (0.51) |
| **12** | 6.33E-2 | (0.33) | **27** | 8.00E-2 | (0.30) | **42** | 7.10E-2 | (0.31) | **57** | 5.24E-2 | (0.37) | **72** | 2.43E-2 | (0.51) |
| **13** | 6.16E-2 | (0.32) | **28** | 6.85E-2 | (0.32) | **43** | 6.44E-2 | (0.31) | **58** | 5.54E-2 | (0.36) | **73** | 2.36E-2 | (0.52) |

| | | | | | | | | | | | | | | | | |
|---|---|---|---|---|---|---|---|---|---|---|---|---|---|---|---|---|
| **14** | 7.54E-2 | (0.30) | **29** | 5.92E-2 | (0.34) | **44** | 8.60E-2 | (0.32) | **59** | 5.28E-2 | (0.36) | **74** | 2.26E-2 | (0.53) |
| **15** | 7.61E-2 | (0.30) | **30** | 6.51E-2 | (0.34) | **45** | 7.50E-2 | (0.33) | **60** | 5.60E-2 | (0.36) | **75** | 2.47E-2 | (0.55) |
| Layer 10 | | | | | | | | | | | | | | |
| **1** | 3.10E-2 | (0.47) | **16** | 4.60E-2 | (0.39) | **31** | 4.95E-2 | (0.37) | **46** | 4.16E-2 | (0.41) | **61** | 4.06E-2 | (0.43) |
| **2** | 3.66E-2 | (0.44) | **17** | 5.06E-2 | (0.38) | **32** | 5.51E-2 | (0.36) | **47** | 3.77E-2 | (0.41) | **62** | 3.03E-2 | (0.45) |
| **3** | 3.44E-2 | (0.45) | **18** | 5.27E-2 | (0.36) | **33** | 5.60E-2 | (0.35) | **48** | 4.32E-2 | (0.40) | **63** | 2.53E-2 | (0.50) |
| **4** | 3.57E-2 | (0.42) | **19** | 6.01E-2 | (0.35) | **34** | 5.93E-2 | (0.35) | **49** | 4.06E-2 | (0.39) | **64** | 2.36E-2 | (0.56) |
| **5** | 4.21E-2 | (0.40) | **20** | 6.71E-2 | (0.33) | **35** | 5.63E-2 | (0.35) | **50** | 4.78E-2 | (0.38) | **65** | 3.70E-2 | (0.45) |
| **6** | 4.07E-2 | (0.41) | **21** | 6.76E-2 | (0.35) | **36** | 5.86E-2 | (0.38) | **51** | 5.04E-2 | (0.38) | **66** | 3.62E-2 | (0.45) |
| **7** | 4.29E-2 | (0.40) | **22** | 4.07E-2 | (0.39) | **37** | 3.85E-2 | (0.40) | **52** | 5.12E-2 | (0.38) | **67** | 3.63E-2 | (0.45) |
| **8** | 4.71E-2 | (0.39) | **23** | 4.80E-2 | (0.38) | **38** | 4.38E-2 | (0.40) | **53** | 6.05E-2 | (0.38) | **68** | 3.53E-2 | (0.46) |
| **9** | 4.93E-2 | (0.38) | **24** | 4.57E-2 | (0.37) | **39** | 4.07E-2 | (0.39) | **54** | 5.29E-2 | (0.41) | **69** | 3.36E-2 | (0.47) |
| **10** | 5.60E-2 | (0.38) | **25** | 5.51E-2 | (0.35) | **40** | 4.87E-2 | (0.38) | **55** | 3.82E-2 | (0.47) | **70** | 2.95E-2 | (0.47) |
| **11** | 4.02E-2 | (0.39) | **26** | 5.22E-2 | (0.34) | **41** | 5.45E-2 | (0.37) | **56** | 4.25E-2 | (0.42) | **71** | 1.92E-2 | (0.57) |
| **12** | 4.75E-2 | (0.38) | **27** | 5.95E-2 | (0.34) | **42** | 5.33E-2 | (0.36) | **57** | 4.01E-2 | (0.42) | **72** | 1.90E-2 | (0.57) |
| **13** | 4.62E-2 | (0.37) | **28** | 5.19E-2 | (0.37) | **43** | 4.91E-2 | (0.36) | **58** | 4.24E-2 | (0.42) | **73** | 1.85E-2 | (0.58) |
| **14** | 5.73E-2 | (0.35) | **29** | 4.48E-2 | (0.39) | **44** | 6.49E-2 | (0.36) | **59** | 4.09E-2 | (0.41) | **74** | 1.77E-2 | (0.60) |
| **15** | 5.72E-2 | (0.35) | **30** | 4.87E-2 | (0.39) | **45** | 5.55E-2 | (0.39) | **60** | 4.35E-2 | (0.41) | **75** | 1.91E-2 | (0.62) |
| Layer 11 | | | | | | | | | | | | | | |
| **1** | 1.85E-2 | (0.56) | **16** | 2.68E-2 | (0.46) | **31** | 2.88E-2 | (0.44) | **46** | 2.59E-2 | (0.47) | **61** | 3.03E-2 | (0.49) |
| **2** | 2.24E-2 | (0.50) | **17** | 2.89E-2 | (0.46) | **32** | 3.13E-2 | (0.44) | **47** | 2.72E-2 | (0.48) | **62** | 1.95E-2 | (0.53) |
| **3** | 2.47E-2 | (0.52) | **18** | 3.06E-2 | (0.43) | **33** | 3.23E-2 | (0.42) | **48** | 2.64E-2 | (0.46) | **63** | 1.82E-2 | (0.59) |
| **4** | 2.08E-2 | (0.50) | **19** | 3.48E-2 | (0.42) | **34** | 3.36E-2 | (0.43) | **49** | 2.90E-2 | (0.46) | **64** | 1.48E-2 | (0.66) |
| **5** | 2.51E-2 | (0.47) | **20** | 3.84E-2 | (0.40) | **35** | 3.43E-2 | (0.41) | **50** | 2.86E-2 | (0.45) | **65** | 2.73E-2 | (0.52) |
| **6** | 2.38E-2 | (0.50) | **21** | 3.78E-2 | (0.42) | **36** | 4.12E-2 | (0.44) | **51** | 2.94E-2 | (0.46) | **66** | 2.68E-2 | (0.52) |
| **7** | 2.52E-2 | (0.47) | **22** | 2.35E-2 | (0.47) | **37** | 2.78E-2 | (0.47) | **52** | 3.64E-2 | (0.45) | **67** | 2.69E-2 | (0.52) |
| **8** | 2.70E-2 | (0.47) | **23** | 2.79E-2 | (0.45) | **38** | 2.70E-2 | (0.46) | **53** | 3.44E-2 | (0.47) | **68** | 2.69E-2 | (0.52) |
| **9** | 2.95E-2 | (0.44) | **24** | 2.61E-2 | (0.45) | **39** | 2.38E-2 | (0.47) | **54** | 2.89E-2 | (0.51) | **69** | 2.56E-2 | (0.54) |
| **10** | 3.98E-2 | (0.45) | **25** | 3.18E-2 | (0.42) | **40** | 2.90E-2 | (0.44) | **55** | 2.22E-2 | (0.57) | **70** | 2.24E-2 | (0.54) |
| **11** | 2.31E-2 | (0.47) | **26** | 2.97E-2 | (0.42) | **41** | 3.09E-2 | (0.44) | **56** | 2.55E-2 | (0.49) | **71** | 1.46E-2 | (0.66) |
| **12** | 2.78E-2 | (0.45) | **27** | 3.45E-2 | (0.40) | **42** | 3.11E-2 | (0.43) | **57** | 2.46E-2 | (0.48) | **72** | 1.45E-2 | (0.66) |
| **13** | 2.71E-2 | (0.44) | **28** | 3.65E-2 | (0.43) | **43** | 3.48E-2 | (0.42) | **58** | 2.60E-2 | (0.49) | **73** | 1.43E-2 | (0.66) |
| **14** | 4.03E-2 | (0.41) | **29** | 2.65E-2 | (0.46) | **44** | 3.79E-2 | (0.43) | **59** | 3.04E-2 | (0.48) | **74** | 1.36E-2 | (0.68) |
| **15** | 3.99E-2 | (0.42) | **30** | 2.80E-2 | (0.47) | **45** | 3.05E-2 | (0.48) | **60** | 3.27E-2 | (0.47) | **75** | 1.26E-2 | (0.71) |
| Layer 12 | | | | | | | | | | | | | | |
| **1** | 1.35E-2 | (0.65) | **16** | 1.94E-2 | (0.53) | **31** | 2.07E-2 | (0.51) | **46** | 1.91E-2 | (0.55) | **61** | 2.25E-2 | (0.57) |
| **2** | 1.65E-2 | (0.58) | **17** | 2.06E-2 | (0.54) | **32** | 2.22E-2 | (0.52) | **47** | 2.01E-2 | (0.55) | **62** | 1.42E-2 | (0.61) |
| **3** | 1.84E-2 | (0.61) | **18** | 2.19E-2 | (0.50) | **33** | 2.30E-2 | (0.49) | **48** | 1.93E-2 | (0.54) | **63** | 1.33E-2 | (0.69) |
| **4** | 1.52E-2 | (0.58) | **19** | 2.46E-2 | (0.50) | **34** | 2.38E-2 | (0.50) | **49** | 2.14E-2 | (0.53) | **64** | 1.05E-2 | (0.78) |
| **5** | 1.83E-2 | (0.55) | **20** | 2.69E-2 | (0.47) | **35** | 2.46E-2 | (0.48) | **50** | 2.06E-2 | (0.52) | **65** | 2.03E-2 | (0.60) |
| **6** | 1.71E-2 | (0.58) | **21** | 2.64E-2 | (0.50) | **36** | 2.98E-2 | (0.52) | **51** | 2.09E-2 | (0.54) | **66** | 2.00E-2 | (0.60) |
| **7** | 1.83E-2 | (0.55) | **22** | 1.68E-2 | (0.55) | **37** | 2.06E-2 | (0.55) | **52** | 2.62E-2 | (0.53) | **67** | 2.02E-2 | (0.60) |
| **8** | 1.95E-2 | (0.55) | **23** | 2.01E-2 | (0.52) | **38** | 1.97E-2 | (0.53) | **53** | 2.41E-2 | (0.55) | **68** | 2.02E-2 | (0.60) |
| **9** | 2.13E-2 | (0.51) | **24** | 1.86E-2 | (0.52) | **39** | 1.71E-2 | (0.55) | **54** | 1.98E-2 | (0.61) | **69** | 1.92E-2 | (0.62) |
| **10** | 2.90E-2 | (0.53) | **25** | 2.26E-2 | (0.49) | **40** | 2.09E-2 | (0.51) | **55** | 1.53E-2 | (0.69) | **70** | 1.69E-2 | (0.62) |
| **11** | 1.66E-2 | (0.56) | **26** | 2.09E-2 | (0.49) | **41** | 2.20E-2 | (0.52) | **56** | 1.86E-2 | (0.57) | **71** | 1.10E-2 | (0.76) |
| **12** | 1.99E-2 | (0.52) | **27** | 2.45E-2 | (0.47) | **42** | 2.22E-2 | (0.50) | **57** | 1.81E-2 | (0.56) | **72** | 1.10E-2 | (0.76) |
| **13** | 1.94E-2 | (0.52) | **28** | 2.63E-2 | (0.51) | **43** | 2.52E-2 | (0.50) | **58** | 1.91E-2 | (0.57) | **73** | 1.07E-2 | (0.76) |

| | | | | | | | | | | | | | | | |
|---|---|---|---|---|---|---|---|---|---|---|---|---|---|---|---|
| **14** | 2.91E-2 | (0.48) | **29** | 1.92E-2 | (0.54) | **44** | 2.68E-2 | (0.51) | **59** | 2.28E-2 | (0.55) | **74** | 1.03E-2 | (0.78) |
| **15** | 2.85E-2 | (0.49) | **30** | 2.01E-2 | (0.55) | **45** | 2.10E-2 | (0.58) | **60** | 2.45E-2 | (0.55) | **75** | 9.44E-3 | (0.82) |
| Layer 13 | | | | | | | | | | | | | | | |
| **1** | 1.01E-2 | (0.75) | **16** | 1.43E-2 | (0.62) | **31** | 1.52E-2 | (0.60) | **46** | 1.41E-2 | (0.63) | **61** | 1.65E-2 | (0.67) |
| **2** | 1.23E-2 | (0.67) | **17** | 1.51E-2 | (0.63) | **32** | 1.61E-2 | (0.61) | **47** | 1.49E-2 | (0.64) | **62** | 1.04E-2 | (0.72) |
| **3** | 1.37E-2 | (0.70) | **18** | 1.60E-2 | (0.59) | **33** | 1.66E-2 | (0.57) | **48** | 1.43E-2 | (0.63) | **63** | 9.61E-3 | (0.81) |
| **4** | 1.12E-2 | (0.68) | **19** | 1.78E-2 | (0.58) | **34** | 1.72E-2 | (0.59) | **49** | 1.58E-2 | (0.62) | **64** | 7.50E-3 | (0.92) |
| **5** | 1.34E-2 | (0.64) | **20** | 1.95E-2 | (0.56) | **35** | 1.79E-2 | (0.56) | **50** | 1.51E-2 | (0.61) | **65** | 1.51E-2 | (0.70) |
| **6** | 1.26E-2 | (0.67) | **21** | 1.91E-2 | (0.59) | **36** | 2.15E-2 | (0.61) | **51** | 1.53E-2 | (0.63) | **66** | 1.49E-2 | (0.70) |
| **7** | 1.35E-2 | (0.64) | **22** | 1.24E-2 | (0.64) | **37** | 1.52E-2 | (0.63) | **52** | 1.90E-2 | (0.62) | **67** | 1.50E-2 | (0.70) |
| **8** | 1.44E-2 | (0.64) | **23** | 1.47E-2 | (0.61) | **38** | 1.46E-2 | (0.62) | **53** | 1.73E-2 | (0.65) | **68** | 1.49E-2 | (0.70) |
| **9** | 1.57E-2 | (0.60) | **24** | 1.36E-2 | (0.61) | **39** | 1.26E-2 | (0.64) | **54** | 1.41E-2 | (0.72) | **69** | 1.42E-2 | (0.72) |
| **10** | 2.13E-2 | (0.62) | **25** | 1.65E-2 | (0.58) | **40** | 1.54E-2 | (0.60) | **55** | 1.09E-2 | (0.82) | **70** | 1.24E-2 | (0.72) |
| **11** | 1.22E-2 | (0.65) | **26** | 1.51E-2 | (0.58) | **41** | 1.60E-2 | (0.61) | **56** | 1.37E-2 | (0.67) | **71** | 8.20E-3 | (0.88) |
| **12** | 1.47E-2 | (0.61) | **27** | 1.77E-2 | (0.56) | **42** | 1.61E-2 | (0.59) | **57** | 1.35E-2 | (0.65) | **72** | 8.15E-3 | (0.88) |
| **13** | 1.41E-2 | (0.60) | **28** | 1.91E-2 | (0.60) | **43** | 1.82E-2 | (0.58) | **58** | 1.42E-2 | (0.66) | **73** | 8.00E-3 | (0.89) |
| **14** | 2.12E-2 | (0.57) | **29** | 1.42E-2 | (0.62) | **44** | 1.93E-2 | (0.60) | **59** | 1.68E-2 | (0.64) | **74** | 7.62E-3 | (0.91) |
| **15** | 2.06E-2 | (0.58) | **30** | 1.47E-2 | (0.64) | **45** | 1.50E-2 | (0.68) | **60** | 1.80E-2 | (0.64) | **75** | 6.97E-3 | (0.95) |
| Layer 14 | | | | | | | | | | | | | | | |
| **1** | 7.50E-3 | (0.88) | **16** | 1.04E-2 | (0.73) | **31** | 1.11E-2 | (0.70) | **46** | 1.03E-2 | (0.74) | **61** | 1.19E-2 | (0.78) |
| **2** | 9.07E-3 | (0.78) | **17** | 1.10E-2 | (0.74) | **32** | 1.18E-2 | (0.71) | **47** | 1.09E-2 | (0.75) | **62** | 7.47E-3 | (0.85) |
| **3** | 1.01E-2 | (0.82) | **18** | 1.17E-2 | (0.69) | **33** | 1.21E-2 | (0.68) | **48** | 1.04E-2 | (0.73) | **63** | 6.85E-3 | (0.95) |
| **4** | 8.22E-3 | (0.79) | **19** | 1.30E-2 | (0.68) | **34** | 1.24E-2 | (0.69) | **49** | 1.14E-2 | (0.73) | **64** | 5.32E-3 | (1.09) |
| **5** | 9.90E-3 | (0.75) | **20** | 1.41E-2 | (0.65) | **35** | 1.28E-2 | (0.66) | **50** | 1.09E-2 | (0.72) | **65** | 1.10E-2 | (0.82) |
| **6** | 9.25E-3 | (0.78) | **21** | 1.38E-2 | (0.70) | **36** | 1.55E-2 | (0.72) | **51** | 1.11E-2 | (0.74) | **66** | 1.08E-2 | (0.82) |
| **7** | 9.91E-3 | (0.75) | **22** | 9.08E-3 | (0.75) | **37** | 1.11E-2 | (0.74) | **52** | 1.36E-2 | (0.73) | **67** | 1.09E-2 | (0.82) |
| **8** | 1.05E-2 | (0.75) | **23** | 1.08E-2 | (0.71) | **38** | 1.07E-2 | (0.72) | **53** | 1.24E-2 | (0.77) | **68** | 1.09E-2 | (0.82) |
| **9** | 1.14E-2 | (0.70) | **24** | 9.89E-3 | (0.72) | **39** | 9.20E-3 | (0.74) | **54** | 1.00E-2 | (0.86) | **69** | 1.03E-2 | (0.85) |
| **10** | 1.54E-2 | (0.72) | **25** | 1.20E-2 | (0.68) | **40** | 1.12E-2 | (0.70) | **55** | 7.69E-3 | (0.97) | **70** | 8.98E-3 | (0.85) |
| **11** | 8.98E-3 | (0.76) | **26** | 1.10E-2 | (0.68) | **41** | 1.16E-2 | (0.72) | **56** | 1.01E-2 | (0.78) | **71** | 6.00E-3 | (1.03) |
| **12** | 1.07E-2 | (0.71) | **27** | 1.28E-2 | (0.66) | **42** | 1.16E-2 | (0.69) | **57** | 9.79E-3 | (0.76) | **72** | 5.93E-3 | (1.03) |
| **13** | 1.03E-2 | (0.71) | **28** | 1.37E-2 | (0.70) | **43** | 1.31E-2 | (0.69) | **58** | 1.03E-2 | (0.77) | **73** | 5.83E-3 | (1.04) |
| **14** | 1.54E-2 | (0.67) | **29** | 1.04E-2 | (0.73) | **44** | 1.39E-2 | (0.71) | **59** | 1.22E-2 | (0.75) | **74** | 5.56E-3 | (1.06) |
| **15** | 1.49E-2 | (0.68) | **30** | 1.08E-2 | (0.74) | **45** | 1.07E-2 | (0.81) | **60** | 1.31E-2 | (0.75) | **75** | 5.09E-3 | (1.11) |
| Layer 15 | | | | | | | | | | | | | | | |
| **1** | 5.49E-3 | (1.03) | **16** | 7.63E-3 | (0.85) | **31** | 8.02E-3 | (0.83) | **46** | 7.37E-3 | (0.88) | **61** | 8.23E-3 | (0.94) |
| **2** | 6.63E-3 | (0.92) | **17** | 8.01E-3 | (0.86) | **32** | 8.51E-3 | (0.84) | **47** | 7.66E-3 | (0.89) | **62** | 5.24E-3 | (1.01) |
| **3** | 7.27E-3 | (0.96) | **18** | 8.41E-3 | (0.81) | **33** | 8.64E-3 | (0.79) | **48** | 7.41E-3 | (0.87) | **63** | 4.74E-3 | (1.15) |
| **4** | 6.03E-3 | (0.92) | **19** | 9.31E-3 | (0.80) | **34** | 8.86E-3 | (0.82) | **49** | 8.06E-3 | (0.87) | **64** | 3.73E-3 | (1.30) |
| **5** | 7.20E-3 | (0.87) | **20** | 1.01E-2 | (0.77) | **35** | 8.96E-3 | (0.79) | **50** | 7.78E-3 | (0.85) | **65** | 7.66E-3 | (0.98) |
| **6** | 6.72E-3 | (0.92) | **21** | 9.89E-3 | (0.82) | **36** | 1.06E-2 | (0.87) | **51** | 7.79E-3 | (0.88) | **66** | 7.47E-3 | (0.98) |
| **7** | 7.25E-3 | (0.87) | **22** | 6.59E-3 | (0.88) | **37** | 7.94E-3 | (0.88) | **52** | 9.37E-3 | (0.88) | **67** | 7.54E-3 | (0.98) |
| **8** | 7.65E-3 | (0.88) | **23** | 7.86E-3 | (0.83) | **38** | 7.65E-3 | (0.86) | **53** | 8.43E-3 | (0.93) | **68** | 7.50E-3 | (0.99) |
| **9** | 8.26E-3 | (0.82) | **24** | 7.16E-3 | (0.84) | **39** | 6.62E-3 | (0.88) | **54** | 7.00E-3 | (1.02) | **69** | 7.20E-3 | (1.01) |
| **10** | 1.10E-2 | (0.85) | **25** | 8.60E-3 | (0.80) | **40** | 8.00E-3 | (0.83) | **55** | 5.38E-3 | (1.16) | **70** | 6.25E-3 | (1.01) |
| **11** | 6.57E-3 | (0.88) | **26** | 7.89E-3 | (0.80) | **41** | 8.28E-3 | (0.85) | **56** | 7.12E-3 | (0.92) | **71** | 4.16E-3 | (1.23) |
| **12** | 7.84E-3 | (0.84) | **27** | 9.14E-3 | (0.78) | **42** | 8.25E-3 | (0.82) | **57** | 6.89E-3 | (0.90) | **72** | 4.15E-3 | (1.23) |
| **13** | 7.44E-3 | (0.83) | **28** | 9.57E-3 | (0.84) | **43** | 8.98E-3 | (0.83) | **58** | 7.23E-3 | (0.92) | **73** | 4.05E-3 | (1.24) |

| | | | | | | | | | | | | |
|---|---|---|---|---|---|---|---|---|---|---|---|---|
| **14** | 1.10E-2 | (0.78) | **29** | 7.50E-3 | (0.86) | **44** | 9.48E-3 | (0.85) | **59** | 8.52E-3 | (0.90) | **74** | 3.85E-3 | (1.27) |
| **15** | 1.06E-2 | (0.80) | **30** | 7.81E-3 | (0.87) | **45** | 7.45E-3 | (0.97) | **60** | 9.03E-3 | (0.90) | **75** | 3.62E-3 | (1.32) |
| Layer 16 | | | | | | | | | | | | | | |
| **1** | 4.03E-3 | (1.20) | **16** | 5.50E-3 | (1.00) | **31** | 5.76E-3 | (0.98) | **46** | 4.98E-3 | (1.05) | **61** | 4.48E-3 | (1.17) |
| **2** | 4.73E-3 | (1.08) | **17** | 5.82E-3 | (1.01) | **32** | 6.07E-3 | (0.99) | **47** | 4.42E-3 | (1.08) | **62** | 3.45E-3 | (1.24) |
| **3** | 4.28E-3 | (1.16) | **18** | 6.04E-3 | (0.95) | **33** | 6.19E-3 | (0.94) | **48** | 5.04E-3 | (1.04) | **63** | 2.77E-3 | (1.39) |
| **4** | 4.38E-3 | (1.08) | **19** | 6.49E-3 | (0.96) | **34** | 6.24E-3 | (0.98) | **49** | 4.60E-3 | (1.06) | **64** | 2.58E-3 | (1.56) |
| **5** | 5.21E-3 | (1.02) | **20** | 7.00E-3 | (0.92) | **35** | 5.92E-3 | (0.96) | **50** | 5.34E-3 | (1.02) | **65** | 4.13E-3 | (1.22) |
| **6** | 4.80E-3 | (1.09) | **21** | 7.01E-3 | (0.97) | **36** | 5.85E-3 | (1.07) | **51** | 5.29E-3 | (1.06) | **66** | 4.04E-3 | (1.23) |
| **7** | 5.26E-3 | (1.02) | **22** | 4.77E-3 | (1.04) | **37** | 4.54E-3 | (1.07) | **52** | 4.96E-3 | (1.10) | **67** | 4.01E-3 | (1.23) |
| **8** | 5.56E-3 | (1.03) | **23** | 5.64E-3 | (0.98) | **38** | 5.24E-3 | (1.02) | **53** | 4.47E-3 | (1.17) | **68** | 3.97E-3 | (1.24) |
| **9** | 5.80E-3 | (0.97) | **24** | 5.16E-3 | (0.99) | **39** | 4.68E-3 | (1.04) | **54** | 4.76E-3 | (1.24) | **69** | 4.72E-3 | (1.24) |
| **10** | 6.31E-3 | (1.03) | **25** | 6.19E-3 | (0.94) | **40** | 5.57E-3 | (0.99) | **55** | 3.75E-3 | (1.39) | **70** | 3.69E-3 | (1.23) |
| **11** | 4.75E-3 | (1.04) | **26** | 5.61E-3 | (0.95) | **41** | 5.84E-3 | (1.01) | **56** | 4.78E-3 | (1.12) | **71** | 2.40E-3 | (1.49) |
| **12** | 5.68E-3 | (0.98) | **27** | 6.42E-3 | (0.92) | **42** | 5.71E-3 | (0.98) | **57** | 4.65E-3 | (1.09) | **72** | 2.37E-3 | (1.50) |
| **13** | 5.22E-3 | (0.99) | **28** | 5.51E-3 | (1.02) | **43** | 4.88E-3 | (1.03) | **58** | 4.72E-3 | (1.12) | **73** | 2.29E-3 | (1.52) |
| **14** | 6.39E-3 | (0.93) | **29** | 5.36E-3 | (1.01) | **44** | 5.17E-3 | (1.04) | **59** | 4.72E-3 | (1.09) | **74** | 2.23E-3 | (1.55) |
| **15** | 6.06E-3 | (0.98) | **30** | 5.60E-3 | (1.03) | **45** | 5.03E-3 | (1.17) | **60** | 4.93E-3 | (1.12) | **75** | 2.48E-3 | (1.59) |
| Layer 17 | | | | | | | | | | | | | | |
| **1** | 2.90E-3 | (1.41) | **16** | 3.97E-3 | (1.18) | **31** | 4.11E-3 | (1.15) | **46** | 3.47E-3 | (1.26) | **61** | 2.98E-3 | (1.42) |
| **2** | 3.44E-3 | (1.27) | **17** | 4.17E-3 | (1.19) | **32** | 4.34E-3 | (1.17) | **47** | 3.04E-3 | (1.29) | **62** | 2.38E-3 | (1.48) |
| **3** | 3.10E-3 | (1.35) | **18** | 4.34E-3 | (1.13) | **33** | 4.39E-3 | (1.12) | **48** | 3.55E-3 | (1.24) | **63** | 1.89E-3 | (1.67) |
| **4** | 3.19E-3 | (1.27) | **19** | 4.64E-3 | (1.13) | **34** | 4.37E-3 | (1.17) | **49** | 3.16E-3 | (1.27) | **64** | 1.80E-3 | (1.87) |
| **5** | 3.77E-3 | (1.21) | **20** | 4.94E-3 | (1.10) | **35** | 4.11E-3 | (1.16) | **50** | 3.67E-3 | (1.22) | **65** | 2.77E-3 | (1.47) |
| **6** | 3.45E-3 | (1.29) | **21** | 4.97E-3 | (1.16) | **36** | 3.94E-3 | (1.30) | **51** | 3.62E-3 | (1.28) | **66** | 2.73E-3 | (1.48) |
| **7** | 3.82E-3 | (1.20) | **22** | 3.41E-3 | (1.22) | **37** | 3.16E-3 | (1.27) | **52** | 3.31E-3 | (1.34) | **67** | 2.69E-3 | (1.49) |
| **8** | 4.02E-3 | (1.22) | **23** | 4.08E-3 | (1.16) | **38** | 3.69E-3 | (1.22) | **53** | 2.99E-3 | (1.42) | **68** | 2.65E-3 | (1.51) |
| **9** | 4.15E-3 | (1.15) | **24** | 3.69E-3 | (1.17) | **39** | 3.30E-3 | (1.24) | **54** | 3.29E-3 | (1.49) | **69** | 3.19E-3 | (1.50) |
| **10** | 4.43E-3 | (1.22) | **25** | 4.41E-3 | (1.11) | **40** | 3.92E-3 | (1.18) | **55** | 2.58E-3 | (1.67) | **70** | 2.51E-3 | (1.49) |
| **11** | 3.44E-3 | (1.22) | **26** | 3.96E-3 | (1.13) | **41** | 4.10E-3 | (1.20) | **56** | 3.29E-3 | (1.35) | **71** | 1.63E-3 | (1.79) |
| **12** | 4.09E-3 | (1.16) | **27** | 4.55E-3 | (1.10) | **42** | 3.97E-3 | (1.18) | **57** | 3.20E-3 | (1.31) | **72** | 1.62E-3 | (1.80) |
| **13** | 3.73E-3 | (1.17) | **28** | 3.75E-3 | (1.23) | **43** | 3.24E-3 | (1.25) | **58** | 3.26E-3 | (1.35) | **73** | 1.58E-3 | (1.82) |
| **14** | 4.52E-3 | (1.10) | **29** | 3.81E-3 | (1.20) | **44** | 3.48E-3 | (1.26) | **59** | 3.20E-3 | (1.31) | **74** | 1.50E-3 | (1.87) |
| **15** | 4.25E-3 | (1.16) | **30** | 4.01E-3 | (1.22) | **45** | 3.46E-3 | (1.41) | **60** | 3.28E-3 | (1.36) | **75** | 1.72E-3 | (1.91) |
| Layer 18 | | | | | | | | | | | | | | |
| **1** | 2.10E-3 | (1.66) | **16** | 2.87E-3 | (1.39) | **31** | 2.91E-3 | (1.37) | **46** | 2.42E-3 | (1.51) | **61** | 2.07E-3 | (1.71) |
| **2** | 2.47E-3 | (1.49) | **17** | 3.00E-3 | (1.40) | **32** | 3.05E-3 | (1.40) | **47** | 2.13E-3 | (1.54) | **62** | 1.63E-3 | (1.80) |
| **3** | 2.23E-3 | (1.59) | **18** | 3.09E-3 | (1.33) | **33** | 3.09E-3 | (1.33) | **48** | 2.48E-3 | (1.48) | **63** | 1.29E-3 | (2.01) |
| **4** | 2.28E-3 | (1.50) | **19** | 3.32E-3 | (1.34) | **34** | 3.09E-3 | (1.39) | **49** | 2.19E-3 | (1.52) | **64** | 1.25E-3 | (2.25) |
| **5** | 2.71E-3 | (1.42) | **20** | 3.54E-3 | (1.30) | **35** | 2.85E-3 | (1.39) | **50** | 2.56E-3 | (1.46) | **65** | 1.90E-3 | (1.77) |
| **6** | 2.50E-3 | (1.51) | **21** | 3.53E-3 | (1.37) | **36** | 2.75E-3 | (1.56) | **51** | 2.52E-3 | (1.54) | **66** | 1.87E-3 | (1.79) |
| **7** | 2.76E-3 | (1.42) | **22** | 2.46E-3 | (1.44) | **37** | 2.23E-3 | (1.52) | **52** | 2.28E-3 | (1.61) | **67** | 1.87E-3 | (1.79) |
| **8** | 2.87E-3 | (1.44) | **23** | 2.90E-3 | (1.37) | **38** | 2.60E-3 | (1.45) | **53** | 2.06E-3 | (1.70) | **68** | 1.85E-3 | (1.80) |
| **9** | 3.00E-3 | (1.35) | **24** | 2.62E-3 | (1.39) | **39** | 2.33E-3 | (1.48) | **54** | 2.28E-3 | (1.79) | **69** | 2.18E-3 | (1.82) |
| **10** | 3.16E-3 | (1.44) | **25** | 3.14E-3 | (1.32) | **40** | 2.76E-3 | (1.41) | **55** | 1.81E-3 | (2.00) | **70** | 1.71E-3 | (1.79) |
| **11** | 2.48E-3 | (1.44) | **26** | 2.82E-3 | (1.34) | **41** | 2.88E-3 | (1.43) | **56** | 2.29E-3 | (1.62) | **71** | 1.16E-3 | (2.13) |
| **12** | 2.94E-3 | (1.37) | **27** | 3.21E-3 | (1.31) | **42** | 2.76E-3 | (1.41) | **57** | 2.22E-3 | (1.57) | **72** | 1.14E-3 | (2.14) |
| **13** | 2.67E-3 | (1.38) | **28** | 2.64E-3 | (1.47) | **43** | 2.24E-3 | (1.51) | **58** | 2.28E-3 | (1.62) | **73** | 1.10E-3 | (2.18) |

| | | | | | | | | | | | | |
|---|---|---|---|---|---|---|---|---|---|---|---|---|
| **14** | 3.24E-3 | (1.30) | **29** | 2.74E-3 | (1.42) | **44** | 2.39E-3 | (1.52) | **59** | 2.18E-3 | (1.58) | **74** | 1.04E-3 | (2.24) |
| **15** | 3.03E-3 | (1.38) | **30** | 2.86E-3 | (1.44) | **45** | 2.40E-3 | (1.70) | **60** | 2.25E-3 | (1.63) | **75** | 1.20E-3 | (2.29) |
| Layer 19 | | | | | | | | | | | | | | |
| **1** | 1.51E-3 | (1.95) | **16** | 2.03E-3 | (1.65) | **31** | 2.05E-3 | (1.63) | **46** | 1.69E-3 | (1.81) | **61** | 1.42E-3 | (2.05) |
| **2** | 1.77E-3 | (1.76) | **17** | 2.15E-3 | (1.66) | **32** | 2.16E-3 | (1.66) | **47** | 1.49E-3 | (1.85) | **62** | 1.10E-3 | (2.17) |
| **3** | 1.59E-3 | (1.89) | **18** | 2.21E-3 | (1.57) | **33** | 2.17E-3 | (1.58) | **48** | 1.74E-3 | (1.77) | **63** | 8.91E-4 | (2.44) |
| **4** | 1.64E-3 | (1.77) | **19** | 2.34E-3 | (1.59) | **34** | 2.17E-3 | (1.65) | **49** | 1.54E-3 | (1.82) | **64** | 8.67E-4 | (2.69) |
| **5** | 1.94E-3 | (1.68) | **20** | 2.52E-3 | (1.54) | **35** | 1.99E-3 | (1.66) | **50** | 1.78E-3 | (1.75) | **65** | 1.34E-3 | (2.14) |
| **6** | 1.79E-3 | (1.79) | **21** | 2.48E-3 | (1.64) | **36** | 1.89E-3 | (1.88) | **51** | 1.75E-3 | (1.85) | **66** | 1.31E-3 | (2.14) |
| **7** | 1.96E-3 | (1.67) | **22** | 1.73E-3 | (1.72) | **37** | 1.56E-3 | (1.81) | **52** | 1.57E-3 | (1.95) | **67** | 1.28E-3 | (2.14) |
| **8** | 2.07E-3 | (1.69) | **23** | 2.06E-3 | (1.63) | **38** | 1.83E-3 | (1.73) | **53** | 1.42E-3 | (2.05) | **68** | 1.27E-3 | (2.17) |
| **9** | 2.13E-3 | (1.60) | **24** | 1.86E-3 | (1.65) | **39** | 1.64E-3 | (1.76) | **54** | 1.59E-3 | (2.16) | **69** | 1.51E-3 | (2.19) |
| **10** | 2.27E-3 | (1.71) | **25** | 2.22E-3 | (1.57) | **40** | 1.92E-3 | (1.68) | **55** | 1.27E-3 | (2.39) | **70** | 1.19E-3 | (2.15) |
| **11** | 1.77E-3 | (1.70) | **26** | 1.99E-3 | (1.60) | **41** | 2.00E-3 | (1.72) | **56** | 1.59E-3 | (1.94) | **71** | 7.93E-4 | (2.59) |
| **12** | 2.11E-3 | (1.61) | **27** | 2.27E-3 | (1.55) | **42** | 1.93E-3 | (1.68) | **57** | 1.54E-3 | (1.89) | **72** | 7.86E-4 | (2.59) |
| **13** | 1.93E-3 | (1.62) | **28** | 1.84E-3 | (1.75) | **43** | 1.55E-3 | (1.81) | **58** | 1.58E-3 | (1.95) | **73** | 7.60E-4 | (2.63) |
| **14** | 2.30E-3 | (1.54) | **29** | 1.92E-3 | (1.69) | **44** | 1.65E-3 | (1.82) | **59** | 1.54E-3 | (1.89) | **74** | 7.18E-4 | (2.71) |
| **15** | 2.13E-3 | (1.63) | **30** | 2.02E-3 | (1.71) | **45** | 1.66E-3 | (2.04) | **60** | 1.57E-3 | (1.96) | **75** | 8.21E-4 | (2.77) |
| Layer 20 | | | | | | | | | | | | | | |
| **1** | 1.07E-3 | (2.31) | **16** | 1.43E-3 | (1.96) | **31** | 1.45E-3 | (1.95) | **46** | 1.20E-3 | (2.15) | **61** | 9.69E-4 | (2.49) |
| **2** | 1.27E-3 | (2.08) | **17** | 1.51E-3 | (1.98) | **32** | 1.52E-3 | (1.98) | **47** | 1.04E-3 | (2.22) | **62** | 7.64E-4 | (2.62) |
| **3** | 1.13E-3 | (2.23) | **18** | 1.56E-3 | (1.87) | **33** | 1.52E-3 | (1.90) | **48** | 1.21E-3 | (2.14) | **63** | 6.05E-4 | (2.94) |
| **4** | 1.16E-3 | (2.09) | **19** | 1.66E-3 | (1.90) | **34** | 1.51E-3 | (1.99) | **49** | 1.06E-3 | (2.19) | **64** | 6.02E-4 | (3.24) |
| **5** | 1.38E-3 | (1.99) | **20** | 1.76E-3 | (1.84) | **35** | 1.39E-3 | (1.98) | **50** | 1.23E-3 | (2.11) | **65** | 9.08E-4 | (2.56) |
| **6** | 1.26E-3 | (2.13) | **21** | 1.74E-3 | (1.95) | **36** | 1.29E-3 | (2.25) | **51** | 1.20E-3 | (2.23) | **66** | 9.05E-4 | (2.57) |
| **7** | 1.39E-3 | (1.99) | **22** | 1.22E-3 | (2.05) | **37** | 1.10E-3 | (2.15) | **52** | 1.07E-3 | (2.35) | **67** | 8.93E-4 | (2.58) |
| **8** | 1.46E-3 | (2.01) | **23** | 1.43E-3 | (1.95) | **38** | 1.30E-3 | (2.07) | **53** | 9.77E-4 | (2.48) | **68** | 8.77E-4 | (2.60) |
| **9** | 1.51E-3 | (1.90) | **24** | 1.32E-3 | (1.97) | **39** | 1.14E-3 | (2.11) | **54** | 1.10E-3 | (2.57) | **69** | 1.02E-3 | (2.65) |
| **10** | 1.59E-3 | (2.05) | **25** | 1.57E-3 | (1.87) | **40** | 1.35E-3 | (2.02) | **55** | 8.82E-4 | (2.88) | **70** | 8.03E-4 | (2.62) |
| **11** | 1.26E-3 | (2.01) | **26** | 1.40E-3 | (1.91) | **41** | 1.40E-3 | (2.06) | **56** | 1.11E-3 | (2.33) | **71** | 5.48E-4 | (3.11) |
| **12** | 1.49E-3 | (1.91) | **27** | 1.58E-3 | (1.86) | **42** | 1.32E-3 | (2.03) | **57** | 1.06E-3 | (2.27) | **72** | 5.43E-4 | (3.09) |
| **13** | 1.37E-3 | (1.93) | **28** | 1.31E-3 | (2.09) | **43** | 1.08E-3 | (2.17) | **58** | 1.08E-3 | (2.35) | **73** | 5.28E-4 | (3.16) |
| **14** | 1.63E-3 | (1.84) | **29** | 1.35E-3 | (2.02) | **44** | 1.14E-3 | (2.20) | **59** | 1.06E-3 | (2.27) | **74** | 4.96E-4 | (3.26) |
| **15** | 1.51E-3 | (1.95) | **30** | 1.41E-3 | (2.06) | **45** | 1.14E-3 | (2.45) | **60** | 1.08E-3 | (2.37) | **75** | 5.57E-4 | (3.36) |
| Layer 21 | | | | | | | | | | | | | | |
| **1** | 7.74E-4 | (2.75) | **16** | 1.01E-3 | (2.34) | **31** | 9.94E-4 | (2.33) | **46** | 8.28E-4 | (2.58) | **61** | 6.56E-4 | (3.03) |
| **2** | 8.90E-4 | (2.48) | **17** | 1.07E-3 | (2.36) | **32** | 1.04E-3 | (2.38) | **47** | 7.20E-4 | (2.66) | **62** | 5.21E-4 | (3.18) |
| **3** | 8.09E-4 | (2.65) | **18** | 1.09E-3 | (2.24) | **33** | 1.05E-3 | (2.28) | **48** | 8.25E-4 | (2.58) | **63** | 4.10E-4 | (3.58) |
| **4** | 8.22E-4 | (2.49) | **19** | 1.16E-3 | (2.26) | **34** | 1.03E-3 | (2.40) | **49** | 7.43E-4 | (2.61) | **64** | 4.02E-4 | (3.94) |
| **5** | 9.70E-4 | (2.37) | **20** | 1.22E-3 | (2.21) | **35** | 9.49E-4 | (2.40) | **50** | 8.50E-4 | (2.55) | **65** | 6.28E-4 | (3.08) |
| **6** | 8.76E-4 | (2.53) | **21** | 1.21E-3 | (2.36) | **36** | 9.03E-4 | (2.70) | **51** | 8.21E-4 | (2.69) | **66** | 6.20E-4 | (3.10) |
| **7** | 9.78E-4 | (2.37) | **22** | 8.57E-4 | (2.45) | **37** | 7.73E-4 | (2.57) | **52** | 7.40E-4 | (2.84) | **67** | 6.10E-4 | (3.10) |
| **8** | 1.04E-3 | (2.39) | **23** | 1.02E-3 | (2.31) | **38** | 9.04E-4 | (2.47) | **53** | 6.64E-4 | (3.01) | **68** | 5.93E-4 | (3.17) |
| **9** | 1.06E-3 | (2.27) | **24** | 9.16E-4 | (2.35) | **39** | 7.94E-4 | (2.54) | **54** | 7.35E-4 | (3.16) | **69** | 5.64E-4 | (3.28) |
| **10** | 1.11E-3 | (2.45) | **25** | 1.09E-3 | (2.24) | **40** | 9.32E-4 | (2.42) | **55** | 5.85E-4 | (3.49) | **70** | 5.35E-4 | (3.20) |
| **11** | 8.91E-4 | (2.41) | **26** | 9.83E-4 | (2.29) | **41** | 9.61E-4 | (2.49) | **56** | 7.57E-4 | (2.80) | **71** | 3.74E-4 | (3.75) |
| **12** | 1.05E-3 | (2.28) | **27** | 1.09E-3 | (2.24) | **42** | 9.10E-4 | (2.45) | **57** | 7.28E-4 | (2.73) | **72** | 3.74E-4 | (3.75) |
| **13** | 9.32E-4 | (2.32) | **28** | 8.70E-4 | (2.54) | **43** | 7.32E-4 | (2.64) | **58** | 7.46E-4 | (2.82) | **73** | 3.63E-4 | (3.77) |

| | | | | | | | | | | | | | | | |
|---|---|---|---|---|---|---|---|---|---|---|---|---|---|---|---|
| **14** | 1.13E-3 | (2.20) | **29** | 9.40E-4 | (2.41) | **44** | 7.78E-4 | (2.66) | **59** | 7.21E-4 | (2.75) | **74** | 3.42E-4 | (3.93) |
| **15** | 1.06E-3 | (2.33) | **30** | 9.89E-4 | (2.45) | **45** | 7.58E-4 | (3.02) | **60** | 7.20E-4 | (2.87) | **75** | 3.27E-4 | (4.03) |
| Layer 22 | | | | | | | | | | | | | | | |
| **1** | 5.17E-4 | (3.33) | **16** | 6.86E-4 | (2.83) | **31** | 6.83E-4 | (2.82) | **46** | 5.60E-4 | (3.15) | **61** | 4.35E-4 | (3.71) |
| **2** | 6.04E-4 | (3.02) | **17** | 7.29E-4 | (2.87) | **32** | 7.07E-4 | (2.90) | **47** | 4.80E-4 | (3.23) | **62** | 3.32E-4 | (3.95) |
| **3** | 5.44E-4 | (3.25) | **18** | 7.41E-4 | (2.71) | **33** | 7.08E-4 | (2.77) | **48** | 5.50E-4 | (3.14) | **63** | 2.74E-4 | (4.39) |
| **4** | 5.58E-4 | (3.02) | **19** | 7.84E-4 | (2.75) | **34** | 6.95E-4 | (2.91) | **49** | 4.89E-4 | (3.21) | **64** | 2.70E-4 | (4.83) |
| **5** | 6.51E-4 | (2.87) | **20** | 8.35E-4 | (2.67) | **35** | 6.37E-4 | (2.93) | **50** | 5.66E-4 | (3.10) | **65** | 4.20E-4 | (3.74) |
| **6** | 5.92E-4 | (3.08) | **21** | 8.23E-4 | (2.85) | **36** | 6.02E-4 | (3.31) | **51** | 5.54E-4 | (3.29) | **66** | 4.19E-4 | (3.80) |
| **7** | 6.81E-4 | (2.85) | **22** | 5.90E-4 | (2.95) | **37** | 5.16E-4 | (3.14) | **52** | 4.93E-4 | (3.45) | **67** | 4.09E-4 | (3.80) |
| **8** | 7.13E-4 | (2.88) | **23** | 6.94E-4 | (2.82) | **38** | 6.04E-4 | (3.00) | **53** | 4.45E-4 | (3.65) | **68** | 3.87E-4 | (3.92) |
| **9** | 7.21E-4 | (2.76) | **24** | 6.22E-4 | (2.85) | **39** | 5.33E-4 | (3.09) | **54** | 4.76E-4 | (3.91) | **69** | 3.62E-4 | (4.06) |
| **10** | 7.68E-4 | (2.96) | **25** | 7.31E-4 | (2.73) | **40** | 6.20E-4 | (2.95) | **55** | 3.85E-4 | (4.29) | **70** | 3.52E-4 | (3.95) |
| **11** | 6.04E-4 | (2.89) | **26** | 6.57E-4 | (2.77) | **41** | 6.43E-4 | (3.03) | **56** | 5.03E-4 | (3.42) | **71** | 2.41E-4 | (4.67) |
| **12** | 7.09E-4 | (2.77) | **27** | 7.32E-4 | (2.72) | **42** | 6.22E-4 | (2.99) | **57** | 4.91E-4 | (3.34) | **72** | 2.48E-4 | (4.59) |
| **13** | 6.36E-4 | (2.83) | **28** | 5.82E-4 | (3.10) | **43** | 4.96E-4 | (3.20) | **58** | 4.97E-4 | (3.46) | **73** | 2.40E-4 | (4.63) |
| **14** | 7.74E-4 | (2.66) | **29** | 6.38E-4 | (2.91) | **44** | 5.15E-4 | (3.26) | **59** | 4.80E-4 | (3.39) | **74** | 2.28E-4 | (4.81) |
| **15** | 7.28E-4 | (2.79) | **30** | 6.78E-4 | (2.96) | **45** | 5.09E-4 | (3.67) | **60** | 4.75E-4 | (3.54) | **75** | 2.19E-4 | (4.92) |
| Layer 23 | | | | | | | | | | | | | | | |
| **1** | 3.24E-4 | (4.20) | **16** | 4.48E-4 | (3.51) | **31** | 4.30E-4 | (3.55) | **46** | 3.58E-4 | (3.93) | **61** | 2.75E-4 | (4.63) |
| **2** | 3.88E-4 | (3.78) | **17** | 4.78E-4 | (3.55) | **32** | 4.51E-4 | (3.62) | **47** | 3.13E-4 | (4.04) | **62** | 2.19E-4 | (4.88) |
| **3** | 3.39E-4 | (4.03) | **18** | 4.74E-4 | (3.40) | **33** | 4.52E-4 | (3.49) | **48** | 3.59E-4 | (3.90) | **63** | 1.73E-4 | (5.44) |
| **4** | 3.54E-4 | (3.78) | **19** | 5.01E-4 | (3.43) | **34** | 4.45E-4 | (3.64) | **49** | 3.18E-4 | (3.99) | **64** | 1.66E-4 | (6.12) |
| **5** | 4.24E-4 | (3.61) | **20** | 5.39E-4 | (3.33) | **35** | 4.07E-4 | (3.67) | **50** | 3.61E-4 | (3.91) | **65** | 2.75E-4 | (4.65) |
| **6** | 3.79E-4 | (3.85) | **21** | 5.24E-4 | (3.53) | **36** | 3.87E-4 | (4.15) | **51** | 3.53E-4 | (4.11) | **66** | 2.63E-4 | (4.78) |
| **7** | 4.37E-4 | (3.56) | **22** | 3.82E-4 | (3.67) | **37** | 3.29E-4 | (3.95) | **52** | 3.20E-4 | (4.31) | **67** | 2.60E-4 | (4.78) |
| **8** | 4.50E-4 | (3.62) | **23** | 4.41E-4 | (3.51) | **38** | 3.85E-4 | (3.75) | **53** | 2.84E-4 | (4.63) | **68** | 2.39E-4 | (4.93) |
| **9** | 4.62E-4 | (3.44) | **24** | 3.96E-4 | (3.57) | **39** | 3.39E-4 | (3.83) | **54** | 3.03E-4 | (4.91) | **69** | 2.26E-4 | (5.13) |
| **10** | 4.91E-4 | (3.66) | **25** | 4.73E-4 | (3.41) | **40** | 3.95E-4 | (3.72) | **55** | 2.46E-4 | (5.40) | **70** | 2.19E-4 | (4.97) |
| **11** | 3.94E-4 | (3.63) | **26** | 4.17E-4 | (3.50) | **41** | 4.13E-4 | (3.82) | **56** | 3.27E-4 | (4.30) | **71** | 1.54E-4 | (5.86) |
| **12** | 4.57E-4 | (3.45) | **27** | 4.71E-4 | (3.38) | **42** | 3.93E-4 | (3.73) | **57** | 3.15E-4 | (4.13) | **72** | 1.55E-4 | (5.81) |
| **13** | 4.13E-4 | (3.52) | **28** | 3.83E-4 | (3.85) | **43** | 3.22E-4 | (4.00) | **58** | 3.19E-4 | (4.31) | **73** | 1.56E-4 | (5.81) |
| **14** | 4.94E-4 | (3.35) | **29** | 4.12E-4 | (3.64) | **44** | 3.38E-4 | (4.05) | **59** | 3.06E-4 | (4.24) | **74** | 1.40E-4 | (6.12) |
| **15** | 4.58E-4 | (3.52) | **30** | 4.42E-4 | (3.69) | **45** | 3.25E-4 | (4.57) | **60** | 2.92E-4 | (4.51) | **75** | 1.31E-4 | (6.34) |
| Layer 24 | | | | | | | | | | | | | | | |
| **1** | 1.97E-4 | (5.45) | **16** | 2.70E-4 | (4.55) | **31** | 2.59E-4 | (4.63) | **46** | 2.06E-4 | (5.18) | **61** | 1.59E-4 | (6.08) |
| **2** | 2.30E-4 | (4.92) | **17** | 2.76E-4 | (4.67) | **32** | 2.64E-4 | (4.75) | **47** | 1.81E-4 | (5.29) | **62** | 1.27E-4 | (6.49) |
| **3** | 1.99E-4 | (5.33) | **18** | 2.84E-4 | (4.46) | **33** | 2.68E-4 | (4.56) | **48** | 2.11E-4 | (5.15) | **63** | 9.84E-5 | (7.31) |
| **4** | 2.13E-4 | (4.94) | **19** | 2.97E-4 | (4.53) | **34** | 2.61E-4 | (4.78) | **49** | 1.87E-4 | (5.28) | **64** | 9.88E-5 | (8.05) |
| **5** | 2.55E-4 | (4.67) | **20** | 3.08E-4 | (4.39) | **35** | 2.39E-4 | (4.85) | **50** | 2.08E-4 | (5.16) | **65** | 1.53E-4 | (6.26) |
| **6** | 2.23E-4 | (5.04) | **21** | 3.00E-4 | (4.68) | **36** | 2.30E-4 | (5.41) | **51** | 2.04E-4 | (5.43) | **66** | 1.49E-4 | (6.32) |
| **7** | 2.61E-4 | (4.65) | **22** | 2.24E-4 | (4.84) | **37** | 1.91E-4 | (5.19) | **52** | 1.84E-4 | (5.74) | **67** | 1.52E-4 | (6.31) |
| **8** | 2.71E-4 | (4.73) | **23** | 2.65E-4 | (4.58) | **38** | 2.28E-4 | (4.95) | **53** | 1.65E-4 | (6.04) | **68** | 1.41E-4 | (6.47) |
| **9** | 2.75E-4 | (4.52) | **24** | 2.31E-4 | (4.69) | **39** | 2.00E-4 | (5.06) | **54** | 1.77E-4 | (6.47) | **69** | 1.30E-4 | (6.79) |
| **10** | 2.83E-4 | (4.81) | **25** | 2.80E-4 | (4.44) | **40** | 2.31E-4 | (4.88) | **55** | 1.40E-4 | (7.22) | **70** | 1.24E-4 | (6.68) |
| **11** | 2.26E-4 | (4.71) | **26** | 2.48E-4 | (4.56) | **41** | 2.40E-4 | (5.01) | **56** | 1.90E-4 | (5.69) | **71** | 8.95E-5 | (7.73) |
| **12** | 2.75E-4 | (4.48) | **27** | 2.77E-4 | (4.47) | **42** | 2.31E-4 | (4.93) | **57** | 1.84E-4 | (5.48) | **72** | 8.82E-5 | (7.68) |
| **13** | 2.42E-4 | (4.58) | **28** | 2.18E-4 | (5.07) | **43** | 1.82E-4 | (5.27) | **58** | 1.88E-4 | (5.65) | **73** | 8.61E-5 | (7.88) |

| | | | | | | | | | | | | |
|---|---|---|---|---|---|---|---|---|---|---|---|---|
| **14** | 2.98E-4 | (4.35) | **29** | 2.47E-4 | (4.75) | **44** | 2.00E-4 | (5.25) | **59** | 1.76E-4 | (5.58) | **74** | 8.03E-5 | (8.11) |
| **15** | 2.69E-4 | (4.62) | **30** | 2.52E-4 | (4.83) | **45** | 1.86E-4 | (6.06) | **60** | 1.73E-4 | (5.92) | **75** | 7.95E-5 | (8.19) |
| Layer 25 | | | | | | | | | | | | | | |
| **1** | 5.20E-5 | (7.39) | **16** | 6.03E-5 | (5.96) | **31** | 5.80E-5 | (5.97) | **46** | 4.77E-5 | (6.60) | **61** | 3.34E-5 | (8.58) |
| **2** | 5.13E-5 | (6.37) | **17** | 6.71E-5 | (6.12) | **32** | 6.10E-5 | (6.33) | **47** | 4.75E-5 | (7.17) | **62** | 2.86E-5 | (9.29) |
| **3** | 5.43E-5 | (7.25) | **18** | 6.67E-5 | (5.68) | **33** | 5.96E-5 | (5.88) | **48** | 4.81E-5 | (6.62) | **63** | 2.31E-5 | (10.33) |
| **4** | 5.56E-5 | (6.75) | **19** | 6.85E-5 | (6.04) | **34** | 5.88E-5 | (6.53) | **49** | 4.69E-5 | (7.27) | **64** | 2.13E-5 | (11.59) |
| **5** | 5.78E-5 | (6.02) | **20** | 6.76E-5 | (6.07) | **35** | 5.35E-5 | (6.25) | **50** | 4.69E-5 | (6.74) | **65** | 3.40E-5 | (8.70) |
| **6** | 5.99E-5 | (6.84) | **21** | 6.80E-5 | (6.41) | **36** | 5.41E-5 | (7.28) | **51** | 4.52E-5 | (7.41) | **66** | 3.26E-5 | (8.59) |
| **7** | 6.08E-5 | (5.97) | **22** | 5.79E-5 | (6.54) | **37** | 5.23E-5 | (6.94) | **52** | 3.87E-5 | (7.96) | **67** | 3.34E-5 | (8.58) |
| **8** | 6.27E-5 | (6.32) | **23** | 6.01E-5 | (5.85) | **38** | 5.21E-5 | (6.31) | **53** | 3.41E-5 | (8.42) | **68** | 3.07E-5 | (9.03) |
| **9** | 6.21E-5 | (5.85) | **24** | 6.35E-5 | (6.23) | **39** | 5.33E-5 | (6.87) | **54** | 3.37E-5 | (9.23) | **69** | 2.82E-5 | (9.36) |
| **10** | 6.84E-5 | (6.44) | **25** | 6.41E-5 | (5.66) | **40** | 5.29E-5 | (6.30) | **55** | 2.59E-5 | (11.20) | **70** | 2.62E-5 | (9.81) |
| **11** | 6.00E-5 | (6.46) | **26** | 6.54E-5 | (6.24) | **41** | 5.64E-5 | (6.61) | **56** | 4.25E-5 | (7.66) | **71** | 2.21E-5 | (10.81) |
| **12** | 6.17E-5 | (5.84) | **27** | 6.21E-5 | (5.88) | **42** | 5.24E-5 | (6.33) | **57** | 4.26E-5 | (7.04) | **72** | 2.17E-5 | (10.66) |
| **13** | 6.42E-5 | (6.22) | **28** | 5.58E-5 | (7.01) | **43** | 4.85E-5 | (7.14) | **58** | 4.30E-5 | (7.57) | **73** | 2.08E-5 | (11.06) |
| **14** | 6.57E-5 | (5.61) | **29** | 5.56E-5 | (6.18) | **44** | 4.59E-5 | (6.79) | **59** | 3.93E-5 | (7.26) | **74** | 1.95E-5 | (11.21) |
| **15** | 6.67E-5 | (6.43) | **30** | 6.07E-5 | (6.41) | **45** | 4.20E-5 | (8.51) | **60** | 3.85E-5 | (8.07) | **75** | 1.84E-5 | (11.77) |

Table A.4: 3D Node Averaged Fission Density (SRI) and MCNP % Uncertainty

| Layer 1 | | | | | | | | | | | | |
|---|---|---|---|---|---|---|---|---|---|---|---|---|
| **1** | 8.64E-3 | (0.65) | **16** | 1.17E-2 | (0.50) | **31** | 1.30E-2 | (0.47) | **46** | 1.06E-2 | (0.52) | **61** | 8.70E-3 | (0.61) |
| **2** | 9.54E-3 | (0.55) | **17** | 1.27E-2 | (0.50) | **32** | 1.46E-2 | (0.47) | **47** | 1.08E-2 | (0.54) | **62** | 6.09E-3 | (0.72) |
| **3** | 9.70E-3 | (0.61) | **18** | 1.30E-2 | (0.47) | **33** | 1.48E-2 | (0.44) | **48** | 1.16E-2 | (0.49) | **63** | 4.00E-3 | (0.88) |
| **4** | 9.98E-3 | (0.57) | **19** | 1.40E-2 | (0.48) | **34** | 1.44E-2 | (0.47) | **49** | 1.19E-2 | (0.52) | **64** | 2.54E-3 | (1.11) |
| **5** | 1.06E-2 | (0.52) | **20** | 1.50E-2 | (0.46) | **35** | 1.20E-2 | (0.49) | **50** | 1.24E-2 | (0.48) | **65** | 9.46E-3 | (0.59) |
| **6** | 1.08E-2 | (0.58) | **21** | 1.60E-2 | (0.48) | **36** | 8.60E-3 | (0.64) | **51** | 1.15E-2 | (0.53) | **66** | 9.33E-3 | (0.59) |
| **7** | 1.12E-2 | (0.51) | **22** | 1.05E-2 | (0.55) | **37** | 7.90E-3 | (0.63) | **52** | 9.00E-3 | (0.60) | **67** | 9.04E-3 | (0.60) |
| **8** | 1.18E-2 | (0.52) | **23** | 1.21E-2 | (0.49) | **38** | 1.08E-2 | (0.51) | **53** | 6.54E-3 | (0.70) | **68** | 8.55E-3 | (0.61) |
| **9** | 1.13E-2 | (0.50) | **24** | 1.30E-2 | (0.50) | **39** | 1.19E-2 | (0.52) | **54** | 4.38E-3 | (0.86) | **69** | 7.28E-3 | (0.66) |
| **10** | 9.63E-3 | (0.61) | **25** | 1.44E-2 | (0.45) | **40** | 1.33E-2 | (0.46) | **55** | 2.77E-3 | (1.13) | **70** | 5.23E-3 | (0.77) |
| **11** | 1.12E-2 | (0.54) | **26** | 1.46E-2 | (0.47) | **41** | 1.43E-2 | (0.48) | **56** | 1.15E-2 | (0.53) | **71** | 5.25E-3 | (0.78) |
| **12** | 1.20E-2 | (0.49) | **27** | 1.50E-2 | (0.44) | **42** | 1.30E-2 | (0.47) | **57** | 1.12E-2 | (0.50) | **72** | 5.14E-3 | (0.78) |
| **13** | 1.17E-2 | (0.52) | **28** | 1.34E-2 | (0.52) | **43** | 1.02E-2 | (0.55) | **58** | 1.14E-2 | (0.53) | **73** | 4.92E-3 | (0.80) |
| **14** | 1.02E-2 | (0.52) | **29** | 8.35E-3 | (0.58) | **44** | 6.70E-3 | (0.64) | **59** | 1.10E-2 | (0.51) | **74** | 4.44E-3 | (0.84) |
| **15** | 1.12E-2 | (0.56) | **30** | 1.17E-2 | (0.52) | **45** | 4.71E-3 | (0.86) | **60** | 1.06E-2 | (0.55) | **75** | 3.63E-3 | (0.93) |
| Layer 2 | | | | | | | | | | | | |
| **1** | 4.36E-2 | (0.43) | **16** | 6.43E-2 | (0.36) | **31** | 7.16E-2 | (0.34) | **46** | 5.82E-2 | (0.38) | **61** | 5.24E-2 | (0.40) |
| **2** | 5.21E-2 | (0.40) | **17** | 7.17E-2 | (0.34) | **32** | 8.21E-2 | (0.32) | **47** | 5.35E-2 | (0.36) | **62** | 3.23E-2 | (0.46) |
| **3** | 4.80E-2 | (0.40) | **18** | 7.21E-2 | (0.34) | **33** | 8.18E-2 | (0.32) | **48** | 6.42E-2 | (0.36) | **63** | 2.14E-2 | (0.57) |
| **4** | 4.98E-2 | (0.38) | **19** | 7.99E-2 | (0.32) | **34** | 8.14E-2 | (0.32) | **49** | 5.93E-2 | (0.34) | **64** | 1.34E-2 | (0.72) |
| **5** | 5.85E-2 | (0.38) | **20** | 9.00E-2 | (0.31) | **35** | 6.64E-2 | (0.35) | **50** | 6.91E-2 | (0.35) | **65** | 5.71E-2 | (0.38) |
| **6** | 5.35E-2 | (0.38) | **21** | 9.43E-2 | (0.31) | **36** | 4.92E-2 | (0.43) | **51** | 6.65E-2 | (0.36) | **66** | 5.51E-2 | (0.39) |
| **7** | 6.12E-2 | (0.37) | **22** | 5.27E-2 | (0.37) | **37** | 3.99E-2 | (0.41) | **52** | 5.40E-2 | (0.39) | **67** | 5.42E-2 | (0.39) |
| **8** | 6.63E-2 | (0.36) | **23** | 6.72E-2 | (0.35) | **38** | 5.95E-2 | (0.37) | **53** | 3.90E-2 | (0.46) | **68** | 5.05E-2 | (0.41) |
| **9** | 6.23E-2 | (0.36) | **24** | 6.46E-2 | (0.33) | **39** | 5.91E-2 | (0.34) | **54** | 2.65E-2 | (0.56) | **69** | 4.42E-2 | (0.43) |
| **10** | 5.48E-2 | (0.41) | **25** | 7.95E-2 | (0.32) | **40** | 7.37E-2 | (0.33) | **55** | 1.52E-2 | (0.71) | **70** | 2.86E-2 | (0.49) |
| **11** | 5.63E-2 | (0.35) | **26** | 7.41E-2 | (0.31) | **41** | 8.03E-2 | (0.32) | **56** | 6.68E-2 | (0.36) | **71** | 2.77E-2 | (0.50) |
| **12** | 6.65E-2 | (0.35) | **27** | 8.32E-2 | (0.31) | **42** | 7.21E-2 | (0.34) | **57** | 6.24E-2 | (0.36) | **72** | 2.71E-2 | (0.51) |
| **13** | 5.84E-2 | (0.35) | **28** | 6.63E-2 | (0.34) | **43** | 5.22E-2 | (0.37) | **58** | 6.57E-2 | (0.36) | **73** | 2.60E-2 | (0.52) |
| **14** | 5.68E-2 | (0.37) | **29** | 4.61E-2 | (0.42) | **44** | 3.77E-2 | (0.46) | **59** | 6.17E-2 | (0.37) | **74** | 2.35E-2 | (0.54) |
| **15** | 5.98E-2 | (0.36) | **30** | 6.59E-2 | (0.36) | **45** | 2.48E-2 | (0.55) | **60** | 6.22E-2 | (0.37) | **75** | 1.91E-2 | (0.60) |
| Layer 3 | | | | | | | | | | | | |
| **1** | 6.99E-2 | (0.34) | **16** | 1.02E-1 | (0.29) | **31** | 1.14E-1 | (0.27) | **46** | 9.24E-2 | (0.30) | **61** | 8.50E-2 | (0.31) |
| **2** | 8.30E-2 | (0.32) | **17** | 1.15E-1 | (0.27) | **32** | 1.31E-1 | (0.25) | **47** | 8.57E-2 | (0.29) | **62** | 5.25E-2 | (0.36) |
| **3** | 7.69E-2 | (0.32) | **18** | 1.15E-1 | (0.27) | **33** | 1.30E-1 | (0.25) | **48** | 1.02E-1 | (0.28) | **63** | 3.52E-2 | (0.44) |
| **4** | 8.01E-2 | (0.30) | **19** | 1.29E-1 | (0.26) | **34** | 1.31E-1 | (0.25) | **49** | 9.51E-2 | (0.27) | **64** | 2.22E-2 | (0.56) |
| **5** | 9.33E-2 | (0.30) | **20** | 1.45E-1 | (0.24) | **35** | 1.06E-1 | (0.28) | **50** | 1.10E-1 | (0.27) | **65** | 9.22E-2 | (0.30) |
| **6** | 8.61E-2 | (0.30) | **21** | 1.53E-1 | (0.25) | **36** | 7.92E-2 | (0.34) | **51** | 1.07E-1 | (0.28) | **66** | 8.88E-2 | (0.31) |
| **7** | 9.73E-2 | (0.29) | **22** | 8.50E-2 | (0.29) | **37** | 6.42E-2 | (0.33) | **52** | 8.77E-2 | (0.31) | **67** | 8.76E-2 | (0.31) |
| **8** | 1.06E-1 | (0.28) | **23** | 1.07E-1 | (0.28) | **38** | 9.47E-2 | (0.29) | **53** | 6.39E-2 | (0.36) | **68** | 8.17E-2 | (0.32) |
| **9** | 9.94E-2 | (0.29) | **24** | 1.04E-1 | (0.26) | **39** | 9.47E-2 | (0.27) | **54** | 4.37E-2 | (0.44) | **69** | 7.16E-2 | (0.34) |
| **10** | 8.83E-2 | (0.32) | **25** | 1.27E-1 | (0.25) | **40** | 1.17E-1 | (0.26) | **55** | 2.51E-2 | (0.56) | **70** | 4.63E-2 | (0.39) |
| **11** | 9.04E-2 | (0.28) | **26** | 1.19E-1 | (0.24) | **41** | 1.29E-1 | (0.25) | **56** | 1.08E-1 | (0.28) | **71** | 4.47E-2 | (0.39) |
| **12** | 1.06E-1 | (0.28) | **27** | 1.33E-1 | (0.25) | **42** | 1.15E-1 | (0.27) | **57** | 9.95E-2 | (0.29) | **72** | 4.38E-2 | (0.40) |
| **13** | 9.38E-2 | (0.27) | **28** | 1.07E-1 | (0.27) | **43** | 8.45E-2 | (0.29) | **58** | 1.06E-1 | (0.28) | **73** | 4.19E-2 | (0.41) |

| | | | | | | | | | | | | |
|---|---|---|---|---|---|---|---|---|---|---|---|---|
| **14** | 9.10E-2 | (0.29) | **29** | 7.37E-2 | (0.33) | **44** | 6.07E-2 | (0.36) | **59** | 9.83E-2 | (0.29) | **74** | 3.81E-2 | (0.43) |
| **15** | 9.72E-2 | (0.28) | **30** | 1.06E-1 | (0.28) | **45** | 4.09E-2 | (0.43) | **60** | 1.00E-1 | (0.29) | **75** | 3.11E-2 | (0.47) |
| Layer 4 | | | | | | | | | | | | | | |
| **1** | 8.84E-2 | (0.30) | **16** | 1.30E-1 | (0.25) | **31** | 1.43E-1 | (0.24) | **46** | 1.16E-1 | (0.27) | **61** | 1.07E-1 | (0.28) |
| **2** | 1.05E-1 | (0.28) | **17** | 1.45E-1 | (0.24) | **32** | 1.65E-1 | (0.23) | **47** | 1.08E-1 | (0.26) | **62** | 6.67E-2 | (0.32) |
| **3** | 9.72E-2 | (0.28) | **18** | 1.44E-1 | (0.24) | **33** | 1.63E-1 | (0.23) | **48** | 1.28E-1 | (0.25) | **63** | 4.51E-2 | (0.39) |
| **4** | 1.01E-1 | (0.26) | **19** | 1.62E-1 | (0.23) | **34** | 1.64E-1 | (0.23) | **49** | 1.19E-1 | (0.24) | **64** | 2.89E-2 | (0.49) |
| **5** | 1.18E-1 | (0.26) | **20** | 1.82E-1 | (0.21) | **35** | 1.34E-1 | (0.25) | **50** | 1.38E-1 | (0.25) | **65** | 1.15E-1 | (0.27) |
| **6** | 1.09E-1 | (0.27) | **21** | 1.91E-1 | (0.22) | **36** | 1.01E-1 | (0.30) | **51** | 1.35E-1 | (0.25) | **66** | 1.11E-1 | (0.27) |
| **7** | 1.23E-1 | (0.26) | **22** | 1.08E-1 | (0.26) | **37** | 8.15E-2 | (0.29) | **52** | 1.11E-1 | (0.27) | **67** | 1.09E-1 | (0.28) |
| **8** | 1.34E-1 | (0.25) | **23** | 1.35E-1 | (0.25) | **38** | 1.20E-1 | (0.26) | **53** | 8.20E-2 | (0.32) | **68** | 1.02E-1 | (0.29) |
| **9** | 1.25E-1 | (0.26) | **24** | 1.31E-1 | (0.23) | **39** | 1.19E-1 | (0.24) | **54** | 5.69E-2 | (0.38) | **69** | 8.94E-2 | (0.31) |
| **10** | 1.11E-1 | (0.29) | **25** | 1.59E-1 | (0.23) | **40** | 1.47E-1 | (0.24) | **55** | 3.30E-2 | (0.49) | **70** | 5.80E-2 | (0.35) |
| **11** | 1.14E-1 | (0.25) | **26** | 1.49E-1 | (0.22) | **41** | 1.62E-1 | (0.23) | **56** | 1.34E-1 | (0.25) | **71** | 5.59E-2 | (0.35) |
| **12** | 1.34E-1 | (0.25) | **27** | 1.66E-1 | (0.22) | **42** | 1.44E-1 | (0.24) | **57** | 1.24E-1 | (0.26) | **72** | 5.48E-2 | (0.36) |
| **13** | 1.18E-1 | (0.24) | **28** | 1.34E-1 | (0.24) | **43** | 1.07E-1 | (0.26) | **58** | 1.32E-1 | (0.25) | **73** | 5.24E-2 | (0.36) |
| **14** | 1.14E-1 | (0.26) | **29** | 9.37E-2 | (0.29) | **44** | 7.77E-2 | (0.32) | **59** | 1.23E-1 | (0.26) | **74** | 4.76E-2 | (0.38) |
| **15** | 1.22E-1 | (0.25) | **30** | 1.34E-1 | (0.25) | **45** | 5.30E-2 | (0.38) | **60** | 1.26E-1 | (0.26) | **75** | 3.89E-2 | (0.42) |
| Layer 5 | | | | | | | | | | | | | | |
| **1** | 9.48E-2 | (0.29) | **16** | 1.39E-1 | (0.24) | **31** | 1.52E-1 | (0.23) | **46** | 1.24E-1 | (0.26) | **61** | 1.12E-1 | (0.27) |
| **2** | 1.12E-1 | (0.27) | **17** | 1.55E-1 | (0.23) | **32** | 1.73E-1 | (0.22) | **47** | 1.14E-1 | (0.25) | **62** | 7.16E-2 | (0.31) |
| **3** | 1.04E-1 | (0.27) | **18** | 1.53E-1 | (0.23) | **33** | 1.71E-1 | (0.22) | **48** | 1.35E-1 | (0.25) | **63** | 4.99E-2 | (0.37) |
| **4** | 1.08E-1 | (0.25) | **19** | 1.70E-1 | (0.22) | **34** | 1.72E-1 | (0.22) | **49** | 1.25E-1 | (0.24) | **64** | 3.32E-2 | (0.46) |
| **5** | 1.26E-1 | (0.26) | **20** | 1.90E-1 | (0.21) | **35** | 1.43E-1 | (0.24) | **50** | 1.44E-1 | (0.24) | **65** | 1.19E-1 | (0.27) |
| **6** | 1.15E-1 | (0.26) | **21** | 1.99E-1 | (0.22) | **36** | 1.10E-1 | (0.29) | **51** | 1.41E-1 | (0.24) | **66** | 1.15E-1 | (0.27) |
| **7** | 1.31E-1 | (0.25) | **22** | 1.17E-1 | (0.25) | **37** | 8.89E-2 | (0.28) | **52** | 1.19E-1 | (0.26) | **67** | 1.13E-1 | (0.27) |
| **8** | 1.42E-1 | (0.24) | **23** | 1.45E-1 | (0.24) | **38** | 1.29E-1 | (0.25) | **53** | 9.14E-2 | (0.30) | **68** | 1.05E-1 | (0.28) |
| **9** | 1.34E-1 | (0.25) | **24** | 1.38E-1 | (0.22) | **39** | 1.26E-1 | (0.24) | **54** | 6.53E-2 | (0.36) | **69** | 9.31E-2 | (0.30) |
| **10** | 1.19E-1 | (0.28) | **25** | 1.67E-1 | (0.22) | **40** | 1.55E-1 | (0.23) | **55** | 3.83E-2 | (0.45) | **70** | 6.13E-2 | (0.34) |
| **11** | 1.22E-1 | (0.24) | **26** | 1.56E-1 | (0.21) | **41** | 1.69E-1 | (0.22) | **56** | 1.39E-1 | (0.25) | **71** | 5.88E-2 | (0.34) |
| **12** | 1.43E-1 | (0.24) | **27** | 1.75E-1 | (0.22) | **42** | 1.52E-1 | (0.23) | **57** | 1.30E-1 | (0.25) | **72** | 5.76E-2 | (0.35) |
| **13** | 1.25E-1 | (0.24) | **28** | 1.42E-1 | (0.23) | **43** | 1.15E-1 | (0.25) | **58** | 1.37E-1 | (0.25) | **73** | 5.52E-2 | (0.35) |
| **14** | 1.22E-1 | (0.25) | **29** | 1.03E-1 | (0.28) | **44** | 8.66E-2 | (0.30) | **59** | 1.28E-1 | (0.25) | **74** | 5.03E-2 | (0.37) |
| **15** | 1.28E-1 | (0.24) | **30** | 1.44E-1 | (0.24) | **45** | 6.07E-2 | (0.35) | **60** | 1.30E-1 | (0.25) | **75** | 4.18E-2 | (0.41) |
| Layer 6 | | | | | | | | | | | | | | |
| **1** | 7.61E-2 | (0.30) | **16** | 1.12E-1 | (0.25) | **31** | 1.20E-1 | (0.24) | **46** | 9.95E-2 | (0.26) | **61** | 8.51E-2 | (0.29) |
| **2** | 9.02E-2 | (0.28) | **17** | 1.21E-1 | (0.24) | **32** | 1.33E-1 | (0.23) | **47** | 9.03E-2 | (0.26) | **62** | 5.96E-2 | (0.32) |
| **3** | 8.25E-2 | (0.28) | **18** | 1.20E-1 | (0.24) | **33** | 1.32E-1 | (0.23) | **48** | 1.06E-1 | (0.25) | **63** | 4.42E-2 | (0.37) |
| **4** | 8.55E-2 | (0.26) | **19** | 1.30E-1 | (0.23) | **34** | 1.32E-1 | (0.23) | **49** | 9.65E-2 | (0.25) | **64** | 3.52E-2 | (0.44) |
| **5** | 9.97E-2 | (0.26) | **20** | 1.43E-1 | (0.22) | **35** | 1.14E-1 | (0.25) | **50** | 1.11E-1 | (0.25) | **65** | 8.86E-2 | (0.28) |
| **6** | 9.06E-2 | (0.27) | **21** | 1.49E-1 | (0.23) | **36** | 9.02E-2 | (0.29) | **51** | 1.08E-1 | (0.26) | **66** | 8.58E-2 | (0.29) |
| **7** | 1.04E-1 | (0.26) | **22** | 9.62E-2 | (0.25) | **37** | 7.41E-2 | (0.28) | **52** | 9.51E-2 | (0.27) | **67** | 8.43E-2 | (0.29) |
| **8** | 1.11E-1 | (0.25) | **23** | 1.17E-1 | (0.24) | **38** | 1.05E-1 | (0.26) | **53** | 9.21E-2 | (0.30) | **68** | 7.89E-2 | (0.30) |
| **9** | 1.05E-1 | (0.25) | **24** | 1.08E-1 | (0.23) | **39** | 9.96E-2 | (0.25) | **54** | 7.05E-2 | (0.34) | **69** | 7.11E-2 | (0.32) |
| **10** | 9.15E-2 | (0.29) | **25** | 1.30E-1 | (0.23) | **40** | 1.21E-1 | (0.24) | **55** | 4.15E-2 | (0.43) | **70** | 4.96E-2 | (0.35) |
| **11** | 9.63E-2 | (0.25) | **26** | 1.20E-1 | (0.22) | **41** | 1.28E-1 | (0.23) | **56** | 1.06E-1 | (0.26) | **71** | 4.77E-2 | (0.36) |
| **12** | 1.13E-1 | (0.25) | **27** | 1.35E-1 | (0.22) | **42** | 1.18E-1 | (0.24) | **57** | 9.98E-2 | (0.26) | **72** | 4.67E-2 | (0.36) |
| **13** | 9.84E-2 | (0.25) | **28** | 1.11E-1 | (0.25) | **43** | 9.33E-2 | (0.25) | **58** | 1.03E-1 | (0.26) | **73** | 4.47E-2 | (0.37) |

| | | | | | | | | | | | | |
|---|---|---|---|---|---|---|---|---|---|---|---|---|
| **14** | 9.48E-2 | (0.26) | **29** | 8.85E-2 | (0.27) | **44** | 8.98E-2 | (0.30) | **59** | 9.78E-2 | (0.27) | **74** | 4.13E-2 | (0.38) |
| **15** | 9.65E-2 | (0.26) | **30** | 1.15E-1 | (0.25) | **45** | 6.72E-2 | (0.34) | **60** | 9.80E-2 | (0.27) | **75** | 4.02E-2 | (0.41) |
| Layer 7 | | | | | | | | | | | | | | |
| **1** | 7.05E-2 | (0.31) | **16** | 1.05E-1 | (0.26) | **31** | 1.12E-1 | (0.25) | **46** | 9.41E-2 | (0.27) | **61** | 7.68E-2 | (0.30) |
| **2** | 8.36E-2 | (0.29) | **17** | 1.12E-1 | (0.25) | **32** | 1.20E-1 | (0.24) | **47** | 8.36E-2 | (0.27) | **62** | 5.56E-2 | (0.33) |
| **3** | 7.62E-2 | (0.29) | **18** | 1.11E-1 | (0.25) | **33** | 1.20E-1 | (0.24) | **48** | 9.67E-2 | (0.26) | **63** | 4.28E-2 | (0.37) |
| **4** | 7.89E-2 | (0.27) | **19** | 1.18E-1 | (0.24) | **34** | 1.20E-1 | (0.24) | **49** | 8.70E-2 | (0.26) | **64** | 3.55E-2 | (0.44) |
| **5** | 9.21E-2 | (0.27) | **20** | 1.28E-1 | (0.23) | **35** | 1.08E-1 | (0.25) | **50** | 1.00E-1 | (0.26) | **65** | 7.88E-2 | (0.30) |
| **6** | 8.32E-2 | (0.28) | **21** | 1.34E-1 | (0.24) | **36** | 1.01E-1 | (0.28) | **51** | 9.75E-2 | (0.27) | **66** | 7.62E-2 | (0.30) |
| **7** | 9.62E-2 | (0.27) | **22** | 9.38E-2 | (0.25) | **37** | 8.32E-2 | (0.27) | **52** | 8.89E-2 | (0.28) | **67** | 7.50E-2 | (0.31) |
| **8** | 1.01E-1 | (0.26) | **23** | 1.10E-1 | (0.25) | **38** | 1.00E-1 | (0.26) | **53** | 9.20E-2 | (0.30) | **68** | 7.04E-2 | (0.32) |
| **9** | 9.71E-2 | (0.26) | **24** | 9.97E-2 | (0.24) | **39** | 9.16E-2 | (0.25) | **54** | 7.31E-2 | (0.34) | **69** | 6.37E-2 | (0.33) |
| **10** | 8.41E-2 | (0.30) | **25** | 1.19E-1 | (0.24) | **40** | 1.10E-1 | (0.25) | **55** | 4.28E-2 | (0.43) | **70** | 4.53E-2 | (0.36) |
| **11** | 8.90E-2 | (0.26) | **26** | 1.08E-1 | (0.23) | **41** | 1.16E-1 | (0.25) | **56** | 9.52E-2 | (0.27) | **71** | 4.32E-2 | (0.37) |
| **12** | 1.04E-1 | (0.26) | **27** | 1.23E-1 | (0.23) | **42** | 1.08E-1 | (0.25) | **57** | 9.03E-2 | (0.27) | **72** | 4.24E-2 | (0.37) |
| **13** | 9.01E-2 | (0.26) | **28** | 1.02E-1 | (0.25) | **43** | 8.84E-2 | (0.26) | **58** | 9.25E-2 | (0.27) | **73** | 4.06E-2 | (0.38) |
| **14** | 8.68E-2 | (0.27) | **29** | 1.05E-1 | (0.26) | **44** | 1.04E-1 | (0.28) | **59** | 8.77E-2 | (0.28) | **74** | 3.77E-2 | (0.40) |
| **15** | 8.70E-2 | (0.27) | **30** | 1.11E-1 | (0.25) | **45** | 8.08E-2 | (0.31) | **60** | 8.73E-2 | (0.28) | **75** | 3.73E-2 | (0.43) |
| Layer 8 | | | | | | | | | | | | | | |
| **1** | 6.49E-2 | (0.32) | **16** | 9.71E-2 | (0.26) | **31** | 1.03E-1 | (0.26) | **46** | 8.79E-2 | (0.28) | **61** | 6.98E-2 | (0.32) |
| **2** | 7.69E-2 | (0.30) | **17** | 1.03E-1 | (0.26) | **32** | 1.09E-1 | (0.25) | **47** | 7.71E-2 | (0.28) | **62** | 5.13E-2 | (0.34) |
| **3** | 7.00E-2 | (0.31) | **18** | 1.01E-1 | (0.26) | **33** | 1.09E-1 | (0.25) | **48** | 8.82E-2 | (0.28) | **63** | 4.04E-2 | (0.38) |
| **4** | 7.24E-2 | (0.29) | **19** | 1.07E-1 | (0.26) | **34** | 1.09E-1 | (0.25) | **49** | 7.88E-2 | (0.27) | **64** | 3.43E-2 | (0.45) |
| **5** | 8.43E-2 | (0.28) | **20** | 1.16E-1 | (0.25) | **35** | 1.00E-1 | (0.26) | **50** | 9.03E-2 | (0.27) | **65** | 7.12E-2 | (0.32) |
| **6** | 7.60E-2 | (0.29) | **21** | 1.21E-1 | (0.25) | **36** | 9.83E-2 | (0.28) | **51** | 8.87E-2 | (0.28) | **66** | 6.89E-2 | (0.32) |
| **7** | 8.81E-2 | (0.28) | **22** | 8.93E-2 | (0.26) | **37** | 8.19E-2 | (0.27) | **52** | 8.26E-2 | (0.29) | **67** | 6.75E-2 | (0.32) |
| **8** | 9.28E-2 | (0.27) | **23** | 1.03E-1 | (0.26) | **38** | 9.43E-2 | (0.27) | **53** | 8.81E-2 | (0.31) | **68** | 6.33E-2 | (0.33) |
| **9** | 8.89E-2 | (0.28) | **24** | 9.13E-2 | (0.25) | **39** | 8.40E-2 | (0.27) | **54** | 7.18E-2 | (0.34) | **69** | 5.74E-2 | (0.35) |
| **10** | 7.67E-2 | (0.31) | **25** | 1.08E-1 | (0.25) | **40** | 9.95E-2 | (0.26) | **55** | 4.20E-2 | (0.43) | **70** | 4.11E-2 | (0.38) |
| **11** | 8.17E-2 | (0.27) | **26** | 9.81E-2 | (0.25) | **41** | 1.05E-1 | (0.26) | **56** | 8.69E-2 | (0.29) | **71** | 3.91E-2 | (0.39) |
| **12** | 9.51E-2 | (0.27) | **27** | 1.12E-1 | (0.25) | **42** | 9.89E-2 | (0.26) | **57** | 8.21E-2 | (0.29) | **72** | 3.82E-2 | (0.39) |
| **13** | 8.25E-2 | (0.27) | **28** | 9.34E-2 | (0.27) | **43** | 8.27E-2 | (0.27) | **58** | 8.37E-2 | (0.29) | **73** | 3.66E-2 | (0.40) |
| **14** | 7.91E-2 | (0.28) | **29** | 1.05E-1 | (0.26) | **44** | 1.03E-1 | (0.28) | **59** | 7.91E-2 | (0.29) | **74** | 3.40E-2 | (0.42) |
| **15** | 7.88E-2 | (0.28) | **30** | 1.05E-1 | (0.26) | **45** | 8.15E-2 | (0.31) | **60** | 7.89E-2 | (0.30) | **75** | 3.38E-2 | (0.45) |
| Layer 9 | | | | | | | | | | | | | | |
| **1** | 5.78E-2 | (0.34) | **16** | 8.66E-2 | (0.28) | **31** | 9.11E-2 | (0.27) | **46** | 7.88E-2 | (0.29) | **61** | 6.17E-2 | (0.34) |
| **2** | 6.85E-2 | (0.32) | **17** | 9.13E-2 | (0.28) | **32** | 9.63E-2 | (0.27) | **47** | 6.87E-2 | (0.29) | **62** | 4.59E-2 | (0.36) |
| **3** | 6.21E-2 | (0.33) | **18** | 8.98E-2 | (0.27) | **33** | 9.55E-2 | (0.27) | **48** | 7.81E-2 | (0.29) | **63** | 3.65E-2 | (0.40) |
| **4** | 6.44E-2 | (0.30) | **19** | 9.45E-2 | (0.27) | **34** | 9.67E-2 | (0.27) | **49** | 6.96E-2 | (0.29) | **64** | 3.13E-2 | (0.47) |
| **5** | 7.51E-2 | (0.30) | **20** | 1.02E-1 | (0.26) | **35** | 8.95E-2 | (0.28) | **50** | 7.95E-2 | (0.29) | **65** | 6.31E-2 | (0.33) |
| **6** | 6.78E-2 | (0.31) | **21** | 1.06E-1 | (0.27) | **36** | 8.91E-2 | (0.30) | **51** | 7.84E-2 | (0.30) | **66** | 6.09E-2 | (0.34) |
| **7** | 7.83E-2 | (0.30) | **22** | 8.02E-2 | (0.27) | **37** | 7.41E-2 | (0.28) | **52** | 7.39E-2 | (0.31) | **67** | 5.96E-2 | (0.34) |
| **8** | 8.24E-2 | (0.29) | **23** | 9.16E-2 | (0.27) | **38** | 8.45E-2 | (0.28) | **53** | 8.00E-2 | (0.32) | **68** | 5.59E-2 | (0.35) |
| **9** | 7.92E-2 | (0.29) | **24** | 8.11E-2 | (0.27) | **39** | 7.44E-2 | (0.28) | **54** | 6.57E-2 | (0.36) | **69** | 5.09E-2 | (0.37) |
| **10** | 6.86E-2 | (0.33) | **25** | 9.50E-2 | (0.27) | **40** | 8.77E-2 | (0.28) | **55** | 3.85E-2 | (0.45) | **70** | 3.65E-2 | (0.40) |
| **11** | 7.27E-2 | (0.29) | **26** | 8.63E-2 | (0.26) | **41** | 9.22E-2 | (0.28) | **56** | 7.71E-2 | (0.30) | **71** | 3.46E-2 | (0.42) |
| **12** | 8.45E-2 | (0.28) | **27** | 9.83E-2 | (0.26) | **42** | 8.74E-2 | (0.28) | **57** | 7.27E-2 | (0.31) | **72** | 3.39E-2 | (0.42) |
| **13** | 7.33E-2 | (0.28) | **28** | 8.28E-2 | (0.28) | **43** | 7.41E-2 | (0.28) | **58** | 7.40E-2 | (0.31) | **73** | 3.24E-2 | (0.43) |

| | | | | | | | | | | | | |
|---|---|---|---|---|---|---|---|---|---|---|---|---|
| **14** | 7.03E-2 | (0.30) | **29** | 9.49E-2 | (0.27) | **44** | 9.34E-2 | (0.30) | **59** | 6.99E-2 | (0.31) | **74** | 3.01E-2 | (0.44) |
| **15** | 6.97E-2 | (0.30) | **30** | 9.42E-2 | (0.27) | **45** | 7.45E-2 | (0.32) | **60** | 6.97E-2 | (0.32) | **75** | 3.00E-2 | (0.48) |
| Layer 10 | | | | | | | | | | | | | | |
| **1** | 4.87E-2 | (0.37) | **16** | 7.23E-2 | (0.31) | **31** | 7.56E-2 | (0.30) | **46** | 6.65E-2 | (0.32) | **61** | 5.28E-2 | (0.36) |
| **2** | 5.80E-2 | (0.34) | **17** | 7.61E-2 | (0.30) | **32** | 7.96E-2 | (0.30) | **47** | 5.82E-2 | (0.32) | **62** | 3.90E-2 | (0.39) |
| **3** | 5.31E-2 | (0.35) | **18** | 7.52E-2 | (0.30) | **33** | 7.91E-2 | (0.29) | **48** | 6.57E-2 | (0.32) | **63** | 3.13E-2 | (0.44) |
| **4** | 5.42E-2 | (0.33) | **19** | 7.97E-2 | (0.30) | **34** | 8.01E-2 | (0.30) | **49** | 5.88E-2 | (0.32) | **64** | 2.68E-2 | (0.51) |
| **5** | 6.35E-2 | (0.33) | **20** | 8.56E-2 | (0.28) | **35** | 7.53E-2 | (0.30) | **50** | 6.69E-2 | (0.32) | **65** | 5.38E-2 | (0.36) |
| **6** | 5.73E-2 | (0.34) | **21** | 8.82E-2 | (0.30) | **36** | 7.55E-2 | (0.32) | **51** | 6.58E-2 | (0.33) | **66** | 5.22E-2 | (0.37) |
| **7** | 6.59E-2 | (0.32) | **22** | 6.63E-2 | (0.30) | **37** | 6.27E-2 | (0.31) | **52** | 6.29E-2 | (0.33) | **67** | 5.11E-2 | (0.37) |
| **8** | 6.93E-2 | (0.32) | **23** | 7.61E-2 | (0.30) | **38** | 7.07E-2 | (0.31) | **53** | 6.72E-2 | (0.35) | **68** | 4.80E-2 | (0.38) |
| **9** | 6.76E-2 | (0.32) | **24** | 6.72E-2 | (0.29) | **39** | 6.20E-2 | (0.31) | **54** | 5.50E-2 | (0.39) | **69** | 4.37E-2 | (0.40) |
| **10** | 6.10E-2 | (0.35) | **25** | 7.90E-2 | (0.29) | **40** | 7.31E-2 | (0.30) | **55** | 3.26E-2 | (0.49) | **70** | 3.15E-2 | (0.43) |
| **11** | 6.06E-2 | (0.31) | **26** | 7.14E-2 | (0.29) | **41** | 7.63E-2 | (0.30) | **56** | 6.46E-2 | (0.33) | **71** | 2.99E-2 | (0.45) |
| **12** | 7.10E-2 | (0.31) | **27** | 8.18E-2 | (0.29) | **42** | 7.30E-2 | (0.30) | **57** | 6.13E-2 | (0.33) | **72** | 2.92E-2 | (0.45) |
| **13** | 6.21E-2 | (0.31) | **28** | 6.98E-2 | (0.31) | **43** | 6.29E-2 | (0.31) | **58** | 6.24E-2 | (0.33) | **73** | 2.80E-2 | (0.46) |
| **14** | 6.22E-2 | (0.32) | **29** | 7.78E-2 | (0.30) | **44** | 7.89E-2 | (0.32) | **59** | 5.96E-2 | (0.34) | **74** | 2.59E-2 | (0.48) |
| **15** | 6.10E-2 | (0.32) | **30** | 7.80E-2 | (0.30) | **45** | 6.24E-2 | (0.35) | **60** | 5.95E-2 | (0.34) | **75** | 2.57E-2 | (0.52) |
| Layer 11 | | | | | | | | | | | | | | |
| **1** | 3.33E-2 | (0.41) | **16** | 4.80E-2 | (0.34) | **31** | 5.00E-2 | (0.33) | **46** | 4.58E-2 | (0.35) | **61** | 4.30E-2 | (0.40) |
| **2** | 4.00E-2 | (0.38) | **17** | 5.01E-2 | (0.34) | **32** | 5.20E-2 | (0.34) | **47** | 4.57E-2 | (0.36) | **62** | 2.88E-2 | (0.42) |
| **3** | 4.23E-2 | (0.39) | **18** | 5.08E-2 | (0.33) | **33** | 5.23E-2 | (0.33) | **48** | 4.54E-2 | (0.35) | **63** | 2.51E-2 | (0.49) |
| **4** | 3.65E-2 | (0.37) | **19** | 5.48E-2 | (0.33) | **34** | 5.27E-2 | (0.33) | **49** | 4.66E-2 | (0.35) | **64** | 1.94E-2 | (0.55) |
| **5** | 4.37E-2 | (0.36) | **20** | 5.86E-2 | (0.32) | **35** | 5.23E-2 | (0.33) | **50** | 4.61E-2 | (0.35) | **65** | 4.41E-2 | (0.40) |
| **6** | 3.92E-2 | (0.38) | **21** | 5.83E-2 | (0.34) | **36** | 5.90E-2 | (0.36) | **51** | 4.48E-2 | (0.36) | **66** | 4.28E-2 | (0.40) |
| **7** | 4.43E-2 | (0.36) | **22** | 4.29E-2 | (0.34) | **37** | 4.90E-2 | (0.35) | **52** | 4.96E-2 | (0.37) | **67** | 4.21E-2 | (0.41) |
| **8** | 4.63E-2 | (0.36) | **23** | 5.01E-2 | (0.33) | **38** | 4.83E-2 | (0.34) | **53** | 4.45E-2 | (0.40) | **68** | 4.03E-2 | (0.42) |
| **9** | 4.78E-2 | (0.34) | **24** | 4.44E-2 | (0.33) | **39** | 4.13E-2 | (0.35) | **54** | 3.56E-2 | (0.45) | **69** | 3.63E-2 | (0.44) |
| **10** | 5.91E-2 | (0.36) | **25** | 5.27E-2 | (0.33) | **40** | 4.92E-2 | (0.34) | **55** | 2.22E-2 | (0.55) | **70** | 2.63E-2 | (0.47) |
| **11** | 4.05E-2 | (0.35) | **26** | 4.73E-2 | (0.33) | **41** | 5.00E-2 | (0.34) | **56** | 4.39E-2 | (0.37) | **71** | 2.51E-2 | (0.49) |
| **12** | 4.78E-2 | (0.34) | **27** | 5.52E-2 | (0.32) | **42** | 4.91E-2 | (0.34) | **57** | 4.26E-2 | (0.36) | **72** | 2.46E-2 | (0.49) |
| **13** | 4.34E-2 | (0.34) | **28** | 5.45E-2 | (0.34) | **43** | 4.95E-2 | (0.34) | **58** | 4.32E-2 | (0.37) | **73** | 2.36E-2 | (0.50) |
| **14** | 6.03E-2 | (0.33) | **29** | 5.03E-2 | (0.34) | **44** | 5.31E-2 | (0.36) | **59** | 4.91E-2 | (0.37) | **74** | 2.17E-2 | (0.52) |
| **15** | 5.70E-2 | (0.34) | **30** | 5.02E-2 | (0.34) | **45** | 4.06E-2 | (0.40) | **60** | 4.90E-2 | (0.38) | **75** | 1.91E-2 | (0.56) |
| Layer 12 | | | | | | | | | | | | | | |
| **1** | 2.71E-2 | (0.46) | **16** | 3.83E-2 | (0.38) | **31** | 3.97E-2 | (0.37) | **46** | 3.68E-2 | (0.39) | **61** | 3.52E-2 | (0.44) |
| **2** | 3.28E-2 | (0.41) | **17** | 4.00E-2 | (0.38) | **32** | 4.12E-2 | (0.38) | **47** | 3.71E-2 | (0.39) | **62** | 2.33E-2 | (0.47) |
| **3** | 3.50E-2 | (0.43) | **18** | 4.12E-2 | (0.37) | **33** | 4.15E-2 | (0.36) | **48** | 3.66E-2 | (0.39) | **63** | 2.04E-2 | (0.54) |
| **4** | 2.97E-2 | (0.41) | **19** | 4.46E-2 | (0.36) | **34** | 4.18E-2 | (0.37) | **49** | 3.81E-2 | (0.39) | **64** | 1.56E-2 | (0.62) |
| **5** | 3.58E-2 | (0.39) | **20** | 4.75E-2 | (0.35) | **35** | 4.20E-2 | (0.37) | **50** | 3.72E-2 | (0.39) | **65** | 3.62E-2 | (0.44) |
| **6** | 3.22E-2 | (0.42) | **21** | 4.67E-2 | (0.37) | **36** | 4.76E-2 | (0.40) | **51** | 3.58E-2 | (0.41) | **66** | 3.53E-2 | (0.44) |
| **7** | 3.60E-2 | (0.39) | **22** | 3.36E-2 | (0.38) | **37** | 3.94E-2 | (0.38) | **52** | 4.00E-2 | (0.42) | **67** | 3.47E-2 | (0.45) |
| **8** | 3.77E-2 | (0.39) | **23** | 3.97E-2 | (0.37) | **38** | 3.85E-2 | (0.38) | **53** | 3.51E-2 | (0.45) | **68** | 3.32E-2 | (0.46) |
| **9** | 3.98E-2 | (0.37) | **24** | 3.53E-2 | (0.37) | **39** | 3.28E-2 | (0.39) | **54** | 2.79E-2 | (0.50) | **69** | 2.99E-2 | (0.48) |
| **10** | 5.21E-2 | (0.38) | **25** | 4.23E-2 | (0.36) | **40** | 3.93E-2 | (0.38) | **55** | 1.75E-2 | (0.61) | **70** | 2.18E-2 | (0.52) |
| **11** | 3.25E-2 | (0.39) | **26** | 3.77E-2 | (0.36) | **41** | 3.96E-2 | (0.38) | **56** | 3.51E-2 | (0.41) | **71** | 2.08E-2 | (0.54) |
| **12** | 3.88E-2 | (0.38) | **27** | 4.41E-2 | (0.36) | **42** | 3.92E-2 | (0.38) | **57** | 3.44E-2 | (0.40) | **72** | 2.03E-2 | (0.54) |
| **13** | 3.58E-2 | (0.37) | **28** | 4.40E-2 | (0.38) | **43** | 3.99E-2 | (0.38) | **58** | 3.49E-2 | (0.41) | **73** | 1.95E-2 | (0.55) |

| | | | | | | | | | | | | |
|---|---|---|---|---|---|---|---|---|---|---|---|---|
| **14** | 5.26E-2 | (0.36) | **29** | 3.91E-2 | (0.38) | **44** | 4.22E-2 | (0.40) | **59** | 4.03E-2 | (0.41) | **74** | 1.79E-2 | (0.57) |
| **15** | 4.93E-2 | (0.36) | **30** | 3.94E-2 | (0.38) | **45** | 3.18E-2 | (0.45) | **60** | 4.03E-2 | (0.42) | **75** | 1.57E-2 | (0.62) |
| Layer 13 | | | | | | | | | | | | | | |
| **1** | 2.25E-2 | (0.50) | **16** | 3.13E-2 | (0.42) | **31** | 3.22E-2 | (0.41) | **46** | 2.98E-2 | (0.44) | **61** | 2.87E-2 | (0.49) |
| **2** | 2.73E-2 | (0.45) | **17** | 3.28E-2 | (0.42) | **32** | 3.35E-2 | (0.42) | **47** | 3.01E-2 | (0.44) | **62** | 1.89E-2 | (0.52) |
| **3** | 2.92E-2 | (0.47) | **18** | 3.39E-2 | (0.40) | **33** | 3.37E-2 | (0.40) | **48** | 2.98E-2 | (0.43) | **63** | 1.64E-2 | (0.60) |
| **4** | 2.46E-2 | (0.45) | **19** | 3.68E-2 | (0.40) | **34** | 3.38E-2 | (0.42) | **49** | 3.09E-2 | (0.43) | **64** | 1.26E-2 | (0.69) |
| **5** | 2.98E-2 | (0.43) | **20** | 3.91E-2 | (0.39) | **35** | 3.39E-2 | (0.41) | **50** | 3.02E-2 | (0.43) | **65** | 2.95E-2 | (0.49) |
| **6** | 2.68E-2 | (0.45) | **21** | 3.82E-2 | (0.41) | **36** | 3.84E-2 | (0.45) | **51** | 2.91E-2 | (0.45) | **66** | 2.88E-2 | (0.49) |
| **7** | 2.98E-2 | (0.43) | **22** | 2.72E-2 | (0.43) | **37** | 3.18E-2 | (0.43) | **52** | 3.23E-2 | (0.46) | **67** | 2.83E-2 | (0.50) |
| **8** | 3.12E-2 | (0.43) | **23** | 3.23E-2 | (0.41) | **38** | 3.12E-2 | (0.42) | **53** | 2.82E-2 | (0.50) | **68** | 2.71E-2 | (0.51) |
| **9** | 3.32E-2 | (0.41) | **24** | 2.89E-2 | (0.41) | **39** | 2.66E-2 | (0.43) | **54** | 2.24E-2 | (0.56) | **69** | 2.44E-2 | (0.54) |
| **10** | 4.36E-2 | (0.42) | **25** | 3.46E-2 | (0.40) | **40** | 3.20E-2 | (0.42) | **55** | 1.40E-2 | (0.69) | **70** | 1.78E-2 | (0.58) |
| **11** | 2.67E-2 | (0.43) | **26** | 3.08E-2 | (0.40) | **41** | 3.21E-2 | (0.43) | **56** | 2.85E-2 | (0.46) | **71** | 1.70E-2 | (0.59) |
| **12** | 3.19E-2 | (0.42) | **27** | 3.59E-2 | (0.39) | **42** | 3.17E-2 | (0.42) | **57** | 2.80E-2 | (0.45) | **72** | 1.66E-2 | (0.60) |
| **13** | 2.97E-2 | (0.41) | **28** | 3.57E-2 | (0.43) | **43** | 3.22E-2 | (0.43) | **58** | 2.85E-2 | (0.46) | **73** | 1.59E-2 | (0.61) |
| **14** | 4.39E-2 | (0.39) | **29** | 3.15E-2 | (0.42) | **44** | 3.41E-2 | (0.45) | **59** | 3.28E-2 | (0.45) | **74** | 1.46E-2 | (0.64) |
| **15** | 4.10E-2 | (0.40) | **30** | 3.19E-2 | (0.43) | **45** | 2.55E-2 | (0.51) | **60** | 3.28E-2 | (0.46) | **75** | 1.28E-2 | (0.68) |
| Layer 14 | | | | | | | | | | | | | | |
| **1** | 1.86E-2 | (0.55) | **16** | 2.55E-2 | (0.47) | **31** | 2.60E-2 | (0.46) | **46** | 2.39E-2 | (0.49) | **61** | 2.29E-2 | (0.55) |
| **2** | 2.25E-2 | (0.50) | **17** | 2.67E-2 | (0.47) | **32** | 2.71E-2 | (0.46) | **47** | 2.41E-2 | (0.49) | **62** | 1.51E-2 | (0.58) |
| **3** | 2.40E-2 | (0.52) | **18** | 2.77E-2 | (0.45) | **33** | 2.73E-2 | (0.45) | **48** | 2.39E-2 | (0.48) | **63** | 1.32E-2 | (0.67) |
| **4** | 2.03E-2 | (0.49) | **19** | 3.01E-2 | (0.44) | **34** | 2.72E-2 | (0.46) | **49** | 2.49E-2 | (0.48) | **64** | 1.00E-2 | (0.77) |
| **5** | 2.46E-2 | (0.47) | **20** | 3.19E-2 | (0.43) | **35** | 2.73E-2 | (0.46) | **50** | 2.42E-2 | (0.48) | **65** | 2.36E-2 | (0.54) |
| **6** | 2.21E-2 | (0.50) | **21** | 3.10E-2 | (0.46) | **36** | 3.07E-2 | (0.50) | **51** | 2.32E-2 | (0.50) | **66** | 2.30E-2 | (0.55) |
| **7** | 2.45E-2 | (0.48) | **22** | 2.21E-2 | (0.47) | **37** | 2.56E-2 | (0.48) | **52** | 2.59E-2 | (0.52) | **67** | 2.27E-2 | (0.55) |
| **8** | 2.57E-2 | (0.47) | **23** | 2.62E-2 | (0.46) | **38** | 2.52E-2 | (0.47) | **53** | 2.25E-2 | (0.56) | **68** | 2.17E-2 | (0.57) |
| **9** | 2.73E-2 | (0.45) | **24** | 2.34E-2 | (0.46) | **39** | 2.14E-2 | (0.48) | **54** | 1.78E-2 | (0.63) | **69** | 1.95E-2 | (0.60) |
| **10** | 3.59E-2 | (0.46) | **25** | 2.81E-2 | (0.44) | **40** | 2.57E-2 | (0.46) | **55** | 1.12E-2 | (0.77) | **70** | 1.43E-2 | (0.64) |
| **11** | 2.19E-2 | (0.48) | **26** | 2.50E-2 | (0.44) | **41** | 2.58E-2 | (0.47) | **56** | 2.28E-2 | (0.51) | **71** | 1.35E-2 | (0.67) |
| **12** | 2.62E-2 | (0.46) | **27** | 2.91E-2 | (0.44) | **42** | 2.55E-2 | (0.47) | **57** | 2.25E-2 | (0.50) | **72** | 1.33E-2 | (0.67) |
| **13** | 2.44E-2 | (0.45) | **28** | 2.88E-2 | (0.47) | **43** | 2.58E-2 | (0.48) | **58** | 2.28E-2 | (0.51) | **73** | 1.28E-2 | (0.68) |
| **14** | 3.61E-2 | (0.43) | **29** | 2.53E-2 | (0.47) | **44** | 2.71E-2 | (0.50) | **59** | 2.63E-2 | (0.51) | **74** | 1.18E-2 | (0.71) |
| **15** | 3.36E-2 | (0.44) | **30** | 2.57E-2 | (0.47) | **45** | 2.03E-2 | (0.57) | **60** | 2.63E-2 | (0.52) | **75** | 1.03E-2 | (0.76) |
| Layer 15 | | | | | | | | | | | | | | |
| **1** | 1.51E-2 | (0.61) | **16** | 2.06E-2 | (0.52) | **31** | 2.10E-2 | (0.51) | **46** | 1.88E-2 | (0.55) | **61** | 1.77E-2 | (0.63) |
| **2** | 1.83E-2 | (0.55) | **17** | 2.15E-2 | (0.52) | **32** | 2.18E-2 | (0.52) | **47** | 1.88E-2 | (0.55) | **62** | 1.18E-2 | (0.66) |
| **3** | 1.93E-2 | (0.57) | **18** | 2.23E-2 | (0.50) | **33** | 2.18E-2 | (0.50) | **48** | 1.88E-2 | (0.54) | **63** | 1.02E-2 | (0.76) |
| **4** | 1.66E-2 | (0.55) | **19** | 2.42E-2 | (0.49) | **34** | 2.16E-2 | (0.52) | **49** | 1.93E-2 | (0.55) | **64** | 7.89E-3 | (0.87) |
| **5** | 2.00E-2 | (0.53) | **20** | 2.56E-2 | (0.48) | **35** | 2.14E-2 | (0.51) | **50** | 1.90E-2 | (0.54) | **65** | 1.80E-2 | (0.62) |
| **6** | 1.81E-2 | (0.55) | **21** | 2.49E-2 | (0.51) | **36** | 2.36E-2 | (0.57) | **51** | 1.82E-2 | (0.57) | **66** | 1.76E-2 | (0.63) |
| **7** | 2.00E-2 | (0.53) | **22** | 1.78E-2 | (0.53) | **37** | 1.99E-2 | (0.54) | **52** | 1.98E-2 | (0.59) | **67** | 1.73E-2 | (0.63) |
| **8** | 2.09E-2 | (0.53) | **23** | 2.11E-2 | (0.51) | **38** | 2.00E-2 | (0.53) | **53** | 1.72E-2 | (0.64) | **68** | 1.66E-2 | (0.65) |
| **9** | 2.21E-2 | (0.50) | **24** | 1.88E-2 | (0.51) | **39** | 1.71E-2 | (0.54) | **54** | 1.39E-2 | (0.71) | **69** | 1.52E-2 | (0.68) |
| **10** | 2.85E-2 | (0.52) | **25** | 2.26E-2 | (0.49) | **40** | 2.04E-2 | (0.52) | **55** | 8.84E-3 | (0.86) | **70** | 1.10E-2 | (0.73) |
| **11** | 1.78E-2 | (0.53) | **26** | 2.01E-2 | (0.50) | **41** | 2.05E-2 | (0.53) | **56** | 1.79E-2 | (0.58) | **71** | 1.04E-2 | (0.76) |
| **12** | 2.13E-2 | (0.51) | **27** | 2.32E-2 | (0.49) | **42** | 2.01E-2 | (0.53) | **57** | 1.76E-2 | (0.57) | **72** | 1.02E-2 | (0.76) |
| **13** | 1.97E-2 | (0.50) | **28** | 2.26E-2 | (0.53) | **43** | 1.99E-2 | (0.54) | **58** | 1.77E-2 | (0.58) | **73** | 9.82E-3 | (0.77) |

| | | | | | | | | | | | | |
|---|---|---|---|---|---|---|---|---|---|---|---|---|
| **14** | 2.87E-2 | (0.48) | **29** | 2.02E-2 | (0.53) | **44** | 2.08E-2 | (0.57) | **59** | 2.02E-2 | (0.57) | **74** | 9.07E-3 | (0.81) |
| **15** | 2.65E-2 | (0.49) | **30** | 2.07E-2 | (0.53) | **45** | 1.58E-2 | (0.64) | **60** | 2.01E-2 | (0.59) | **75** | 8.13E-3 | (0.85) |
| Layer 16 | | | | | | | | | | | | | | |
| **1** | 1.23E-2 | (0.68) | **16** | 1.67E-2 | (0.58) | **31** | 1.66E-2 | (0.58) | **46** | 1.43E-2 | (0.63) | **61** | 1.12E-2 | (0.73) |
| **2** | 1.47E-2 | (0.62) | **17** | 1.74E-2 | (0.58) | **32** | 1.73E-2 | (0.58) | **47** | 1.25E-2 | (0.63) | **62** | 8.63E-3 | (0.77) |
| **3** | 1.33E-2 | (0.65) | **18** | 1.79E-2 | (0.55) | **33** | 1.73E-2 | (0.56) | **48** | 1.42E-2 | (0.62) | **63** | 6.88E-3 | (0.86) |
| **4** | 1.34E-2 | (0.61) | **19** | 1.90E-2 | (0.55) | **34** | 1.69E-2 | (0.59) | **49** | 1.26E-2 | (0.63) | **64** | 6.09E-3 | (0.99) |
| **5** | 1.59E-2 | (0.59) | **20** | 2.00E-2 | (0.54) | **35** | 1.59E-2 | (0.59) | **50** | 1.43E-2 | (0.62) | **65** | 1.12E-2 | (0.73) |
| **6** | 1.45E-2 | (0.62) | **21** | 1.97E-2 | (0.58) | **36** | 1.50E-2 | (0.66) | **51** | 1.36E-2 | (0.65) | **66** | 1.09E-2 | (0.73) |
| **7** | 1.62E-2 | (0.59) | **22** | 1.42E-2 | (0.59) | **37** | 1.33E-2 | (0.61) | **52** | 1.24E-2 | (0.69) | **67** | 1.07E-2 | (0.74) |
| **8** | 1.69E-2 | (0.59) | **23** | 1.69E-2 | (0.57) | **38** | 1.53E-2 | (0.60) | **53** | 1.08E-2 | (0.74) | **68** | 1.02E-2 | (0.76) |
| **9** | 1.76E-2 | (0.56) | **24** | 1.51E-2 | (0.57) | **39** | 1.35E-2 | (0.60) | **54** | 1.06E-2 | (0.81) | **69** | 1.11E-2 | (0.79) |
| **10** | 1.88E-2 | (0.59) | **25** | 1.81E-2 | (0.55) | **40** | 1.59E-2 | (0.59) | **55** | 6.81E-3 | (0.98) | **70** | 7.34E-3 | (0.83) |
| **11** | 1.44E-2 | (0.59) | **26** | 1.60E-2 | (0.56) | **41** | 1.61E-2 | (0.60) | **56** | 1.35E-2 | (0.66) | **71** | 6.79E-3 | (0.87) |
| **12** | 1.72E-2 | (0.57) | **27** | 1.81E-2 | (0.55) | **42** | 1.54E-2 | (0.60) | **57** | 1.31E-2 | (0.65) | **72** | 6.67E-3 | (0.87) |
| **13** | 1.56E-2 | (0.56) | **28** | 1.51E-2 | (0.61) | **43** | 1.27E-2 | (0.63) | **58** | 1.30E-2 | (0.67) | **73** | 6.42E-3 | (0.89) |
| **14** | 1.91E-2 | (0.54) | **29** | 1.59E-2 | (0.59) | **44** | 1.32E-2 | (0.65) | **59** | 1.28E-2 | (0.66) | **74** | 6.00E-3 | (0.92) |
| **15** | 1.76E-2 | (0.56) | **30** | 1.64E-2 | (0.59) | **45** | 1.18E-2 | (0.74) | **60** | 1.28E-2 | (0.68) | **75** | 6.21E-3 | (0.98) |
| Layer 17 | | | | | | | | | | | | | | |
| **1** | 9.96E-3 | (0.75) | **16** | 1.33E-2 | (0.65) | **31** | 1.31E-2 | (0.65) | **46** | 1.10E-2 | (0.71) | **61** | 8.36E-3 | (0.84) |
| **2** | 1.18E-2 | (0.68) | **17** | 1.39E-2 | (0.65) | **32** | 1.36E-2 | (0.65) | **47** | 9.54E-3 | (0.72) | **62** | 6.59E-3 | (0.88) |
| **3** | 1.06E-2 | (0.72) | **18** | 1.43E-2 | (0.62) | **33** | 1.36E-2 | (0.64) | **48** | 1.11E-2 | (0.71) | **63** | 5.21E-3 | (0.99) |
| **4** | 1.08E-2 | (0.68) | **19** | 1.50E-2 | (0.62) | **34** | 1.33E-2 | (0.66) | **49** | 9.62E-3 | (0.72) | **64** | 4.70E-3 | (1.12) |
| **5** | 1.28E-2 | (0.65) | **20** | 1.58E-2 | (0.61) | **35** | 1.23E-2 | (0.67) | **50** | 1.09E-2 | (0.71) | **65** | 8.33E-3 | (0.84) |
| **6** | 1.17E-2 | (0.69) | **21** | 1.56E-2 | (0.65) | **36** | 1.13E-2 | (0.76) | **51** | 1.04E-2 | (0.75) | **66** | 8.14E-3 | (0.85) |
| **7** | 1.30E-2 | (0.65) | **22** | 1.13E-2 | (0.66) | **37** | 1.02E-2 | (0.70) | **52** | 9.37E-3 | (0.79) | **67** | 7.96E-3 | (0.85) |
| **8** | 1.36E-2 | (0.65) | **23** | 1.35E-2 | (0.64) | **38** | 1.20E-2 | (0.68) | **53** | 8.11E-3 | (0.85) | **68** | 7.67E-3 | (0.87) |
| **9** | 1.40E-2 | (0.63) | **24** | 1.20E-2 | (0.64) | **39** | 1.06E-2 | (0.68) | **54** | 8.20E-3 | (0.92) | **69** | 8.44E-3 | (0.90) |
| **10** | 1.47E-2 | (0.66) | **25** | 1.43E-2 | (0.62) | **40** | 1.25E-2 | (0.67) | **55** | 5.28E-3 | (1.12) | **70** | 5.57E-3 | (0.95) |
| **11** | 1.16E-2 | (0.65) | **26** | 1.26E-2 | (0.62) | **41** | 1.26E-2 | (0.68) | **56** | 1.03E-2 | (0.75) | **71** | 5.13E-3 | (1.00) |
| **12** | 1.38E-2 | (0.63) | **27** | 1.43E-2 | (0.62) | **42** | 1.19E-2 | (0.68) | **57** | 9.94E-3 | (0.74) | **72** | 5.04E-3 | (1.00) |
| **13** | 1.24E-2 | (0.63) | **28** | 1.16E-2 | (0.69) | **43** | 9.58E-3 | (0.72) | **58** | 9.93E-3 | (0.76) | **73** | 4.85E-3 | (1.02) |
| **14** | 1.50E-2 | (0.61) | **29** | 1.25E-2 | (0.67) | **44** | 9.98E-3 | (0.75) | **59** | 9.64E-3 | (0.76) | **74** | 4.54E-3 | (1.06) |
| **15** | 1.37E-2 | (0.64) | **30** | 1.30E-2 | (0.67) | **45** | 9.12E-3 | (0.84) | **60** | 9.56E-3 | (0.78) | **75** | 4.72E-3 | (1.12) |
| Layer 18 | | | | | | | | | | | | | | |
| **1** | 7.94E-3 | (0.84) | **16** | 1.06E-2 | (0.72) | **31** | 1.04E-2 | (0.73) | **46** | 8.54E-3 | (0.81) | **61** | 6.45E-3 | (0.95) |
| **2** | 9.46E-3 | (0.77) | **17** | 1.10E-2 | (0.72) | **32** | 1.07E-2 | (0.74) | **47** | 7.40E-3 | (0.81) | **62** | 5.06E-3 | (1.00) |
| **3** | 8.46E-3 | (0.81) | **18** | 1.13E-2 | (0.70) | **33** | 1.06E-2 | (0.72) | **48** | 8.58E-3 | (0.80) | **63** | 4.02E-3 | (1.12) |
| **4** | 8.64E-3 | (0.76) | **19** | 1.19E-2 | (0.70) | **34** | 1.04E-2 | (0.75) | **49** | 7.47E-3 | (0.81) | **64** | 3.64E-3 | (1.28) |
| **5** | 1.02E-2 | (0.73) | **20** | 1.25E-2 | (0.68) | **35** | 9.53E-3 | (0.76) | **50** | 8.40E-3 | (0.81) | **65** | 6.40E-3 | (0.96) |
| **6** | 9.26E-3 | (0.77) | **21** | 1.22E-2 | (0.73) | **36** | 8.73E-3 | (0.86) | **51** | 8.01E-3 | (0.85) | **66** | 6.23E-3 | (0.97) |
| **7** | 1.04E-2 | (0.73) | **22** | 8.96E-3 | (0.74) | **37** | 8.00E-3 | (0.79) | **52** | 7.23E-3 | (0.90) | **67** | 6.14E-3 | (0.97) |
| **8** | 1.08E-2 | (0.73) | **23** | 1.06E-2 | (0.72) | **38** | 9.38E-3 | (0.77) | **53** | 6.26E-3 | (0.97) | **68** | 5.90E-3 | (1.00) |
| **9** | 1.12E-2 | (0.70) | **24** | 9.49E-3 | (0.72) | **39** | 8.28E-3 | (0.77) | **54** | 6.30E-3 | (1.05) | **69** | 6.50E-3 | (1.03) |
| **10** | 1.17E-2 | (0.75) | **25** | 1.13E-2 | (0.70) | **40** | 9.70E-3 | (0.75) | **55** | 4.12E-3 | (1.26) | **70** | 4.28E-3 | (1.09) |
| **11** | 9.17E-3 | (0.73) | **26** | 9.95E-3 | (0.70) | **41** | 9.78E-3 | (0.77) | **56** | 7.94E-3 | (0.86) | **71** | 3.95E-3 | (1.13) |
| **12** | 1.10E-2 | (0.71) | **27** | 1.12E-2 | (0.70) | **42** | 9.28E-3 | (0.77) | **57** | 7.66E-3 | (0.85) | **72** | 3.91E-3 | (1.14) |
| **13** | 9.84E-3 | (0.71) | **28** | 9.07E-3 | (0.78) | **43** | 7.39E-3 | (0.82) | **58** | 7.70E-3 | (0.87) | **73** | 3.74E-3 | (1.16) |

| | | | | | | | | | | | | |
|---|---|---|---|---|---|---|---|---|---|---|---|---|
| **14** | 1.19E-2 | (0.68) | **29** | 9.86E-3 | (0.75) | **44** | 7.70E-3 | (0.85) | **59** | 7.42E-3 | (0.86) | **74** | 3.51E-3 | (1.20) |
| **15** | 1.08E-2 | (0.72) | **30** | 1.02E-2 | (0.75) | **45** | 7.04E-3 | (0.96) | **60** | 7.29E-3 | (0.90) | **75** | 3.63E-3 | (1.28) |
| Layer 19 | | | | | | | | | | | | | | |
| **1** | 6.30E-3 | (0.94) | **16** | 8.37E-3 | (0.82) | **31** | 8.09E-3 | (0.83) | **46** | 6.61E-3 | (0.92) | **61** | 4.93E-3 | (1.09) |
| **2** | 7.51E-3 | (0.86) | **17** | 8.68E-3 | (0.82) | **32** | 8.34E-3 | (0.83) | **47** | 5.70E-3 | (0.93) | **62** | 3.88E-3 | (1.14) |
| **3** | 6.71E-3 | (0.91) | **18** | 8.87E-3 | (0.79) | **33** | 8.27E-3 | (0.82) | **48** | 6.62E-3 | (0.91) | **63** | 3.08E-3 | (1.29) |
| **4** | 6.83E-3 | (0.85) | **19** | 9.33E-3 | (0.79) | **34** | 8.06E-3 | (0.85) | **49** | 5.72E-3 | (0.93) | **64** | 2.80E-3 | (1.45) |
| **5** | 8.09E-3 | (0.82) | **20** | 9.80E-3 | (0.77) | **35** | 7.36E-3 | (0.87) | **50** | 6.49E-3 | (0.92) | **65** | 4.90E-3 | (1.09) |
| **6** | 7.32E-3 | (0.87) | **21** | 9.58E-3 | (0.82) | **36** | 6.75E-3 | (0.98) | **51** | 6.14E-3 | (0.97) | **66** | 4.78E-3 | (1.10) |
| **7** | 8.19E-3 | (0.82) | **22** | 7.06E-3 | (0.84) | **37** | 6.22E-3 | (0.89) | **52** | 5.51E-3 | (1.03) | **67** | 4.69E-3 | (1.11) |
| **8** | 8.56E-3 | (0.82) | **23** | 8.40E-3 | (0.81) | **38** | 7.26E-3 | (0.87) | **53** | 4.77E-3 | (1.11) | **68** | 4.52E-3 | (1.14) |
| **9** | 8.77E-3 | (0.79) | **24** | 7.43E-3 | (0.81) | **39** | 6.41E-3 | (0.88) | **54** | 4.83E-3 | (1.20) | **69** | 4.97E-3 | (1.18) |
| **10** | 9.20E-3 | (0.84) | **25** | 8.80E-3 | (0.79) | **40** | 7.54E-3 | (0.86) | **55** | 3.12E-3 | (1.45) | **70** | 3.27E-3 | (1.24) |
| **11** | 7.21E-3 | (0.83) | **26** | 7.78E-3 | (0.80) | **41** | 7.56E-3 | (0.88) | **56** | 6.09E-3 | (0.98) | **71** | 3.03E-3 | (1.30) |
| **12** | 8.65E-3 | (0.80) | **27** | 8.66E-3 | (0.80) | **42** | 7.14E-3 | (0.88) | **57** | 5.88E-3 | (0.97) | **72** | 2.97E-3 | (1.30) |
| **13** | 7.71E-3 | (0.80) | **28** | 6.99E-3 | (0.89) | **43** | 5.70E-3 | (0.93) | **58** | 5.91E-3 | (0.99) | **73** | 2.86E-3 | (1.33) |
| **14** | 9.32E-3 | (0.77) | **29** | 7.68E-3 | (0.85) | **44** | 5.91E-3 | (0.97) | **59** | 5.72E-3 | (0.98) | **74** | 2.67E-3 | (1.38) |
| **15** | 8.44E-3 | (0.81) | **30** | 8.00E-3 | (0.85) | **45** | 5.37E-3 | (1.10) | **60** | 5.63E-3 | (1.02) | **75** | 2.80E-3 | (1.45) |
| Layer 20 | | | | | | | | | | | | | | |
| **1** | 4.91E-3 | (1.07) | **16** | 6.46E-3 | (0.93) | **31** | 6.23E-3 | (0.94) | **46** | 5.07E-3 | (1.05) | **61** | 3.72E-3 | (1.25) |
| **2** | 5.85E-3 | (0.97) | **17** | 6.72E-3 | (0.93) | **32** | 6.40E-3 | (0.95) | **47** | 4.38E-3 | (1.06) | **62** | 2.94E-3 | (1.31) |
| **3** | 5.22E-3 | (1.03) | **18** | 6.89E-3 | (0.89) | **33** | 6.36E-3 | (0.93) | **48** | 5.01E-3 | (1.05) | **63** | 2.35E-3 | (1.47) |
| **4** | 5.31E-3 | (0.97) | **19** | 7.25E-3 | (0.89) | **34** | 6.17E-3 | (0.97) | **49** | 4.35E-3 | (1.06) | **64** | 2.11E-3 | (1.67) |
| **5** | 6.32E-3 | (0.93) | **20** | 7.52E-3 | (0.88) | **35** | 5.65E-3 | (0.99) | **50** | 4.97E-3 | (1.05) | **65** | 3.72E-3 | (1.25) |
| **6** | 5.73E-3 | (0.98) | **21** | 7.35E-3 | (0.94) | **36** | 5.14E-3 | (1.12) | **51** | 4.70E-3 | (1.11) | **66** | 3.63E-3 | (1.27) |
| **7** | 6.39E-3 | (0.93) | **22** | 5.46E-3 | (0.95) | **37** | 4.78E-3 | (1.02) | **52** | 4.21E-3 | (1.17) | **67** | 3.53E-3 | (1.28) |
| **8** | 6.66E-3 | (0.93) | **23** | 6.48E-3 | (0.92) | **38** | 5.59E-3 | (0.99) | **53** | 3.63E-3 | (1.27) | **68** | 3.39E-3 | (1.31) |
| **9** | 6.81E-3 | (0.90) | **24** | 5.76E-3 | (0.93) | **39** | 4.92E-3 | (1.00) | **54** | 3.67E-3 | (1.37) | **69** | 3.65E-3 | (1.36) |
| **10** | 7.11E-3 | (0.96) | **25** | 6.80E-3 | (0.90) | **40** | 5.76E-3 | (0.98) | **55** | 2.39E-3 | (1.66) | **70** | 2.46E-3 | (1.43) |
| **11** | 5.63E-3 | (0.94) | **26** | 5.97E-3 | (0.91) | **41** | 5.79E-3 | (1.00) | **56** | 4.64E-3 | (1.12) | **71** | 2.28E-3 | (1.49) |
| **12** | 6.71E-3 | (0.91) | **27** | 6.67E-3 | (0.91) | **42** | 5.48E-3 | (1.00) | **57** | 4.51E-3 | (1.10) | **72** | 2.26E-3 | (1.50) |
| **13** | 6.00E-3 | (0.91) | **28** | 5.40E-3 | (1.01) | **43** | 4.34E-3 | (1.06) | **58** | 4.49E-3 | (1.14) | **73** | 2.17E-3 | (1.53) |
| **14** | 7.19E-3 | (0.87) | **29** | 5.93E-3 | (0.97) | **44** | 4.49E-3 | (1.11) | **59** | 4.33E-3 | (1.13) | **74** | 2.03E-3 | (1.58) |
| **15** | 6.55E-3 | (0.92) | **30** | 6.15E-3 | (0.97) | **45** | 4.08E-3 | (1.26) | **60** | 4.23E-3 | (1.17) | **75** | 2.08E-3 | (1.68) |
| Layer 21 | | | | | | | | | | | | | | |
| **1** | 3.75E-3 | (1.22) | **16** | 4.88E-3 | (1.07) | **31** | 4.72E-3 | (1.08) | **46** | 3.80E-3 | (1.21) | **61** | 2.77E-3 | (1.45) |
| **2** | 4.46E-3 | (1.11) | **17** | 5.06E-3 | (1.07) | **32** | 4.81E-3 | (1.10) | **47** | 3.28E-3 | (1.23) | **62** | 2.23E-3 | (1.51) |
| **3** | 3.98E-3 | (1.17) | **18** | 5.22E-3 | (1.03) | **33** | 4.76E-3 | (1.08) | **48** | 3.77E-3 | (1.21) | **63** | 1.75E-3 | (1.70) |
| **4** | 4.08E-3 | (1.10) | **19** | 5.49E-3 | (1.03) | **34** | 4.64E-3 | (1.12) | **49** | 3.27E-3 | (1.23) | **64** | 1.57E-3 | (1.94) |
| **5** | 4.80E-3 | (1.07) | **20** | 5.70E-3 | (1.01) | **35** | 4.21E-3 | (1.14) | **50** | 3.69E-3 | (1.22) | **65** | 2.78E-3 | (1.45) |
| **6** | 4.33E-3 | (1.13) | **21** | 5.55E-3 | (1.08) | **36** | 3.86E-3 | (1.29) | **51** | 3.51E-3 | (1.29) | **66** | 2.70E-3 | (1.47) |
| **7** | 4.86E-3 | (1.07) | **22** | 4.12E-3 | (1.09) | **37** | 3.60E-3 | (1.17) | **52** | 3.16E-3 | (1.35) | **67** | 2.64E-3 | (1.48) |
| **8** | 5.06E-3 | (1.07) | **23** | 4.89E-3 | (1.06) | **38** | 4.24E-3 | (1.14) | **53** | 2.71E-3 | (1.46) | **68** | 2.46E-3 | (1.54) |
| **9** | 5.19E-3 | (1.03) | **24** | 4.35E-3 | (1.06) | **39** | 3.70E-3 | (1.15) | **54** | 2.75E-3 | (1.59) | **69** | 2.29E-3 | (1.60) |
| **10** | 5.40E-3 | (1.09) | **25** | 5.14E-3 | (1.04) | **40** | 4.32E-3 | (1.13) | **55** | 1.81E-3 | (1.91) | **70** | 1.79E-3 | (1.67) |
| **11** | 4.29E-3 | (1.08) | **26** | 4.48E-3 | (1.05) | **41** | 4.36E-3 | (1.15) | **56** | 3.48E-3 | (1.30) | **71** | 1.71E-3 | (1.73) |
| **12** | 5.08E-3 | (1.04) | **27** | 5.02E-3 | (1.05) | **42** | 4.11E-3 | (1.16) | **57** | 3.36E-3 | (1.28) | **72** | 1.67E-3 | (1.74) |
| **13** | 4.55E-3 | (1.04) | **28** | 4.07E-3 | (1.16) | **43** | 3.23E-3 | (1.23) | **58** | 3.35E-3 | (1.32) | **73** | 1.61E-3 | (1.77) |

| | | | | | | | | | | | | |
|---|---|---|---|---|---|---|---|---|---|---|---|---|
| **14** | 5.46E-3 | (1.00) | **29** | 4.50E-3 | (1.11) | **44** | 3.39E-3 | (1.28) | **59** | 3.20E-3 | (1.31) | **74** | 1.46E-3 | (1.86) |
| **15** | 4.93E-3 | (1.06) | **30** | 4.62E-3 | (1.12) | **45** | 3.08E-3 | (1.45) | **60** | 3.09E-3 | (1.37) | **75** | 1.37E-3 | (1.94) |
| Layer 22 | | | | | | | | | | | | | | |
| **1** | 2.76E-3 | (1.43) | **16** | 3.57E-3 | (1.25) | **31** | 3.43E-3 | (1.27) | **46** | 2.77E-3 | (1.42) | **61** | 1.99E-3 | (1.71) |
| **2** | 3.30E-3 | (1.30) | **17** | 3.72E-3 | (1.25) | **32** | 3.51E-3 | (1.29) | **47** | 2.39E-3 | (1.43) | **62** | 1.58E-3 | (1.79) |
| **3** | 2.95E-3 | (1.37) | **18** | 3.80E-3 | (1.20) | **33** | 3.47E-3 | (1.26) | **48** | 2.74E-3 | (1.42) | **63** | 1.26E-3 | (2.02) |
| **4** | 3.00E-3 | (1.29) | **19** | 3.99E-3 | (1.21) | **34** | 3.35E-3 | (1.32) | **49** | 2.36E-3 | (1.44) | **64** | 1.15E-3 | (2.28) |
| **5** | 3.54E-3 | (1.25) | **20** | 4.15E-3 | (1.18) | **35** | 3.07E-3 | (1.34) | **50** | 2.66E-3 | (1.44) | **65** | 2.00E-3 | (1.71) |
| **6** | 3.21E-3 | (1.31) | **21** | 4.04E-3 | (1.27) | **36** | 2.80E-3 | (1.53) | **51** | 2.53E-3 | (1.51) | **66** | 1.96E-3 | (1.73) |
| **7** | 3.59E-3 | (1.24) | **22** | 3.00E-3 | (1.29) | **37** | 2.61E-3 | (1.38) | **52** | 2.27E-3 | (1.60) | **67** | 1.90E-3 | (1.74) |
| **8** | 3.73E-3 | (1.25) | **23** | 3.55E-3 | (1.24) | **38** | 3.05E-3 | (1.34) | **53** | 1.95E-3 | (1.73) | **68** | 1.77E-3 | (1.80) |
| **9** | 3.82E-3 | (1.20) | **24** | 3.16E-3 | (1.25) | **39** | 2.70E-3 | (1.35) | **54** | 2.00E-3 | (1.86) | **69** | 1.60E-3 | (1.91) |
| **10** | 3.94E-3 | (1.28) | **25** | 3.73E-3 | (1.21) | **40** | 3.15E-3 | (1.32) | **55** | 1.31E-3 | (2.24) | **70** | 1.28E-3 | (1.98) |
| **11** | 3.13E-3 | (1.26) | **26** | 3.28E-3 | (1.22) | **41** | 3.16E-3 | (1.36) | **56** | 2.51E-3 | (1.53) | **71** | 1.24E-3 | (2.03) |
| **12** | 3.71E-3 | (1.22) | **27** | 3.66E-3 | (1.23) | **42** | 2.98E-3 | (1.36) | **57** | 2.43E-3 | (1.51) | **72** | 1.21E-3 | (2.05) |
| **13** | 3.32E-3 | (1.22) | **28** | 2.95E-3 | (1.37) | **43** | 2.35E-3 | (1.45) | **58** | 2.42E-3 | (1.55) | **73** | 1.17E-3 | (2.07) |
| **14** | 3.99E-3 | (1.18) | **29** | 3.27E-3 | (1.30) | **44** | 2.43E-3 | (1.51) | **59** | 2.29E-3 | (1.56) | **74** | 1.06E-3 | (2.19) |
| **15** | 3.64E-3 | (1.24) | **30** | 3.39E-3 | (1.31) | **45** | 2.25E-3 | (1.71) | **60** | 2.20E-3 | (1.63) | **75** | 9.82E-4 | (2.28) |
| Layer 23 | | | | | | | | | | | | | | |
| **1** | 1.91E-3 | (1.72) | **16** | 2.44E-3 | (1.51) | **31** | 2.34E-3 | (1.53) | **46** | 1.86E-3 | (1.73) | **61** | 1.35E-3 | (2.08) |
| **2** | 2.24E-3 | (1.57) | **17** | 2.53E-3 | (1.51) | **32** | 2.38E-3 | (1.56) | **47** | 1.62E-3 | (1.74) | **62** | 1.08E-3 | (2.17) |
| **3** | 2.00E-3 | (1.66) | **18** | 2.59E-3 | (1.46) | **33** | 2.34E-3 | (1.53) | **48** | 1.86E-3 | (1.72) | **63** | 8.51E-4 | (2.44) |
| **4** | 2.05E-3 | (1.56) | **19** | 2.71E-3 | (1.46) | **34** | 2.25E-3 | (1.60) | **49** | 1.60E-3 | (1.75) | **64** | 7.53E-4 | (2.79) |
| **5** | 2.42E-3 | (1.51) | **20** | 2.82E-3 | (1.44) | **35** | 2.07E-3 | (1.63) | **50** | 1.80E-3 | (1.75) | **65** | 1.35E-3 | (2.08) |
| **6** | 2.19E-3 | (1.59) | **21** | 2.73E-3 | (1.54) | **36** | 1.88E-3 | (1.85) | **51** | 1.69E-3 | (1.85) | **66** | 1.31E-3 | (2.10) |
| **7** | 2.44E-3 | (1.51) | **22** | 2.06E-3 | (1.55) | **37** | 1.79E-3 | (1.66) | **52** | 1.53E-3 | (1.95) | **67** | 1.30E-3 | (2.12) |
| **8** | 2.54E-3 | (1.51) | **23** | 2.43E-3 | (1.51) | **38** | 2.09E-3 | (1.63) | **53** | 1.32E-3 | (2.11) | **68** | 1.20E-3 | (2.21) |
| **9** | 2.60E-3 | (1.46) | **24** | 2.15E-3 | (1.52) | **39** | 1.84E-3 | (1.64) | **54** | 1.34E-3 | (2.28) | **69** | 1.08E-3 | (2.32) |
| **10** | 2.70E-3 | (1.55) | **25** | 2.54E-3 | (1.47) | **40** | 2.13E-3 | (1.61) | **55** | 8.67E-4 | (2.75) | **70** | 8.66E-4 | (2.40) |
| **11** | 2.14E-3 | (1.52) | **26** | 2.24E-3 | (1.48) | **41** | 2.13E-3 | (1.65) | **56** | 1.70E-3 | (1.85) | **71** | 8.28E-4 | (2.48) |
| **12** | 2.54E-3 | (1.47) | **27** | 2.47E-3 | (1.49) | **42** | 2.00E-3 | (1.66) | **57** | 1.65E-3 | (1.83) | **72** | 8.08E-4 | (2.50) |
| **13** | 2.28E-3 | (1.48) | **28** | 1.98E-3 | (1.66) | **43** | 1.60E-3 | (1.75) | **58** | 1.63E-3 | (1.88) | **73** | 7.83E-4 | (2.53) |
| **14** | 2.74E-3 | (1.42) | **29** | 2.22E-3 | (1.58) | **44** | 1.64E-3 | (1.84) | **59** | 1.55E-3 | (1.89) | **74** | 7.15E-4 | (2.65) |
| **15** | 2.44E-3 | (1.50) | **30** | 2.29E-3 | (1.59) | **45** | 1.48E-3 | (2.10) | **60** | 1.48E-3 | (1.98) | **75** | 6.52E-4 | (2.81) |
| Layer 24 | | | | | | | | | | | | | | |
| **1** | 1.17E-3 | (2.19) | **16** | 1.50E-3 | (1.94) | **31** | 1.40E-3 | (1.99) | **46** | 1.14E-3 | (2.22) | **61** | 7.93E-4 | (2.72) |
| **2** | 1.36E-3 | (2.02) | **17** | 1.53E-3 | (1.95) | **32** | 1.43E-3 | (2.02) | **47** | 9.61E-4 | (2.27) | **62** | 6.21E-4 | (2.85) |
| **3** | 1.20E-3 | (2.14) | **18** | 1.56E-3 | (1.88) | **33** | 1.42E-3 | (1.99) | **48** | 1.11E-3 | (2.23) | **63** | 5.00E-4 | (3.20) |
| **4** | 1.21E-3 | (2.02) | **19** | 1.60E-3 | (1.91) | **34** | 1.36E-3 | (2.08) | **49** | 9.56E-4 | (2.27) | **64** | 4.41E-4 | (3.64) |
| **5** | 1.46E-3 | (1.94) | **20** | 1.67E-3 | (1.87) | **35** | 1.24E-3 | (2.11) | **50** | 1.08E-3 | (2.27) | **65** | 7.93E-4 | (2.71) |
| **6** | 1.32E-3 | (2.05) | **21** | 1.63E-3 | (2.00) | **36** | 1.12E-3 | (2.40) | **51** | 1.00E-3 | (2.40) | **66** | 7.79E-4 | (2.74) |
| **7** | 1.48E-3 | (1.94) | **22** | 1.23E-3 | (2.01) | **37** | 1.05E-3 | (2.17) | **52** | 9.00E-4 | (2.53) | **67** | 7.57E-4 | (2.76) |
| **8** | 1.53E-3 | (1.96) | **23** | 1.47E-3 | (1.94) | **38** | 1.25E-3 | (2.10) | **53** | 7.78E-4 | (2.74) | **68** | 7.00E-4 | (2.88) |
| **9** | 1.57E-3 | (1.88) | **24** | 1.28E-3 | (1.96) | **39** | 1.09E-3 | (2.12) | **54** | 7.61E-4 | (3.01) | **69** | 6.39E-4 | (3.02) |
| **10** | 1.62E-3 | (2.00) | **25** | 1.54E-3 | (1.90) | **40** | 1.29E-3 | (2.07) | **55** | 5.00E-4 | (3.63) | **70** | 5.10E-4 | (3.14) |
| **11** | 1.29E-3 | (1.96) | **26** | 1.32E-3 | (1.93) | **41** | 1.27E-3 | (2.14) | **56** | 1.02E-3 | (2.41) | **71** | 4.79E-4 | (3.26) |
| **12** | 1.53E-3 | (1.89) | **27** | 1.49E-3 | (1.93) | **42** | 1.22E-3 | (2.15) | **57** | 9.88E-4 | (2.37) | **72** | 4.71E-4 | (3.26) |
| **13** | 1.36E-3 | (1.90) | **28** | 1.19E-3 | (2.16) | **43** | 9.48E-4 | (2.29) | **58** | 9.59E-4 | (2.46) | **73** | 4.57E-4 | (3.32) |

| | | | | | | | | | | | | |
|---|---|---|---|---|---|---|---|---|---|---|---|---|
| **14** | 1.65E-3 | (1.84) | **29** | 1.34E-3 | (2.04) | **44** | 9.78E-4 | (2.39) | **59** | 9.33E-4 | (2.44) | **74** | 4.10E-4 | (3.49) |
| **15** | 1.46E-3 | (1.95) | **30** | 1.39E-3 | (2.06) | **45** | 8.52E-4 | (2.74) | **60** | 8.77E-4 | (2.56) | **75** | 3.85E-4 | (3.66) |
| Layer 25 | | | | | | | | | | | | | | |
| **1** | 2.61E-4 | (3.21) | **16** | 3.02E-4 | (2.55) | **31** | 2.80E-4 | (2.63) | **46** | 2.23E-4 | (2.97) | **61** | 1.52E-4 | (3.88) |
| **2** | 2.78E-4 | (2.67) | **17** | 3.19E-4 | (2.69) | **32** | 2.94E-4 | (2.80) | **47** | 2.26E-4 | (3.20) | **62** | 1.32E-4 | (4.20) |
| **3** | 2.79E-4 | (3.05) | **18** | 3.13E-4 | (2.48) | **33** | 2.83E-4 | (2.62) | **48** | 2.18E-4 | (2.97) | **63** | 1.01E-4 | (4.79) |
| **4** | 2.85E-4 | (2.84) | **19** | 3.29E-4 | (2.65) | **34** | 2.80E-4 | (2.87) | **49** | 2.20E-4 | (3.22) | **64** | 8.97E-5 | (5.49) |
| **5** | 2.92E-4 | (2.57) | **20** | 3.22E-4 | (2.67) | **35** | 2.48E-4 | (2.81) | **50** | 2.16E-4 | (3.01) | **65** | 1.52E-4 | (3.88) |
| **6** | 3.06E-4 | (2.90) | **21** | 3.20E-4 | (2.87) | **36** | 2.30E-4 | (3.38) | **51** | 2.03E-4 | (3.36) | **66** | 1.52E-4 | (3.89) |
| **7** | 2.98E-4 | (2.57) | **22** | 2.83E-4 | (2.85) | **37** | 2.42E-4 | (3.06) | **52** | 1.76E-4 | (3.61) | **67** | 1.45E-4 | (3.99) |
| **8** | 3.17E-4 | (2.70) | **23** | 2.93E-4 | (2.58) | **38** | 2.48E-4 | (2.80) | **53** | 1.51E-4 | (3.92) | **68** | 1.39E-4 | (4.05) |
| **9** | 3.12E-4 | (2.49) | **24** | 3.02E-4 | (2.75) | **39** | 2.53E-4 | (3.00) | **54** | 1.36E-4 | (4.43) | **69** | 1.21E-4 | (4.31) |
| **10** | 3.38E-4 | (2.81) | **25** | 3.05E-4 | (2.52) | **40** | 2.55E-4 | (2.75) | **55** | 9.76E-5 | (5.55) | **70** | 1.06E-4 | (4.64) |
| **11** | 3.00E-4 | (2.78) | **26** | 3.05E-4 | (2.73) | **41** | 2.65E-4 | (2.96) | **56** | 2.04E-4 | (3.37) | **71** | 1.02E-4 | (4.78) |
| **12** | 3.10E-4 | (2.50) | **27** | 2.89E-4 | (2.58) | **42** | 2.41E-4 | (2.84) | **57** | 1.96E-4 | (3.15) | **72** | 1.01E-4 | (4.76) |
| **13** | 3.19E-4 | (2.68) | **28** | 2.78E-4 | (3.06) | **43** | 2.14E-4 | (3.26) | **58** | 1.92E-4 | (3.45) | **73** | 9.63E-5 | (4.93) |
| **14** | 3.25E-4 | (2.45) | **29** | 2.72E-4 | (2.70) | **44** | 1.90E-4 | (3.19) | **59** | 1.86E-4 | (3.23) | **74** | 8.76E-5 | (5.12) |
| **15** | 3.25E-4 | (2.83) | **30** | 2.88E-4 | (2.83) | **45** | 1.87E-4 | (4.02) | **60** | 1.75E-4 | (3.62) | **75** | 8.07E-5 | (5.38) |

# APPENDIX B

# SUPPLEMENTAL DATA – HTTR 1D BENCHMARK

Table B.1: 1D HTTR Geometric Parameters

| | | Material | Width (cm) |
|---|---|---|---|
| Fuel Bundles (blocks 2,3,4) | Fuel Pin Cell | Graphite | 0.9046 |
| | | He Gas | 0.3819 |
| | | Sleeve | 0.3492 |
| | | Fuel | 0.4190 |
| | | He Gas | 0.1455 |
| | | Fuel | 0.4190 |
| | | Sleeve | 0.3492 |
| | | He Gas | 0.3819 |
| | | Graphite | 0.9046 |
| | Center Cell | Graphite | 4.2550 |
| | Outer Regions | Graphite+BP | 4.0090 |
| Control Bundles (blocks 1,5) | Outer Regions | Graphite | 3.7013 |
| | Tube | He/Grph | 1.0285 |
| | Control | $B_4C$/Grph | 11.9991 |
| | Center Cell | Graphite | 2.2879 |
| Reflector | Entire Cell | Graphite | 37.8027 |

Number densities for material regions of the HTTR 1D Benchmark problem are presented in Table B.2. For block 3, (C) and (UC) represent the controlled and uncontrolled block respectively.

Table B.2: HTTR Material Number Densities (part/bcm)

| | U235 | U238 | B10 | B11 | C-nat | O16 | Si28 | He4 |
|---|---|---|---|---|---|---|---|---|
| Graphite | | | 7.8482E-09 | 3.1590E-08 | 8.8745E-02 | | | |
| CentCRB Tube | | | 4.4964E-09 | 1.8098E-08 | 5.0843E-02 | | | |
| CentCRB Rod | | | 1.9945E-04 | 8.0789E-04 | 4.6763E-02 | | | |
| Sleeve | | | 7.1811E-09 | 2.8905E-08 | 8.8745E-02 | | | |
| He | | | | | | | | 2.5649E-05 |
| Grph+BP | | | 3.6590E-06 | 1.4468E-05 | 8.7422E-02 | | | |
| Fuel 1 | 8.8371E-05 | 1.8340E-03 | 2.3030E-08 | 9.2697E-08 | 7.5868E-02 | 3.8447E-03 | 2.0737E-03 | |
| Block 3 Grph (UC) | | | 6.1945E-09 | 2.4934E-08 | 7.0046E-02 | | | |
| Block 3 Grph (C) | | | 1.0006E-05 | 4.0529E-05 | 6.6170E-02 | | | |
| Block 3 Grph+BP (UC) | | | 1.8322E-06 | 7.2449E-06 | 7.3991E-02 | | | |
| Block 3 Grph+BP (C) | | | 9.3686E-06 | 3.7771E-05 | 7.1070E-02 | | | |
| Fuel 2 | 1.0467E-04 | 1.8123E-03 | 2.2597E-08 | 9.0955E-08 | 7.5749E-02 | 3.8340E-03 | 2.0487E-03 | |
| Fuel 3 | 1.2458E-04 | 1.7872E-03 | 2.2202E-08 | 8.9367E-08 | 7.5846E-02 | 3.8236E-03 | 2.0336E-03 | |
| OuterCRB Tube | | | 6.1723E-09 | 2.4844E-08 | 6.9794E-02 | | | |
| OuterCRB Rod | | | 7.4800E-05 | 3.0298E-04 | 6.8264E-02 | | | |

# REFERENCES


Bell, G.I., and Glasstone, S. Nuclear Reactor Theory, Krieger Publishing Company. Malabar, FL, (1970).

Cathalau, S, LeFebvre, J.C., West, J.P."Proposal for a Second Stage of the Benchmark on Power Distributions within Assemblies", NEA/NSC/DOC(96)2 (1996)

Challifour, John, Generalized Functions and Fourier Analysis: An Introduciton. W.A.Benjamin. Reading, MA (1972).

deBoor, Carl, "On Calculations with B-Splines," *J. Approx. Theory,* Volume 6, pp 50-62 (1972).

deBoor, Carl, A Practical Guide to Splines. Springer. New York (2001).

Douglass, S. and Rahnema, F. "Analysis of cross section condensation in PWR simulations." PHYSOR-2010: Advances in Reactor Physics to Power the Nuclear Renaissance, Pittsburgh, PA, May 9-14 (2010).

Douglass, S. and Rahnema, F. "Cross section recondensation method via generalized energy condensation theory." *Annals of Nuclear Energy*, Volume 38, Issue 9, pp 2105-2110 (2011a).

Douglass, S. and Rahnema, F. "Specification for a 1-dimensional gas-cooled reactor benchmark problem for neutron transport." Am. Nucl. Soc. 2011 National Meeting, Hollywood, FL - Trans. of the Am. Nucl. Soc., Volume 104, pp 74-78 (2011b).

Douglass, S. and Rahnema, F. "Consistent generalized energy condensation theory." *Annals of Nuclear Energy*, Volume 40, Issue 1, pp 200-214 (2012a).

Douglass, S. and Rahnema, F. "Cross Section Recondensation as a Spectral Correction for Non-Fissionable Lattices in VHTR Cores," Am. Nucl. Soc. 2012 National Meeting, Chicago, IL, Accepted. (2012b).

Kelly, D.J., "Depletion of a BWR Lattice Using the RACER Continuous Energy Monte Carlo Code," *Proceedings of the International Conference on Mathematics and Computations, Reactor Physics and Environmental Analyses*, Portland, Oregon, April 30-May 4, Vol. 2, p. 1011, American Nuclear Society (1995).

Kozlowski, T. and Downar, T. J., "OECD/NEA and U.S. NRC PWR MOX/UO2 Core Transient Benchmark," NEA/NSC/DOC(2003)20, (2003)

LANL, "The NJOY Nuclear Data Processing System, Version 91," LA-12740-M, Los Alamos National Laboratory (1994).

LANL, X-5 Monte Carlo Team, “MCNP-A General Monte Carlo N-Particle Transport Code, Version 5”, Los Alamos National Laboratory (2005).

Lewis, E.E. and Miller, W.F., Jr. (1993), Computational Methods of Neutron Transport, *American Nuclear Society*, La Grange Park, Illinois.

McKinley, M.S. and Rahnema, F. “Higher-Order Boundary Condition Perturbation Theory for the Diffusion Approximation,” *Nucl. Sci. and Eng.* Volume 136, pp 15-33. (2000).

Mosher S., “A Variational Transport Theory Method for Two-Dimensional Reactor Core Calculations,” PhD Dissertation, Georgia Institute of Technology, Atlanta, GA (2004).

Mosher, S. and Rahnema, F. “The Incident Flux Response Expansion Method for Heterogeneous Coarse Mesh Transport Problems,” *Transport Theory and Statistical Physics* Volume 35, pp 55-86 (2006).

Nath, R.J., Ed., PWR Technology Manual, WCAP-7730, PWR Systems Division, Westinghouse Nuclear Energy Systems. (1971).

Nojiri, N., Nakano, M., Fujimoto, N. et al., "Benchmark Problem’s Data for HTTR’s Start-up Core Physics Experiments." JAERI-memo 10-1005, JAERI, (2008).

Pounders, J. and Rahnema, F. “Moment-Conserving Histopolating B-Splines for Continuous Tally Estimation.” *PHYSOR2010 – Advances in Reactor Physics to Power the Nuclear Renaissance,* Pittsburgh, PA. American Nuclear Society (2010).

Rahnema, F., Douglass, S., and Forget, B., “Generalized energy condensation theory.” *Nucl. Sci. and Eng.*, Volume 160, Issue 1, pp 41-58 (2008).

Rahnema, F. and McKinley, M.S. “High-Order Cross Section Homogenization Method,” *Annals of Nuclear Energy,* Volume 29, pp 875-899 (2002).

Rose, P.F. and Dunford, C.L. Eds., "*ENDF-102, Data Formats and Procedures for the Evaluated Nuclear Data File, ENDF-6*," Brookhaven National Laboratory report BNL-NCS-44945 (1990).

Silver, R.N., Roeder, H., Voter, A.F. and Kress, J.D. “Kernel Polynomial Approximations for Densities of States and Spectral Functions,” *J. Comput. Phys.* Volume 124, pp 115-130 (1996).

Simeonov, T., “Release Notes – Helios System Version 1.8,” Studsvik Scandpower Report, SSP-03/221, November 26 (2003).

Smith, K.S., “Spatial Homogenization Methods for Light Water Reactor Analysis,” Ph.D. Thesis, Massachusetts Institute of Technology (1980).

Smith, K.S., “Assembly Homogenization Techniques for Light Water Reactor Analysis,” *Progress in Nuclear Energy,* Volume 17, pp 303-335. (1994)

Solis, J, Ivanov, K., and Sarikaya, B . “Boiling Water Reactor Turbine Trip (TT) Benchmarks; Volume I: Final Specifications,” NEA/NSC/DOC(2001)1 (2001)

Sutton, B. (Private Communication), (2007).

Taiwo, T.A., Kim, T.K., Yang, W.S., Khalil, H.S. "Evaluation of the High Temperature Engineering Test Reactor (HTTR) Start-up Experiments." ANL-GenIV-059 (2005).

Williams, M.L. “Pointwise Energy Solution of the Boltzmann Transport Equation for Thermal Neutrons,” DOE/ID/13765, (2001)

Williams, M.L. and Asgari, M “Computation of Continuous-Energy Neutron Spectra with Discrete Ordinates Transport Theory”, *Nucl. Sci. and Eng.* Volume 121, 173-201 (1995).

Won, J.H. and Cho, N.Z. “Discrete Ordinates method-like transport computation with equivalent group condensation and angle-collapsing for local/global iteration”, *Annals of Nuclear Energy,* Volume 38, pp 846-852 (2011).

Yamashita, K. et. al., "Nuclear Design of the High Temperature Engineering Test Reactor (HTTR)," Nuclear Science and Engineering, Volume 122, Issue 1, pp 212-228 (1996).

Zerkle, M.L., “Theory and Application of Deterministic, Multidimensional, Pointwise Energy Lattice Physics Methods,” *B-T-3287*, Bettis Atomic Power Library (1999).

Zerkle, M. L., Abu-Shumays, I. K., Ott,M. W., and Winwood, J. P. “Theory and Application of the RAZOR Two-Dimensional Continuous Energy Lattice Physics Code,” *Proceeding of the Joint International Conference on Mathematical Methods and Supercomputing for Nuclear Applications,* Saratoga Springs, New York, October 5-9, 1997, Vol. 1, pp. 417-428, American Nuclear Society (1997).

Zhang, Z. et al, “Simplified two and three dimensional HTTR benchmark problems.” Annals of Nuclear Energy, Volume 38, Issue 5, pp 1172-1185 (2011).

Zhu, L. and Forget, B., “A Discrete Generalized Energy Expansion Theory,” Nuclear Science and Engineering, Volume 166, Issue 3, pp 239-253 (2010).

Zhu, L. and Forget, B., "An energy recondensation method using the discrete generalized multigroup energy expansion theory," Annals of Nuclear Energy, Volume 38, Issue 8 pp 1718-1727 (2011).

# VITA

## STEVEN JAMES DOUGLASS

DOUGLASS was born in San Antonio, TX, and attended public school in Canton, GA. He received a B.S. in Physics in 2005 and an M.S. in Nuclear Engineering in 2007, both from the Georgia Institute of Technology. During his undergraduate career he became a member of the Georgia Tech Band and Kappa Kappa Psi National Honorary Band Fraternity. He began his doctoral work at Georgia Tech in the Computational Reactor and Medical Physics Lab immediately after his M.S., working towards a PhD in Nuclear Engineering. When not pursuing research, Mr. Douglass enjoys running, watching baseball, and playing racquetball.